CAPITAL REGION HEAT POLLUTION REDUCTION

Atmospheric Modeling for the Development of a Regional Heat Pollution Reduction Plan

Technical Project Report

Prepared for

Shelley Jiang
Sacramento Metropolitan Air Quality Management District
777 12th Street
Sacramento, CA 95814

Julia Kim and Helena Rhim
Local Government Commission
980 9th Street
Sacramento, CA 95814

Prepared by

Haider Taha
Altostratus Inc.
940 Toulouse Way
Martinez, CA 94553
haider@altostratus.com

February 26, 2020

Altostratus Inc.

ACKNOWLEDGEMENTS

TABLE OF CONTENTS

LIST OF TABLES

ACRONYMS AND ABBREVIATIONS

AGL   Above ground level
Cal/EPA   California Environmental Protection Agency
CCSM4   Community Climate System Model (fourth generation)
CES 3.0   CalEnviroScreen version 3.0
DAC   Disadvantaged communities
DH   Degree-hours
DH hr^{-1} Degree-hour per hour
DOT   Department of Transportation
EDC   El Dorado County
EDCAQMD   El Dorado County Air Quality Management District
FDDA   Four-dimensional data assimilation
FRAQMD   Feather River Air Quality Management District
JJAS   June, July, August, and September
LGC   Local Government Commission
MJJAS   May, June, July, August, and September
modUCM   An Altostratus Inc.-modified version of an urban canopy model
MTP   Metropolitan transportation plan
NNRP   NCEP-NCAR Reanalysis Project
NO$_2$ Nitrogen dioxide
O$_3$ Ozone
PAN   Peroxyacetyl nitrate
PCAPCD   Placer County Air Pollution Control District
RCP   Representative concentration pathway
SACOG   Sacramento Area Council of Governments
SacRT   Sacramento regional transit district
SMAQMD   Sacramento Metropolitan Air Quality Management District
SMUD   Sacramento Municipal Utility District
SoCAB   South Coast Air Basin
TAC   Technical Advisory Committee
UCM   Urban canopy model
UHI   Urban heat island (also see the Glossary)
UHII   Urban heat island index (also see the Glossary)
MPE   Model performance evaluation
WRF   Weather Research and Forecasting model
WSP   WSP Global Inc.
YSAQMD   Yolo-Solano Air Quality Management District
ZEV   Zero emissions vehicles

Altostratus Inc.

GLOSSARY

Albedo: Reflectivity integrated over a range of wavelengths and over the hemisphere

DH: Degree-hours

DH hr^{-1}:   Degree-hour per hour (temperature equivalent of UHII)

DH/15 days: Total number of degree-hours summed up over a period of 15 days

Heat wave:
                A period of time during which the National Weather Service Heat Index (NWS HI) is within or exceeds the values of 105 – 110 ºF on at least two consecutive days.

Probing points:
                Points of interest added to the analysis in locations where there are no weather stations – the goal is to increase the spatial data coverage and bridge the gap in areas with sparse monitoring networks

RCP: Representative concentration pathway (defined in detail in the report) is an indicator to the effects of emissions on future climates. Two scenarios (RCP 4.5 and RCP 8.5) are used in this study. Units are W m^{-2} in radiative forcing, e.g., 4.5 or 8.5 W m^{-2}.

UHI: Urban heat island: instantaneous temperature difference between an urban location and a non-urban reference point (e.g., at a single hour). Units are ºC.

UHII   Urban heat island index: a cumulative (total) temperature difference between an urban location and a non-urban reference point calculated over a determined time interval, e.g., several hours or several days, etc. Units are ºC · hr.

Time-varying upwind non-urban temperature reference points:
                In the approach applied in this study, the upwind non-urban temperatures needed to calculate the UHI or UHII are obtained from reference points that are dynamically identified at each hourly or sub-hourly interval (time-dependent) based on wind approach direction at that hour or interval.

EXECUTIVE SUMMARY

E.0 PREAMBLE

Detailed atmospheric modeling was undertaken in this study with the goal of informing and prioritizing the development of a heat mitigation plan for the Capital region, including the counties of Sacramento, El Dorado, Placer, Yuba, Sutter, and Yolo. The study, funded by SB-1 (Caltrans), was carried out to evaluate the effects of various mitigation measures on urban heat in these six counties.

The modeling was carried out to characterize and rank several proposed heat-mitigation measures in terms of their effectiveness in modifying local microclimates, i.e., in producing urban cooling. The study also addressed the potential negative impacts, albeit smaller, that could arise from implementation of these measures and the factors to consider in order to prevent or minimize any such effects.

An important consideration in this study was to design strategies of urban-heat mitigation that are reasonable and realistic, i.e., measures that are readily found and applied in the region, not hypothetical or extreme levels of modifications. These mitigation levels and characterizations of the interactions with the heat island effect were also designed as a refinement to the California UHI Index developed by Altostratus Inc. for the California Environmental Protection Agency (https://calepa.ca.gov/2015/09/16/urbanheat/).

The mitigation strategies (whether in standalone fashion or in combinations) evaluated in this effort were also based on feedback received from the participating counties, cities, and communities in the region. The main measures were:

- Cool roofs;
- Cool pavements;
- Vegetation canopy cover;
- Vehicles electrification / EV ownership;
- Solar PV; and
- Cool walls.

Six major tasks, each with several subtasks, were completed in this study:

1. Land-use and land-cover analysis (current conditions and future projections);
2. Observational meteorological data analysis (mesonet weather data);
3. Base modeling and model performance evaluation;
4. Modeling of mitigation measures in current climates and land use;
5. Modeling of mitigation measures in future climates and land use; and
6. Reporting and dissemination of results.

Two aspects are discussed in this report. The first is how practices in and modifications to the transportation system, e.g., pavements, roadways, and heat emissions, can affect the microclimate of surrounding areas and communities. The second is how practices in urban areas, e.g., implementation of cool surfaces, vegetation cover, fleet electrification, and other measures, can affect the transportation sector, including impacts on roadways and pavements temperatures.

This Executive Summary provides brief pointers to characterizations and findings from the modeling and analysis tasks. Details on all tasks can be found in the Project Technical Report which follows this summary.

E.1 THE UHI INDEX

To begin this discussion of heat mitigation, a distinction between the terms "urban heat" and "urban heat island" (UHI) or "urban heat island index" (UHII) needs to be made and the concepts clarified (see the Glossary). To re-state the obvious, the goal of this and similar studies is to design and implement measures that reduce urban heat, not urban heat islands per se. In other words, the goal is to cool down the ambient air in any hot urban area, regardless of how much hotter or cooler it may be compared to some other urban areas or some non-urban reference points (the latter being the definition of the urban heat island). Thus, if so, what is the purpose of characterizing urban heat islands (or the UHII) in this study? The simple answer is that the UHI and UHII are just quantitative indicators or yardsticks that tell us how much cooling we can reasonably expect to achieve at a certain urban location. In other words, the UHI (or UHII) simply is an indicator as to how much cooling is needed to bring the temperature at a certain urban location down to that of a nearby non-urban area. This, by definition, is the amount of cooling that could realistically be expected at that location (of course the actual cooling that is achievable could be smaller or larger than the UHI or UHII, as will be shown later in this report).

Having established this general understanding of urban heat and the purpose of computing the UHI or UHII, we can now proceed with the characterization of urban heat in the Capital region.

Based on the definition of time-varying upwind non-urban temperature reference points for each area (see the Glossary) and the hourly calculations of temperatures at each model grid cell per coincident wind direction, the urban heat island index (UHII) was computed for years (2013 – 2016), periods (May through September), and regions of interest in this study. The UHII was calculated for all hours, specific hours, as well as for a range of hours. A graphical example for the all-hours UHII is shown in Figure EX-1a where, additionally, several AB617 communities defined by the Sacramento Metropolitan AQMD are highlighted.

In this example, the UHII is for the period July 16 – 31, 2015 for which the all-hours averaged temperature equivalent (DH hr^{-1}) is as follows (shown with bold numbers on the figure for selected AB617 communities): A: 3.3 °C; B: 3.6 °C; C: 2.1 °C; D: 3.9 °C; E: 2.1 °C; G: 1.5 °C; and H: 2.7 °C. Other UHII temperature equivalents during this period are Davis: 2.1 °C; Woodland: 1.5 °C;

Yuba City: 2.2 °C; Placerville: 1.8 °C; Auburn: 4.5 °C; and Roseville-Lincoln: 4.7 °C, as seen in the figure.

In Figure EX-1a, the UHII in each of the six tiles (rectangles) is calculated independently from the others based on wind direction and different upwind reference points, even though all tiles are shown together as a mosaic on the same map. It is to be emphasized that this is a UHII map, not an absolute temperature field. Thus, in areas such as Auburn and Lincoln, the UHII can be elevated at times because of day/night variations in temperature of the natural surroundings, higher elevations, or heat transport from upwind urban areas.

The same UHII information is provided again in Figure EX-1b, but with urban and city boundaries outlined (with a black line) to provide a visual reference to areas of interest.

Figure EX-1a: Composite of UHII tiles, July 16-31, 2015 for all-hours averages in six tiles in the Capital region (A – H are some of the AB617 communities in this region). The UHII range in this example is 0 to 2176 °C·hr/15 days and each step change in color is equivalent to 155 °C·hr/15 days. The numbers in bold are the all-hours temperature equivalents (°C) of the UHII at the selected AB617 communities.
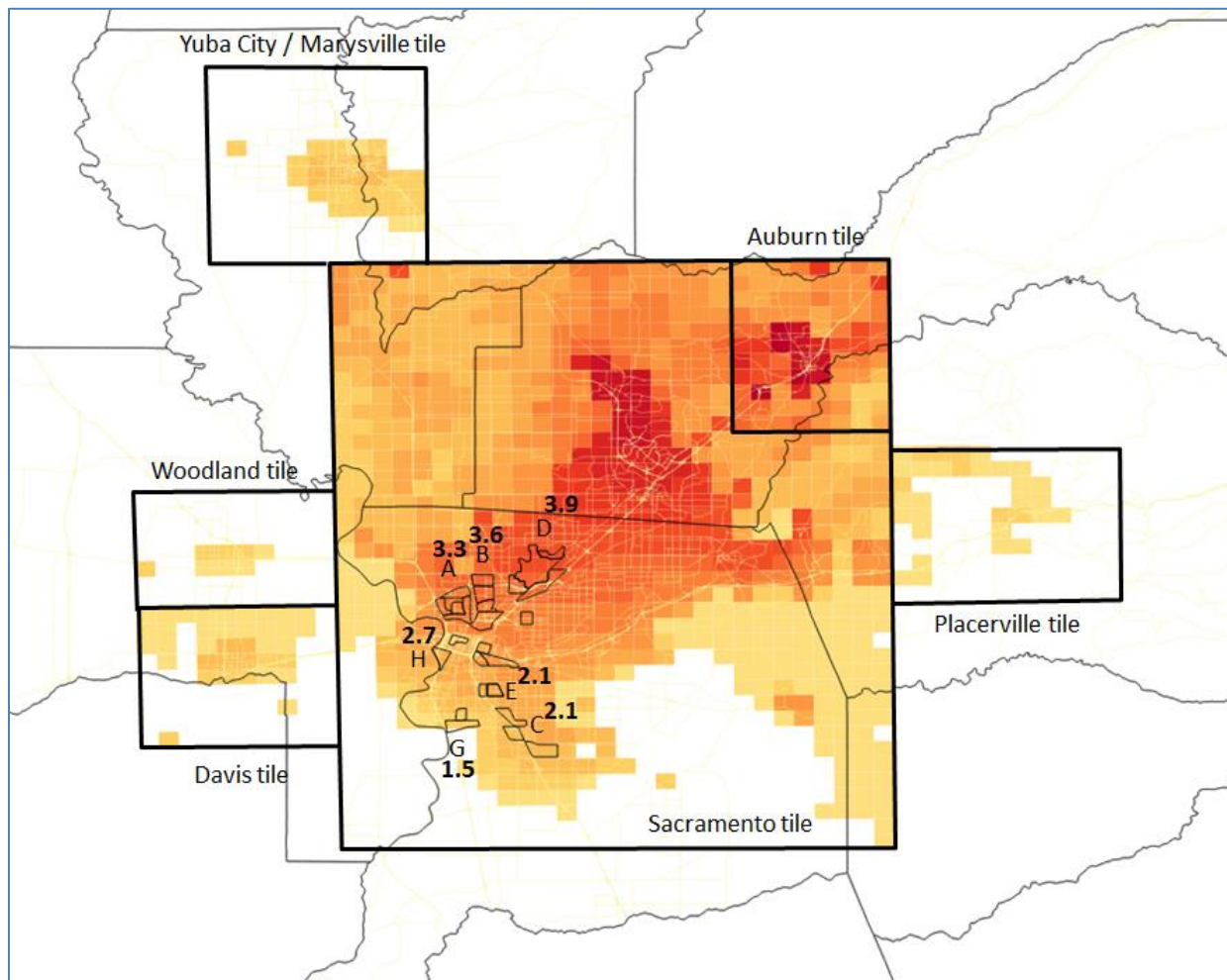
Figure EX-1b: As in Figure EX-1a, above, but with urban / city boundaries outlined.
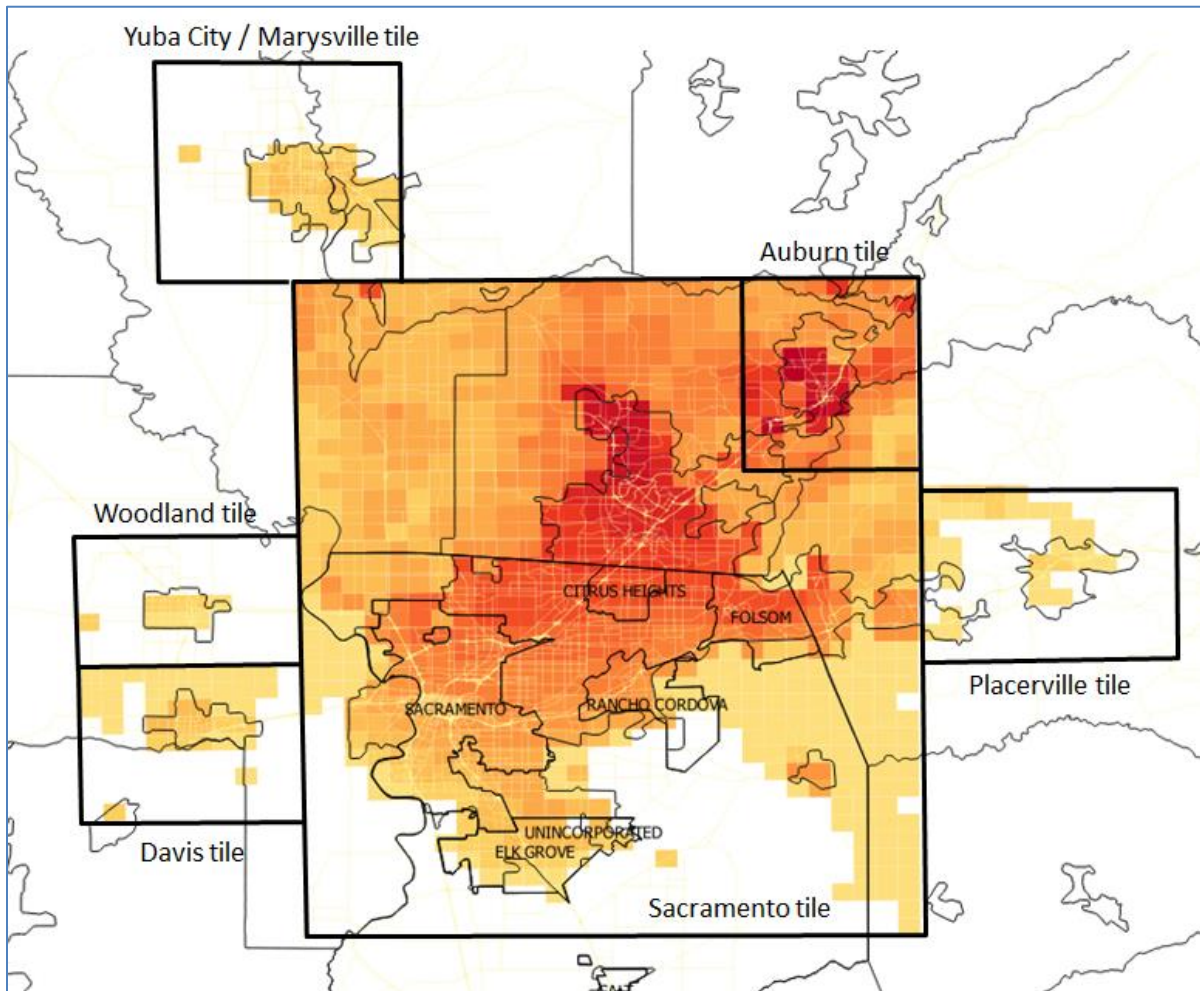
E.2 CHARACTERIZING URBAN HEAT IN RELATION TO CALTRANS PROJECTS

Some attributes of the current-climate urban heat and the UHII may be of interest to Caltrans, local jurisdictions, cities, transit providers, and communities as they can affect various aspects of paving, maintenance of roadways, aging of materials, and the transportation infrastructure in general. The impacts of UHI-mitigation measures on surface temperature (that can provide benefits to pavements' initial construction and long-term maintenance and aging) are discussed in the technical report. Here, a qualitative assessment of Caltrans's facilities and roadway projects locations in relation to the UHII is provided as an initial characterization of areas where urban-cooling measures might need to be introduced first (among other considerations). Those facilities and roadways that fall within the boundaries of the study domains are superimposed on the UHII and shown in Figure EX-2, including locations of airports, Amtrak stations, and state highways within the UHII tiles modeled in this region.

An important point to keep in mind, one that is re-iterated throughout this report, is that urban heat indicators (e.g., UHI and UHII) addressed and calculated in this study are air-temperature-based, not derived from skin surface temperature such as shown in many "urban hot-spot" studies or assessments based on satellite / remote-sensing data or imagery. Hence, the spatial patterns of urban heat analyzed in this study and presented in this report differ significantly from those seen in satellite imagery.

In Figure EX-2, the all-hours UHII for July 16 – 31, 2015, is shown in the background (other years and intervals provide similar information). The UHII range in this example is from 0 to 2176 °C·hr per 15 days and each step change in color is equivalent to 155 °C·hr per 15 days. Considering the information shown in this figure, a rough, initial ranking of Caltrans facilities can be formulated based on the UHII, from highest (most severe) to lowest (less severe):

- Airports rankings (highest to lowest UHII):
  - Auburn Municipal (AUN), Lincoln Regional (LHM), Sacramento McClellan (MCC), Rio Linda (L36), Sacramento International (SMF), Sacramento Executive (SAC), Sutter County (O52), Yuba County (MYV), Rancho Murieta (RIU), UC Davis (EDU), Yolo County (DWA), Placerville (PFV), and Woodland (O41);
- Amtrak stations rankings (highest to lowest UHII):
  - Auburn (ARN), Rocklin (RLN), Roseville (RSV), Marysville (MRV), Sacramento (SAC), State Capitol (SCS), Davis (DAV), Placerville (PCV), and Elk Grove (EKG);
- State highways rankings (highest to lowest UHII):
  - 65, 80, 244, 50, and 51; and
- Rankings based on traffic volume versus the UHII and the main routes in the region.

Figure EX-2: All-hours average UHII (July 16-31, 2015) versus Caltrans roadways and facilities locations. Data source for facilities and roadways: Caltrans (2019).
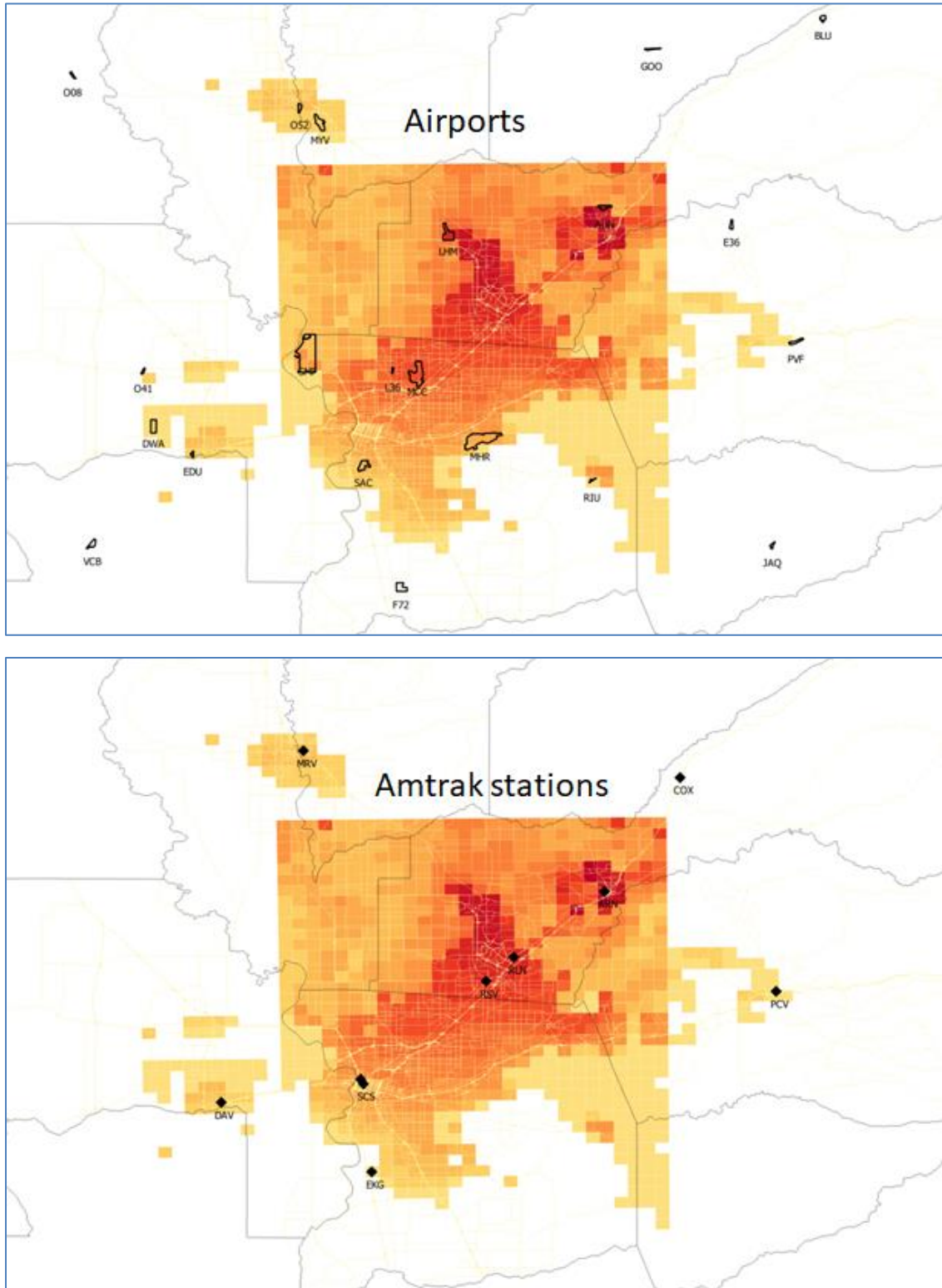
Figure EX-2, continued.
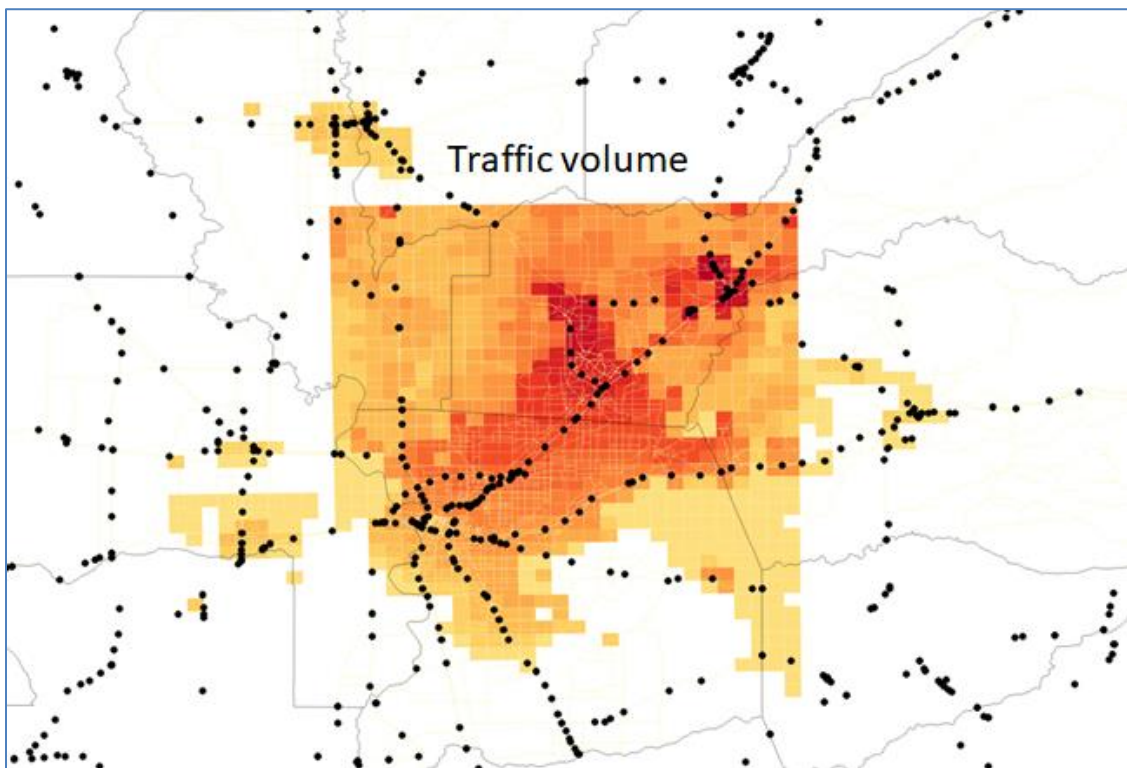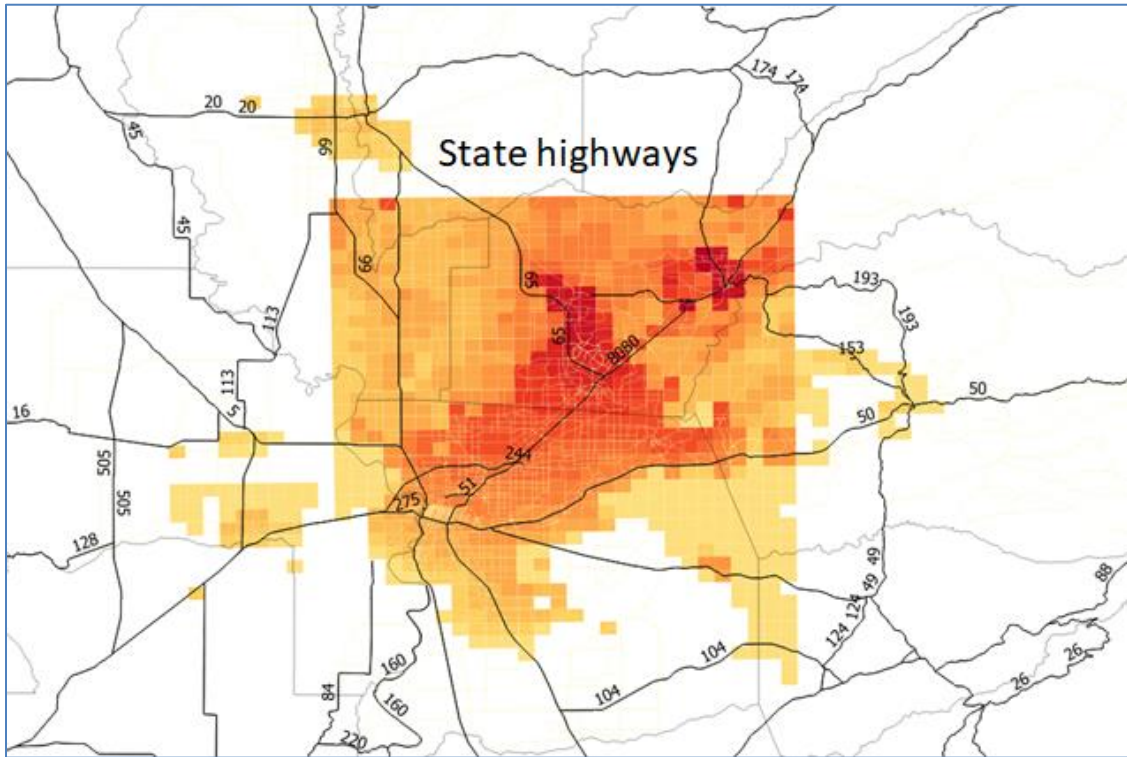
E.3 CALCULATING A TEMPERATURE-WEIGHTED UHII SCORE

The goal of this analysis is to provide additional layers of information, e.g., microclimate data, that could be used in conjunction with other datasets, such as CES 3.0, to help prioritize geographical areas for deployment of UHI mitigation measures, i.e., to offset the UHII. For this purpose, an initial scoring of areas was developed based on the modeled UHII at the regional scale, i.e., the 6-counties Capital region. The first set of scores (Figure EX-3a) is based solely on the UHII regardless of air temperature. In other words, this scoring may be used, for example, by Caltrans and urban planners to develop regional action plans. However, the reductions in absolute temperature, regardless of the UHII, are equally welcomed in all areas.

Thus, the purpose of scoring various geographical areas, such as shown in Figure EX-3a, is to provide additional information to cities and communities when allocating resources. The figure shows five tiers based on UHII intervals of 1 °C including for non-urban areas (heat transport). As with CES 3.0, the higher the UHII score (or tier), the worse the conditions are, i.e., larger urban heat. To reiterate, this scoring is based on climate as the sole criterion, no socio-economic factors are taken into account. If, for example, the UHII score is compared to CES 3.0 scores (last graph in Figure EX-3a), then the UHII score shifts relatively more towards central and south Sacramento, in areas where AB617 communities A, B, and D are located (which occur in UHII Tiers 3 and 4) as well as community C and it surroundings (which occur in UHII Tier 2). Areas near Auburn and Yuba City / Marysville also have high CES 3.0 scores.

With UHII as the sole basis for scoring, the areas including Yuba City / Marysville, Woodland, Davis, and Placerville occur in Tiers 1 and 2 (the lowest and second-to-lowest scores). Most of north and south Sacramento and AB617 communities C, E, and G and others nearby occur in Tier 2 (second score). Central Sacramento, AB617 communities A, B, and D, through Folsom and El Dorado Hills occur in Tiers 3 and 4. Northeast Sacramento, Roseville, Rocklin, Granite Bay, Lincoln, parts of Folsom, and areas west of Auburn occur in Tier 4. Finally, an area from Roseville to Lincoln and a small area over Auburn fall into Tier 5 (the highest score).

However, using only the UHII as an indicator to mitigation priorities and scoring various areas can provide an overall picture that may be counter-intuitive. Thus, the scoring discussed above and shown in Figure EX-3a can be done differently, per data users' specific application or considerations. For example, the above can be repeated but this time using both UHII and absolute air temperature as basis (Figure EX-3b). The goal is to provide relatively more intuitive rankings or scoring, ones that also take into account how hot an area is, not just how large its UHII. This is discussed in detail in the report but it is briefly mentioned here that areas with both large UHII and high temperatures get a higher score than areas with small UHII and lower temperatures. Of course, a range of various combinations exists in-between these two ends.

Figure EX-3b shows an example of urban-area scoring based on both all-hour UHII and all-hour temperature averages for the years and intervals modeled in this study. As can be seen, the pattern differs from that of UHII-only basis (in Figure EX-3a). The lowest score (Tier 1) includes AB617

communities D, G, H and surroundings, peripheral areas in Woodland and Davis, small areas in Marysville, Placerville, and parts of El Dorado Hills.

The second score (Tier 2) includes south and southeast Sacramento, some western parts of downtown Sacramento and surroundings, areas to the south of the American River, peripheral areas in Yuba City / Marysville, northwest Woodland, and central Davis. Some areas in Granite Bay are also included in this tier.

The next-to-top score (Tier 3) includes AB617 communities A, B, D, north Sacramento and parts of downtown, and an area extending east to include south Folsom and El Dorado Hills. Also included in this tier are parts of Lincoln and Auburn.

The top score (Tier 4) includes parts of AB617 community "D", parts of northeast Sacramento, Folsom, El Dorado Hills, Roseville, Rocklin, Lincoln, central parts of Yuba City / Marysville, and parts of Auburn.

Appendix D-2 provides a larger version of these maps.

Figure EX-3a: UHII score for implementing UHI-reduction measures at the regional scale: Tiers 1 through 5 (lowest to highest scores) using UHII as the sole criterion. The CES 3.0 score (last graph) is such that areas with higher score are more vulnerable to various environmental factors.
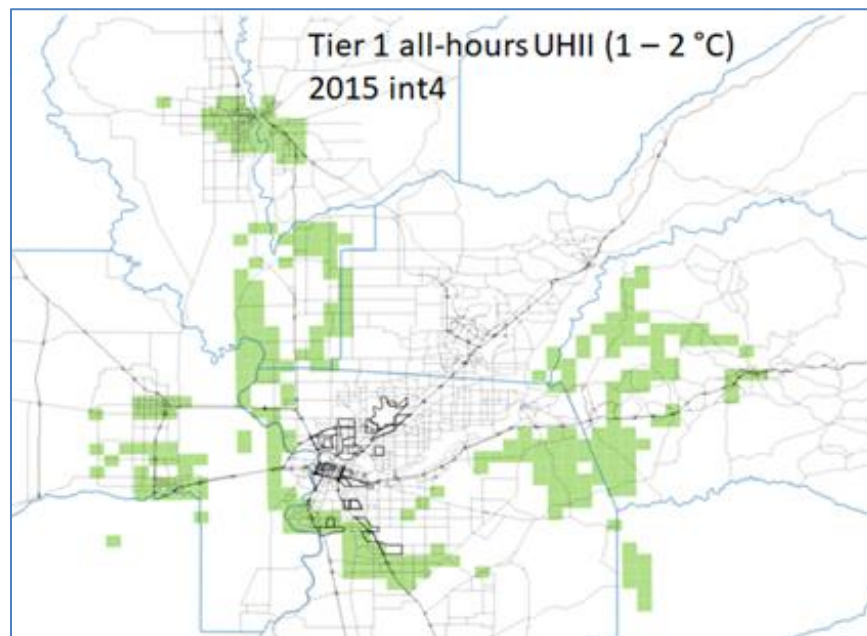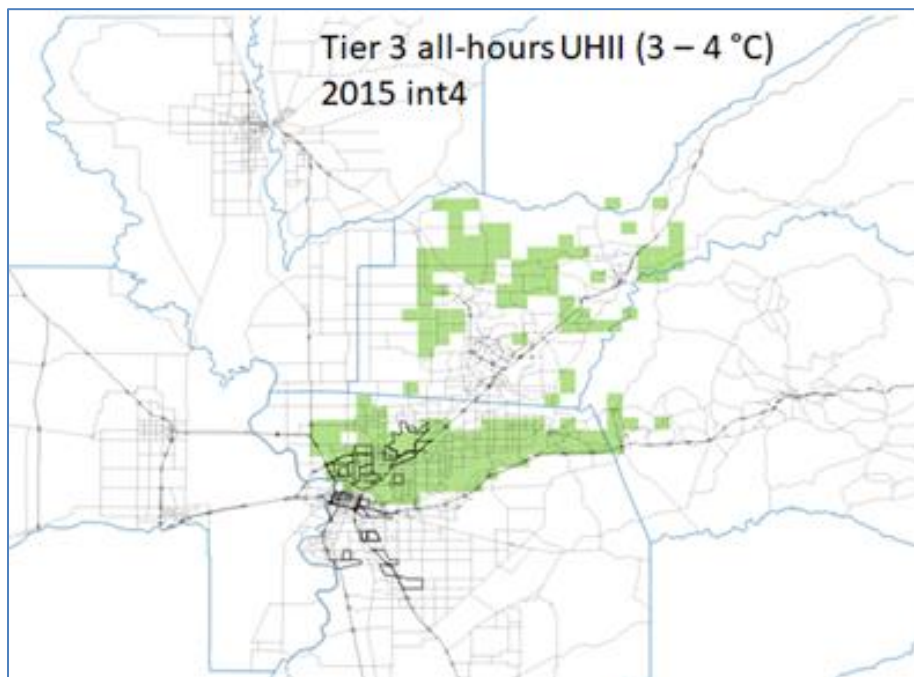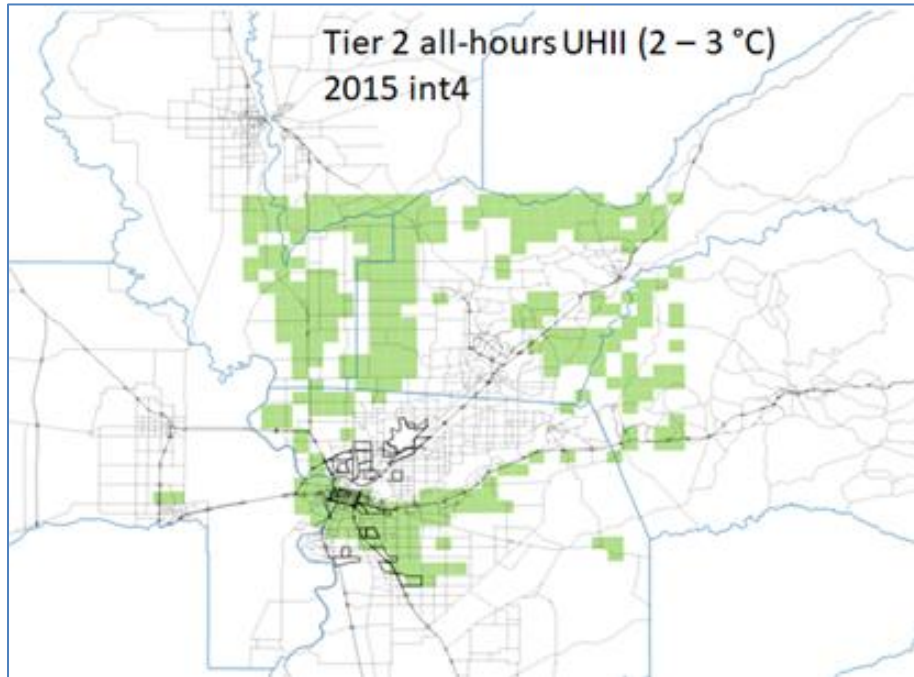
Figure EX-3a, continued.

Figure EX-3a, continued.

Tier 4 all-hours UHII (4 – 5 °C)
2015 int4

Tier 5 all-hours UHII (5 – 6 °C)
2015 int4
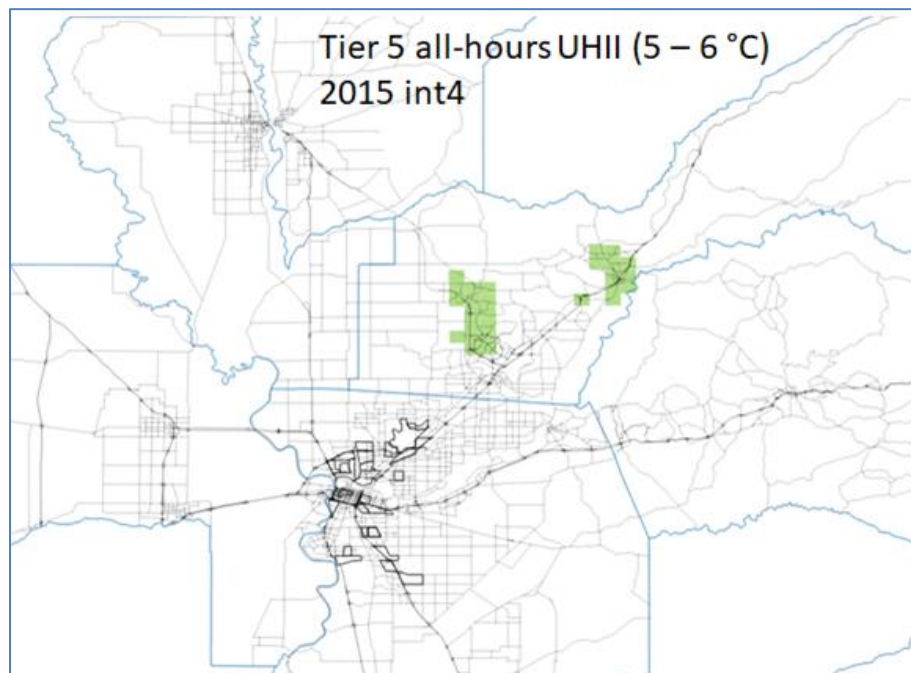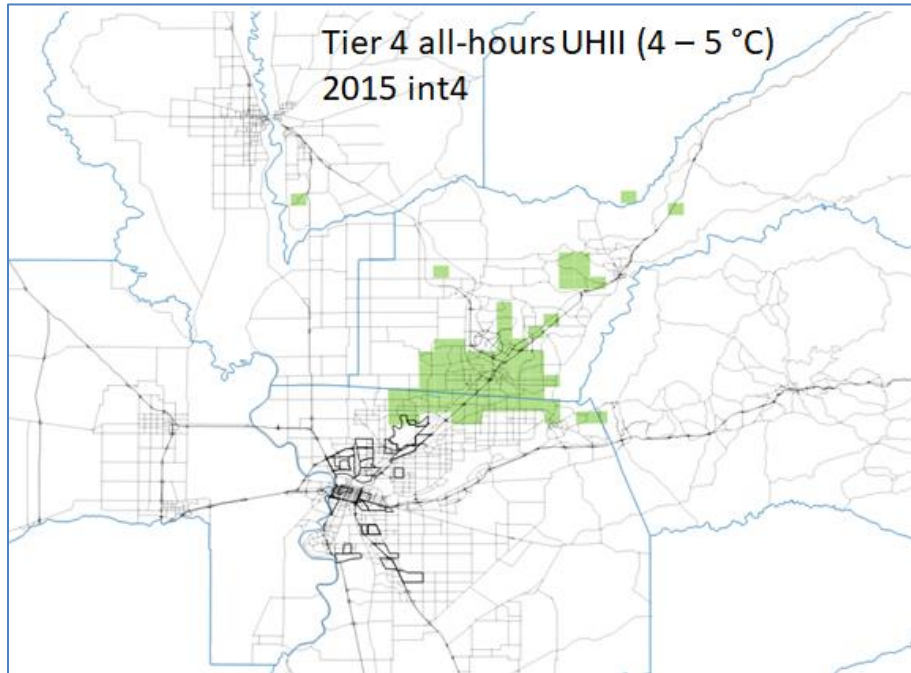
Figure EX-3a, continued.
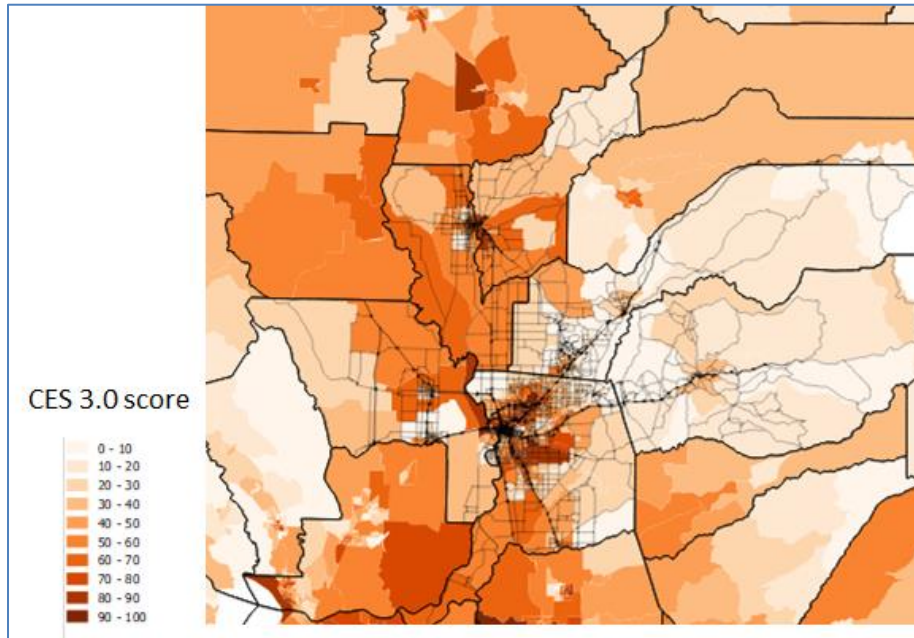
Figure EX-3b: Temperature-weighted UHII score (tiers 1 through 4 are lowest to highest scores). The weighted UHII score, wuSCORE, is discussed in the report.
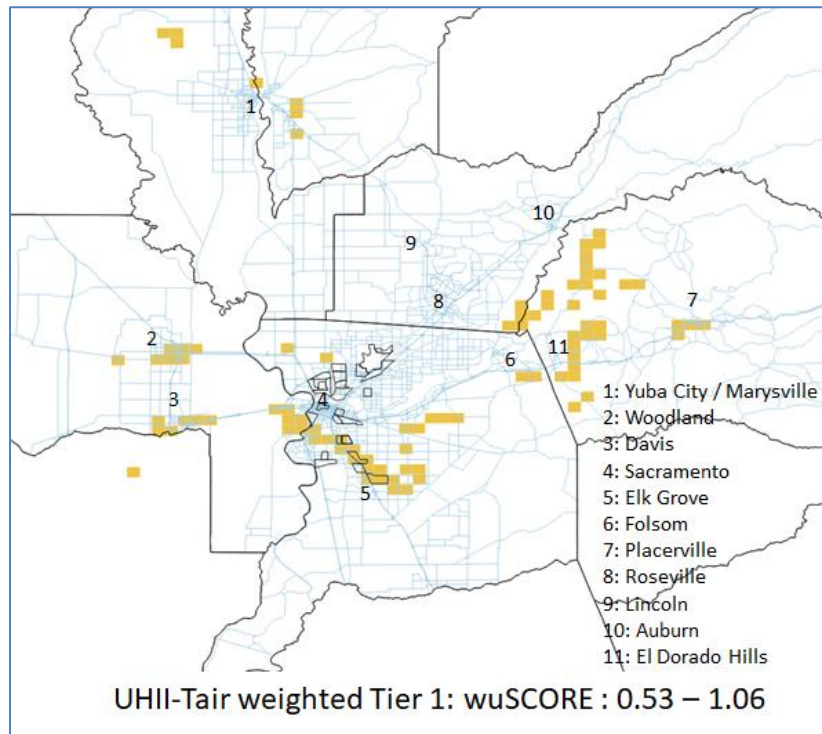
Figure EX-3b, continued.

UHII-Tair weighted Tier 2: wuSCORE : 1.06 − 1.60

1: Yuba City / Marysville
2: Woodland
3: Davis
4: Sacramento
5: Elk Grove
6: Folsom
7: Placerville
8: Roseville
9: Lincoln
10: Auburn
11: El Dorado Hills

UHII-Tair weighted Tier 3: wuSCORE : 1.60 − 2.13

1: Yuba City / Marysville
2: Woodland
3: Davis
4: Sacramento
5: Elk Grove
6: Folsom
7: Placerville
8: Roseville
9: Lincoln
10: Auburn
11: El Dorado Hills

1: Yuba City / Marysville
2: Woodland
3: Davis
4: Sacramento
5: Elk Grove
6: Folsom
7: Placerville
8: Roseville
9: Lincoln
10: Auburn
11: El Dorado Hills

UHII-Tair weighted Tier 4: wuSCORE : 2.13 – 2.66

E.4 DEFINING URBAN-HEAT MITIGATION MEASURES AT THE REGIONAL SCALE

At the course, regional scale, i.e., the 6-counties Capital region, measures related to cool surfaces and vegetation-canopy cover were defined as follows. These were determined based on results from prior studies indicating the feasibility and reasonability of such measures.

case10:   Small increase in albedo -- an increase of 0.15 on impervious surfaces. At this scale (2-km resolution), there is no distinction between roof and pavement albedo changes. Difference between this case and the base case is labeled "del10".

case20:   Larger increase in albedo -- an increase of 0.25 on impervious surfaces. Difference between this case and the base case is labeled "del20".

case01:   A first-level increase in canopy cover (about 2.5 – 3 million trees throughout the 6-counties Capital region, which is about a 12% increase in canopy cover, i.e., an additional 12% of a cell's area is covered with canopy. Difference between this case and the base case is labeled "del01".

case02:   This is a second-level (extreme) increase in canopy cover (~20% cover or adding 5 million trees throughout the entire 6-counties Capital region), i.e., an additional 20% of a cell's area is covered with canopy. This is not a realistic or practical

Altostratus Inc.

scenario at this time, and thus not used in the combined scenario (case31, below) or in some of the analysis in this report. This scenario is included only as a test for potential upper-bound effects, per suggestions from local tree organizations. Difference between this case and the base case is labeled "del02".

case31: A realistic-high scenario of combined albedo and canopy-cover increases. The increase in impervious albedo is slightly larger (0.35 increase) than in case20 and the increase in canopy cover corresponds to that of case01. Difference between this case and the base case is labeled "del31".

E.5 QUANTIFYING THE EFFECTS OF HEAT-MITIGATION MEASURES AT THE REGIONAL SCALE

E.5.1 Instantaneous and averaged effects of mitigation measures in current climate and land use

A random sample from snapshots of instantaneous effects of mitigation measures is provided in Figure EX-4. The purpose of presenting instantaneous effects is to help formulate a general impression as to spatial characteristics of changes in the temperature field that can be expected to result from implementing urban-cooling measures in the 6-counties Capital region. Thus, this is a general sketch of the geographical extent, locations, and levels of changes in temperature that could be anticipated in the region at coarse scale (2-km resolution).

In Figure EX-4, the instantaneous temperature impacts of five mitigation measures (defined in Section E.4, above) are presented for the random hour at 1300 PDT, July 28, 2015. These temperature perturbations result from case01, case02, case10, case20, and case31, respectively (A – E).

For this sample hour, the temperature reductions reach up to 0.7, 1.4, 1.5, 2.4, and 3.9 °C, respectively, for the measures and scenarios listed above and are larger for the cases involving cool surfaces than those with only vegetation-cover increase (during the daytime). The spatial pattern of cooling follows the urban boundaries and the magnitude of cooling increases with built-up density. We note here that the mitigation measures can also inadvertently cause some warming outside of the modified areas, generally downwind of the urban land use. However, the warming is small compared to the cooling effect both in magnitude (maximum of 0.3 °C) and in the geographical extent affected by the temperature changes, as seen in Figure EX-4.

Furthermore, different measures produce different spatial patterns of cooling. For example, vegetation canopy measures (case01 and case02) produce an effect that is somewhat spatially

uniform throughout the modified urban areas (figures A and B), whereas the albedo measures (case10 and case20, figures C and D) produce more distinguishable features or spatially differentiated patterns in the temperature field. For example, areas along the American River and surroundings (the lighter-colored curved path seen in figures C and D, in the middle of the Sacramento region) do not get as much cooling in the albedo scenarios because of the relatively smaller built-up fraction in those areas (i.e., less roofs and paved surfaces available for albedo modifications).

Lastly, the area affected by cooling increases from the lower scenarios to the higher ones, e.g., compare case31 (figure E) to any other of the graphs. This is caused not only by the larger local temperature reductions but also by the increased transport of cooler air downwind from the modified urban areas (this is discussed in detail in the technical report following this summary).

To provide a different perspective, Figure EX-5 shows the all-hours average impacts from mitigation measures for a period of interest (June – September, 2013 -2016). The areas of Davis, Sacramento, Woodland, and Yuba City see larger cooling effects and also the larger inter-quartile ranges of temperature change. Excluding case02 (extreme increases in canopy cover) it can be seen that albedo (case20) and canopy (case01) measures have generally comparable effects and that the combination scenario (case31) is the most effective in cooling the urban areas. The all-hours metric is skewed towards the vegetation-canopy effects (rather than albedo) because of the nighttime cooling effects of vegetation (a time at which the albedo modifications have small or no effects). Thus, the order (i.e., efficacy) of cooling measures is different during daytime hours or at times of peak temperature than at night. In the Project Technical Report, following this Executive Summary, information is provided in detail for other time periods, scenarios, combinations, and locations.

Figure EX-4 (A – E): Instantaneous differences in air temperature (°C) at a random hour and date for five different mitigation scenarios.
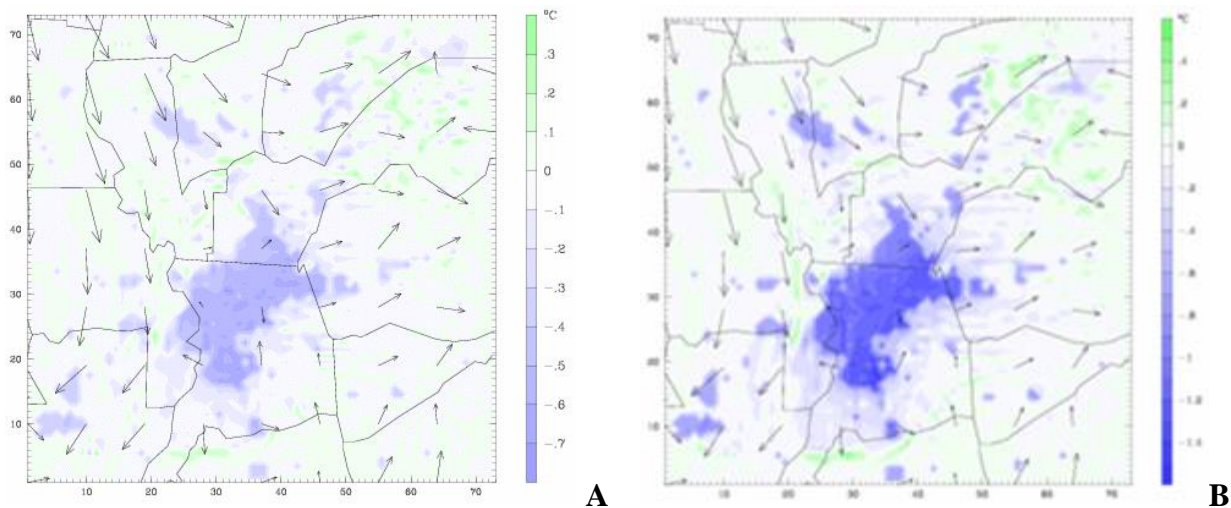
A

B

Left: del01: 1300 PDT, July 28, 2015, horizontal wind vector (base) at 2 m AGL, Maximum change at this hour: -0.7 °C. Right: same but for del02, maximum change at this hour: -1.4 °C.

Figure EX-4, continued.
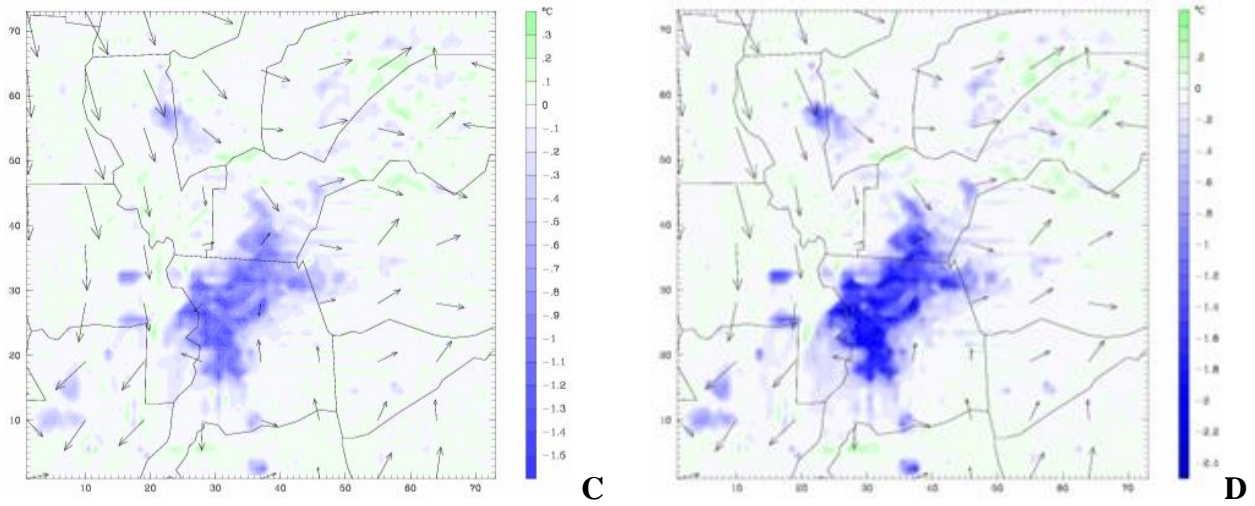
C

D

Left: del10: 1300 PDT, July 28, 2015, horizontal wind vector (base) at 2 m AGL, Maximum change at this hour: -1.5 °C. Right: same but for del20, maximum change at this hour: -2.4 °C.

E
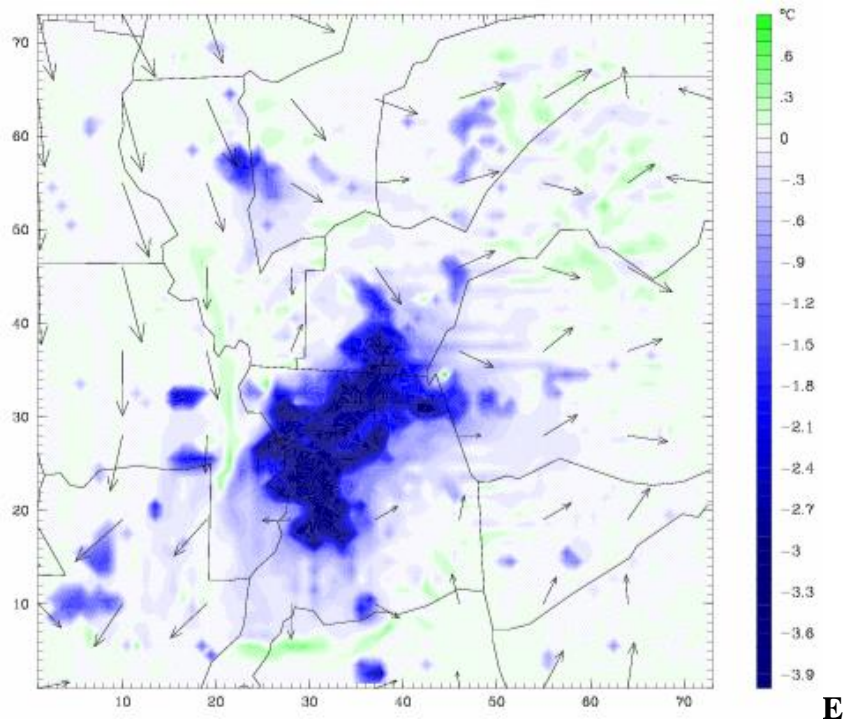
del31: 1300 PDT, July 28, 2015, horizontal wind vector (base) at 2 m AGL, Maximum change at this hour: -3.9 °C.

Figure EX-5: Summary of all-hour average temperature changes from five mitigation scenarios. Median, quartiles, and maxima/minima are shown with box-and-whisker plots.
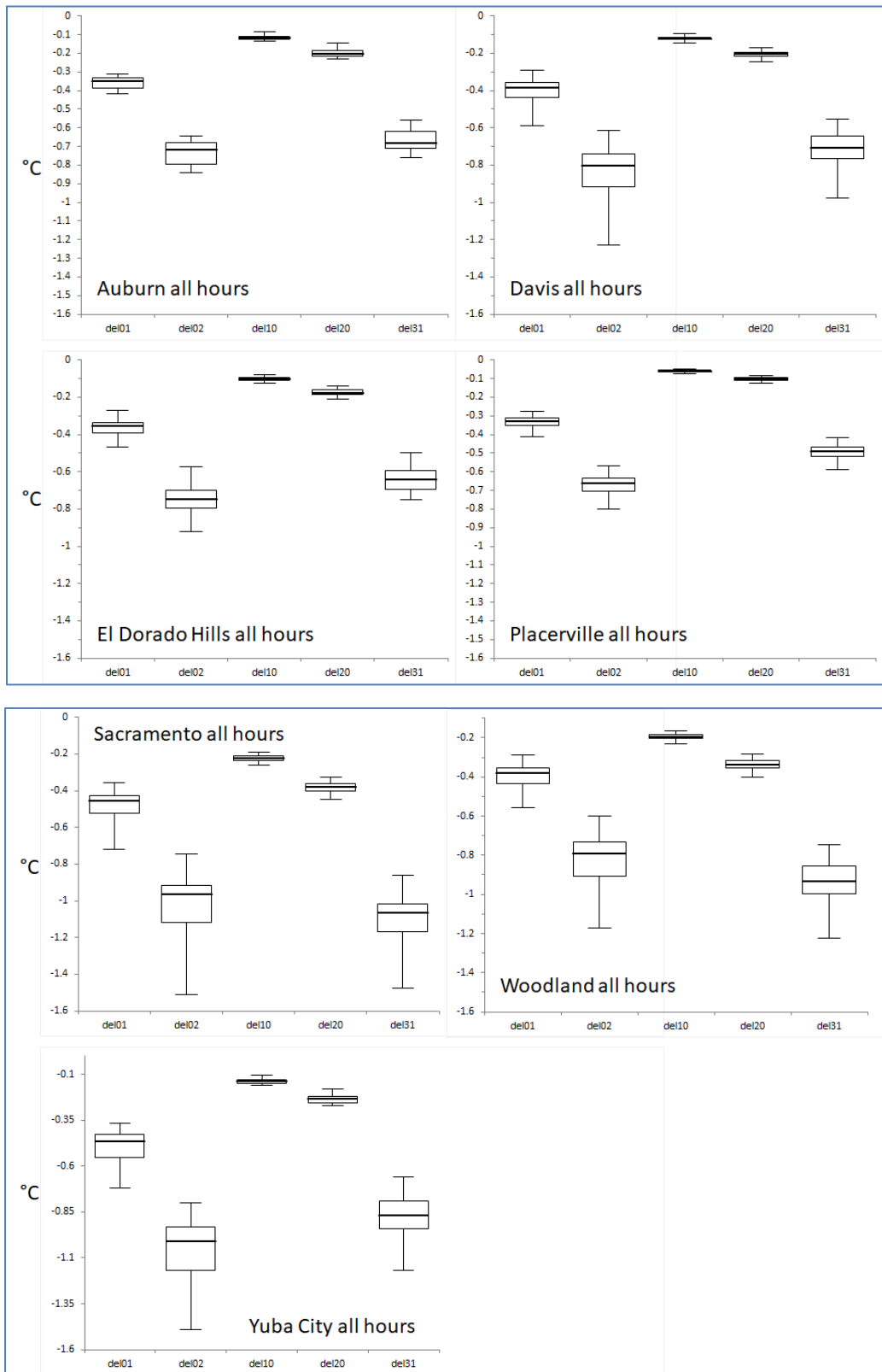
E.5.2 Quantifying the impacts of heat-mitigation measures on outdoor thermal conditions and heat exposure in current climate

Because of their significant cooling potentials, UHI-mitigation measures can affect various public-health heat indicators – for example, they can help decrease or offset exceedances in the National Weather Service Heat Index (NWS HI) above critical warning thresholds and reduce the number of heat-wave or excessive heat-event days. Table EST-1 provides an example from the analysis for the hour at 1700 PDT in terms of average potentials for reductions in the NWS HI levels resulting from case31 (defined in Section E.4). In the table, cumulative metrics (i.e., % change in degree-hours above specified warning thresholds) are provided. For each selected probing point (P0001 through P0032; see Glossary) throughout the 6-counties Capital region, the table gives the percent reduction in degree-hours (DH) above the NWS HI thresholds 106 °F (Danger), 91 °F (Extreme caution), and 80 °F (Caution). Of note – in this report, the NWS HI is the only instance where °F is used; the report in its entirety uses SI units and °C.

Results in Table EST-1 indicate that the combination measure (case31) can reduce the NWS HI exceedances above 106 °F (Danger) by between 50% and 100% (except for one location) and the exceedances above 91 °F (Extreme Caution) by between 18% and 36%.

Table EST-1: Reductions in exceedances (DH) above three NWS HI levels at 1700 PDT (averages over all intervals) in current climate for selected probing locations (P####) defined in the report. All numbers in the table are percentages.

	HI threshold	Probing location						
		P0001	P0004	P0008	P0011	P0013	P0014	P0018
% reduction in DH above thresholds	Caution (%)	-5.8	-5.0	-5.2	-9.4	-4.9	-6.1	-4.7
	Extreme caution (%)	-31.9	-28.6	-30.5	-28.0	-33.5	-36.2	-27.0
	Danger (%)	-66.2	-49.7	-100.0	N/A	-79.8	-83.2	-85.5

	HI threshold	Probing location					
		P0020	P0022	P0026	P0028	P0029	P0032
% reduction in DH above thresholds	Caution (%)	-4.8	-4.8	-4.2	-4.8	-2.6	-3.5
	Extreme caution (%)	-31.9	-23.3	-22.3	-18.7	-22.1	-29.5
	Danger (%)	-100.0	N/A	-79.7	-1.1	-58.7	-75.6

In terms of locally mitigating the effects of excessive heat events or heat waves (see Glossary), Table EST-2 provides a summary of the mitigation potential of case31. The table shows the number of days with NWS HI of 105 – 110 °F at each selected probing location and for three heat-wave events identified in this study (listed in the table). The reduction in the number of heat-wave days at each location (as a result of implementing case31) is also shown.

Altostratus Inc.

Table EST-2: Number of consecutive days with NWS HI 105 – 110 ºF during three time periods.

Probing location	Heat wave?	Number of days with NWS HI 105 – 110 ºF					
		6/30 – 7/4, 2013		6/30 – 6/31, 2016		7/28 – 7/30, 2016	
		base	case31	base	case31	base	case31
P0001 AB617 (Sac)	yes	5	1	0	0	2	0
P0004 AB617 (Sac)	yes	3	1	0	0	2	0
P0008 AB617 (Sac)		1	0	0	0	0	0
P0011 AB617 (Sac)		1	0	0	0	0	0
P0013 Citrus Heights	yes	5	1	1	0	1	0
P0014 Roseville	yes	5	2	1	0	2	0
P0018 Lincoln	yes	4	3	1	0	2	0
P0020 El Dorado Hills		1	0	0	0	0	0
P0022 Placerville		0	0	0	0	0	0
P0026 Woodland	yes	3	0	0	0	0	0
P0028 Davis	yes	4	0	0	0	0	0
P0029 Marysville	yes	4	4	2	0	3	2
P0032 Yuba City	yes	4	4	2	0	3	1

As seen in Table EST-2, all areas can locally offset the heat-wave effects, except for one period in each of the Yuba City and Marysville locations. During the 6/30 – 7/3, 2013 heat wave, case31 reduces the number of heat-event days from 5 or 4 to 1 or 0 in most locations, except for Marysville and Yuba City. During the 6/30 – 6/31, 2016 heat event, case31 reduces the number of days to zero in all locations. The same occurs during the interval 7/29 – 7/30, 2016, i.e., heat-wave days are reduced to zero, except for Marysville and Yuba City where they are reduced from 3 to 2 and from 3 to 1 days, respectively.

Considerations to minimize or prevent any potential inadvertent health impacts from thermal or air-quality changes resulting from UHI-mitigation measures are discussed in the report.

E.5.3 Ranking the effectiveness of heat-mitigation measures at the regional scale under current climate and land use

Figure EX-6a is a high-level summary of the regional-scale UHI-mitigation potentials of the five measures defined in Section E.4 in current climate and land use / land cover conditions. Information in this chart can be used to rank the measures for implementation in each area. Thus, for example, once an area's weighted UHII score is identified (from Section E.3, Figure EX-3b) the chart in Figure EX-6a can be used to obtain an initial assessment of the efficacy of measures per a given location, i.e., as defined at the top of the chart. Thus, the combined information is shown in Figure EX-6b, which is essentially a combination of Figure EX-3b and Figure EX-6a. However, this does not mean that a city or local jurisdiction is obligated to adopt such rankings for implementation purposes. As will be seen later in Section E.8 (and Table EST-4) the effectiveness

of measures in attaining the UHII is further provided as an additional layer of information for jurisdictions to develop their own UHI-mitigation priorities or "mix and match" several measures.

As explained in the technical report, case02 is an extreme scenario of vegetation-cover increase and should be disregarded for practical purposes. However, it is included here as a test for upper bounds (largest cooling effects) per suggestions from local tree organizations.

Of note, Figure EX-6a does not provide the spread (e.g., inter-quartile ranges) of the cooling effects from a particular measure nor how close various measures are to each other (or how far apart they are in terms of their cooling effects). The chart simply shows the ranking of measures even if differences between one measure and another are very small or almost tied in some instances (these details are discussed in the report). Cases that are tied are indicated in Figure EX-6a with a repeated number and color code. It is important to note that these rankings are based on air-temperature changes averaged over 2-km and that they can differ at the finer scales (500 m) where the magnitudes of the temperature reductions also get larger when averaged at finer resolutions.

In Figure EX-6a (and EX-6b), the various time bands may be of interest in different applications. For example, the 0600 PDT and allHRS bands could be of interest from a heat-wave perspective, the 1400-2000 PDT band may be of interest to utilities, the 1500-PDT band could be used in relation to peak cooling demand analysis, and the band at 1300 PDT may be of relevance to assessments of measures around solar noon.

The modeling of future climates, as discussed in the report, shows that except for a number of instances, the ranking (and ordering) of measures shown in Figure EX-6a remains largely unchanged into the future. That is, the ranking of measures in terms of their effectiveness in current climates and LULC is the same to mitigate urban heat under conditions of future climate and urbanization. While the ranking (order) can be relatively similar, the magnitudes of the cooling effects can differ.

Table EST-3 provides the numerical values of the cooling associated with these rankings (values are averaged over all grid cells in each region and for the given time period) with case02 excluded, as explained above. The chart below the table is simply a graphical representation of the values listed. Table EST-3 and the chart exclude case02 to provide a fairer comparison among measures. At the finer scales (i.e., specific projects and 500-m resolution), the cooling effects are significantly larger than the 2-km averaged effects reported in Table EST-3.

Thus, it can be noted from Figure EX-6a and Table EST-3 that albedo scenarios (e.g., cool roofs and cool pavements) are the top choice for reducing daytime urban air temperature. But because the vegetation canopy cover can cool the air both during the day and at night, its impacts are dominant in the 24-hour average metrics and early-morning averages. It can also be seen that case31 generally produces the largest cooling regardless of time of day, whereas the ranking of the other measures does vary from one part of the day to another. For instance, and aside from case31, case01 produces the largest cooling at night whereas case20 the largest cooling during the daytime. Lastly, some of the urban areas seem to consistently experience larger cooling effects, e.g.,

Altostratus Inc.

Sacramento, among others in the Capital region especially in case31. This is mainly a result of the larger areas available for implementing UHI-mitigation measures

Figure EX-6a: Summary of urban-heat mitigation potential: ranking of measures case01 through case31 by cooling effectiveness in current climate (1 to 5, or darker to lighter = largest to smallest cooling)**. Note that case02 should be excluded in some analysis. Also note that these are impacts on temperature, not UHII.

		Auburn	Davis	El Dorado Hills	Placerville	Sacramento	Woodland	Yuba City
0600 PDT	case01	3	3	3	3	3	3	3
	case02	1	1	1	1	1	1	1
	case10	5	5	5	5	5	5	5
	case20	4	4	4	4	4	4	4
	case31	2	2	2	2	2	2	2
1300 PDT	case01	4	5	4	3	5	5	4
	case02	2	2	2	2	3	3	2
	case10	5	4	5	4	4	4	5
	case20	3	3	3	3	2	2	3
	case31	1	1	1	1	1	1	1
1400 - 2000 PDT	case01	4	4	4	3	5	4	4
	case02	2	2	2	2	2	2	2
	case10	5	5	5	5	4	3	5
	case20	3	3	3	4	3	2	3
	case31	1	1	1	1	1	1	1
1500 PDT	case01	4	5	4	4	5	5	4
	case02	2	2	2	2	3	3	2
	case10	4	4	4	5	4	4	4
	case20	3	3	3	3	2	2	3
	case31	1	1	1	1	1	1	1
allHRS	case01	3	3	3	3	3	3	3
	case02	1	1	1	1	2	2	1
	case10	5	5	5	5	5	5	5
	case20	4	4	4	4	4	4	4
	case31	2	2	2	2	1	1	2

** Scenarios were defined earlier in Section E.4. As a recap, case01: realistic-high increases in canopy cover; case02: extreme increases in canopy cover; case10: small increases in albedo; case20: larger increases in albedo; case31: combined albedo and canopy-cover scenario.

Figure EX-6b: Combining the temperature-weighted UHII score with the area-specific ranking of measures efficacies. See the technical report for a full discussion of this approach. The ribbons in this figure are slices from the chart in Figure EX-6a, above.
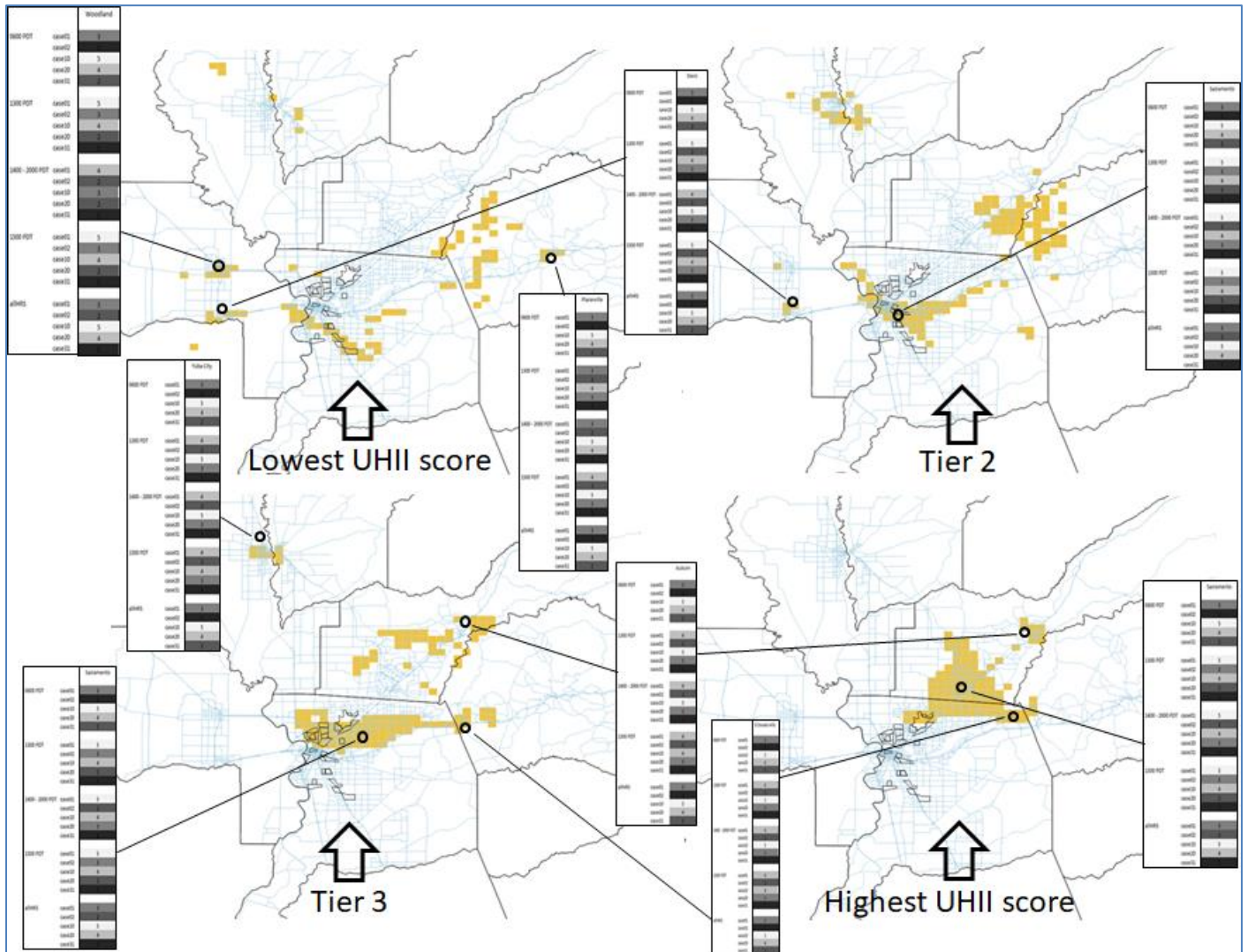
Table EST-3: Numerical values (°C) corresponding to the rankings in Figure EX-6. In this table, case02 has been excluded.

		Auburn	Davis	El Dorado Hills	Placerville	Sacramento	Woodland	Yuba City
0600 PDT	case01	-0.40	-0.60	-0.50	-0.50	-0.70	-0.60	-0.75
	case10	-0.08	-0.15	-0.09	-0.09	-0.10	-0.10	-0.10
	case20	-0.10	-0.20	-0.10	-0.10	-0.20	-0.20	-0.20
	case31	-0.50	-0.90	-0.60	-0.55	-1.00	-0.90	-1.00
1300 PDT	case01	-0.20	-0.18	-0.22	-0.12	-0.25	-0.18	-0.22
	case10	-0.20	-0.20	-0.20	-0.08	-0.40	-0.30	-0.20
	case20	-0.30	-0.30	-0.30	-0.12	-0.65	-0.50	-0.33
	case31	-0.60	-0.60	-0.70	-0.32	-1.30	-0.95	-0.70
1400 - 2000 PDT	case01	-0.22	-0.19	-0.22	-0.18	-0.23	-0.16	-0.20
	case10	-0.20	-0.15	-0.15	-0.10	-0.25	-0.22	-0.15
	case20	-0.32	-0.25	-0.30	-0.15	-0.47	-0.35	-0.25
	case31	-0.72	-0.55	-0.70	-0.40	-1.00	-0.76	-0.60
1500 PDT	case01	-0.18	-0.14	-0.21	-0.14	-0.20	-0.13	-0.17
	case10	-0.18	-0.15	-0.21	-0.10	-0.33	-0.25	-0.18
	case20	-0.30	-0.27	-0.36	-0.16	-0.55	-0.45	-0.30
	case31	-0.64	-0.52	-0.80	-0.37	-1.10	-0.80	-0.60
allHRS	case01	-0.35	-0.40	-0.35	-0.32	-0.45	-0.38	-0.47
	case10	-0.12	-0.17	-0.10	-0.05	-0.20	-0.20	-0.15
	case20	-0.20	-0.20	-0.18	-0.10	-0.37	-0.33	-0.22
	case31	-0.65	-0.70	-0.60	-0.50	-1.06	-0.92	-0.85

E.6 DEFINING HEAT-MITIGATION MEASURES AT THE COMMUNITY SCALE OR PROJECT LEVEL

In addition to the regional (2-km averaged) assessments discussed above, this study also evaluated the localized, site-specific effects of UHI-mitigation measures in areas of interest and at specific MTP (Metropolitan Transportation Plan) roadway project locations. The following reasonable and realistic scenarios were modeled at the community scale (500-m resolution) for current climate and LULC conditions depending on domain and/or specific requests received from the project participants, cities, SMAQMD / LGC, and the project Technical Advisory Committee (TAC). All of these scenarios are discussed in detail in the Project Technical Report and are briefly summarized below. The various measures have different impacts and effectiveness that vary from one location or project to another. The efficacy and rankings of these measures in each area are summarized later in Section E.8.

- Albedo scenarios:
  - For MTP projects, the roadway albedo is increased from a mean of 0.12 (average for current conditions) to 0.35. This is a cap to minimize glare issues.
  - For AB617 communities and other urban areas of interest, such as downtown or specific projects, the roof albedo is increased from a current mean of 0.17 to 0.5 and the roadway albedo from a mean of 0.12 to 0.30. These are caps to minimize potential glare or radiative concerns at pedestrian level.

- Heat-emission scenarios:
  - A vehicle-electrification scenario is applied in designated areas or in transportation corridors of interest. Time- and location-dependent heat emissions from mobile sources are reduced by up to 25% (per CEC and SMAQMD studies that propose an electric-vehicle ownership level of 25%). This scenario also involves quantifying the impacts of electrification per SMAQMD's ZEV Readiness Plan.

- Vegetation-canopy scenarios:
  - Increases in canopy cover are applied in areas of interest defined by the SMAQMD, LGC, and project TAC, including AB617 communities, downtown areas, and other disadvantaged communities (DAC). As an estimate, about 300 large trees are added to a neighborhood of ~ 0.25 km^2, which is equivalent to a cover increase of 8% of a model grid-cell area.

- Cool-wall scenarios:
  - In addition to other cool-surface measures, the albedo of walls is increased in this scenario from an existing average of 0.15 to a maximum of 0.40.

- Solar PV scenarios:
  - Solar PV panels are added to roof- or ground-based surfaces, e.g., parking lots, with different coverages, conversion efficiencies, background albedo, and other parametric considerations, as discussed in the Project Technical Report. In this analysis, the focus is on ground-based solar PV.

- Combination scenarios:
  - These are scenarios combining cool surfaces, vegetation cover, and tailpipe heat emission reductions.

E.7 IDENTIFYING PROJECT AREAS AT THE COMMUNITY SCALE

Unlike the UHII priority areas and rankings that were defined at the regional scale (2-km level) based solely on climate criteria (as shown, for example, in Figure EX-3a,b), the 500-m level priority areas were additionally defined per local project requirements. This was based on areas or projects proposed by the TAC, cities, and SMAQMD / LGC, as well as MTP roadway projects some of which were identified by WSP. In these areas and project sites, the above-defined measures (Section E.6) were applied. Of note, the background grid of dark dots in Figures EX-7 through EX-12 is of no relevance to the discussion in this section (and these mean different things in different contexts) but are discussed in detail in the technical report. Further, the domain labels used in this discussion, i.e., D05 through D10, are also defined in the report (and in Appendix A-2). Note that the following figures are not to the same scale.

Domain D05 (Yuba City / Marysville)

Figure EX-7 depicts the MTP project locations and areas of interest in domain D05. The yellow outline is downtown Marysville, an area designated of interest per project TAC, the orange lines are roadway and bridge projects identified by the City of Yuba City, and the red lines are MTP project locations. The major highways of relevance to electrification scenarios are highlighted with bold black lines.

Figure EX-7: Locations of roadway projects and areas of interest in the Yuba City / Marysville domain.
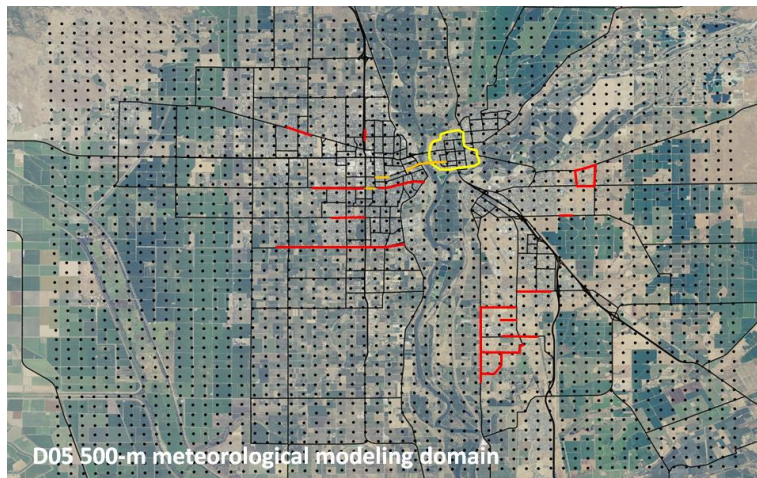
Domain D06 (Woodland)

Figure EX-8 depicts the roadway project and areas of interest in and near the City of Woodland. The yellow line highlights an area of interest (per TAC) in the northwestern part where future urbanization is expected to intensify. The red lines depict the MTP roadway projects and the highways of interest to electrification scenarios are highlighted with bold black lines.

Figure EX-8: Locations of roadway projects and areas of interest in the Woodland area.
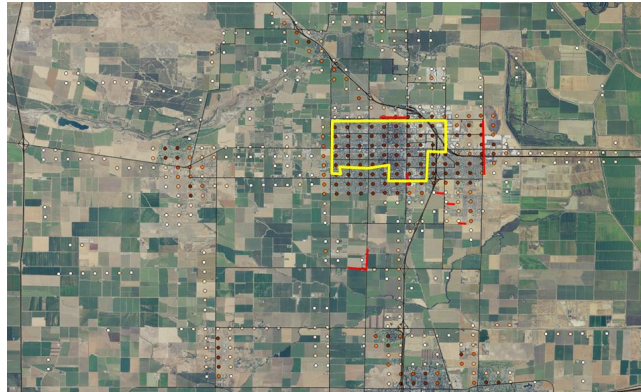
Domain D07 (Sacramento)

The yellow areas in Figure EX-9 are AB617 communities defined by SMAQMD that also are of interest to the project TAC and the cities in this area. The red lines are MTP projects identified by WSP and the major highways of interest in electrification scenarios are highlighted with bold black lines.

Figure EX-9: Locations of roadway projects and areas of interest in the Sacramento area.
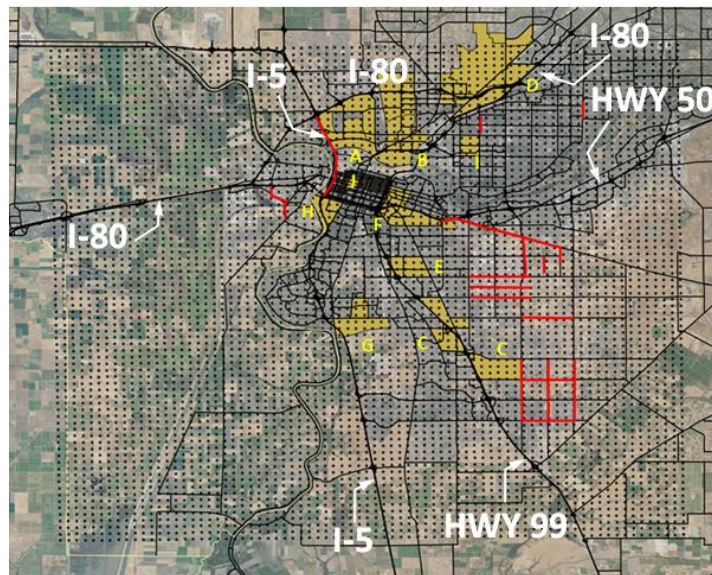
Domain D08 (Sacramento – Roseville – Granite Bay)

In the Sacramento – Roseville – Granite Bay region (Figure EX-10) the yellow area is AB617 community "D" defined by SMAQMD. The red lines are MTP roadway projects and the major highways of relevance to electrification are highlighted with white lines.

Figure Ex-10: Locations of projects and areas of interest in Sacramento – Roseville – Granite Bay area.
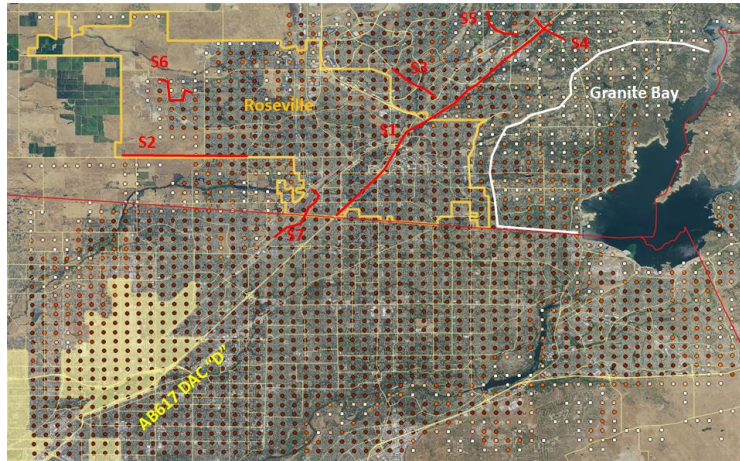
Domain D09 (Folsom – El Dorado Hills)

Figure EX-11 shows the roadway projects and areas of interest in the Folsom – El Dorado Hills region, including the MTP projects (red lines) and the urban areas in both cities. The highways of interest in electrification scenarios are highlighted in white.

Figure EX-11: Locations of roadway projects and areas of interest in the Folsom – El Dorado Hills area.
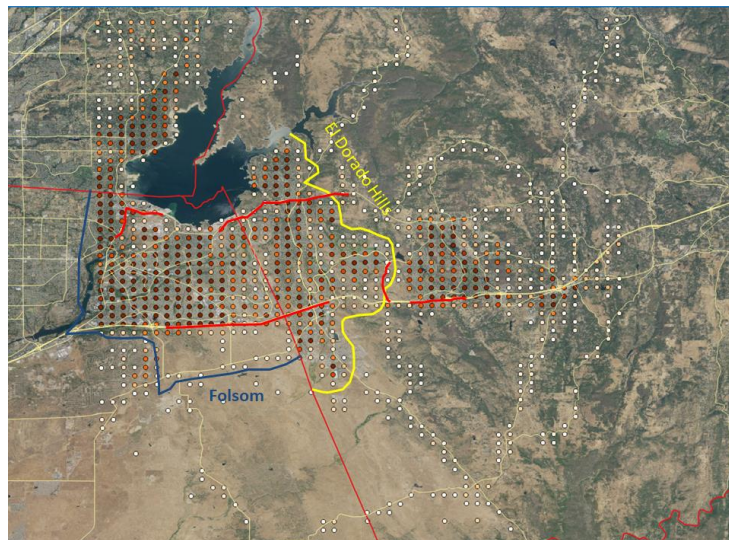
Domain D10 (Placerville – Diamond Springs)

The roadway project locations in the Placerville – Diamond Springs region are highlighted in red in Figure EX-12. The yellow lines delineate the urban areas of interest and the highways of relevance to electrification scenarios are also identified.

Figure EX-12: Locations of roadway projects and areas of interest in Placerville – Diamond Springs area.
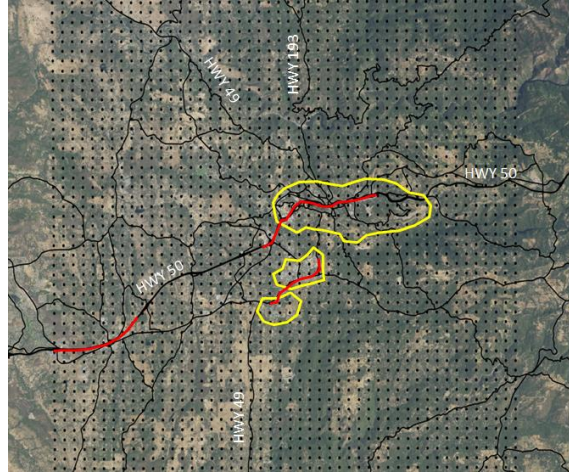
E.8 ATTAINMENT OF THE UHII AT COMMUNITY AND PROJECT SCALES IN CURRENT CLIMATE AND LAND USE

One way to evaluate and inter-compare the mitigation efficacies of various project- or area-specific measures is to quantify their potential to offset the local UHII, i.e., its value at the specific location where the measures are being implemented and evaluated. Thus, the effects of mitigation measures at community level (500-m scale) were compared to the local all-hours UHII computed for current climate conditions and urbanization levels, such as shown earlier in the example in Figure EX-1a. The UHII offset via each UHI-mitigation measure was evaluated for two situations: (1) a scenario where only the community implements the measure and no other nearby communities take any action, and (2) a scenario where both the community <u>and</u> its upwind neighbors implement the measures. In this second situation, the community will benefit from cooler air transported from upwind areas in addition to the local cooling resulting from implementation of its own UHI-mitigation strategies. This is akin to "doubling" the local cooling effects.

The evaluations are summarized in Table EST-4 for each measure in standalone fashion. The total effects of combinations of measures are non-linear (i.e., cannot be computed as simple sums) and are smaller than the sum of the individual components. Still, the information in Table EST-4 can provide Caltrans and urban planners with rough magnitudes of the cooling effects that can be anticipated if measures were combined.

Table EST-4: Potential of local projects in mitigating the all-hours UHII in current climate and land use.

Project area	All-hours Tair UHII (°C)**		Localized/no advection UHII attainment local mitigation only	Localized+advection UHII attainment local mitigation+advection
D05 Yuba City / Marysville Downtown YC and M	2.41	Cool roofs / pavements	-58%	-82%
		Cool pavements	-46%	-70%
		Electric vehicles	-7%	-31%
		Vegetation cover	-71%	-95%
D06 Woodland DAC census tracts	2.14	Cool roofs / pavements	-60%	-93%
		Cool pavements	-69%	-101%
		Electric vehicles	-7%	-39%
		Vegetation cover	-51%	-84%
D07 Sac / SE Sac AB617 A, B, D	4.48	Cool roofs / pavements	-29%	-63%
		Cool pavements	-31%	-65%
		Electric vehicles	-6%	-39%
		Vegetation cover	-33%	-67%
D07 Sac / SE Sac AB617 C, E, G	2.33	Cool roofs / pavements	-56%	-93%
		Cool pavements	-60%	-97%
		Electric vehicles	-11%	-48%
		Vegetation cover	-63%	-101%

Project area	All-hours Tair UHII (°C)**		Localized/no advection UHII attainment local mitigation only	Localized+advection UHII attainment local mitigation+advection
D08 Granite Bay	5.07	Cool roofs / pavements	-28%	-48%
		Cool pavements	-34%	-54%
		Electric vehicles	-6%	-27%
		Vegetation cover	-21%	-41%
D08 Roseville	5.83	Cool roofs / pavements	-24%	-52%
		Cool pavements	-30%	-57%
		Electric vehicles	-5%	-33%
		Vegetation cover	-18%	-46%
D09 El Dorado Hills	4.91	Cool roofs / pavements	-30%	-47%
		Cool pavements	-34%	-51%
		Electric vehicles	-4%	-20%
		Vegetation cover	-23%	-39%
D09 Folsom	4.86	Cool roofs / pavements	-31%	-52%
		Cool pavements	-35%	-56%
		Electric vehicles	-4%	-25%
		Vegetation cover	-23%	-44%
		Doubled cover increase	-40%	-61%
D10 Placerville / Diamond Springs / El Dorado City	1.36	Cool roofs / pavements	-88%	-113%
		Cool pavements	-118%	-143%
		Electric vehicles	-6%	-31%
		Vegetation cover	-96%	-121%

**Averaged over three periods: 2015_int1 (lower range), 2016_int5 (mid-range), and 2013_int3 (upper range).

As shown in Table EST-4, some measures, even in standalone fashion, can completely offset the local UHII. Furthermore, when neighboring communities also implement UHI-mitigation strategies, the local benefits increase significantly -- but of course vary from one measure and location to another. It is to be re-emphasized that these are localized effects, i.e., temperature changes at or near the surface of the modified roadways or air temperature within the urban canyons of the selected communities. Thus, in table EST-4, the effects of cool pavements alone can sometimes be larger than the effects of combined cool pavements and cool roofs because the levels of increase in pavement albedo for the main highways and freeways in the region are larger than for the local roadways in the selected communities (see definitions in Section E.6). In addition, there is a shading effect in the canyons that can reduce the effectiveness of cool pavements in those communities compared to the wide-open freeways where there is minimal shading and a large modifiable area for implementing cool pavements.

E.9 ADDITIONAL COMMUNITY-LEVEL MEASURES

This section presents some additional community-level measures that were not included in the analysis above (in Table EST-4) and that were requested by SMAQMD, LGC, the project TAC, or the cities in the Capital region.

E.9.1 Electrification per SMAQMD ZEV Readiness Plan

Fine-scale modeling was carried out to evaluate the potential temperature impacts from heat-emission reductions following the SMAQMD's ZEV Readiness Plan. Figure EX-13 shows the locations of proposed charging facilities in the region (per SMAQMD) superimposed on the UHII tiles of the Capital region. The type of information shown in the figure can provide SMAQMD with general priorities for implementing the charging stations assuming the UHII is sole criterion.

In this modeling assessment, a zone was defined by a 10-km radius of influence around each station. A Cressman weighting scheme was then applied within each influence zone to decrease electrification levels from 25% at the station locations to zero at the perimeter of each influence zone. This was then used in quantifying the atmospheric impacts from ZEV ownership.

In Table EST-5, sample results are presented from this analysis of the air temperature ($Tair$) and surface temperature ($Tsfc$) impacts of implementing the SMAQMD's ZEV Readiness Plan. While reported separately in this table, $Tair$ and $Tsfc$ should actually be averaged to get a better representation of the temperature effects from reduced tail-pipe heat emissions via electrification. The "average max cooling" column in the table is the average of the largest daily surface cooling over all days in the given period. The "1700 PDT" averages in the table are averages of all 1700 PDT hours and the "all hours" column entries are averages over every hour in the given period. The modeling and analysis were applied to the Sacramento region (domains D07 and D08 defined in the report) for the time periods identified in Table EST-5.

Figure EX-13: Charging/H2 stations vs. UHII composite tiles in July 16-31, 2015.
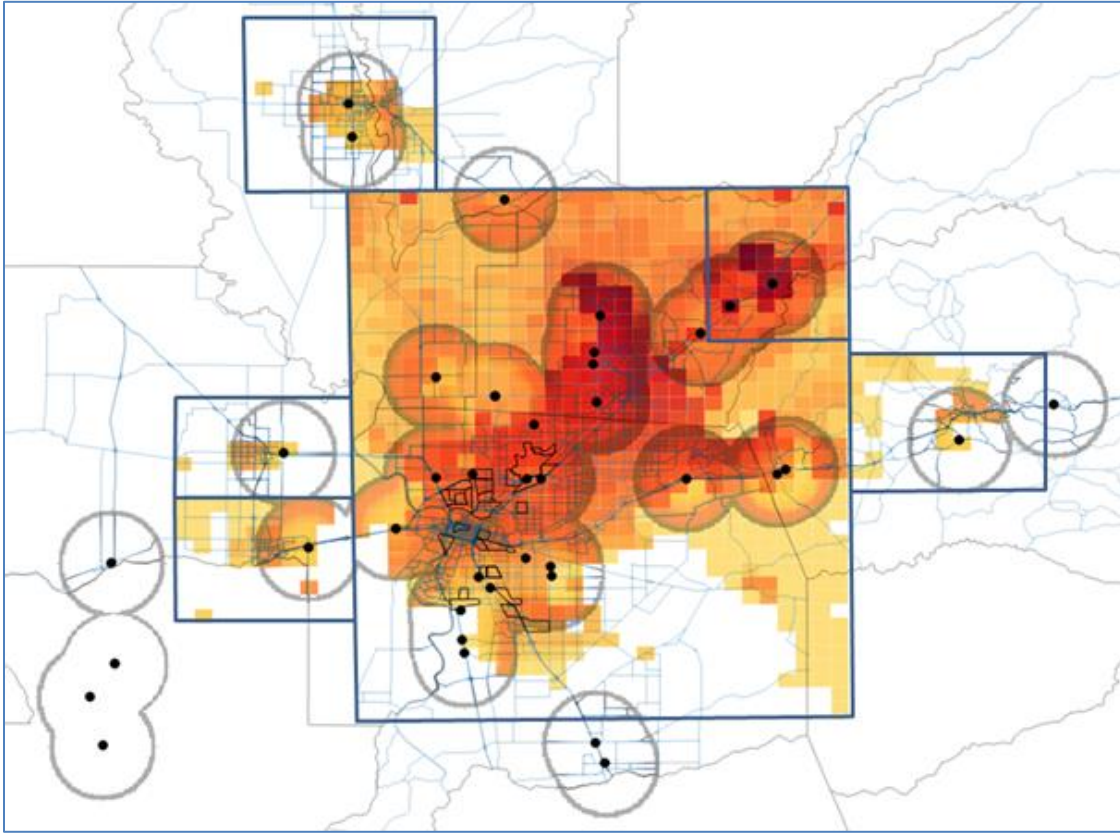
Table EST-5: SMAQMD ZEV Readiness Plan impact on temperature (changes in °C)

Domain and interval	1700 PDT			all hours		
	averages		average max. cooling (Tsfc)	averages		average max. cooling (Tsfc)
	Tair	Tsfc		Tair	Tsfc	
D07						
Jul 1-15, 2013	-0.32	-0.55	-2.97	-0.17	-0.28	-0.87
Jun 1-15, 2015	-0.20	-0.37	-2.81	-0.16	-0.27	-0.84
Aug 1-15, 2016	-0.24	-0.41	-3.34	-0.16	-0.27	-0.86
D08						
Jul 1-15, 2013	-0.27	-0.44	-1.58	-0.18	-0.29	-0.73
Jun 1-15, 2015	-0.25	-0.42	-2.17	-0.17	-0.27	-0.74
Aug 1-15, 2016	-0.26	-0.45	-1.79	-0.18	-0.30	-0.74

E.9.2 Installation of solar PV

Per interest from the City of Folsom and the SMAQMD, the potential impacts of solar PV arrays on near-surface temperature, that is, temperature near the ground, were evaluated and compared to the effects of tree canopies on parking lots. Various parameters were considered in evaluating the standalone effects of ground-based (e.g., parking lots) and roof-based solar PV. The Project Technical Report discusses this measure in additional detail along with the various parameters considered in the analysis.

As there can be a number of possible combinations of such parameters as well as their evolution over time and under future climates and urban surface properties, Table EST-6 lists a subset of the scenarios that were modeled and discussed here. Table EST-7 presents a summary of results for the near-surface temperature impacts from solar PV deployment in the Folsom area.

Table EST-6: Scenarios of solar PV implementation (ε is conversion efficiency; c is cover).

	Surface = roof (#0)			Surface = paved / parking lot (0#)		
Scenario	roof albedo	ε	c	paved albedo	ε	c
casePV10	f(LULC) ~ 0.17 – 0.20	0.15	40%	-	-	-
casePV20	f(LULC) ~ 0.17 – 0.20	0.30	40%	-	-	-
casePV30	0.50	0.30	60%	-	-	-
casePV01	-	-	-	f(LULC) ~ 0.10 – 0.12	0.15	60%
casePV02	-	-	-	f(LULC) ~ 0.10 – 0.12	0.30	60%
casePV03	-	-	-	0.30	0.30	80%
casePV22	f(LULC) ~0.17 – 0.20	0.30	40%	f(LULC) ~ 0.10 – 0.12	0.30	60%

Table EST-7: Changes in near-surface temperatures (°C) within the urban canopy layer resulting from various solar PV scenarios in the Folsom area. Note that scenarios PV03 and PV30 also include significant increases in background albedo, not only installation of solar PV.

	PV scenario							
	PV01	PV02	PV03	PV10	PV20	PV30	PV22	PV30vsAA
1500 PDT average								
Near-surface temperature	-1.17	-2.44	-4.04	-0.03	-0.08	-0.20	-2.49	+0.18
All hours average								
Near-surface temperature	-0.52	-1.18	-1.89	-0.01	-0.03	-0.09	-1.19	+0.08

As expected, the analysis indicates that urban canopy temperatures near the ground are affected more by ground-based PV panels – e.g., those installed over parking lots – than those installed at roof level. This is because (1) the effects from roof modifications occur at generally higher elevations above street level (or urban canyon) and as such, have smaller impacts on temperature near the ground, (2) because the albedo of roofs and the effective albedo of the solar panels are more comparable and both higher than albedo of pavements at ground level, and (3) the effects of shading the ground on near-surface temperatures, e.g. parking lots, is larger than shading at roof level (which sometimes is non-existent). However, near the top of the canopy layer and above roof level, both roof-based and ground-based solar PV have significant and similar effects on air temperature.

With respect to current typical albedo of roofs and pavements, the solar PV scenarios PV01 and PV02 (ground-based PV) produce average all-hours near-surface temperature reductions (localized cooling) of 0.52 and 1.18 °C, respectively. This can reach a maximum of 1.17 and 2.44 °C, respectively, during peak hours. As discussed in the report, other studies found larger cooling at night than during the day from roof-based panels, but in this analysis, the effect of albedo and shading at ground level were evaluated (for the reasons explained above) and found to be dominant and larger during daytime.

The larger cooling in case PV02 relative to that in case PV01 is entirely caused by increased PV conversion efficiency (ε) from 0.15 to 0.30, and represents the range of possible cooling effects from today's PV technology in today's typical albedo ranges in urban areas. The reductions in near-surface temperature as a result of roof-based solar PV installations (cases PV10 and PV20) are smaller, roughly up to 0.1 °C, for the reasons listed above. Nevertheless, these numbers show that the electric benefits from solar PV installations at roof level can be attained without incurring negative atmospheric effects, i.e., increasing air temperature at street level. As discussed in the report, the temperature effects reported here are generally comparable to those from other studies.

In a scenario where both roof- and ground-based solar PV are implemented, e.g., case PV22, the cooling is slightly larger than in case PV02, but by a small amount. In this scenario, reductions in 1500-PDT and all-hours temperatures of 2.49 and 1.19 °C, respectively, are predicted.

In cases PV03 and PV30, the background albedo (of roofs and pavements) is also increased significantly in addition to installing solar PV – hence the resulting large cooling effects are attributable mostly to the increases in background albedo. These scenarios represent future conditions where roof albedo, pavement albedo, PV cover, and conversion efficiency all have increased. Finally, case PV30vsAA demonstrates the potential negative effects of solar PV if implemented widely in the future when cool roofs and cool pavements also would have been deployed at a larger scale. In this case, the installation of solar PV can have the potential to increase near-surface temperature by an average of 0.08 °C (all-hours) and 0.18 °C at the time of the peak (1500 PDT) relative to if only cool roofs and pavements were installed, although still cooler than in the base scenario.

Altostratus Inc.

E.9.3 Smart growth measures

Per SMAQMD's interest, this study evaluated a scenario of smart urban growth whereby 15% less urbanization occurs by 2050 relative to a business-as-usual scenario (BAU). Figure EX-14 depicts the BAU and smart-growth cases as represented on the 2-km grid of the model. The green areas are current urban and the pink areas are new urban by 2050. The current urban LULC was defined based on NLCD 2011-2016 datasets and the BAU scenario based on USGS LUCAS projections, as discussed in detail in the technical report.

While there are several ways the impacts of smart growth could be quantified, including averaging over an entire region or over different sub-domains, here the impacts were evaluated mainly at those locations where urbanization was prevented (Figure EX-14). Clearly, this criterion would result in greater cooling relative to averaging over larger areas, i.e., including currently-urbanized regions.

Figure EX-14: BAU (left) and smart-growth (right) urbanization by 2050 on the model 2-km grid
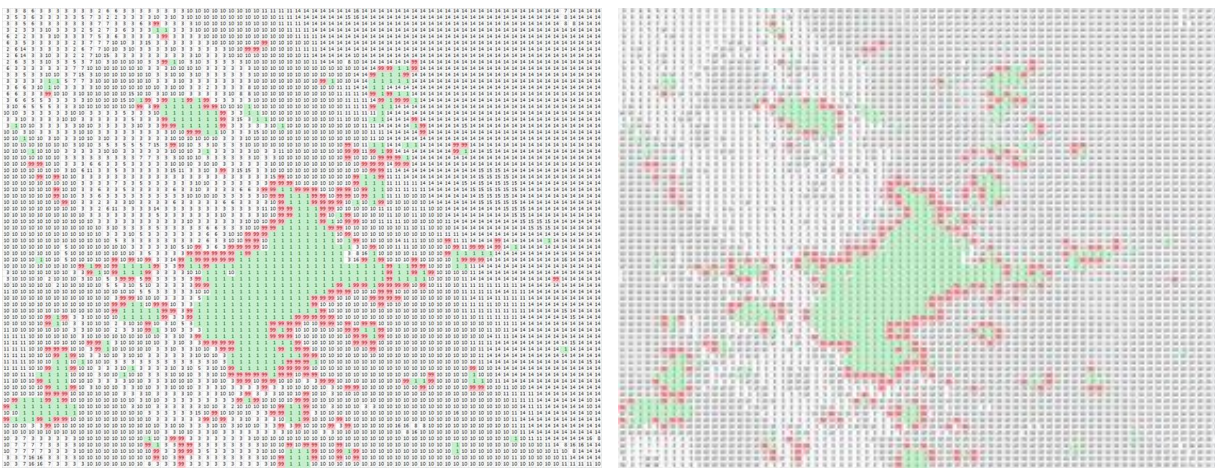
The model results indicate that while there are variations by area and time interval, the overall average avoided warming at 0600 PDT is about 2 °C in those areas where urbanization was prevented or minimized. On the other hand, if averaged over each subdomain, the effects of smart growth are smaller, e.g., an avoided warming of between 0.05 and 0.15 °C region-wide. At 1300 PDT, the avoided warming ranges from an average of 0.05 °C in Davis to up to an average of 0.4 °C in Auburn. If averaged over each subdomain, the effects of smart growth are an avoided warming of between 0.05 and 0.1 °C region-wide.

For the hours between 1400 and 2000 PDT, and similar to 1300 PDT, there are more variations in avoided warming across the regions than is the case at 0600 PDT. At 1400 – 2000 PDT, the avoided warming ranges from an average of 0.6 °C in Davis to up to an average of 1.2 °C in Auburn. Again,

if averaged over each subdomain, the effects of smart growth are smaller, e.g., an avoided warming of between 0.05 and 0.15 °C region-wide

At 1500 PDT, the avoided warming ranges from an average of 0.20 °C in Davis to up to an average of 0.6 °C in Auburn and Yuba City and, if averaged over each subdomain, the effects of smart growth are an avoided warming of between 0.08 and 0.15 °C area-wide. Finally, for all-hour averages, the smart growth scenario shows that except for Auburn and El Dorado Hills, there is less variation across the regions and relatively similar avoided warming of between 1.2 and 1.6 °C.

One observation that can be made from this analysis is that the impacts of smart growth measures are larger (i.e., larger avoided warming) during the nighttime than during the day. This is a direct result of urbanization affecting nighttime temperatures more than those during the daytime, i.e., the classical definition of the urban heat island effect.

E.9.4 Combinations of measures

As discussed above, several mitigation measures were evaluated at the community scale (500-m resolution) in standalone mode. Combinations of measures were not presented as there would be a large number of arbitrary possibilities. However, per interest from the City of Elk Grove, an example of a combination scenario was evaluated, as presented in Figure EX-15.

This assessment was conducted based on fine-scale modeling of the combined measures in D07, a domain containing the City of Elk Grove (see Figure EX-9, above). The results indicate that the combination of measures provides significantly larger cooling benefits than each measure in standalone mode but, with two small exceptions, the total cooling (of combination of measures) is smaller than the sum of the individual components (cooling from each standalone measure). In this domain, and for the modeled periods, the total effect of the combination scenario (green bars in the chart) is about 5 – 15% smaller than the simple sum of the individual cooling effects.

Figure EX-15 summarizes these findings and also shows the significant cooling benefits for the roadway surfaces ("Roadway temperature") during daytime hours, as well as for the 24 hours average. The other columns in this figure are as follows: "UCL temperature" is the air temperature within the urban canopy layer (canyon) and "surface temperature" is the average temperature of various surfaces making up the ground cover. The red bars in Figure EX-15 represent the effects of vegetation canopy alone; the blue bars represent the effects of cool surfaces alone; and the green bars represent their combined effects plus the effects of heat-emission reductions from electrification.

Figure EX-15: Temperature effects of combination of measures in D07. Vertical axis is change in temperature in degrees C.
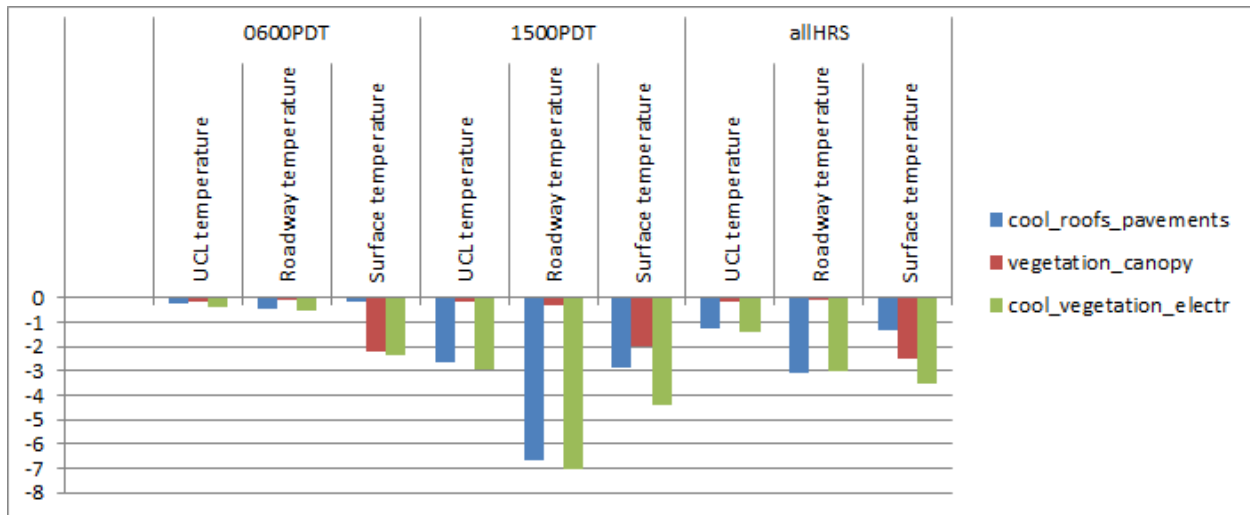
E.9.5 Cool walls

The potential impacts of cool walls were quantified for a scenario where wall albedo was increased from a current average of 0.15 to a maximum value (capped at) 0.40. Figure EX-16 shows the cooling effects as averaged over time intervals (periods) of interest, representing various summer conditions in the City of Elk Grove. As expected, the wall albedo effects are largest during the daytime reaching up to a maximum average localized cooling of 1.4 °C.

Figure EX-16: Averaged temperature effects of cool walls.
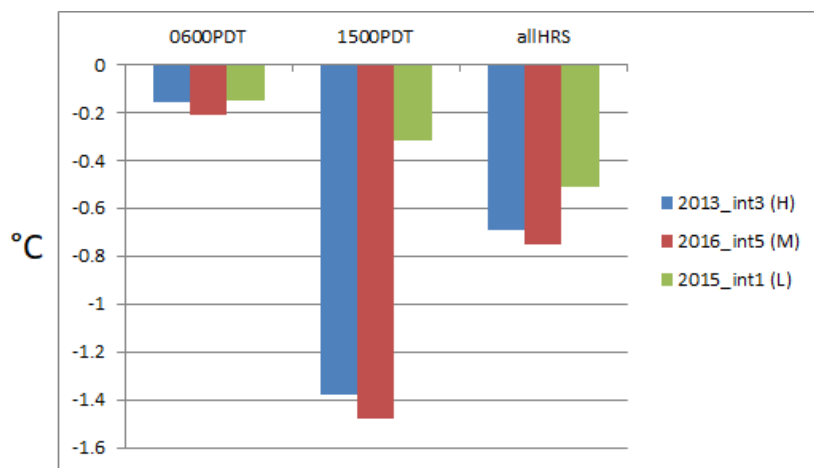
E.10 CHARACTERIZING THE IMPACTS OF CHANGES IN CLIMATE AND URBANIZATION ON THE FUTURE UHII

The changes in local meteorology corresponding to conditions of future climate were evaluated by applying the Altostratus-modified urban WRF in dynamically downscaling the 2050 RCP 4.5 and RCP 8.5 CCSM4 climate-model fields and using them along with future urbanization and land-use change projections (per USGS LUCAS).

The characteristics of the future UHII are dictated mainly by two effects: (1) in areas currently urbanized, the main impacts on the temperature field and the UHII are those from local climate-change effects, whereas (2) in areas that will be urbanizing between now and 2050, the impacts on air temperature will result from both changes in land use (urbanization) and changes in climate. In general, the UHII in 2050 RCP 8.5 is larger than in RCP 4.5, as one would like to expect – however, there are deviations from this tendency, as seen in Table EST-8 and Figure EX-17, in the areas of Yuba City / Marysville and Woodland (first two sets of bars in the figure).

What the results suggest for these two areas may seem counter-intuitive at first, i.e., that the UHII can be slightly smaller (in this example time period) in RCP 8.5 than in RCP 4.5. The reason is that the non-urban areas surrounding Yuba City / Marysville and Woodland warm up faster (on the long run) than the urban areas in these two regions. This might be the result of lower vegetation cover in the non-urban areas than in the urban ones in these two regions (discussed in the report). Since these non-urban areas warm up slightly faster than the urban ones in this case, the UHII, by definition, becomes smaller – despite the fact that the absolute urban temperatures are higher in RCP 8.5 than in RCP 4.5. In all other parts and areas of the study domain, the RCP 8.5 UHII is larger than the RCP 4.5 UHII, as seen in Table EST-8 and Figure EX-17.

Table EST-8. All-hours UHII and changes (temperature equivalent in °C).

Domain	Area	All-hours UHII (temperature equivalent °C)		
		2013-2016	2050 RCP 4.5	2050 RCP 8.5
D05	Yuba City / Marysville	2.41	2.96	2.64
D06	Woodland	2.14	2.80	2.57
D07	Sacramento AB617 A, B, D	4.48	5.00	5.13
D07	Sacramento AB617 C, E, G	2.33	2.67	2.99
D08	Granite Bay	5.07	5.55	5.72
D08	Roseville	5.83	6.42	6.63
D09	El Dorado Hills	4.91	5.02	5.22
D09	Folsom	4.86	5.46	5.62
D10	Placerville	1.36	1.59	1.60

Figure EX-17: Changes (increases) in the UHII from current climate and LULC to 2050.
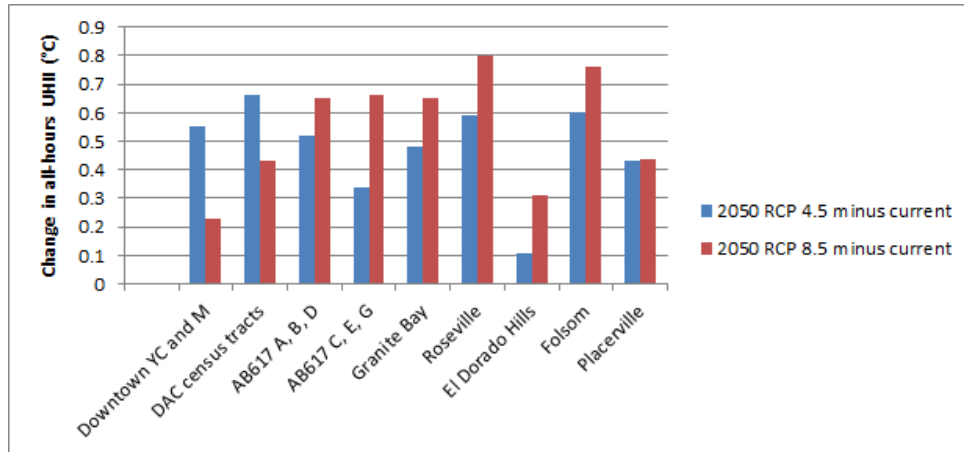
E.11 QUANTIFYING THE LOCAL OFFSETS TO THE UHII IN FUTURE CLIMATES AND URBANIZATION

The effects of local, community-scale heat-mitigation measures (i.e., at the 500-m level) were re-evaluated as in Section E.8, but this time in the context of future climate and land use. The goal was to assess the effectiveness of local mitigation measures in offsetting the future-climate UHII, e.g., as characterized in Table EST-8. In Tables EST-9 and EST-10, the future-climate all-hours UHII in 2050 is presented for each of the areas identified earlier and for RCP 4.5 and RCP 8.5, respectively, along with the effects of mitigation measures in a standalone mode of implementation (if combined, the effects can be larger, as discussed earlier, but are not linear).

The model results show that the effectiveness of the mitigation measures in 2050 is similar to their effectiveness in the current climate. In other words, the UHII attainment levels for various measures are of the same magnitudes in 2050 (RCP 4.5 and RCP 8.5) as in current climate – compare the last two columns in Tables EST-9 and EST-10 with the last two columns in Table EST-4. This is because the increased extent of urbanization, while contributing to additional local warming, also means an increase in technical potential (i.e., area available) for the deployment of mitigation measures, thus keeping the UHII offset levels similar to those in current climates or slightly larger in some cases.

As was the case for current conditions, shown earlier in Table EST-4, some measures in future climates (Tables EST-9 and EST-10), even in standalone fashion, can completely offset the local future-climate UHII. And, as before, when neighboring communities also implement UHI mitigation measures, the local benefits increase significantly. It is reiterated here that these are localized effects, i.e., temperature changes at or near the surface of the modified roadways or air temperature within the urban canyons of the selected communities, which can explain the different effectiveness of cool pavements alone versus combinations of cool roofs and pavements, as discussed in Section E.8, above.

Table EST-9: Potential of local projects in mitigating the all-hours UHII in future climate (2050 RCP 4.5) and urban land use.

Project area	All-hours Tair UHII (°C)**		Localized/no advection UHII attainment local mitigation only	Localized+advection UHII attainment local mitigation+advection
D05 Yuba City / Marysville Downtown YC and M	2.96	Cool roofs / pavements	-47%	-73%
		Cool pavements	-37%	-63%
		Electric vehicles	-6%	-31%
		Vegetation cover	-57%	-83%
D06 Woodland DAC census tracts	2.80	Cool roofs / pavements	-46%	-80%
		Cool pavements	-53%	-87%
		Electric vehicles	-5%	-39%
		Vegetation cover	-39%	-73%
D07 Sac / SE Sac AB617 A, B, D	5.00	Cool roofs / pavements	-26%	-62%
		Cool pavements	-28%	-64%
		Electric vehicles	-5%	-41%
		Vegetation cover	-30%	-66%
D07 Sac / SE Sac AB617 C, E, G	2.67	Cool roofs / pavements	-49%	-87%
		Cool pavements	-52%	-90%
		Electric vehicles	-9%	-47%
		Vegetation cover	-55%	-93%
Project area	All-hours Tair UHII (°C)**		Localized/no advection UHII attainment local mitigation only	Localized+advection UHII attainment local mitigation+advection
D08 Granite Bay	5.55	Cool roofs / pavements	-25%	-50%
		Cool pavements	-31%	-56%
		Electric vehicles	-6%	-30%
		Vegetation cover	-19%	-44%
D08 Roseville	6.42	Cool roofs / pavements	-22%	-54%
		Cool pavements	-27%	-59%
		Electric vehicles	-5%	-37%
		Vegetation cover	-16%	-48%
D09 El Dorado Hills	5.02	Cool roofs / pavements	-30%	-50%
		Cool pavements	-34%	-54%
		Electric vehicles	-4%	-24%
		Vegetation cover	-22%	-43%
D09 Folsom	5.46	Cool roofs / pavements	-27%	-53%
		Cool pavements	-31%	-57%
		Electric vehicles	-4%	-29%
		Vegetation cover	-20%	-46%
D10 Placerville / Diamond Springs / El Dorado City	1.59	Cool roofs / pavements	-75%	-99%
		Cool pavements	-101%	-125%
		Electric vehicles	-5%	-29%
		Vegetation cover	-82%	-106%

Table EST-10: Potential of local projects in mitigating the all-hours UHII in future climate (2050 RCP 8.5) and urban land use.

Project area	All-hours Tair UHII (°C)**		Localized/no advection UHII attainment local mitigation only	Localized+advection UHII attainment local mitigation+advection
D05 Yuba City / Marysville Downtown YC and M	2.64	Cool roofs / pavements	-53%	-79%
		Cool pavements	-42%	-67%
		Electric vehicles	-6%	-32%
		Vegetation cover	-64%	-90%
D06 Woodland DAC census tracts	2.57	Cool roofs / pavements	-50%	-83%
		Cool pavements	-57%	-91%
		Electric vehicles	-6%	-39%
		Vegetation cover	-42%	-76%
D07 Sac / SE Sac AB617 A, B, D	5.13	Cool roofs / pavements	-25%	-61%
		Cool pavements	-27%	-63%
		Electric vehicles	-5%	-40%
		Vegetation cover	-29%	-64%
D07 Sac / SE Sac AB617 C, E, G	2.99	Cool roofs / pavements	-43%	-83%
		Cool pavements	-47%	-86%
		Electric vehicles	-8%	-47%
		Vegetation cover	-49%	-88%

Project area	All-hours Tair UHII (°C)**		Localized/no advection UHII attainment local mitigation only	Localized+advection UHII attainment local mitigation+advection
D08 Granite Bay	5.72	Cool roofs / pavements	-25%	-48%
		Cool pavements	-30%	-54%
		Electric vehicles	-5%	-29%
		Vegetation cover	-18%	-42%
D08 Roseville	6.63	Cool roofs / pavements	-21%	-53%
		Cool pavements	-26%	-57%
		Electric vehicles	-5%	-36%
		Vegetation cover	-16%	-47%
D09 El Dorado Hills	5.22	Cool roofs / pavements	-29%	-47%
		Cool pavements	-32%	-51%
		Electric vehicles	-4%	-22%
		Vegetation cover	-21%	-40%
D09 Folsom	5.62	Cool roofs / pavements	-27%	-51%
		Cool pavements	-30%	-55%
		Electric vehicles	-3%	-28%
		Vegetation cover	-20%	-44%
D10 Placerville / Diamond Springs / El Dorado City	1.6	Cool roofs / pavements	-75%	-100%
		Cool pavements	-100%	-125%
		Electric vehicles	-5%	-30%
		Vegetation cover	-81%	-106%

E.12 SUMMARY RANKING OF HEAT-MITIGATION MEASURES IN FUTURE CLIMATES AND LAND USE

The following chart in Figure EX-18 summarizes the rankings of measures discussed above for 2050 RCP 4.5 and RCP 8.5 and provides a comparison to the rankings under the current climate and land use / urbanization levels that were summarized in Figure EX-6. The chart is color-coded so that black is most effective and near-white is least effective. Again, the caveat regarding case02 should be reiterated (an extreme measure) and that it should be excluded from this comparison to a certain extent.

From Figure EX-18, the following can be observed in terms of ranking the cooling potential of various measures:

1. For the 0600-PDT UHII:

    a. The rankings of mitigation measures (order) are similar and consistent across all regions.

    b. Within each region, the rankings are similar across current and future climates.

2. For the 1300-PDT UHII:

    a. The rankings are different across the regions.

    b. In Davis and Sacramento, the rankings are different in future climate than they are in current climate (but are similar in RCP 4.5 and 8.5).

3. For the 1400 – 2000 PDT UHII:

    a. The rankings are different across the regions.

    b. In Woodland, the rankings are different in future climate than they are in current climate (but are similar in RCP 4.5 and 8.5).

4. For the 1500 PDT UHII:

    a. The rankings are different across the regions.

    b. In Auburn, Davis, El Dorado Hills, and Yuba City, the rankings are different in future climate than they are in current climate (but are similar in RCP 4.5 and 8.5).

5. For the all-hours UHII:

    a. The rankings are different across the regions.

    b. Within each region, the rankings are similar across current and future climates.

This type of information may be useful to planners if they need to specifically target certain times of day, e.g., peak temperatures, or are interested in mitigating all-hour UHII averages for a particular region.

Figure EX-18: Summary of urban-heat mitigation potential: ranking of measures case01 through case31 by cooling effectiveness (darker to lighter = largest to smallest cooling) in future climate (2050). Note that case02 should be excluded in some analysis. Also note that this is impacts on air temperature, not UHII.
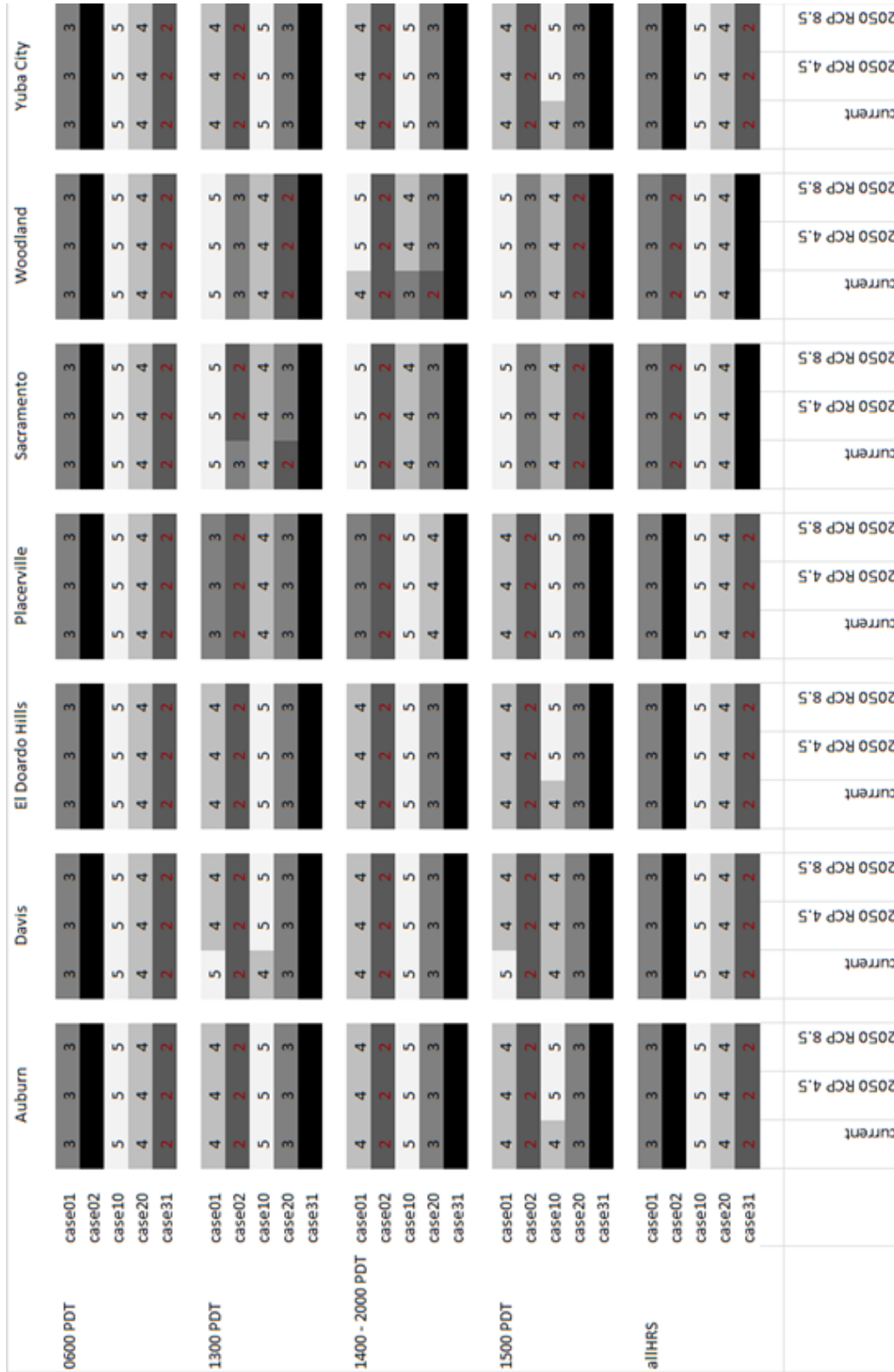
E.13 CONCLUSION AND QUALITATIVE TAKEAWAYS

In concluding this Executive Summary, a few qualitative talking points, or takeaways, from the foregoing discussion are provided, in no particular order:

1. Significant urban-heat pollution exists throughout the 6-counties Capital region. The UHI and the UHII are larger in urban areas that are (1) more densely built up, (2) cover a larger geographical area, (3) located at the downwind end of an urban zone (trajectory-wise), (4) located at higher elevations, and (5) surrounded by non-urban areas that cool down significantly faster at night.

2. While temperatures in the region generally increase from current climate to future (e.g., to 2050 RCP 4.5 and then to 2050 RCP 8.5), the corresponding UHII also increases in this direction except for two urban areas where the UHII can be smaller in RCP 8.5 than in RCP 4.5 (although still larger than in current climate). This is a result of accelerated warming in the surrounding non-urban areas.

3. It is possible and highly feasible to mitigate the current UHI and offset the UHII (in some cases completely) using materials and practices that are reasonable and readily used throughout the 6-counties Capital region. The proposed UHI mitigation measures are reasonable – meaning they do not require some hypothetical or extreme implementation levels, only what is already available and used in the existing market and current practices.

4. Mitigation measures can offset the local UHII in standalone fashion, in some cases completely. Various combinations of measures can further attain or further offset the UHII, although the total effects of combinations of measures are not linear (not simple sums) and generally smaller than the sums of the individual cooling effects of various components.

5. The measures can have significant beneficial effects in terms of public heat health as indicated by their ability to lower the warning levels in the National Weather Service Heat Index (NWS HI). This was assessed by modeling various UHI-mitigation scenarios in this study, in both current and future climates.

6. The cooling measures can significantly reduce or completely erase the number of heat-wave days during several excessive-heat event periods identified in the study.

7. The mitigation measures are as effective under conditions of future climate and land use as they are under current conditions.

8. Different mitigation measures affect urban heat and temperature differently during different times of the day. Hence it is possible to target certain specific time intervals, e.g., peaks, night, day, or all hours (per a community or city's needs) by choosing a specific mitigation measure or combinations of measures.

9. If, in addition to a community's heat-mitigation actions, neighboring communities also implement UHI-mitigation measures, the local cooling effects could double (although there is a range of effects depending on location, time, specific measures, etc.).

10. Some measures that are not conventionally associated with urban cooling (or urban heat island mitigation), such as (1) vehicle electrification, (2) solar PV installations, and (3) smart urban growth, all appear to have significant urban-cooling effects.

11. The cooling effects are beneficial across various urban areas in the Capital region, including AB617 and disadvantaged communities, which can help improve thermal comfort, reduce emissions of air pollutants, and improve air quality.

12. In this modeling study, ranking of mitigation efficacy was done for each region, each measure, and each time interval (e.g., specific hours, a range of hours, or 24 hours, etc.) for current and future climates and land use. Some areas or time intervals have a consistent ranking of measures, others vary by location, and others vary in future climate relative to current conditions.

13. Information generated in this modeling study can be used by Caltrans, SMAQMD, LGC, the cities and communities in the Capital region to prioritize projects and implementation of various measures or in the allocation of resources per urban-heat criteria under current climate conditions as well as for future climate and land use.

1. INTRODUCTION

Hot weather can cause a myriad of unwanted effects including heat-health impacts, increased cooling energy demand, higher emissions of air pollutants, and worsening air quality (Taha 2015a; Alfaro et al. 2004, 2006; Founda and Santamouris 2017; Gershunov et al. 2009; Li and Bou-Zeid 2013). Thus, urban areas in the warmer parts of the world have implemented or begun to implement various measures to combat heat, whether urban or not. In the context of heat-mitigation measures, it is useful to distinguish between the terms "urban heat" and "urban heat island" (UHI) or "urban heat island index" (UHII) and clarify some of the concepts involved.

To re-state the obvious, the goal of this and similar studies is to design and implement measures that reduce urban heat, not urban heat islands per se. In other words, the goal is to cool down the ambient air in any hot urban area, regardless of how much hotter or cooler it may be compared to some other urban areas or some non-urban reference points (the latter being the definition of the urban heat island). Thus, if so, what is the purpose of characterizing urban heat islands (or the UHII)? The simple answer is that the UHI and UHII are just quantitative indicators or yardsticks that tell us how much cooling we can reasonably expect to achieve at a certain urban location. In other words, the UHI (or UHII) simply is an indicator as to how much cooling is needed to bring the temperature of a certain urban location down to that of a nearby non-urban area (Taha 2013a, 2017). Of course, the actual cooling that is achievable at a certain location could be smaller or larger than the UHI or UHII, as will be discussed later in this report.

Furthermore, there is a subtle difference between the UHI and the UHII, as used in this study, that can be defined as follows:

UHI: Urban heat island, is an instantaneous temperature difference between an urban location and a non-urban reference point (e.g., an instantaneous measurement). Thus, the units of UHI are °C.

UHII   Urban heat island index, is a cumulative (total) temperature difference between an urban location and a non-urban reference point calculated over a determined time interval, e.g., several hours or several days, etc. The units of UHII are degree-hours, e.g., °C · hr, or degree-days, and so on.

An important point to emphasize here is that urban heat indicators quantified in this study (including UHI and UHII, for example) are air-temperature-based, not derived from skin-surface temperature (such as shown in many studies of "urban hot spots" that are basically satellite / thermal remote-sensing imageries) also referred to as "surface-temperature urban heat island", or SUHI. Hence, the spatial patterns of urban heat analyzed in this study and presented in this report differ from those seen in satellite imagery most of which simply shows hot roofs and roadways surrounded by cooler vegetation or pervious surfaces. This is discussed in some more detail later in Section 3.4.

Altostratus Inc.

Having established this basic understanding of urban heat and the purpose of computing the UHI (or UHII), we can now proceed with discussing the characterization of the UHI and UHII in the Capital region.

In 2015, the California Environmental Protection Agency (Cal/EPA) developed a first-of-its-kind Urban Heat Island Index (UHII) for the state of California (Taha and Freed 2015). In that effort, four levels of the UHII were defined (Taha 2017), as shown in Figure 1-1. However, only the Level-1 UHII was developed and modeled in that undertaking (additional information can be found at https://calepa.ca.gov/wp-content/uploads/sites/6/2016/10/UrbanHeat-Report-Report.pdf).

Essentially, the various levels were defined such that the progression of the UHII, as an indicator or metric, goes from characterizing the problem (Level-1) to characterizing the mitigation (Level-4).

Figure 1-1: UHII levels (source: Taha 2017).
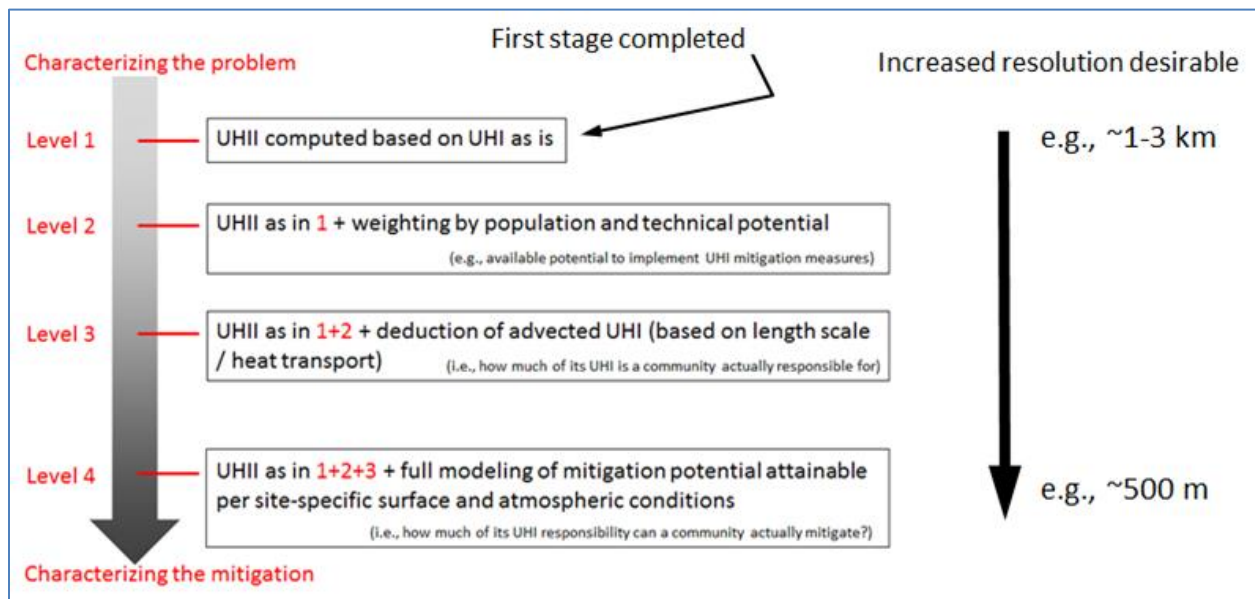
In consultation with the Cal/EPA and the stakeholders in that study, the Level-1 UHII was defined in its simplest form as in equation (1-1):

$$UHII = \sum_{h=1}^{H(JJA)} \left[T_{u(k),h} - min\left(T_{u(k),h}, T_{nu(k),h}\right) \right]$$

(1-1)

where the *UHII* (C·hr) is computed over several time periods, e.g., June, July, and August (JJA) over several years, T_u is urban air temperature at a specific location k, T_{nu} is non-urban, upwind, reference temperature corresponding to (i.e., paired with) urban location k, and h is the time index,

e.g., hour. The non-urban temperature (T_{nu}) corresponding to each urban point k is time-varying and depending on wind approach direction, that is, the direction from which the wind is approaching the urban location k.

The same definition of the UHII was used in this study, except that it was applied to longer and different time periods in years 2013 through 2016. In the simplest terms, per Equation 1-1, the UHII is the temperature difference between an urban location k at hour h and its corresponding upwind non-urban reference point (at the same hour), but only when the urban temperature is larger than the non-urban reference temperature.

In the present study, several aspects of the UHII beyond Level-1 were directly or indirectly addressed and discussed in the report. To evaluate UHII Levels 2 – 3, i.e., heat generation and transport, the following factors were considered:

- Heat that is generated at the transportation system (corridors, roadways, facilities, infrastructure, stations, rail, airports, maintenance yards, etc.) and transported to other areas -- quantified by accounting for surface physical properties of roadways and infrastructure, as well as heat emissions from motor vehicles;
- Urban heat advected to the transportation system -- quantified by evaluating the effects of surface physical characteristics in urban areas, morphological / geometrical properties, and heat emissions; and
- Urban heat generation and transport throughout the region -- a result of large-scale climate effects and forcings.

When mitigating or reversing urban-heat effects, which entails the development of a Level-4 assessment of the changes in UHII, the following factors were considered:

- Direct effects, e.g., impacts on structural integrity / lifespan of pavement and on transportation infrastructure as indicated by changes in surface temperature and other related variables;
- Indirect effects, e.g., impacts on air temperature in urban corridors and the advection of cooler air into the surrounding urban areas (which has implications on thermal conditions, emissions, and air quality);
- Thermal and environmental comfort of the transportation system's users, as quantified by changes in air temperature near the ground and in the urban canopy layer; and
- Emissions impacts, e.g., lower pavement temperatures and shading of parking lots and structures (with solar PV or vegetation canopy) thus reducing evaporative / fugitive hydrocarbon emissions, as quantified by changes in surface and air temperatures in areas affected by mitigation measures.

Urban-heat mitigation measures can benefit both the transportation system and the communities which they serve. Urban cooling, i.e., reductions in surface and air temperatures, can benefit the transportation sector in some or all of the following ways, depending on scale and proximity to areas where the mitigation measures are implemented:

≡ Reducing the impacts of heat stress on roadways (in current climate, heat events, and future climate), which has benefits in terms of slowing the aging of bitumen, the stiffness of asphalt, deformation and rutting, i.e., past certain surface temperature thresholds, as well as reducing tensile stresses, cracking, and impacts on expansion joints;

≡ Reducing surface traffic restrictions as urban cooling can bring down air temperature below the thresholds that dictate roadways closures (e.g., asphalt temperature threshold for roadways to remain open to traffic), as well as potential reductions in wildfires in nearby areas;

≡ Minimizing impacts on operations at stations, parking lots, facilities and the impacts on users of the transportation system, by reducing heat and radiation (comfort, energy), reducing impacts on vehicles air conditioners, tires, overheating, evaporative emissions, reducing heat effects on railways (buckling or failure), and reducing impacts on aircraft operations, e.g., required runway length for takeoffs and landings; and

≡ City-wide impacts on transportation infrastructure.

The urban-cooling measures can also benefit the communities by improving summer thermal comfort, reducing heat stress, reducing cooling energy demand, air-pollutant emissions, and improving public air-quality and heat health.

Considering all of the above factors, the SMAQMD, with interest from communities in the area, as well as SMUD, LGC, the cities, and local organizations, participated in this SB-1/Caltrans-funded effort to build upon the Cal/EPA Level-1 UHII and address the needs and impacts of the transportation sector. Thus, the overarching objectives of this project were to:

≡ Characterize and quantify urban heat in current and future climates in the 6-counties Capital region (including the counties of Sacramento, El Dorado, Placer, Yuba, Sutter, and Yolo);

≡ Identify urban areas and transportation-system zones that are subject to higher temperatures under conditions of current and future climate and land use (urbanization); and

≡ Evaluate and quantify the effectiveness of urban-cooling measures and rank their potentials in mitigating heat (in current and future climates).

Various cooling measures have been investigated in the past via either modeling or observations (or some combinations thereof), e.g., Taha (2007, 2015a,b), Akbari et al. (1999), Georgescu et al. (2014), Gilbert et al. (2017), and Levinson et al. (2007), among many other U.S. and international

Altostratus Inc.

studies, too numerous to list here. In this study, the following measures were evaluated and modeled:

- ≡ For area-wide transportation and non-transportation urban cooling, that is, to achieve regional effects benefiting urban areas as a whole in the 6-counties Capital region, the measures considered in this study and evaluated at the coarse (2-km) scale included:

    - ≡ Cool roofs and cool pavements;
    - ≡ Vegetation canopy cover;
    - ≡ Combinations of measures; and
    - ≡ Smart growth (for future climate), i.e., infill or greenfield developments.

- ≡ For localized effects at community scale, transportation corridors, specific roadway projects, and specific neighborhoods, i.e., to achieve localized benefits regardless of whether any actions are taken by other communities at the regional scale, the following measures were considered (these were modeled at 500-m resolution):

    - ≡ Cool roofs;
    - ≡ Cool pavements;
    - ≡ Vegetation canopy cover;
    - ≡ Vehicle electrification;
    - ≡ Solar PV; and
    - ≡ Cool walls.

Green roofs were not considered in this study in response to recommendations from the project TAC because of their high initial and maintenance costs, as well as effectiveness issues.

It is important to note that the urban-heat mitigation measures and mitigation levels proposed and modeled in this study, and whose effects are presented in this report, are reasonable, i.e., can already be found in the study region and are not some hypothetical or extreme measures as is sometimes assumed in this type of studies. Thus:

1. The reasonability of the measures means that the scenarios studied in this project are based on reasonable increases in albedo, vegetation cover, vehicles electrification, etc. This means that we are simply encouraging people to use more of the measures and products that are already available and easily implemented locally, not some extreme levels or hypothetical mitigation measures that are impractical. In other words, this is simply encouraging a wider use of materials and methods that already exist in the current market and in current construction and building practices.

2. Keeping the modification levels reasonable also means minimizing any potential negative effects on the atmosphere, e.g., air quality impacts, that could result from decreased mixing (venting), increased UV albedo, increased biogenic emissions, or increasing visual

environmental concerns such as glare (these factors will be discussed in Section 5.6). Thus, the mitigation levels assumed in this study were also meant to be kept below "city-specific" thresholds in each area, if identifiable, as discussed in Taha (2005, 2007).

2. LAND USE AND LAND COVER ANALYSIS

2.1 OBJECTIVES OF LULC ANALYSIS

The main purposes of land-use and land-cover (LULC) analysis in this project were to (1) define study domains and modeling grids for the project area with focus on the 6-counties Capital region, (2) acquire most recent LULC datasets as needed, (3) reformat and recast the data into direct and derived parameters for input to the land-surface and atmospheric models used in this study, (4) characterize LULC change and urbanization over time, e.g., through 2050 or beyond, and (5) develop technical potentials for deployment of mitigation measures in various parts of the region.

This task entailed assembling and analyzing LULC data for current conditions (by merging various sources of information, as discussed in Section 2.3, below) and future growth scenarios. The task also involved characterization of urban morphology / geometry, transportation system, roadways, infrastructure, and deriving the surface physical properties of relevance to urban heat, e.g., albedo, canopy cover, roughness length, soil moisture, shade factor, various plan-, top-, and frontal-area densities for calculations of various building and vegetation-canopy parameters, and anthropogenic heat emissions, using a bottom-up approach discussed in the following sections. Another product from the LULC analysis is technical potential for the development of mitigation scenarios and identification of implementation levels

2.2 SELECTION OF MODELING DOMAINS

This study used a version of the WRF modeling system that is continuously modified, updated, and customized at Altostratus Inc., as described elsewhere (e.g., Taha 2017, 2008a-c; Taha et al. 2018). An analysis and modeling domain structure was configured for this study (Figure 2-1) based on a nested-grid system of 54, 18, 6, 2, and 0.5 km resolutions. The 2-km grid is used to model and analyze the impacts of heat mitigation measures at the regional scale in the Capital region, i.e., the effects that will result from region-wide implementation of certain strategies. The 500-m grids, on the other hand, are used to evaluate localized mitigation measures at the project or community scales (independently of actions taken collectively at the regional scale) and to evaluate in more detail their localized impacts. The 500-m grids (Figure 2-2) were configured based on LULC analysis and feedback received from the SMAQMD and LGC. The grids also contain all areas of interest, current and future, that were identified by the project TAC. For each of these 2-km and 500-m modeling grids, LULC was thoroughly characterized and data were generated for input to the land-surface and atmospheric models, as discussed below.

Figure 2-1: Ten-domain atmospheric-model grids configuration (D01-D10). Domain D04, shown again in yellow in Figure 2-2, below, encompasses the Capital region.
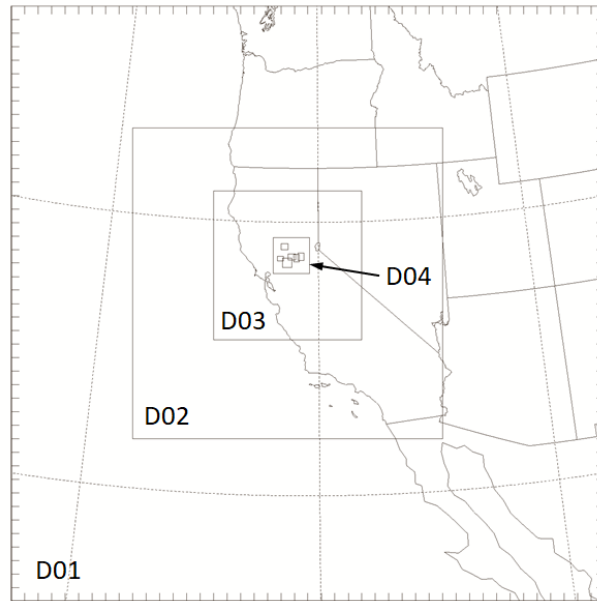
Figure 2-2: 2-km domain (yellow rectangle, D04), for the Capital region, and 500-m grids (white rectangles, D05-D10) for detailed simulations of localized heat-mitigation measures. Also shown in the figure are areas deemed of interest by the project TAC and participating cities and organizations (blue, red, and grey overlays and blue markers). The latitude/longitude coordinates of the 2-km domain corners are also shown.
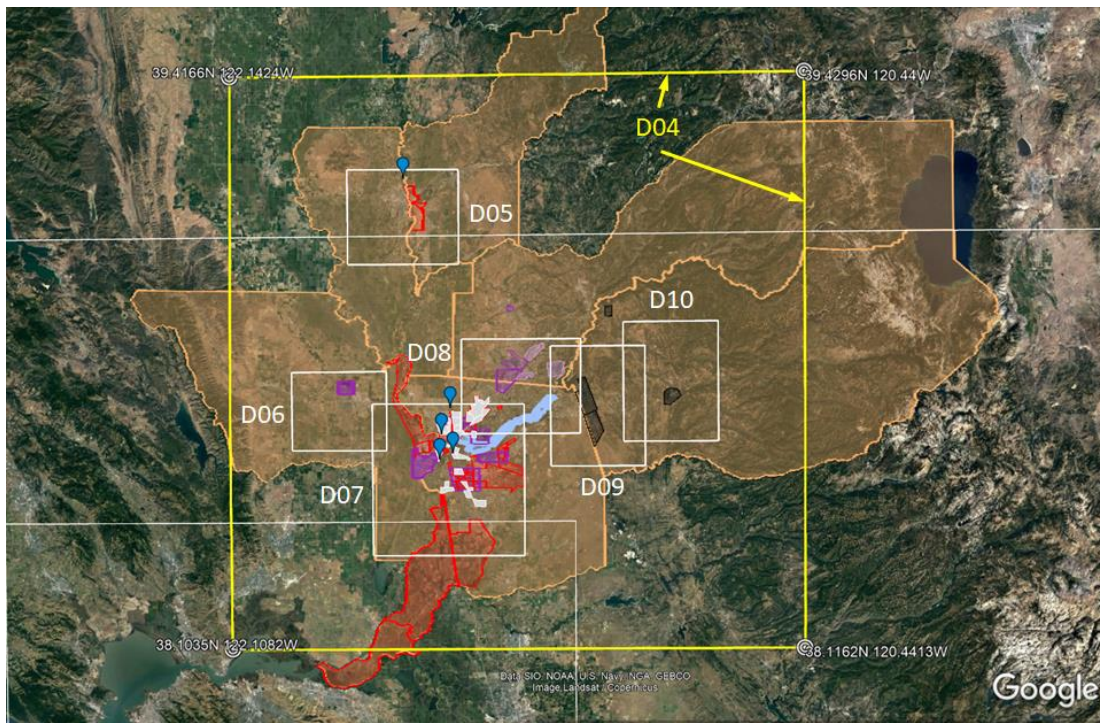
Figure 2-3 shows the actual positions of the model grid points (also known as mass points or cell centers) in the study region. The white dots represent the 2-km domain (D04) grid points and the smaller dots are those of the 500-m domains (D05 – D10). They are difficult to distinguish in Figure 2-3 because of their close spacing – thus Figure 2-4 is provided as an example to show the detail of how the 500-m grids mesh with the 2-km grid, in this case how D07 (red dots) meshes with D04 (white dots). Viewing these figures at a magnification of ~300% allows for a better distinction of various features and grid points.

Each point in these 2-km and 500-m domains was characterized in terms of LULC and surface physical properties based on a detailed bottom-up approach developed at Altostratus Inc. (Taha 2017, 2013a,b). At the finer scales, this approach is more accurate and area-specific than the common urban surface characterizations used in atmospheric modeling such as NUDAPT / WUDAPT (Ching et al. 2009) or similar other approaches used with the WRF modeling system. Depending on available information, some characterizations are reverted to default, others are extremely grid-specific, that is, based on data available from cities, counties, or other GIS data sources, as well as from in-situ observations. The detailed bottom-up surface characterization approach used in this study is discussed in the following sections.

Throughout this report, and aside from the coarse domains D01 – D03 (Figure 2-1), the finer-scale domains are identified and referred to as follows:

D04:   This is a 2-km grid encompassing all six counties in the Capital region (yellow rectangle in Figure 2-2 and white dots in Figure 2-3)
D05:   500-m grid for the Yuba City / Marysville area (in Yuba and Sutter counties)
D06:   500-m grid encompassing Woodland (in Yolo County)
D07:   500-m grid for various areas in Sacramento (in Sacramento County)
D08:   500-m grid for the Roseville and Granite Bay areas (in Sacramento and Placer counties)
D09:   500-m grid encompassing Folsom, El Dorado Hills, and surrounds (in Sacramento and El Dorado counties)
D10:   500-m grid for the Placerville area (in El Dorado County).

As mentioned above, the fine-scale domains were selected per recommendations received from the project TAC, SMAQMD, and LGC (see markups in Figure 2-2). In addition, SMAQMD (2018) identified ten AB617 communities (DACs) in the Sacramento area, as shown in Figure 2-5. Thus, domains D07 and D08 were also designed to encompass these communities.

Figure 2-3: Locations of atmospheric-model mass points in the study region. D04 is 2-km in resolution and all other domains (D05 – D10) are at 500-m resolution.
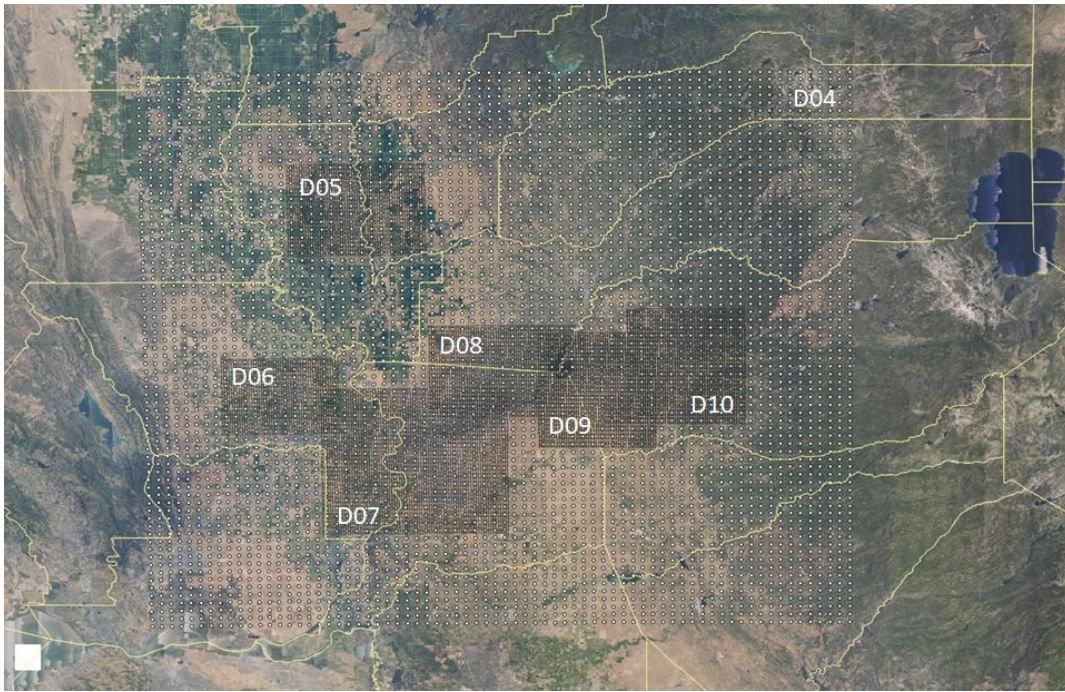
Figure 2-4: Example showing details of meshing between a 500-m grid (D07, small red points) and a 2-km grid (D04, white circles).
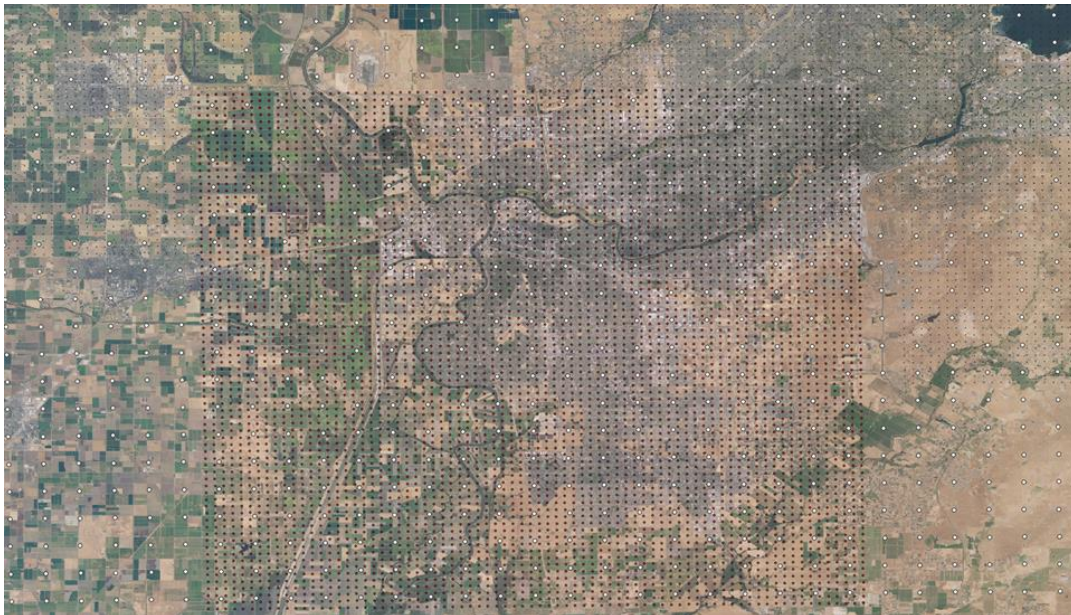
Figure 2-5: AB617 disadvantaged communities A – J, per SMAQMD (2018).
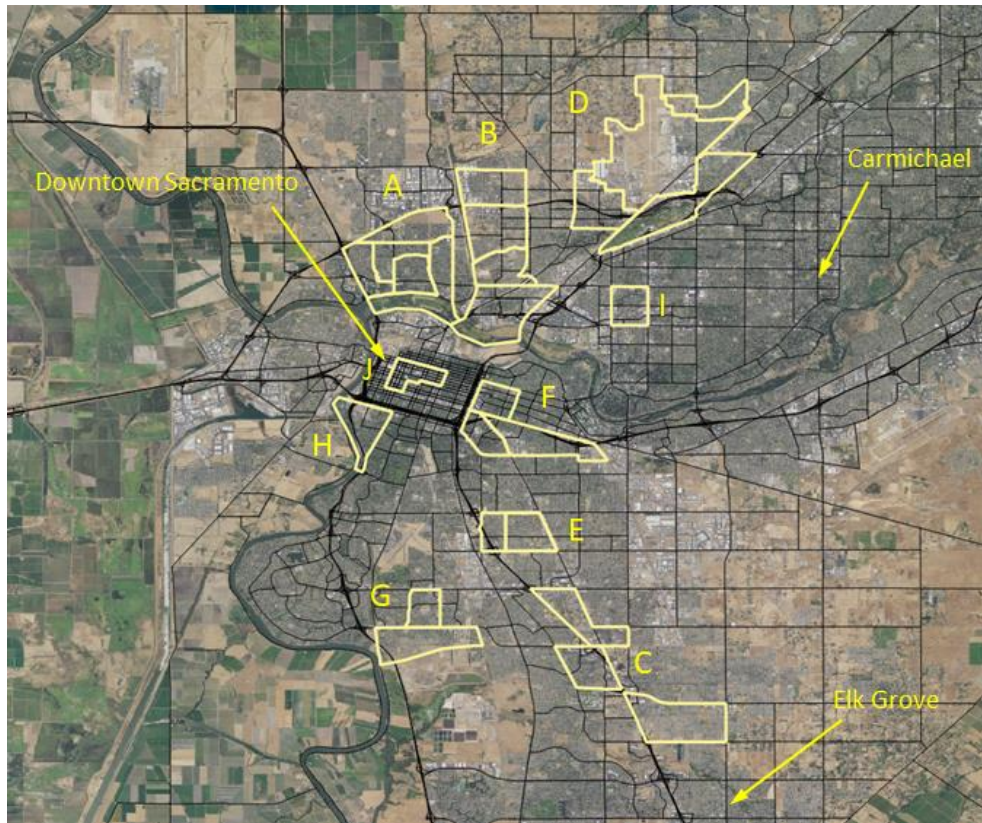
2.3 LULC AND SURFACE-PROPERTIES DATASETS

To develop a detailed, bottom-up surface physical characterization input to the meteorological model, several LULC data types were used in this project. These included:

- ≡ 30-m National Land Cover Data (NLCD 2011 / 2016) for current LULC (MRLC 2011);
- ≡ 30-m NLCD 2011 / 2016 impervious cover, for current conditions (MRLC 2011);
- ≡ 30-m USGS Anderson Level-II and Level-IV LULC, for current conditions (Anderson et al. 2001);
- ≡ USGS LUCAS datasets for future-year LULC projections through year 2100 (Sleeter et al. 2017a,b);
- ≡ 1-m to 30-m USGS Anderson Level-IV LULC, from SACOG for current conditions (data.sacog.gov);
- ≡ Google Earth Pro urban morphological and land-cover data for specific area characterizations of urban morphology (google.com);

- 1-m aerial photography-based roof albedo characterizations (Lawrence Berkeley National Laboratory) for current conditions, https://heatisland.lbl.gov/projects/projects-california-roof-albedo (Ban-Weiss et al. 2015);
- 1-m area-specific urban morphological and geometrical data (National Urban Datasets and Portal Tool N/WUDAPT) for current conditions (Burian et al. 2003; Ching et al.2009);
- 1-m Earth Define / CAL FIRE urban tree canopy cover datasets (www.earthdefine.com);
- 1-m Quick Bird UFORE urban tree canopy dataset (UC Davis / USFS) for urban areas in the Sacramento region, current conditions (Simpson and McPherson 2007);
- MRLC canopy cover (30-m resolution) for current conditions (MRLC 2011); and
- MODIS albedo for current conditions (MRLC 2011).

In addition to the above, area-specific datasets were also used as suitable from the following sources:

- CALTRANS GIS: www.dot.ca.gov/hq/tsip/gis/datalibrary;
- SACOG regional GIS clearinghouse: https://www.sacog.org/regional-gis-clearninghouse;
- CalEnviroScreen 3.0: https://oehha.ca.gov/calenviroscreen (OEHHA 2013);
- Sacramento County: http://generalmap.gis.saccounty.net/JSViewer/county_portal.html#;
- Sacramento County general plan: http://www.per.saccounty.net/PlansandProjectsIn-Progress/Pages/GeneralPlan.aspx;
- City of Sacramento: http://data.cityofsacramento.org/datasets/general-plan;
- Sacramento County GIS: http://data-sacramentocounty.opendata.arcgis.com/;
- El Dorado County GIS: http://gem.edcgov.us/ugotnetextracts/;
- Sacramento County Building footprints: //data-sacramentocounty.opendata.arcgis.com/; and
- Sacramento County parcels information: //data-sacramentocounty.opendata.arcgis.com/.

The LULC datasets were analyzed and model parameters were calculated based on characterizations from the above-listed data sources. These datasets were used to develop grid cell-by-cell surface characterizations, as discussed in the following sections. Furthermore, crosswalks among different datasets were also established as needed to bridge the gaps in data coverage and provide parameters required as input to the atmospheric models. The crosswalks will be discussed later in this report.

2.3.1 Calculations of urban tree canopy cover based on Earth Define / CAL FIRE data

Calculations specific to this dataset were performed in this study to derive tree-canopy cover in those areas defined as urban (per Earth Define, www.earthdefine.com) in the domains of interest. Figure 2-6 (A) shows the data extent in this study domain and depicts the 1-m resolution canopy cover toggle (tree/no tree) in urban areas of the 6-counties region.

The data obtained from CAL FIRE / Earth Define were recast, vectorized, and modified (and used in combination with other data sources) to derive the model-input parameters related to vegetation cover that are needed in this study, including cover, leaf-area index, height, and geometrical properties of the canopy. The calculations were carried out at the 2-km level (D04) and then repeated at the 500-m resolution for domains D05 – D10. After vectorizing and aggregating, the data was re-gridded into the model's map projection for the specific domains to derive additional vegetation-related parameters such as albedo, roughness length, soil moisture, and shade factor (Taha 20-8a-c, 2017).

Examples from these calculations are shown in Figure 2-6 (B – h), where the caption below each figure identifies the corresponding domain. This canopy cover information is merged with the tree-cover data derived from NLCD 2011 / 2016 as well as from specific Sacramento-area datasets (discussed further below) to develop full-domain tree canopy characterizations.

Figure 2-6: (A) 1-m resolution urban tree canopy cover toggle (tree / no tree) based on Earth Define / CAL FIRE datasets for the study region and an example detail; (B – H) computed gridded tree cover in domains D04 – D10 (only in grid cells defined as "urban").

2-6.A

CALFIRE tree cover in D04 (2 km domain). Cover is only in urban land use.

2-6.B

CALFIRE tree cover in D05 (500 m domain). Cover is only in urban land use. Black lines are approximate urban boundaries.

2-6.C

CALFIRE tree cover in D06 (500 m domain). Cover is only in urban land use. Black lines are approximate urban boundaries.

2-6.D

CALFIRE tree cover in D07 (500 m domain). Cover is only in urban land use. Black lines are approximate urban boundaries.

2-6.E

CALFIRE tree cover in D08 (500 m domain). Cover is only in urban land use. Black lines are approximate urban boundaries.

2-6.F

CALFIRE tree cover in D09 (500 m domain). Cover is only in urban land use. Black lines are approximate urban boundaries.

2-6.G

Altostratus Inc.

CALFIRE tree cover in D10 (500 m domain). Cover is only in urban land use. Black lines are approximate urban boundaries.

2-6.H

The maps in Figure 2-6 (B – H) show some discontinuity in coverage, areas of unusually large cover, or blank areas because of the distributions of urban cells in the domains (i.e., the CAL FIRE data exist only in urban cells). In other words, those blank areas in the figure actually contain vegetation cover in various amounts, e.g., crops, forests, open spaces, etc., but they don't appear in these figures because they are not in cells classified as urban. Areas with unusual cover were handled separately or excluded from the analysis as outliers.

Considering only those cells with vegetation cover greater than 0.01, i.e., urban cells as defined here, the median and range of vegetation cover are shown in Figure 2-7 and summarized in Table 2-1 (for the 500-m domains). Medians and quartiles are shown as boxes superimposed upon the scatter plots in each graph.

Thus, according to this dataset, the bulk of the canopy cover in urban areas of the Capital region rarely exceeds 0.26. The highest values are found in domains D07 and D08 representing central Sacramento and immediate surroundings. These may be in fact why central Sacramento and areas near downtown are generally cooler than other parts of the greater Sacramento region (as will be discussed in Section 3.4). This is also the reason why certain scenarios of canopy-cover increase in urban areas (larger than case01, see Section 5.5), are deemed to be hypothetical and unfeasible at this time.

Table 2-1: Median and range of canopy cover in urban cells of 500-m domains D05 through D10 (based on CAL FIRE / Earth Define datasets). The range in this table is not specified as difference between maximum and minimum values but, rather, the range of the bulk of the canopy cover values in the specified domains, as seen in Figure 2-7.

Domain (500-m grid)	Median of canopy cover	Range of canopy-cover bulk
D05	0.068	0.01 – 0.20
D06	0.055	0.01 – 0.15
D07	0.059	0.01 – 0.24
D08	0.059	0.01 – 0.26
D09	0.045	0.01 – 0.22
D10	0.027	0.01 – 0.14

Figure 2-7: Distribution of canopy cover in 500-m domains D05 – D10 (only in grid cells defined as urban) computed based on Earth Define / CAL FIRE data. Superimposed boxes show median and quartiles.
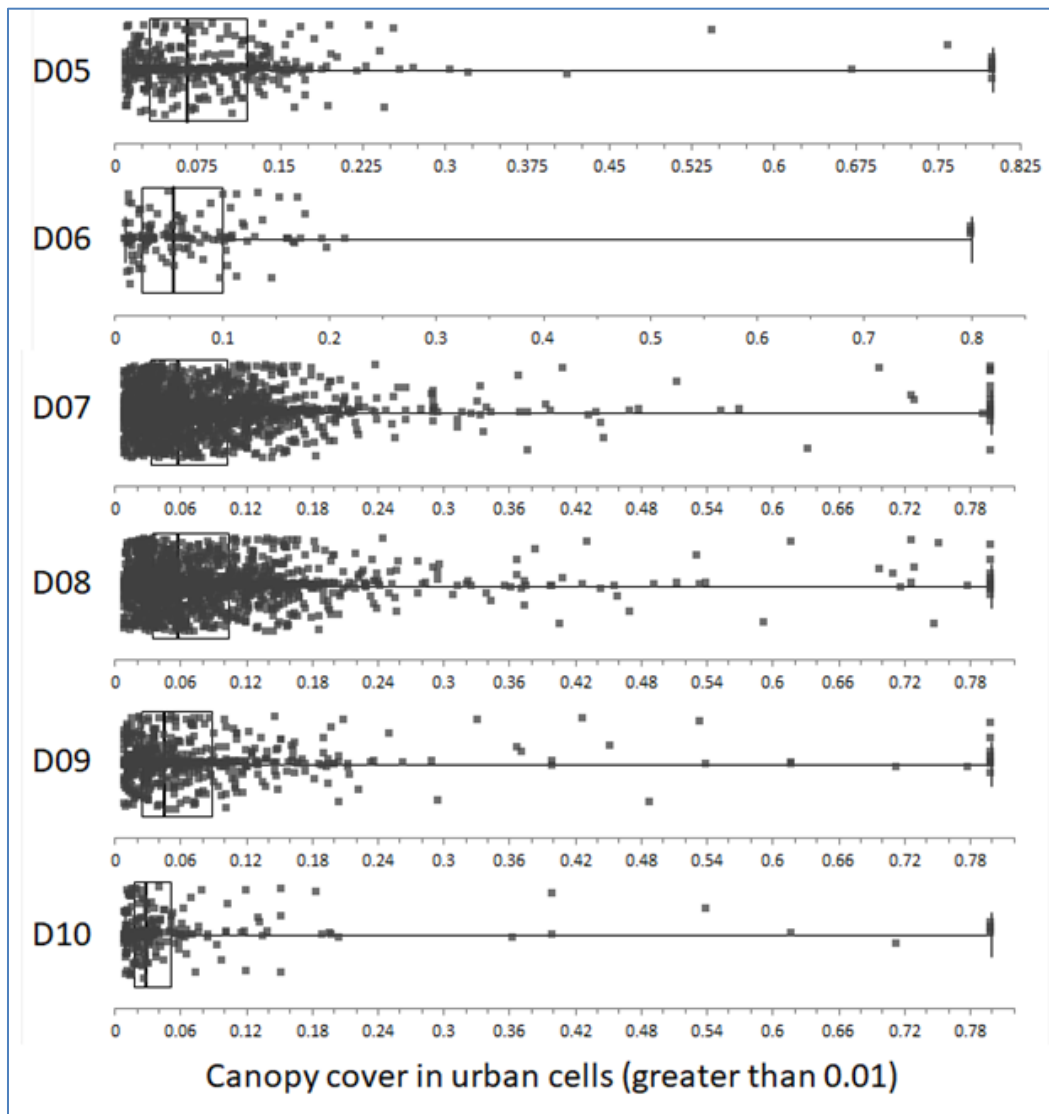
2.3.2 Calculation of canopy cover based on NLCD 2011 / 2016

To enhance the tree-cover characterizations beyond the Earth Define / CAL FIRE datasets (discussed above) and to bridge the data gap with canopy-cover information in non-urban areas, additional calculations were carried out using 30-m resolution NLCD 2011 / 2016 data (MRLC 2011) for the 500-m domains. The canopy-cover dataset in NLCD 2011 / 2016, developed by the U.S. Forest Service (USFS), covers both urban and nonurban areas.

Thus, the NLCD data were processed to remap and re-grid the information per the domain configurations used in this study. Examples from these calculations are shown in Figure 2-8 (A – H), where the computed cover is for the 2-km grid (D04) and for 500-m grids D05 - D10 (the caption below each figure identifies the domain). The results are also summarized in Figure 2-9.

Figure 2-8 (A – H): Gridded canopy cover computed from 30-m NLCD 2011, USFS datasets.
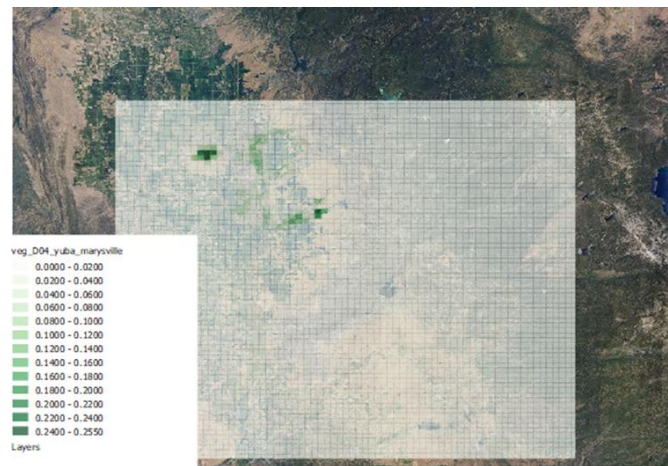
NLCD 2011-based calculations of canopy cover in D04 Yuba City / Marysville   **2-8.A**
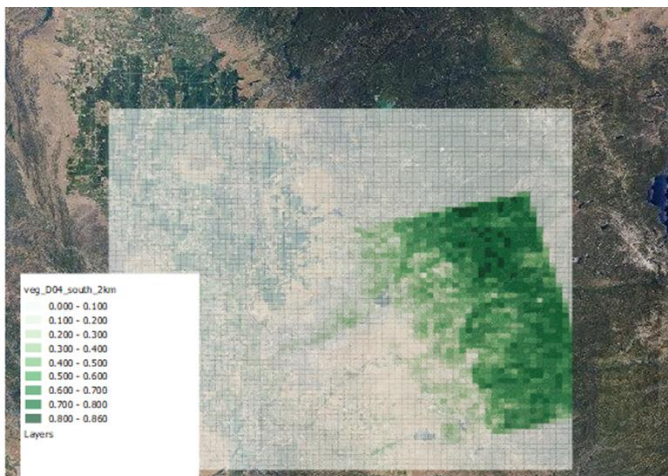
NLCD 2011-based calculations of canopy cover in D04 south 2km   **2-8.B**

NLCD 2011-based calculations of canopy cover in D05 500 m domain   **2-8.C**

NLCD 2011-based calculations of canopy cover in D06 500 m domain   **2-8.D**
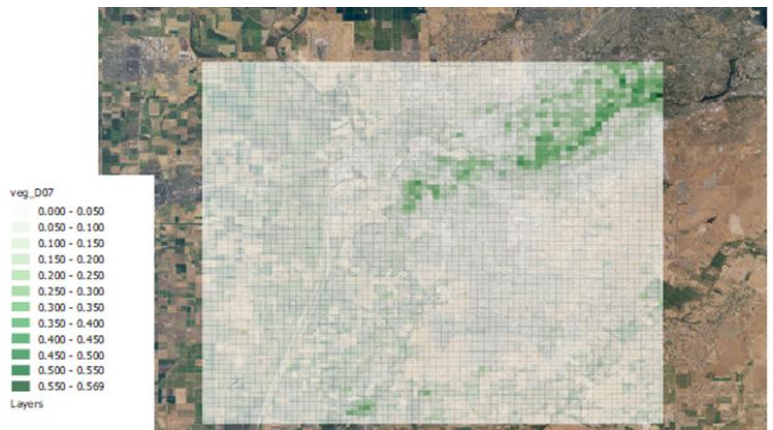
NLCD 2011-based calculations of canopy cover in D07 500 m domain   **2-8.E**

NLCD 2011-based calculations of canopy cover in D08 500 m domain

2-8.F
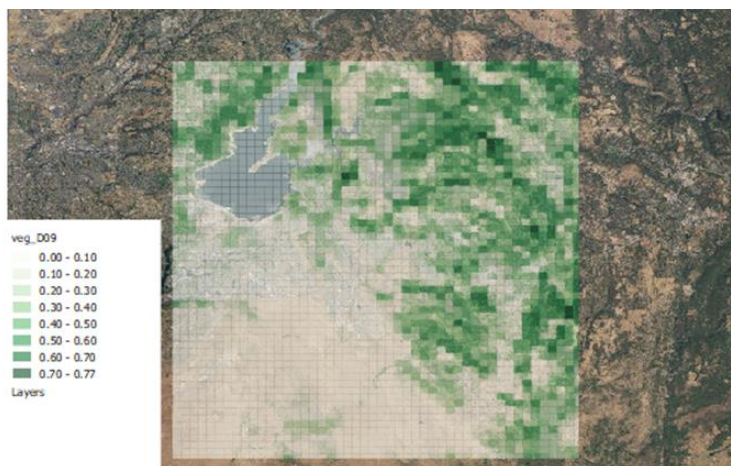
NLCD 2011-based calculations of canopy cover in D09 500 m domain

2-8.G
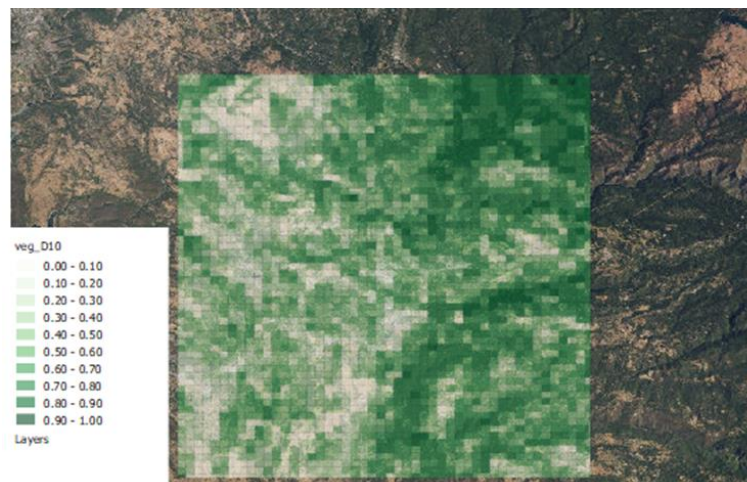
NLCD 2011-based calculations of canopy cover in D10 500 m domain

2-8.H

Figure 2-9: Distribution of computed canopy cover in 500-m domains D05 – D10 (in urban and non-urban cells) based on NLCD 2011 / USFS data. Superimposed boxes show medians and quartiles.
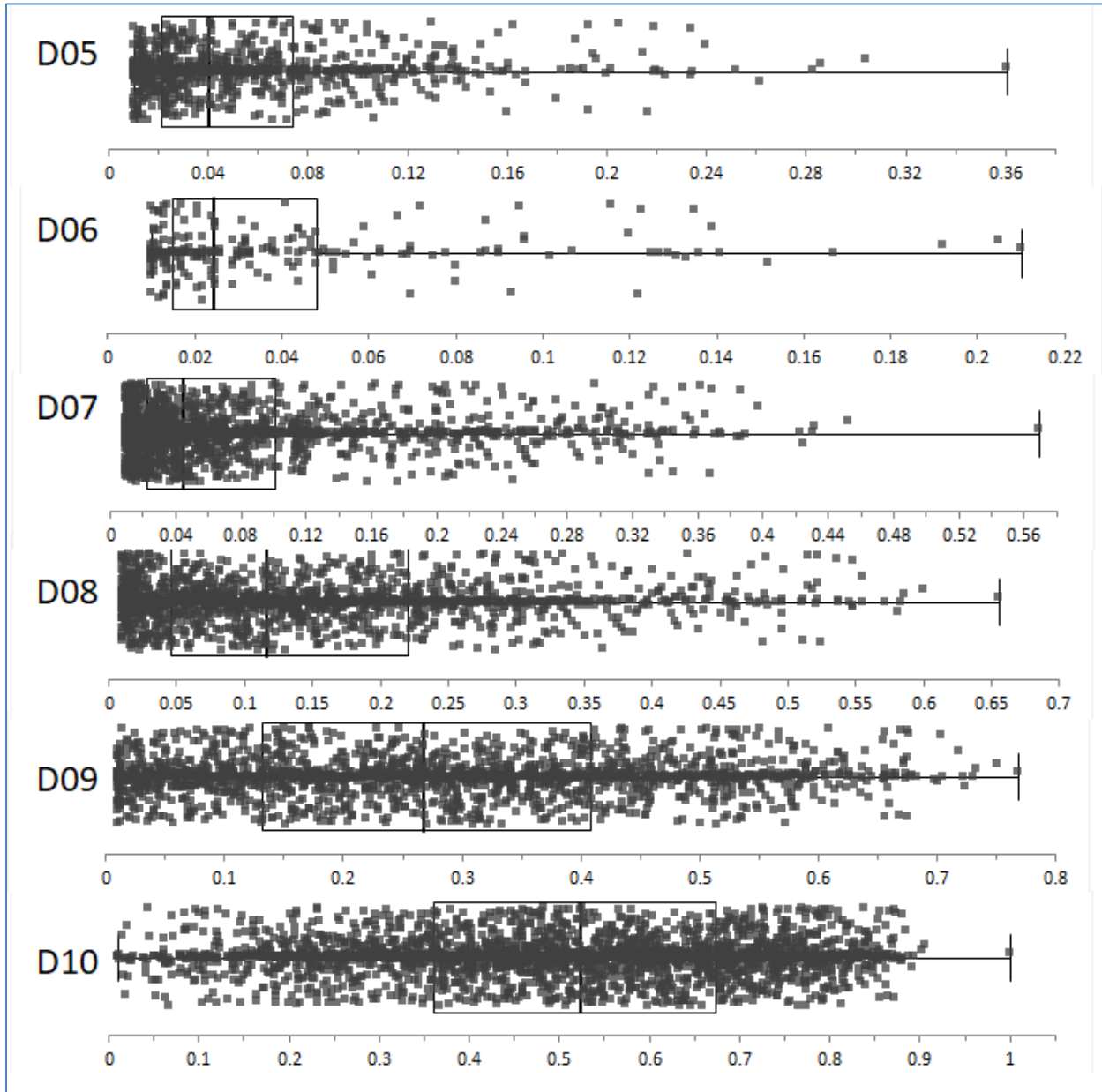
Canopy cover in urban and non-urban cells (greater than 0.01)

Compared to the urban-only canopy cover (from the CAL FIRE dataset, see Section 2.3.1), the inclusion of non-urban canopy cover in the analysis (Figure 2-9 and Table 2-2) shows that non-urban areas have larger canopy cover than their corresponding urban areas, in general, although a smaller canopy is seen in some cases, e.g., in the Yuba City / Marysville and the Woodland regions where non-urban canopy cover is smaller than the urban one (compare Tables 2-2 and 2-1).

This could be one reason why the non-urban areas in these two domains (D05 and D06) warm up faster than their corresponding urban areas, in future climate, producing a smaller UHII in 2050 RCP 8.5 than in 2050 RCP 4.5, as discussed in Section 6.6.

Combining the information from both sources discussed above serves as basis for the cell-by-cell characterization of canopy cover, i.e., following the bottom-up approach that directly characterizes cover without using LULC information as proxy (Taha 2008a-c; Taha 2017). As will be seen later, in some cases, additional information on tree cover, e.g., for a specific street or project site, can also be gleaned from Google Earth Pro.

Table 2-2: Medians and ranges of canopy cover in urban and non-urban cells in 500-m domains D05 through D10 based on NLCD 2011 / 2016 (USFS datasets). The range, in this table, is not specified as difference between maximum and minimum values but, rather, the range of the bulk of the canopy cover values in the specified domains, as seen in Figure 2-9.

Domain (500-m grid)	Median of canopy cover	Range of canopy-cover bulk
D05	0.040	0.01 – 0.160
D06	0.025	0.01 – 0.070
D07	0.045	0.01 – 0.360
D08	0.120	0.01 – 0.525
D09	0.260	0.01 – 0.650
D10	0.525	0.01 – 0.900

2.3.3 Calculations of impervious cover

Impervious cover in the NLCD 2011 / 2016 dataset (MRLC 2011) consists of roofs and ground-based paved surfaces at a resolution of 30 m. This is an important parameter to characterize in this study as it can provide an assessment of technical potential for the deployment of high-albedo materials on roadways and buildings. It can also provide a basis for computing dynamics- and physics-related parameters input to the models indirectly, e.g., roughness length or drag coefficients, soil moisture, anthropogenic heat emissions (tailpipe exhaust), and heat capacity. Gridded impervious fraction was computed for each domain as shown in the following examples (Figure 2-10), as identified by the captions below each figure.

The impervious cover information is also merged with the vegetation cover data to develop cell-by-cell characterizations of mitigation potential, particularly in the areas designated of interest by the project TAC.

Figure 2-10 (A – F): Gridded impervious cover computed based on NLCD 2011 datasets.
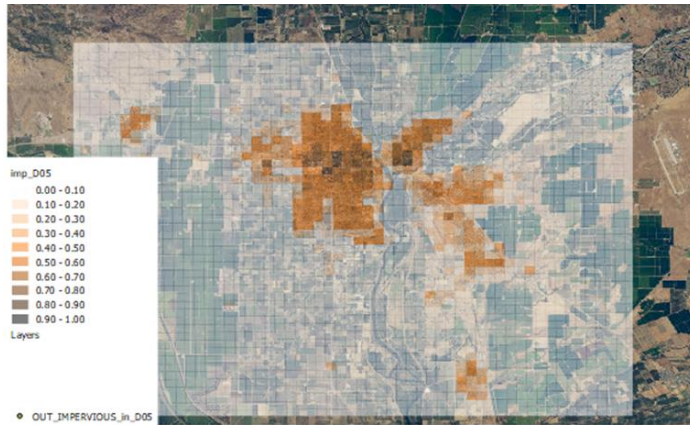
NLCD2011-based calculation of impervious cover: D05 500-m

2-10.A
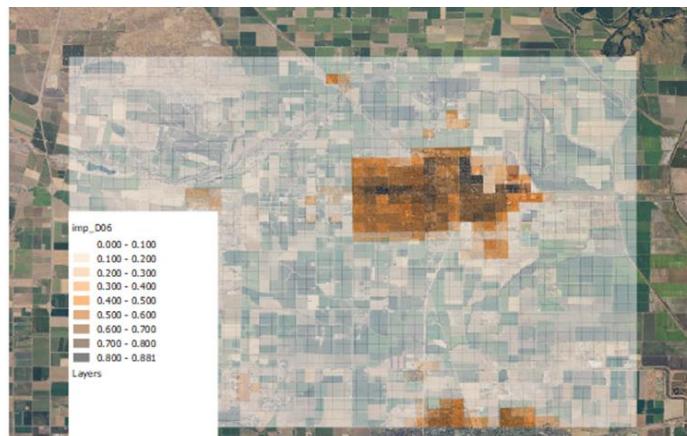
NLCD2011-based calculation of impervious cover: D06 500-m

2-10.B
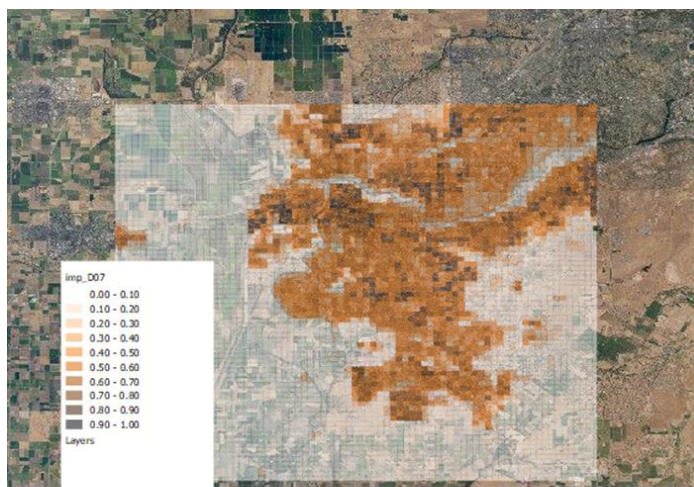
NLCD2011-based calculation of impervious cover: D07 500-m

2-10.C
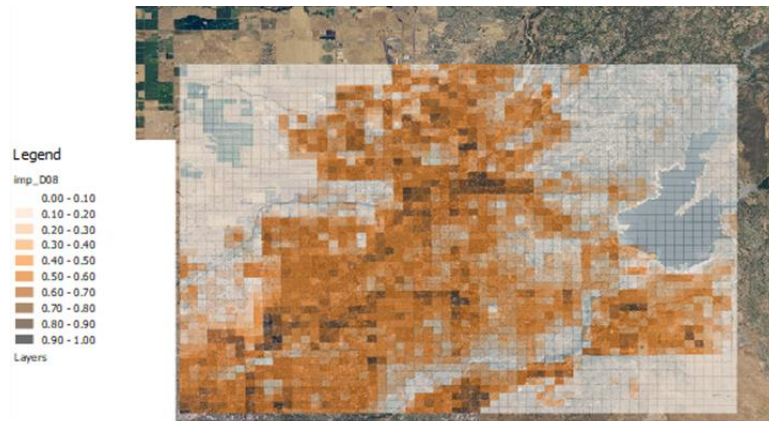
NLCD2011-based calculation of impervious cover: D08 500-m

2-10.D

NLCD2011-based calculation of impervious cover: D09 500-m

2-10.E
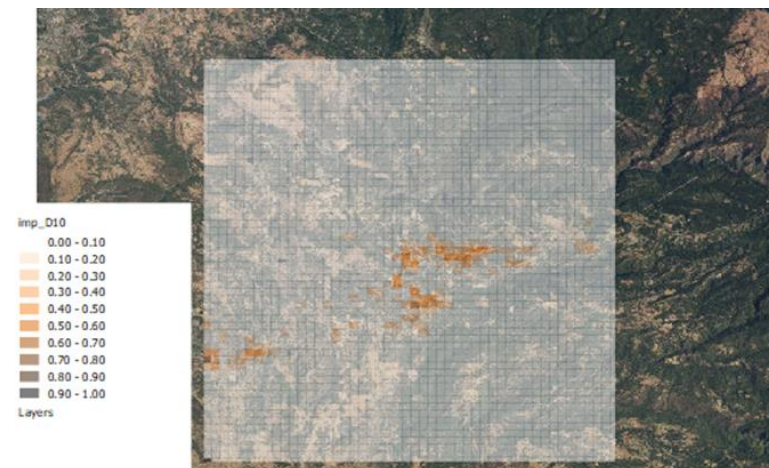
NLCD2011-based calculation of impervious cover: D10 500-m

2-10.F

To characterize the distribution of impervious cover in the 500-m domains, values greater than 1% in each cell were examined. This analysis is visualized in Figure 2-11 and Table 2-3. It can be seen that except for domains D07 and D08 (the main urban Sacramento area), all other urban areas in the 6-counties Capital region have impervious cover below 28% (medians and inter-quartile ranges are indicated with superimposed boxes). In domains D07 and D08, the bulk of impervious cover is generally up to about 50%. Also, as a general estimate, roughly half of impervious cover is made up of roofs and the other half of pavements and roadways (Akbari et al. 1999; Rose et al. 2003). Cleary at any specific location it may be different but as an average over the domains, this is a sufficiently accurate characterization.

Figure 2-11: Distribution of impervious cover in 500-m domains D05 – D10 (in urban and non-urban cells) computed based on NLCD 2011 / 2016 data. Superimposed boxes show medians and quartiles.
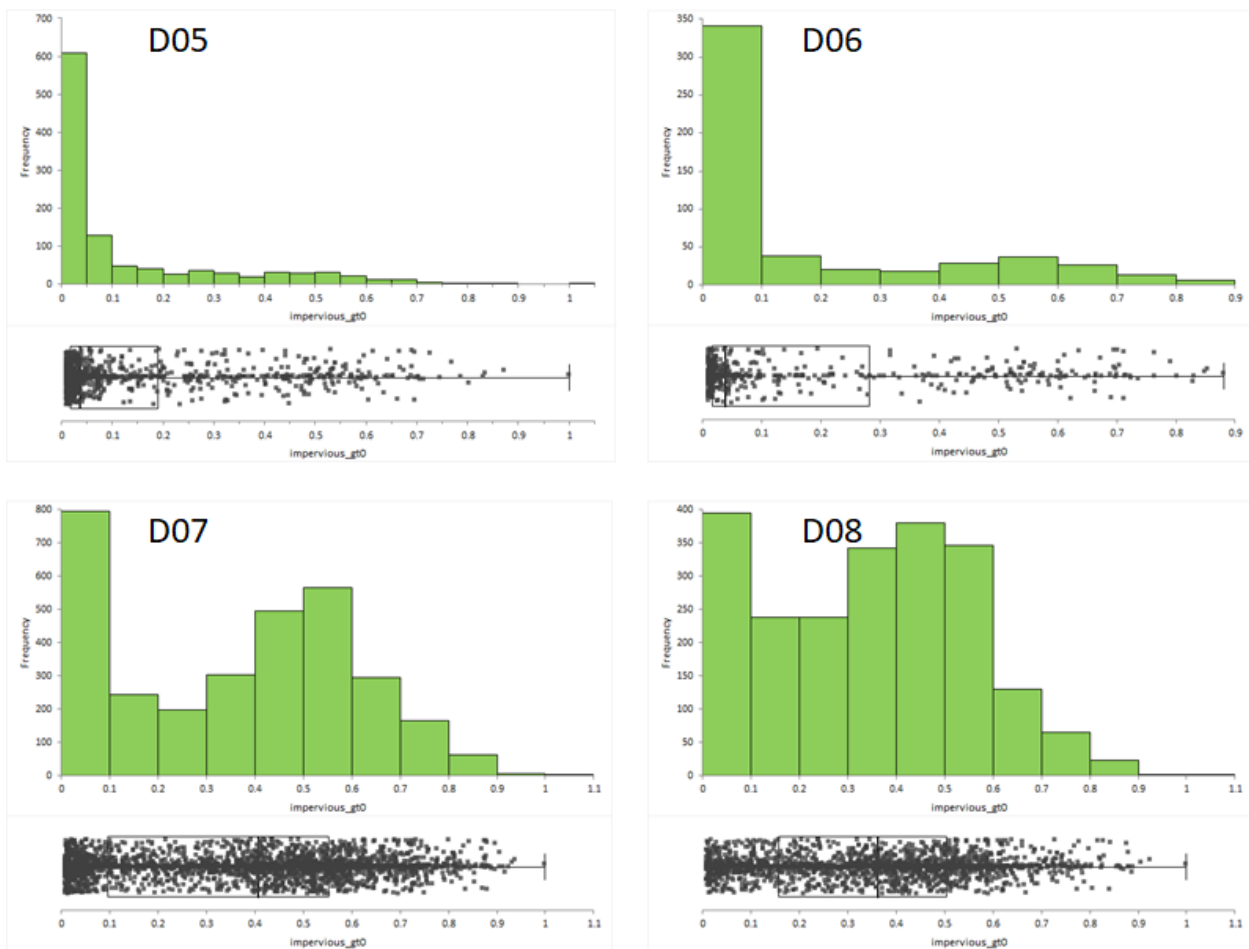
Figure 2-11, continued.
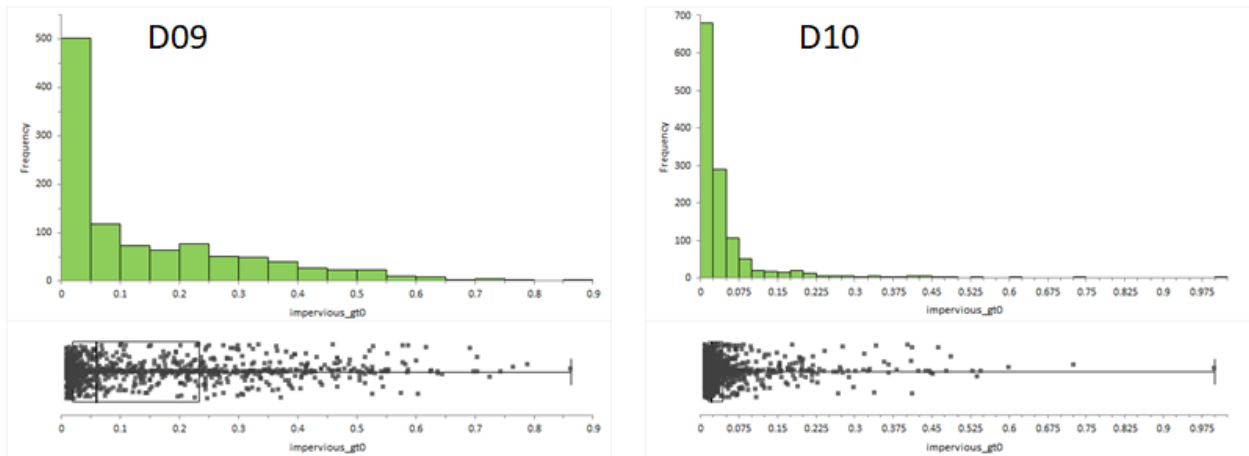
Table 2-3: Median, bulk ranges, and maxima of impervious cover in urban and non-urban cells in 500-m domains D05 through D10 based on NLCD 2011 datasets. The range in this table is not specified as difference between maximum and minimum values but, rather, the range of the bulk of the canopy cover values in the specified domains, as seen in Figure 2-11.

Domain (500-m grid)	Median of impervious cover	Range of impervious-cover bulk	Bulk maximum
D05	0.037	0.01 – 0.19	0.7
D06	0.040	0.01 – 0.28	0.8
D07	0.400	0.01 – 0.55	0.9
D08	0.360	0.01 – 0.51	0.8
D09	0.060	0.01 – 0.23	0.5
D10	0.020	0.01 – 0.04	0.2

Figure 2-12 shows the main transportation routes and their densities in the 6-counties Capital region. It is clear that the density of roadways is proportional to the impervious cover computed above. The transportation routes are a major component of LULC characterization and input to the atmospheric / land-surface models and have a significant impact on surface and air temperatures. In many of the figures in the following sections, these major routes stand out with different values of thermo-physical properties relative to those of the background.

We will also see later when discussing modeling results that urban heat is proportional to impervious fraction as is heat emission from mobile sources. Conversely, the cooling from increased albedo (e.g., cool roofs and pavements) also is proportional to impervious cover.

Figure 2-12: Main transportation routes in the study domain (data source: SACOG).

Black lines: Major highways
Purple lines: Major roads
Red lines: Light rail
Green circles: Amtrak stations
Black dots :   Bus stops
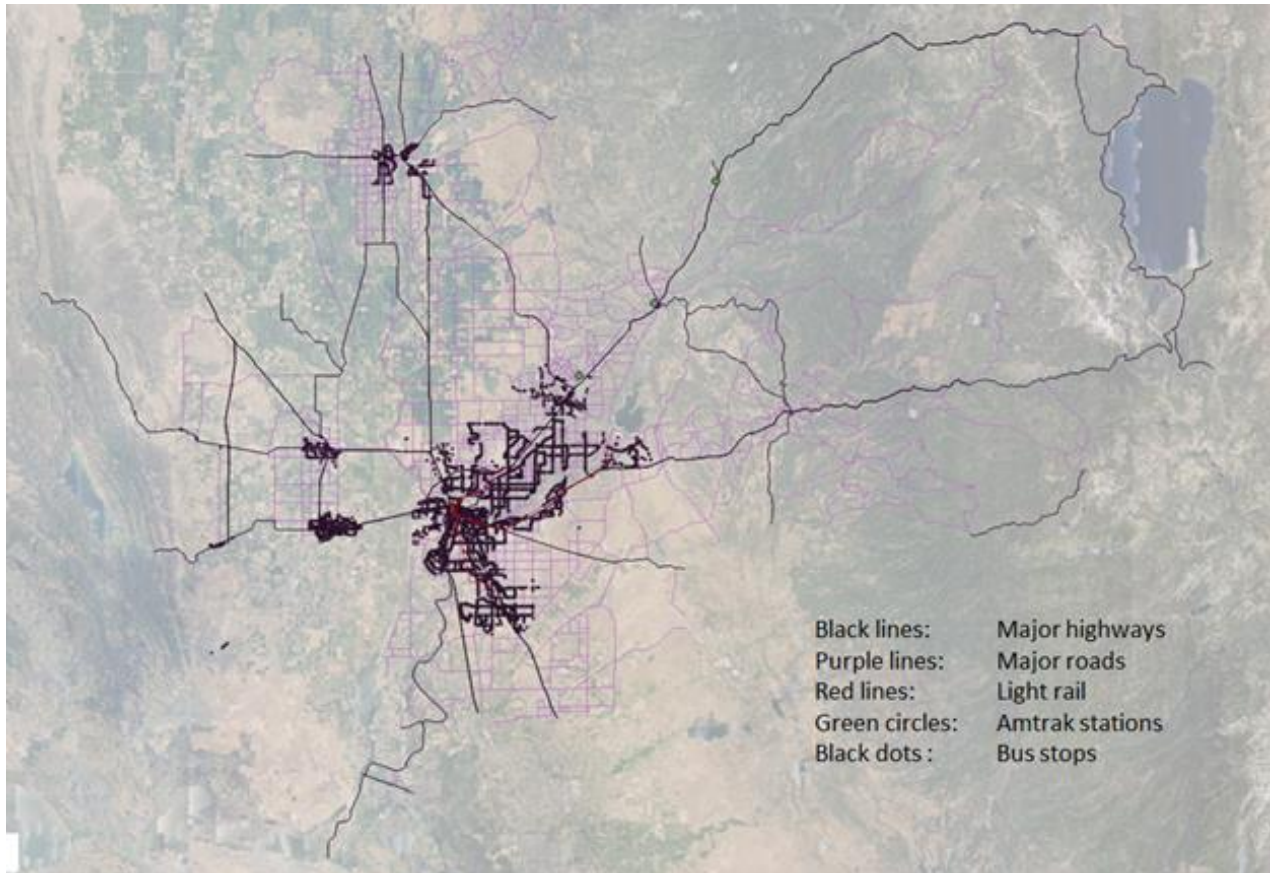
2.3.4 Calculations of thermo-physical parameters

Various thermo-physical parameters, depending on modeling scheme or parameterizations, are required to characterize the surface in the atmospheric models. In the 2-km domain, where the Altostratus AREAMOD approach was applied (Taha 2005, 2007, 2017), most of the needed parameters are standard, meaning similar to those used in standard WRF model, except that their derivation, pre-processing, and ingestion in the various model components are done differently from the standard WRF. In the AREAMOD approach, site-specific bottom-up characterization of model grid cells is carried out individually using any and all information that is available for each cell. At the 500-m level, on the other hand, additional parameters are needed beyond these standard variables, as discussed elsewhere in this report (i.e., in developing input to the urban WRF and the Altostratus-modified version of the urban canopy model, per Taha 2008a-c, 2017, 2019).

In this section, the calculations of some of the standard parameters are presented. Since these multi-parameter calculations are repeated for each of domains D04 to D10, figures resulting from this exercise will occupy considerable space. Thus, only the calculations for D04 (2 km) and D07 (500

m) are shown here as examples. Maps of variables and parameters for the other domains are included in Appendix A-1. Of these parameters, the most relevant to heat mitigation measures at the regional, 2-km level, are (1) urban fraction, (2) surface albedo, (3) vegetation cover / soil moisture, (4) roughness length, and (5) shade factor. These are relevant because the mitigation measures of interest usually involve perturbing one or more of these properties.

In this study, the parameters were computed based on different sources of information and spatial resolutions (listed above in Section 2.3) then scaled up to 500 m or 2 km depending on the domain. The actual process of deriving these parameters is quite lengthy and is discussed in Taha (2008a-c). Examples from this analysis are shown in Figure 2-13. Figures A – E are for domain D04 and Figures F – J are for domain D07 (as indicated above, other domains are presented in Appendix A-1). In the 500-m domains, these properties are further weighted by the non-urban fraction in each grid cell and the urban-fraction properties are based on site-specific information.

Figure 2-13 (A – J): Examples of computed gridded parameters for domains D04 and D07

NLCD2011_GIRAS-based calculation of urbfrac (0 - 1) in D04 (2 km domain)

A

Figure 2-13, continued.

NLCD2011_GIRAS-based calculation of albedo in D04 (2 km domain)

B

NLCD2011_GIRAS-based calculation of soil moisture content in D04 (2 km domain)

C

NLCD2011_GIRAS-based calculation of roughness length (m) in D04 (2 km domain)

D

Figure 2-13, continued.
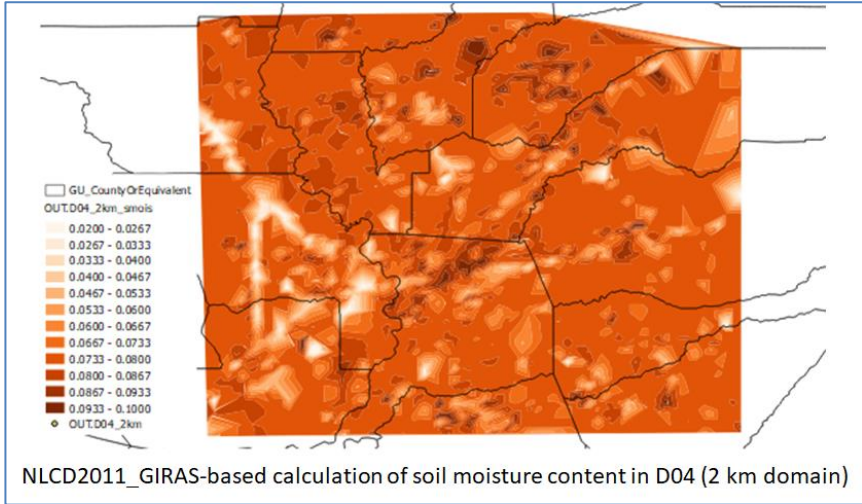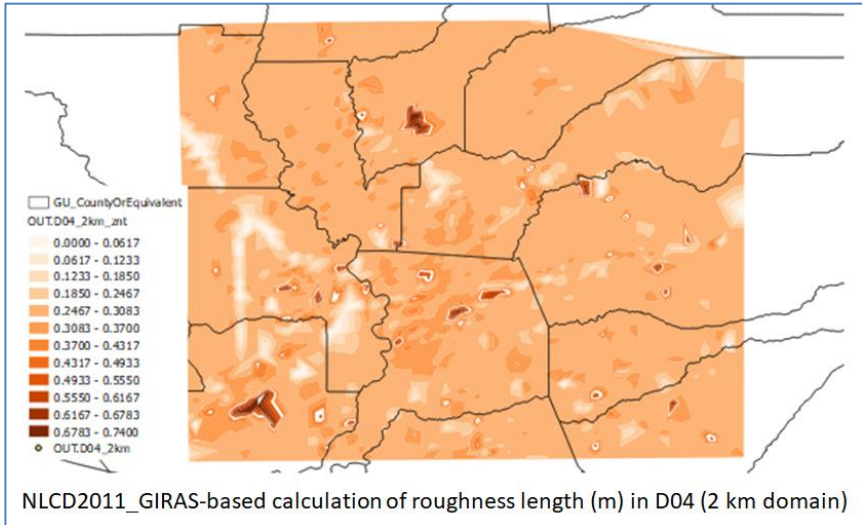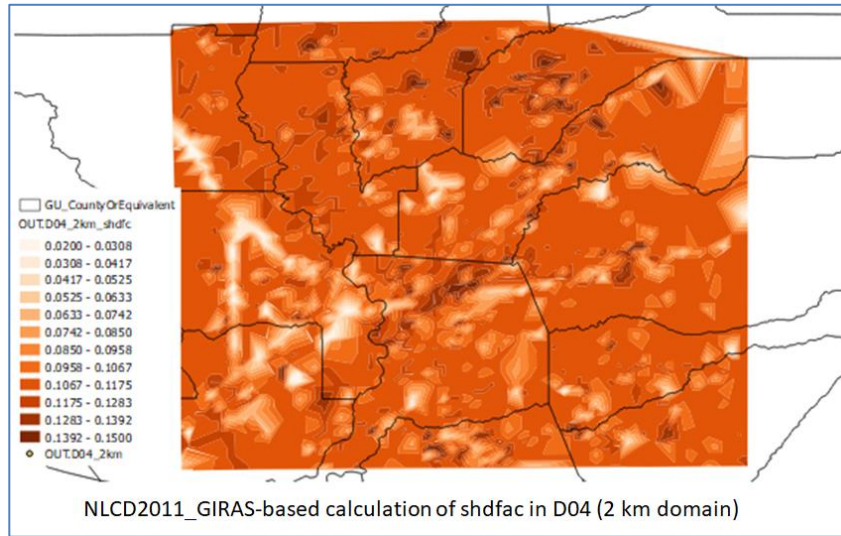
NLCD2011_GIRAS-based calculation of shdfac in D04 (2 km domain) **E**

NLCD2011_GIRAS-based calculation of urbfrac (0 - 1) in D07 (500 m domain) **F**
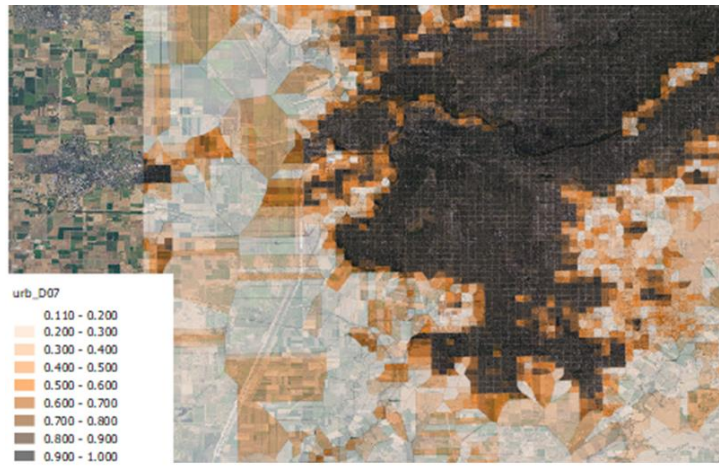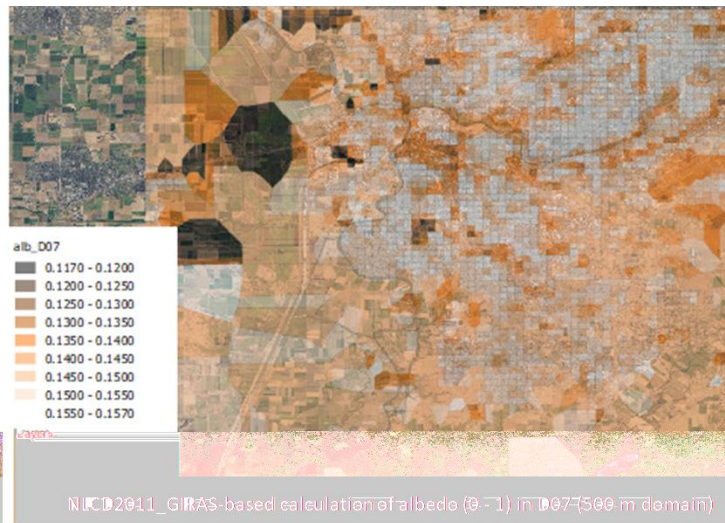
NLCD2011_GIRAS-based calculation of albedo (0 - 1) in D07 (500 m domain) **G**

Figure 2-13, continued.

NLCD2011_GIRAS-based calculation of soil moisture content in D07 (500 m domain)   **H**
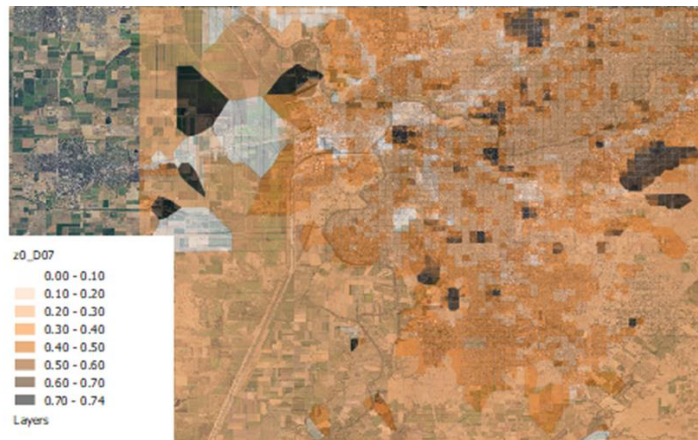
NLCD2011_GIRAS-based calculation of roughness length (m) in D07 (500 m domain)   **I**

NLCD2011_GIRAS-based calculation of shdfac in D07 (500 m domain)   **J**

2.4 DEVELOPMENT OF CROSSWALKS AND URBAN GEOMETRY PARAMETERS

Because the geographical extent (coverage) varies from one data type to another, and some datasets have large gaps or are sparse in coverage, a crosswalk among different datasets becomes necessary at some point to develop continuous physical characterizations of the surface. One particular such instance occurs in the derivation of urban geometry parameters (e.g., heights, frontal-, plan-, and top-area densities, sky view factor, and drag and roughness length parameters) from building footprint information. It is often the case that building footprint datasets are more limited in coverage than more general LULC data (see for example Figure 2-14) -- in such cases a crosswalk between building morphometric characteristics and LULC classes is necessary to extend the areal coverage of data with building information. It is acknowledged here that derivation of such parameters from crosswalks relies on certain assumptions being made and thus can lead to biases or inaccuracies. However, short of any other feasible approach to characterize large areas with gaps in data, this probably is the most optimal methodology.

As seen in Figure 2-14, for example, the publicly-available building footprint information for Sacramento County covers only a part of the region. Thus, a correlation with LULC is developed, in this case, for gridded building plan (λ_p) and frontal (λ_f) area densities to compute the roughness length parameter (z0) per MacDonald et al. (1998) and Grimmond and Oke (1999), as well as other variables.

Figure 2-14: Spatial coverage of available building-footprint datasets for Sacramento County.

Assignment of centroids to joined LULC and buildings footprints datasets
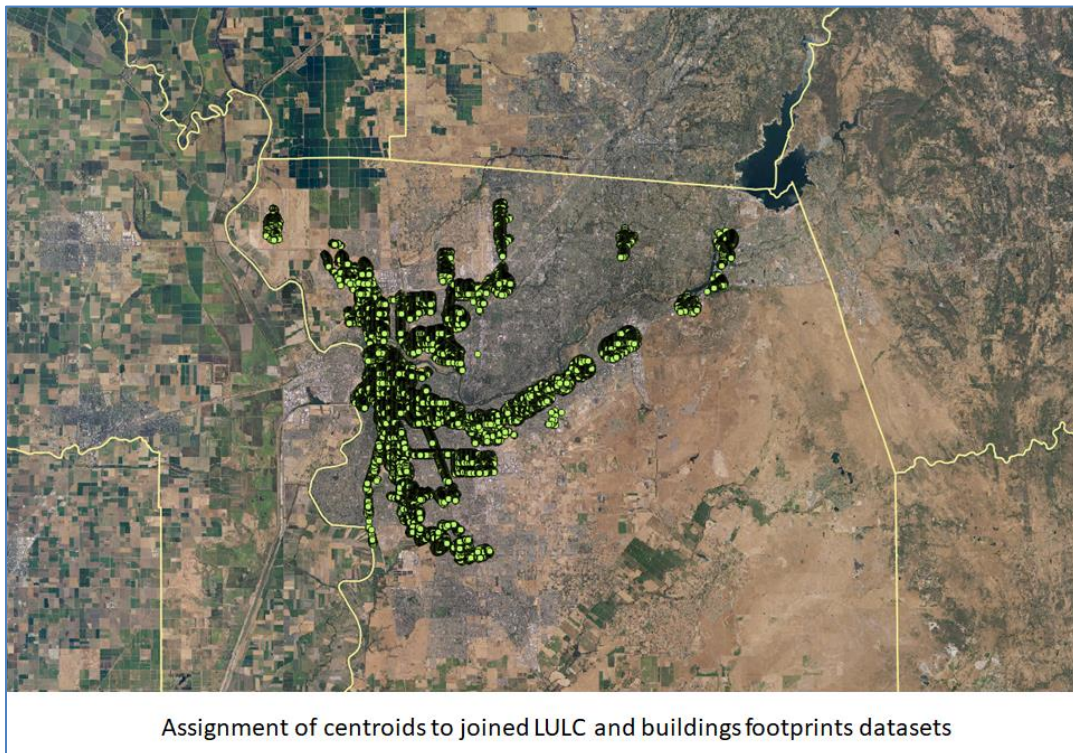
Figures 2-15 and 2-16 (A – D) show samples from this analysis. Figure 2-15 is an example from building footprint and geometry characterizations for the downtown Sacramento area. This figure is a blow-up from Figure 2-14, centered over downtown Sacramento, showing building outlines and footprints that are used in developing the gridded 3-dimensional properties input to the urban atmospheric model (Taha 2008a-c, 2017, 2018). Building heights, spacings, street orientations, street widths, and floor-plan areas are used in combination with other information to derive urban canyon properties and various geometrical parameters input to the meteorological model.

In each pair of graphs in Figure 2-16, the top two show the distributions of λp (vertical axis) for various LULC classes (on horizontal axis). In the bottom graphs of each figure, the distribution of parameter λf is plotted on the vertical axis and the LULC classes on the horizontal. This analysis is done for a large number of LULC classes (thus a small sample is shown in Figure 2-16) and used to develop crosswalks. In Table 2-4, the LULC classes are identified and the corresponding computed parameter values are listed.

For the 500-m domains, as simulated with the Altostratus-updated urban model (modUCM, Taha 2017, 2018), additional geometrical parameters are needed beyond those for the standard WRF, including detailed 3-dimensional morphological characterizations, as discussed in the following sections. Parameters derived from building footprint datasets include building plan-, top-, and frontal-area densities, sky-view factor, building heights, canyon orientation and geometry, street width, roughness length, and technical potential for deployment of project-specific UHI mitigation measures in each community.

Figure 2-15: Building footprints: example detail from downtown Sacramento. Data source: County and City of Sacramento.

Figure 2-16 (A – D): Development of crosswalks between LULC and building footprint characteristics in Sacramento County: a sample from the analysis and derivation of λp and λf parameters (top and bottom graphs in each figure, respectively).

Partial sample from the analysis of Sac County building footprints and parcels/LULC datasets

A

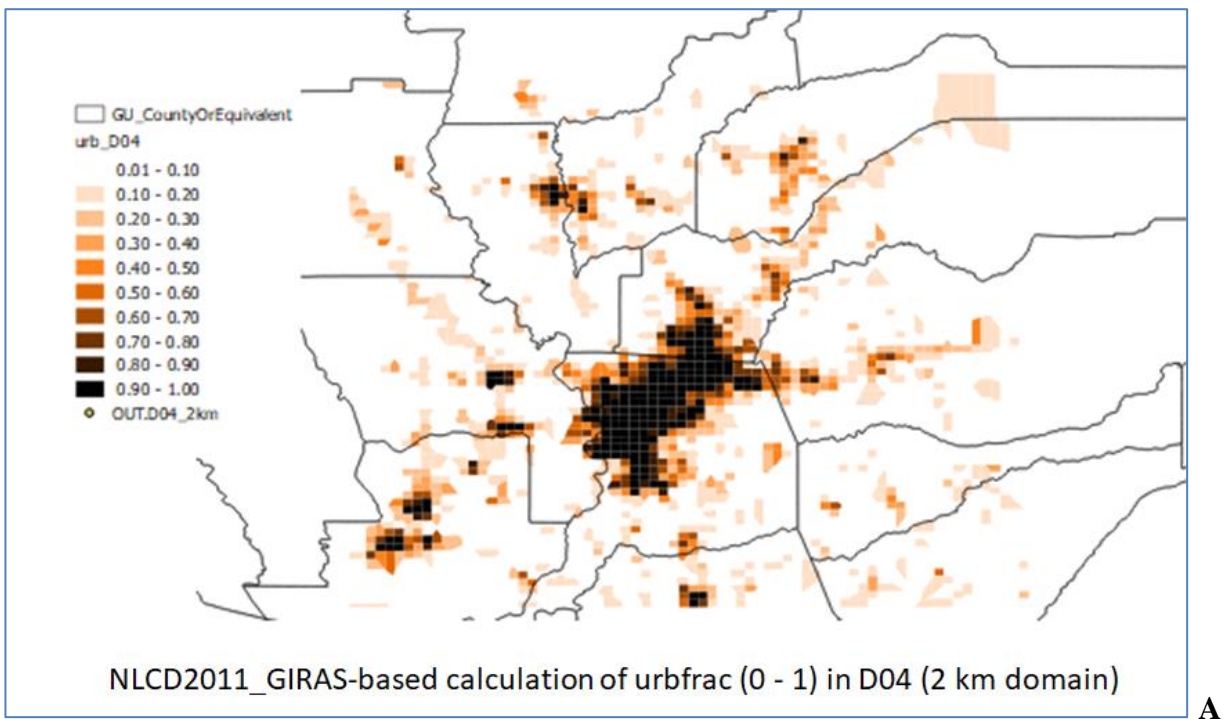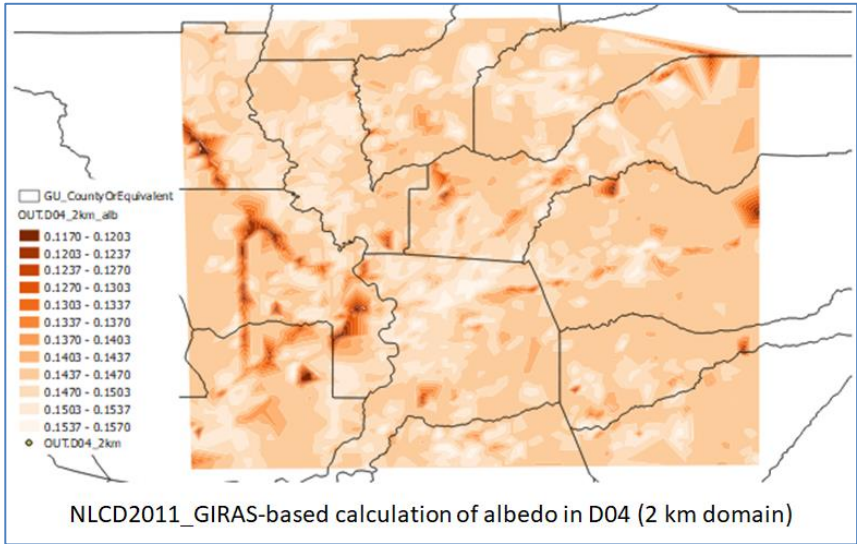Partial sample from the analysis of Sac County building footprints and parcels/LULC datasets
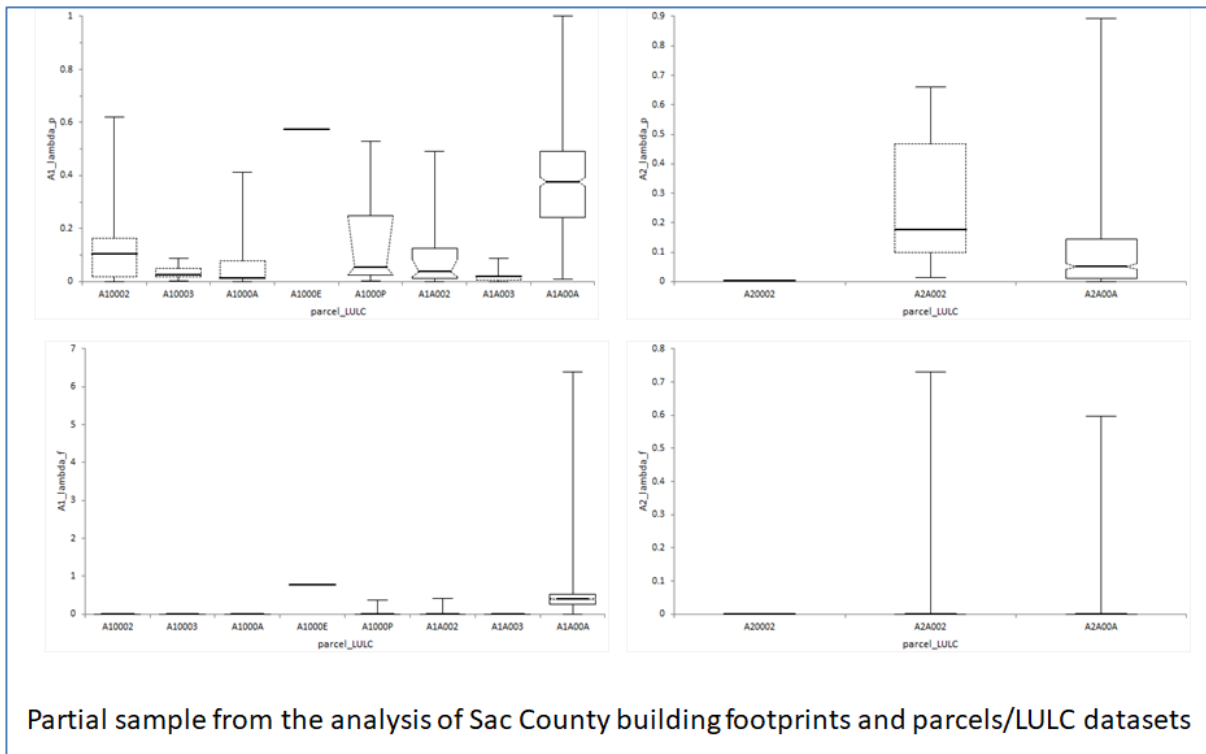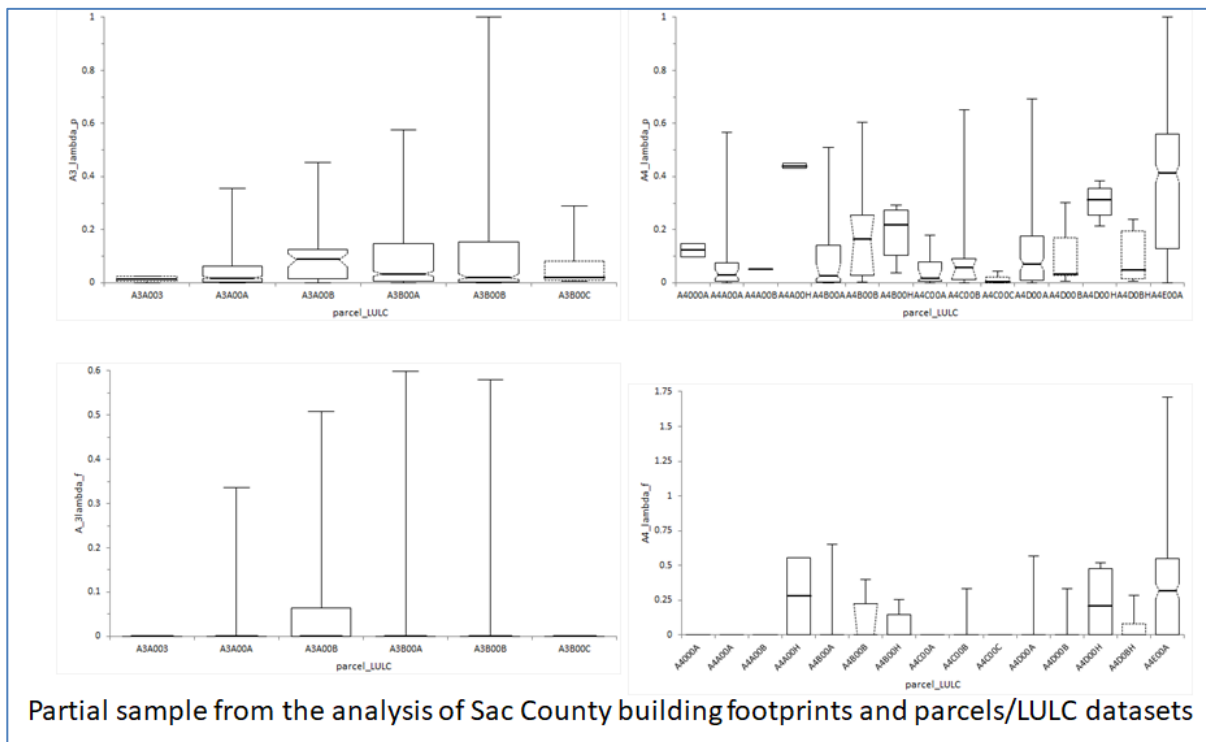
B

Figure 2-16, continued.

Partial sample from the analysis of Sac County building footprints and parcels/LULC datasets

C
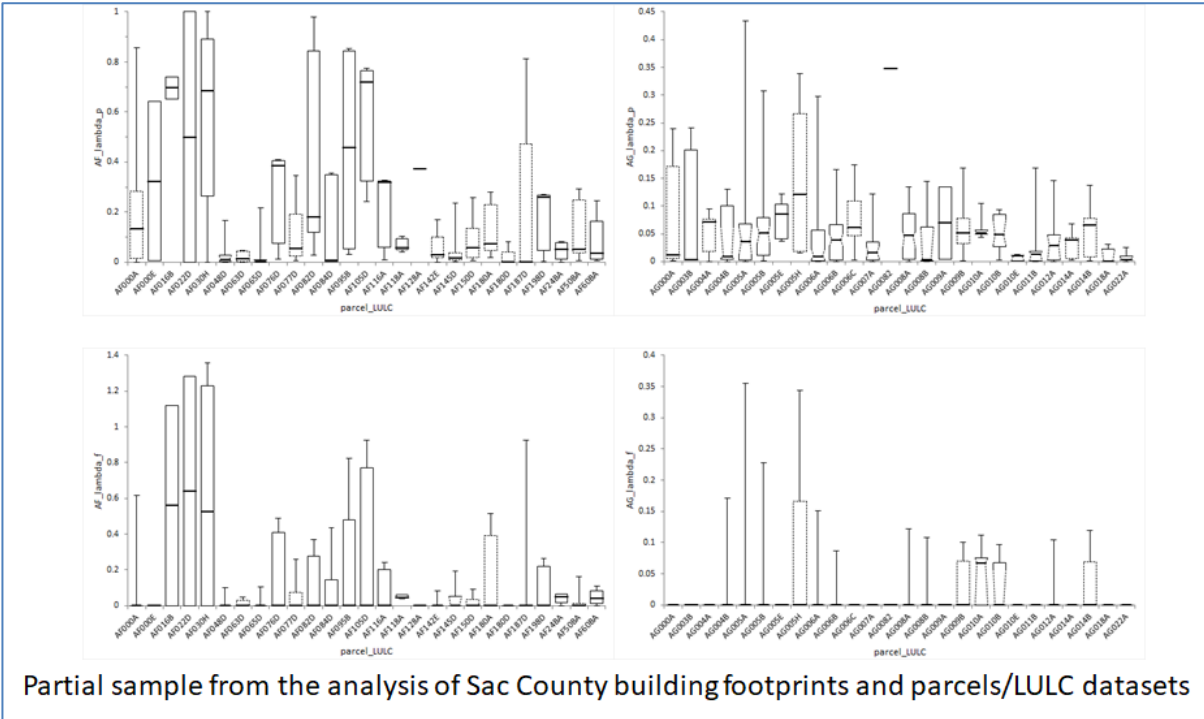
Partial sample from the analysis of Sac County building footprints and parcels/LULC datasets

D

Table 2-4: LULC classes in calculation of building geometrical parameters for Sacramento County.

		λp	λf		Zd/Zh	Z0/Zh	Zh	Z0
A1	single family residential	0.342	0.441		0.605	0.044	9.0	0.40
A2	two family residential	0.097	0.283		0.218	0.111	10.0	1.11
A3	three family residential	0.077	0.244		0.176	0.107	12.0	1.28
A4	four family residential	0.237	0.470		0.463	0.087	12.0	1.04
A5		0.229	0.438		0.451	0.085		
AE	low-rise apartments	0.161	0.362		0.340	0.101	16.0	1.62
AF	high-rise apartments	0.142	0.265		0.305	0.082	42.0	3.45
AG	residential court	0.046	0.094		0.110	0.038	0.5	0.02
AH	mobile home park	0.001	0.000		0.003	0.000	3.5	0.05
AJ	hotel	0.081	0.482		0.186	0.188	24.0	4.52
AK	boarding house	0.292	0.576		0.541	0.077	12.5	0.96
AL	rooming house	0.149	0.331		0.318	0.099	12.5	1.24
AN	motel	0.061	0.222		0.141	0.105	8.0	0.84
AQ	residential common area	0.062	0.156		0.145	0.069	0.5	0.03
AR	bed and breakfast	0.187	0.408		0.384	0.099	9.0	0.89
AT	mobile home	0.066	0.003		0.154	0.000	3.0	0.05

		λp	λf		Zd/Zh	Z0/Zh	Zh	Z0
B0	retail / commercial	0.011	0.004		0.028	0.000	5.0	0.10
BA	small retail	0.179	0.430		0.371	0.108	4.0	0.43
BB	store-office combo	0.199	0.451		0.405	0.101	16.0	1.62
BC	restaurant	0.131	0.448		0.286	0.141	6.0	0.85
BD	large retail	0.056	0.138		0.132	0.062	12.0	0.74
BE	shopping center	0.048	0.388		0.114	0.185	6.0	1.11
BF	vehicle-oriented	0.118	0.240		0.259	0.084	5.0	0.42
BG		0.002	0.001		0.006	0.000		
BI		0.026	0.004		0.062	0.000		
BQ		0.054	0.005		0.127	0.000		
CA	office (general)	0.194	0.318		0.397	0.074	14.0	1.04
CB	office / large, single tenant	0.097	1.143		0.217	0.297	12.0	3.56
CC	bank	0.106	0.261		0.236	0.098	8.0	0.78
CD	savings and loan	0.072	0.112		0.167	0.041	8.0	0.33
CE	broadcasting / radio / TV	0.081	0.241		0.184	0.103	20.0	2.06
CF	post office	0.045	0.069		0.107	0.022	7.0	0.16
CG	medical / dental	0.127	0.253		0.276	0.085	15.0	1.27
CH	veterinarian	0.035	0.183		0.083	0.098	6.0	0.59
CJ	office / residential conversion	0.207	0.378		0.417	0.083	12.0	0.99
CQ	office / common area	0.032	0.004		0.077	0.000	3.0	0.05

Table 2-4, continued.

		λp	λf		Zd/Zh	Z0/Zh	Zh	Z0
DA	acute care hospital	0.016	0.049		0.038	0.014	25.5	0.35
DB	skilled nursing facility	0.073	0.248		0.168	0.110	11.0	1.21
DC	health / residential care facility	0.110	0.318		0.245	0.116	5.0	0.58
DD	retirement home	0.134	0.675		0.291	0.188	12.5	2.36
DE	day nursery	0.112	0.297		0.249	0.108	4.0	0.43
DF	mortuary / cemetery	0.054	0.316		0.126	0.153	0.5	0.08
EE	church	0.084	0.216		0.191	0.090	25.0	2.25
EF	church / private school	0.050	0.131		0.117	0.059	15.5	0.92
EK	church / private social service agency	0.057	0.249		0.135	0.120	4.5	0.54
FA	golf course	0.006	0.001		0.015	0.000	0.2	0.02
FB		0.331	0.008		0.591	0.000		
FC		0.263	0.006		0.501	0.000		
FE	marina	0.006	0.004		0.014	0.000	0.2	0.00
FF	theater	0.120	0.363		0.263	0.125	36.0	4.51
FG	private club	0.125	0.272		0.273	0.093	4.0	0.37
FH	sports court / field / stadium	0.024	0.045		0.058	0.011	25.0	0.28
G0	industrial	0.013	0.004		0.031	0.000		
GA	light industrial	0.086	0.326		0.195	0.135	10.0	1.35
GB	heavy industrial	0.029	0.008		0.071	0.000	15.0	
GC	industrial warehouse	0.124	0.288		0.272	0.098	15.0	1.47
GD	industrial / building materials	0.054	0.179		0.127	0.086	10.0	0.86
GE	industrial / aerospace	0.019	0.006		0.047	0.000	25.0	
GF	industrial / truck or transit terminal	0.032	0.194		0.078	0.105	8.0	0.84
GG	industrial / food processing	0.085	0.239		0.194	0.100	8.0	0.80
GI	industrial	0.002	0.001		0.004	0.000	5.0	
GJ	industrial	0.012	0.002		0.030	0.000	5.0	
GK	industrial	0.021	0.006		0.052	0.000	5.0	
GL	industrial / mini storage	0.044	0.089		0.104	0.035	3.0	0.11
GM	industrial / multi tenant	0.094	0.005		0.213	0.000	9.0	
GQ		0.052	0.002		0.123	0.000		

		λp	λf		Zd/Zh	Z0/Zh	Zh	Z0
IA	vacant / residential	0.086	0.528		0.197	0.197	2.0	0.39
IB	vacant / commercial / retail	0.116	0.380		0.255	0.133	2.0	0.27
IC	vacant / office	0.159	0.426		0.336	0.118	2.0	0.24
ID	vacant / care / health	0.011	0.008		0.026	0.000	2.0	0.00
IF	vacant / recreational	0.051	0.169		0.121	0.081	2.0	0.16
IG	vacant / industrial	0.041	0.190		0.097	0.099	2.0	0.20
IH	vacant / agricultural	0.010	0.004		0.025	0.000	2.0	0.00
MA		0.116	3.606		0.255	0.426		
MB		0.006	0.001		0.016	0.000		
MD		0.011	0.008		0.028	0.000		
ML		0.010	0.008		0.024	0.000		
MP		0.040	0.273		0.095	0.143		
MR		0.103	0.277		0.230	0.106		
MS		0.130	3.913		0.284	0.414		
MU		0.053	0.288		0.125	0.141		
MW		0.069	0.006		0.160	0.000		
WA	public/utilities federal	0.027	0.598		0.065	0.274	35.0	9.60
WB	public/utilities state	0.029	0.109		0.070	0.052	25.5	1.34
WC	public/utilities county	0.029	0.316		0.070	0.171	20.0	3.43
WD	public/utilities city	0.060	0.183		0.141	0.085	25.5	2.17
WF	public/utilities public school	0.011	0.096		0.027	0.048	15.0	0.73
WG	public/utilities special district	0.034	0.009		0.081	0.000	8.0	0.00
WH	public/utilities SBE property	0.026	0.260		0.064	0.146	8.0	1.17

3. OBSERVATIONAL WEATHER DATA

3.1 OBJECTIVES OF OBSERVATIONAL METEOROLOGICAL ANALYSIS

The main objectives of observational meteorological analysis were to (1) acquire weather data from a dense network of mesonet monitors in the 6-counties Capital region, (2) quality-check and recast the data, (3) use the observational data in initial characterization of microclimates and the temperature field in the region, (4) recast the data for use in 4-dimensional assimilation in the meteorological model (FDDA), and (5) prepare the observations for use in thorough statistical model performance evaluation (as discussed in Section 4).

Thus, data were acquired from various sources, as discussed next, and summer months (May through September) of years 2013 – 2016 were analyzed. The purpose was also to identify intra-urban variability in meteorological fields based on observations.

3.2 OBSERVATIONAL METEOROLOGICAL DATA

Several datasets were identified, evaluated for use in this study, and acquired as suitable. Datasets were examined at multiple spatial resolutions and geographical coverages including both point and gridded data (analysis). The following observational meteorological data were considered. Overlap exists, sometimes completely, among these datasets and, in such cases, only a subset was used in this study.

- MADIS (Meteorological Assimilation Data Input System; madis-data.ncep.noaa.gov): An extensive and comprehensive repository of hourly weather datasets maintained by the National Centers for Environmental Prediction (NOAA / NCEP). It consists of and synthesizes data from various providers and, as such, was used as the main source of observational data in this study.

- URBANET / National mesonet: An urban-monitors hourly dataset by the National Centers for Environmental Prediction that can be partially or fully accessed via MADIS (depending on a user's access privileges).

- National Weather Service / NOAA Cooperative Observer Program (COOP): A dataset of annual averages and daily maximum and minimum temperatures and precipitation (nws.noaa.gov/om/coop/).

- Daymet (daymet.ornl.gov and urs.earthdata.nasa.gov): Gridded datasets at 1-km resolution of parameters including daily maximum and minimum air temperature, humidity, and precipitation. The data is prepared and maintained by the Oak Ridge National Laboratory (ORNL).

- WeatherBug (weatherbug.com): A commercial dataset consisting overwhelmingly of citizen weather observing program (CWOP) monitors. While both coverage and the spatial resolution

of the monitoring network are relatively high, data quality is difficult to ascertain and/or check via post-processing.

- Weather Underground (wunderground.com): A commercial dataset covering swathes of urban areas at relatively higher coverages and resolutions in some parts but, as with the WeatherBug datasets, the quality is not consistently checked and most monitors are privately owned, i.e., CWOP – thus not always subject to WMO-standard siting criteria, maintenance, and/or calibration.

- NOAA MesoWest (wrh.noaa.gov/mesowest): Map-based surface meteorology (point observations). Areas covered in California include the San Francisco Bay Area, Sacramento, San Diego, Los Angeles region, and the Fresno – Bakersfield areas. MesoWest also provides historical data (climate and daily weather information) as well as specific weather-station data.

- PRISM Climate Group (prism.oregonstate.edu) and PRISM UCAR (climatedataguide.ucar.edu): Gridded (analysis) historical meteorology datasets including daily temperature maxima, minima, and precipitation.

- NCAR dataset 472.0: Hourly historical point weather observations at airports or near airways. The dataset is developed and maintained by NCAR and made available for use as input to atmospheric models. This dataset also is useful in model performance evaluation.

- MesoWest mesonet (mesowest.utah.edu/): Mesonet data covering most of California and other western states. This dataset is also included in the MADIS system.

- NOAA daily datasets: National gridded datasets of daily temperature maxima and minima, and other daily variables, e.g., precipitation, based mainly on the NOAA COOP observations. Available for several decades to present with a spatial resolution of 6 km (data.ncdc.noaa.gov).

- California Irrigation Management Information System (CIMIS): A dataset developed mainly for agricultural applications with limited observations in urban areas.

- Network-specific California datasets: Data from various California agencies including the Air Resources Board and Air Quality Management Districts. e.g., SMAQMD, FRAQMD, YSAQMD, EDCAQMD, and PCAPCD.

- California Climate Data Archive, CALCLIM (calclim.dri.edu): A climate monitoring and data access website for the state of California, sponsored by the California Energy Commission as a joint effort with the Scripps Institute of Oceanography and the Western Regional Climate Center (WRCC). CALCLIM lists many of the same networks found in MADIS and other data sources listed above. Other useful climate datasets at WRCC can be accessed from wrcc.dri.edu/coop-inventory/ and wrcc.dri.edu/climate-maps.

The monitor locations (~400 stations) in the study domain, i.e., the 6-counties Capital region and surrounding areas, are shown in Figure 3-1 along with a listing of the main data providers. Figure 3-2 shows the locations of mesonet and metar monitors that are closest to AB617 communities in Sacramento County, as defined by the Sacramento Metropolitan Air Quality District (SMAQMD 2018).

Figure 3-1: Weather monitor locations in the study domain and MADIS data providers.
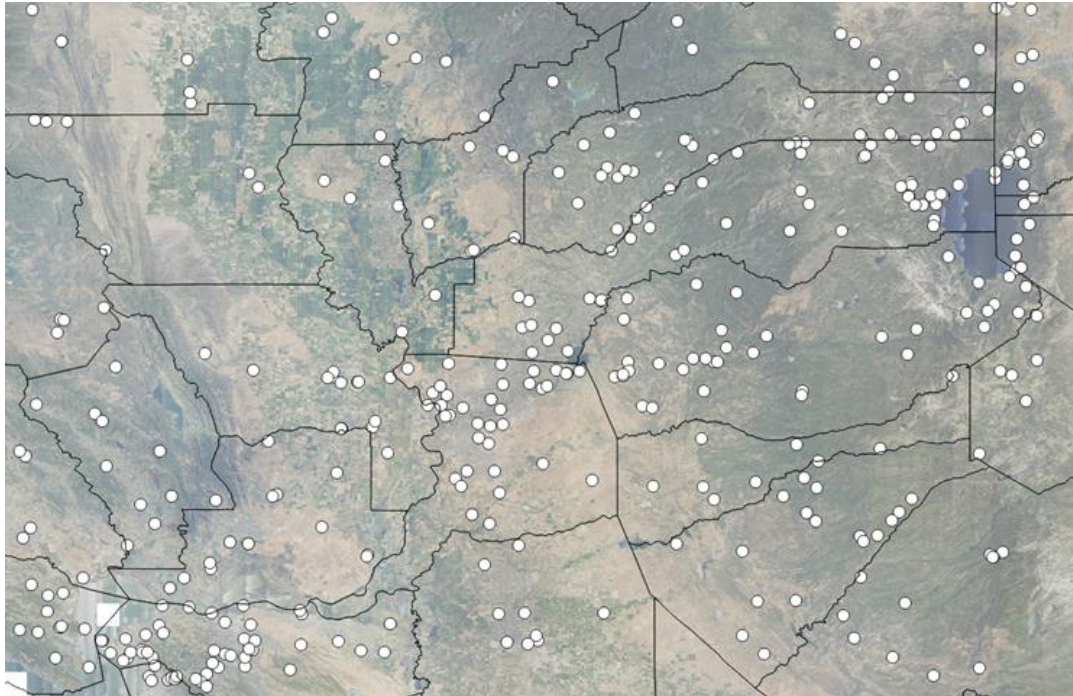
AWOS (Automated weather observing system)
APRSWXNET (Automatic position reporting system)
RAWS (Remote automated weather stations)
HADS (Hydro-meteorological automated data system)
CA-HYDRO (California hydro-meteorological networks)
MesoWest (Automated environmental monitoring)
AirNow (U.S. EPA monitoring networks)
ASOS (Automated surface observing systems (airways))

Data acquired from each of these monitors include (among an extensive number of variables) the following parameters: (1) air temperature, (2) dew point, (3) relative humidity, (4) wind speed, (5) wind direction, (6) wind gusts, (7) solar radiation, (8) atmospheric pressure, (9) precipitation, (10) geopotential height, (11) virtual temperature (12) visibility, (13) cloud base, and (14) soil moisture / temperature. In addition to use in analysis of observed meteorology, the acquired datasets were recast for use in model performance evaluation as will be discussed in Section 4. The data were also reformatted for input to meteorological model, i.e., in 4-dimensional data assimilation (FDDA) as needed.

The data were quality-checked to ensure suitability. MADIS allows for various levels of data screening based on: (1) static, station-specific verifications and (2) spatial analysis of observations at the target monitor relative to nearest-neighbor stations (analysis) which, in this case, generally includes some 4-6 stations surrounding the target (buddy check).

Altostratus Inc.

Figure 3-2: Locations of mesonet and metar monitors closest to AB617 communities in Sacramento County.
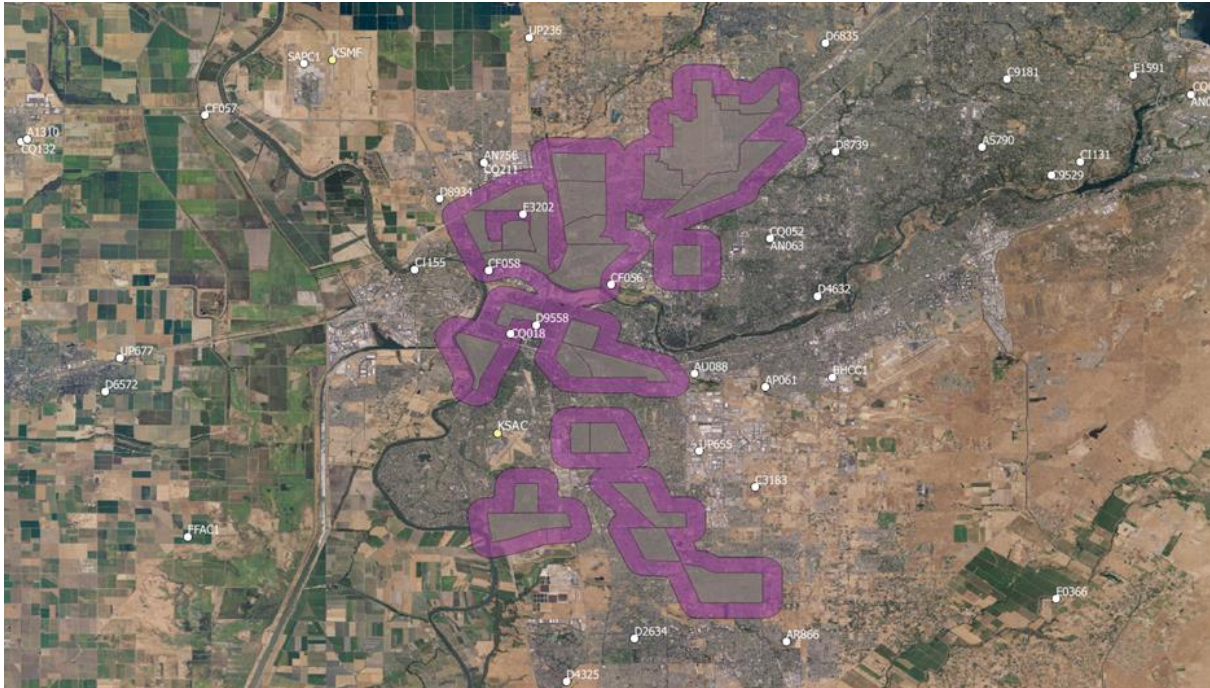
Figure 3-2 shows the following stations and proximities to AB617 communities or zones in the Sacramento area:

- o Station E3202 is in area "A";
- o Station CF056 is close to area "B";
- o Stations UP655 and C3183 are close to areas "C" and "E";
- o Station AU088 is close to area "F";
- o Station KSAC is close to area "H";
- o Stations CQ052 and AN063 are close to area "I"; and
- o Stations D9558 and CQ018 are in area "J".

These station locations will be referenced when evaluating the potential impacts of and benefits from various UHI-mitigation measures in subsequent discussions in this report.

3.3 CHARACTERIZATION OF THE OBSERVATIONAL TEMPERATURE FIELD

The analysis of observed meteorology was carried out with focus on the temperature field in the 6-counties Capital region. To keep the discussion relatively compact in this section, the temperature field is presented as cumulative metrics, such as degree-hours, and localized tendencies, i.e., warming and cooling at each station location. Since the data is quite extensive, only a few snapshot examples are presented here.

In Figure 3-3, the graphs captioned "YYYYMM_dhpd" show examples from the cumulative analysis of temperature. In each figure, YYYYMM denotes the year and month and "dhpd" indicates degree-hours per day (°C · hr day^{-1}) as averaged for the given month. Thus, for example, "201306_dhpd" indicates an all-hours averaged temperature computed as DH day^{-1} for the month of June in 2013 (this is a non-threshold DH day^{-1} metric). In these figures, the progression of color codes from light to dark indicates lower to higher temperatures or DH day^{-1}. The dhpd metric is computed at each mesonet station, for all hours, and averaged for the given month and year.

Similarly, the figures labeled "YYYYMM_1400PDT" and YYYYMM_0200PDT" show examples from the analysis of the temperature field near the time of the daily maximum and near the time of minimal nighttime activity, respectively. In each figure, "1400PDT" or "0200PDT" indicates that the figures show the average of all 1400 or 0200 PDT hours in the given month and year.

Although the daily maximum temperature can occur anytime between 1200 and 1800 PDT depending on weather conditions, here, 1400 PDT is selected as an indicator to daily peaks. Thus, in Figure 3-3, the average of all 1400 PDT hours is shown for each mesonet station for the given month and year (YYYYMM_1400PDT). Similarly, the daily minimum typically occurs just before sunrise but here 0200 PDT (YYYYMM_0200PDT) is examined since this is a time with lower nighttime activity. Of note, this is a characterization at coarse scales and is meant to provide a general picture of the temperature field in the 6-counties Capital region. The study focuses on much finer resolutions in the modeling and analysis tasks discussed later in this report.

Overall, there are significant variations from month to month and year to year, as well as between the DHPD, 1400 PDT, and 0200 PDT metrics. However, some general semi-persistent patterns in the temperature field can be observed. In Sacramento County, the eastern and northern parts are generally warmer than the central-western parts in DHPD and the 1400-PDT time frame. At 0200 PDT, on the other hand, the western and north-western parts of Sacramento County are generally warmer, i.e., areas closer to downtown and more urbanized parts of Sacramento are relatively warmer at night, which is a typical nighttime UHI situation. The boundary between Sacramento and Placer counties, i.e., North Highlands and areas to its northeast, such as Rocklin and Roseville, is significantly warmer than the rest of the county in most conditions (across months and years). The area immediately near downtown Sacramento is generally either average compared to or cooler than the rest of the county during the day (1400 PDT) but can be slightly warmer at night (0200 PDT). The northwestern part of Sacramento County also is generally warmer than the central or southern parts.

In El Dorado County, topography causes the western parts to be warmer than the others. However, the temperature contrast between the western and eastern parts of this county are larger during the day than at night. Within the western parts, the DHPD indicator and the temperature field during the day (1400 PDT) show that the areas of Placerville and El Dorado Hills are consistently warmer than their surroundings in that part of the county. Furthermore, Placerville can be warmer than El

Dorado Hills, even though it is located further east and surrounded by denser forests. In Placer County, as with El Dorado, topography causes the western parts to be warmer than the eastern higher-elevation areas. Within the western part, there are some variations in the temperature field as well. For example, the area near Lincoln is consistently warmer than other parts in western Placer County. The temperature field also suggests that Granite Bay is warmer than its surroundings and that Roseville is also warmer at times.

In Yuba County, an area (monitor) about 5 km south of Marysville (in Olivehurst) appears to be consistently warmer than other monitors in that region during the day. At night, it can be warmer during some periods and cooler during others. It is interesting to note that the atmospheric model also produces an isolated large UHII just to the south of that monitor location (it can be seen in most figures in Section 5).

In Sutter County, the monitor at Yuba City shows that it is consistently warmer than areas to the south. Compared to a monitor in Sutter (city), the data suggests that Yuba City is sometimes similar to and at other times cooler than Sutter. However, the small number of monitors in Yuba and Sutter counties may render these assessments biased. Finally, in Yolo County, the monitor at Woodland indicates that it is consistently warmer than or similar to Davis. However, both of Davis and Woodland are generally cooler than areas in the western parts of Yolo County.

All of these observations suggest significant urban-generated heat in the region. As will be discussed in the modeling sections, further below, the observations also support the modeling results and the model characterization of the temperature field in the Capital region.

Figure 3-3: Observational temperature field as DH day^{-1} (ºC · hr day^{-1}), 1400 PDT, or 0200 PDT averages (ºC) for the 6-counties Capital region. Figures are labeled YYYYMM_*.

201306_dhpd   201307_dhpd
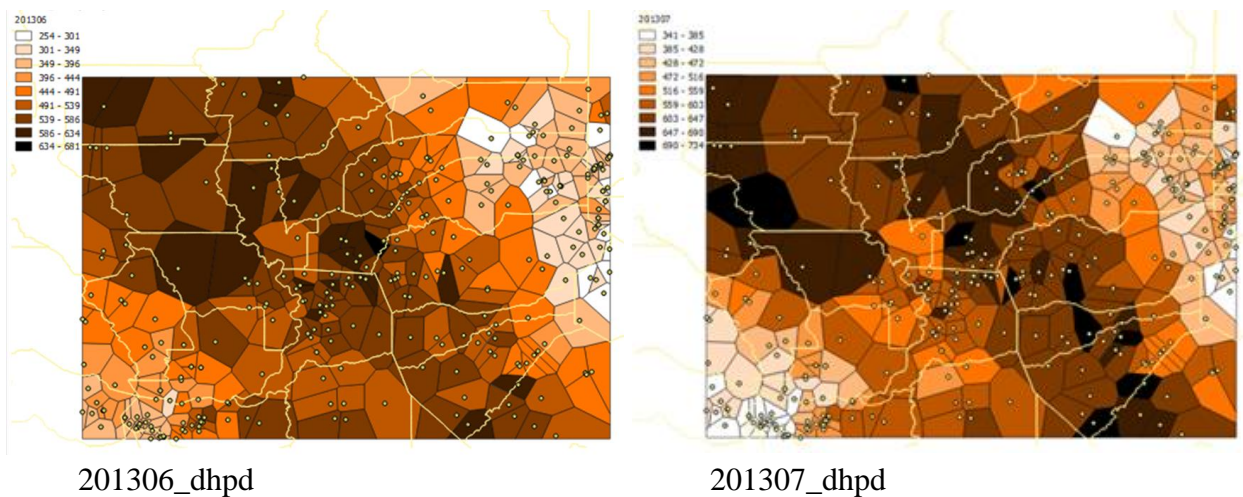
Figure 3-3. continued.
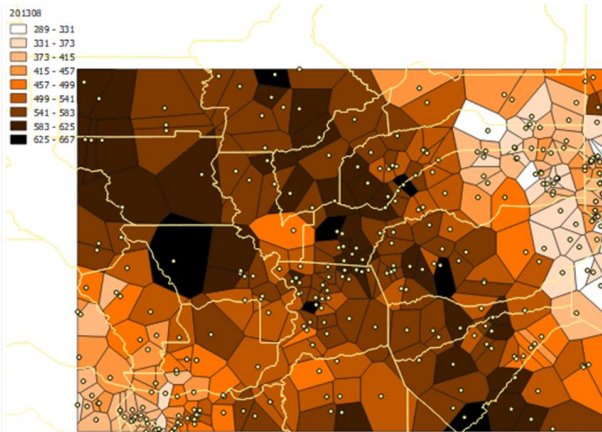
201308_dhpd
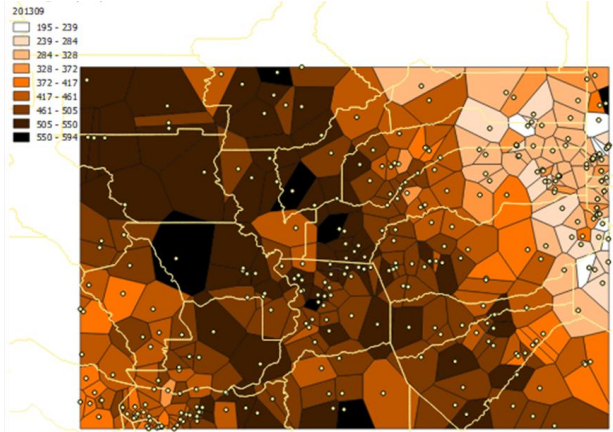
201309_dhpd
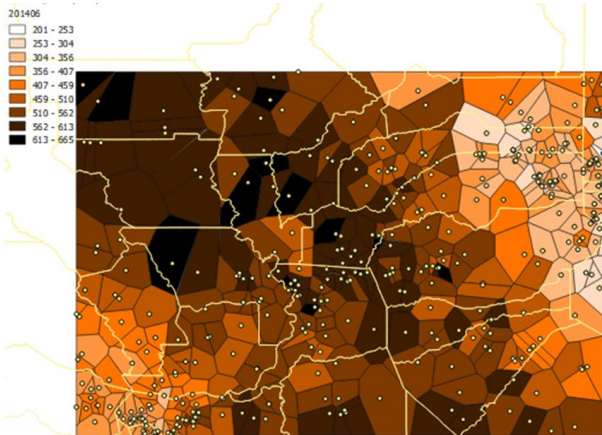
201406_dhpd
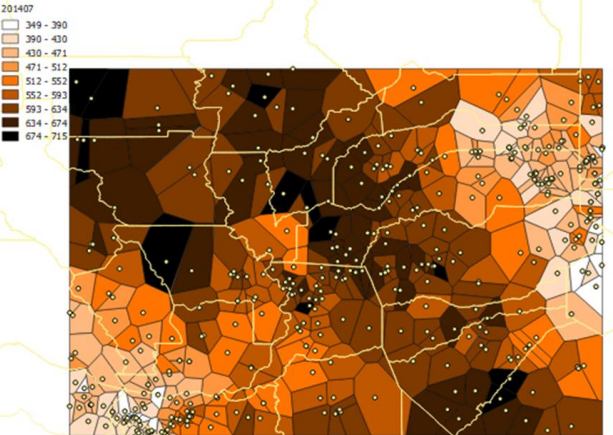
201407_dhpd
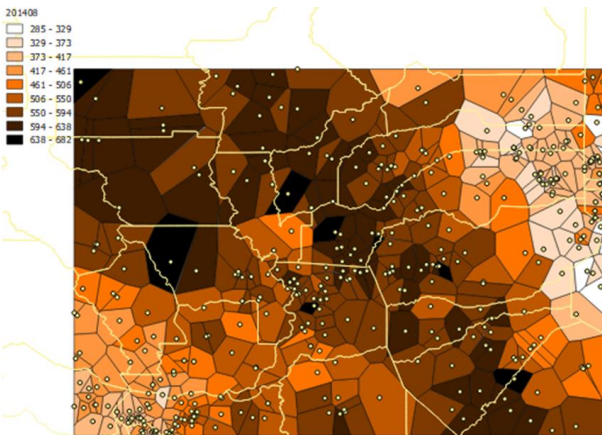
201408_dhpd
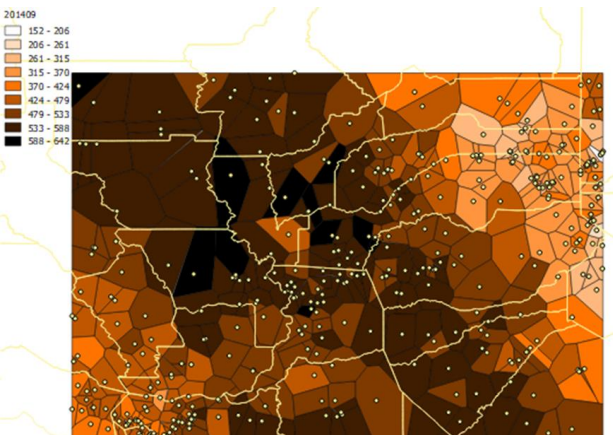
201409_dhpd

Figure 3-3. continued.
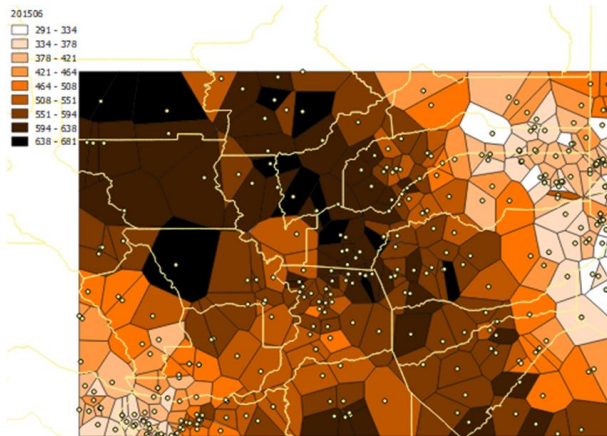
201506_dhpd
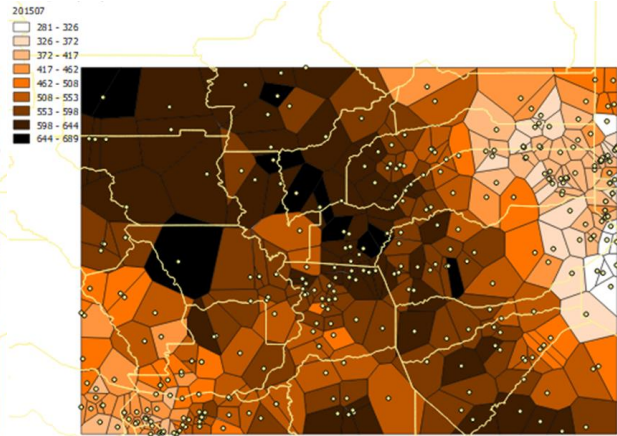
201507_dhpd
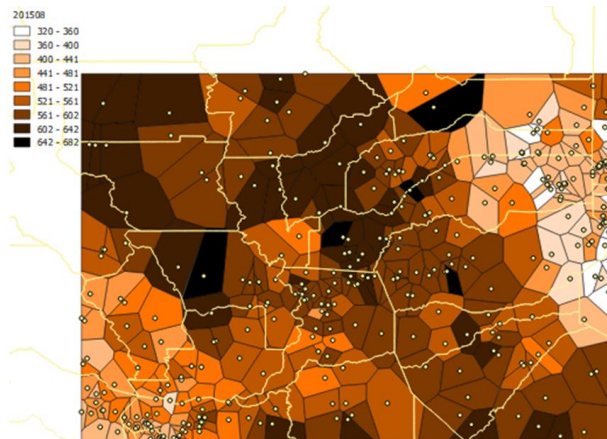
201508_dhpd
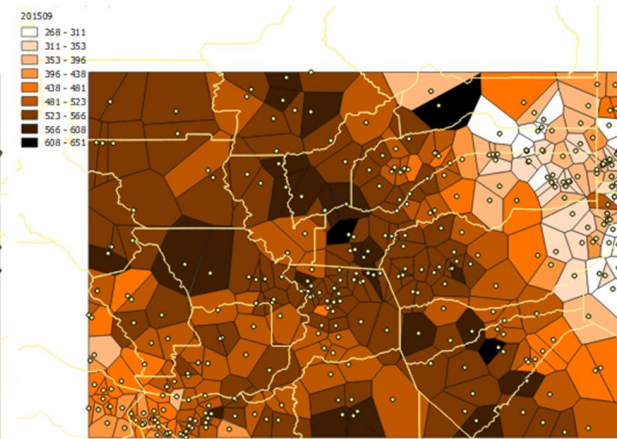
201509_dhpd

201606_dhpd

201607_dhpd

Altostratus Inc.

Capital Region Heat Pollution Reduction | 102
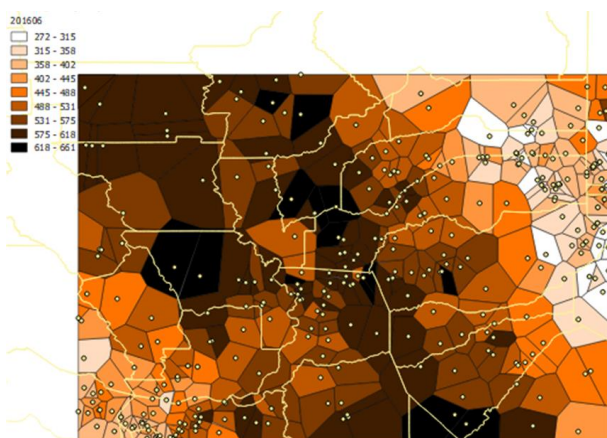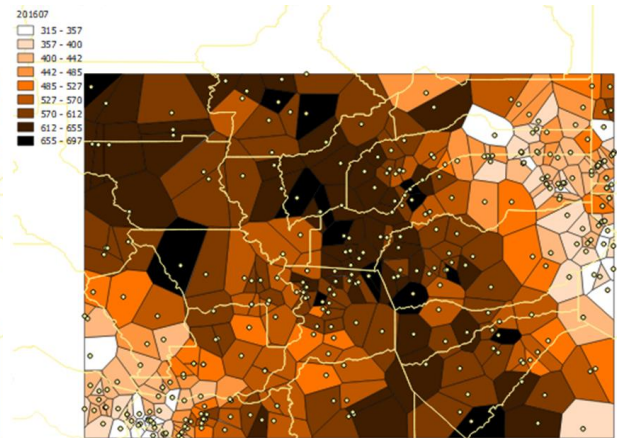
Figure 3-3. continued.
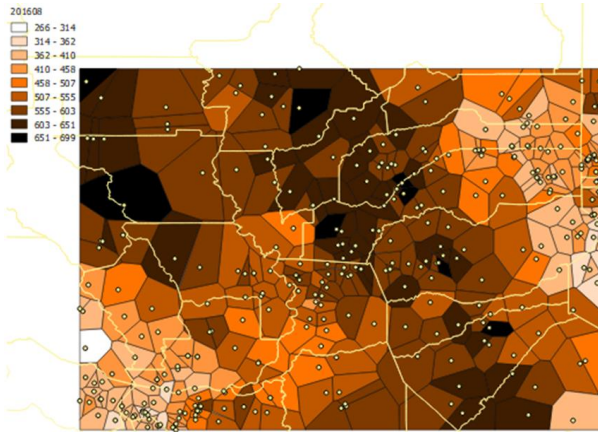
201608_dhpd
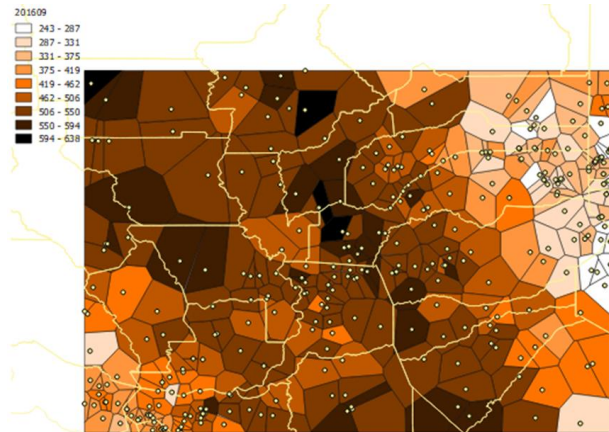
201609_dhpd
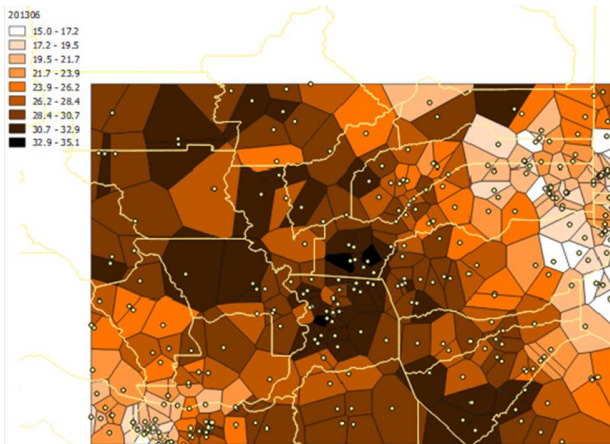
201306_1400PDT
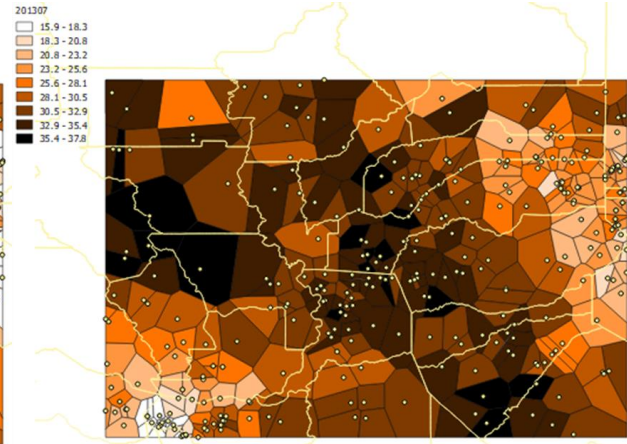
201307_1400PDT
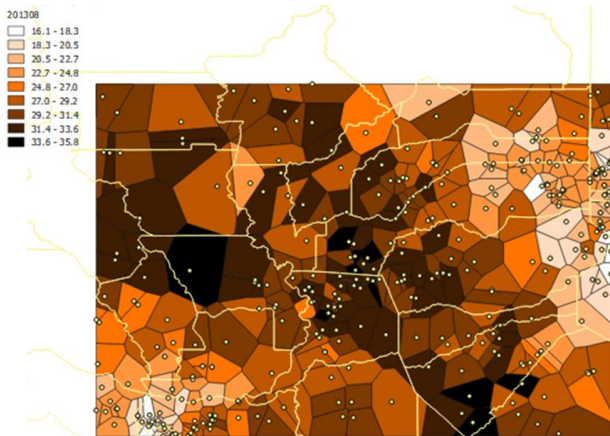
201308_1400PDT
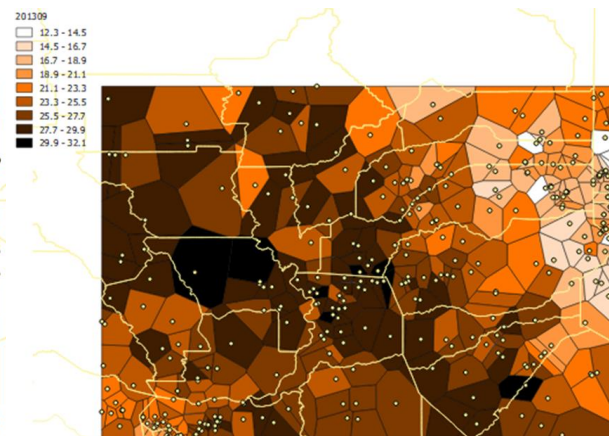
201309_1400PDT

Figure 3-3. continued.
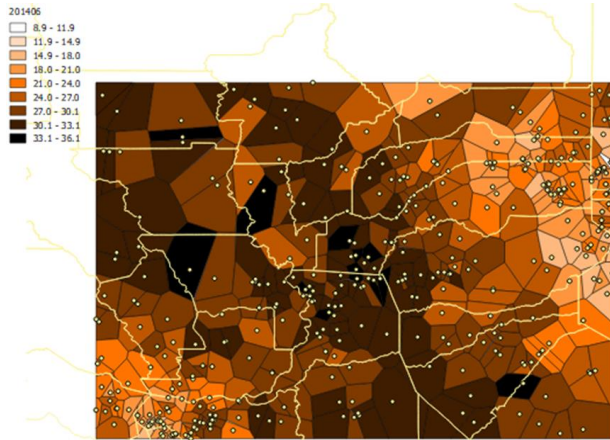
201406_1400PDT
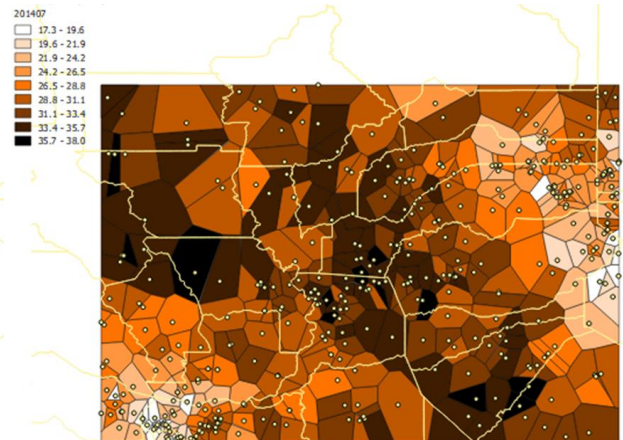
201407_1400PDT
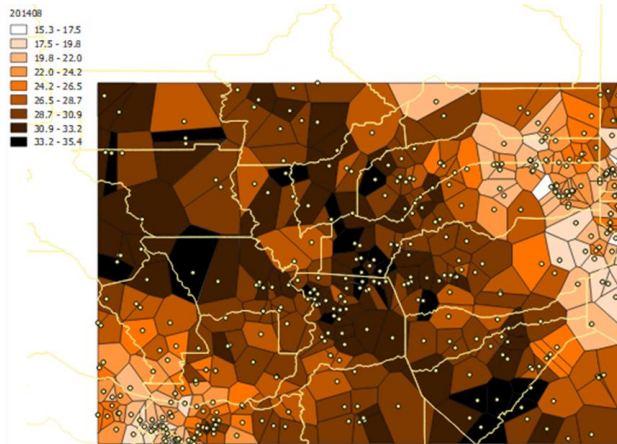
201408_1400PDT
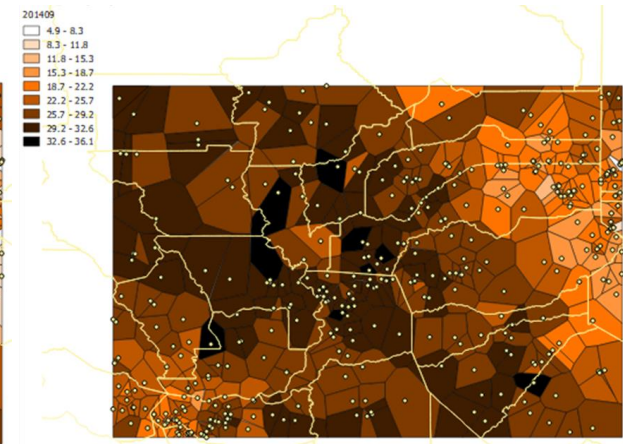
201409_1400PDT
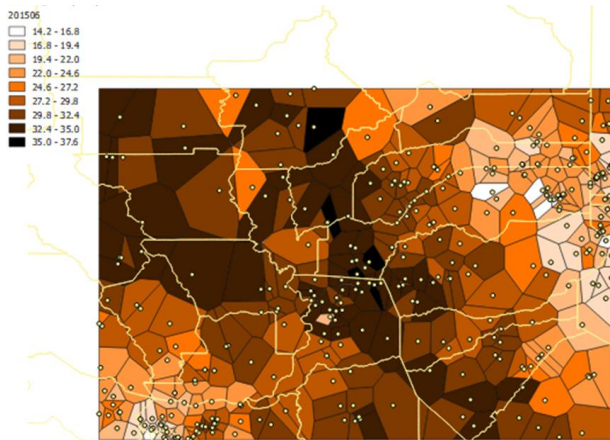
201506_1400PDT
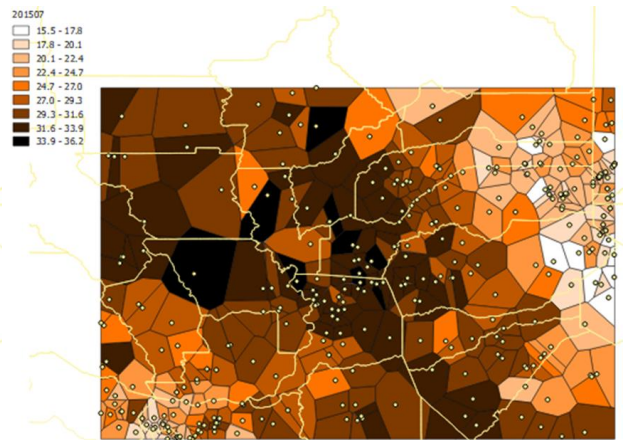
201507_1400PDT

Figure 3-3. continued.
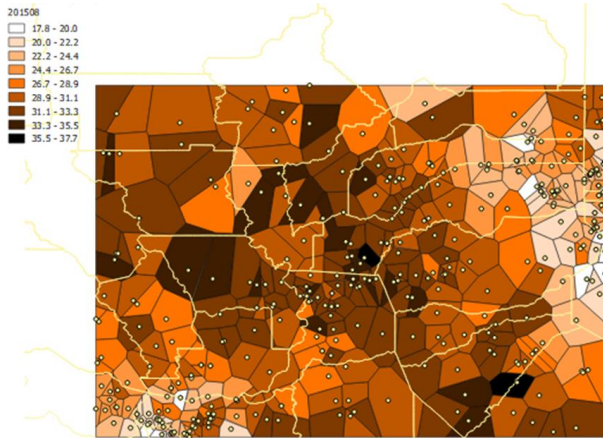
201508_1400PDT
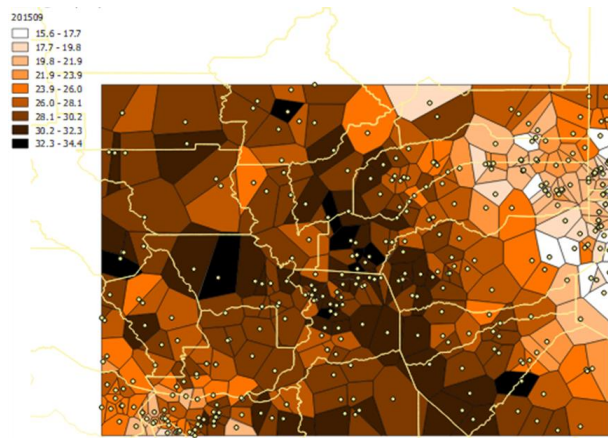
201509_1400PDT
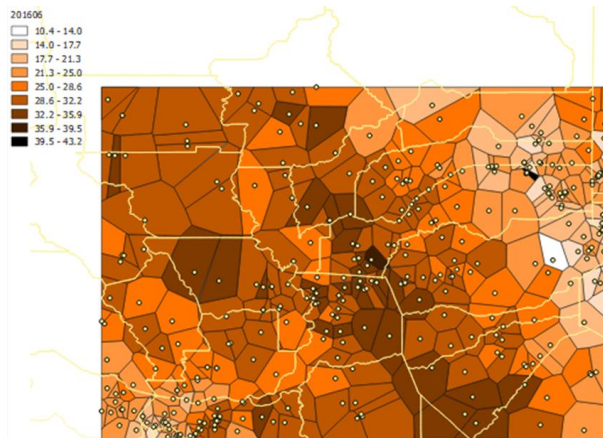
201606_1400PDT
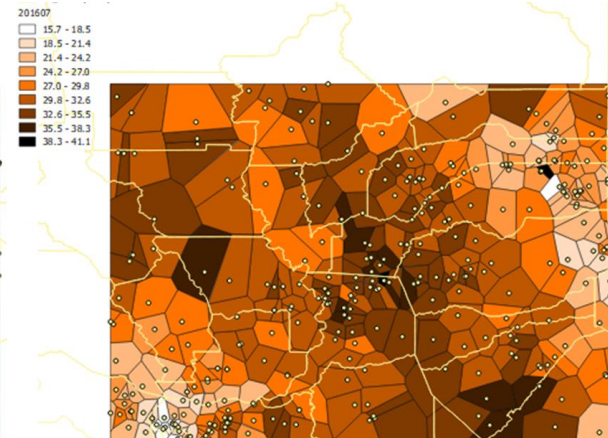
201607_1400PDT
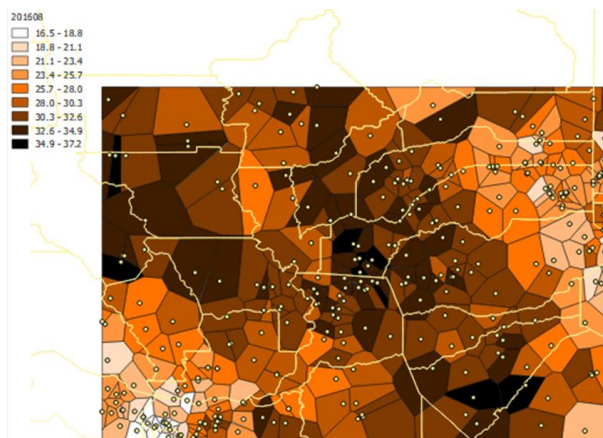
201608_1400PDT
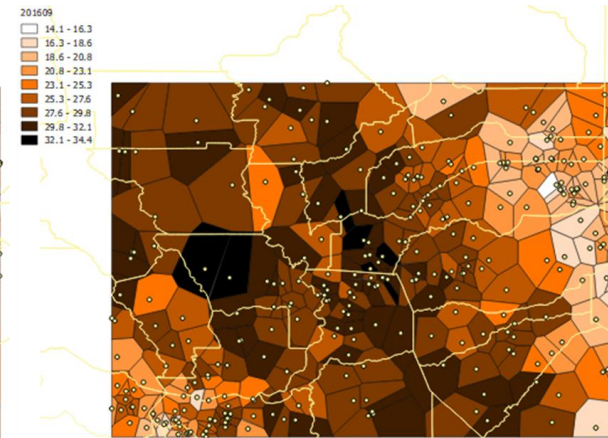
201609_1400PDT

Figure 3-3. continued.
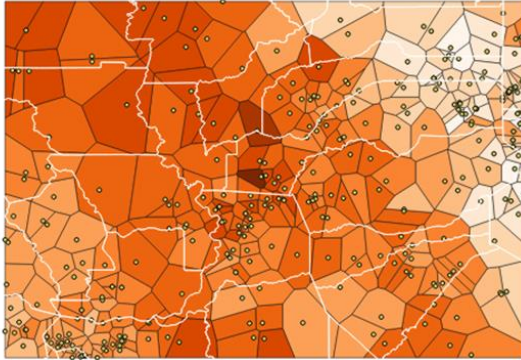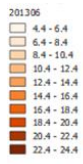
201306_0200PDT
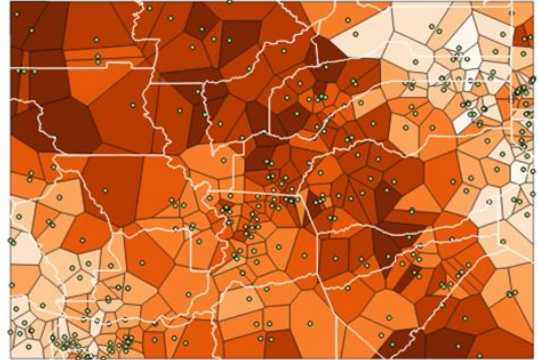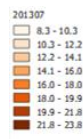
201307_0200PDT
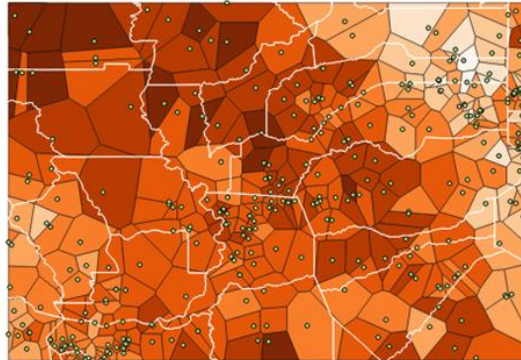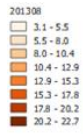
201308_0200PDT
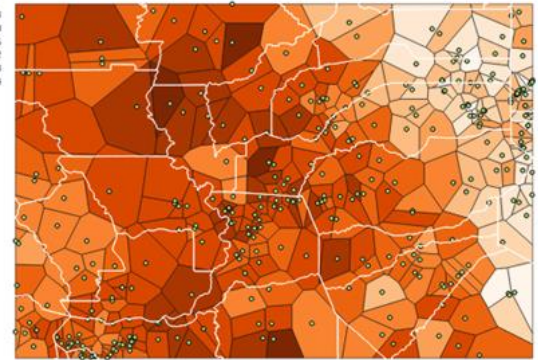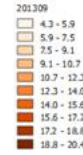
201309_0200PDT
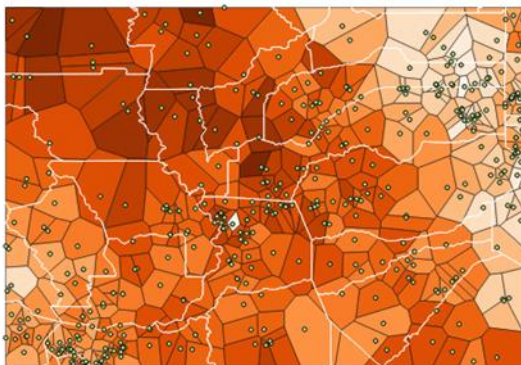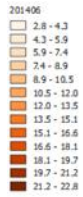
201406_0200PDT
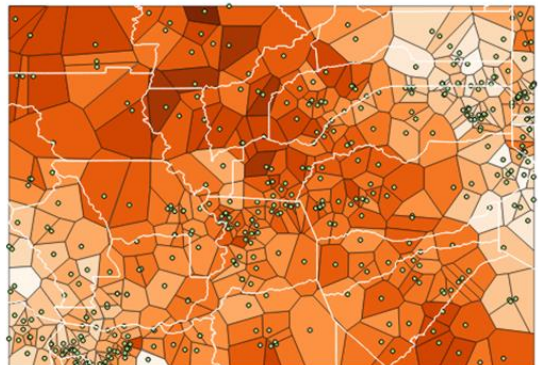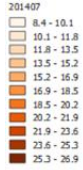
201407_0200PDT

Figure 3-3. continued.
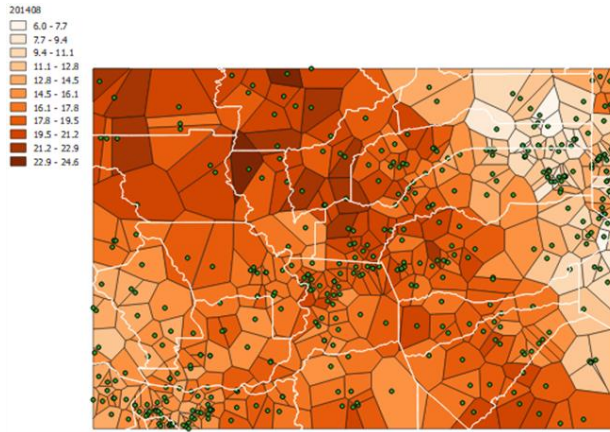
201408_0200PDT
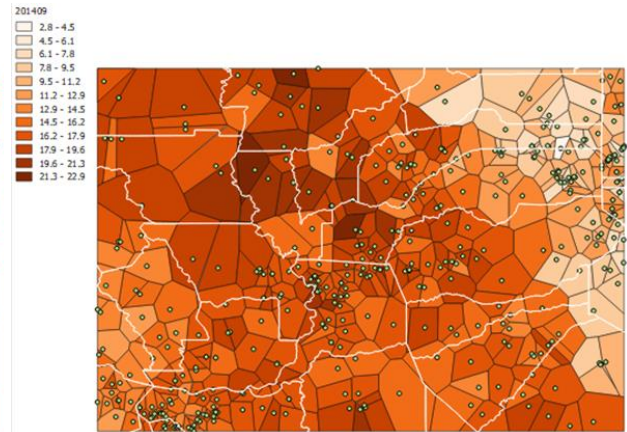
201409_0200PDT
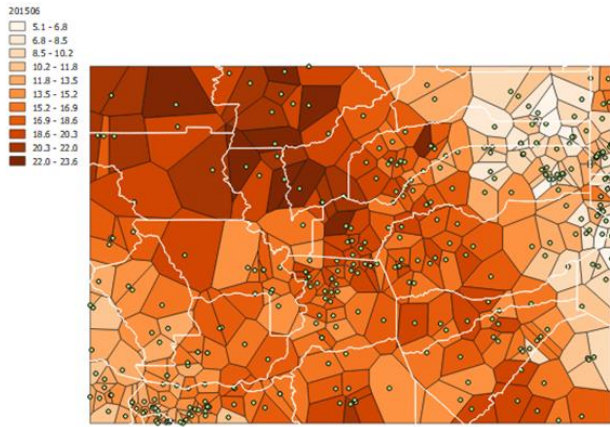
201506_0200PDT
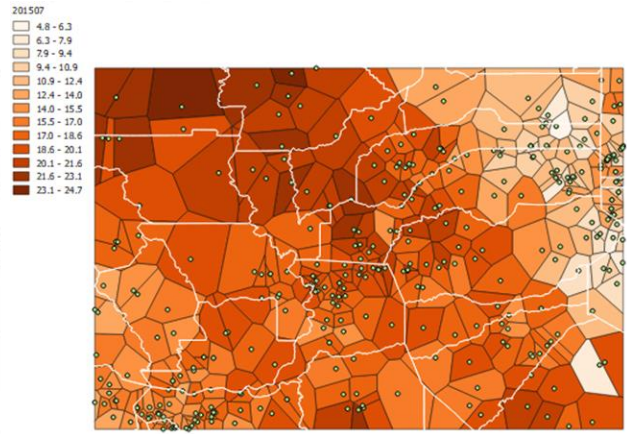
201507_0200PDT
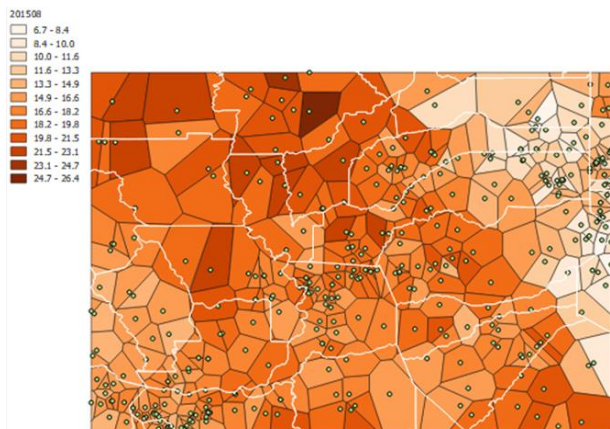
201508_0200PDT
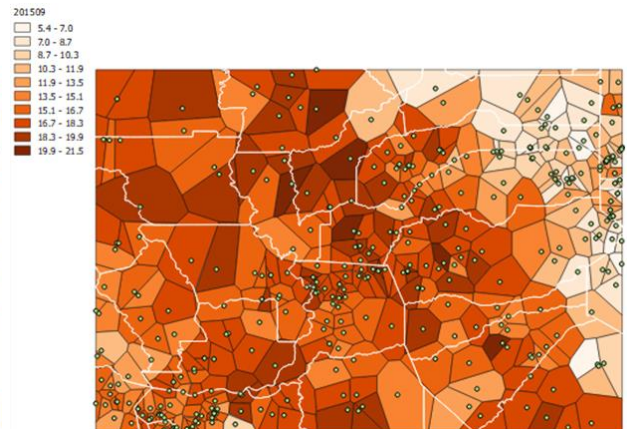
201509_0200PDT

Figure 3-3. continued.

201606_0200PDT

201607_0200PDT

201608_0200PDT

201609_0200PDT
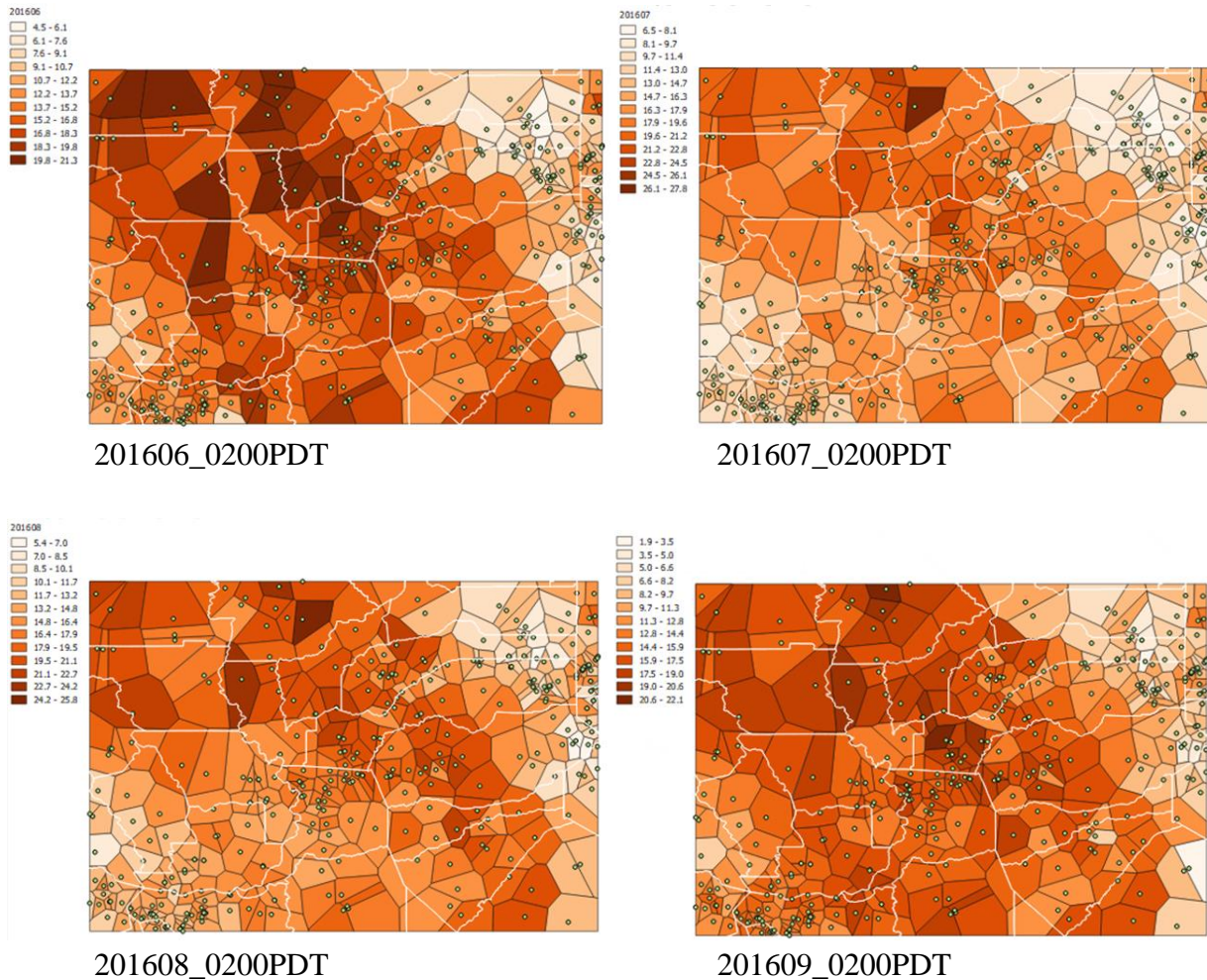
3.4 URBAN HEAT IN RELATION TO URBAN CORE AREAS

As discussed earlier in this report, the urban heat indicators, including the UHI and the UHII, characterized and quantified in this study are air-temperature-based, not derived from skin surface temperature such as shown in some urban "hot-spot" assessments from satellite / remote-sensing data or imagery, sometimes referred to as "surface temperature urban heat island", or SUHI. Thus, the spatial patterns of urban heat presented in this report can differ significantly from those seen in satellite imagery. For example, heat plumes and air-temperature peaks can be displaced downwind from urban cores. Furthermore, the SUHI is irrelevant to characterizing air-pollutant emissions rates, air quality (chemistry), and transport of heat from one area to another.

It has become almost an unshakable impression or thinking that downtown areas are the epicenters of heat islands. In reality, this is not always the case and the confusion may be a result of

misinformation from said "hot-spot" surface temperature characterizations. In effect, however, hot roofs in downtown or in high-rise areas can be high enough above ground that their influence on street-level air temperature is small to nil. In addition, the streets and urban canyons are well shaded by the tall buildings and likely receive no more than an hour or two of direct sunlight every day (depending on orientation), and sometimes none. The tall walls are exposed to sunlight, one or two directions at a time, but can dissipate heat rather efficiently because of the lower temperatures, stronger winds, and mixing at higher elevations away from the ground. By the same token, increased turbulence of air flowing over the rough downtown area increases mixing of temperature and accelerates cooling. Thus, an area such as downtown Sacramento can be warm but not necessarily the warmest all the times. Furthermore, in the specific case of Sacramento, the downtown area is heavily treed (see again Figure 2-7, domain D07) which helps keep it cooler than its surrounds. The observational meteorological data from the Sacramento area, e.g., Figures 3-3 and 3-4, support this argument.

Taha (2017) shows that this also is the case in the Los Angeles urban climate archipelago. However, he also demonstrates that smaller, low-rise downtown areas, such as in Fresno or Bakersfield, do indeed get warmer than their surrounds. In the Sacramento area the warmest parts stretch from AB617 communities A, B, and D east to Folsom and El Dorado Hills and northeast to Rocklin, Roseville, and Lincoln. In the discussion of model results, later in this report, the same will be seen – that the hotter parts of the Sacramento area are displaced to the east and northeast and that the downtown area is relatively cooler than some of the surrounds. This was also observed in the Level-1 Cal/EPA UHII (Taha 2017; Taha and Freed 2015).

Figure 3-4: Observational mesonet all-hour average air temperature contours. Left: 201306; Range: 306 – 646 ℃·hr day^{-1}. Right: 201307; Range: 389 – 701 ℃·hr day^{-1}
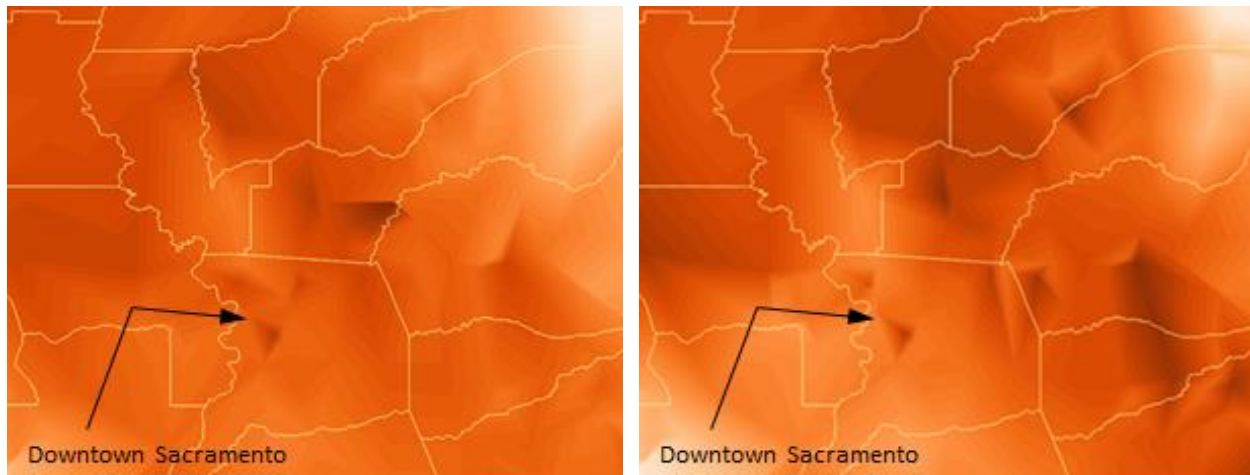
3.5 OBSERVATIONAL INTRA-URBAN TEMPERATURE RANGE

To provide an "at a glance" characterization of the temperature field across the study domain shown in Figures 3-3 and 3-4, above, the observed air temperature across the region is plotted, in Figure 3-5, as a cumulative distribution function (solid line, CDF) along with a 95% confidence band (dashed lines). While this exercise can be done for any time period or time of day, various averages, and so on, here we examine the CDF of monthly averages of the 1400-PDT observed air temperature. The labels on each graph of Figure 3-5 are YYYYMM. Thus, the figure provides a quick visual comparison of the temperature field across various years and months.

It can be seen that regardless of the actual intra-urban temperature range, the CDF signature is relatively similar throughout all periods except in some cases such as June and September 2014, and June and July 2016 that show a slightly steeper CDF. This indicates that the <u>spatial</u> characteristics of the temperature field, and hence the UHI and UHII, are relatively similar, in general, across the various summer weather conditions (but, of course, the absolute temperature differs from month to month and year to year). This implies that the design (spatial pattern of deployment) of mitigation measures will be equally valid and effective throughout different summer months and seasons.

The analysis also shows that relative to a specified threshold, e.g., 35 °C (which will be used later in evaluating impacts per electric utilities criteria) the observational data for the years and periods examined here indicate that 9% of the weather stations in this domain exceed the threshold in July 2013, 2% in June 2014, 5% in July 2014, 1% in both August and September 2014, 2% in both June and July 2015, 1% in August 2015, 1% in June 2016, 6% in July 2016, and 2% in August 2016. Considering that these are month-long averages of 1400 PDT temperatures, these exceedances are quite significant and indicative of a serious overheating problem in the region. Furthermore, the observational analysis shows that the warmest period (of the intervals studied in this effort) is July 2013, followed by July 2016 and July 2014. All of these indicators are taken into consideration when selecting modeling periods at the fine scales (500 m) as will be discussed later in this report.

Figure 3-5: Cumulative distribution function (CDF) and 95% confidence band for month-averaged observational air temperature at 1400 PDT.
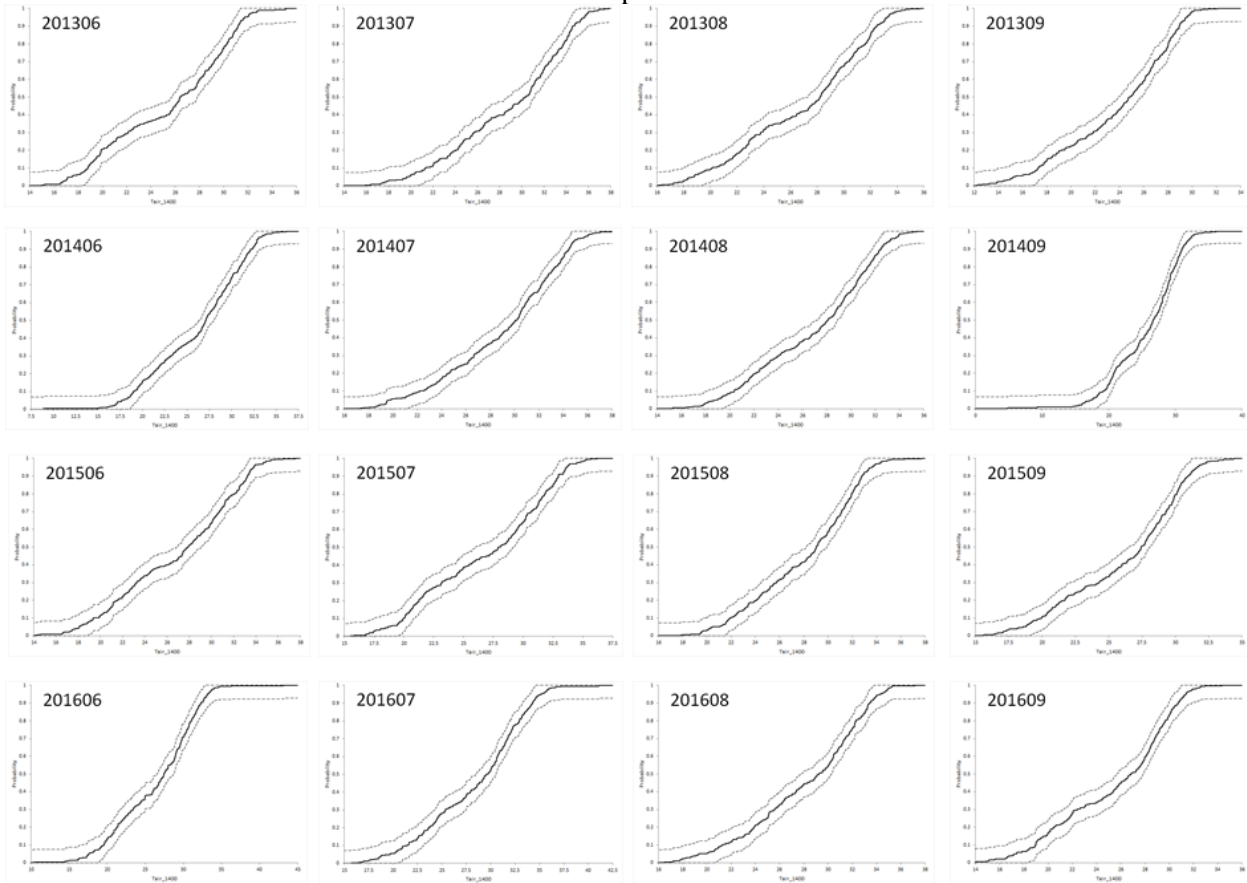
3.6 ANALYSIS OF OBSERVED LOCAL TENDENCIES

As discussed in Section 3.5, the general signature of the temperature field is relatively similar across the summer months and years examined in this study. However, there were also some month-to-month variations (as can be expected) producing different signatures in Figure 3-5. In this section, the spatial aspects of these variations in profiles are examined, i.e., identifying the geographical areas affected by those departures from the "typical" profiles in Figure 3-5.

To crudely characterize (based on observational data) the intra-seasonal magnitudes of warming or cooling in different parts of the domain as the background weather changes, local tendencies were computed at each mesonet station location relative to its own conditions during the month of June, as reference. Thus, for example, Figure 3-6 (A – F) shows the averaged changes in 1400 PDT temperatures (at each station relative to its own location) for July, August, and September in years 2013 and 2016, relative to June of 2013 or 2016, respectively.

To reiterate, what is shown in Figure 3-6 is not an absolute temperature field that can be compared across the domain (i.e., the figures cannot be used to evaluate which area is warmer or cooler than another) – each figure is a mosaic that only shows how much each area (weather station location) warms up or cools down relative to its own conditions in June (here, the month of June is used as reference, but any other reference would be equally useful). Thus, graphs A – C are for July, August, and September of 2013 (relative to June 2013) and graphs D – F are for July, August, and September of 2016 (relative to June 2016). They all show the averaged tendencies at 1400 PDT at each station for each given month. The caption below each figure provides the actual range of temperature change in each month and year. The following is a brief discussion.

July 2013 minus June 2013 (Figure 3-6 A): In July, the entire Sacramento County area warms up relative to June, but the eastern and southeastern parts warm up relatively more than the rest of the county. There is also larger warming in the North Highlands area and northeast of it into Placer County. A monitor south of Sacramento also registers higher-than-average warming. In El Dorado County, most areas warm up but the central parts of the county warm up more, including Placerville and surrounding areas. In El Dorado Hills, the warming is relatively smaller than at Placerville. In Placer County, the eastern parts warm up more than the western parts that are closer to Sacramento County. Areas near Lincoln and Roseville, while still warming up, do not heat up as much as the eastern parts of the county. In Yuba County, the eastern parts warm up more than the areas near Marysville. Yuba City, in Sutter County, warms up more than Sutter (City) and more than Marysville. Finally, in Yolo County, there is moderate warming, and it is larger in Woodlands than in Davis.

August 2013 minus June 2013 (Figure 3-6 B): The eastern and southeastern parts of Sacramento County warm up more than the rest of the county. Areas along the boundary between Sacramento and Placer counties also warm up more than its surroundings. There is a cooling signal in the southern part of the domain, relative to June. In El Dorado County, most areas warm up, but the central parts warm up more, including Placerville and surrounding areas. In El Dorado Hills, the warming is negligible relative to June. In Placer County, the eastern parts warm up more than the western parts. However, southern parts of the county, i.e., at the boundary with Sacramento County, including areas near Roseville warm up as well. The areas near Lincoln have negligible change relative to June. In Yuba and Sutter counties, the areas to the north and south of Yuba City and Marysville warm up, but at these two locations, there is relatively small change compared to June. In Yolo County, there is moderate warming, and, again, it is larger in Woodlands than in Davis.

September 2013 minus June 2013 (Figure 3-6 C): In September, the region is cooler than in June except for a few monitor locations around the San Francisco Bay Area. In general, all areas appear to cool down uniformly relative to June, except for some sporadic monitors where there is larger cooling than at others.

In general, the eastern parts of the 6-counties region cool down more (relative to June) than central or western areas.

July 2016 minus June 2016 (Figure 3-6 D): The entire area of Sacramento County warms up relative to June but, in this case, the largest warming is found in the western parts (rather than eastern), south of Sacramento, and in southern areas of the county. There is also large warming in the Roseville area. In El Dorado County, all monitor locations, except for two, appear to warm up uniformly. The area around Placerville still warms up slightly more than areas near El Dorado Hills. In Placer County, all monitors appear to warm up uniformly, except for larger warming in the Roseville area. In Lincoln, the warming also is larger than in its surroundings. In Yuba and Sutter counties, the warming is uniform across all monitor locations except for one cooling and one larger heating. Yuba City and Marysville warm up in similar amounts. Finally, in Yolo County, Woodlands warms up more than it surroundings and more than Davis.

August 2016 minus June 2016 (Figure 3-6 E): The spatial pattern of warming in the 6-counties region is similar to that in July-minus-June (Figure D) albeit at slightly different absolute temperatures.

September 2016 minus June 2016 (Figure 3-6 F): As with 2013 September-minus-June, there is relatively uniform cooling across monitors in this domain. There are, of course, some monitor locations that cool down more than others and some warm up slightly, but are outside of the urban areas of interest in this discussion.

Thus, to summarize the foregoing discussion, the meteorological observations indicate that while absolute air temperature changes significantly from month to month and between urban and non-urban areas, there are small intra-urban variations across the months. In other words, urban areas warm up or cool down in a relatively similar fashion. Independently from this, some of the largest departures (whether warming or cooling) are also found along the foothills and higher elevations in the eastern half of the domain as well as in some non-urban areas in the Yuba City and Woodland regions.

Thus, conversely, it can be argued that the impacts of the UHI-mitigation measures (in urban areas), spatially, should remain relatively similar across the different summer months and years. This will be discussed in more detail later in this report, when comparing the rankings of various measures across different geographical areas and in the different current and future climates.

Figure 3-6: Local monthly tendencies in temperature.

2013 July minus June difference (°C) in averaged 1400 PDT temperature. Actual
range is -2.64 to +6.99 °C. Based on observations from mesonet stations.

A

2013 August minus June difference (°C) in averaged 1400 PDT temperature. Actual
range is -2.71 to +5.38 °C. Based on observations from mesonet stations.

B

2013 September minus June difference (°C) in averaged 1400 PDT temperature.
Actual range is -9.06 to +5.07 °C. Based on observations from mesonet stations.

C

Figure 3-6, continued.

2016 July minus June difference (°C) in averaged 1400 PDT temperature. Actual range is -3.91 to +11.63 °C. Based on observations from mesonet stations.

D

2016 August minus June difference (°C) in averaged 1400 PDT temperature. Actual range is -10.4 to +12.78 °C. Based on observations from mesonet stations.

E

2016 September minus June difference (°C) in averaged 1400 PDT temperature. Actual range is -7.69 to +10.65 °C. Based on observations from mesonet stations.

F

4. BASE ATMOSPHERIC MODELING

4.1 OBJECTIVES OF BASE MODELING

In this study, atmospheric modeling was conducted with the WRF system (Skamarock et al. 2008) and an Altostratus Inc.-modified and updated version of its urban canopy model (Taha 2017; Martilli et al. 2002; Chen et al. 2010). This advanced version, applied at the 500-m level, will be referred to as "modUCM" in the rest of this report to distinguish it from the standard versions of the WRF model. This is in addition to the coarse-scale Altostratus AREAMOD approach, applied at the 2-km level, which was introduced earlier in Section 2.3.4.

The Altostratus modifications include improvements to the urban-canopy layer and land-surface parametrizations, as well as modifications to the single and multi-layer models (UCM and BEP/BEP-BEM) of WRF (Martilli et el. 2002; Salamanca and Martilli 2009). The modifications also involve innovative trigger mechanisms that call the urbanized modules at specified locations in the model domains (Taha 2018). Furthermore, Altostratus also uses different data preparation, surface characterization, and parameter-ingestion schemes (in the AREAMOD approach) than the standard WRF pre-processing system, resulting in more cell-specific characterizations in the LULC bottom-up approach discussed earlier in this report.

Thus, a base modeling task was performed at the beginning of this project to test any further model updates and evaluate model performance. The following was carried out:

- ≡ Configure, modify, and customize the atmospheric model's urban modules and parameterizations for study-domain specifics, such as available data and domain characteristics;
- ≡ Develop cell-specific surface-characterization input using the bottom-up approach discussed earlier along with available current-conditions urban morphology and geometry datasets;
- ≡ Develop current-climate meteorological input (initial, boundary, and surface conditions) based on observational weather data (MADIS) and reanalysis (NNRP; Kistler et al. 2001);
- ≡ Perform current-climate simulations, for the years 2013 – 2016, focusing on summer seasons (May – September, MJJAS);
- ≡ Define point-forecast locations, regional means, or other metrics for developing the reference-state meteorology;
- ≡ Carry out statistical model performance evaluation based on modeling-community-recommended benchmarks; and
- ≡ Diagnose model results to quantify the urban-heat effects of interest, per various metrics and thresholds defined later in Section 5.9.

Another objective of the base modeling was to evaluate length scales (fetch effects) of surface perturbations, e.g., albedo increase, to assess the Level-3 UHII implications in this region. This will be discussed in Section 5.8.

4.2 URBAN REPRESENTATIONS IN THE ATMOSPHERIC MODEL

Sub-grid or sub-filter scale parameterizations that are used to "urbanize" a meteorological model are as follows, per DuPont et al. (2005), Martilli et al. (2002), and Taha (2008a-c). Note that some or all of these parameterizations are used and implemented per model configuration and specific application.

$$\frac{\partial \rho u_i}{\partial t} = F_{g(ui)} + F_{ui}^j + \sum_j D_{ui}^j \tag{4-1}$$

$$\frac{\partial \rho \theta}{\partial t} = F_{g(\theta)} + H_j + Q_f \tag{4-2}$$

$$\frac{\partial \rho q}{\partial t} = F_{g(q)} + S_j \tag{4-3}$$

$$\frac{\partial E}{\partial t} = \frac{\partial u_i E}{\partial x_i} + \left\{ k_m \left[\left(\frac{\partial u}{\partial z}\right)^2 + \left(\frac{\partial v}{\partial z}\right)^2 \right] S_{air} + F_E^{bui} \right\} + \left\{ \frac{g}{\theta_v} \langle w\theta_v \rangle + H_E \right\}$$
$$- \frac{1}{\rho} \frac{\partial (\rho \langle wE \rangle)}{\partial z} - \varepsilon + \sum_j w_E^j - \sum_j D_E^j \tag{4-4}$$

Equations 4-1 – 4-4 are for momentum, heat, mass (water vapor), and turbulent kinetic energy (TKE), respectively.

In equations (4-1) – (4-3), the terms Fg are the general forcing terms (i.e., original model dynamics and physics) and the additional terms represent the urban parameterizations, i.e., subgrid-scale terms to account for the effects of urban land use and morphology. The two additional terms in equation (4-1) are (a) friction forces by the horizontal surface of buildings, roofs, and vegetation canopies, and (b) drag forces resulting from the vertical surfaces of buildings, obstacles, and vegetation canopies. The additional two terms in equation (4-2) are (a) sensible heat fluxes from buildings/roofs, pavements/streets, and vegetation, and (b) sensible heat flux from anthropogenic sources, e.g., motor vehicles and building cooling towers. The additional term in equation (4-3) is evapotranspiration from vegetation surfaces and evaporation from roofs and pavements. In equation (4-4), there are four additional terms (terms *F, H, W, and D*) that represent (a) shear

Altostratus Inc.

production of TKE by horizontal buildings and vegetation canopy surfaces, (b) buoyancy production of TKE by heat flux from building and vegetation and from anthropogenic heating (e.g., motor vehicles), (c) wake production by buildings and vegetation canopies, and (4) accelerated dissipation (cascade / sink), respectively.

For a detailed discussion of these terms and model urbanization, the reader is referred to DuPont et al. (2005), Martilli et al. (2002), and Taha (2008a-c).

4.3 INITIAL REGIONAL 2-km SIMULATIONS

One of the first objectives in this study was to enhance the representation of urban areas in the atmospheric model so as to improve performance and increase area-specificity of the simulations and results. This was done via (1) improving input to the model, i.e., more site- and area-specific surface characterizations, and (2) updating model parameterizations and calculations as presented above.

As discussed in Section 2, the LULC input to the model was improved via use of a bottom-up approach in characterizing the surface. An immediate result of this improvement can be seen in the more responsive temperature field to a better representation of the urban areas in the modeled domains. As an example, Figure 4-1 (left) shows the difference in the simulated temperature field at a random hour (1600 PDT on May 30th, 2013) between a run using the standard WRF model and a run using the Altostratus Inc. AREAMOD approach.

As can be seen in the figure, the standard WRF misses the urban areas highlighted in blue and underpredicts urban air temperature by up to 3.5 ℃ in those areas. In other words, the standard WRF model does not "see" these urban areas shown in blue but they are captured in the AREAMOD approach (per more recent LULC input and more accurate bottom-up characterization of surface). This is a significant difference, especially since this study is about modifications to urban areas with UHI-mitigation measures. Thus, the correct capture of urban extent is necessary.

Compare the left graph in Figure 4-1 with the right one showing the updated urban LULC from the analysis in Section 2. The central, "hollow" areas in many urban zones in the left figure, especially in the Sacramento metropolitan area, is what actually exists in the standard WRF and the blue areas are the additional representations in the AREAMOD approach (Taha 2017). As we will see later, this has a very significant effect on the modeled meteorology, UHII, and the impacts of further urban expansion in future climates (e.g., 2050).

It is likely that urban modelers will not use the standard WRF as is "out of the box" and will improve urban representation in some fashion – still, the purpose here is to show the AREAMOD approach's effectiveness in improving the WRF simulations. Furthermore, Altostratus Inc. also continually improves and customizes the fine-scale models, such as UCM of Kusaka and Chen (Chen et al 2010; Kusaka et al. 2001) by extensively expanding their ability for site-specific modeling, resulting in the "modUCM" version introduced above (Taha 2017, 2018). Figure 4-2

shows a comparison between the temperature fields produced by the standard UCM and the modUCM. It can be seen that modUCM captures features that the standard UCM is unable to, including, for example, the main roadways in the area (some of which were purposefully made cooler in this example for the Sacramento 500-m domain, D07), which is relevant to the transportation aspect of this study.

Figure 4-1. Left: Temperature difference between standard and Altostratus-modified WRF. Right: urban land use per most recent datasets.

NLCD2011_GIRAS-based calculation of urbfrac (0 - 1) in D04 (2 km domain)
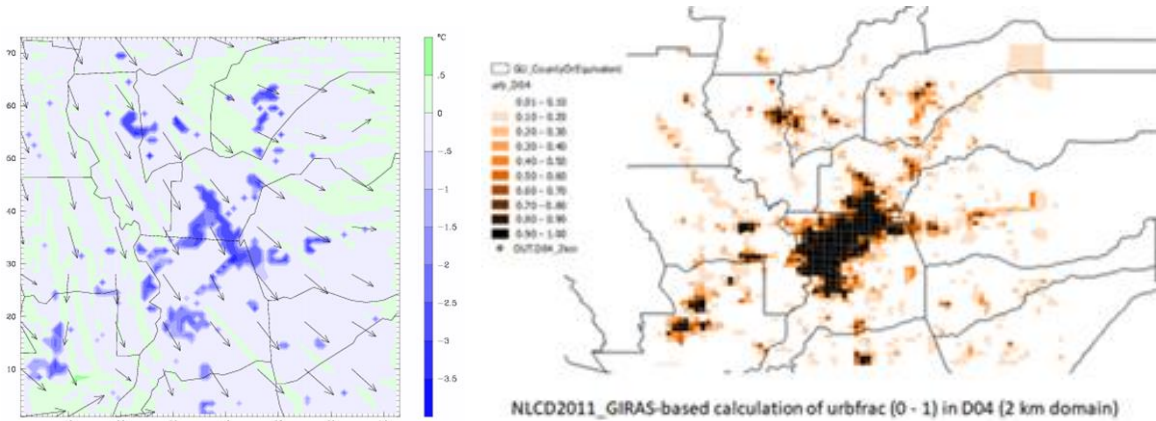
Figure 4-2. Temperature difference between standard and Altostratus-modified urban canopy model simulations of the Sacramento area.
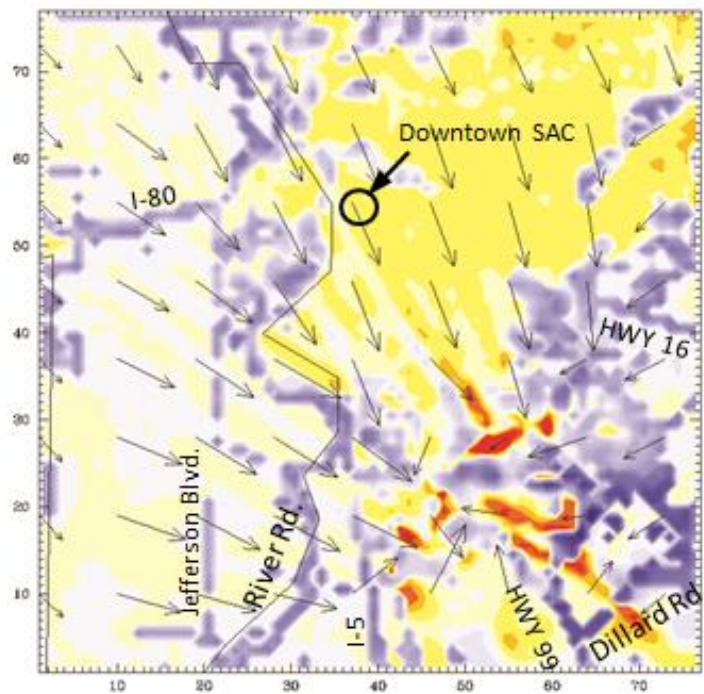
4.4 COARSE GRIDS SIMULATIONS (D01 – D03)

As discussed earlier in Section 2.2 (and shown in Figure 2-1), the atmospheric model was run on a multi-domain configuration that included 10 different grids at horizontal resolutions of 54 km (one domain), 18 km (one domain), 6 km (one domain), 2 km (one domain), and 500-m (six domains). Random samples from the 6-km domain (D03) simulations are shown in Figure 4-3.

The first three domains (D01 – D03) were run using the standard WRF model and pre-processors (Sakamarock et al. 2008), with some of the more relevant options being Kain-Fritsch for microphysics, TKE boundary-layer scheme MYJ, WSM 3 class, and the NOAH land-surface model (other details are explained elsewhere). In the 2-km domain (D04), Altostratus Inc.'s AREAMOD approach, configurations, and pre-processing were applied (Taha 2015b, 2017, 2018). In the 500-m domains (D05 – D10) Altostratus Inc.'s modUCM model in combination with AREAMOD were used as part of the urbanized WRF system.

The atmospheric model was run with 27 or 55 vertical level as needed per models and parameterizations being applied in each domain. Domains D01 – D04 were run with two-way feedback, whereas the 500-m grids (D05 – D10) were run via one-way nesting (Taha 2017, 2018).

In this report, results from domains D01, D02, and D03 are not presented. However, the results were evaluated against surface and upper-air observational meteorological data to ensure that the model captured the synoptic features during selected time intervals and that it produced the corresponding spatial patterns of temperature and wind flow throughout the region. Note that the quantitative model performance evaluation via thorough statistical analysis was done at the 2-km level (D04) as presented later in Section 4.5.3). In this report, only the results from the 2-km resolution domain (D04) and the 500-m resolution domains D05 through D10 are presented.

Figure 4-3: Sample model results (at random hours) from the 6-km resolution domain D03 for a summer and winter set of simulations. 2-m air temperature and 10-m winds at 1700 PDT, August 13, 2016 (left) and at 1600 PST, January 31, 2016 (right).
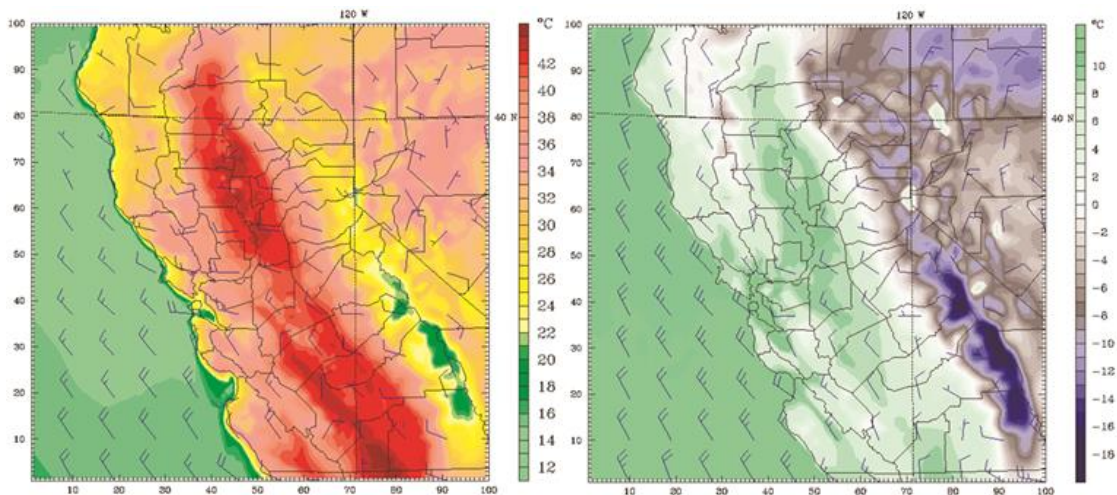
4.5 RESULTS FROM BASE MODELING OF THE 2-km DOMAIN (D04)

As discussed earlier in the analysis of observational weather data in Section 3, the mesonet network in this domain is relatively dense – yet there still are significant gaps in coverage over urban areas that need to be evaluated in this effort. To do so, a number of "probing" points or locations were added in this study to the network of mesonet monitors in order to increase the number of locations where model output can be evaluated in urban areas. Figure 4-4 shows the locations of the mesonet stations (white circles) and the additional probing locations (blue circles). Both sets of points are used in model output analysis but, obviously, only the locations with observations (mesonet – white circles) are used in model performance evaluation, as will be discussed in Section 4.5.3. The probing points were added to several locations in urban areas deemed of interest by the project TAC, SMAQMD, and LGC.

Figure 4-4 also shows a random sample from the model temperature field highlighting the higher temperatures in and around urban areas and the locations of mesonet stations and probing points relative to urban heat plumes in this region. In this example, the field is for all-hours average air temperature at 2 m above ground level for June 15 – 30, 2016 at a resolution of 2 km. In this example, the range of average temperature (from light color to dark) is 13.7 – 28.6 °C and each color level (interval) is 0.5 °C.

Figure 4-4: Locations of mesonet weather stations (white circles) and additional probing point locations (blue circles) in relation to urban heat plumes in the 6-counties Capital region.
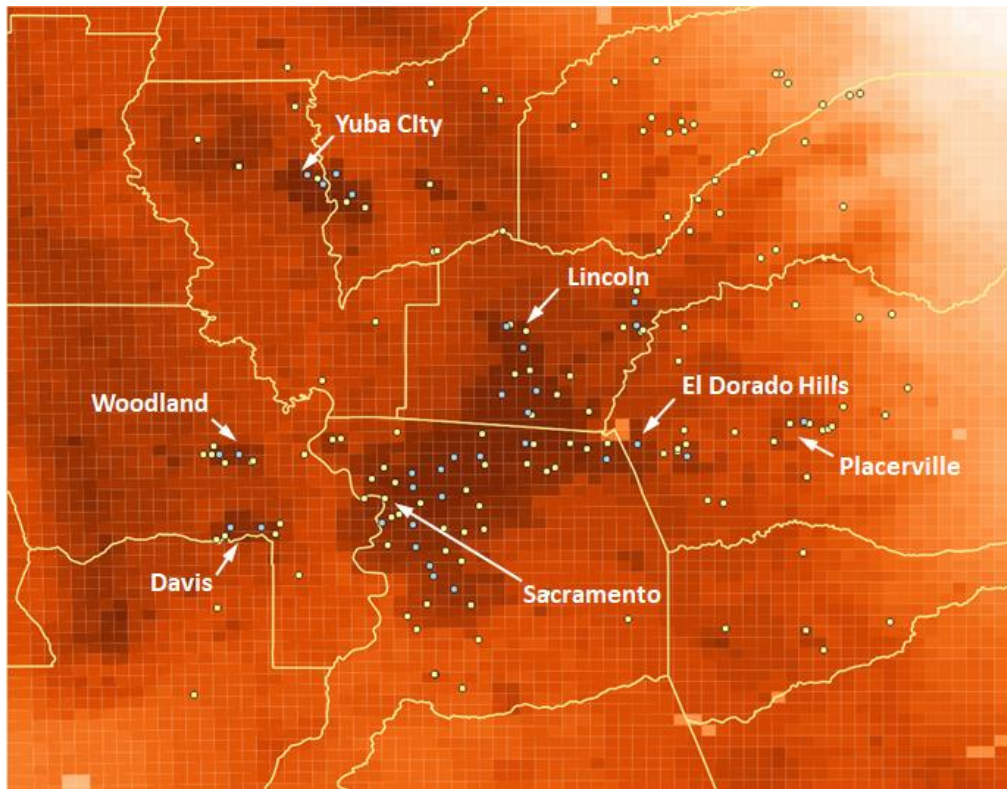
4.5.1 Sample daytime results at 2 km

Figure 4-5 provides a sample of results for the 2-km domain simulated with 55 vertical levels using the Altostratus Inc. AREAMOD approach. Random daytime hours from the simulations of June 2013 are presented. The first figure simply shows the locations of various cities of interest in this study. The subsequent figures provide model temperature fields at 2 m AGL (above ground level) along with the horizontal wind vector (at the lowest atmospheric level) for sample time stamps identified below each figure A – F between 1500 and 1900 PDT. The purpose of Figure 4-5 is to highlight the daytime UHI characteristics and the displacement of heat plumes with wind direction.

It can be seen that urban heat plumes are pushed to the south and southeast by the northwesterly wind (A), to the east by westerly wind (B), and to the east and southeast by westerly and northwesterly wind (C). In figures D, E, and F, the heat plumes are pushed to the north and northeast by the mostly southwesterly wind.

While the general spatial pattern of temperature over the urban areas in this region is relatively similar across different random time stamps, there are significant intra-urban variations in the temperature field from one time interval to another. Thus, whereas the UHI is easily identifiable in all time stamps in the areas of Yuba City / Marysville, Woodland, Davis, and Placerville, the UHI pattern in the central area (the greater Sacramento region) varies from one period to another. For example, in figures A, B, and C the UHI extends throughout the large urban area, whereas in figures D, E, and F, the hottest parts are seen north of the Sacramento-Placer counties boundary line, i.e., in the areas of Rocklin, Roseville, and Lincoln. It can also be seen that the higher temperatures are transported significant distances downwind from urban areas to non-urban, rural, and agricultural land use. The length scale for urban heat transport will be discussed in Section 5.8.

Figure 4-5: Model 2-m temperature field during daytime hours in the 2-km domain.
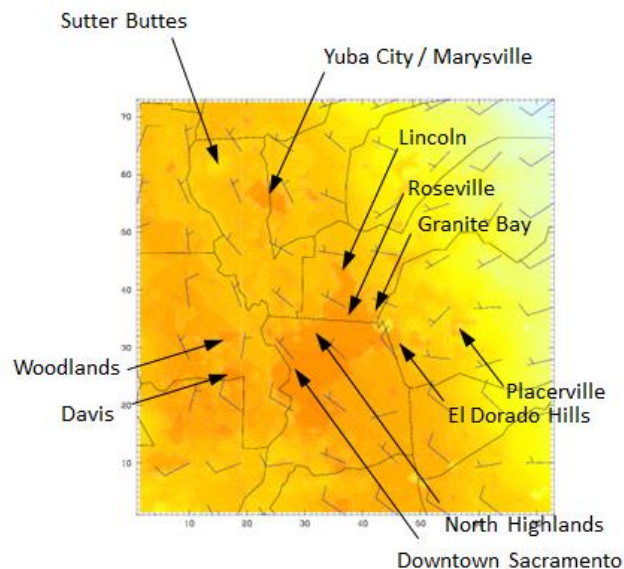
Figure 4-5, continued.
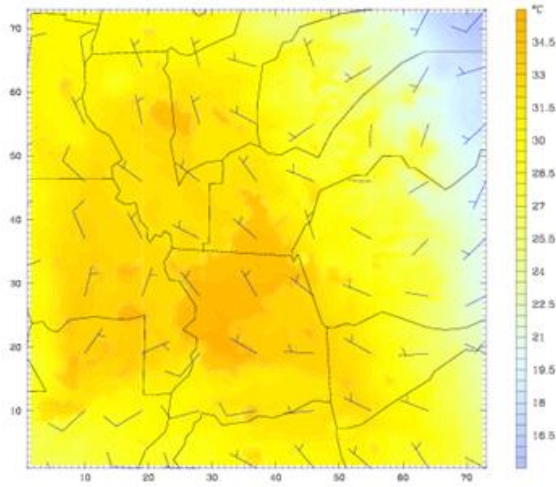
A: 1900 PDT, June 1ˢᵗ, 2013
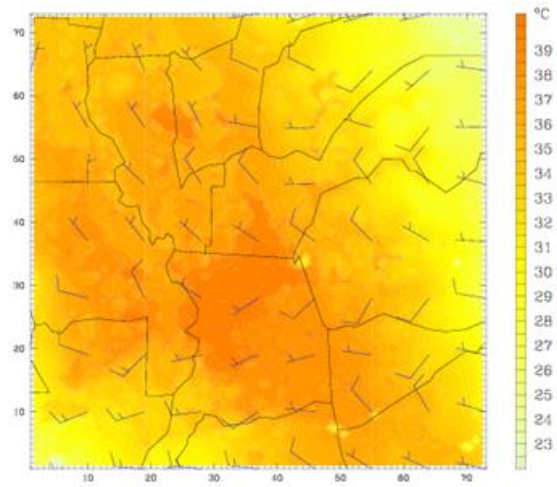
B: 1500 PDT, June 3ʳᵈ, 2013
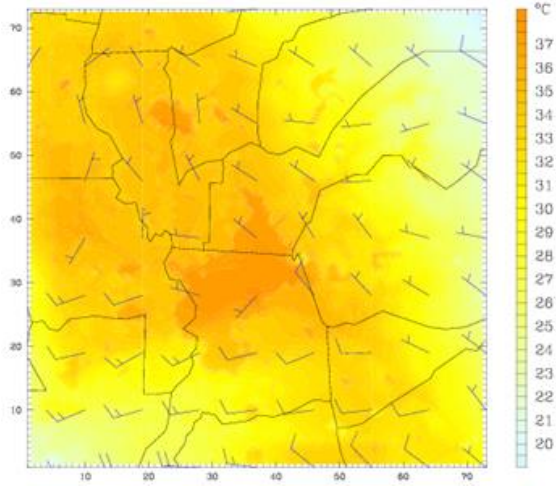
C: 1800 PDT, June 3ʳᵈ, 2013
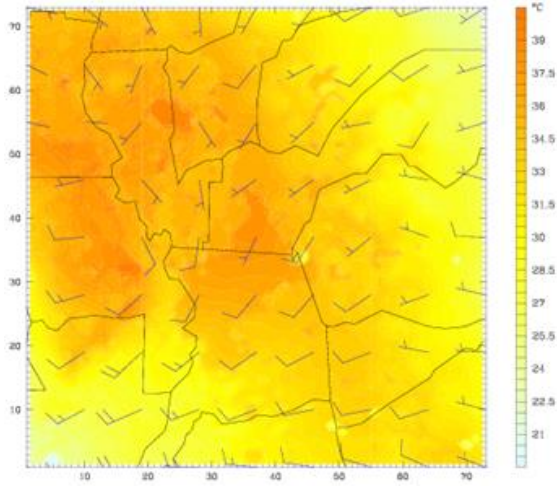
D: 1500 PDT, June 4ᵗʰ, 2013
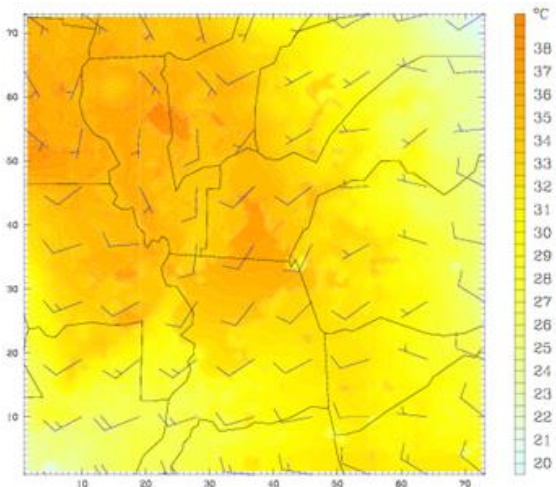
E: 1700 PDT, June 4ᵗʰ, 2013
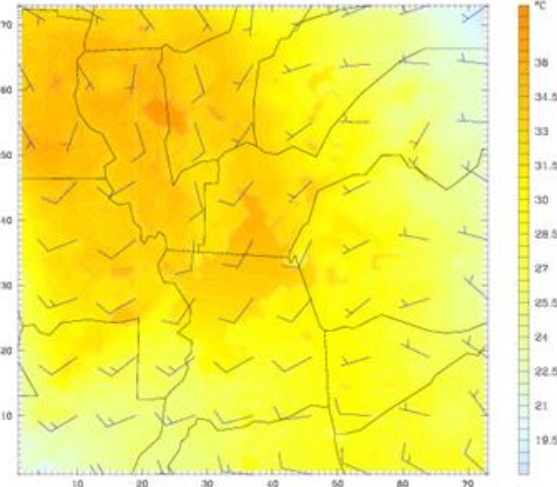
F: 1800 PDT, June 4ᵗʰ, 2013

4.5.2 Sample early morning results

Figure 4-6 is a sample snapshot from the model temperature field at 0700 PDT on two different days, provided here as examples. The figure shows that various areas are warmer than their surroundings, but for different reasons. The central parts of the domain are warmer because they are urban (the outlines of urban areas are clearly identifiable and the UHI is well-defined) whereas the eastern one-third of the domain is warmer because of the higher elevations (nighttime inversion). This is also the reason that the Sutter hills (in the northwestern part of the domain) are warner as are the mountain ranges at the western edge of the domain. These higher elevations are cooler, as expected, during daytime (see Figure 4-5).

Figure 4-6: Model 2-m temperature field during early morning hours in the 2-km domain.

0700 PDT, June 4th, 2013   0700 PDT, June 15th, 2013
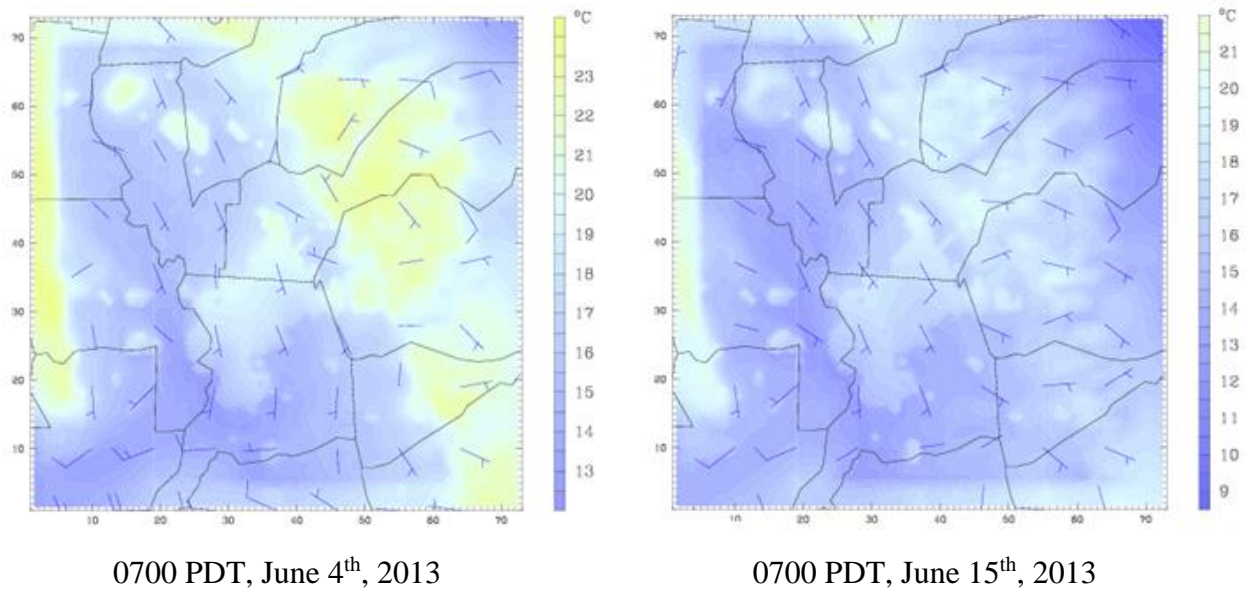
4.5.3 Model performance evaluation

Model performance evaluation (MPE) is typically carried out in most modeling projects and, thus, has been historically discussed in a large number of studies, e.g., Tesche et al. (2001). The science and operational basis for MPE will not be repeated here, nor the metrics or benchmarks – only a brief summary of findings is discussed in this section.

In this study, MPE was carried out at the 2-km level for each year and interval at hourly time scales (each interval is 2-weeks long, after removing spin-up days). Variables that were evaluated at each weather station location (Figure 4-4) were (1) air temperature (°C), (2) relative humidity (%), (3) wind speed (m s^{-1}), and (4) wind direction (°).

For 2-m AGL air temperature, two parameters were evaluated: (1) 4-D air temperature (denoted below as "Tair_2m" or "Tair2m") which is interpolated between surface and air temperature at the first ½ eta level of the model and (2) a relatively more "diagnostic" air temperature (denoted as "T2"), computed based on surface temperature and heat-transfer coefficient. Both Tair_2m and T2 were used in this study, depending on MPE results that are area-specific as well as the mitigation measure in question. Some measures require evaluation with T2, others require Tair2m, and, yet, some require use of surface temperature.

MPE statistics that were calculated include mean bias, mean absolute error, root mean squared error, and index of agreement for temperature, humidity, wind speed, and wind direction. Each of the statistics was computed at every station and all hours of model and observations (hours when observations were available at a weather station).

Table 4-1 is a condensed summary of MPE statistics for the 2-km grid. In the table, mean bias (MB), mean error (mean absolute error) (MAE), and RMSE statistics are provided for each of the variables listed above. RMSE is a more stringent indicator than MAE as it is much more sensitive to outliers because of its squared term and, thus, MAE may be a better indicator of performance. In Figure 4-7, the metrics and their ranges are shown with box-and-whiskers plots. The center horizontal line is the median, first to third quartiles shown as a box, and minima and maxima as whiskers with caps. The 95% confidence interval for the median is shown as a notch on the box.

The metrics values for each variable were found to be reasonable and comparable to results from many other studies of California that had good model performance. Of interest to this study is air temperature, where this MPE suggests that Tair_2m is a slightly better indicator than T2 (2.5 °C MAE median versus 2.75 °C) but that both can be used equally well in this application. These values are comparable to recommended benchmarks of 2 - 3 °C as seen in a large number of studies for California.

In terms of relative humidity (RH), in Figure B, there are no specific community-recommended benchmarks, rather, there are some benchmarks for water vapor mixing ratio. However, the RH metrics shown in this figure are reasonable (a median MAE of about 10%) considering the range of RH encountered in the large and varied study domain.

Wind speed statistics (Figure C) show a median MAE of 2 m s^{-1} which is reasonable per community-recommended benchmarks of 2 m s^{-1}. Finally, wind-direction statistics (Figure D) indicate a median MAE of less than 90°. This is considered reasonable as it generally represents the correct flow direction. The recommended benchmarks are between 30° and 60° and in this modeling effort, the median MAE is 55°, which is considered reasonable especially in light of the varied land cover and topography in the region.

Table 4-1: Condensed summary of MPE for D04.

interval	RH_MB	RH_MAE	RH_RMSE	T2_MB	T2_MAE	T2_RMSE	Tair2m_MB	Tair2m_MAE	Tair2m_RMSE	wdr_MB	wdr_MAE	wdr_RMSE	wsp_MB	wsp_MAE	wsp_RMSE
2013_int1	-8.58	11.53	14.19	2.29	2.88	3.52	1.49	2.77	3.38	30.20	70.35	98.66	1.79	2.05	2.40
2013_int2	-10.06	12.15	15.42	1.97	2.53	3.10	0.58	2.13	2.64	25.15	67.36	93.37	1.78	2.05	2.36
2013_int3	-5.84	9.54	12.18	2.46	2.89	3.60	1.40	2.53	3.22	5.69	56.69	76.80	1.75	1.98	2.26
2013_int4	-4.84	9.39	12.02	2.07	2.81	3.37	0.89	2.40	3.01	2.45	47.30	62.82	1.86	2.06	2.30
2013_int5	-8.26	11.26	13.97	2.49	2.89	3.47	1.00	2.22	2.76	0.32	49.64	65.50	1.76	1.97	2.26
2013_int6	-12.34	13.57	16.31	2.02	2.71	3.30	0.76	2.37	2.96	-1.16	53.83	71.88	1.74	2.00	2.30
2013_int7	-13.40	14.65	18.29	1.94	2.81	3.59	0.62	2.38	2.98	-1.69	58.40	82.08	1.56	1.81	2.06
2014_int1	-9.65	11.96	15.41	2.42	2.78	3.31	1.92	2.79	3.45	27.61	72.71	100.24	1.77	2.11	2.47
2014_int2	-5.06	8.88	11.22	1.92	2.62	3.11	0.75	2.25	2.76	20.28	63.22	88.51	1.69	2.05	2.40
2014_int3	-6.58	9.09	11.49	2.44	2.90	3.62	1.78	2.68	3.50	10.68	55.67	75.33	1.91	2.14	2.44
2014_int4	-5.98	9.59	12.27	1.59	2.62	3.27	0.25	2.09	2.62	5.62	52.57	72.46	1.92	2.10	2.39
2014_int5	-8.44	12.12	15.53	2.26	3.04	3.95	0.97	2.55	3.25	-7.38	54.56	73.28	1.74	1.98	2.25
2014_int6	-8.55	10.36	12.81	2.05	2.64	3.23	0.73	2.04	2.52	2.01	53.31	72.49	1.49	1.78	2.03
2014_int7	-14.21	15.44	18.70	2.32	2.84	3.38	1.64	2.64	3.17	2.75	69.29	91.65	1.36	1.66	1.93
2015_int1	-8.15	11.97	15.90	2.13	2.79	3.62	1.11	2.51	3.21	11.13	63.20	86.43	1.67	2.02	2.34
2015_int2	-4.92	8.61	11.03	2.18	2.69	3.20	1.21	2.53	3.17	6.37	54.08	73.39	1.78	2.01	2.28
2015_int3	-3.20	9.08	11.74	1.25	2.49	3.08	-0.04	2.27	2.83	1.17	44.28	58.37	1.89	2.12	2.41
2015_int4	-6.18	10.95	13.76	2.44	2.78	3.38	1.81	2.66	3.40	13.27	61.23	84.22	1.84	2.12	2.41
2015_int5	-5.28	9.36	11.85	2.08	2.67	3.32	0.75	2.22	2.77	-0.80	47.16	65.91	1.69	1.95	2.21
2015_int6	-7.60	10.29	13.00	1.89	2.56	3.25	0.68	2.20	2.86	1.84	54.92	76.61	1.41	1.71	1.96
2015_int7	-7.34	10.96	13.68	2.07	2.76	3.42	1.20	2.63	3.27	4.72	66.40	95.50	1.38	1.79	2.11
2015_int1	-5.94	10.67	13.54	1.86	2.62	3.20	0.98	2.50	3.11	14.51	61.54	86.59	1.55	1.98	2.30
2015_int2	-11.01	12.86	16.13	1.83	2.56	3.17	1.35	2.72	3.45	20.31	73.59	99.71	1.48	1.83	2.14
2015_int3	-7.17	9.64	11.65	2.47	2.83	3.34	1.58	2.54	3.12	9.72	53.02	73.88	1.78	2.06	2.34
2015_int4	-9.57	10.97	13.23	2.54	2.85	3.36	1.80	2.55	3.10	6.12	51.73	71.01	1.74	2.00	2.29
2015_int5	-8.54	11.24	13.74	2.51	2.84	3.32	1.52	2.38	2.92	5.51	53.76	72.06	1.62	1.87	2.16
2015_int6	-11.48	13.62	16.98	2.52	3.02	3.61	1.55	2.60	3.18	-1.67	46.79	61.87	1.58	1.82	2.06
2015_int7	-10.87	13.51	16.36	2.39	2.84	3.39	1.26	2.31	2.84	3.97	62.90	86.65	1.56	1.87	2.14

Altostratus Inc.

Figure 4-7. MPE metrics for 2-km domain (D04)
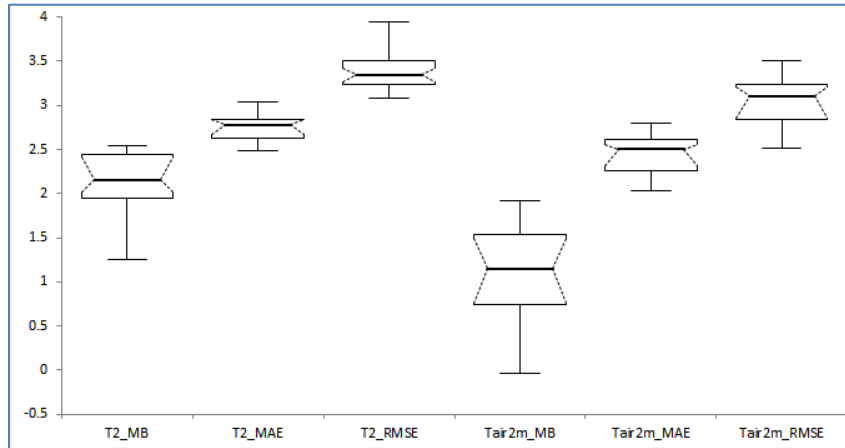
A: Air temperature statistics (int1-int7, 2013-2016); vertical axis is °C.
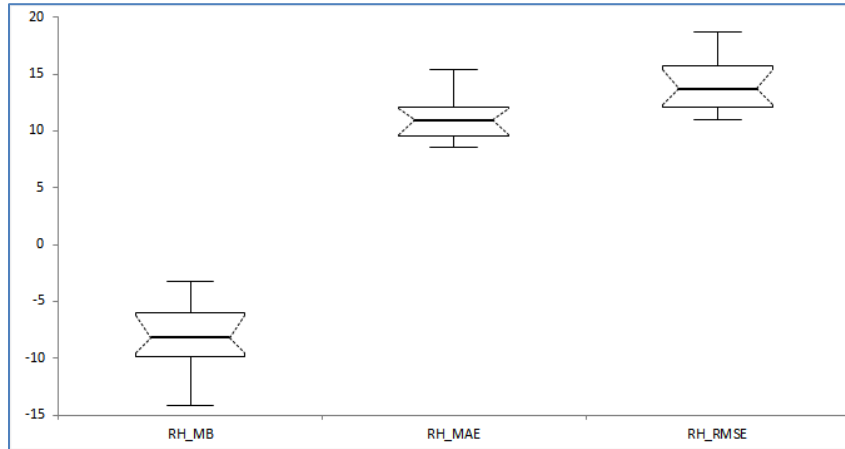
B: RH statistics (int1-int7, 2013-2016); vertical axis is %.
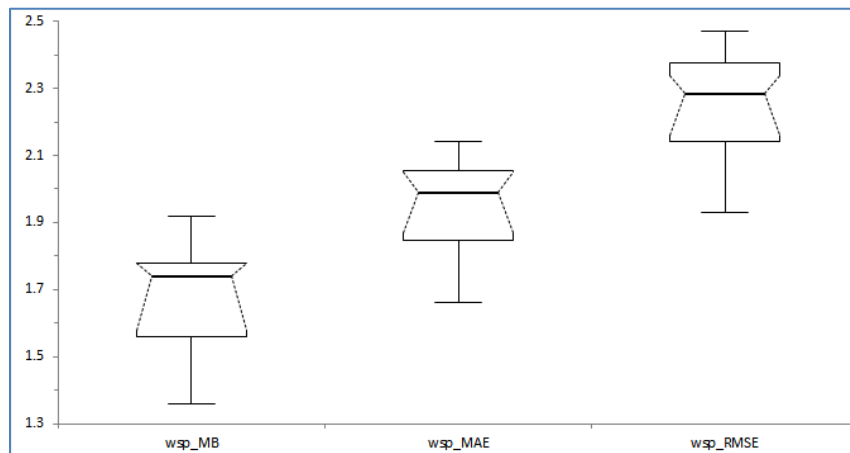
C: Wind speed statistics (int1-int7, 2013-2016); vertical axis is m s^{-1}.

Figure 4-7, continued.
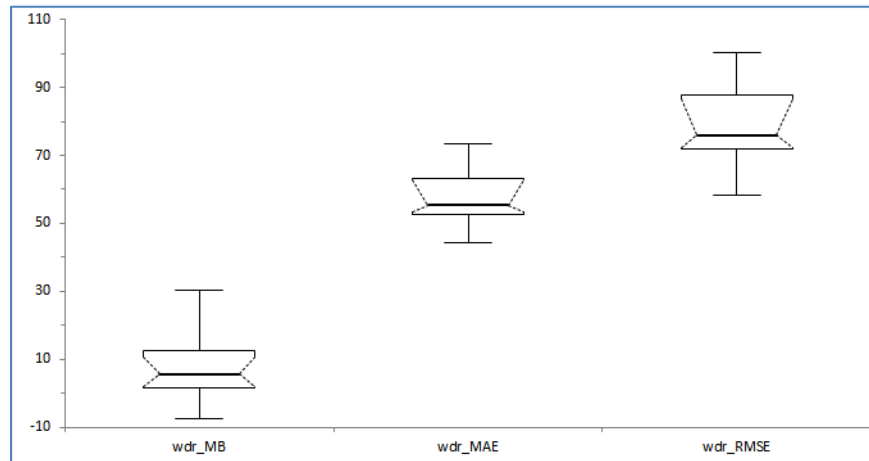
D: Wind direction statistics (int1-int7, 2013-2016); vertical axis is °.

5. EFFECTS OF MITIGATION MEASURES IN CURRENT CLIMATE AND LAND USE

5.1 OBJECTIVES OF MODELING MITIGATION MEASURES IN CURRENT CONDITIONS

Following the establishment of base meteorology and carrying out model performance evaluation as discussed in Section 4, the main objectives of the next steps were to:

- ≡ Customize area- and cell-specific characterizations and model input:
    - ≡ Present -day meteorological input, initial and boundary conditions
    - ≡ Present-day land-use/land-cover
    - ≡ Current-conditions urban morphology and surface thermo-physical properties
    - ≡ Technical potential for deployment of mitigation measures;

- ≡ Perform additional present-day base-case meteorological simulations to characterize current climate conditions, metrics, and UHII as well as develop a more detailed basis against which the mitigation measures are compared;

- ≡ Perform present-day simulations of mitigation measures, combinations of measures, and characterize various levels of the UHII;

- ≡ Develop metrics and thresholds and apply them in quantification of benefits, e.g., in terms of urban-heat reduction; and

- ≡ Develop derivatives and metrics for translation of meteorological model results into planning guidelines for the transportation system and the communities that were selected in the study region.

In this section, results from two modeling components are presented: (1) modeling and analysis at 2-km resolution for the domain encompassing the 6-counties Capital region to evaluate mitigation measures region-wide and (2) modeling and analysis at the 500-m scale to evaluate the potential benefits of localized and project-specific mitigation measures at the community or neighborhood scales.

It is to be noted here that Section 5 (this section) addresses only current conditions of climate and LULC. Future climates and LULC, their effects, and mitigation, are discussed in Section 6.

In this section and in the rest of this report, time intervals 1 – 7 are defined as follows:

Interval 1: June 1 – 15; Interval 2: June 16 – 30; Interval 3: July 1 – 15; Interval 4: July 16 – 31; Interval 5: August 1 – 15; Interval 6: August 16 – 31; and Interval 7: September 1 – 15. The time

periods are also abbreviated as YYYY_int#, for example: 2013_int6, meaning August 16 – 31, 2013.

5.2 MODELING CURRENT CONDITIONS: 2-m TEMPERATURE FIELD

As the model output is very large, this and the following sections focus on and provide some samples from the 2-m AGL temperature field as a subset from the simulation results. In Appendixes B-1 and B-2, averages over intervals 2, 4, and 6 (June 16-30, July 16-31, August 16-31) of each year (2013 – 2018) are presented for all hours and for 1500 PDT. For other times of day, or other intervals, the data is included in the model output but not discussed in this section, nor plotted in the figures.

As discussed in Section 4, modeling of the 2-km regional domain (and the output discussed in this section) was carried out with Altostratus Inc's AREAMOD approach. And while there are many ways, variables, and derivatives that could be presented, here the 2-m AGL temperature field is shown for a few example snapshots as an introduction. Later in this report, various metrics and threshold analyses at the 2-km scale will be presented.

The range of current-climate, modeled 2-m air-temperature across the 6-counties Capital region is summarized in Table 5-1 for intervals 2, 4, and 6. In general, those time intervals with the highest all-hour average temperatures also are the intervals with the highest daily maximum temperatures, e.g., at 1500 PDT. The model temperature ranges and absolute values discussed here compare well with the results from analysis of observational data (from mesonet networks) discussed in Section 3.

Table 5-1: Model temperature range (°C) across the 6-counties region during various time intervals.

	Model temperature range across the 6-counties domain	
	All-hours average (°C)	1500-PDT average (°C)
2013, June 16 - 30	11.52 – 26.18	14.59 – 32.23
2013, July 16 - 31	16.98 – 29.12	18.59 – 36.99
2013, August 16 - 31	15.28 – 28.50	18.43 – 36.29
2014, June 16 - 30	11.91 – 26.70	15.68 – 33.66
2014, July 16 - 31	17.78 – 28.51	19.41 – 36.91
2014, August 16 - 31	14.75 – 27.70	18.07 – 35.64
2015, June 16 - 30	16.91 – 30.20	20.01 – 37.41
2015, July 16 - 31	14.89 – 30.03	17.71 – 37.41
2015, August 16 - 31	16.77 – 28.86	19.77 – 36.46
2016, June 16 - 30	13.71 – 28.55	17.71 – 35.60
2016, July 16 - 31	17.30 – 31.02	20.84 – 39.17
2016, August 16 - 31	17.52 – 28.79	19.06 – 37.57

A random example from the model temperature field is presented in Figures 5-1 – 5-4 as (1) all-hour averages and (2) 1500 PDT averages for selected periods. Figures 5-1 and 5-2 show a sample from the all-hours model temperature field in the 6-counties region, e.g., the all-hour average field for the periods 2013_int2 and 2013_int4, respectively. These periods exhibit two different but common spatial patterns of the temperature field that are seen in many other periods and time intervals as well.

Thus, whereas the absolute temperature range differs between these two periods, the more remarkable difference is in the spatial pattern of urban heat, i.e., temperature field in and around urban areas in the Capital region. The differences arise because of the different dominant wind directions – for example, in Figure 5-1, the dominant wind is mainly northwesterly, northerly, and northeasterly whereas in Figure 5-2, the dominant wind is mostly westerly and southwesterly. It can be seen in the latter case that the temperature contrast in Sacramento County, as well as in the areas of Woodland and Davis, is diminished relative to surrounding areas (compared to Figure 5-1). In this case, most of the higher temperatures are found in areas from Rocklin and Roseville to Lincoln, in Placerville, and Yuba City / Marysville. The relatively consistent higher urban heat in the Rocklin-Roseville area (relative to different wind directions) is one reason why the UHI Index (Taha 2017) for this area is pushed northeast of the central Sacramento area, including downtown Sacramento. This was also seen in the UHI Index developed for the Cal/EPA (Taha and Freed 2015).

To examine this aspect further, Figures 5-3 and 5-4 show the 1500-PDT average temperature field corresponding to the same two periods examined in Figures 5-1 and 5-2. Although now the intra-urban temperature contrast is less obvious at 1500 PDT (relative to all-hours field discussed above), a similar observation can be made with respect to Sacramento County, Davis, and Woodland in that their temperatures are less differentiated from their surroundings, e.g., Figure 5-4 (westerly and southwesterly wind) relative to Figure 5-3 (northwesterly, northerly, and northeasterly wind).

As described in Section 3, the white circles in the figures represent locations of mesonet monitors in the region and the blue circles are the locations of additional probing points used in the analysis of the temperature (and other) fields.

Figure 5-1: All hours, non-threshold, average 2-m AGL air temperature (°C); 2-km domain; Year 2013, interval 2; 30 temperature levels, Δ ≈ 0.5 °C; Actual range: 11.5 – 26.2 °C
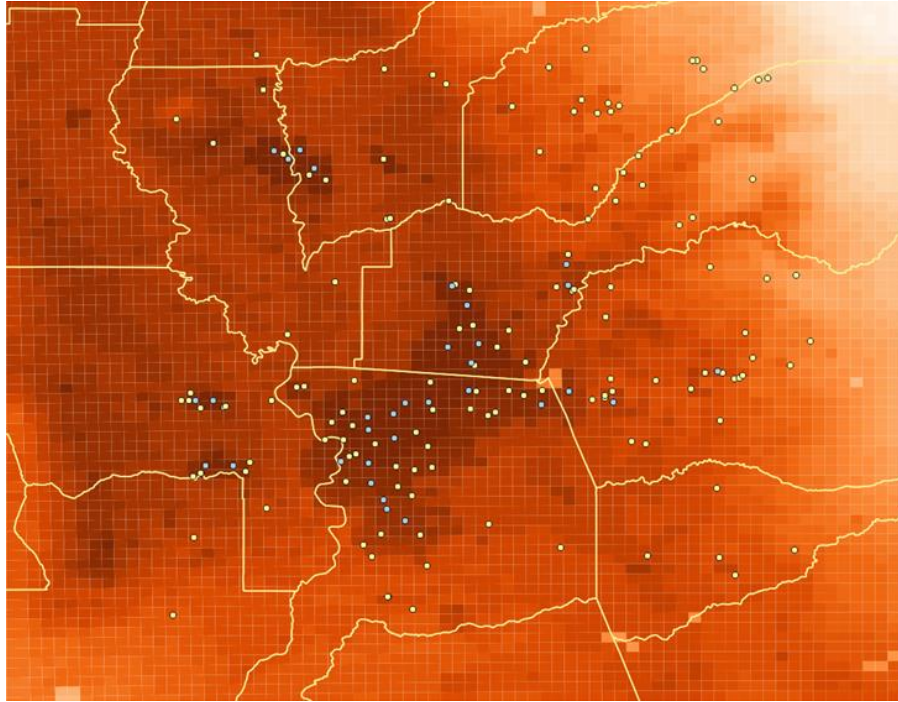
Figure 5-2: All hours, non-threshold, average 2-m AGL air temperature (°C); 2-km domain; Year 2013, interval 4; 25 temperature levels, Δ ≈ 0.5 °C; Actual range: 17.0 – 29.1 °C
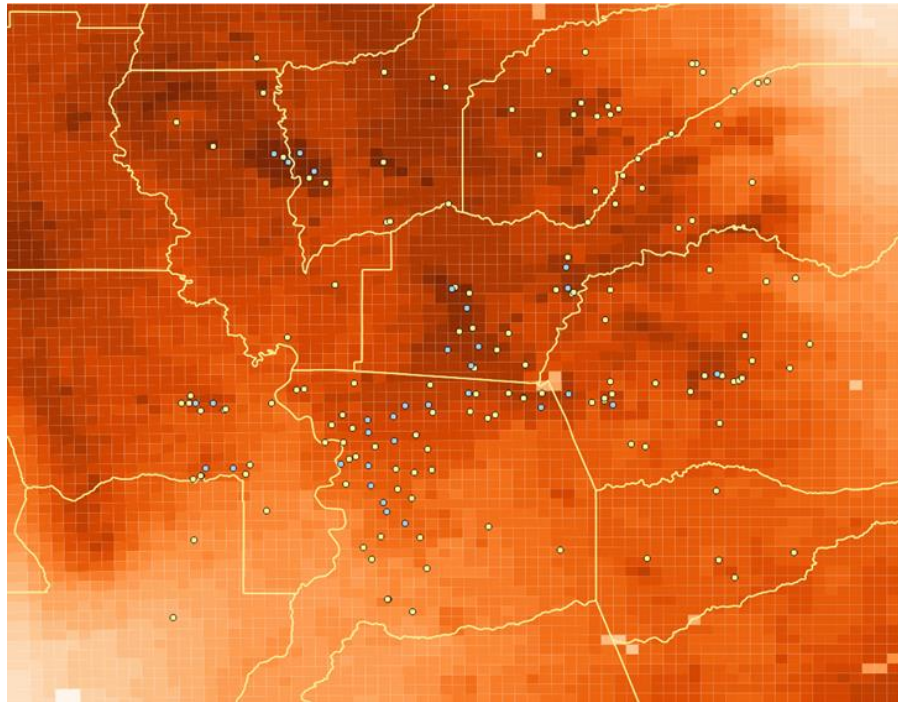
Figure 5-3: 1500 PDT, non-threshold, average 2-m AGL air temperature (°C); 2-km domain; Year 2013, interval 2; 30 temperature levels, Δ ≈ 0.5 °C; Actual range: 14.6 – 32.2 °C
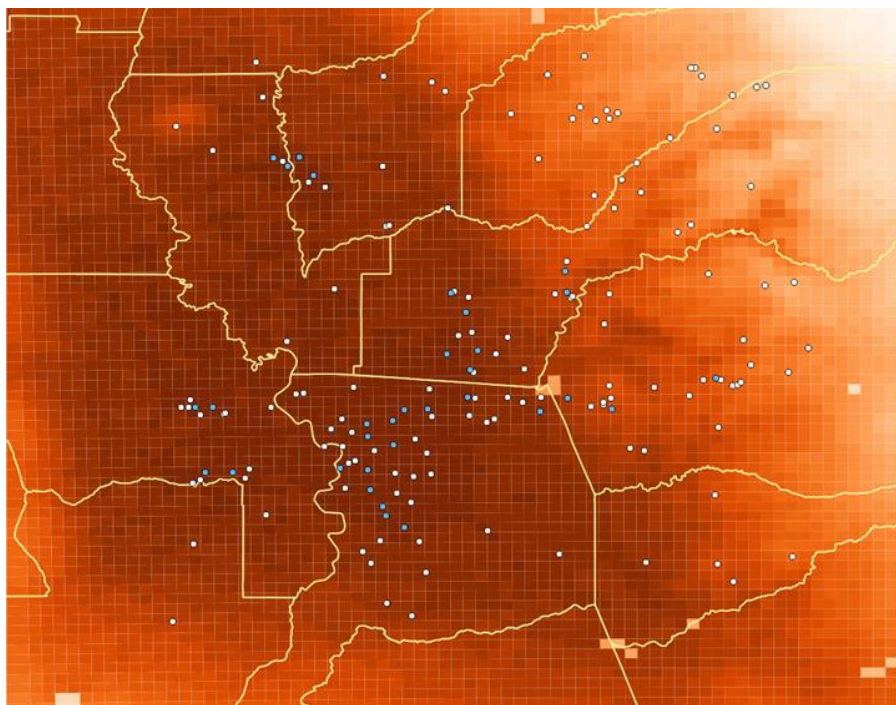
Figure 5-4: 1500 PDT, non-threshold, average 2-m AGL air temperature (°C); 2-km domain; Year 2013, interval 4; 35 temperature levels, Δ ≈ 0.5 °C; Actual range: 18.6 – 37.0 °C
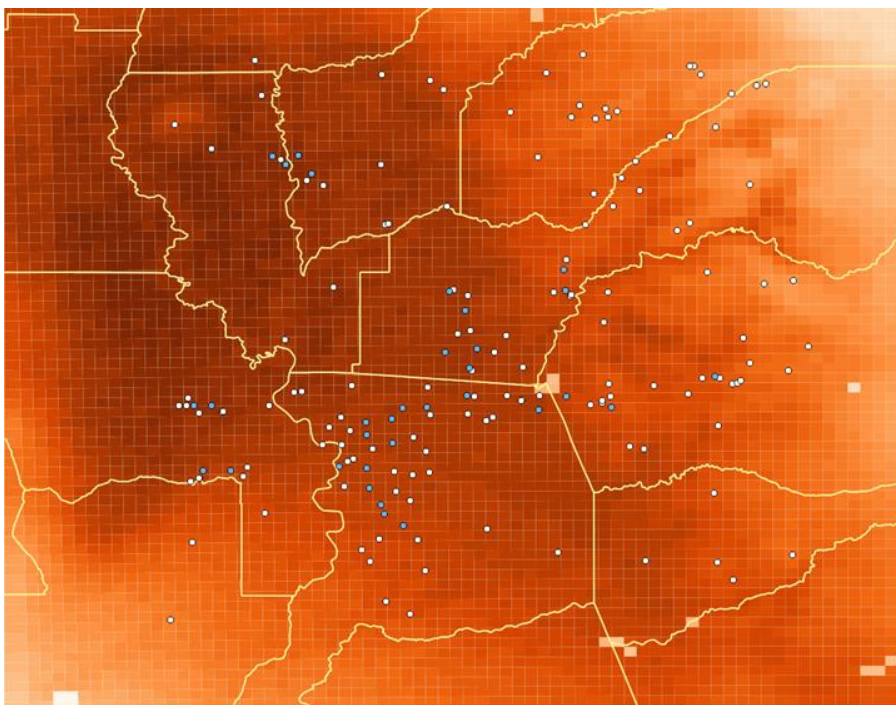
5.3 CHARACTERIZATION OF THE UHI INDEX (UHII) IN CURRENT CLIMATE

The goal of this sub-task was to establish the base-case conditions, as represented by the UHII, resulting from effects of current LULC properties in current climate. This serves both to characterize urban heat and to form a basis against which the benefits (or effects) of mitigation measures can be compared. The model results discussed in this section are for the regional 6-counties Capital region domain, including a separate UHII "tile" for each subregion as shown in Figure 5-5.

Summer months May to September (MJJAS) of years 2013 – 2016 inclusive were modeled. Throughout this report, some results are provided for specific hours or random intervals/times, and other results are presented as averages or cumulatives over the entire modeled periods and/or over various sub-domains.

To increase the accuracy of the simulations, a "leap frog" technique (Taha 2017, 2018; Taha and Freed 2015) was used. This approach minimizes model drift in long simulations and allows the capture of signals in the reanalysis (e.g., NNRP, Kistler et al. 2001) that may no longer be "seen" or refreshed during long simulations. Thus, while this approach increases computational burden by about 15% to 20%, it increases model accuracy over long periods of time. After removal of spin-up days in each interval, the results are presented as "net" 15- or 16-day blocks of time throughout the modeled seasons. In this report, these intervals are labeled int1, int2, int3, and so on, as defined earlier in Section 5.1.

In order to compute the UHII, the 6-counties Capital region was divided into six "tiles" or sub-domains each of which has its corresponding non-urban, upwind temperature reference points (as shown in Figure 5-5). The reason for assigning different, separate reference points for each sub-domain is to cancel out the large-scale, regional climate effects, i.e., the changes in the background temperature across the region. For example, areas to the north of Sacramento (such as Yuba City / Marysville) are generally warmer than south-west Sacramento simply because of changes in the synoptic weather and reduced impacts from the sea breeze (from the San Francisco Bay Area), and this regional heat pattern is unrelated to urban effects. Thus, using separate non-urban reference points for different tiles can address and compensate for these regional climate differences. Furthermore, the UHII at any location (i.e., at each grid cell) within each tile is computed relative to a time-varying, wind-direction-dependent upwind reference point. As it is possible that, at any given time, the wind approach direction is different in various tiles, the UHII is computed per different directions within the region. This approach, while more accurate than standard methodologies of using static reference points, can sometimes produce counter-intuitive spatial patterns of the UHI and UHII.

Figure 5-5: UHII-computation tiles and upwind reference points in the 6-counties Capital region (superimposed on a random-hour temperature field).

The upwind temperature reference points, a subset of which is shown in Figure 5-5, were selected to be outside of the urban heat plumes for each wind direction. This was determined after results from an ensemble of base model runs was examined to characterize the plumes and their variations with time and wind direction. This also took into account the temperature length scales discussed later in Section 5.8.

Counter clock-wise from top in Figure 5-5, the tiles are for the regions of: Yuba City / Marysville, Woodland, Davis, Sacramento, Placerville, and Auburn. At each hourly or sub-hourly interval of the AREAMOD / WRF simulations, the wind approach direction at each grid cell in the tiles is evaluated and the UHII computed per upwind reference point for each tile independently of others.

Based on these reference points and hourly calculations at each grid cell relative to coincident wind direction, the UHII was computed for all years, periods (intervals), and regions. It was calculated for all hours, as well as for specific hours, e.g., early morning, evening, and times of peaks, as well as for a range of hours, e.g., 1400 to 2000 PDT. A graphical example for all-hours UHII is shown in Figure 5-6 where, additionally, several AB617 communities defined by the Sacramento Metropolitan AQMD are highlighted (SMAQMD 2018).

Figure 5-6: Composite of UHII tiles, July 16-31, 2015 all-hours averaged UHI Index for six tiles in the Capital region (A – H are selected AB617 communities).
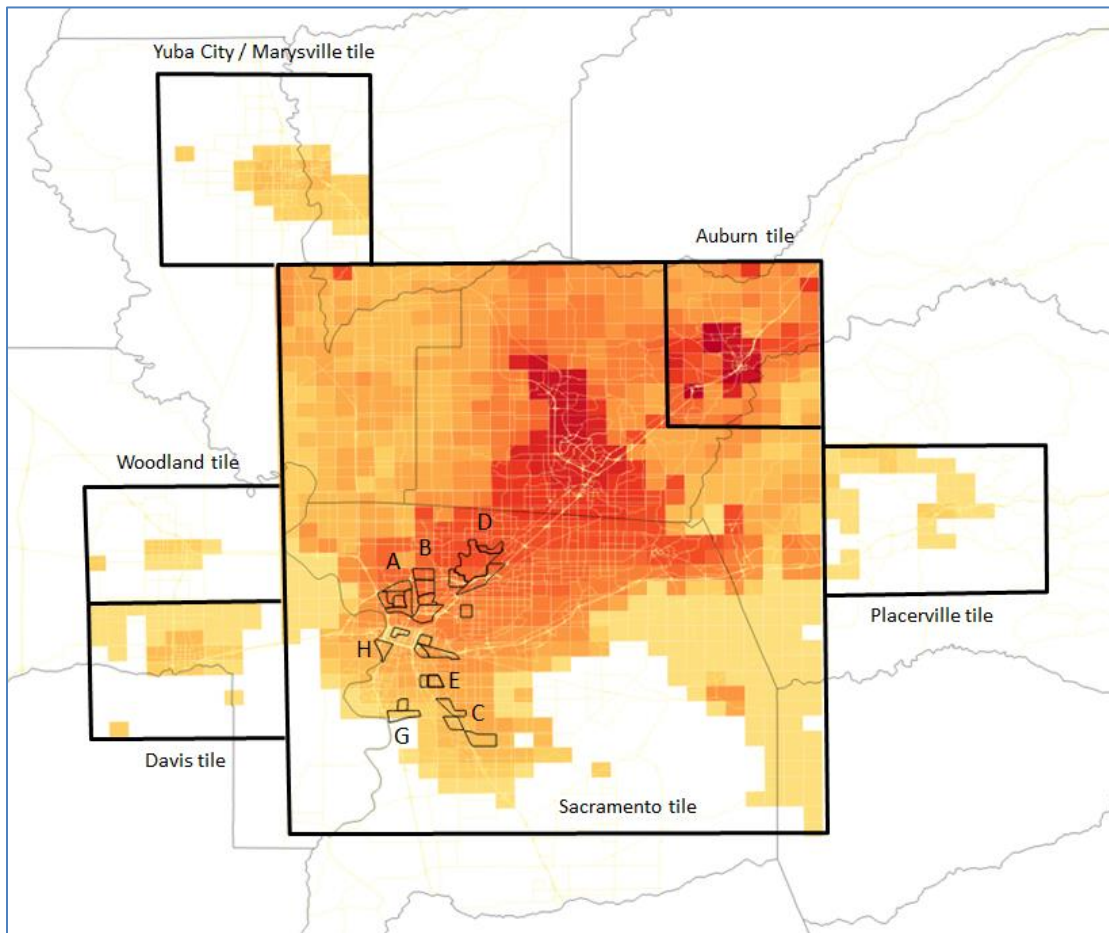
In this example (Figure 5-6), the UHII is computed for the period July 16 – 31, 2015 for which, the all-hours averaged temperature equivalent (i.e., DH hr^{-1}) is as follows (for selected AB617 communities):

A: 3.3 °C; B: 3.6 °C; C: 2.1 °C; D: 3.9 °C; E: 2.1 °C; G: 1.5 °C; and H: 2.7 °C. Other UHII temperature equivalents shown in this figure are Davis: 2.1 °C; Woodland: 1.5 °C; Yuba City: 2.2 °C; Placerville: 1.8 °C; Auburn: 4.5 °C; and Roseville-Lincoln: 4.7 °C. Recall, again, that each tile is independent of the others, even though they are merged and plotted together on the same map shown in the figure.

In areas such as Auburn and Lincoln, the UHII can be elevated at times because of day/night variations in temperature of the natural surroundings, higher elevations (Auburn), or heat transport from upwind urban areas (Lincoln). The latter effect can be explained as follows. As the Taylor series expansion or the total derivative of temperature (*T*) tells us (equation 5-1), the change in air

temperature at any location on Earth (e.g., a point in an urban area) is the sum of (1) temperature change resulting from local heat generation or physical processes and (2) change resulting from transport of heat from upwind sources, e.g., upwind urban areas. The local heat generation could be from anthropogenic origins such as motor vehicles, buildings, etc., or resulting from heat fluxes caused by certain surface physical properties of roofs, pavements, roadways, and so on.

$$\frac{dT}{dt} = \frac{\partial T}{\partial t} + u \cdot \nabla T$$

(5-1)

The LHS of Equation 5-1 is total derivative for temperature, the first term on RHS is local temperature change, e.g., a result of local sources / sinks of temperature or heat generation, and the last term is advection of temperature from upwind areas, e.g., upwind urban land use or from some other sources of heat.

Thus, if the local heat-generation term were held constant at any given time interval, the change in local temperature becomes proportional to heat transported to the area which, in turn, is proportional to the time and distance an air mass travels over an urban area (for example) before arriving at the location of interest. Figure 5-7 shows an example depicting back trajectories arriving at three locations in the greater Sacramento region, computed based on the Altostratus Inc. AREAMOD / WRF approach. While wind direction varies from day to day and hour to hour, in this example a significant percentage of the approach directions is from the southwest, i.e., from the San Francisco Bay Area.

As seen in the figure, air masses typically travel over mostly crop, natural, and agricultural lands before arriving at AB617 community C, but other air masses travel slightly longer over urban areas before arriving at communities A and B. However, air masses arriving at Rocklin travel for almost 4 hours over urban areas before arriving there. Per Equation 5-1, this partly explains why the UHII is larger in communities A and B than in community C and also why it is significantly larger in the Rocklin area than in communities A and B.

As will be shown later in this report, this is also the reason why reducing the UHII (i.e., cooling) with mitigation measures, assuming region-wide deployment, also increases in this direction. That is, the cooling at Rocklin is generally greater than cooling at communities A and B, and greater than cooling at community C, because the air arriving at Rocklin, for example, is already cooler because of brushing over a longer upwind stretch of cooled urban areas.

Figure 5-7: Back trajectories example, July 16 – 31, 2015, arriving at 1400 PDT on 13 different days. The "4" marker is the position of the air mass four hours prior to arrival, i.e., its position at 1000 PDT. Urban areas are highlighted with brown or orange background.

Arriving AB617 communities "A","B" and community "C" at 1400 PDT on 13 different days

Arriving Rocklin area at 1400 PDT on 13 different days
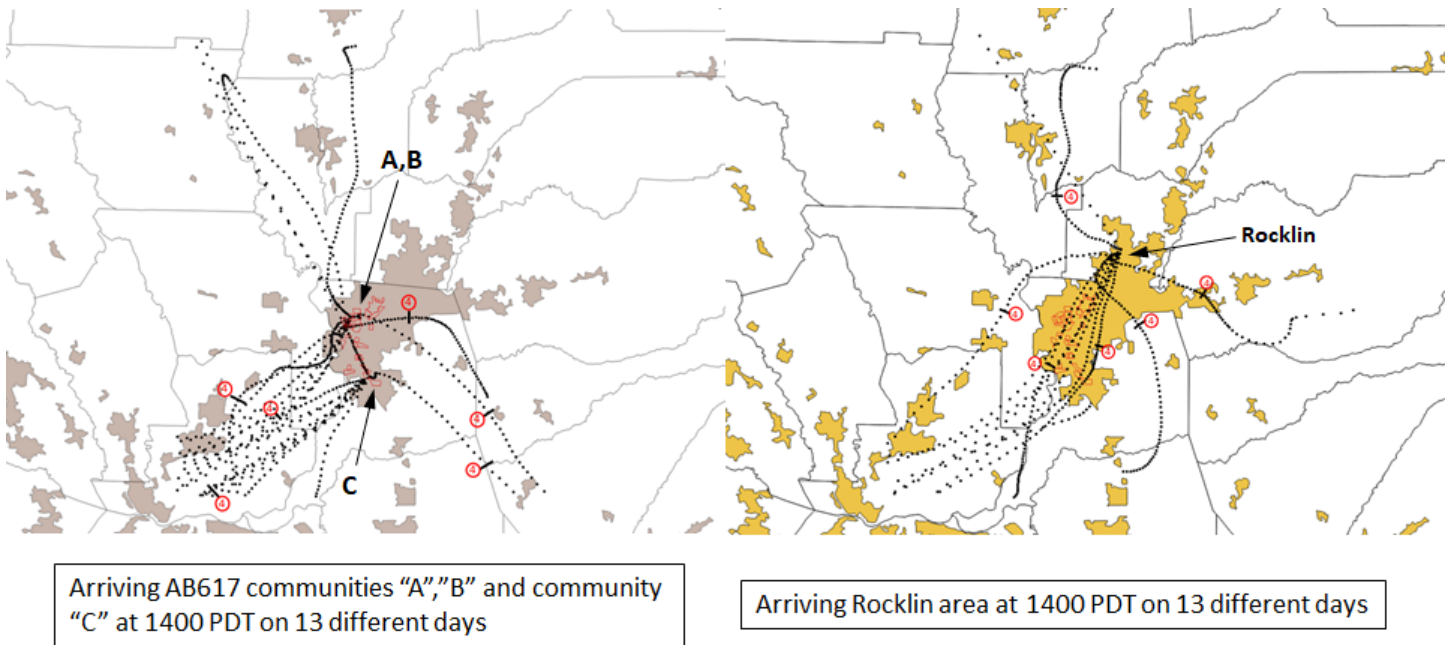
5.4 UHII VERSUS CES 3.0 AND CALTRANS FACILITIES AND ROADWAY PROJECTS

The UHII was computed based on current climate (2013 – 2016) and compared to the CalEnviroScreen (CES 3.0, OEHHA 2013) scores for various areas in the study region (this analysis will be discussed in more detail in Section 5.17). Figure 5-8a provides a qualitative comparison between the two datasets using the UHII for the period July 16 – 31, 2015 as an example. One can see that in the UHII tiles of Yuba City / Marysville, Woodland, Davis, and Placerville, there is a good agreement between the two, that is, the higher the CES score, the higher the UHII. In the larger Sacramento Metro area and in some areas near Auburn, the correlations are mixed because of the significant variability of temperature in the large region. Thus, whereas in the western half of this urban region there is positive correlation between UHII and CES 3.0 score, especially in the AB617 communities (outlined with black lines), in the eastern part, the UHII is high but the CES score is low. Thus, in terms of mitigation, this suggests, at least qualitatively, that the western half is more of a priority for deployment of urban cooling measures.

It is important to re-emphasize that Figures 5-6, 5-8a, and similar others, represent the UHII (in various tiles) and not the absolute temperature as a continuous field. As a result, one might be tempted to conclude, for example, that Auburn is hotter than some parts of Sacramento, say communities A, B, and D (see Figure 5-6). However, this can be misleading -- what the UHII Figures 5-6 and 5-8a show is that the temperature <u>difference</u> between urban and non-urban areas in Auburn is larger than the temperature <u>difference</u> between communities A, B, D, and some non-

urban areas in Sacramento. To clarify this further, Figure 5-8b shows the continuous temperature field (not UHII) for the region, averaged over the period 1400-2000 PDT during the same sample interval (July 16 – 31, 2015). The continuous temperature field shows that Auburn is actually cooler than communities A, B, and D (while its UHII is larger). Some differences are computed as an example (and listed in Figure 5-8b) relative to a single reference point for all areas in this domain, not tiled or wind-direction-dependent as with the UHII (this is done for illustration purposes only) and it can be seen that Auburn is 1.3 °C warmer than the reference point whereas communities A, B, and D are 3.2 to 3.6 °C warmer than that point. In other words, Auburn is about 2.1 °C cooler on average than communities A, B, and D even though its UHII is larger than that of these communities.

Another point that is emphasized throughout this report is that urban heat indicators (e.g., UHI or UHII) addressed in this study are air-temperature-based, not derived from skin surface temperature. Hence, the spatial patterns of urban heat presented in this report (e.g., Figure 5-8a) can differ significantly from those seen in other datasets, e.g., from satellite imagery.

Figure 5-8a: All-hours UHII (2015 int4) versus CES 3.0 scores (percentages). White circles are 0% and dark brown are 100% (highest) CES scores. The UHII ranges from white (0) to dark red (2176 DH/15 days), each step is 155 DH/15 days.
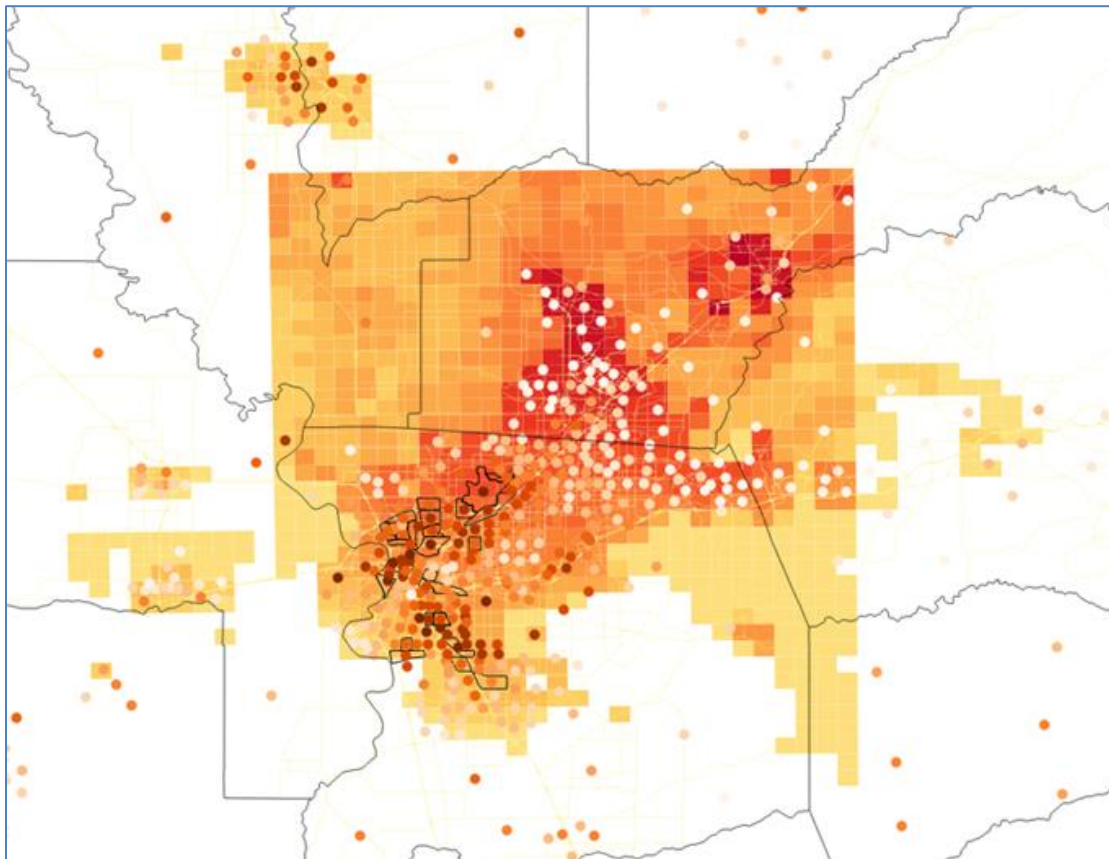
Figure 5-8b: Air-temperature field averaged over hours 1400 – 2000 PDT for July 16 – 31, 2015.
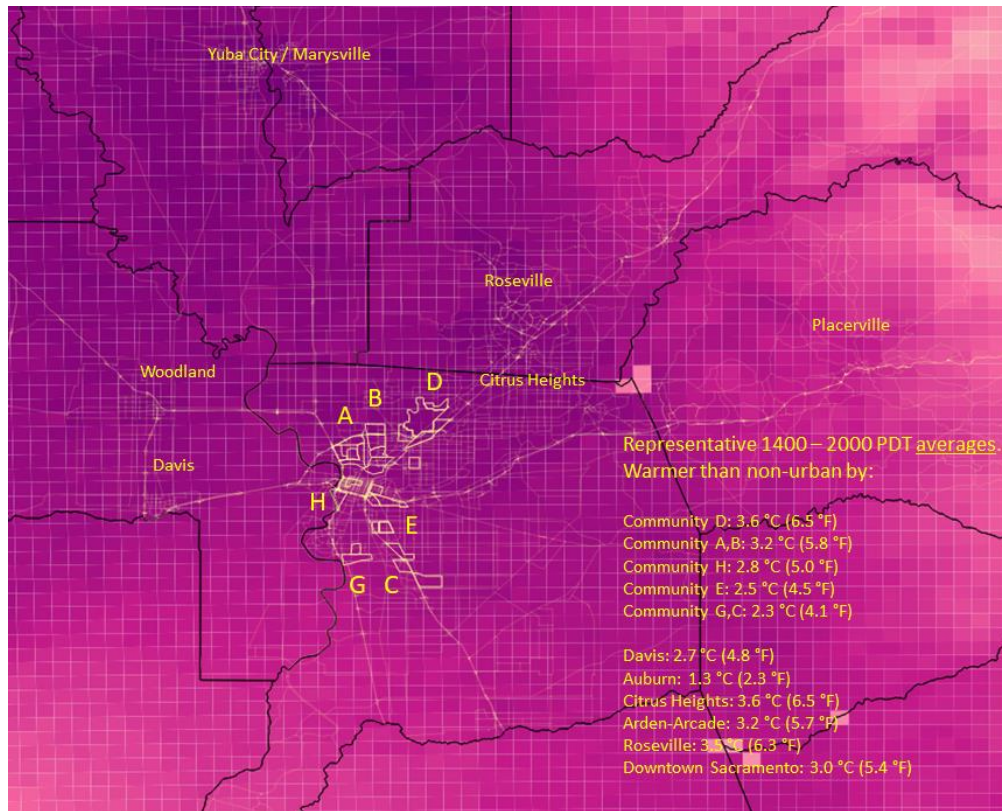
Furthermore, various attributes of urban heat and the UHII may be of interest to Caltrans, cities, local jurisdictions, and communities as they affect various aspects of paving, maintenance of roadways, aging of materials, and the transportation infrastructure in general. The impacts of UHI-mitigation measures on skin surface temperature (that can provide benefits during pavements' initial construction and in long-term maintenance and aging) will be discussed later in this report when presenting results from the fine-scale simulations. Here, in this section, a qualitative assessment of Caltrans's facilities and roadway projects locations in relation to the UHII is provided as an initial prioritization of where urban-cooling measures might need to be introduced first (among other considerations).

Those facilities and roadways that fall within the boundaries of the study domains are superimposed upon the UHII and shown in Figure 5-9. These include locations of airports, Amtrak stations, state highways, and traffic volume within the UHII tiles modeled in this region (tiles were defined above).

This, of course, is only a climate/meteorology basis for geographically prioritizing the mitigation measures, which is one of many considerations. In Figure 5-9, the all-hours UHII for July 16 – 31, 2015, is shown in the background (other years and intervals provide similar information). The UHII range in this example is from 0 to 2176 °C·hr per 15 days and each step change in color is

equivalent to 155 °C·hr per 15 days. Considering the information shown in Figure 5-9, a rough, initial ranking of Caltrans facilities can be formulated based on the UHII, from highest (most severe) to lowest (less severe):

≡ Airports rankings (highest to lowest UHII):

  o Auburn Municipal (AUN), Lincoln Regional (LHM), Sacramento McClellan (MCC), Rio Linda (L36), Sacramento International (SMF), Sacramento Executive (SAC), Sutter County (O52), Yuba County (MYV), Rancho Murieta (RIU), UC Davis (EDU), Yolo County (DWA), Placerville (PFV), and Woodland (O41);

≡ Amtrak stations rankings (highest to lowest UHII):

  o Auburn (ARN), Rocklin (RLN), Roseville (RSV), Marysville (MRV), Sacramento (SAC), State Capitol (SCS), Davis (DAV), Placerville (PCV), and Elk Grove (EKG);

≡ State highways rankings (highest to lowest UHII):

  o 65, 80, 244, 50, and 51; and

≡ Priorities based on traffic density (represented by the closeness of dots in the figure) versus the UHII and the main routes in the region.

Figure 5-9: UHII versus Caltrans roadways and facilities locations. Data sources for facilities and roadway locations: Caltrans 2019.
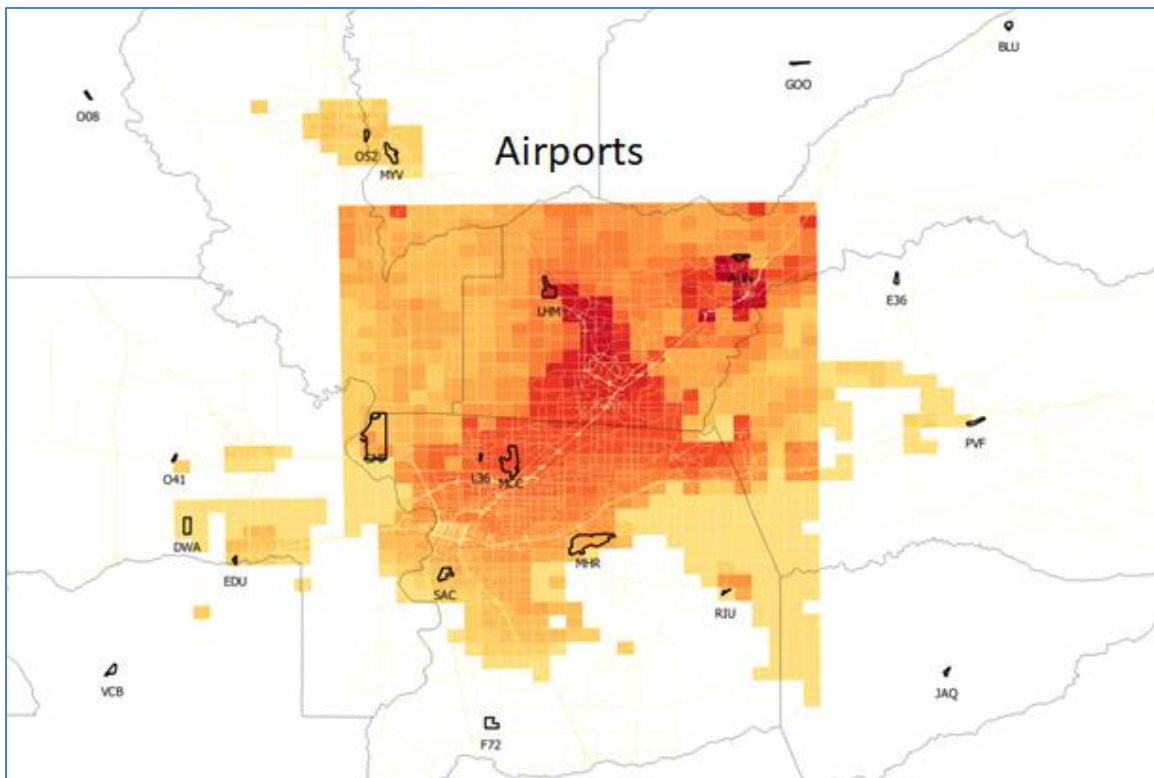
Figure 5-9, continued.
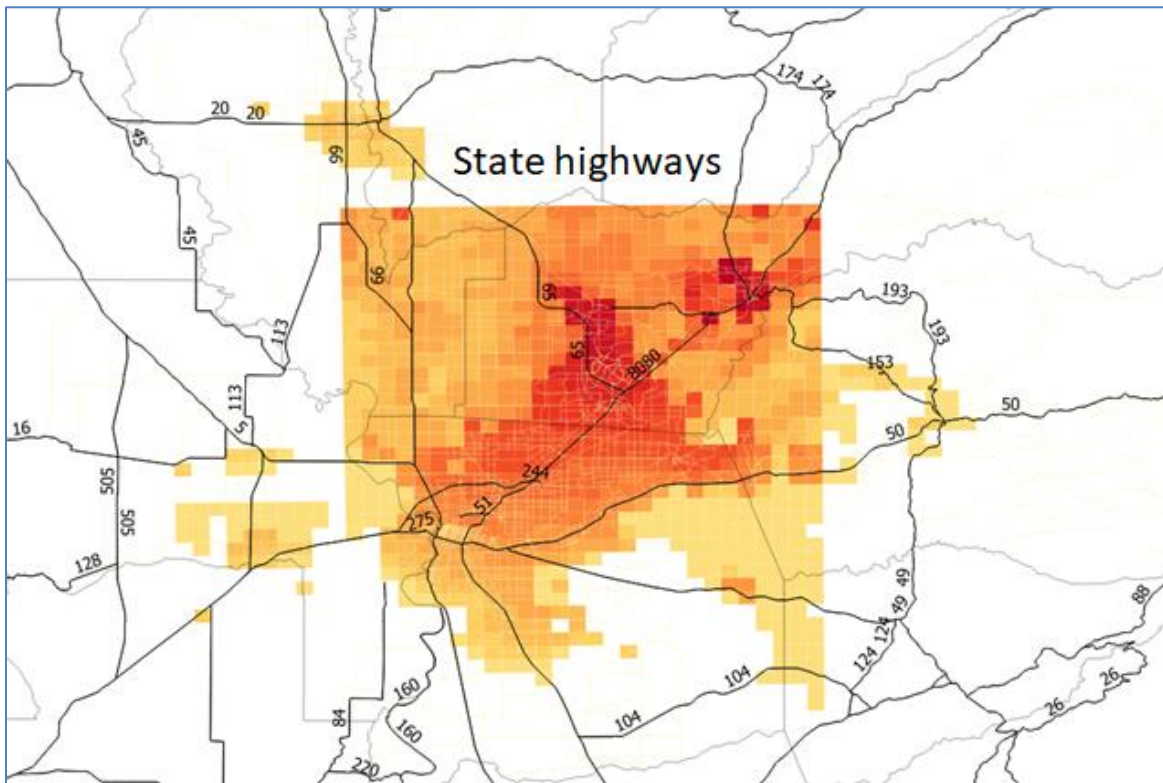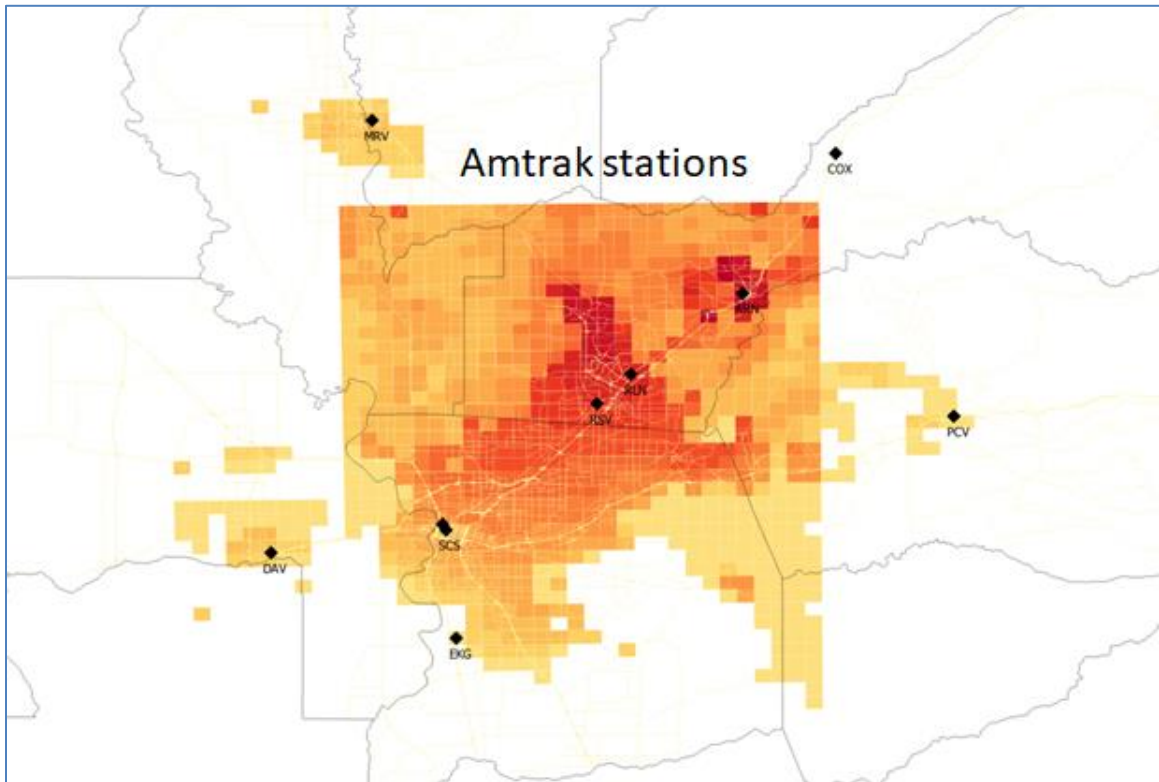
Figure 5-9, continued.
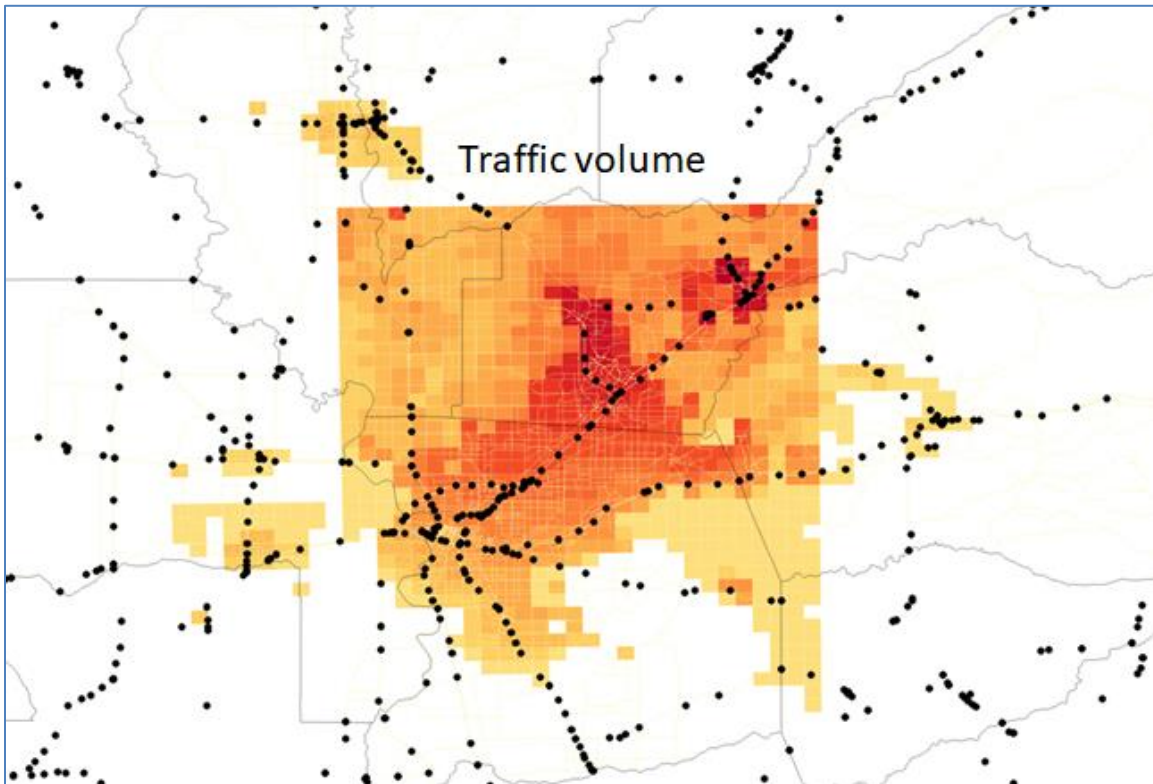
5.5 DEFINITION OF MITIGATION MEASURES AT THE REGIONAL SCALE (2 km)

At the 2 km level, i.e., the Capital-region domain, the mitigation measures modeled in this study included (1) albedo modifications, (2) increases in canopy cover, and (3) a combination of measures. Note that at the community scale, 500-m level, additional measures were modeled as will be discussed later in this report.

Thus, at the regional scale, the following scenarios were defined:

case10:   Small increase in albedo -- an increase of 0.15 on impervious surfaces. At this scale (2-km resolution), there is no distinction between roof and pavement albedo changes. Difference between this case and the base case is labeled "del10".

case20:   Larger increase in albedo -- an increase of 0.25 on impervious surfaces. Difference between this case and the base case is labeled "del20".

case01:   A first-level increase in canopy cover, about 2.5 – 3 million trees throughout the entire 6-counties region, which is about a 12% increase in cover, i.e., an additional 12% of a cell's area. Previous studies, e.g., Simpson and McPherson (2007) and Taha et al. (2011, 2015) estimated that the established urban-forest canopy in

Sacramento is ~14% and that many newer, urbanizing areas have canopy cover that needs to be brought up from ~5% to 14%, hence the 12% increase. To put this increase into context, in a previous study by Altostratus Inc. for the SMAQMD, a control measure of 650,000 replacement trees in the Sacramento Federal Non-Attainment area (SFNA) was assumed (Taha et al. 2011, 2015). Difference between this case and the base case is labeled "del01".

case02:   A second (and extreme) level of increase in canopy cover (~20% - 25% cover increase or adding 5 – 6 million trees throughout the entire 6-counties Capital region, i.e., an additional 20% of a cell's area). This is not a realistic scenario nor considered feasible at this time, and thus not used in the combined scenario (case31, below) or some analysis later in this report. However, this scenario is included as a test for potential upper-bound effects per suggestions from local tree organizations. Compared to findings from many other studies, this increase is still smaller than what is typically proposed (canopy increase of 40%) to exert a significant impact on air temperature. Difference between this case and the base case is labeled "del02".

case31:   This is a realistic-high case of combined albedo and canopy-cover increases. The increase in albedo is slightly larger (+0.35) than in case20 and the increase in canopy cover corresponds to that of case01. Difference between this case and the base case is labeled "del31".

In addition, and per a request from the City of Sacramento, several intermediate levels of canopy cover were also modeled at the 2-km scale to evaluate the incremental effects of canopy growth (or additional canopy) on air temperature and water usage. Studies by the City of Sacramento and Davey Inc. (Davey 2018), estimate that the canopy cover increases by about 1% per year. Thus, as a crude estimate, the assumptions of going from current cover to ~25% increase would take some 25 years (per literature, a large tree is 65 m^2 in crown area; medium tree 30 m^2; and a small tree 10 m^2).

These additional scenarios mesh with case01 and case02 (defined above) as follows:

- case01A: increase of +3.4% of cell area
- case01B: increase of +7.7% of cell area
- **case01**:   increase of +12.0% of cell area
- case02A: increase of +16.3% of cell area
- case02B: increase of +20.6% of cell area
- **case02**:   increase of +25.0% of cell area

Thus, the final (maximum) amount of increase in canopy cover (case02) corresponds to +25% which is in line with estimates made by the Sacramento Tree Foundation for a total target canopy

cover of 35% (Torin Dunnavant, SacTree, personal communication). That is, an increase of 25% (of the area) in canopy cover added to an existing cover of between 4% and 15%, will bring the total to 35%. However, as seen above, an increase in cover larger than case01 (+12%) is considered rather too large to be practically implementable at this time and, thus, in some of the analysis in this report, cases larger than case01 (e.g., case02) are not discussed.

The increase in canopy cover in case01 can also be considered a realistic upper bound because it will bring the total canopy cover to about 14% which is the average of the established cover in Sacramento (Simpson and McPherson 2007). In the future, concerted efforts might be followed to reach canopy cover that is similar to cases 02A, 02B and case02.

In terms of albedo increases, e.g., implementation of cool surfaces, the levels assumed here (case10 and case20) are realistic and reasonable – they translate into the surface-specific increases in albedo as summarized in Table 5-2.

Table 5-2: Upper bounds for realistic surface-specific increases in albedo

	Case10 max	Case20 max
Residential roof	+ 0.10	+ 0.25
Commercial roof	+ 0.20	+ 0.30
Roadway	+ 0.15	+ 0.20
Sidewalks/paved	+ 0.10	+ 0.20
Parking lots	+ 0.15	+ 0.25

In Figure 5-10, the translations of surface-specific albedo changes from Table 5-2 to gridded values of albedo increase at the 2-km level are summarized for 495 urban cells in D04 (the 6-counties Capital region domain). As seen in this figure, the albedo changes at 2-km level for case10 are mostly between +0.02 and +0.08, with a small number of cells affected by albedo increases of greater than 0.08. Case20 has a similar distribution except for roughly double the amount of increase in albedo. These are realistic levels of increase and represent materials already found in this region and used in current construction and building practices. Note that the scenarios modeled at finer scales (500-m level) are described later in this report.

Figure 5-10: Translation of surface-specific albedo increase into grid-level increase.
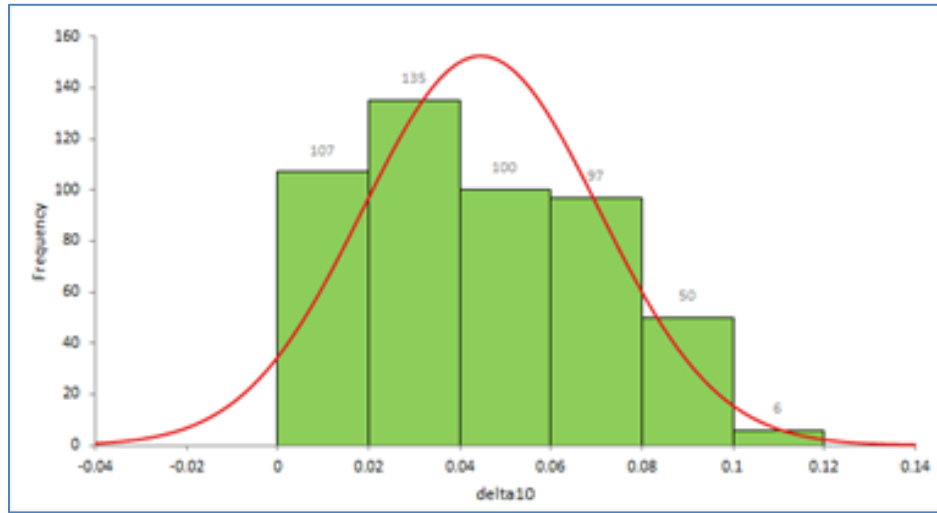
In order to answer some oft-posed questions such as (1) "how many roofs do we need to modify?" or (2) "how many trees do we need to plant?", the following very rough estimates are provided for the 2-km domain (D04). Caveats to keep in mind are the various assumptions made in the following discussion. For the 500-m grids, different project-specific numbers are provided and discussed later in this report.

Domain D04 consists of a total of 5184 cells. Out of these, 3154 cells have an urban fraction greater than zero, but the cells where UHI mitigation measures are actually applied (where urban fraction is greater than 30%) number only 495 cells, in 2015, and 495+360 cells in 2050. Recall that case10, case20, and case31 increase impervious albedo (of roofs and pavements) by +0.15, +0.25, and +0.35, respectively, as discussed above.

The total impervious area in 2015 (based on NLCD 2011 and USGS Level-II data discussed in Section 2) in the 495 urban cells is 630 km^2, which is about 31% of the total area of those 495 cells (and 3% of the entire domain D04). At the 2-km level, it is realistic to assume that, on average, half of the impervious area is pavements and roadways and the other half is roofs -- which is supported by examination of aerial photographs and Google Earth PRO imagery, as well as studies by Akbari et al. (1999) and Rose et al. (2003).

Roofs

Thus 315 km^2 of roof area is available for modification (to varying degrees) in the 6-counties Capital region. Assuming 60% of the total roof area is residential and that a residential (housing unit) roof is 200 m^2 on average, this translates into 945,000 housing units throughout domain D04. A comparison with the number of housing units per census information (census.gov) in Table 5-3 suggests that almost all of the housing units must use cool roofs, if a low level of albedo increase is applied. In other words,

A. to achieve <u>case10</u>, 945,000 roofs (which is nearly all of the residential roofs) in the 6-counties Capital region need to have their albedos increased by a very modest amount of +0.15, or half of the residential roofs will need their albedos increased by +0.30, or one third of residential roofs will need to increase their albedo by +0.45 (all of these scenarios assume that pavements and commercial roof albedos are increased by +0.15). This scenario translates into an albedo increase of +0.046 over the 395 urban cells and +0.0045 over domain D04.

B. To achieve <u>case20</u>, 945,000 roofs in the 6-counties Capital region need to have their albedos increased by +0.25, or half of the residential roofs will need their albedos increased by +0.50 (these two scenarios assume that pavements and commercial roof albedos are increased by +0.25). This scenario translates into an albedo increase of +0.077 over the 395 urban cells and +0.0075 over the regional D04 domain.

C. To achieve case31, 945,000 roofs in the 6-counties Capital region need to have their albedos increased by +0.35, or half of the residential roofs will need their albedos increased by +0.70 (these scenarios assume that pavements and commercial roof albedos are increased by +0.35). This scenario translates into an albedo increase of +0.1 over the 395 urban cells and +0.01 over the D04 domain.

It should be noted that the effects of, say, doubling or tripling the increase in roof albedo while simultaneously halving or reducing the affected roof area to one third is nonlinear. However, the linearity assumption is made here to provide very rough estimates in answering the above question.

Table 5-3: Housing units in the Capital region counties

County	No. of housing units
Sacramento	564,349
El Dorado	89,286
Placer	159,667
Yuba	28,225
Sutter	34,204
Yolo	76,916
TOTAL	952,647

Pavements

In terms of roadways and highways, assuming an overall average road width of 30 m across all types (including curbs, where they exist), then 315 km^2 (from above NLCD-based impervious cover calculations) is equivalent to 10,500 km of roadways available for modification (note:

Altostratus Inc.

typical widths of freeways: 60 m, typical widths of streets and avenues in commercial areas: 25 m, and typical widths of roadways in residential areas: 18 m).

Compare with the following:

- Total CA roadways: 631,000 km
- CA public roads: 282,000 km
- SAC DOT roadways: 3,520 km (in Sacramento County only, not including the other 5 counties in the Capital region)

Or, alternatively, the roadways albedo (for case01) could be increased by 0.3 over 5,250 km in the 6-counties Capital region.

Tree cover

As for the needed tree cover, or equivalent number of trees, it can be estimated very crudely as follows (for the 2-km domain):

- case01: +7300 trees per 4 km^2, which equates to about +12% of cell area subject to forestation. This corresponds to up to 3.6 M new trees, depending on size, throughout the 6-counties Capital region.

- case02: + 12000 to +15300 trees per 4 km^2, which is equivalent to +20% to +25% of cell area subject to forestation. This translates into 5 – 7 M new trees, depending on size, throughout the 6-counties Capital region. Again, case02 is considered a relatively extreme scenario in this analysis.

5.6 SELECTING UHI-MITIGATION MEASURES: POSSIBLE IMPACTS ON BVOC EMISSIONS, UV ALBEDO, MIXING, AND THERMAL / VISUAL ENVIRONMENT

As with many environmental control measures, the implementation of urban-cooling strategies can in some cases result in unintended consequences, that is, produce both positive and negative effects (Taha 2013a). The opposing impacts can be seen in meteorology (e.g., cooling and warming), emissions (decrease or increase), and in air quality (e.g., decrease and increase in formation and/or transport of ozone or particulate matter). In this section, factors to consider when designing or selecting UHI-mitigation measures are discussed.

5.6.1 Albedo increase and UV radiation

Taha (2005, 2007) discussed the air-quality effects of changes in UV albedo in detail. Here, some highlights are presented but largely follow that discussion. For the purposes of implementing cool surfaces, the albedo of interest is in the range of 0.28 to 2.8 μm, that is, "solar" albedo. By definition, this includes radiation in the UV, visible, and NIR spectra. Thus, in addition to the main effect of changing visible and NIR albedo, there is the possibility of inadvertently increasing UV

albedo as a result of implementing measures of cool surfaces (Fallmann et al. 2016; Epstein et al. 2017). This may be of concern because the energy in the UV wavelength can influence some of the important photodissociation reactions, e.g., those of NO_2, O_3, and PAN (peroxyacetyl nitrate), that can have potential negative implications, i.e., increasing ozone concentrations. However, in reality, the proposed measures of cool roofs and pavements may have little or no effect on UV albedo as many reflective materials incur no increase in albedo in that wavelength range. In fact, some high-albedo materials actually have lower UV albedo than conventional materials (Berdahl et al. 2002; Berdahl and Bretz 1997, Levinson et al. 2007).

Regardless of whether or not reflective materials actually change UV albedo, the effects of UV radiation changes (e.g., UV-B) on ozone formation are not easy to discern. Increased UV-B in areas with high NOx emissions (e.g., urban and industrial areas) can increase ozone formation (Gery et al. 1988, Thompson 1992, 1991) and the opposite can be true in areas with low NOx emissions, e.g., suburban or rural regions (Liu and Trainer 1988).

The issue of potential UV albedo increase actually involves more than just how much UV radiation is modified; it also involves actinic irradiance and species-specific characteristics such as quantum yield and absorption cross sections (all of which determine the rates of photodissociation for a particular chemical species). But the focus here is on albedo because it is the one parameter that is changing from one surface-modification scenario to another.

Generally, the UV spectrum is defined as UV-A (0.315-0.400 μm), UV-B (0.280-0.315 μm), and UV-C (0.100-0.280 μm). Stratospheric oxygen absorbs UV radiation in the range 0.17-0.24 μm and photodissociates to produce ozone, via:

$$O_2 + h\nu \rightarrow 2\ O\ (^3P) \qquad\qquad (5\text{-}2)$$

$$O\ (^3P) + O_2 + M \rightarrow O_3 + M \qquad\qquad (5\text{-}3)$$
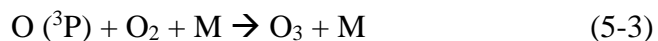
where M = air = N_2, O_2, etc. This leaves mostly UV-B and UV-A radiation to reach the troposphere because the ozone produced in the above process absorbs UV at and below 0.29 μm. Thus, in the troposphere, wavelengths of relevance to photochemical reactions are 0.30 μm and longer (Seinfeld and Pandis 1998) but still short enough to contain part of the high energy spectrum.

Of the smog-related photochemical reactions in the polluted urban boundary layer, photodissociation pathways of importance to the strategy of increasing albedo are mainly those of NO_2, O_3, and PAN. NO_2 absorbs at wavelengths of 0.45 μm or shorter, but because there is little UV radiation reaching the troposphere at or shorter than 0.29 μm, the theoretical critical UV range of interest for NO_2 is thus between 0.30 and 0.45 μm (Cooper and Alley 1994). Further narrowing this range is the fact that 90% of the NO_2 molecules absorb UV energy below 0.4 μm (Stern et al. 1984) and as a result, the practical range of importance for NO_2 photodissociation is 0.3 to 0.37

μm (Seinfeld 1975). For O_3, the critical UV wavelength range is 0.315 μm or shorter (Harrison 1990) and for PAN, the cutoff is 0.35 μm or shorter (Seinfeld and Pandis 1998). Thus, the inclusive range of 0.3 to 0.37 μm is the overall "envelope" that needs to be considered when modifying surface albedo. This envelope is shown by the area to the left of the vertical red line (and red arrow) in Figure 5-11.

The information shown in Figure 5-11 indicates that it is possible to select reflective materials that do not increase UV albedo, e.g., compare curves B, D, and E that show increase in overall albedo without much changing (if not decreasing) the UV albedo. Furthermore, some high-albedo materials reflect less in the UV range than their low-albedo counterparts, as seen in Figure 5-12. For example, if a cedar shake roof is replaced by either a TiO_2-painted roof or a limestone-based product, the UV albedo actually decreases from about 0.58 to 0.15 while the overall albedo increases from about 0.35 to 0.7.

In Figure 5-11, material A has a very low albedo (~0.05). By moving to material B or C, the overall albedo increases to about 0.25 and 0.60, respectively, whereas the changes in UV albedo are relatively smaller, e.g., from 0.05 to 0.06 or 0.09, respectively. However, materials D and E have much higher solar albedos, e.g., 0.7 and 0.82, respectively, but their UV albedos are similar to (unchanged from) that of material B. In fact, the UV albedo of materials D or E can be lower than that of B. On the other hand, there could be high-albedo materials such as F and G (about 0.7) that also have high UV albedo, e.g., up to about 0.4. Thus, from a photochemistry perspective, careful selection of reflective materials is critical, but it is very possible to select high-albedo materials without altering the UV albedo.

Some earlier studies by Berdahl and Bretz (1997) provided reflectance measurements and albedo values for a variety of materials (some examples shown in Table 5-4). The materials presented in this table are of similar structure, construction, and texture but different albedo. As seen in the table, it is possible to increase solar albedo in the visible and NIR ranges without changing the UV albedo by any significant amount. In some cases, such as the single-ply example, UV albedo actually decreases while visible and NIR albedos increase. For asphalt shingles, there is no change in UV albedo, while overall albedo increases from 0.08 to 0.21.

In summary, it is possible to increase visible and NIR albedo without increasing UV albedo. Thus, it is possible to maximize the expected benefits from lower air temperatures without the inadvertent photochemical effects that might be associated with increases in UV albedo. This is an implicit assumption made in developing albedo scenarios in this modeling study. That is, in the meteorological simulations of modified albedo scenarios, solar albedo is increased whereas UV albedo is assumed unchanged in the photochemical simulations. This is a reasonable and conservative assumption because, as seen above, we could actually decrease UV albedo and incur further air-quality benefits.

Figure 5-11: Spectral reflectance of selected materials based on measurements by Berdahl et al. (2001) and Berdahl and Bretz (1997). The vertical black lines delineate the boundaries of the UV, visible, and NIR ranges, also shown with two-headed arrows at the bottom of the figure. The vertical red line (at left) and arrow show the UV range of practical relevance to photodissociation (in terms of albedo modifications). Other labels are discussed in the text. Figure source: Taha (2004).
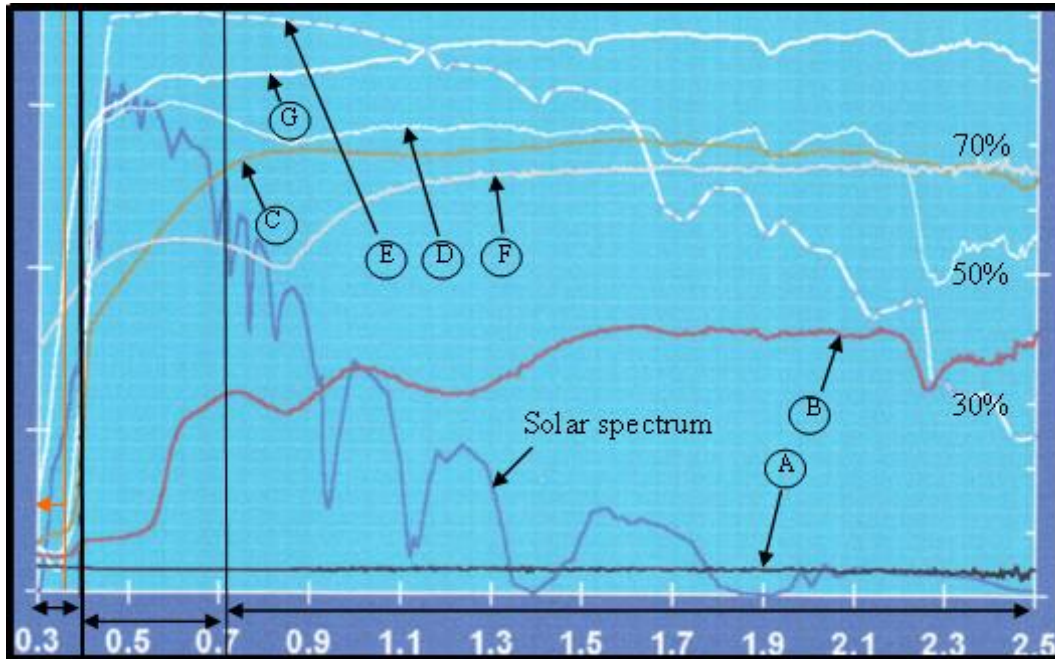
Figure 5-12. Spectral reflectivity characteristics of selected roofing materials. A leaf is also included for comparison. Source: Levinson et al. (2004).
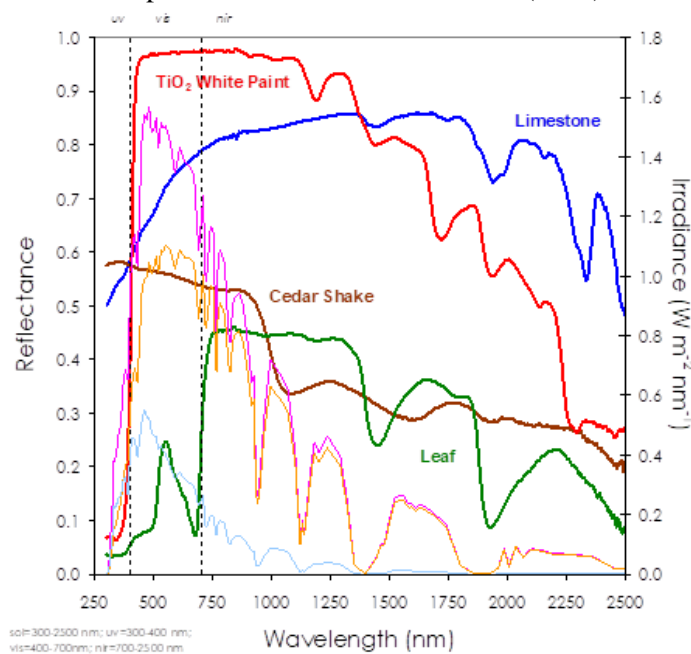
Table 5-4. Albedo of selected materials (commercial product names are not given). Based on Berdahl and Bretz (1997).

	Albedo			
	Solar	UV	VIS	NIR
Coatings (in order of increasing solar albedo)				
Product 1	0.74	0.10	0.79	0.76
Product 2	0.83	0.11	0.89	0.85
Product 3	0.85	0.12	0.90	0.87
Single ply membranes (in order of increasing solar albedo)				
Product 1	0.77	0.25	0.80	0.79
Product 2	0.80	0.19	0.87	0.79
Product 3	0.83	0.14	0.91	0.82
Asphalt shingles (in order of increasing solar albedo)				
Product 1	0.08	0.05	0.08	0.09
Product 2	0.08	0.06	0.08	0.09
Product 3	0.12	0.06	0.12	0.12
Product 4	0.20	0.06	0.22	0.19
Product 5	0.21	0.06	0.24	0.21

5.6.2 Vegetation-cover increase and biogenic hydrocarbon emissions

Vegetation cover affects the soil-atmosphere environment via several complex pathways. Stated in the simplest terms, the effects of vegetation canopies can be seen in their impacts on (1) air and surface temperatures, (2) wind speed and turbulent kinetic energy, (3) emissions of biogenic volatile organic compounds (BVOC), (4) dry and wet deposition of air pollutants, and (5) atmospheric humidity.

All of these pathways affect air quality and ozone production via different mechanisms and to varying degrees. Here, we discuss one issue of relevance to photochemical production of ozone, which is the potential increase in BVOC emissions, i.e., those of isoprene and monoterpenes, from increasing urban vegetation cover. In general, the guidance is to use non- or low-emitting vegetation species to avoid negative air-quality consequences. In an earlier modeling study, for example, Taha (1996) showed that for the Los Angeles Basin, tree species emitting at a rate higher than 2 μg g^{-1} hr^{-1} (per dry leaf mass) of isoprene and/or monoterpenes could bring adverse effects on air quality when introduced in large numbers (millions of trees). That study also pointed out that numerous zero-emitting vegetation species exist that could be used in such applications (Benjamin et al. 1996). Thus, when implementing urban forestation strategies, careful selection of tree species is an important factor.

Furthermore, Taha et al. (2015) modeled the effects of converting 650,000 current-mix trees in the Sacramento Federal non-attainment area for ozone (SFNA) into low emitters of BVOC as a voluntary or emerging control measures for maintenance of the 8-hour ozone standard in the area. The results indicated that the daily reductions in ozone from species replacement alone can reach

up to 3 ppb. The 8-hour average peak ozone is reduced by 2%. If canopy cooling effects were also accounted for, the air-quality impacts could be 10 times as large as those of only replacing the tree species (emissions control measure).

In this modeling study, and as discussed in later sections of this report, the additional vegetation introduced in urban areas is assumed to be non-emitting or emitting less than 2 $\mu g \ g^{-1} \ hr^{-1}$ of isoprene and/or monoterpenes (Taha 1997, 2017). In this context, Table 5-5 provides some general information on emissions rates for consideration when implementing urban forestation in the Sacramento region. The air quality ratings in the table are based on the ozone forming potential of each species (Simpson and McPherson 2007). It is also assumed that the planted species do not vary much in albedo from the current species (0.18 – 0.22 albedo).

Table 5-5: BVOC emission rates for species with "excellent", "good", and "fair" air quality ratings, per Simpson and McPherson (2007), US EPA, and Sacramento Tree Foundation (2015).

Tree Common Name	Tree Scientific Name	Isop g tree^{-1} day^{-1}	Terp g tree^{-1} day^{-1}	Air Quality Rating
Bottle tree	Brachychiton populneus	0.0	0.0	Excellent
Cape chestnut	Calodendrum capense	0.0	0.0	Excellent
Chitalpa	Chitalpa x tashkentensis 'Morning Cloud'	0.0	0.0	Excellent
Chitalpa	Chitalpa x tashkentensis 'Pink Dawn'	0.0	0.0	Excellent
Fan-Tex ash	Fraxinus velutina 'Rio Grande'	0.0	0.0	Excellent
Canary Island pine	Pinus canariensis	0.0	0.0	Excellent
Aleppo pine	Pinus halepensis	0.0	0.0	Excellent
Italian stone pine	Pinus pinea	0.0	0.0	Excellent
Fern pine	Podocarpus gracilior	0.0	0.0	Excellent
Evergreen pear	Pyrus kawakamii	0.0	0.0	Excellent
South African sumac	Rhus lancea	0.0	0.0	Excellent
Frontier elm	Ulmus parvifolia 'Frontier'	0.0	0.0	Excellent
Bottle tree	Brachychiton populneus	0.0	0.0	Excellent
Calabrian pine	Pinus brutia	0.0	0.0	Excellent
Afghan pine	Pinus eldarica	0.0	0.0	Excellent
Southern live oak	Quercus virginiana	0.0	0.0	Excellent
Oregon ash	Fraxinus latifolia	0.0	0.0	Excellent
Interior live oak	Quercus wislizenii	0.0	0.0	Excellent
Columnar Red Maple	Acer platanoides 'Crimson Sentry'	0.0	0.0	Excellent
European hackberry	Celtis australis	0.0	0.0	Excellent
Eastern redbud	Cercis canadensis	0.0	0.0	Excellent
Crape myrtle	Lagerstroemia indica	0.0	0.0	Excellent
Flowering pear	Pyrus calleryana	0.0	0.0	Excellent
Capital Pear	Pyrus calleryana 'Capital'	0.0	0.0	Excellent
Chanticleer Pear	Pyrus calleryana 'Chanticleer'	0.0	0.0	Excellent
Blue oak	Quercus douglasii	0.0	0.0	Excellent
Bur oak	Quercus macrocarpa	0.0	0.0	Excellent
Upright English oak	Quercus robur 'Fastigiata'	0.0	0.0	Excellent

Tree Common Name	Tree Scientific Name	Isop g tree⁻¹ day⁻¹	Terp g tree⁻¹ day⁻¹	Air Quality Rating
Zelkova	Zelkova serrata	0.0	0.0	Excellent
Narrow zelkova	Zelkova serrata 'Musashino	0.0	0.0	Excellent
Princeton elm	Ulmus americana 'Princeton'	0.0	0.0	Excellent
Valley Forge elm	Ulmus americana 'Valley Forge'	0.0	0.0	Excellent
Accolade elm	Ulmus japonica x wilsoniana 'Accolade'	0.0	0.0	Excellent
Washington hawthorn	Crataegus phaenopyrum	0.0	0.0	Excellent
Japanese crabapple	Malus floribunda	0.0	0.0	Excellent
Prairie fire crabapple	Malus hybrid 'Prairifire'	0.0	0.0	Excellent
Robinson crabapple	Malus hybrid 'Robinson'	0.0	0.0	Excellent
Bechtel crabapple	Malus ioenis 'Plena'	0.0	0.0	Excellent
Japanese Flowering Cherry	Prunus serrulata 'Amanogawa'	0.0	0.0	Excellent
Flowering plum	Prunus cerasifera	0.0	0.0	Excellent
Australian willow	Geijera parviflora	0.0	0.0	Excellent
Bronze loquat	Eriobotrya deflexa	0.0	0.0	Excellent
Loquat	Eriobotrya japonica	0.0	0.0	Excellent
Red leaf photinia	Photinia x fraseri	0.0	0.0	Excellent
Sweet bay	Laurus nobilis	0.0	0.1	Excellent
Saratoga sweetbay	Laurus nobilis 'Saratoga'	0.0	0.1	Excellent
Sassafras	Sassafras albidum	0.0	0.1	Excellent
Trident maple	Acer buergerianum	0.0	0.1	Excellent
Paperbark maple	Acer griseum	0.0	0.1	Excellent
Shantung maple	Acer truncatum	0.0	0.1	Excellent
Chinese wingnut	Pterocarya stenoptera	0.0	0.1	Excellent
Cork oak	Quercus suber	0.0	0.1	Excellent
Maidenhair tree	Ginkgo biloba	0.0	0.1	Excellent
Male ginkgo	Ginkgo biloba 'Fairmont'	0.0	0.1	Excellent
Male ginkgo	Ginkgo biloba 'Princeton Sentry'	0.0	0.1	Excellent
Dawn redwood	Metasequoia glyptostroboides	0.0	0.1	Excellent

Tree Common Name	Tree Scientific Name	Isop g tree⁻¹ day⁻¹	Terp g tree⁻¹ day⁻¹	Air Quality Rating
Desert willow	Chilopsis linearis	0.0	0.3	Good
Chinese fringe tree	Chionanthus retusus	0.1	0.0	Good
Hedge maple	Acer campestre	0.0	0.4	Good
Norwegian Sunset maple	Acer saccharum ssp. nigrum	0.0	0.4	Good
Tartarian maple	Acer tartaricum	0.0	0.4	Good
Norwegian Sunset maple	Acer truncatum 'Norwegian Sunset'	0.0	0.4	Good
Pacific Sunset shantung maple	Acer truncatum 'Pacific Sunset'	0.0	0.4	Good
Deodar cedar	Cedrus deodara	0.0	0.5	Good
Japanese snowbell	Styrax japonicus	0.2	0.1	Good
Japanese lilac tree	Syringa reticulata 'Ivory Silk'	0.2	0.1	Good
Chaste tree	Vitex agnus-castus	0.2	0.1	Good
Red maple	Acer rubrum	0.0	0.5	Good
Bohall Maple	Acer rubrum 'Bohall'	0.0	0.5	Good
Columnar red maple	Acer rubrum x freemani 'Armstrong'	0.0	0.5	Good
California Incense cedar	Calocedrus decurrens	0.0	0.6	Good

Altostratus Inc.

Tree Common Name	Tree Scientific Name	Isop g tree⁻¹ day⁻¹	Terp g tree⁻¹ day⁻¹	Air Quality Rating
California buckeye	Aesculus californica	0.3	0.1	Good
Bailey acacia	Acacia baileyana	0.0	0.8	Good
Southern magnolia	Magnolia grandiflora	0.0	0.9	Good
Saucer magnolia	Magnolia soulangiana	0.0	0.9	Good
Kentucky coffee tree	Gymnocladus dioica	0.3	0.1	Good
Katsura tree	Cercidiphyllum japonicum	0.4	0.1	Good
His majesty amur cork tree	Phellodendron amurense 'His Majesty'	0.4	0.1	Good
Macho amur cork tree	Phellodendron amurense 'Macho'	0.4	0.1	Good
Eye stopper amur cork tree	Phellodendron lavallei 'Longenecker'	0.4	0.1	Good
True Shade locust	Gleditsia tricanthos inerm	0.4	0.1	Good
Japanese pagodatree	Sophora japonica	0.4	0.2	Good
Valley oak	Quercus lobata	0.5	0.0	Good
Pistache	Pistacia chinensis	0.0	1.2	Good
Brisbane box	Lophostemon confertus	0.5	0.1	Good
Briotti red horse chestnut	Aesculus x carnea 'Briotti'	0.5	0.2	Good
Italian alder	Alnus cordata	0.5	0.2	Good
River birch	Betula nigra	0.5	0.2	Good
Japanese white birch	Betula platyphylla japonica	0.5	0.2	Good
Pyramidal European hornbeam	Carpinus betulus 'Fastigiata'	0.5	0.2	Good
Bald Cypress	Taxodium distichum	0.0	1.5	Good
Tulip tree	Liriodendron tulipifera	0.4	0.8	Good
Hardy rubber tree	Eucommia ulmoides	0.7	0.2	Good
Chinese parasol tree	Firmiana simplex	0.7	0.2	Good
Littleleaf linden	Tilia cordata	0.7	0.2	Good
Cajeput tree	Melaleuca quinquenervia	0.8	0.1	Good
Pink trumpet tree	Tabebuia impetiginosa	0.0	2.1	Good
Tristania var. 'Elegant'	Tristania laurina 'Elegant'	0.9	0.1	Good
Mountain silverbell	Halesia monticola	1.0	0.3	Good
Japanese Stewartia	Stewartia pseudocamellia	1.0	0.3	Good

Tree Common Name	Tree Scientific Name	Isop g tree⁻¹ day⁻¹	Terp g tree⁻¹ day⁻¹	Air Quality Rating
Tupelo	Nyssa sylvatica	1.6	0.5	Fair
American hophornbeam	Ostrya virginiana	1.6	0.5	Fair
Carob tree	Ceratonia siliqua	1.6	0.7	Fair
California buckeye	Aesculus californica	1.8	0.5	Fair
Red oak	Quercus rubra	2.2	0.4	Fair
Sawtooth oak	Quercus acutissima	2.3	0.1	Fair
Shumard oak	Quercus shumardii	2.3	0.1	Fair
Goldenrain tree	Koelreuteria bipinnata	2.4	0.0	Fair
Chinese flame tree	Koelreuteria paniculata	2.4	0.0	Fair
California sycamore	Platanus racemosa	2.7	0.0	Fair
Coast redwood	Sequoia sempervirens	0.0	6.4	Fair
European beech	Fagus sylvatica	2.7	0.1	Fair
Silver linden	Tilia tomentosa	2.5	0.7	Fair
American linden	Tilia americana	2.5	0.7	Fair

Altostratus Inc.

Willow oak	Quercus phellos	3.0	0.0	Fair
Southern live oak	Quercus virginiana	3.0	0.1	Fair
Scarlet oak	Quercus coccinea	3.0	0.7	Fair
Holly oak	Quercus ilex	3.7	0.1	Fair
Chestnut leaf oak	Quercus castaneifolia	3.7	0.2	Fair
Bunya-bunya	Araucaria bidwillii	3.7	1.1	Fair
London plane	Platanus X acerifolia	4.7	0.0	Fair
Lombardy poplar	Populus nigra 'Italica'	4.7	0.0	Fair
Black oak	Quercus kelloggii	5.0	0.1	Fair
Coast live oak	Quercus agrifolia	5.2	0.0	Fair
Turkey oak	Quercus cerris	7.7	0.4	Fair

5.6.3 Urban cooling and reduced mixing

Urban cooling can affect both vertical and horizontal mixing, advection, and flow patterns. In coastal areas of California, urban cooling can also weaken the sea-breeze, thus affecting the flushing of air pollutants. Reduced vertical mixing can cause increased ozone concentrations under certain conditions whereas reduced horizontal mixing (venting) can result in higher temperatures downwind of urban cooling and thus potentially higher ozone in these areas (Taha 2007). Reduced vertical mixing and venting can also increase the concentrations of particulate matter (Epstein et al.2017; Fallmann et al. 2016).

Taha (2013a, 2005, 2007) suggested that there exists a city-specific cooling threshold for effects of changes in temperature and mixing, that, if heeded, can maximize the benefits from reduced air temperature without inadvertently impacting air quality. Another aspect of importance, especially beyond the urban scale, i.e., at regional and global scales, is the potential impact of heat-island mitigation on convective cloud enhancement. Some of these negative effects have been evaluated on the global scale by Jacobson and TenHoeve (2011) and at the regional scale by Georgescu et al. (2014). However, these are not critical factors in the coastal and semi-arid climates of California where rain occurs during winter and is not dependent on convective activity.

In this modeling assessment for the Capital region, these competing positive and negative effects of mitigation measures were accounted for in the detailed simulations at 2-km and 500-m scales and, thus, the final results embody these various possible outcomes. While the study did not include an air-quality modeling component similar to Taha (2015b, 2013a,b, 2008a,c), the potential negative impacts on air quality were minimized or averted, hypothetically, by defining optimal levels of urban cooling. Thus, avoiding those negative impacts was addressed indirectly in this study by (1) constraining the increases in albedo and/or canopy cover (as well as other measures) to reasonable amounts (at the 2-km level), i.e., avoiding the extreme hypothetical increases that can result in larger urban cooling, and (2) by evaluating the changes in heat fluxes and temperature at the top of the urban boundary layer and assessing the net effects. If there is roughly similar cooling and warming at the top of this layer, as a result of implementing mitigation measures, then

this may imply that there are close to zero net effects throughout the planetary boundary layer, i.e., relatively unchanged vertical mixing and venting.

5.6.4 Reflective materials, glare, and possible pedestrian concerns

In addition to imposing some constraints on UHI-mitigation levels to avoid any potential negative air-quality impacts, as discussed above, such constraints are also imposed to prevent possible issues related to the visual/thermal environment at street level. In order to minimize or avoid potential problems with glare in the lowest parts of the urban canopy layer, the highest albedo of roadways and pavements is limited to a maximum of 0.30 or 0.35, depending on location (as defined earlier in Section 5.5 for the 2-km scale and later in Section 5.19 for the 500-m scale). These are reasonable and realistic increase levels that should not cause glare issues. For the same reasons, the maximum roof albedo is assumed to be 0.50.

A question arises in some situations with regard to cool pavements and potential negative impacts on pedestrian thermal comfort. The argument is that increasing the albedo of pavements would increase radiation reflected onto subjects in the area. This is discussed with some physical and geometrical insight.

From a physical perspective, i.e., heat transfer between two objects, these effects should be evaluated on a site-by-site basis. When the albedo of pavements is increased, it affects several factors, most notably convective and radiative heat transfer. Increased pavement albedo results in lower skin-surface temperature which, in turn, results in lower air temperature. Increased albedo also means increased reflected visible and NIR radiation onto surrounding objects (the concern in this case is pedestrians) but, also, because the surface is cooler, there is smaller heat gained by subjects because of reduced long-wave radiation. Furthermore, with regard to shortwave radiation, the amount of heat gained depends on a myriad of factors down to the albedo of the clothing worn by subjects, as well as other biophysical characteristics.

Thus, the tradeoffs between cooling effects (from reduced surface and air temperatures and reduced longwave radiation) and heating effects (from increased shortwave radiation) will have to be evaluated on a case by case basis. Several studies, e.g., Gilbert et al. (2017) and Levinson et al. (2017), have examined these effects. However, this assessment is based purely on a heat-transfer exercise that does not take into account any implementation or geometry/location aspects that are likely to be the overriding factors in this context.

Thus, more important than the physical considerations discussed above are the practical considerations, levels and locations of implementation, and geometrical aspects when implementing cool pavements. To begin with, the highest priorities for cool pavements deployment should be assigned to major freeways and highways, as well as main routes and roads through the areas of interest. This includes, for example, I-5, I-80, HWY 50, HWY 99, and so on, where there is practically non-existent pedestrian traffic. However, in reality, even suburban

residential neighborhoods have little pedestrian activity during the day. A benefit of targeting the main freeways and highways is their large areas available for albedo modification which is especially relevant in light of their continuous exposure to solar radiation throughout the daytime.

On the other hand, in areas with significant pedestrian traffic, say, downtown Sacramento as an example, or some commercial areas, cool pavements are not desirable in the first place because the urban geometry (e.g., taller buildings and canyon orientations) limit exposure of roadway surfaces to the sun to only a few hours during the daylight and sometimes not at all (i.e., completely shaded). Hence, it serves no purpose implementing cool pavements in such places as they will have little or no effects on temperature. Thus, in areas with tall buildings and high pedestrian volume, we assume no cool-pavement measures.

Finally, an important factor is the sensible level of increase in pavement albedo, as discussed above. All of the foregoing discussion should be viewed in the context of the actual increases in albedo, e.g., such as assumed in this study. The increases are modest (new albedo capped at 0.35 in freeways / highways and 0.30 in residential areas) -- essentially similar to some light-colored cement or concrete pavements that already exist in the region (also see Table 5-6, below). It is not being assumed in this study that extremely reflective materials will be used.

5.6.5 Cool pavement materials

This report provides a quantitative assessment of the effects of various modifications to pavement albedo on surface and air temperatures and their impacts on neighboring communities, e.g., AB617 and disadvantaged populations. The effectiveness of pavements / cool roadways is also compared to that of other measures.

However, it was not part of the scope of work in this project to evaluate cost and life-cycle aspects of implementing cool pavements. This is another significant layer of information altogether, which was addressed in other major studies, e.g., Levinson et al. (2017) and Gilbert et al. (2017). Thus, the choice of materials based on cost or construction-related information is not evaluated here, only the selection based on climate criteria and impacts of pavements on urban heat.

To provide some brief information on the possible pavements choices and materials that could be used to attain the cooling goals set forth in this study, e.g., a maximum pavement albedo of 0.30 or 0.35 (see definitions in Section 5.19), some data is provided in Table 5-6, which is a very simplified and abridged version of information from Levinson et al. (2017). The table shows that some pavement materials currently on the market do have sufficiently high albedo to achieve the cooling effects discussed in this report and with minimal glare issues, per discussion above. Table 5-6 lists a small sample of conventional and relatively more reflective surface types for pavements. It also provides information on expected service life for a sample from the larger dataset of Levinson et al. (2017).

Thus, to achieve the target cooling defined by cool-pavement scenarios in this study, surface types with an albedo range of 0.20 to 0.30 in Table 5-6 would be suitable for application in the Capital region per modeling results (discussed in following sections). Such pavement types will also satisfy the above-discussed glare issue by capping pavement albedo to a maximum of 0.30 or 0.35.

Table 5-6: Sample of pavement surface types and treatment materials. Abridged from and simplified based on Levinson et al. (2017).

Pavement surface type	Albedo range	Service-life range (years)
Bonded Concrete Overlay on Asphalt	0.20 - 0.35	10 - 20
Cape Seal	0.05 - 0.15	2 - 15
Chip Seal	0.10 - 0.24	1 - 10
Fog Seal	0.04 - 0.07	1 - 5
Conventional Asphalt Concrete	0.05 - 0.15	5 - 20
Conventional Interlocking Concrete Pavement (Pavers)	0.20 - 0.35	5 - 20
Permeable Asphalt Concrete	0.08 - 0.15	5 - 20
Permeable Portland Cement Concrete	0.20 - 0.30	5 - 20
Permeable Rubberized Asphalt Concrete	0.08 - 0.15	5 - 20
Permeable Asphalt Concrete	0.08 - 0.15	5 - 20
Permeable Portland Cement Concrete	0.20 - 0.30	5 - 20
Permeable Rubberized Asphalt Concrete	0.08 - 0.15	5 - 20
Portland Cement Concrete	0.20 - 0.30	10-60 depending on design
Reflective Coating - Bisphenol A	0.20 - 0.30	-
Reflective Coating - Polyester Styrene	0.20 - 0.30	-
Reflective Coating – Polyurethane	0.20 - 0.30	-
Reflective Coating - Styrene Acrylate	0.20 - 0.30	-
Rubberized Asphalt Concrete (mill and fill)	0.04 - 0.13	5 - 20
Rubberized Asphalt Concrete (overlay)	0.04 - 0.13	5 - 20
Sand Seal	0.07 - 0.10	1 - 6
Slurry Seal	0.07 - 0.10	1 - 10

5.7 IMPACTS OF MITIGATION MEASURES ON WINTERTIME OUTDOOR AIR TEMPERATURE

Before proceeding with the presentation of summertime impacts from UHI-mitigation measures, a brief revisit to the potential wintertime effects on temperature is in order. Among some of the concerns regarding potential negative effects occurring inadvertently from implementing urban-cooling measures, several were discussed in Section 5.6. An additional concern may be the potential penalties in terms of heating needs during the winter season.

<u>Albedo</u>

The purpose of the brief discussion in this section is to demonstrate that during winter, cooling measures such as increased albedo have small or no impacts on air temperature, hence small or no negative effects on heating energy needs. It should be noted, however, that there may be negative effects at the building scale if, for example, a cool roof is applied that can affect the heating energy needs of the space (floor) directly beneath it. Such effects would have to be evaluated on a case-by-case basis, although these impacts have been shown to be small (e.g., Akbari and Konopacki 2005) because of larger air mass (lower sun angle), increased cloudiness, and snow cover in winter. Thus, the net year-round effects of cool roofs are a significant reduction in energy use. Furthermore, in the Sacramento region, winters are not particularly cold compared to other parts of the country.

In this study, the effects of mitigation measures on wintertime ambient urban air temperature were examined briefly. The modeling and analysis indeed show small or non-existent cooling effects in winter (a result of smaller solar altitude angle and larger cloud cover). An example from this analysis is summarized in Figure 5-13 showing results from the Altostratus Inc. AREAMOD / WRF modeling approach for two summer and two wintertime intervals. The temperature differences presented in this example correspond to the cooling effects of case10, a scenario of small increases in albedo, as defined earlier in Section 5.5. The figure shows the impacts on air temperature at the time of the maximum effect from the albedo measures, i.e., around midday.

In this example, whereas case10 decreases the summertime midday temperature by 1 °C or slightly more in large and well-defined areas that are affected by cooling (top two graphs in Figure 5-13), the wintertime effects are either non-existent or small (e.g., up to 0.5 °C) and impacting very small areas that also are not as well-defined as in summer (bottom two graphs). The analysis suggests that the albedo-increase levels proposed in this study would result in no significant negative impacts during the winter. Higher levels of albedo increase (hypothetical and not modeled in this study) might result in negative wintertime effects. As such it is important to constrain the albedo increases to reasonable levels, i.e., as defined in this study.

<u>Canopy cover</u>

In terms of vegetation cover (not shown in Figure 5-13), the same conclusion applies as most trees shed their leaves in winter thus reducing cooling effects from shading and evapotranspiration. For evergreen trees, the lower incoming solar radiation (increased cloudiness and larger air mass) and lower air temperatures reduce the trees' cooling effects via shading and evapotranspiration, respectively. As with the albedo modifications, the results suggest small or no effects during the wintertime, depending on location and scenario.

Figure 5-13: Cooling from case10 (increase in albedo) in summer (top figures) and winter (bottom figures) for random hours as examples.

(SUMMER) 1200 PDT, June 3rd, 2013

(SUMMER) 1500 PDT, June 4th, 2013

(WINTER) 1500 PST, January 31st, 2016

(WINTER) 1300 PST, January 28th, 2016
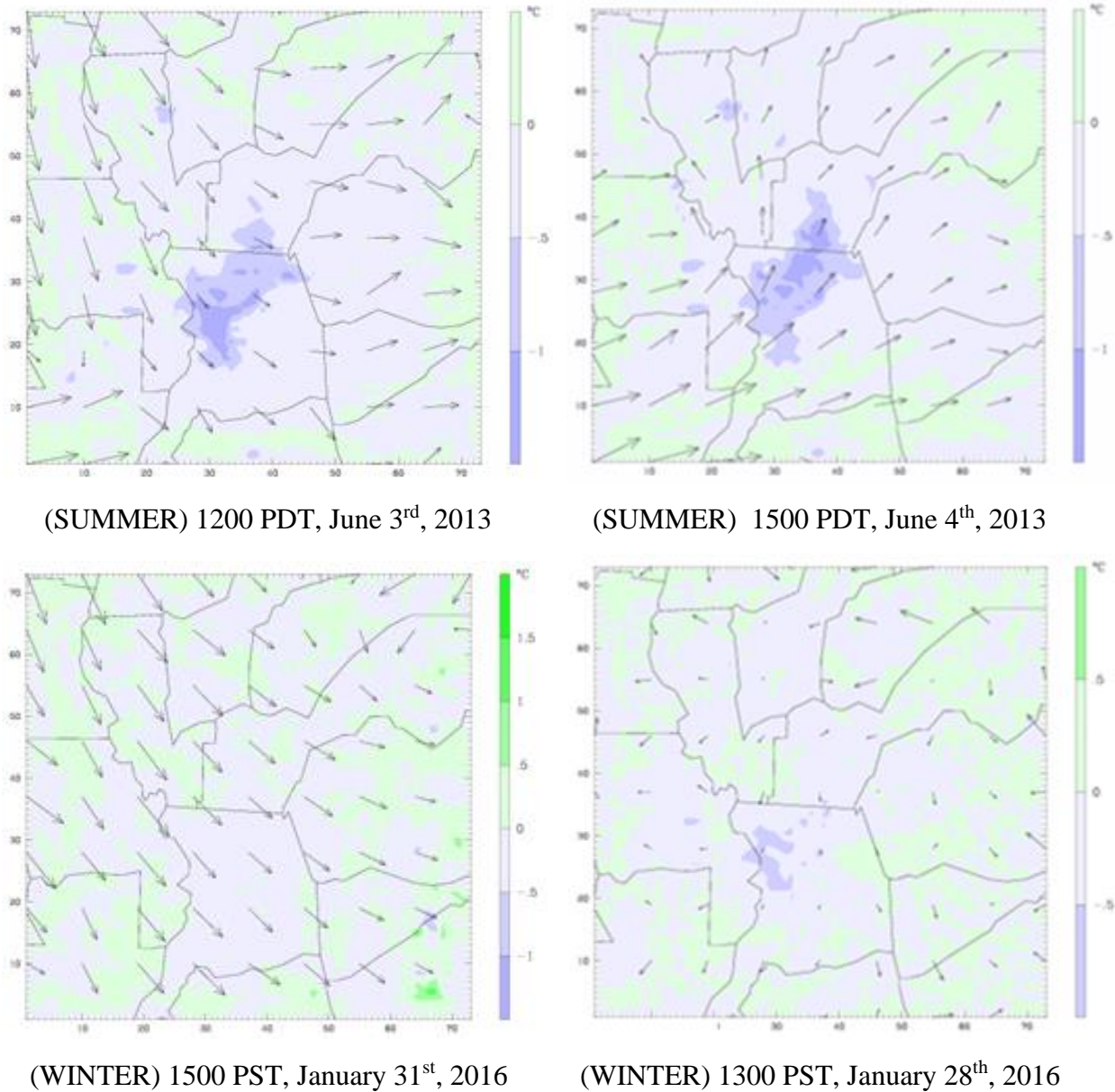
5.8 COOLING EFFECTS AND WIND: ESTIMATION OF A LENGTH SCALE

Taha (2017) defined four levels of the UHII for characterization, quantification, and modeling, as discussed in Section 1 and shown graphically in Figure 1-1. The third level (Level 3) involves defining a community's "responsibility" for its local UHII, i.e., how much heat is locally generated versus transported from upwind sources. Hence there is interest in estimating a length scale for urban heat transport. Such length scale is also of relevance in the selection of UHI reference points and locating them outside of urban heat plumes (as introduced in Section 5.3).

Thus, in this study, a modeling exercise was undertaken to characterize the fetch or length scale of a reverse effect, i.e., cooling effects from a mitigation measure. A "reverse" Level-3 length scale is an indicator to the impacts of an urban area on a downwind location. As expected, this depends on the level of surface modification, weather conditions, wind speed and direction, the upwind distance over which an air parcel travels over hot or cooled surfaces, and the desired downwind temperature threshold or lifetime, i.e., how large the temperature reduction is relative to an original upwind value, Δ_o, by the time it reaches the downwind point of interest.

To establish a downwind temperature-change threshold, several metrics could be used, for example, e-folding ($1/e\ \Delta_o$) or half lifetime ($\frac{1}{2}\ \Delta_o$), or some other measure. In this discussion, a temperature-reduction half-lifetime ($\frac{1}{2}\ \Delta_o$) is presented, meaning the time or distance downwind where temperature reduction reaches half of the original temperature depression (Δ_o) at the edge of the urban area.

Figure 5-14 shows an example from this analysis for 2-m AGL temperature difference corresponding to case10 at different time intervals. These are results from Altostratus Inc.'s AREAMOD / WRF modeling approach. The sample hours in this figure were selected to show different wind patterns and directions for demonstration purposes. The cool-air plumes are shown for the coincident wind directions in the domain (depicted in the upper-left part of each figure).

The small circles are the grid cells where albedo was actually modified (the darker the circle, the larger the albedo increase, per legend on each figure). The shades of blue are the changes in air temperature (per legend) – the darker blue means larger cooling. As can be seen, there are areas that have become cooler even though no changes in albedo were applied at those locations. Thus, these are areas affected by the transport of cooler air from the modified grid cells.

Averaging over the wind speed range (per each direction), temperature reduction, and albedo change (in this example), the half-lifetime for temperature reduction was found at 2 to 4 km downwind (the "average" qualifier is important to note here, as the fetch can be longer under certain conditions). In other words, for the current-climate summer conditions studied in this effort (MJJAS 2013-2016), an air mass cooled by flowing over an urban area where mitigation measures have been implemented can retain half of its cooling by the time it reaches 2 to 4 km downwind from the edge of the urban area (where temperature depression = Δ_o). The reverse is also true for warming of an air parcel flowing over a hot urban area.

Figure 5-14: Length scales associated with cooling from increased albedo for case10. Examples provided for several time intervals with different flow patterns.
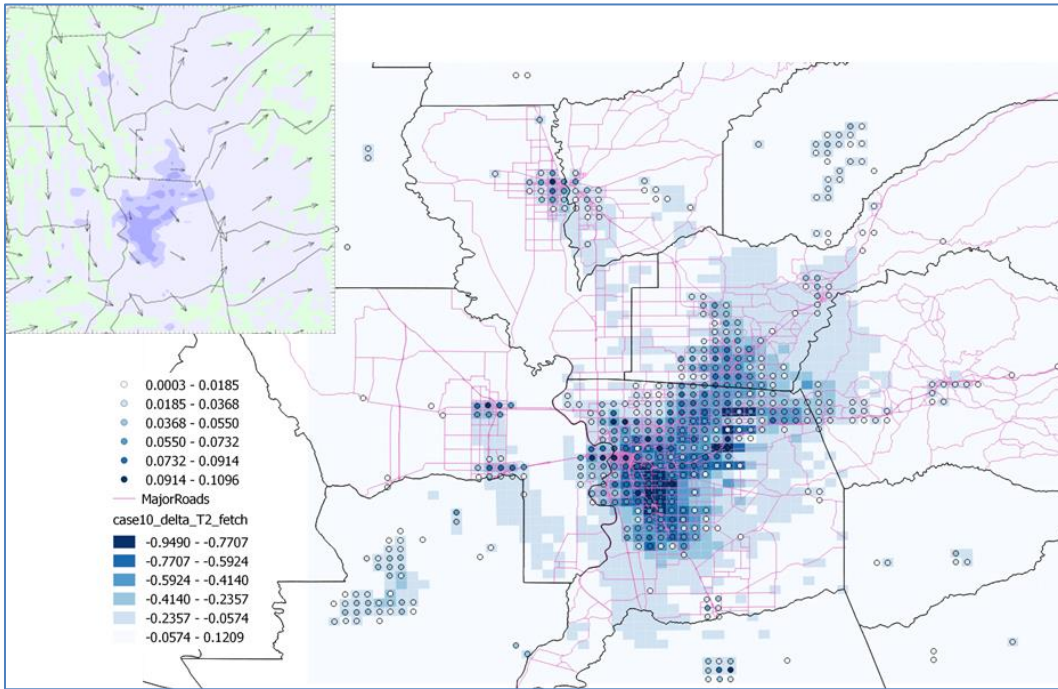
1400 PDT, June 1st, 2013
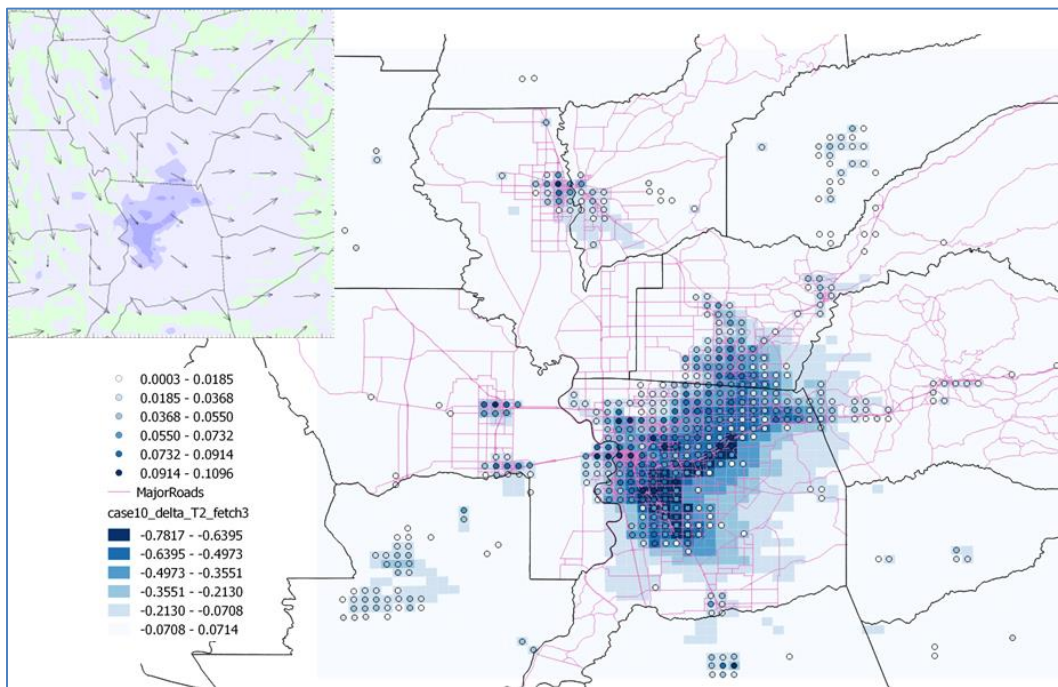
1200 PDT, June 3rd, 2013

Figure 5-14, continued.
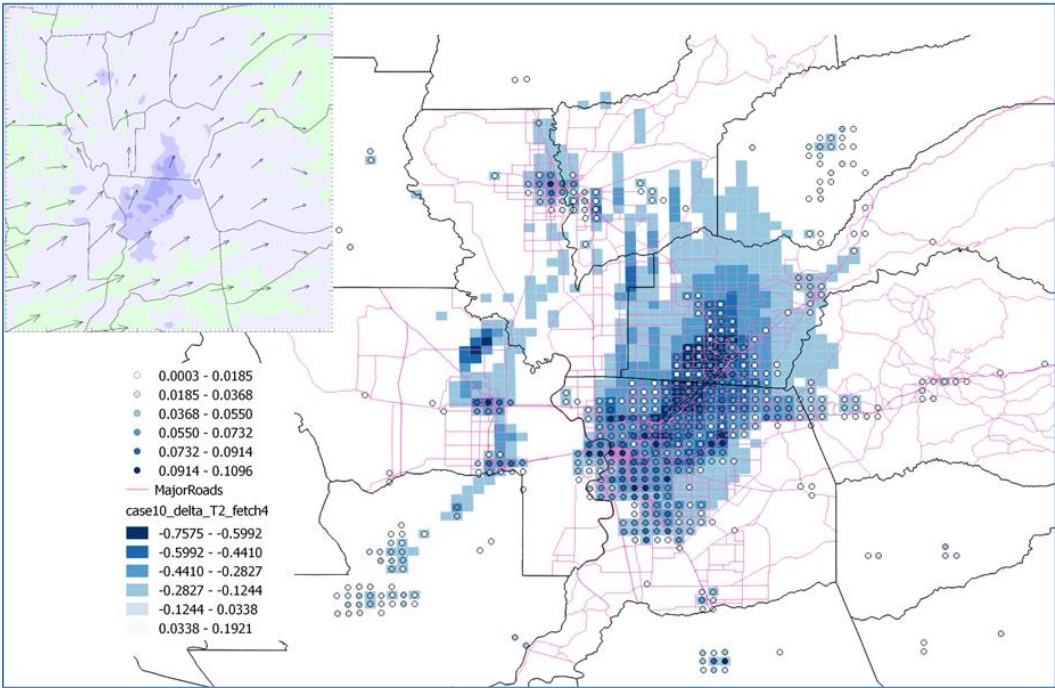
1500 PDT, June 4th, 2013
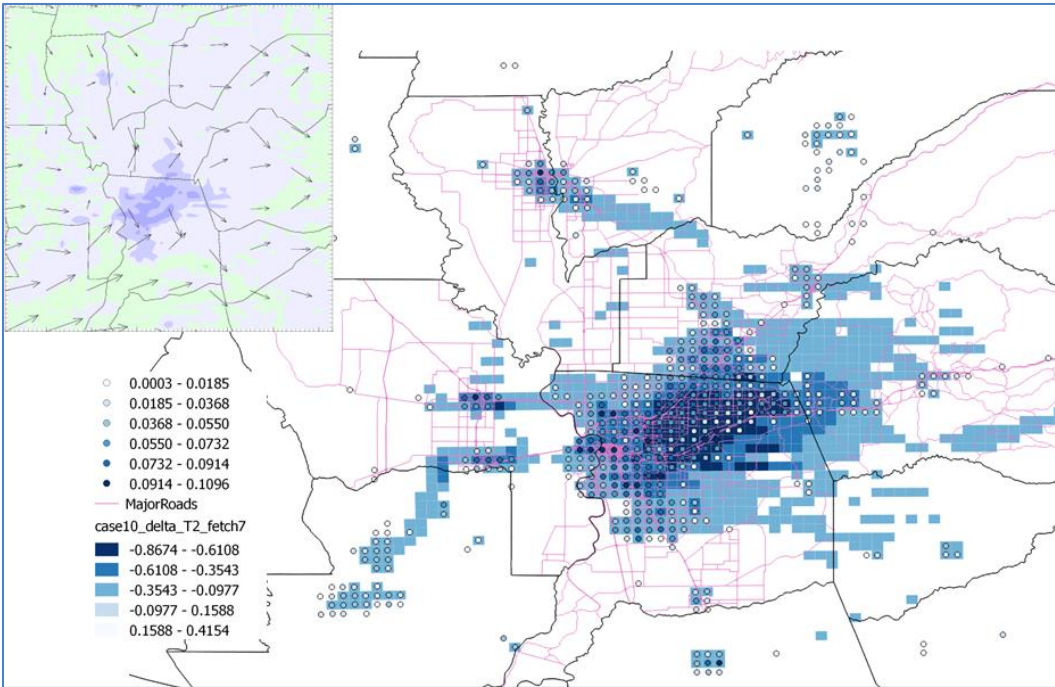
1500 PDT, June 6th, 2013

Figure 5-14, continued.
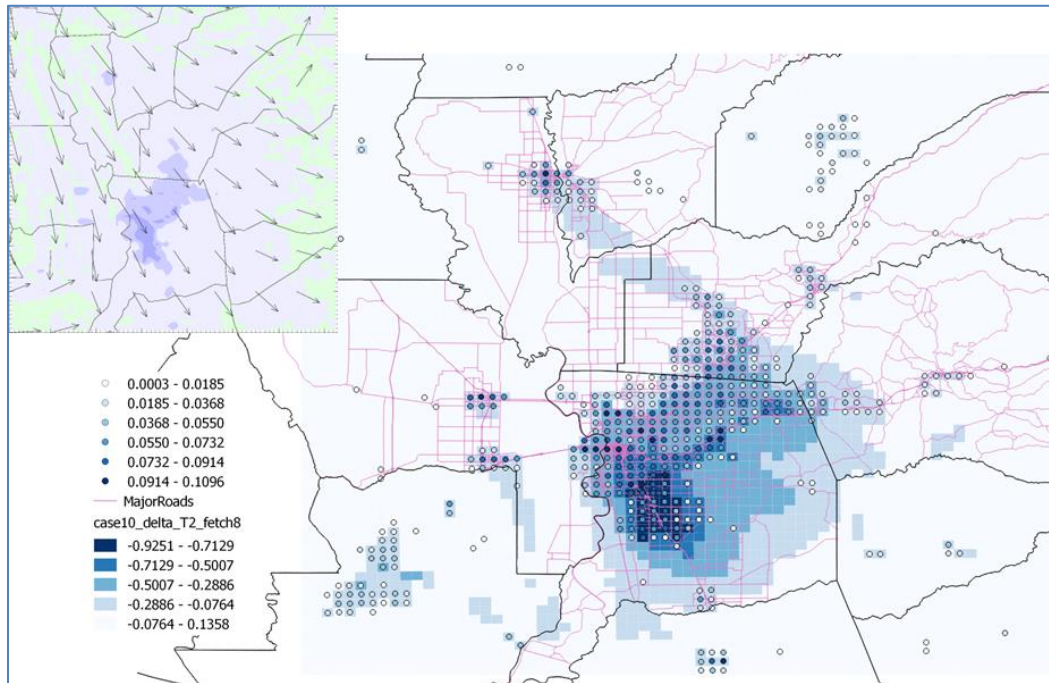
1300 PDT, June 7th, 2013

5.9 METRICS AND THRESHOLDS

To provide an assessment of the urban-heat mitigation potentials of various measures, several metrics and thresholds were defined in consultation with the SMAQMD, LGC, and project TAC:

Metrics at the 2-km level: all hours, all months (MJJAS), all years (2013-2016):

- ≡ Instantaneous, 4-dimensional, hourly analysis
- ≡ 0600 PDT average 2-km temperature (~minimum temperature)
- ≡ 0600 PDT 2-km UHII
- ≡ 1300 PDT average 2-km temperature (~solar noon)
- ≡ 1400-to-2000 PDT average 2-km temperature
- ≡ 1500 PDT average 2-km temperature (~peak temperatures)
- ≡ 1500 PDT 2-km UHII
- ≡ All-hours 2-km UHII
- ≡ All-hours average 2-km temperature
- ≡ Degree-hours over 35 °C threshold
- ≡ Degree-hours over 38 °C threshold
- ≡ National Weather Service Heat Index exceedances
- ≡ National Weather Service Heat Index time series

Metrics at the 500-m level (specific locations and roadway projects at community scale):

≡ Instantaneous, 4-dimensional, hourly analysis

≡ 0600 PDT (daily minima)

≡ 1300 PDT (daily peaks)

≡ 1500 PDT (daily peaks)

≡ All hours / cumulatives

≡ 0700 PDT (morning commute peak)

≡ 1700 PDT (evening commute peak)

5.9.1 Metrics

In this modeling effort, metrics were computed at each model grid cell or station location for (1) base scenarios (for current and future climates / land use) to characterize urban heat and the UHI / UHII, as well as other indicators, and (2) mitigation scenarios (for current and future climates / land use), per each 2-week interval (from May 30th through September 16th of each year). These metrics include the following (in no particular order):

i. Simple averages (non-UHII), <u>non-threshold</u>:

    a. All-hour averages and all-hour degree-hours (DH).

    b. Peak temperature averages (hours between 1400 and 1800 PDT; and 1400 – 2000 PDT, of interest to area utilities).

    c. Daily minimum temperature averages, e.g., at 0600 PDT.

ii. Thresholds-based, non-UHII cumulatives, DH_{TH}:

    Degree-hours (per specified intervals) computed when urban air temperatures exceed certain predefined static or dynamic temperature threshold, TH (this is not a UHII).

iii. Level-3 UHII:

    Based on the UHI signal from (i and ii) above, develop a Level-3 UHII estimate. Or, conversely, based on the impacts of mitigation measures (i.e., cooling signal), develop a "reverse" Level-3 UHII as discussed, above, in Section 5.8. Either way, the goal is to characterize the length scale of interest in urban areas within the 6-counties region, so that the UHI / UHII reference points can be selected outside of the heat plume's influence (as was discussed in Section 5.3).

iv. UHI Index (UHII), non-threshold:

    a. All hours UHII (see *UHII; UHII_b* in equations 5-4 and 5-5).

    b. Peaks (see *UHII_d* in equation 5-7), for 1400 – 1800 PDT; through 2000 PDT for utilities.

    c. Minima (see *UHII_d* in equations below) for 0600 PDT.

Altostratus Inc.

v. Thresholds-based UHII:

Regardless of date/interval or time of day, this threshold-based UHII (*UHII_c* in Equation 5-6) is computed for each hour the urban air temperature exceeds a certain threshold.

Note that in Equation 5-6 we compute the metrics when <u>urban</u> air temperature is higher than the specified threshold, regardless of whether or not the <u>rural</u> reference temperatures are below or above the threshold. The Cal/EPA proposed an equation where the threshold applied to both urban and non-urban temperatures (which is a more stringent criterion), here, we apply it only to urban temperature because we'd want to quantify the potential for cooling urban areas (i.e., to make them as cool as possible) during a heat event or when temperature is above a certain threshold.

vi. National Weather Service Heat Index (*HI*)

This is defined with Equation 5-8 and the subsequent calculations in Equation 5-9. In addition to computing changes in *HI* with Equation 5-8, the potential "shift down" from one *HI* warning level to a lower one (per NWS– see Figure 5-15) will be assessed and used to demonstrate potential benefits from UHI mitigation techniques, e.g., shifting the *HI* down from "Extreme Danger" to "Danger" level, or from "Danger" to "Extreme Caution". Note that Figure 5-15 is a variant of the *HI* -- it was developed for areas that are generally hot but with relatively lower humidity, which is suitable for the Capital Region.

Note: the NWS Experimental *HeatRisk* index was not used in this study since it relies on climatology (e.g., temperatures from 1985 to 2015) and thus will require an additional, extensive level of effort to produce (climatological analysis is not part of this study). Thus, the NWS *HI* is used instead (practically, the main difference between *HeatRisk* and *HI* is that the former has a climatology context added to it).

Equation 5-4 represents the form used in computing the Level-1 UHI Index (UHII) for the state of California that was developed for Cal/EPA (Taha 2017) to satisfy AB 296 requirements in that the index captured both the *severity* (magnitude) and *extent* (duration) of the urban-nonurban temperature differential. In the following equations, $T_{u(k),h}$ is the urban temperature at time step (hour) h, $T_{nu(k),h}$ is the nonurban temperature at time-step h, and H is the number of time-steps, in this case, the number of hours in the period MJJAS of a given year, or *int#* (interval) per year. Here, k is a location index representing a pair of points, one urban and one reference, that is, $u(k)$ is the urban point of the pair k, and $nu(k)$ is the non-urban, reference point of the pair k. Note that there is no temperature threshold associated with the UHII definition in Equation 5-4.

In Equation 5-6 the threshold temperature is denoted as $T_{TH,h}$ indicating a dynamic, time-dependent threshold. If the threshold is static (constant across all hours), then the threshold temperature will simply reduce to T_{TH}.

$$UHII = \sum_{h=1}^{H(JJA)} \left[T_{u(k),h} - min\left(T_{u(k),h}, T_{nu(k),h}\right)\right] \qquad (5-4)$$

$$UHII\_b = \sum_{h=1}^{H(int\#)} \left[T_{u(k),h} - T_{nu(k),h}\right] \qquad (5-5)$$

$$UHII\_c = \begin{cases} \sum_{h=1}^{H(int\#)}\left[T_{u(k),h} - T_{nu(k),h}\right], & T_{u(k),h} > T_{TH,h} \\ \\ 0, & T_{u(k),h} \leq T_{TH,h} \end{cases} \qquad (5-6)$$

$$UHII\_d = \sum_{h=1}^{H(int\#)} \left[T_{u(k),h} - T_{nu(k),h}\right], \quad H_{start} \leq h \leq H_{end} \qquad (5-7)$$

Per NWS Technical Attachment (SR 90-23) the Heat Index (*HI*) is given by Equation 5-8, where *T* is temperature in °F and *H* is relative humidity (%):

$HI = -42.379 + 2.04901523\ T + 10.14333127\ H - .22475541\ T\ H - .00683783\ T^2 - .05481717\ H^2 + .00122874\ T^2\ H + .00085282\ T\ H^2 - .00000199\ T^2\ H^2$

$$(5-8)$$

Thus, if we partially differentiate *HI* with respect to temperature (*T*), we obtain (per Taha 2015):

$$\frac{\partial HI}{\partial T} = c_2 - c_4\ H - 2c_5\ T + 2c_7\ T\ H + c_8\ H^2 - 2c_9\ T\ H^2 \qquad (5-9)$$

where c_2=2.04901, c_4=0.224755, c_5=0.006837, c_7=0.001228, c_8=0.000852, and c_9=0.00000199, and where *HI* and *T* are in degree °F, in this case, and *H* (relative humidity) is in percent. Thus for example, during relatively mild heat conditions, e.g., 85°F (29.4°C) and 40% relative humidity, $\partial HI/\partial T$ from equation (5-9) is 1.06°F °F[-1] (1.9°F °C[-1]) whereas during a relatively more severe

Altostratus Inc.

heat episode, say 94°F (34.4°C) and 70% relative humidity, $\partial HI/\partial T$ is 3.53°F °F^{-1} (6.4°F °C^{-1}), showing the relatively different influence of a one degree change in temperature in different weather conditions. This type of dependence was used in this study to evaluate the potential of mitigation measures in alleviating heat stress.

Note that the NWS HI is the only instance in this study and report where degrees F are used. Otherwise, the entirety of the report uses SI units and °C.

Figure 5-15 shows the NWS Heat Index warning levels developed for areas with generally high temperatures but relatively lower humidity, which is suitable for the Capital Region. In this project, this information was used to evaluate the potential of cooling measures in "shifting down" the HI from one warning level to a lower one.

5.9.2 Thresholds

The following temperature thresholds were used in this analysis and in conjunction with the metrics defined above:

    i.   35 °C (95 °F) for DH_{TH}
    ii.   38.3 °C (101 °F) for DH_{TH}, per SMUD (extreme heat days)
    iii.   35 °C (95 °F) for equation 5-6 (for static T_{TH})
    iv.   NWS HI 95 °F + humidity (for equations 5-8 and 5-9)
    v.   NWS HI 105-110 °F exceeded for at least two consecutive days, which is the definition of a heat wave.

Figure 5-15: NWS HI for hot areas with lower humidity. Source:
https://www.wrh.noaa.gov/psr/general/safety/heat/heatindex.png
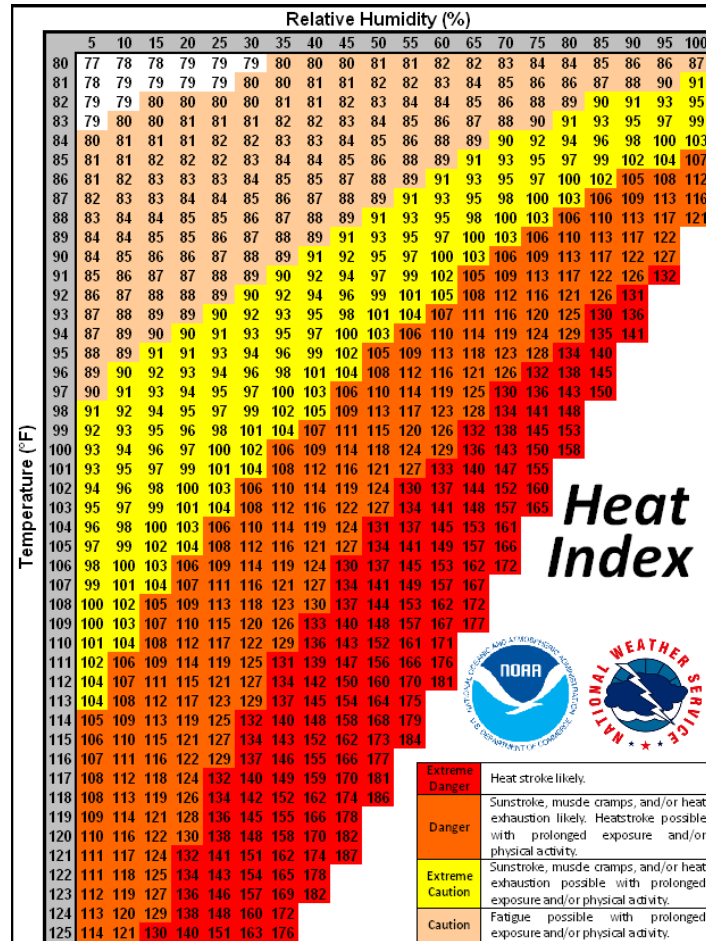
5.10 EFFECTS OF MITIGATION MEASURES IN CURRENT CLIMATES AND LAND USE: INSTANTANEOUS TEMPERATURE DIFFERENCES

To begin the presentation of effects from various mitigation measures, a brief snapshot from the temperature-difference field is provided as an introduction. The examples for a random hour from the studied periods are provided here to help formulate a general idea as to the spatial characteristics of the changes in the temperature field in the Capital region. This is a general sketch of the extent, geographical locations, and levels of changes in temperature that can be expected in the region as a result of implementing UHI-mitigation measures.

Thus, in Figure 5-16, the instantaneous temperature impacts of five mitigation measures are presented for the scenarios defined earlier in Section 5.5 and for a random hour at 1300 PDT, July 28, 2015. These temperature perturbations result from cases 01, 02, 10, 20, and 31.

At this snapshot hour, the temperature reductions reach up to 0.7, 1.4, 1.5, 2.4, and 3.9 °C, respectively, for the measures and scenarios listed above. The spatial pattern of these reductions follows the urban boundaries as well as the downwind transport of cool air, as discussed in Section 5.8. The magnitude of cooling increases with built-up density and the size of the urban area being modified. Of note, the mitigation measures can also cause some warming, generally downwind of the modified urban areas. However, the warming is small compared to the cooling effect both in magnitude and the size of the areas affected.

Furthermore, different measures produce different spatial patterns of cooling. For example, vegetation canopy measures (case01 and case02) produce an effect that is somewhat spatially uniform across the affected urban areas (first two graphs), whereas the albedo measures (case10 and case20, second two graphs in Figure 5-16) produce some more distinguishable or spatially differentiated patterns in the cooling effect. It can be seen, for example, that the American River and surrounding areas (the lighter-colored curved pattern in the middle of the Sacramento region) do not get as much cooling in the albedo scenarios because of the relatively smaller built-up fraction in those areas (i.e., less roofs and paved surface available for modification). Compare the second two graphs in this figure with the impervious fraction characterized earlier in Figures 2-10.C and 2-10.D (in Section 2.3.3).

Figure 5-16: Instantaneous differences in air temperature at a random hour and date for five different mitigation scenarios in the 6-counties Capital region. The temperature differences (del01 through del31) were defined in Section 5.5.
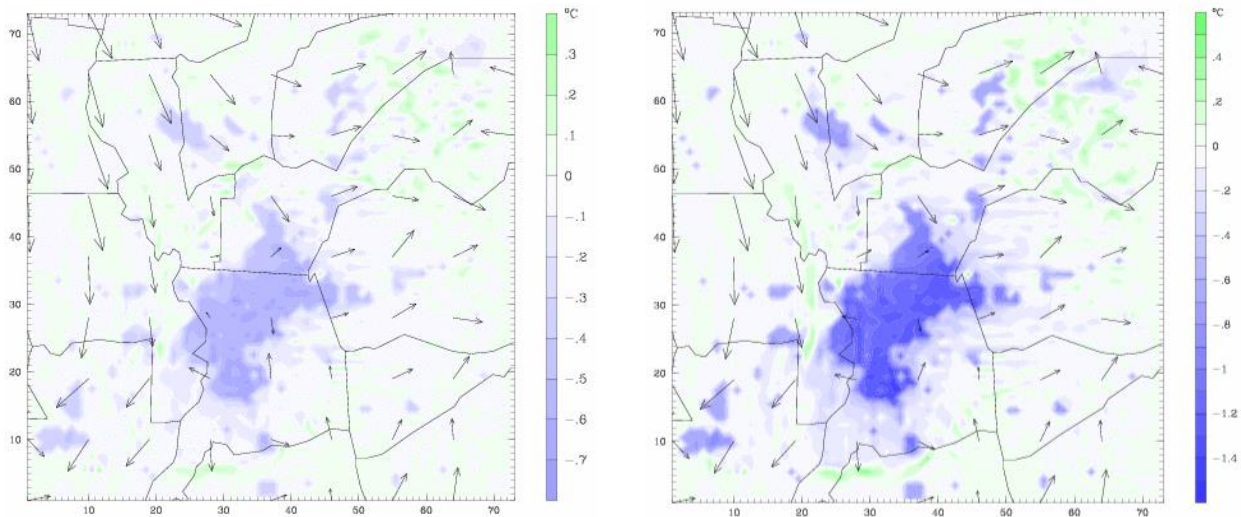
Left: del01:1300 PDT, July 28, 2015, horizontal wind vector (base) at 2 m AGL, maximum change at this hour: -0.7 °C. Right: same but for del02, maximum change at this hour: -1.4 °C.

Figure 5-16, continued.
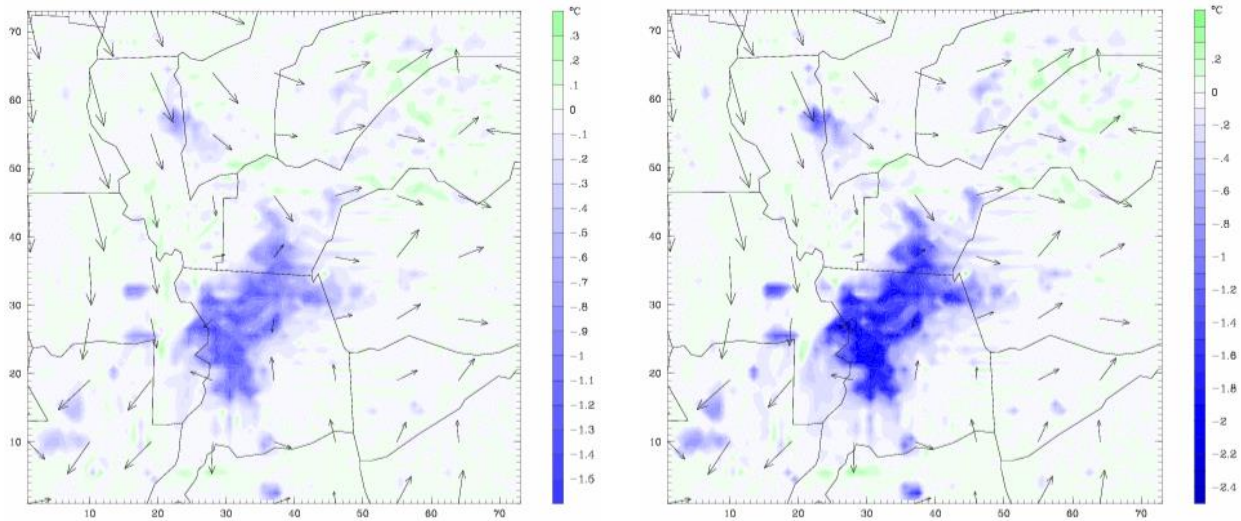
Left: del10: 1300 PDT, July 28, 2015, horizontal wind vector (base) at 2 m AGL, maximum change at this hour: -1.5 °C. Right: same but for del20, maximum change at this hour: -2.4 °C.
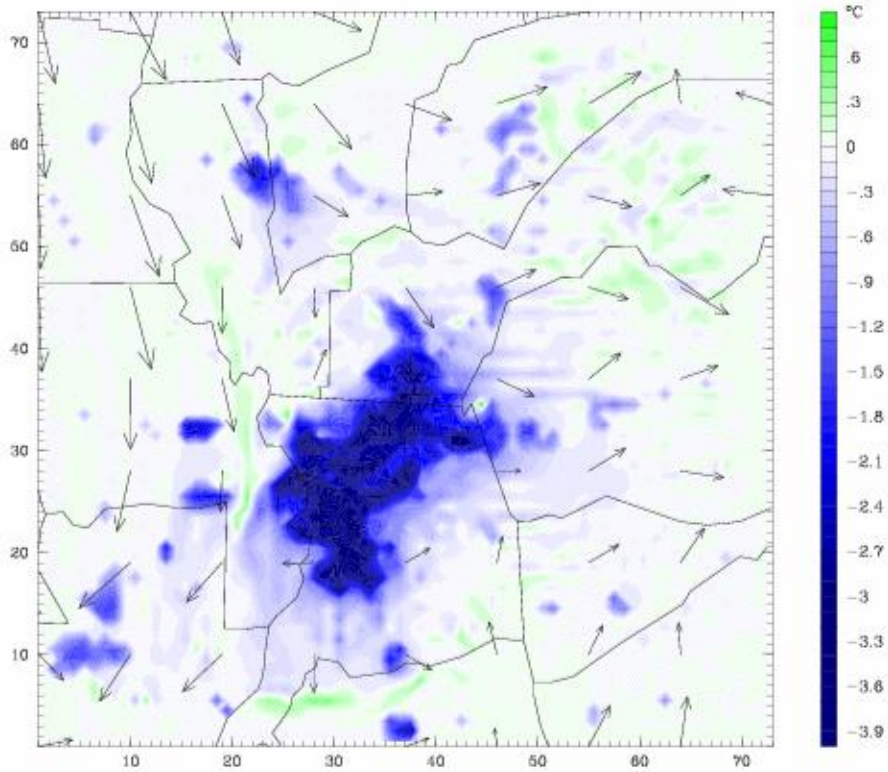
del31:1300 PDT, July 28, 2015, horizontal wind vector (base) at 2 m AGL, maximum change at this hour: -3.9 °C.

5.11 IMPACTS OF MITIGATION MEASURES ON THE TEMPERATURE FIELD AND THEIR RANKING AT THE REGIONAL SCALE

In the following sections, the impacts of mitigation measures on the temperature field are presented. It is important to note that the ranking of various measures in terms of their cooling potential can differ by area and time interval (i.e., hour or range of hours). Thus, the implementation and deployment of measures (e.g., selecting the top priorities) depends on the goal to be achieved at a particular locale. For example, if the goal were to reduce daytime maxima in temperature, then the ranking could differ from if all-hour temperature averages were to be reduced or if, for some reason, nighttime temperature were to be modified.

We note again here that case02 is an extreme scenario of vegetation canopy increase in urban areas and should perhaps be disregarded in some parts of this analysis – it is included here as a maximum possible effect from urban reforestation (per request from project participants). As discussed earlier, case01 is likely an upper bound for realistic implementation of canopy-cover measures.

Thus, aside from case02, the other mitigation levels evaluated at the 2-km level are realistic and relatively moderate. Furthermore, the localized impacts (e.g., cooling) and ranking (i.e., relative effectiveness) of various measures and levels can differ from on subdomain to another because the advective effects are significant at this scale. Recall that this analysis is for current climate (MJJAS 2013 – 2016) and for current land-use conditions and urbanization levels.

5.11.1 Impacts on the temperature field at 0600 PDT

In Figure 5-17, the average temperature reductions at 0600 PDT are presented. This is temperature reduction averaged over all 0600-PDT hours (in each period) and over the urban grid cells in each specified sub-domain. It can be seen that the ranking (i.e., the order of measures' effectiveness listed at right on each figure) at this hour is consistent across all regions but that the magnitudes of reductions in temperature differ by location. Furthermore, the intra-measure differences within each area are also different, i.e., how close or far apart are the reductions from different measures.

Whereas Figure 5-17 shows the variations in cooling levels across different time periods (for each region), Figure 5-18 summarizes the averages of those effects. It can be seen that the effects of canopy-cover are larger than those of albedo, as expected, since there is no significant amount of sunlight at 0600 PDT. The cooling effects associated with albedo measures at this hour are mostly carry-overs from the previous day's daytime hours, i.e., smaller long-wave re-radiation of heat at night. The areas in Davis, Sacramento, Woodland, and Yuba City have larger cooling at this hour and larger inter-quartile ranges (spread) of cooling effects. The most effective scenario, excluding case02, is the combination case31.

Figure 5-17: Average temperature reduction (°C) at 0600 PDT. Time periods are identified on the horizontal axis and the ranking of measures on the right side of each graph.

Figure 5-17, continued.

Sacramento 0600 PDT

Woodland 0600 PDT

Yuba City 0600 PDT
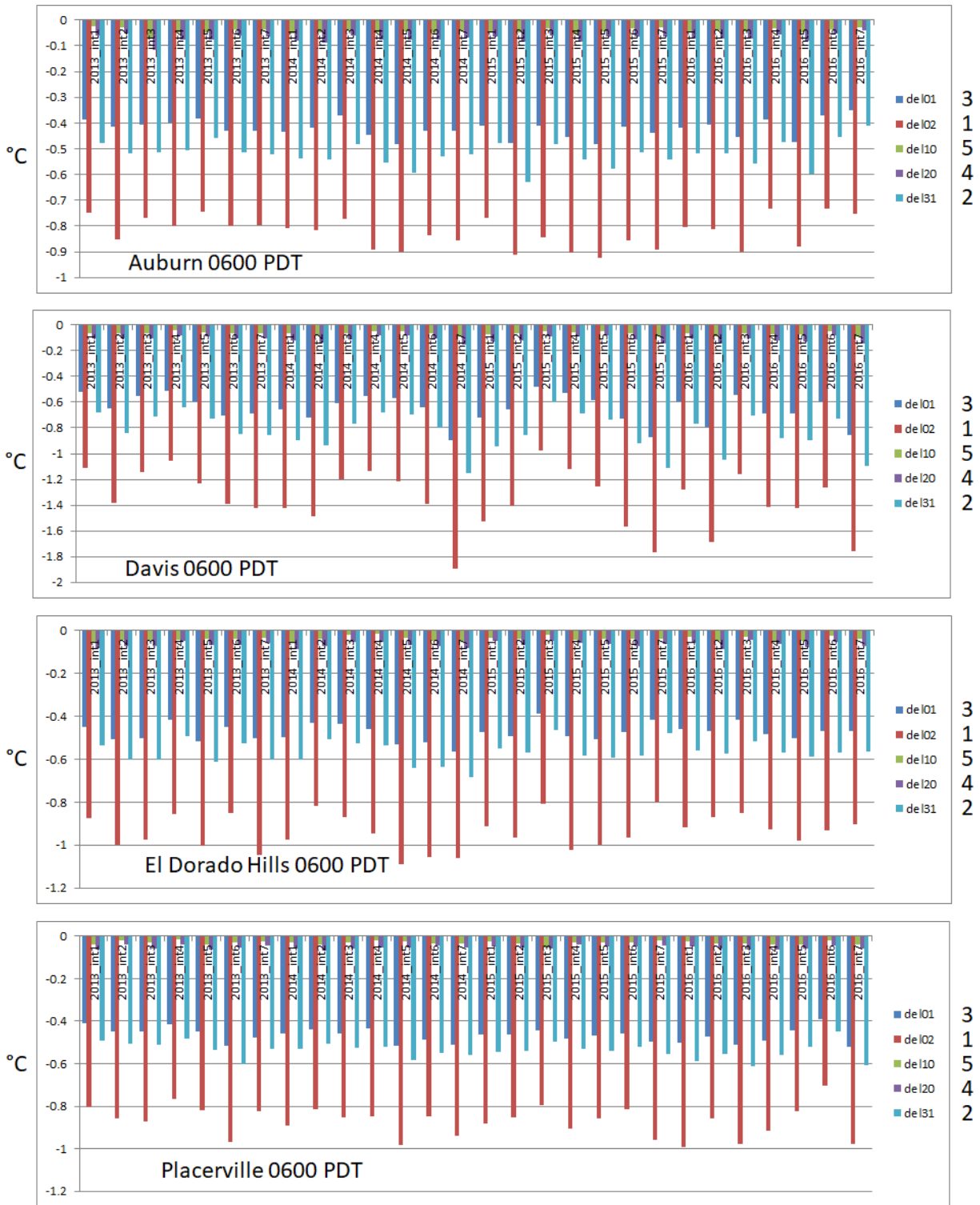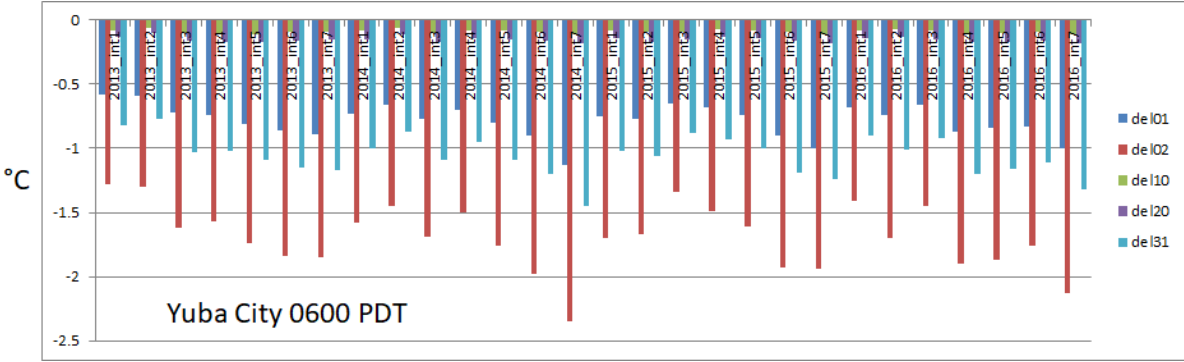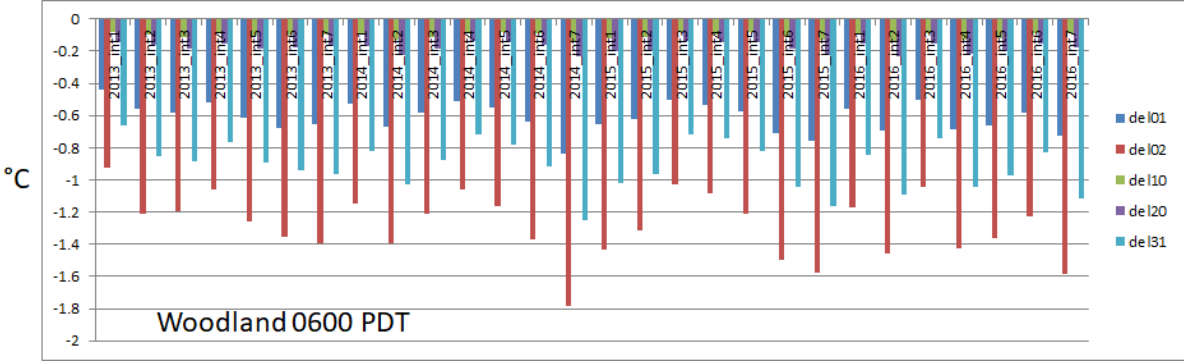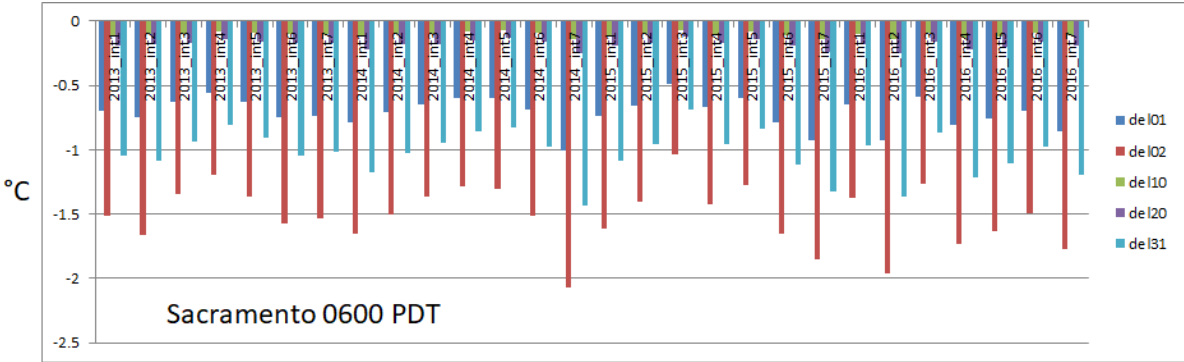
Figure 5-18: Summary of averaged temperature impacts at 0600 PDT. Median, quartiles, and maxima/minima are shown with box and whisker plots.
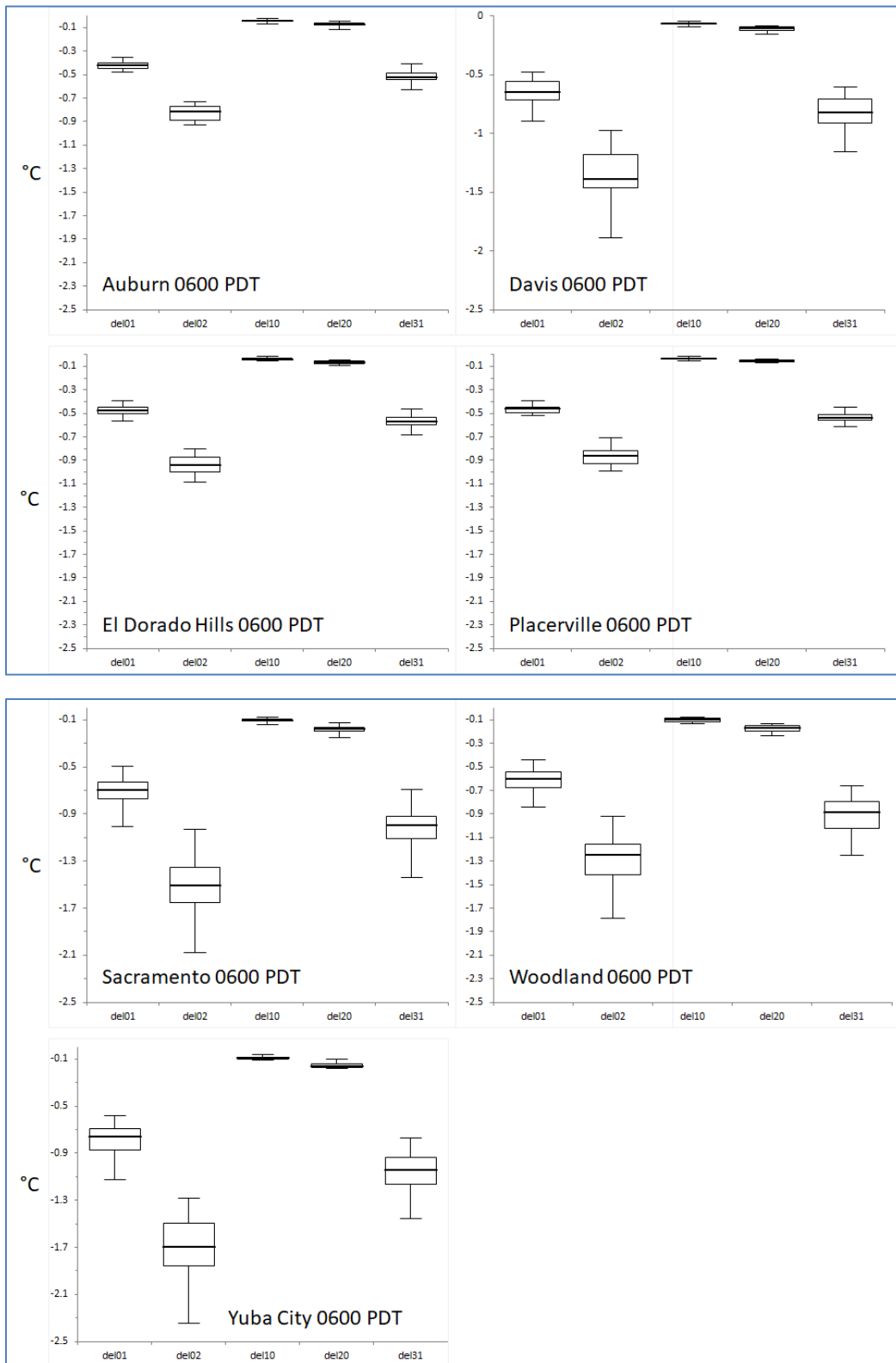
5.11.2 Impacts on the temperature field at 1300 PDT

In Figure 5-19, the average temperature reductions at 1300 PDT are shown (i.e., reductions averaged over all 1300 PDT hours in each time period) and also averaged over urban grid cells in each specified sub-domain. The figure shows that the ranking (i.e., the order of measures' effectiveness) at this time interval is (1) different from that at 0600 PDT, discussed above, and (2) varies across different regions, unlike at 0600 PDT where they were similar across all sub-domains. As this is a daylight hour close to solar noon (1300 PDT), the effects of albedo measures are larger than those of canopy cover. The magnitudes of reductions in temperature differ by location and so do the intra-measure differences within each area, i.e., how close or far apart are the reductions from different measures. There are also situations where some of the measures are tied in terms of their cooling potentials, as seen in Figure 5-19 (e.g., case01 and case20 in Placerville, as indicated by the bracket at the right end of the figure).

Figure 5-20 summarizes the averages of those effects at 1300 PDT over all time periods. The areas in El Dorado Hills, Sacramento, and Woodland have some of the larger cooling effects at this hour as well as the larger inter-quartile ranges of temperature reductions. At 1300 PDT, the albedo measures are more effective than canopy-cover increases (excluding the extreme case02), which is the inverse of the ranking at 0600 PDT. The albedo effects can also be larger than case02 in some domains, i.e., Sacramento and Woodland. Finally, the most effective scenario is case31.

Figure 5-19: Average temperature reduction (°C) at 1300 PDT. Time periods are identified on the horizontal axis and the ranking of measures on the right side of each graph.

Figure 5-19, continued.

El Dorado Hills 1300 PDT

Placerville 1300 PDT

Sacramento 1300 PDT

Woodland 1300 PDT

Figure 5-19, continued.

Yuba City 1300 PDT

Figure 5-20: Summary of averaged temperature impacts at 1300 PDT. Median, quartiles, and maxima/minima are shown with box and whisker plots.
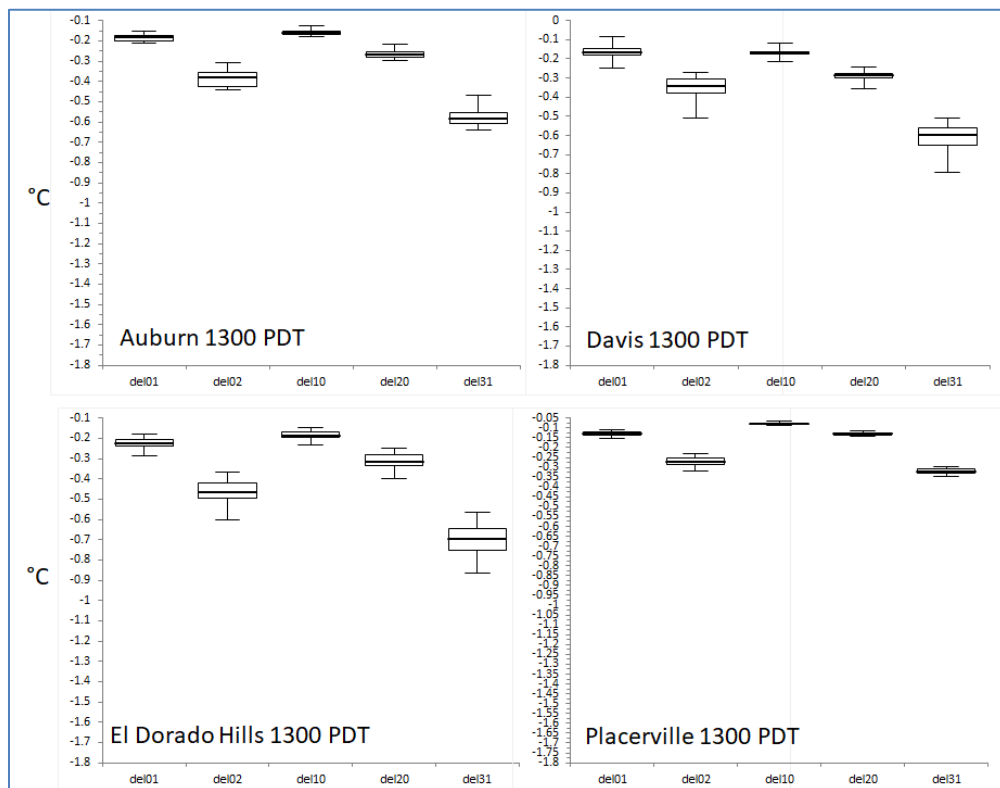
Figure 5-20, continued.
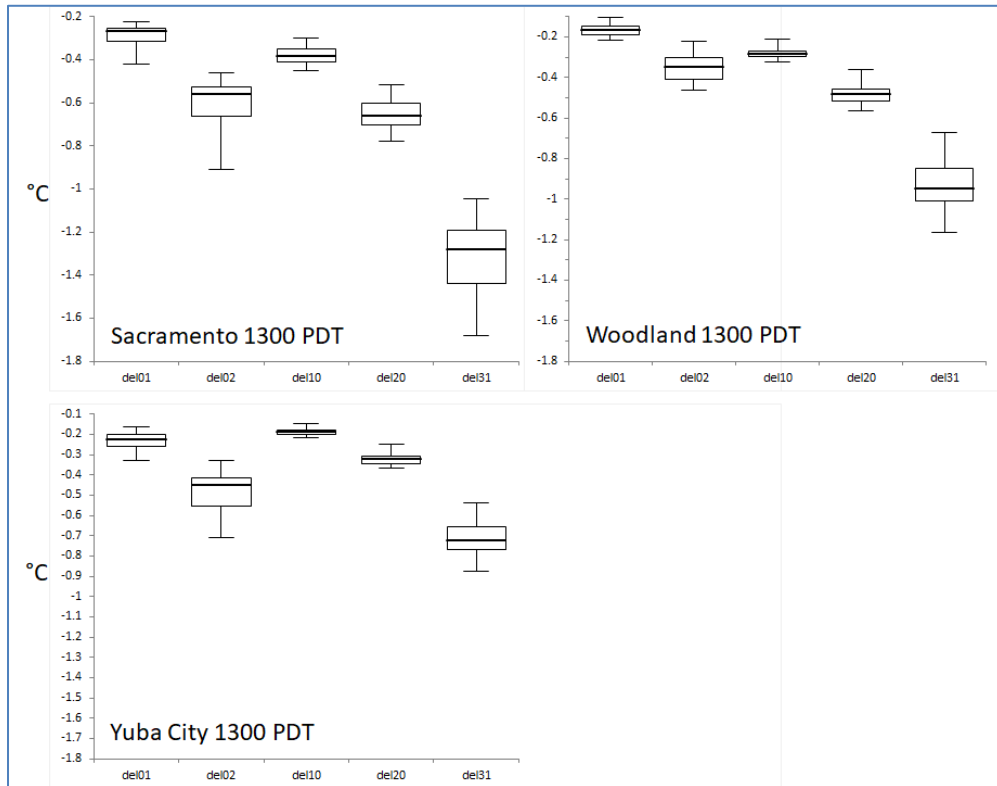
5.11.3 Impacts on the temperature field during hours 1400 – 2000 PDT

Figure 5-21 shows the average temperature reductions for the hour range 1400 - 2000 PDT (i.e., temperature reductions averaged over all 1400 to 2000 PDT hours in each time period) and also averaged over urban grid cells in each specified sub-domain. This range of hours is of interest to local utilities, i.e., SMUD, for peak electric load planning and management. The figure shows that the order of measures' effectiveness during this hourly range is (1) different from that at 0600 and 1300 PDT (although more similar to 1300 PDT) and (2) also varies across different regions, unlike at 0600 PDT. During this range of hours (1400 – 2000 PDT), the effects of albedo measures again are larger than those of canopy cover, excluding case02, because of it being mostly daylight. The magnitudes of reductions in temperature and the intra-measure differences within each area differ by location, as was seen at hour 1300 PDT, above, in Section 5.1.2. There are also instances where some of the measures are tied in terms of their cooling potentials, as seen in Figure 5-21 (e.g., case02 and case20 in Woodland). This indicates that the effects of albedo are very significant during this range of hours (and are equivalent to the effects of an extreme canopy-cover measure).

Figure 5-22 summarizes the cooling effects averaged for the hours 1400 – 2000 PDT over all time periods. In this case, the cooling effects are more uniform across all regions (less contrasts)

although some areas, such as Sacramento, see the largest cooling. During this hourly range, the albedo and vegetation measures, when averaged over all periods, have relatively the same cooling potential (excluding case02). Albedo scenario case20 produces larger cooling than vegetation scenario case01, and the most effective measure is, again, the combined scenario case31.

Figure 5-21: Average temperature reduction (°C) during hours 1400 – 2000 PDT. Periods are identified on the horizontal axis and the ranking of measures on the right side of each graph.

Figure 5-21, continued.

Placerville 1400 – 2000 PDT

Sacramento 1400 – 2000 PDT

Woodland 1400 – 2000 PDT

Yuba City 1400 – 2000 PDT
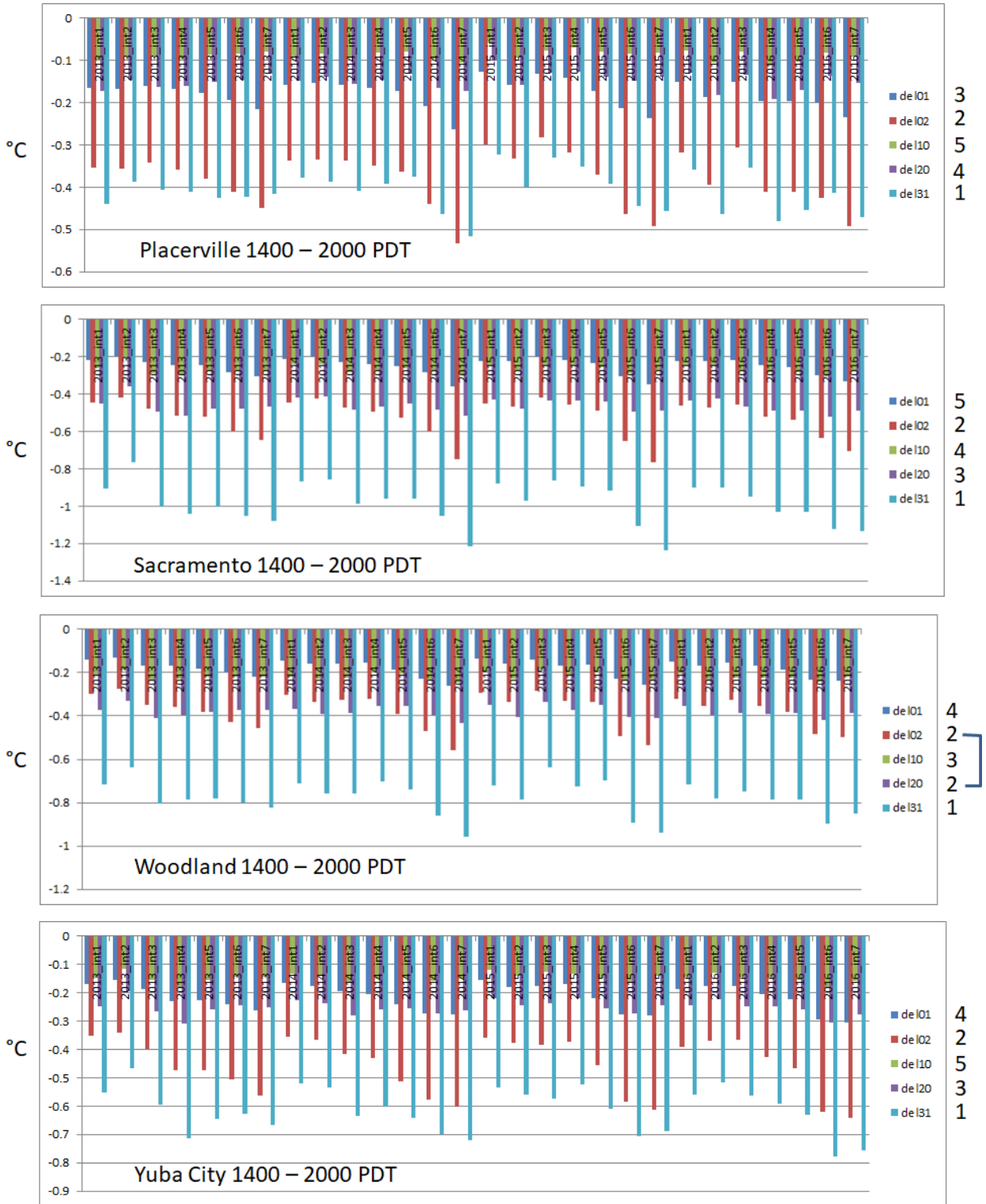
Figure 5-22: Summary of averaged temperature impacts at 1400 - 2000 PDT. Median, quartiles, and maxima/minima are shown with box and whisker plots.
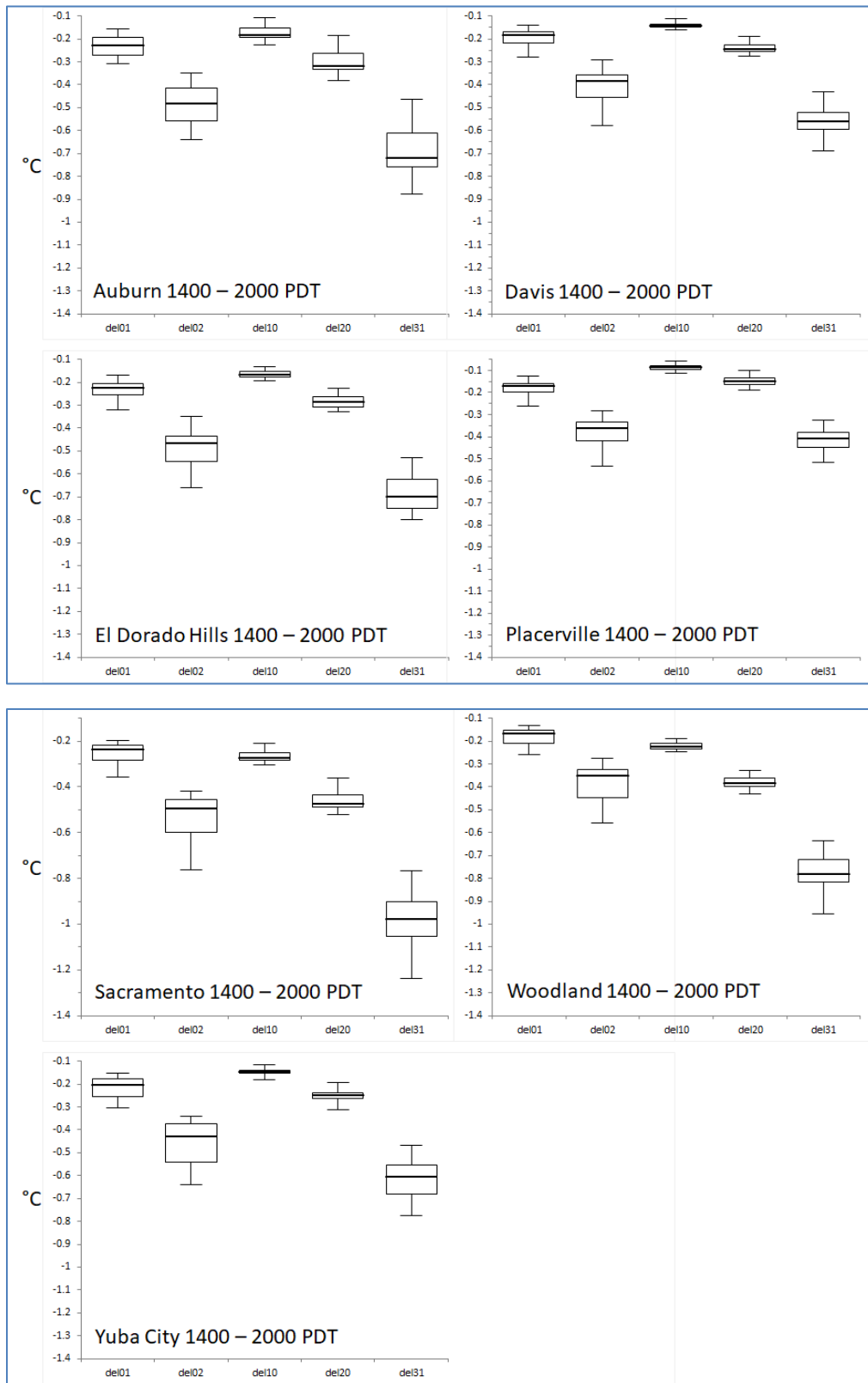
5.11.4 Impacts on the temperature field at 1500 PDT

An analysis similar to that for 1300 PDT (~solar noon) was repeated for 1500 PDT, which is closer to the time of peak air temperatures. Figure 5-23 shows the average temperature reductions at this hour (i.e., reductions averaged over all 1500-PDT hours in each period) that are also averaged over urban grid cells in each specified sub-domain. The ranking of measures at 1500 PDT is relatively similar to that at 1300 PDT, although differences do exist. At 1500 PDT, the effects of albedo measures during this daylight hour are larger than those of canopy cover (excluding case02). Some albedo measures (case20) even have a larger cooling effect than the extreme canopy cover scenario (case02). The magnitudes of reductions in temperature and the intra-measure differences within each area, i.e., how close or far apart are the reductions from different measures, also differ from one area to another. There also are cases with ties in terms of cooling potential, as seen in Figure 5-23 (e.g., case01 and case10 in Auburn, El Dorado Hills, and Yuba City).

Figure 5-24 provides a summary of the averaged effects at 1500 PDT. The areas in El Dorado Hills, Sacramento, and Woodland see relatively larger cooling effects at this time interval – these are also the areas with the larger inter-quartile ranges (spread) of temperature reductions. At this time interval, the albedo measures are more effective than canopy measures and the most effective scenario is the combination case31.

Figure 5-23: Average temperature reduction (°C) at 1500 PDT. Periods are identified on the horizontal axis and the ranking of measures on the right side of each graph.
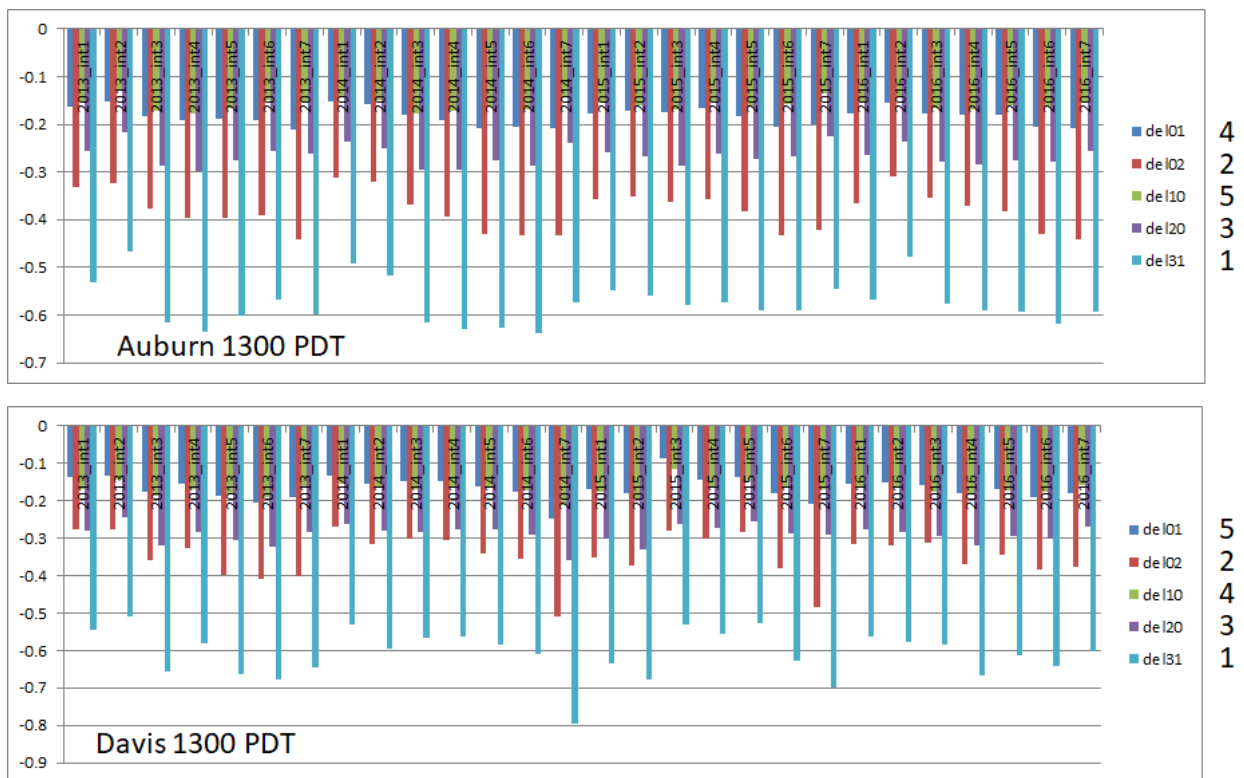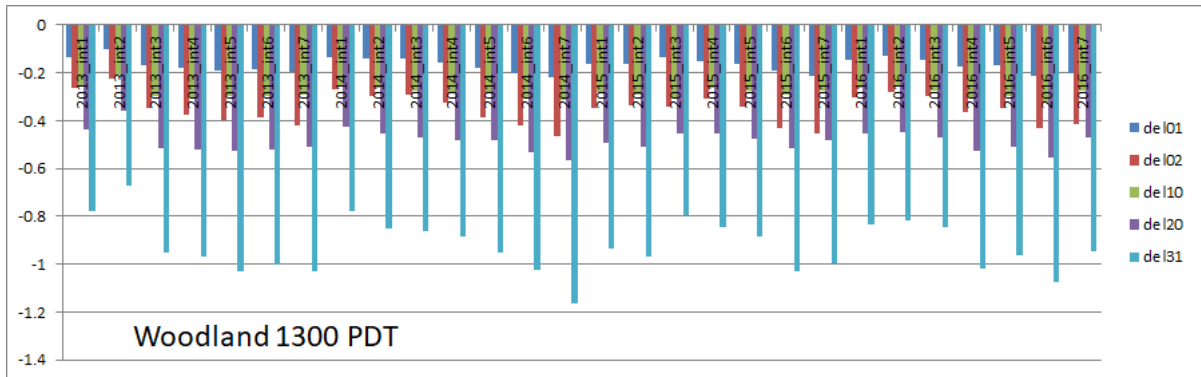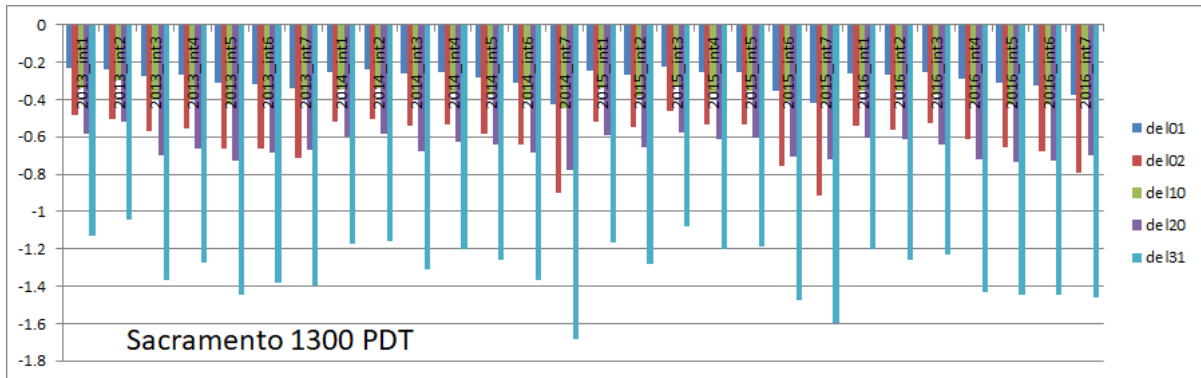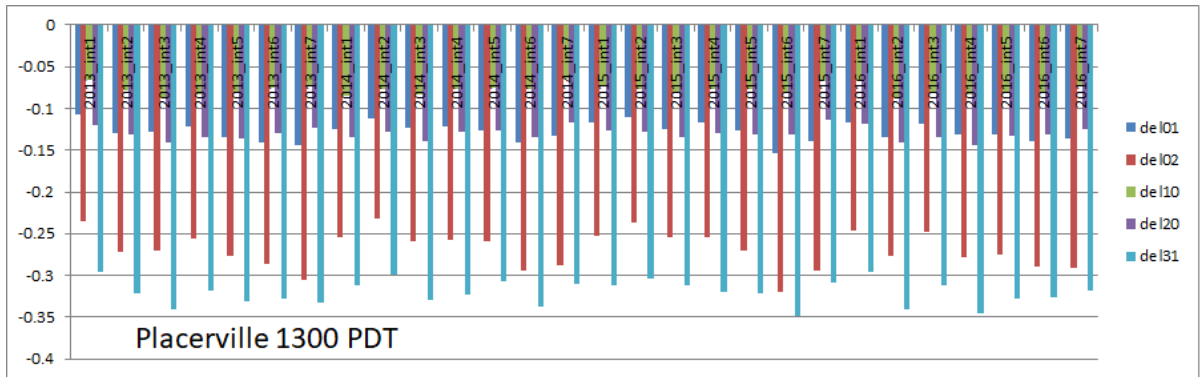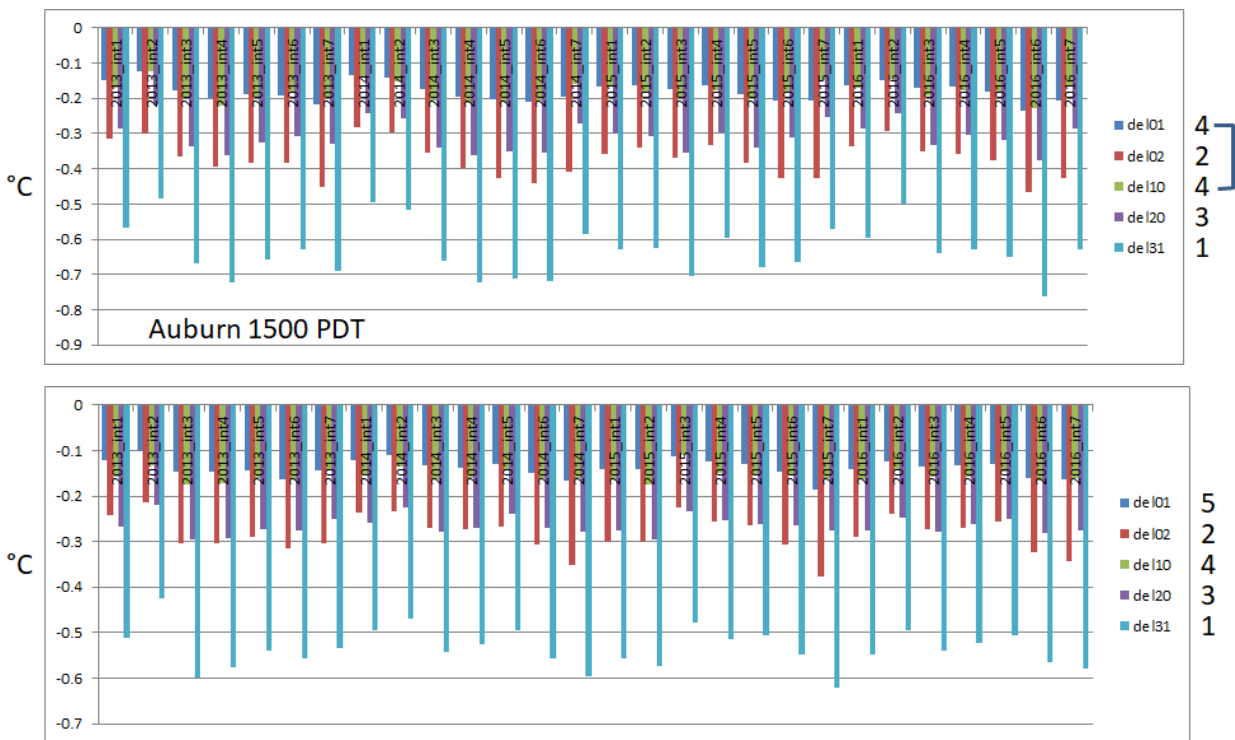
Figure 5-23, continued.
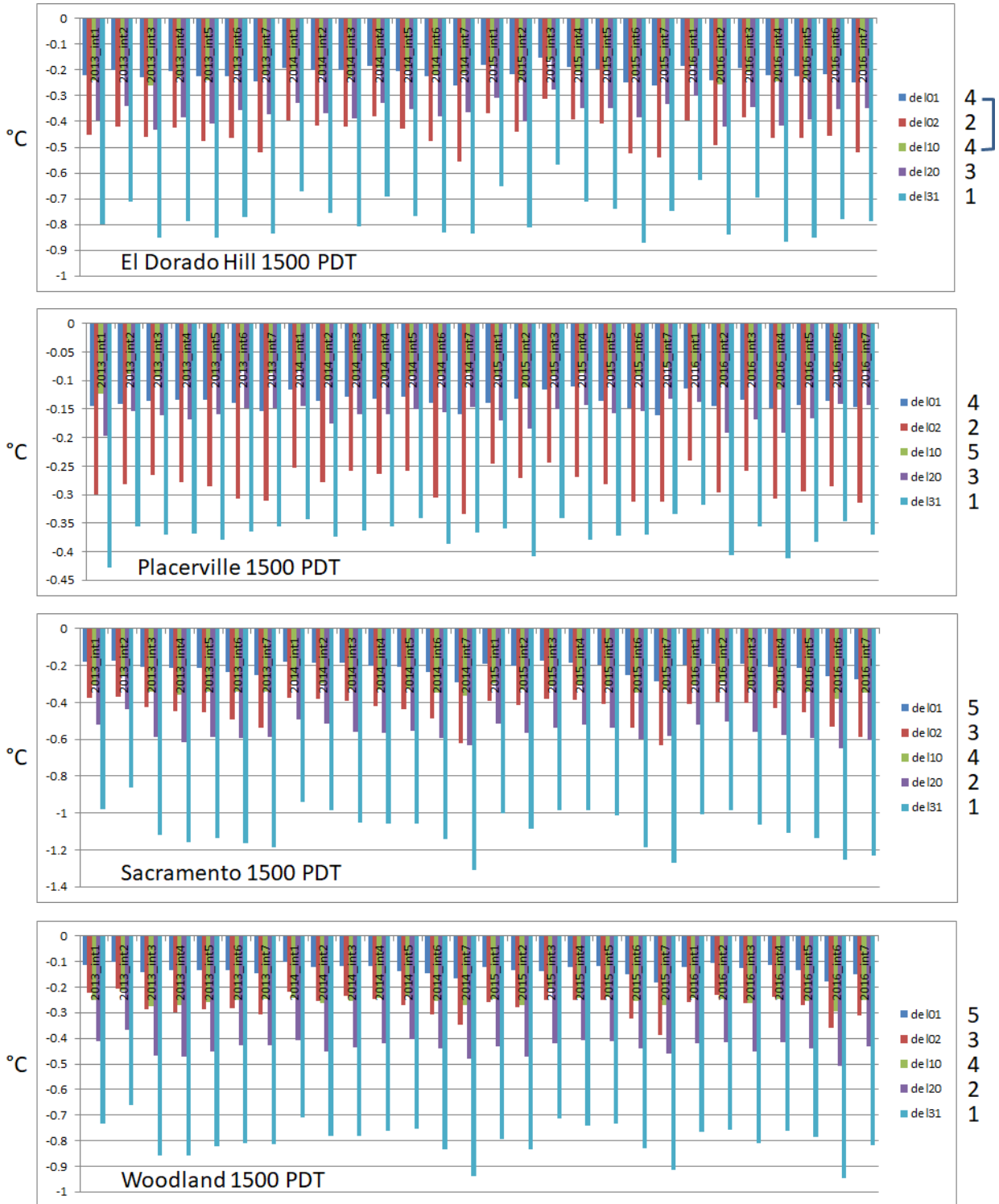
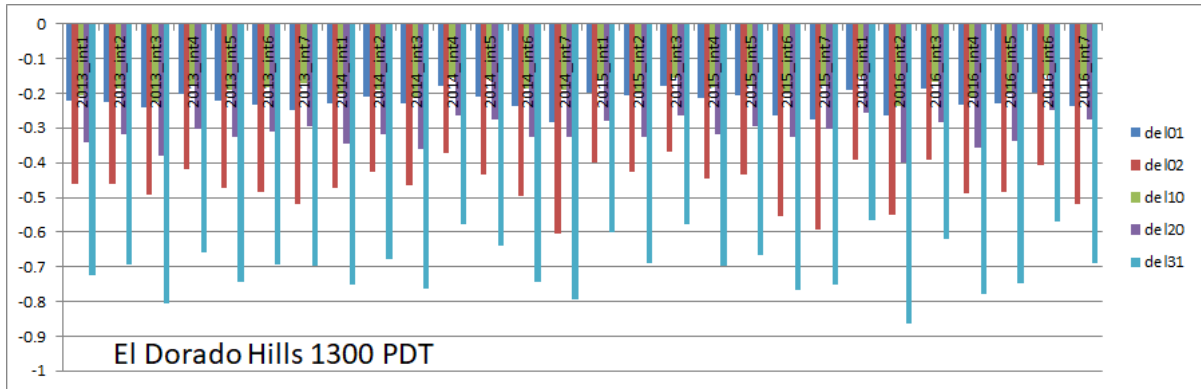Figure 5-23, continued.
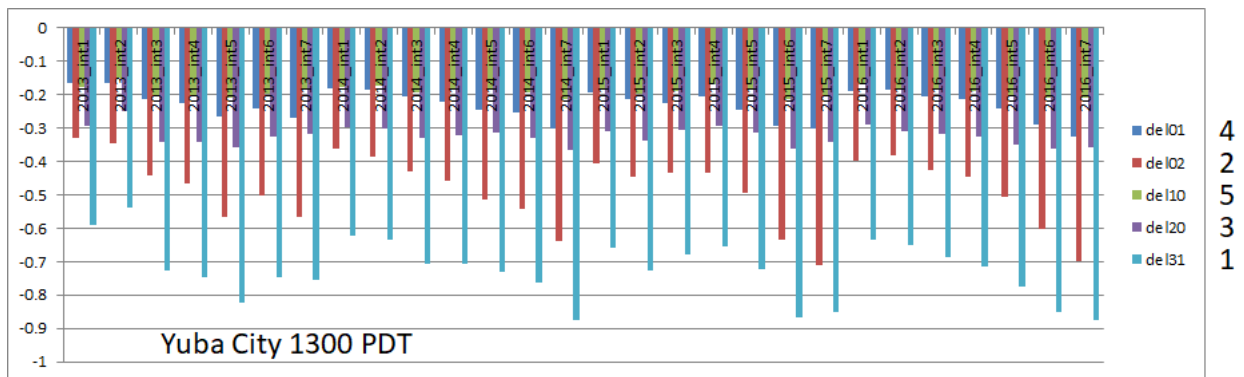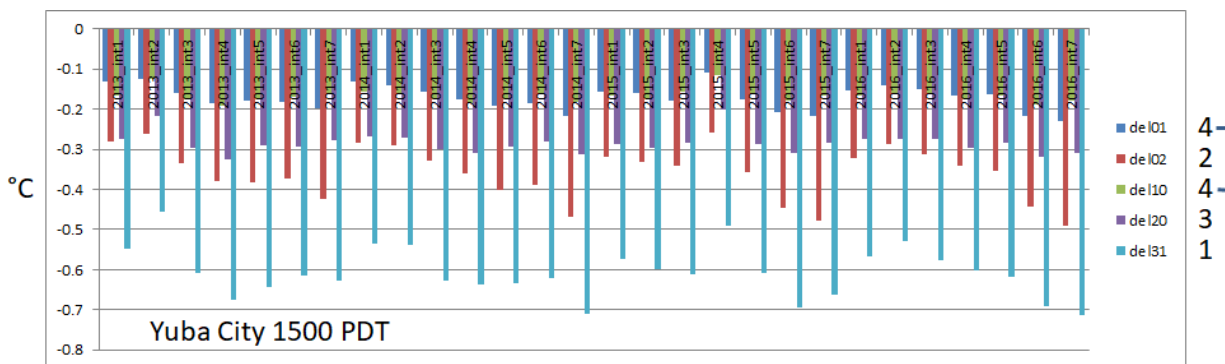

Figure 5-24: Summary of temperature impacts at 1500 PDT. Median, quartiles, and maxima/minima are shown with box and whisker plots.
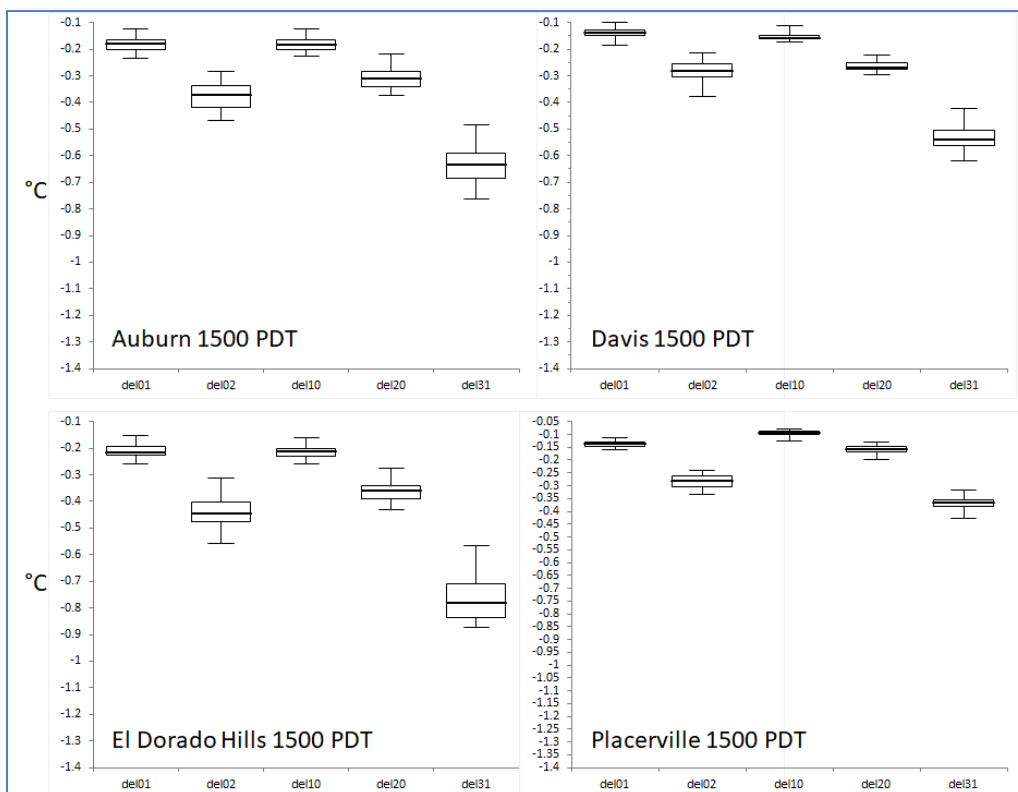
Figure 5-24, continued.
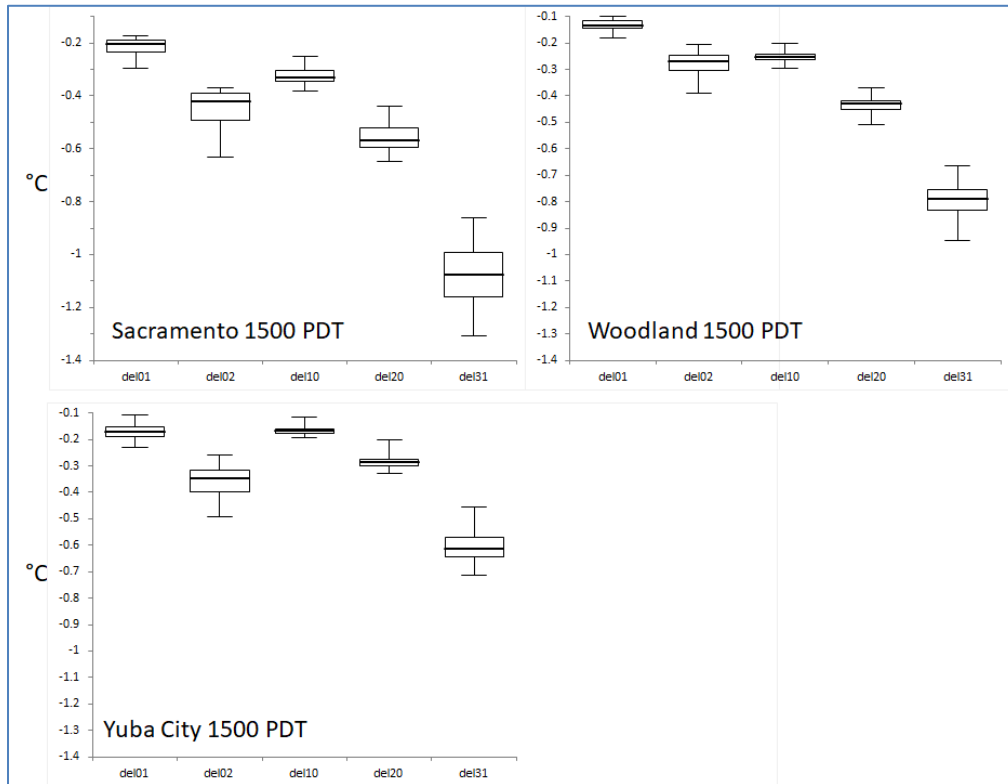
5.11.5 Impacts on the all-hours temperature field

Figure 5-25 shows the all-hours average temperature reductions (i.e., averaged over all hours in each period) and also averaged over urban grid cells in the specified sub-domains. The ranking of measures for this range of hours is biased towards (influenced by) nighttime effects of vegetation cover and thus may not be a good indicator for use in daytime urban heat-reduction planning. In fact, as the figure shows, and except for one or two instances, the ranking (i.e., the order of measures' effectiveness) at all hours is same as the ranking at 0600 PDT (the magnitude is different, however).

Figure 5-26 summarizes the all-hours cooling effects averaged again over all modeled periods. The areas of Davis, Sacramento, Woodland, and Yuba City see the larger cooling effects, which is comparable to 0600 PDT. The most effective scenario is case02 – if this scenario is excluded, then the next most effective one is the combination measure (case31).

Figure 5-25: Average all-hours temperature reduction (°C). Periods are identified on the horizontal axis and the ranking of measures on the right side of each graph.
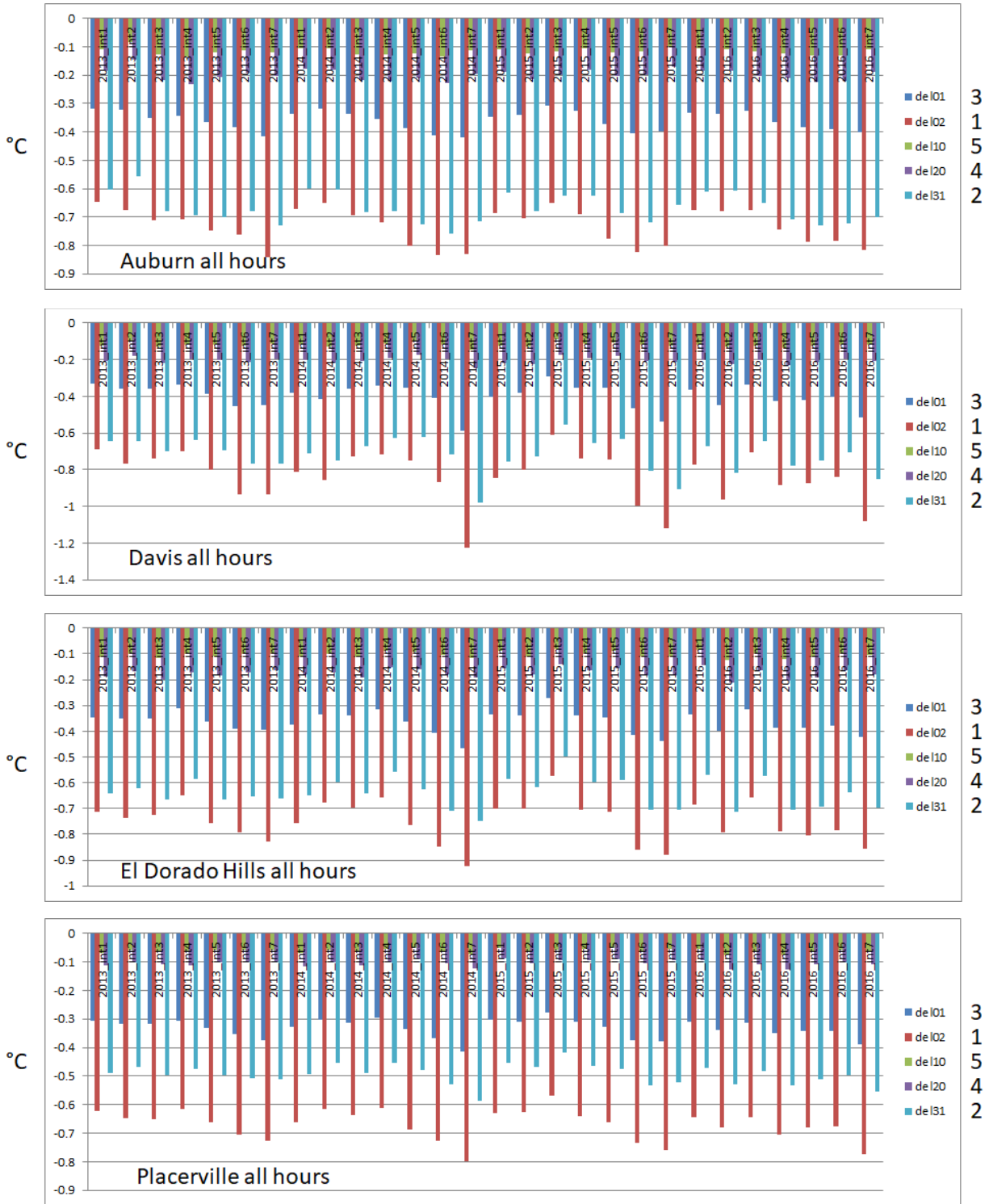
Figure 5-25, continued.
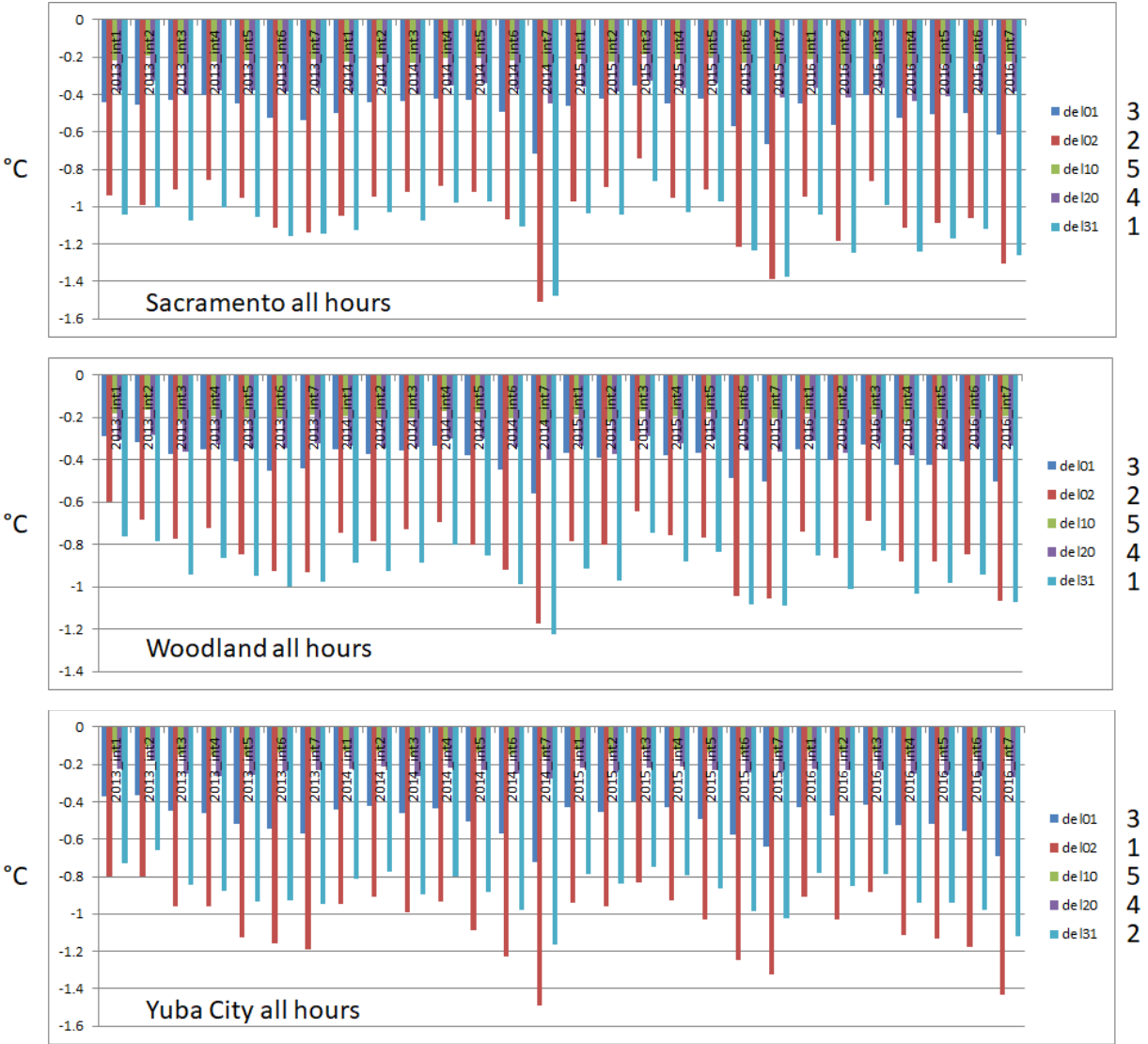
Figure 5-26: Summary of all-hour average temperature impacts. Median, quartiles, and maxima/minima are shown with box and whisker plots.
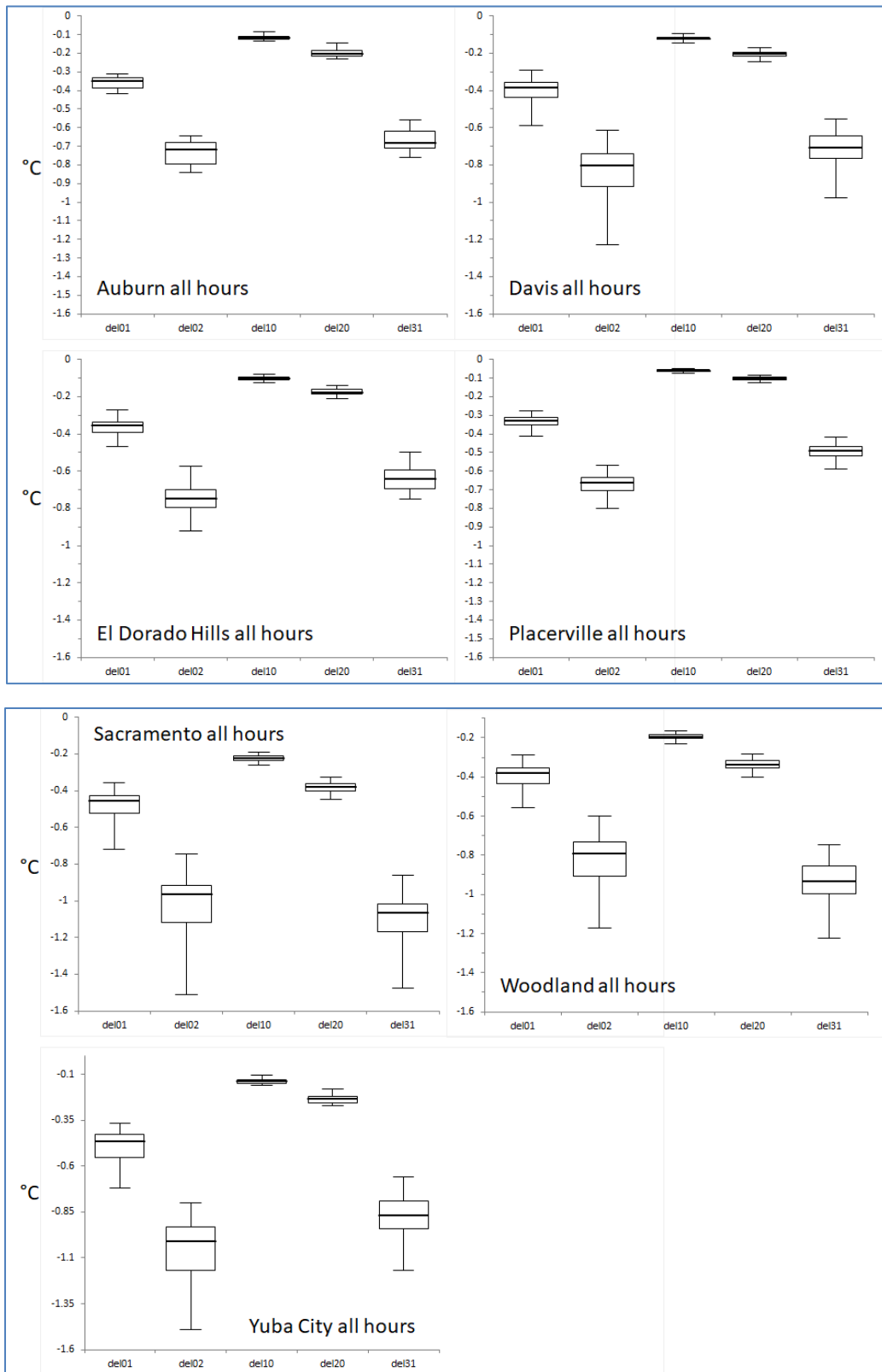
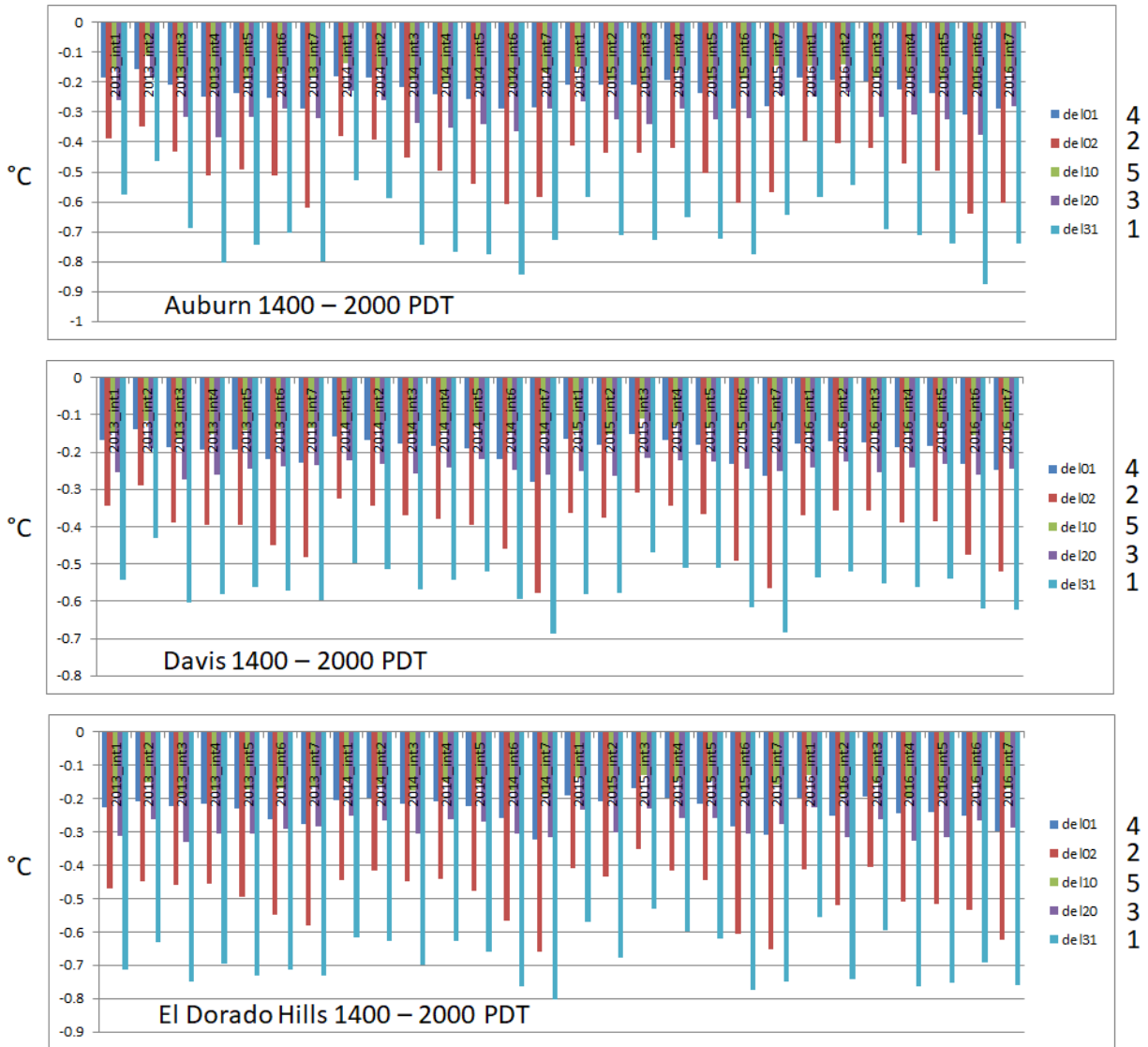## 5.12 SUMMARY OF RANKINGS

To provide an "at a glance" comparison among various scenarios, Chart 5-1 summarizes the ranking of the five measures (defined earlier) in each region and for various hours or times of day. This is a high-level summary of the UHI-mitigation potentials of these measures in current climate and land-use / land-cover conditions. As explained earlier, case02 is an extreme scenario of vegetation-cover increase and should be disregarded. It is included here only as a test for upper bounds, i.e., largest cooling, per suggestions from local tree organizations.

Chart 5-1: Summary of urban-heat mitigation potential: ranking of measures case01 through case31 by cooling effectiveness in current climate (1 – 5, darker to lighter gray = largest to smallest cooling). Note that case02 should be excluded in some analysis. Also note that these are impacts on temperature, not UHII.

		Auburn	Davis	El Dorado Hills	Placerville	Sacramento	Woodland	Yuba City
0600 PDT	case01	3	3	3	3	3	3	3
	case02	1	1	1	1	1	1	1
	case10	5	5	5	5	5	5	5
	case20	4	4	4	4	4	4	4
	case31	2	2	2	2	2	2	2
1300 PDT	case01	4	5	4	3	5	5	4
	case02	2	2	2	2	3	3	2
	case10	5	4	5	4	4	4	5
	case20	3	3	3	3	2	2	3
	case31	1	1	1	1	1	1	1
1400 - 2000 PDT	case01	4	4	4	3	5	4	4
	case02	2	2	2	2	2	2	2
	case10	5	5	5	5	4	3	5
	case20	3	3	3	4	3	2	3
	case31	1	1	1	1	1	1	1
1500 PDT	case01	4	5	4	4	5	5	4
	case02	2	2	2	2	3	3	2
	case10	4	4	4	5	4	4	4
	case20	3	3	3	3	2	2	3
	case31	1	1	1	1	1	1	1
allHRS	case01	3	3	3	3	3	3	3
	case02	1	1	1	1	2	2	1
	case10	5	5	5	5	5	5	5
	case20	4	4	4	4	4	4	4
	case31	2	2	2	2	1	1	2

The chart does not provide information on the spread (e.g., inter-quartile ranges) of the cooling effects from a particular measure nor how close various measures are to each other (or how far apart they are in terms of cooling effects). It simply shows the ranking even if differences between one measure and another can be very small or almost tied in some instances. Cases (scenarios) that are tied are indicated by a repeated number (and color code). It is important to note that the rankings are based on temperature changes averaged over 2-km. These rankings can differ at the finer scales

(500 m) and the magnitudes of the temperature reductions also get larger when averaged at finer resolutions. In Chart 5-1, the various time bands may be of interest to different applications. For example, the 0600 PDT and allHRS bands could be of interest from a heat-wave perspective, the 1400-2000 PDT band may be of interest to utilities, the 1500-PDT band could be used in relation to peak cooling demand analysis, and the band at 1300 PDT is of relevance to assessments of measures around solar noon.

The modeling of future climates, e.g., year 2050 RCP 4.5 and RCP 8.5, discussed later, shows that except for a number of instances, the current-climate ranking (and ordering) of measures remains generally unchanged into the future. That is, the ranking of measures in terms of their cooling effectiveness in current climates and LULC remains relatively the same in the future. While the ranking (order) can be relatively similar in current and future years, the magnitudes of the cooling effects differ. Table 5-7 provides the numerical values of the cooling associated with Chart-1 (values are averaged over all grid cells in each region and for the given time period), with case02 excluded. The additional chart below the table simply is a graphical representation of the values listed.

Table 5-7: Temperature changes (°C) corresponding to Chart 5-1 (case02 has been excluded).

		Auburn	Davis	El Dorado Hills	Placerville	Sacramento	Woodland	Yuba City
0600 PDT	case01	-0.40	-0.60	-0.50	-0.50	-0.70	-0.60	-0.75
	case10	-0.08	-0.15	-0.09	-0.09	-0.10	-0.10	-0.10
	case20	-0.10	-0.20	-0.10	-0.10	-0.20	-0.20	-0.20
	case31	-0.50	-0.90	-0.60	-0.55	-1.00	-0.90	-1.00
1300 PDT	case01	-0.20	-0.18	-0.22	-0.12	-0.25	-0.18	-0.22
	case10	-0.20	-0.20	-0.20	-0.08	-0.40	-0.30	-0.20
	case20	-0.30	-0.30	-0.30	-0.12	-0.65	-0.50	-0.33
	case31	-0.60	-0.60	-0.70	-0.32	-1.30	-0.95	-0.70
1400 - 2000 PDT	case01	-0.22	-0.19	-0.22	-0.18	-0.23	-0.16	-0.20
	case10	-0.20	-0.15	-0.15	-0.10	-0.25	-0.22	-0.15
	case20	-0.32	-0.25	-0.30	-0.15	-0.47	-0.35	-0.25
	case31	-0.72	-0.55	-0.70	-0.40	-1.00	-0.76	-0.60
1500 PDT	case01	-0.18	-0.14	-0.21	-0.14	-0.20	-0.13	-0.17
	case10	-0.18	-0.15	-0.21	-0.10	-0.33	-0.25	-0.18
	case20	-0.30	-0.27	-0.36	-0.16	-0.55	-0.45	-0.30
	case31	-0.64	-0.52	-0.80	-0.37	-1.10	-0.80	-0.60
allHRS	case01	-0.35	-0.40	-0.35	-0.32	-0.45	-0.38	-0.47
	case10	-0.12	-0.17	-0.10	-0.05	-0.20	-0.20	-0.15
	case20	-0.20	-0.20	-0.18	-0.10	-0.37	-0.33	-0.22
	case31	-0.65	-0.70	-0.60	-0.50	-1.06	-0.92	-0.85

Table 5-7 excludes case02 to provide a fairer comparison among measures. At the finer scales (i.e., specific projects evaluated at 500-m resolution), the cooling effects are significantly larger than the 2-km averaged effects reported here.

It can be concluded from this discussion (Chart 5-1 and Table 5-7) that albedo scenarios (e.g., cool roofs and cool pavements) are the top choice for reducing daytime urban air temperature. Because the vegetation canopy cover can cool the air both during the day and at night, its impacts are dominant in the 24-hour average metrics and early-morning averages.

5.13 IMPACTS OF COOLING MEASURES ON THE URBAN HEAT ISLAND INDEX IN CURRENT CLIMATE

Following the calculations and establishment of the UHII for the Capital region, as discussed earlier in Section 5.3, the potential of various mitigation measures in offsetting or mitigating the index was quantified. In this section, an overview is presented for the regional scale (2 km) for current climate and LULC. A similar assessment will be presented at the fine scale (500 m), later in this report.

The examples shown here are for cases 01, 02, 10, 20, and 31, as defined earlier, for hours 0600 PDT, 1500 PDT, and the all-hour average UHII. It is reiterated that the maps shown in this discussion are composites (not a continuous field) made up of six different tiles, each with its own upwind reference points (see Section 5.3). It is equally important to note here that the changes discussed in the following sections are changes in the UHII (which, itself, is a temperature *difference*) not in absolute temperature.

5.13.1 Impacts on the UHII at 0600 PDT

Figures 5-27 and 5-28 summarize the potential of heat-mitigation measures for fully or partially offsetting the UHII at 0600 PDT. Figure 5-27 also shows the spatial characteristics of the UHII offsets, i.e., where the cooling effect is largest within each of the tiles. A temperature equivalent (DH hr^{-1} in units of C·hr hr^{-1}) is also provided on each figure. This example is for the period July 16 – 31, 2015.

As discussed earlier, all cases are presented in Figure 5-28, however, vegetation-canopy scenarios above case01 may not be realistically feasible at this time. It can be seen from Figure 5-28 that at 0600 PDT, the most effective measures are those that include canopy-cover increase, which, as previously highlighted, is because (1) the effects of albedo changes are small, as there is little solar radiation at this hour -- except for reduced long-wave re-radiation of heat at night, and (2) that vegetation canopies cool the air continuously during the day and night.

While all regions benefit from significant UHII offset at this hour, the areas of Woodland, Davis, and Sacramento see the largest reductions, percentage-wise (Figure 5-28). The largest reduction is produced by case31 (up to -2.1 °C in temperature equivalent) as seen in the last graph of Figure 5-27.

Figure 5-27: Change in 0600-PDT UHII (composite 2 km domain). Example for period July 16 – 31, 2015 (DH = °C · hr)

Figure 5-27, continued.

Example: 2015_int4, Case31 range of UHII change (white to dark blue: 0 to -32.1 DH / 15 days)
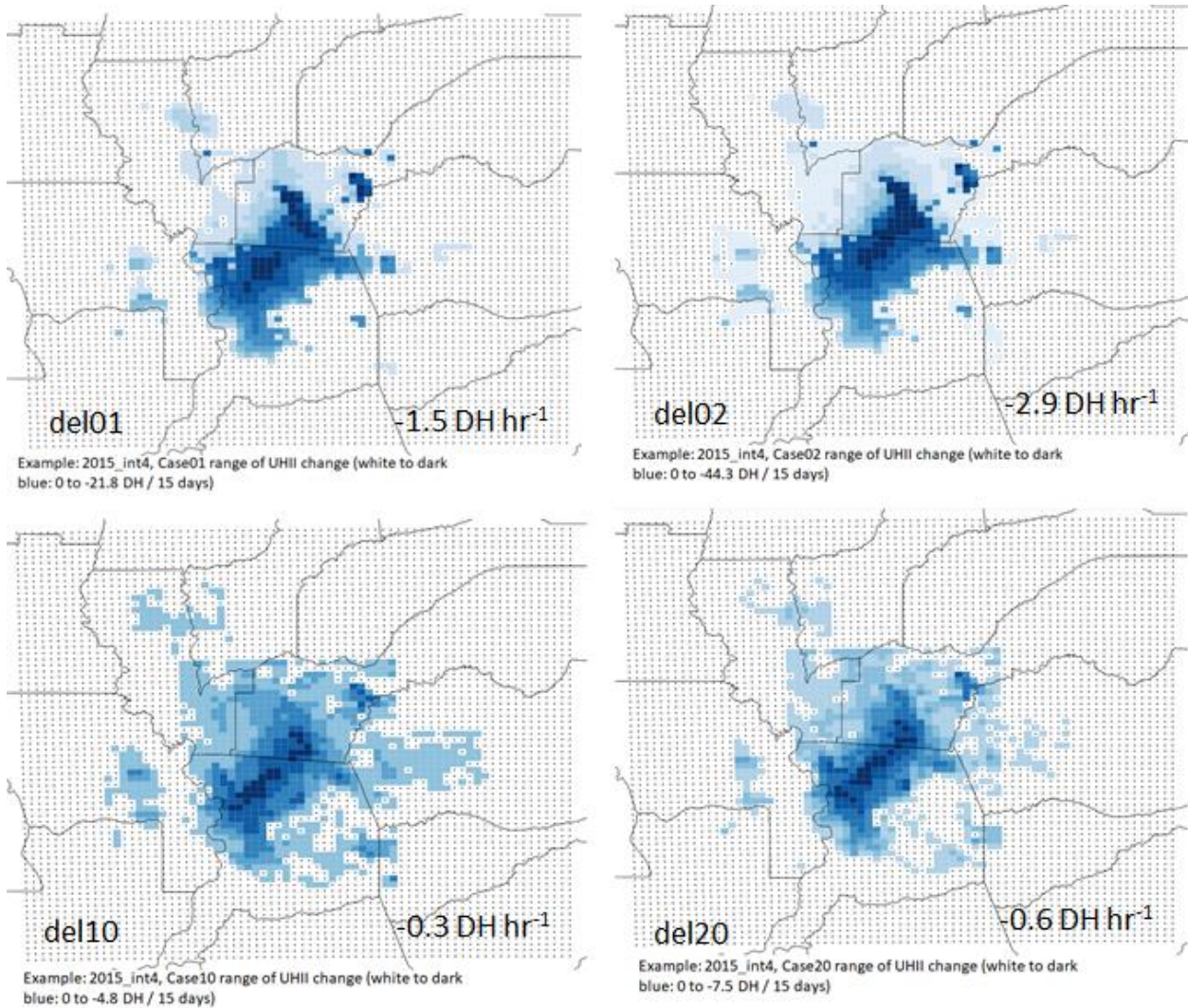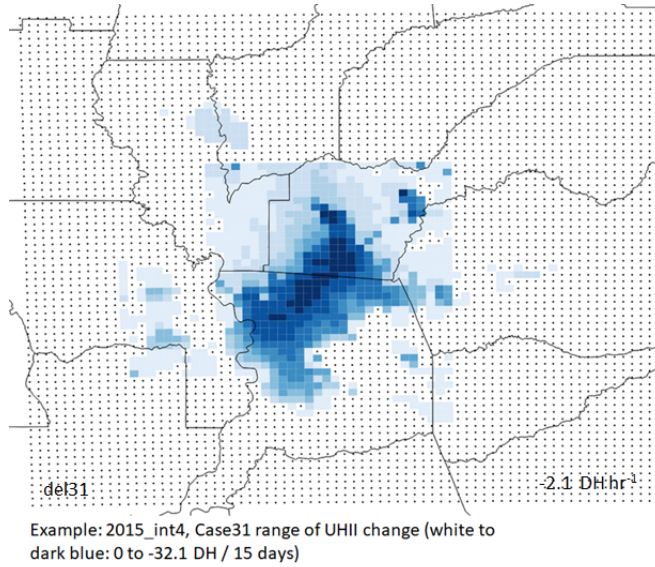
Figure 5-28: Reduction (%) in 0600-PDT UHII for the period July 16 – 31, 2015 (DH = °C · hr)
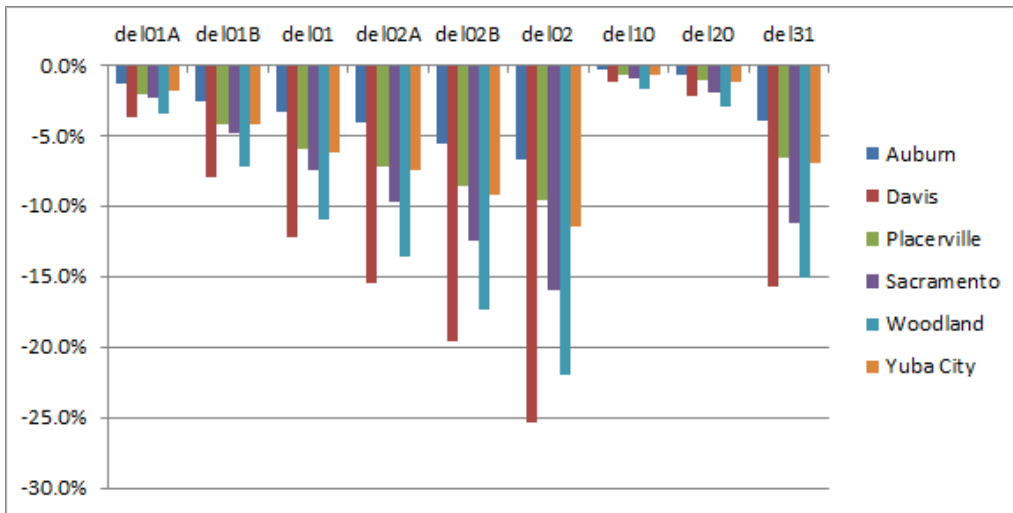
5.13.2 Impacts on the UHII at 1500 PDT

In a similar manner, Figures 5-29 and 5-30 summarize the potential of heat-mitigation measures in offsetting the UHII at 1500 PDT for an example period (July 16 – 31, 2015). Figure 5-29 shows the spatial characteristics of UHII offsets – the effects of albedo measures are now dominant during daylight hours, which is the reverse of what occurs at 0600 PDT (Section 5.13.1). Furthermore, the spatial characteristics of cooling at this hour are more varied than at 0600 PDT because the effects of albedo are more pronounced than the effects of canopy cover. As discussed earlier, features such as the American River and surrounding areas, for example, now appear

conspicuously in the figures, since these are areas where albedo changes are the smallest, because of small impervious cover.

In Figure 5-30, it can be seen that albedo measures are more effective than canopy measures during daylight hours (excluding case02 and similar). The most effective scenario at reducing the UHII is that of a combination of measures (case31). While the UHII offset is significant in all areas, Sacramento, Auburn, and Placerville see the larger reductions (percentage wise) in the UHII, which is different from the areas at 0600 PDT.

There also is a negligible increase in the UHII in case01B in Yuba City (Figure 5-30). In past studies, e.g., Taha (2013a,b), such increases were observed resulting from non-linear effects and attributed to changes in the wind and mixing fields under certain daytime conditions. But the occurrence is negligible (as seen in the figure) and the area affected by the increase is small, as discussed earlier in Section 5.10.

Figure 5-29: Change in 1500-PDT UHII (composite 2 km domain). Example for period July 16 – 31, 2015 (DH = °C · hr)

del01   -0.4 DH hr^{-1}

Example: 2015_int4, Case01 range of UHII change (white to dark blue: 0 to -6.3 DH / 15 days)

del02   -0.6 DH hr^{-1}

Example: 2015_int4, Case02 range of UHII change (white to dark blue: 0 to -8.6 DH / 15 days)

del10   -0.4 DH hr^{-1}

Example: 2015_int4, Case10 range of UHII change (white to dark blue: 0 to -6.3 DH / 15 days)

del20   -0.7 DH hr^{-1}

Example: 2015_int4, Case20 range of UHII change (white to dark blue: 0 to -10.3 DH / 15 days)

del31   -1.1 DH hr⁻¹

Example: 2015_int4, Case31 range of UHII change (white to dark
blue: 0 to -15.9 DH / 15 days)

Figure 5-30: Reduction (%) in 1500-PDT UHII for the period July 16 – 31, 2015 (DH = °C · hr)
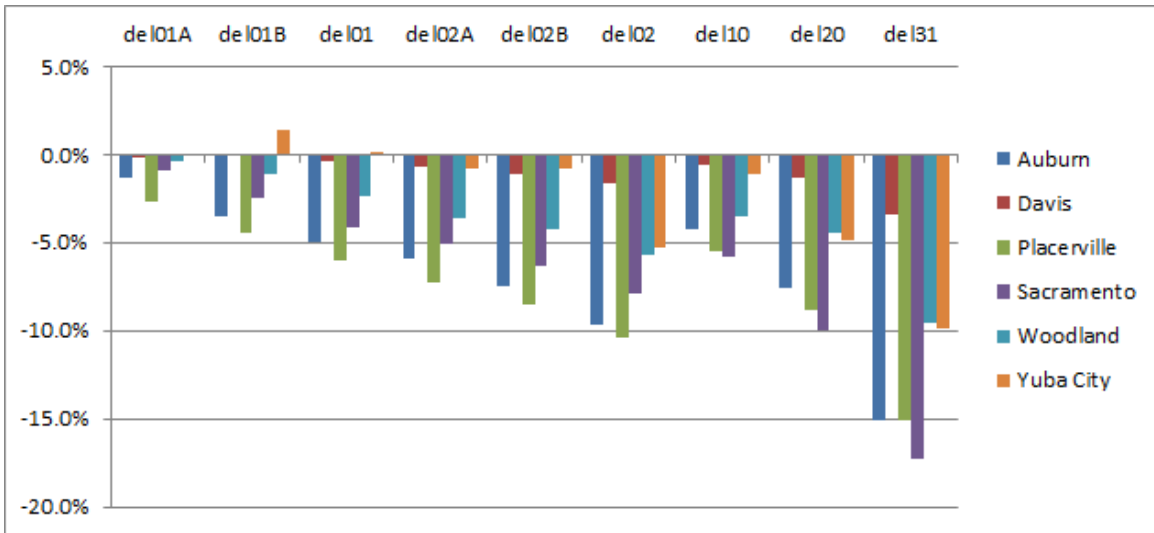
5.13.3 Impacts on the all-hours UHII

Some aspects of the all-hours UHII mitigation are presented in this section. Figures 5-31 and 5-33 summarize the potential of heat-mitigation measures in offsetting the UHII as an all-hour average for the sample period July 16 – 31, 2015. Figure 5-31 shows the spatial characteristics of UHII offsets which, again, are skewed relatively more towards the effects of canopy cover (since they include nighttime effects). For comparison, Figure 5-32 is the Cal/EPA all-hours UHII (Taha

2017). One can see that (1) the spatial pattern of UHII mitigation is in general such that the greater offsets are in locations of larger UHII (which is both expected and desirable) and (2) that case31 (as well as case02) can offset most if not all of the all-hours UHII in terms of temperature equivalent (DH hr^{-1}).

The most effective measures (excluding case02 and similar) are the combination scenario and the vegetation-cover case01. The albedo measures are still effective and significant, but because this metric includes nighttime effects, vegetation canopy has a more dominant effect. Finally, while all areas benefit significantly from mitigation measures at all hours, Woodland, Sacramento, and Davis see the largest (percentage-wise) reductions in the all-hours UHII.

Figure 5-31: Change in all-hours UHII (composite 2 km domain). Example for period July 16 – 31, 2015 (DH = °C · hr)

del01   -0.8 DH hr^{-1}

Example: 2015_int4, Case01 range of all-hours UHII change (white to dark blue: 0 to -286 DH / 15 days)

del02   -1.7 DH hr^{-1}

Example: 2015_int4, Case02 range of all-hours UHII change (white to dark blue: 0 to -596 DH / 15 days)

del10   -0.3 DH hr^{-1}

Example: 2015_int4, Case10 range of all-hours UHII change (white to dark blue: 0 to -114 DH / 15 days)

del20   -0.5 DH hr^{-1}

Example: 2015_int4, Case20 range of all-hours UHII change (white to dark blue: 0 to -192 DH / 15 days)

del31   1.6 DH hr⁻¹

Example: 2015_int4, Case31 range of all-hours UHII change (white to dark blue: 0 to -549 DH / 15 days)

Figure 5-32: Level-1 Cal/EPA UHII (Taha 2017; Taha and Freed 2015), not encompassing the entire 6-counties region. Areas with the largest UHII also have some of the largest potentials for cooling.

2.0 DH hr⁻¹

1.2 DH hr⁻¹
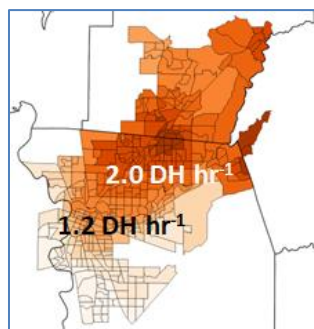
Finally, Figure 5-34 summarizes the reductions in the UHII (DH exceedances) relative to 35 °C (95 °F) which is a threshold commonly used by the electric utilities in calculating summertime cooling loads. The pattern of reductions in UHII (DH) above this threshold looks generally similar to the pattern of reductions in the all-hours UHII (see Figure 5-33). Excluding the extreme case02 and related scenarios, the most effective measure at reducing UHII above 35 °C is again case31 followed by albedo (case20) and vegetation-canopy cover (case01). Here, they are both of relatively similar magnitudes. However, the order of areas with most benefits (percentage-wise) is Placerville, Auburn, and Sacramento.

It is important to reiterate again that the changes discussed in this section are changes in UHII not in absolute temperature.

Figure 5-33: Reduction (%) in all-hours UHII for the period July 16 – 31, 2015 (DH = °C · hr)
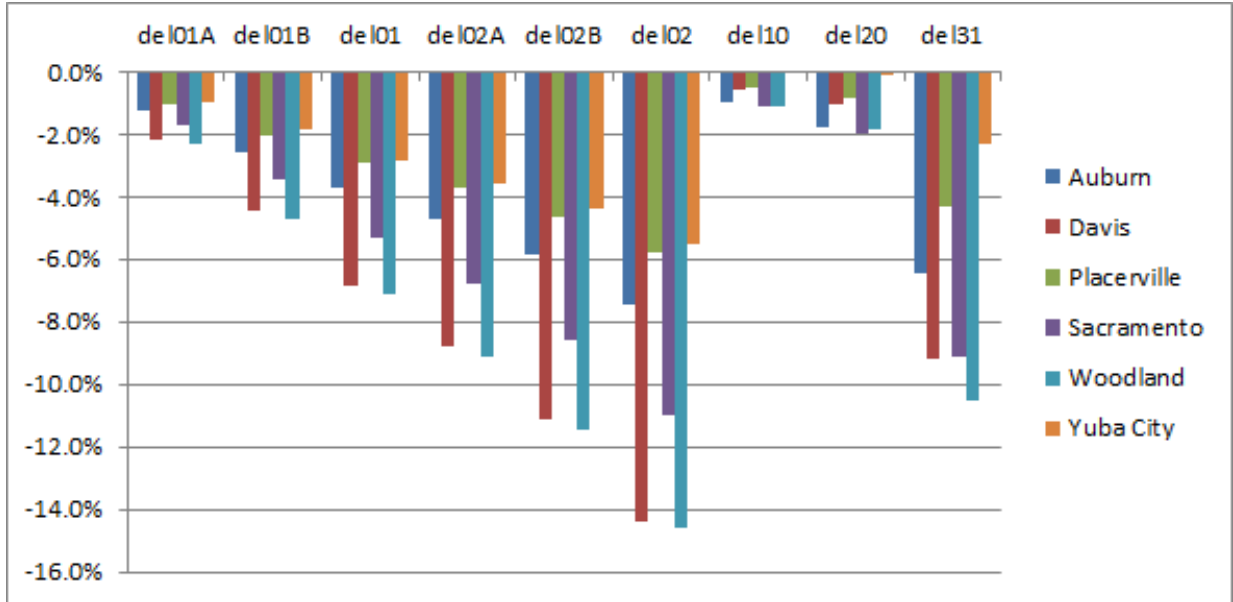
Figure 5-34: Reduction (%) in UHII above a 35 °C threshold, for all periods.
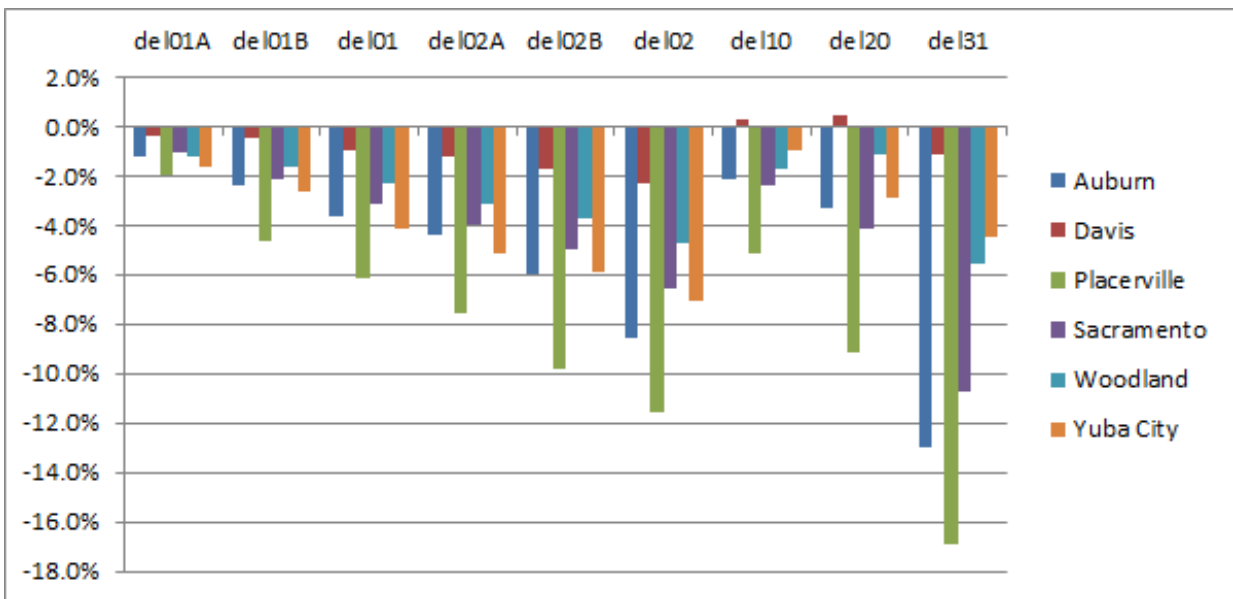
5.14 CHANGES IN TEMPERATURE EXCEEDANCES OVER THRESHOLDS

In this section, the changes in temperature, e.g., cumulative DH, above thresholds of 35 and 38 °C are presented. It is noted here that this analysis of temperature (DH) versus thresholds is different from a similar analysis of DH in terms of the National Weather Service Heat Index (NWS HI, discussed in Section 5.15) in that the NWS HI also includes humidity in the calculations. Thus, the analysis in this section may be more useful to applications by utilities -- the threshold of 38 °C, for example, is of interest to utilities in the region (SMUD) in planning for electric demand. On the other hand, the NWS HI analysis is used in the assessment of potential heat-health impacts of mitigation measures.

35 °C threshold

Figure 5-35 shows the degree-hour (°C·hr) exceedances above 35 °C in the sub-domains of interest and for all modeled times. For each time period, indicated on the horizontal axis, a base case and five scenarios or measures are plotted to provide an indication as to their heat-mitigation potentials. While the range of exceedances (absolute values) varies by region, certain features are consistent across all domains. For instance, the periods 2013_int3, 2014_int3, and 2016_int4 have consistently larger exceedances than other time periods in all sub-domains (these are periods containing heat-wave/heat-event days, as discussed in Section 5.15, Table 5-12). Also, relative to the base scenario, it can be seen that all measures can reduce exceedances by a significant amount.

Table 5-8 summarizes the percentage-wise reductions in exceedances averaged over all periods for each region. Excluding case02 (an extreme scenario), it can be seen that the albedo measures are either similar in effect to or better than the vegetation-canopy measures since the 35 °C threshold is a daytime-high temperature (i.e., a time of day when albedo measures are effective). The scenario producing the largest reductions in exceedances is case31, which is consistent with results from other analysis of metrics and threshold.

Figure 5-35: Temperature exceedance (DH) over a 35 °C threshold, for all periods.

Figure 5-35, continued.

Woodland DH over 35 °C threshold

Yuba City DH over 35 °C threshold
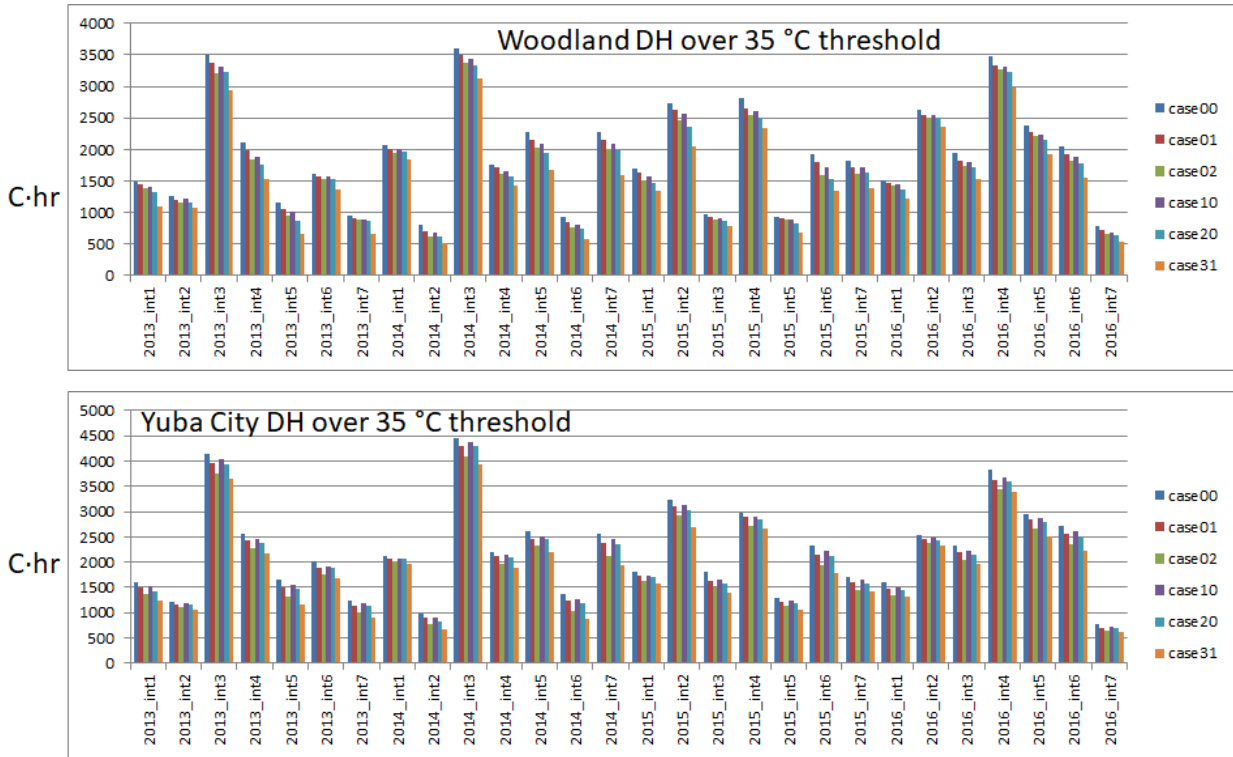
Table 5-8: Reduction in exceedances over 35 °C, current climate, averaged over all intervals and years (2013 – 2016) and over urban areas in the given sub-domains.

	Canopy scenarios		Albedo scenarios		Combination
	del01	del02	del10	del20	del31
Auburn	-8.1%	-16.3%	-6.8%	-11.2%	-23.7%
Davis	-5.4%	-10.9%	-4.5%	-7.9%	-16.7%
El Dorado Hills	-9.6%	-18.6%	-7.7%	-12.6%	-27.4%
Placerville	-6.9%	-14.1%	-3.9%	-6.7%	-16.4%
Sacramento	-7.7%	-15.2%	-8.5%	-14.1%	-28.9%
Woodland	-4.7%	-9.5%	-6.6%	-11.3%	-21.3%
Yuba City	-5.4%	-12.1%	-3.9%	-6.9%	-16.5%

38 °C threshold

Figure 5-36 represents the degree-hour (ºC·hr) exceedances above 38 °C in all sub-domains and for all time intervals. As in the preceding discussion, for each time interval a base case and five scenarios or mitigation measures are plotted. As discussed above, certain features are consistent

across all domains, e.g., periods 2013_int3, 2014_int3, and 2016_int4 (heat-wave/heat events) have consistently larger exceedances than other time periods in all sub-domains.

In Table 5-9, the percentage-wise reductions in exceedances above 38 °C, averaged over all periods for each region, are summarized. It is to be noted, as elsewhere in this analysis, that case del02 is an extreme and that case31 represents a more realistic level of canopy cover increase paired with a relatively high, but realistic increase in albedo. Thus, excluding case02, one can see that the albedo measures are either similar to (in effect) or better than the vegetation-canopy measures, as this is a daytime temperature threshold. Furthermore, the scenario producing the largest reductions in exceedances is case31, which is consistent with other results presented earlier in this report.

Figure 5-36: Temperature exceedance (DH) over a 38 °C threshold, for all periods.
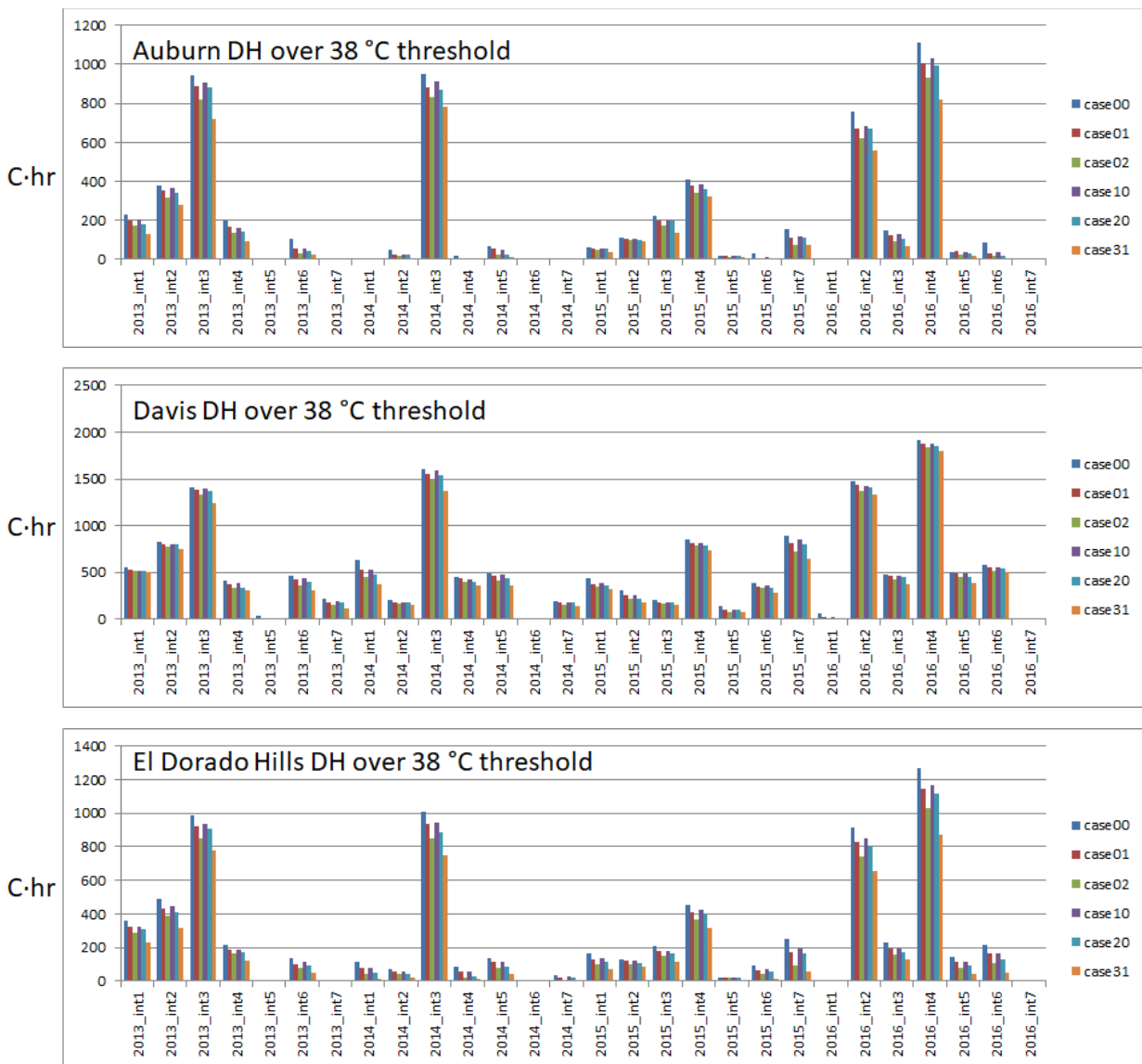
Figure 5-36, continued.

Table 5-9: Average reduction in exceedances over 38 °C, current climate, averaged over all intervals and years (2013 – 2016).
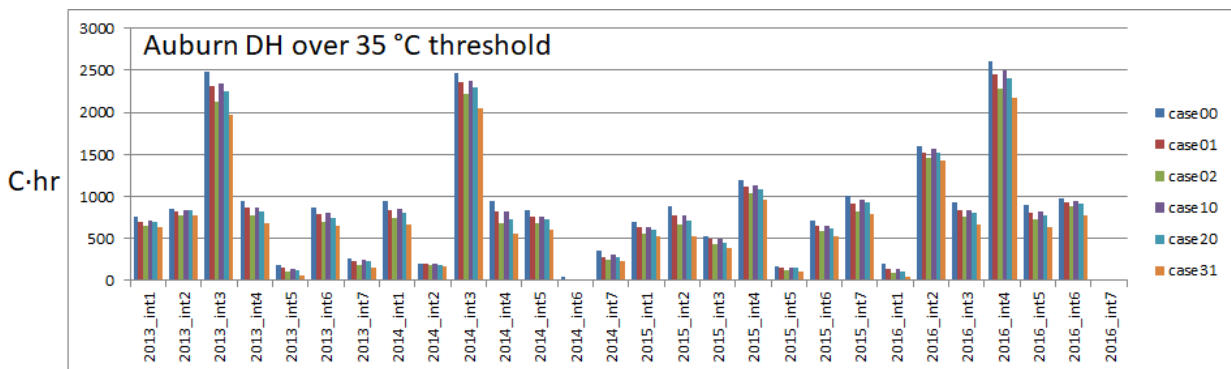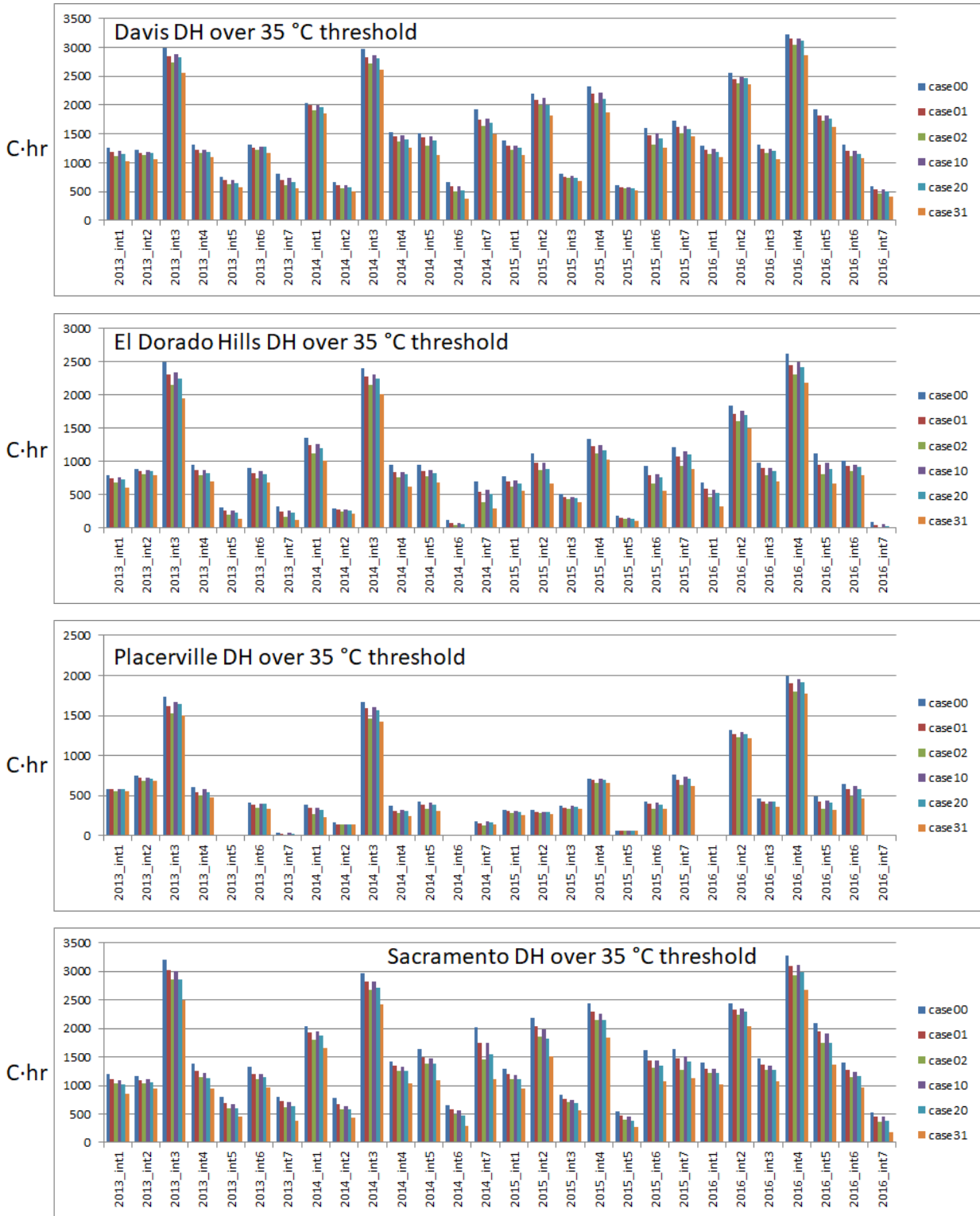
	Canopy scenarios		Albedo scenarios		Combination
	del01	del02	del10	del20	del31
Auburn	-11%	-21%	-10%	-15%	-31%
Davis	-6%	-12%	-5%	-9%	-19%
El Dorado Hills	-13%	-25%	-11%	-18%	-38%
Placerville	-12%	-25%	-8%	-15%	-32%
Sacramento	-10%	-20%	-11%	-19%	-36%
Woodland	-6%	-12%	-10%	-16%	-28%
Yuba City	-7%	-14%	-6%	-10%	-20%

5.15 REDUCTIONS IN THE NATIONAL WEATHER SERVICE HEAT INDEX (NWS HI) WARNING LEVELS

One interesting aspect of UHI-mitigation measures, at least in theory, is their potential to improve public heat health among other benefits. To characterize these effects, the potential of measures in reducing exposure to excessive heat, e.g., above various warning levels of the National Weather Service Heat Index (NWS HI), was quantified in this study. The NWS HI was defined earlier in Section 5.9.1 (Equation 5-8) – it is computed based on both temperature and humidity but reported in degrees F (i.e., as an effective temperature).

The goal of the analysis presented in this section was to quantify the potential of heat-mitigation measures in "shifting down" the NWS HI from one warning level to a lower one, e.g., from "Danger" to "Extreme Caution" or from "Extreme Caution" to "Caution", and to reduce exposure to heat-wave conditions (see Glossary). Several metrics are discussed below that provide an assessment of these potential effects – some are specific to certain time intervals; others are more general indicators of averages. These metrics were calculated at a number of probing locations identified in Figure 5-37.

As an example, Table 5-10 shows the number of hours at 1700 PDT (through all intervals in 2013-2016) that are over the "Danger" and "Extreme Caution" levels and how that number is reduced with a scenario of combined albedo increase and canopy cover (case31). It can be seen that the number of hours above the "Danger" level can be reduced by half or more and that the number of hours above the "Extreme Caution" level can be reduced by between 18% and 35% with case31.

As discussed below and shown in Table 5-12, the mitigation measures can also reduce the number of heat-wave days and the exposure to heat-wave conditions.

Figure 5-37: Locations of probing points for the analysis of changes in the NWS Heat Index.
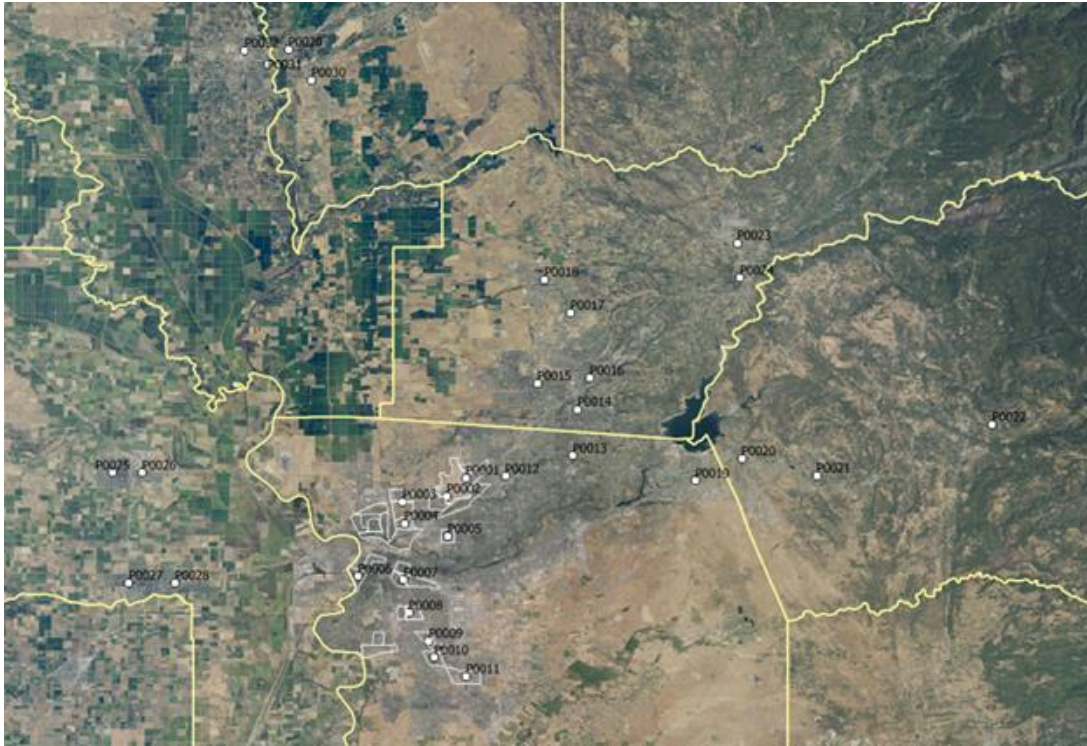
Table 5-10: Changes in the number of hours when the NWS Heat Index exceeds the specified thresholds for "Danger" and "Extreme Caution".

Probing station	Number of hours above NWS HI "Danger" **		Number of hours above NWS HI "Extreme Caution" **		Reduction
	case00	case31	case00	case31	Case31-00
P0001 AB617 (SAC)	4	2	180	124	31%
P0004 AB617 (SAC)	3	2	171	123	28%
P0008 AB617 (SAC)	2	1	140	98	30%
P0011 AB617 (SAC)	1	1	124	90	27%
P0013 Citrus Heights	6	2	177	119	33%
P0014 Roseville	7	2	189	122	35%
P0018 Lincoln	8	2	210	154	27%
P0020 El Dorado Hills	2	1	114	78	32%
P0022 Placerville	1	1	40	31	23%
P0026 Woodlands	6	2	193	151	22%
P0028 Davis	2	2	149	122	18%
P0029 Marysville	13	6	245	192	22%
P0032 Yuba City	13	4	251	178	29%

** At 1700 PDT hours during the period 2013 – 2016 intervals 1 – 7.

The NWS HI "Danger" level is defined as above the threshold of 106 °F (41.1 °C) and "Extreme Caution" above a threshold of 91 °F (32.8 °C). The "Caution" level is set at 80 °F (26.7 °C). These thresholds are shown as dashed lines in Figure 5-38. A heat wave is defined when the NWS HI is within or exceeds 105-110 ℉ for at least two consecutive days. Per this definition, and as seen in Figure 5-38, the model correctly captures heat events/heat waves in the Capital region during the intervals of (1) June 30 – July 4, 2013 (day counter 30-34 in Figure 5-38), (2) June 30 – July 1, 2016 (day counter 345-346), and (3) July 28 – 29, 2016 (day counter 373-374).

Two types of information can be gleaned from Figure 5-38:

1. whether there are exceedances above certain HI warning levels or thresholds, e.g., above the dashed lines. For example, in the first graph of Figure 5-38, there are exceedances in 1700-PDT HI above 106 °F between June 30th and July 4th, 2013 (day counter 30-34), which is one of three heat waves identified above, and there are several exceedances above 91 °F, some of which are highlighted with the vertical green arrows; and

2. whether there are instances where the cooling measure (case31) "shifts down" the HI from one warning level to a lower one. Some such instances are shown at the locations of the green arrows in the first graph of Figure 5-38 where the HI goes from the "Extreme Caution" level (blue series) to the "Caution" level (red series). The cumulative HI reductions (e.g., DH above thresholds) are discussed later in this section.

Figure 5-38: NWS HI at all 1700-PDT hours (for case00, case31) for JJAS at probing locations identified in Figure 5-37.

Figure 5-38, continued.

Location: P0004 AB617 community, Sacramento
NWS HI (°F) at hour 1700 PDT, 2013 − 2016, int1 − int7 (420 hours)

Location: P0008 AB617 community, Sacramento
NWS HI (°F) at hour 1700 PDT, 2013 − 2016, int1 − int7 (420 hours)

Location: P0011 AB617 community, Sacramento
NWS HI (°F) at hour 1700 PDT, 2013 − 2016, int1 − int7 (420 hours)

Figure 5-38, continued.

Location: P0013 Citrus Heights
NWS HI (°F) at hour 1700 PDT, 2013 − 2016, int1 − int7 (420 hours)

Location: P0014 Roseville
NWS HI (°F) at hour 1700 PDT, 2013 − 2016, int1 − int7 (420 hours)

Location: P0018 Lincoln
NWS HI (°F) at hour 1700 PDT, 2013 − 2016, int1 − int7 (420 hours)

Figure 5-38, continued.

Location: P0020 El Dorado Hills
NWS HI (°F) at hour 1700 PDT, 2013 – 2016, int1 – int7 (420 hours)

Location: P0022 Placerville
NWS HI (°F) at hour 1600 PDT, 2013 – 2016, int1 – int7 (420 hours)

Location: P0026 Woodlands
NWS HI (°F) at hour 1700 PDT, 2013 – 2016, int1 – int7 (420 hours)

Figure 5-38, continued.

Location: P0028 Davis
NWS HI (°F) at hour 1700 PDT, 2013 – 2016, int1 – int7 (420 hours)

Location: P0029 Marysville
NWS HI (°F) at hour 1700 PDT, 2013 – 2016, int1 – int7 (420 hours)

Location: P0032 Yuba City
NWS HI (°F) at hour 1700 PDT, 2013 – 2016, int1 – int7 (420 hours)

Table 5-11 provides additional information for the hours at 1700 PDT in terms of exceedances and potentials for reduction of the NWS HI levels by the mitigation measures (in this example, case31). In this table, cumulative metrics (i.e., % change in degree-hours above the thresholds) are provided. Thus, for each selected probing point (P0001 through P0032), the first three rows provide the percentages of DH above the given thresholds and the following three rows give the percent reduction in DH above those thresholds. Thus, it can be seen that the mitigation measure (case31) has a significant impact and can reduce exceedances above 106 °F by between 50% and 100% (except for one location) and the exceedances above 91 °F by between 18% and 36%.

Table 5-11: Exceedances (DH) above three NWS HI levels (1700 PDT averages over all intervals) in current climate for selected probing locations (P####) defined in Figure 5-37. All numbers in the table are percentages. (Note: DH = °F · hr).

	HI threshold	Probing location						
		P0001	P0004	P0008	P0011	P0013	P0014	P0018
% of DH	>80 °F (%)	93.0	92.8	90.6	90.1	92.3	93.4	93.9
above	> 91 °F (%)	45.6	43.5	36.0	32.1	44.8	47.7	52.7
thresholds	> 106 °F (%)	0.9	0.6	0.3	0.0	1.4	1.7	2.0
% reduction in	>80 °F (% ↓)	-5.8	-5.0	-5.2	-9.4	-4.9	-6.1	-4.7
DH above	> 91 °F (%↓)	-31.9	-28.6	-30.5	-28.0	-33.5	-36.2	-27.0
thresholds	> 106 °F (%↓)	-66.2	-49.7	-100.0	N/A	-79.8	-83.2	-85.5

	HI threshold	Probing location					
		P0020	P0022	P0026	P0028	P0029	P0032
% of DH	>80 °F (%)	89.0	71.3	94.1	92.1	94.6	94.8
above	> 91 °F (%)	29.3	10.4	48.7	38.2	61.0	62.5
thresholds	> 106 °F (%)	0.3	0.0	1.4	0.3	3.4	3.4
% reduction	>80 °F (% ↓)	-4.8	-4.8	-4.2	-4.8	-2.6	-3.5
in DH above	> 91 °F (%↓)	-31.9	-23.3	-22.3	-18.7	-22.1	-29.5
thresholds	> 106 °F (%↓)	-100.0	N/A	-79.7	-1.1	-58.7	-75.6

In terms of locally countering or offsetting the effects of excessive heat events or heat waves (per above definitions), Table 5-12 provides a summary of the mitigation potential for case31. The table shows the number of days with NWS HI of 105 – 110 ºF at each selected probing location and for the three heat-wave events identified above. The table also shows the reduction in the number of heat-wave days at each location as a result of implementing case31 – the heat-wave effects are-locally offset everywhere except for one period in each of the Yuba City and Marysville locations.

Altostratus Inc.

During the 6/30 – 7/3, 2013 heat wave, case31 reduces the number of heat-wave days from 5 or 4 to 1 or 0 in most locations, except for Marysville and Yuba City. During the 6/30 – 6/31, 2016 heat event, case31 reduces the number of days to zero at all locations. The same occurs during the interval 7/29 – 7/30, 2016, i.e., heat-wave days are reduced to zero, except for Marysville and Yuba City where they are reduced from 3 to 2 and from 3 to 1, respectively.

Table 5-12: Number of consecutive days with NWS HI 105 – 110 ºF in three time periods.

Probing location	Heat wave?	Number of days with NWS HI 105 – 110 ºF					
		6/30 – 7/4, 2013		6/30 – 6/31, 2016		7/28 – 7/30, 2016	
		base	case31	base	case31	base	case31
P0001 AB617 (Sac)	yes	5	1	0	0	2	0
P0004 AB617 (Sac)	yes	3	1	0	0	2	0
P0008 AB617 (Sac)		1	0	0	0	0	0
P0011 AB617 (Sac)		1	0	0	0	0	0
P0013 Citrus Heights	yes	5	1	1	0	1	0
P0014 Roseville	yes	5	2	1	0	2	0
P0018 Lincoln	yes	4	3	1	0	2	0
P0020 El Dorado Hills		1	0	0	0	0	0
P0022 Placerville		0	0	0	0	0	0
P0026 Woodland	yes	3	0	0	0	0	0
P0028 Davis	yes	4	0	0	0	0	0
P0029 Marysville	yes	4	4	2	0	3	2
P0032 Yuba City	yes	4	4	2	0	3	1

Whereas some of the foregoing discussion, e.g., Figure 5-38 and Table 5-11, summarized the effects of UHI mitigation in terms of the 1700-PDT NWS HI, Figure 5-39 provides additional information for the hours from 1400 to 2000 PDT. Thus, the following charts summarize the average reductions (percentage-wise) in DH exceedances above the three warning thresholds of the NWS HI (Caution, Extreme Caution, and Danger) for case31 at thirteen selected probing points (defined earlier) and for seven individual hours (from 1400 to 2000 PDT) averaged over all such hours in the modeled periods (i.e., a total of 420 hours for each computed hour average). In other words, Figure 5-39 provides an average for all 1400-PDT hours during JJAS of 2013-2016, all 1500-PDT hours during JJAS 2013-2016, and so on, as identified in the legend of each figure. If no data is shown for certain hours in the graphs, this means that there were no exceedances of the thresholds to begin with.

From Figure 5-39, it can be seen that the mitigation measure can offset exceedances above various thresholds at all locations and hours, sometimes fully (100%) offsetting the exceedances over the "Danger" threshold. Furthermore, and except for the "Danger" level, the reductions in the other two levels exhibit a rough "inverted U" pattern suggesting that the cooling measure decreases the

HI relatively more on both sides of 1700 PDT. That is, the HI is reduced most (percentage-wise) at 1400 and 2000 PDT, then at 1500 and 1900 PDT, then at 1600 and 1800 PDT, and finally at 1700 PDT. Thus, in a way, the foregoing discussion of the hour at 1700 PDT might in fact be a presentation of the smallest beneficial effects of the cooling measures (i.e., the benefits can be larger at other hours, or it could be because the heat index is smaller at those hours than at 1700 PDT). For the "Danger" level, this argument does not apply as there is no clear pattern in HI reductions and the cooling measure can be equally effective at different hours.

Figure 5-39: Percentage-wise reductions in the NWS HI exceedances (DH) over the specified thresholds for case31 relative base scenario for all hours during JJAS at probing locations identified in Figure 5-37.
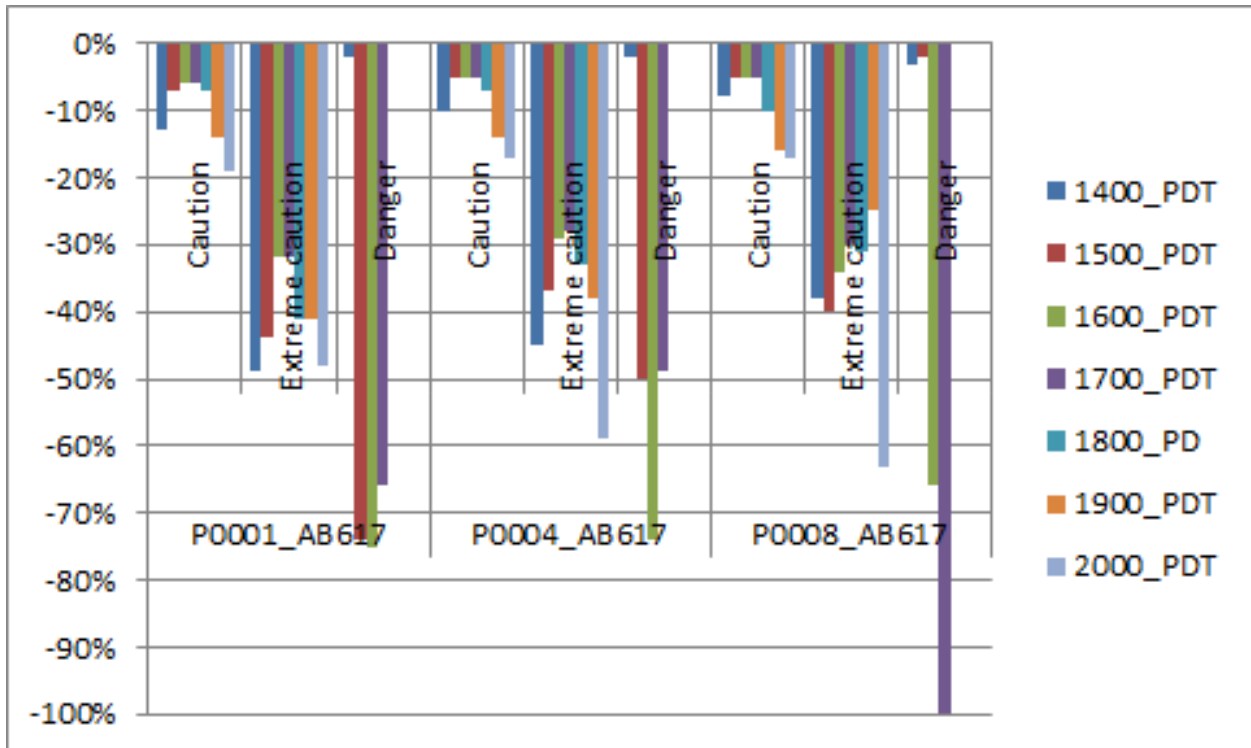
Figure 5-39, continued.
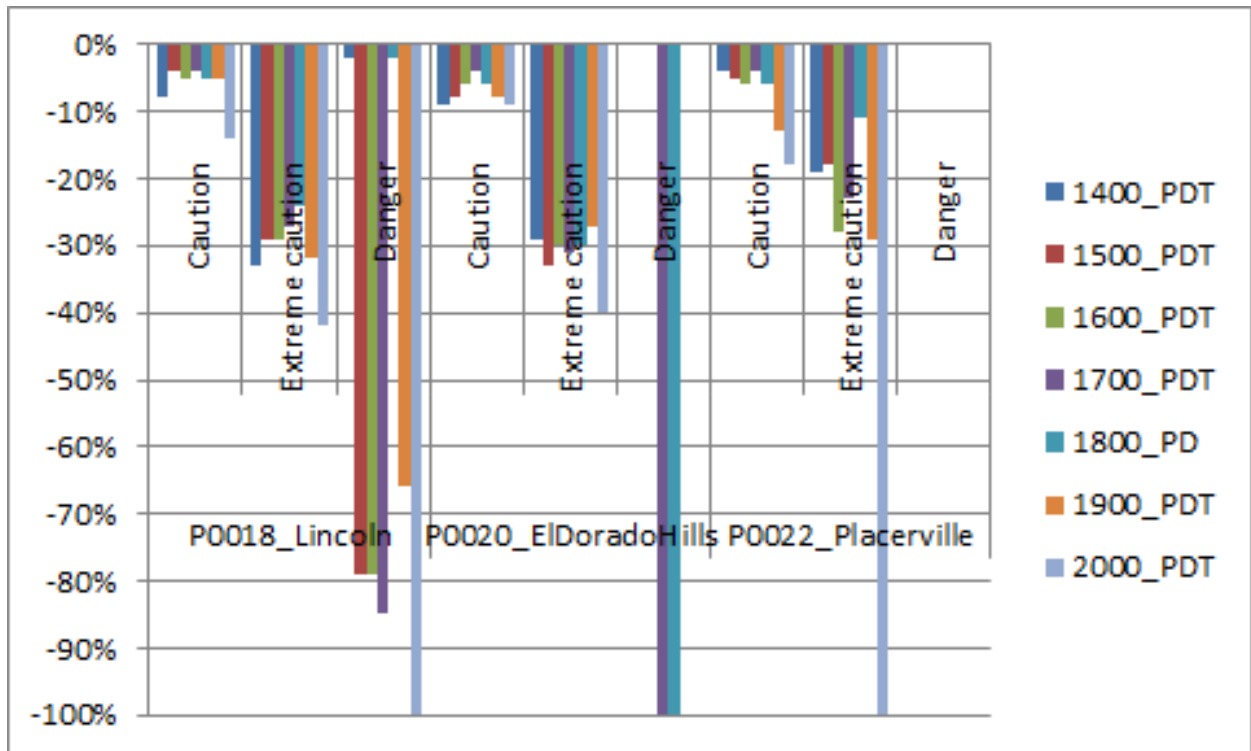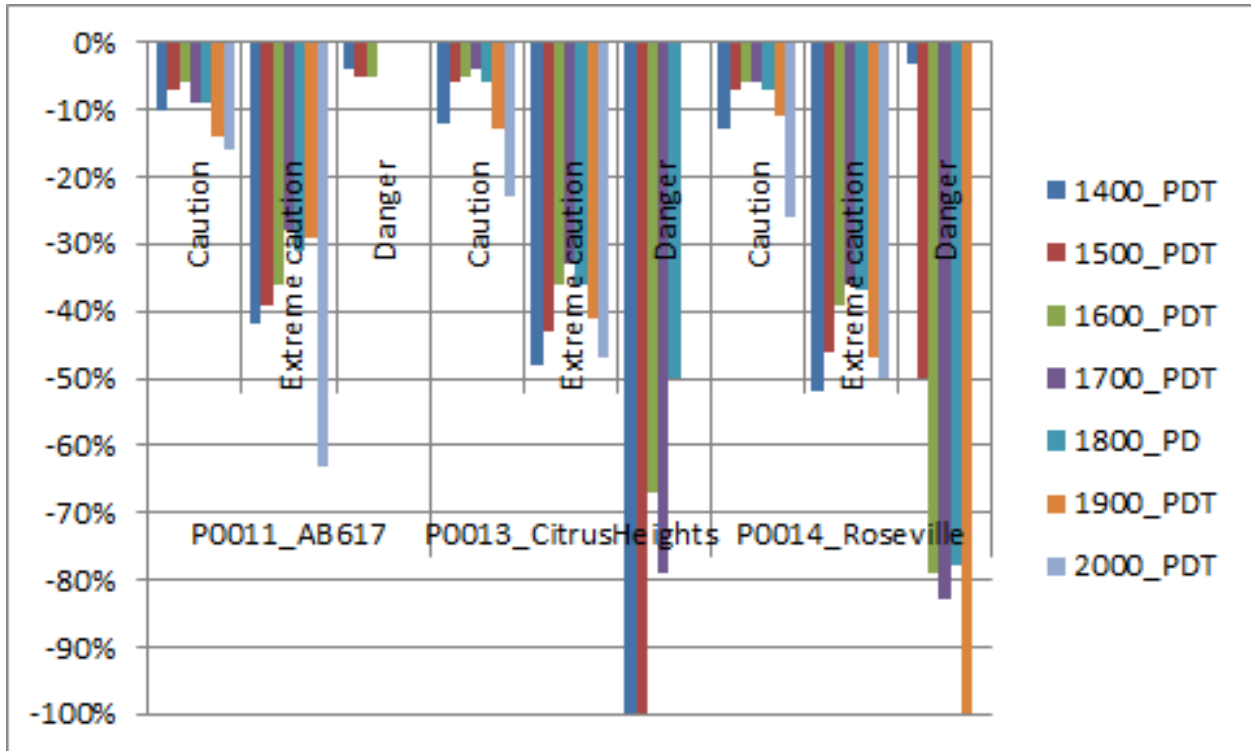
Figure 5-39, continued.
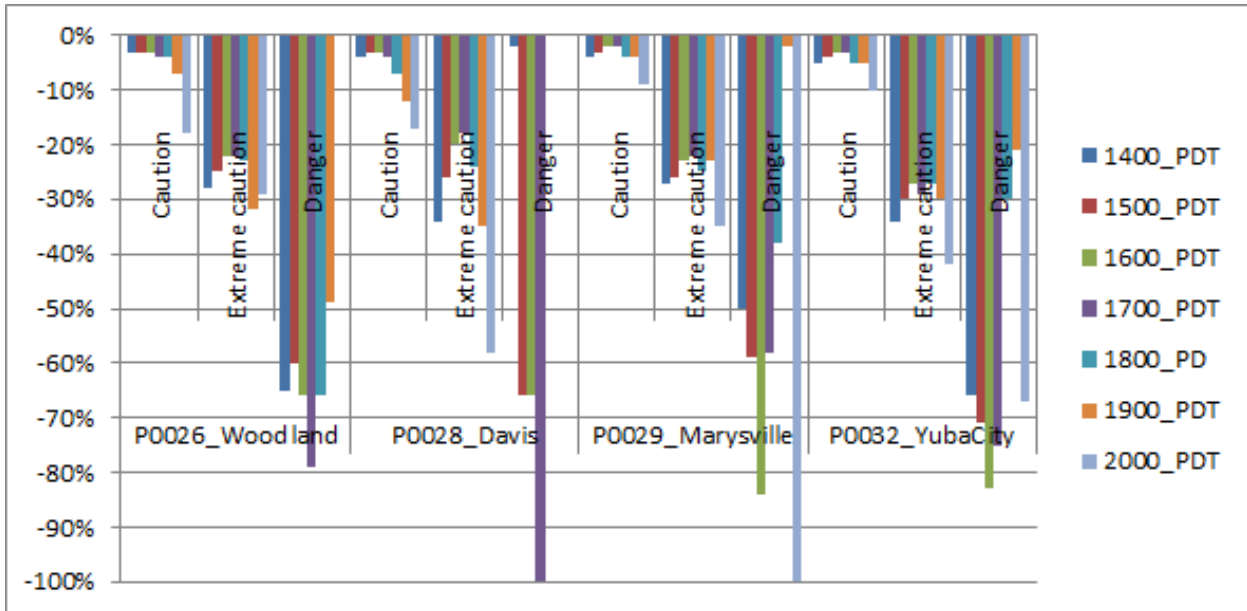
5.16 IMPACTS OF INCREMENTAL INCREASES IN CANOPY COVER

In this section, the impacts of incremental increases in canopy cover on air temperature are discussed in addition to providing an estimate of the corresponding water usage. The increase in cover could be a result of canopy growth and/or planting additional urban trees over time. For this purpose, additional, intermediate scenarios to case01 and case02 (that were presented earlier in Section 5-5) were introduced and modeled. These are cases 01A, 01B, 02A, and 02B, as defined in Table 5-13.

Table 5-13: Definition of canopy-cover incremental cover.

Scenario	01A	01B	**01**	02A	02B	**02**
Cover **increase** (percent of cell area)	3.4%	7.7%	12.0%	16.3%	20.6%	25.0%
Possible equivalent time frame	2018	2022	2026	2030	2033	2037

It is re-iterated here that scenarios with tree cover increases larger than case01, i.e., 02A, 02B, and 02, are likely not feasible at this time as they will require a very large amount of tree planting. As alluded to earlier, case01 can be considered an upper bound that includes increasing canopy cover by 12% (area-wise) and bringing the total cover in many areas to about 14% which is the average of the established canopy cover in Sacramento. By comparison, case02 would bring the total cover to 35%, which, while technically doable, is a relatively more extreme scenario. Nevertheless, all

of the cases are considered in the analysis to provide various estimates of cooling effects and water consumption.

The following tabulations and figures summarize the effects in each sub-domain of the 6-counties Capital region. These are averages (spatially) over each area as well as temporally over the specified hours or hourly intervals during years 2013-2016 and intervals 1-7 within each. Information is also provided to show the degree-hours (°C·hr) exceedances over specified thresholds, e.g., 35 and 38 °C, and percent-wise changes (reductions) relative to these thresholds for each canopy scenario.

The results presented in this section are for a few sample hour intervals during daylight as well as over all-hour periods. This is an important point to keep in mind since the effects of canopy cover are continuous (during day and night) unlike the effects of albedo that occur during the day or the effects of vehicle electrification and heat-emission control that are seen mostly during rush hours. This is also important from heat-health / heat-wave perspectives since nighttime cooling can contribute to relieving heat stress.

Table 5-14 is a listing of average base and perturbation-scenario temperatures and average reductions resulting from the various incremental canopy scenarios. This information is also presented graphically in Figure 5-40, where it can be seen that as canopy cover increases, the net cooling effect becomes larger, which is what is generally expected. However, the increase is not linear although it appears to be close to that.

Modeling the incremental increases in canopy cover suggests different sensitives in temperature response to changes in cover (Figure 5-40). To discuss this point, we examine the changes in all-hours average cooling (which is the last graph in Figure 5-40) as an example. In Auburn (for instance), going from a 3.4% increase in canopy cover (percent of cell area) to 25% increase, that is, going from case01A to case02, results in all-hours average cooling going from 0.1 to 0.7 °C. On the other hand, the same canopy cover increase, i.e., going from +3.4% to +25% in Sacramento, results in all-hours average cooling going from 0.15 to 1.0 °C, meaning a larger response or sensitivity to the same changes in canopy cover. The main reason, aside from geographical, LULC, and microclimatic differences, is the size of the urban area affected by canopy-cover increase. In Sacramento, larger areas are affected by tree cover than in Auburn and, thus, areas in Sacramento can benefit from the transport of cooler air from upwind locations, hence the additional cooling benefit. The same observation applies to other time intervals and hours.

Table 5-14: Average temperature and change (°C) from incremental increase in canopy cover

1300 PDT

1300PDT	case00	case01A	case01B	case01	case02A	case02B	case02	del01A	del01B	del01	del02A	del02B	del02
Auburn	29.3128	29.256	29.1965	29.1356	29.0867	29.0269	28.9451	-0.05676	-0.11624	-0.17717	-0.22603	-0.2859	-0.36762
Davis	31.3363	31.2855	31.2319	31.1764	31.1315	31.0769	31.0011	-0.05087	-0.10443	-0.15992	-0.20483	-0.25944	-0.33524
El Dorado Hills	29.5428	29.4745	29.4024	29.3275	29.2682	29.1946	29.0935	-0.06836	-0.14045	-0.21537	-0.27462	-0.34822	-0.44933
Placerville	28.8258	28.786	28.7448	28.7022	28.6677	28.6253	28.566	-0.03978	-0.08095	-0.12362	-0.15803	-0.20047	-0.25978
Sacramento	30.8787	30.7906	30.6966	30.5997	30.5218	30.4253	30.292	-0.08811	-0.18218	-0.279	-0.35689	-0.4534	-0.58672
Woodland	31.8151	31.7639	31.7083	31.6526	31.6083	31.5533	31.4742	-0.05126	-0.10678	-0.1625	-0.20679	-0.26181	-0.34088
Yuba City	31.5444	31.4748	31.3992	31.3216	31.2603	31.1831	31.0765	-0.06962	-0.1452	-0.22281	-0.28407	-0.36129	-0.46788

1400 to 2000 PDT

1400 to 2000PDT	case00	case01A	case01B	case01	case02A	case02B	case02	del01A	del01B	del01	del02A	del02B	del02
Auburn	30.33	30.2598	30.1842	30.1063	30.0437	29.9676	29.8617	-0.07017	-0.14583	-0.22366	-0.28628	-0.36245	-0.46828
Davis	31.5302	31.4704	31.4081	31.3434	31.2918	31.2281	31.1418	-0.05983	-0.1221	-0.18676	-0.23845	-0.30207	-0.38837
El Dorado Hills	30.4984	30.4277	30.3522	30.2737	30.2102	30.1326	30.0244	-0.07071	-0.14621	-0.2247	-0.28819	-0.36575	-0.47393
Placerville	28.9496	28.8949	28.8364	28.7765	28.7272	28.6663	28.5821	-0.05469	-0.11319	-0.17315	-0.22241	-0.28332	-0.36751
Sacramento	31.8764	31.7998	31.7182	31.6339	31.5662	31.4824	31.3658	-0.07659	-0.15819	-0.24249	-0.31024	-0.39398	-0.51064
Woodland	32.4665	32.411	32.3526	32.292	32.2442	32.1839	32.1013	-0.05547	-0.11393	-0.17449	-0.22231	-0.28258	-0.36517
Yuba City	33.2518	33.1866	33.1154	33.0444	32.9852	32.9123	32.8106	-0.06526	-0.13648	-0.20748	-0.26661	-0.33951	-0.44126

1500 PDT

1500PDT	case00	case01A	case01B	case01	case02A	case02B	case02	del01A	del01B	del01	del02A	del02B	del02
Auburn	31.0863	31.0314	30.9729	30.9126	30.8646	30.8077	30.7264	-0.05497	-0.11345	-0.17372	-0.22176	-0.27869	-0.35997
Davis	33.063	33.0208	32.976	32.9288	32.8929	32.8488	32.7894	-0.04219	-0.08707	-0.13417	-0.17012	-0.21426	-0.27366
El Dorado Hills	31.4745	31.4091	31.3396	31.268	31.2114	31.1418	31.0453	-0.06536	-0.13486	-0.20646	-0.26306	-0.3327	-0.42916
Placerville	30.0235	29.9812	29.9371	29.8914	29.8563	29.8119	29.7508	-0.04223	-0.08633	-0.13203	-0.16715	-0.21151	-0.27262
Sacramento	33.0852	33.0199	32.9501	32.8785	32.8207	32.7497	32.651	-0.06529	-0.13514	-0.20671	-0.26453	-0.33548	-0.43419
Woodland	33.7661	33.7267	33.6823	33.6387	33.6041	33.5592	33.5003	-0.03941	-0.08379	-0.12739	-0.16202	-0.20694	-0.26577
Yuba City	33.9507	33.8995	33.8422	33.7855	33.7388	33.6811	33.6046	-0.05114	-0.10845	-0.16514	-0.21191	-0.26953	-0.34612

All hours

allHRS	case00	case01A	case01B	case01	case02A	case02B	case02	del01A	del01B	del01	del02A	del02B	del02
Auburn	26.3181	26.2066	26.0893	25.9703	25.8753	25.7615	25.608	-0.11159	-0.22879	-0.34786	-0.44286	-0.55666	-0.7101
Davis	25.1114	24.989	24.8585	24.724	24.616	24.4835	24.301	-0.12239	-0.25288	-0.38736	-0.49535	-0.62788	-0.8104
El Dorado Hills	25.7303	25.6179	25.4992	25.378	25.2816	25.1641	25.0053	-0.11241	-0.23114	-0.35234	-0.44876	-0.56621	-0.725
Placerville	25.4063	25.3032	25.1945	25.0848	24.9993	24.8962	24.7585	-0.10307	-0.21177	-0.32151	-0.40698	-0.51014	-0.64776
Sacramento	25.7256	25.5786	25.4209	25.2567	25.124	24.9594	24.7307	-0.14699	-0.30467	-0.46885	-0.60159	-0.76621	-0.99484
Woodland	25.6928	25.5717	25.4429	25.3115	25.2053	25.0744	24.8944	-0.12108	-0.24985	-0.38128	-0.48749	-0.61838	-0.79832
Yuba City	27.0336	26.8848	26.723	26.5552	26.4187	26.2497	26.0161	-0.14887	-0.31061	-0.47847	-0.61496	-0.78393	-1.01756

Figure 5-40: Average reduction in air temperature (ºC) for various intervals, canopy scenarios, and regions. Time periods are given a top left of each graph. Vertical axis is degrees C.
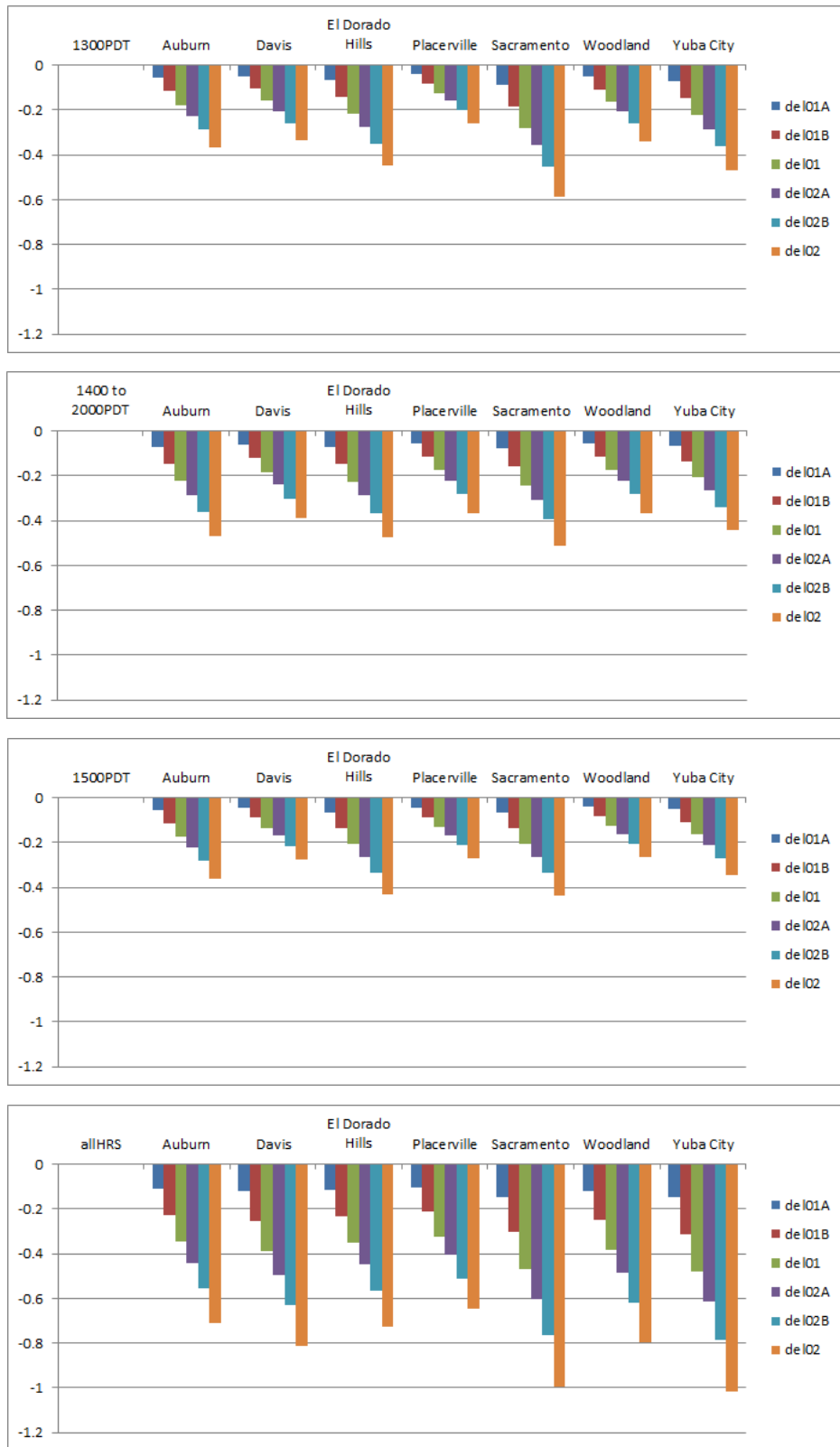
Table 5-15 summarizes the cumulative exceedances (DH) above 35 and 38 °C and their changes (reductions) for various canopy-cover incremental scenarios. The reductions (percentage-wise) of total DH above thresholds are also represented in Figure 5-41. In general, the pattern in these figures is similar to those in Figure 5-40 (average reductions in temperature). The urban-cooling measures can decrease the DH exceedances above 35 °C by up to 18% and above 38 °C by up to 25%, depending on region.

Table 5-15: Degree-hours (°C · hr) and changes from incremental canopy cover over specified thresholds

Threshold: 35 °C

totDH above 35	case00	case01A	case01B	case01	case02A	case02B	case02	del01A	del01B	del01	del02A	del02B	del02
Auburn	846.87	825.321	801.814	778.072	760.713	739.514	708.931	-21.5493	-45.0556	-68.7983	-86.1566	-107.356	-137.939
Davis	1511.72	1483.96	1456.31	1429.56	1408.89	1382.86	1346.71	-27.7615	-55.4101	-82.1601	-102.838	-128.861	-165.018
El Dorado Hills	961.836	932.987	902.124	869.72	848.722	821.346	782.901	-28.8486	-59.7119	-92.1156	-113.114	-140.49	-178.935
Placerville	526.077	514.036	499.851	489.87	481.431	467.883	451.701	-12.0406	-26.2261	-36.2069	-44.6463	-58.1943	-74.3753
Sacramento	1537.63	1497.72	1458.12	1419.34	1389.32	1353.65	1303.5	-39.9079	-79.5081	-118.295	-148.311	-183.981	-234.132
Woodland	1845.11	1816.34	1786.45	1758.56	1733.35	1706	1670.69	-28.7717	-58.6578	-86.5431	-111.76	-139.112	-174.422
Yuba City	2160.07	2123.17	2081.81	2042.36	2005.14	1959.6	1898.84	-36.8973	-78.2571	-117.703	-154.924	-200.462	-261.225

Threshold: 38 °C

totDH above 38	case00	case01A	case01B	case01	case02A	case02B	case02	del01A	del01B	del01	del02A	del02B	del02
Auburn	210.152	202.176	194.193	185.563	179.782	173.696	165.93	-7.97576	-15.9589	-24.5886	-30.3697	-36.4562	-44.2216
Davis	543.194	533.002	521.248	509.497	501.32	491.254	476.541	-10.1921	-21.9468	-33.6973	-41.8747	-51.9404	-66.6531
El Dorado Hills	267.096	256.243	244.945	233.087	224.251	214.774	200.056	-10.8531	-22.1518	-34.009	-42.8458	-52.322	-67.0405
Placerville	86.0162	82.1139	78.538	75.6212	73.394	70.9801	66.2296	-3.90225	-7.47823	-10.395	-12.6222	-15.0361	-19.7865
Sacramento	552.711	535.437	516.826	498.535	484.765	467.099	444.554	-17.2742	-35.8851	-54.1766	-67.9465	-85.6122	-108.157
Woodland	658.175	643.615	630.917	616.891	607.585	595.145	579.582	-14.5597	-27.2581	-41.284	-50.5896	-63.0298	-78.5925
Yuba City	806.334	787.241	766.083	748.25	733.734	717.912	692.357	-19.0924	-40.2505	-58.0832	-72.6	-88.4211	-113.976

Figure 5-41: Average reduction in DH exceedances above 35 and 38 °C for incremental canopy cover.
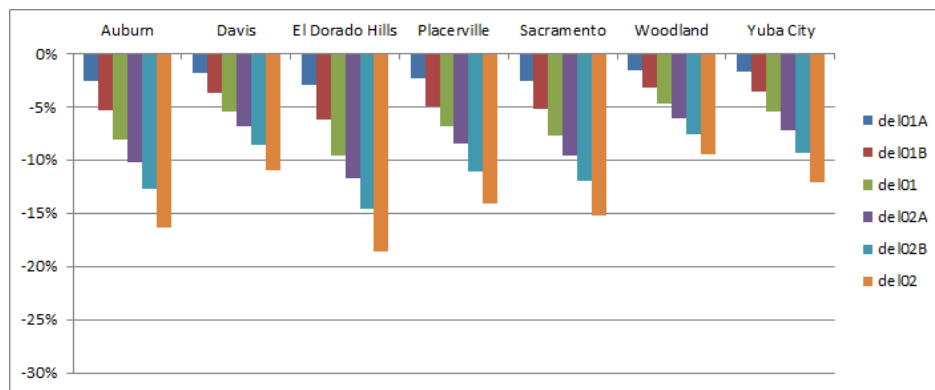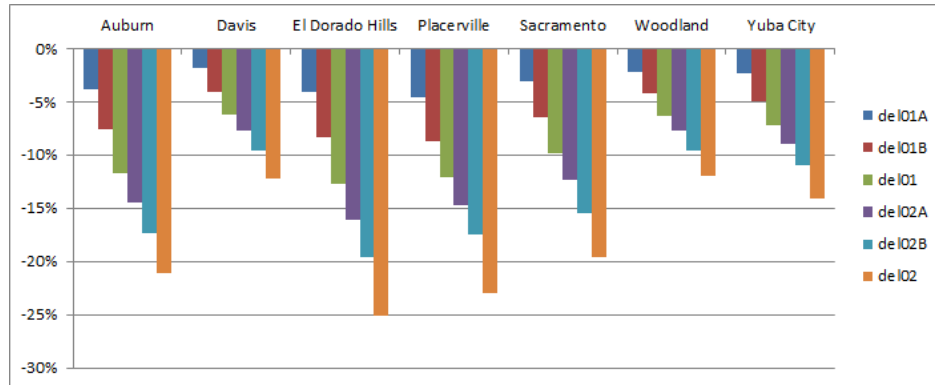
Total DH above 35 °C

Figure 5-41, continued.

Total DH above 38 °C

In terms of water usage by the canopy, the following <u>crude</u> estimates were developed via quantification of evapotranspiration. The estimates are provided as water needed by the canopy in order to achieve an all-hours average cooling of 0.5 °C in each of the sub-regions.

While the discussion above clearly indicates a wide range of cooling potential across different scenarios and across different regions, here a cooling of 0.5 °C is used as a common denominator to provide equivalence, i.e., the same basis for comparison across different regions. The 0.5 ℃ cooling is an average over all urban cells in the given area and over all hours of the day (not just daytime or specific hour). The corresponding water usage is estimated by calculating evapotranspiration over years 2013-2016 and intervals 1-7 within each year. Table 5-16 is a summary of these estimates, in liters per year (L yr^{-1}) of water per neighborhood. In this calculation, a neighborhood is assumed to cover an area of 0.25 – 0.5 km^2.

Table 5-16: Water use equivalents to achieve an area average of 0.5 °C reduction in all-hours average temperature.

Area	H$_2$O (L yr^{-1}) per neighborhood (~ 0.25 – 0.5 km^2)
Auburn	117,905,000
Davis	94,500,000
El Dorado Hills	106,276,320
Placerville	118,260,000
Sacramento	74,740,320
Woodland	94,608,000
Yuba City	74,600,200

Altostratus Inc.

To put these estimates into some context, we compare against a few examples:

(1) Per U.S. EPA, a typical family of four uses 144,000 gallons of water per year, which is 545,040 liters per year (L yr^{-1}). Thus, the water usage range in Table 5-16 (per neighborhood of 0.25 to 0.5 km^2) would correspond to the annual water usage of some 130 – 200 households. To provide further context, a census tract in urban California is about 1 km^2 on average and has about 5000 people (which is about 1250 households), and the neighborhood calculations at 0.25 – 0.5 km^2 would translate to between 312 and 625 households. Thus, per this calculation, the tree water usage in a neighborhood is equivalent to the annual water usage of some 130 – 200 households out of 312 – 625 households (to achieve an all-hours and area-wide average cooling of 0.5 °C), which is about one third of the households.

(2) A brief literature review of crops evapotranspiration shows (after various conversions) that, for example, alfalfa uses 350,462,900 L yr^{-1} per 0.25 km^2 per season, which is 3 to 5 times more than the evaporation from the canopy scenarios in table above. For wheat, the usage is 101,634,250 L yr^{-1} per 0.25 km^2.

(3) For the purpose of comparing water-usage estimates, as computed above, against the literature and values from observational studies, the following example is provided. Various organizations have measured or estimated water consumption by trees and found that evapotranspiration is correlated to trunk diameter at breast height (DBH), e.g., Pretzsch et al. (2015). Measurements show that for typical mature large trees with DBH of 30 cm (12 inches), evapotranspiration ranges from 120 to 150 gallons of water per day per tree. This is respectively equivalent to 82,554,240 and 103,192,800 L yr^{-1} per 0.25 km^2 and is of the same magnitude as the values reported in Table 5-16, thus lending additional credence to these estimates.

5.17 IDENTIFYING GEOGRAPHICAL AREAS FOR IMPLEMENTING URBAN-COOLING MEASURES BASED ON THE UHII SCORE

The goal of this analysis is to produce additional layers of information, e.g., that could be used in conjunction with other datasets, including CES 3.0 (OEHHA 2013), to help identify and prioritize geographical areas for deployment of UHI-mitigation measures.

For this purpose, an initial scoring of areas was developed based on the modeled UHII at the regional scale. As with the CES 3.0 score, the higher the UHII score, the worse is urban heat and the higher the priority is for action. The first set of scores (e.g., Figure 5-41) was developed based on the local UHII regardless of absolute air temperature. However, the cooling measures are welcome in all regions, regardless of the score, as residents would benefit from these effects no

matter how they rank relative to some other areas. That is, the reductions in absolute temperature are equally welcomed everywhere.

Thus, the purpose of the scoring such as shown in Figure 5-41 is to provide Caltrans and urban planners with additional information when allocating resources. The figure shows five tiers or ranks based on UHII intervals of 1 °C in the 6-counties Capital region (the higher the score, the worse is the condition). The UHII scoring presented here is based on climate as the sole criterion -- no socio-economic factors were taken into consideration. If, for example, the UHII tiers were weighted by CES 3.0 scores (last graph in Figure 5-41), the UHII score would shift relatively more towards central and south Sacramento, in areas with AB617 communities A, B, and D (which occur in UHII Tiers 3 and 4) as well as community C and its surroundings (which occur in UHII Tier 2). Additional information is provided in Appendix D-1.

Thus, if only UHII is used as basis, the areas including Yuba City / Marysville, Woodland, Davis, and Placerville occur in UHII Tiers 1 and 2. Most of north and south Sacramento and AB617 communities C, E, and G and others nearby occur in Tier 2. Central Sacramento, AB617 communities A, B, and D, and an area extending to Folsom and El Dorado Hills occur in Tiers 3 and 4. Northeast Sacramento, Roseville, Rocklin, Granite Bay, Lincoln, parts of Folsom, and areas west Auburn occur in Tier 4. Finally, an area from Roseville to Lincoln and a small area over Auburn fall into Tier 5. Again, the higher the tier (or UHII score), the worse is the UHII. Of note, this also includes some non-urban areas because of heat transport.

Figure 5-41: UHII score for implementing UHI-reduction measures at the regional scale: Tiers 1 through 5 (lowest to highest score) using UHII as the sole criterion.

Figure 5-41, continued

Tier 2 all-hours UHII (2 – 3 °C)
2015 int4

Tier 3 all-hours UHII (3 – 4 °C)
2015 int4

Tier 4 all-hours UHII (4 – 5 °C)
2015 int4
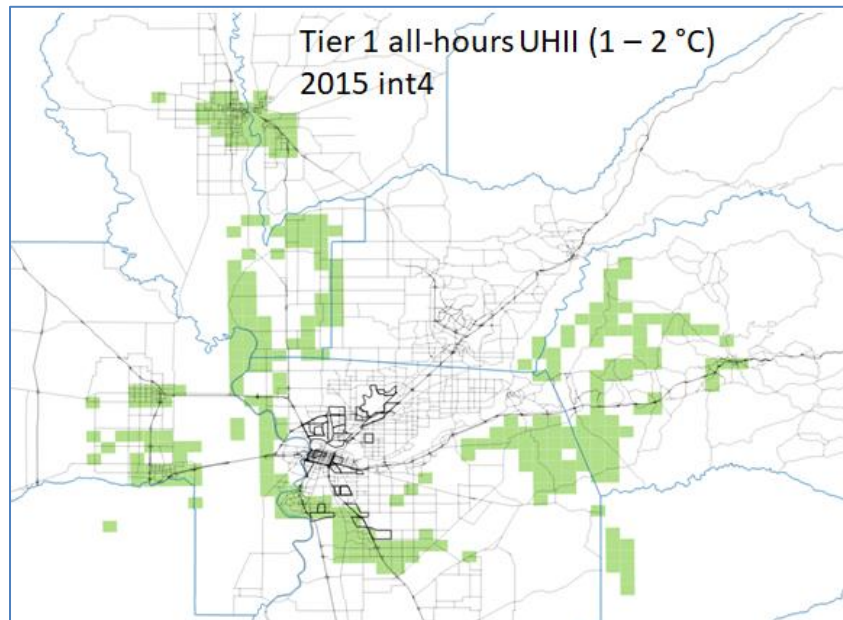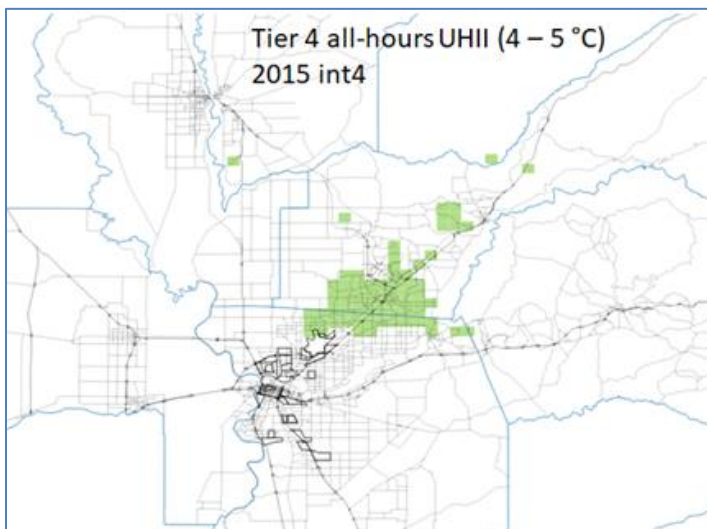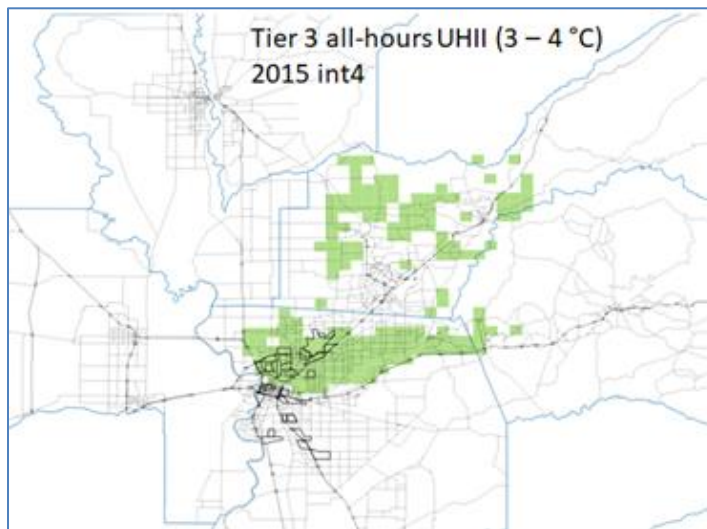
Figure 5-41, continued

However, using only the UHII as an indicator to mitigation priorities can provide an overall picture that may be counter-intuitive at times. Thus, the above scoring is repeated, but this time using both UHII and absolute air temperature as basis, to provide relatively more intuitive rankings. That is, areas with both large UHII and high absolute temperatures get a higher score than areas with small

UHII and lower temperatures. Of course, a range of possible combinations exists in-between these two ends.

To develop a temperature-weighted UHII score, i.e., *wuSCORE*, (here, for all hours and all intervals) a tier was assigned to each of the UHII and absolute temperature ranges as follows:

$$1.0 \leq UHII < 2.0, \quad UHII_{tier} = 1$$
$$2.0 \leq UHII < 3.0, \quad UHII_{tier} = 2$$
$$3.0 \leq UHII < 4.0, \quad UHII_{tier} = 3$$
$$4.0 \leq UHII < 5.0, \quad UHII_{tier} = 4$$
$$5.0 \leq UHII < 6.0, \quad UHII_{tier} = 5$$

and,

$$25.0 \leq Tair < 26.0, \quad Tair_{tier} = 1$$
$$26.0 \leq Tair < 27.0, \quad Tair_{tier} = 2$$
$$27.0 \leq Tair < 28.0, \quad Tair_{tier} = 3$$
$$28.0 \leq Tair < 29.0, \quad Tair_{tier} = 4$$
$$29.0 \leq Tair < 30.0, \quad Tair_{tier} = 5$$

where, the units of Tair are °C and the units for UHII are °C·hr hr^{-1}. Then, for cells where UHII > 1 and Tair > 25 °C, the weighted UHII score (*wuSCORE*) for a given grid cell is computed as:

$$wuSCORE = LOG\ (UHII_{tier} \times Tair_{tier}) \qquad (5\text{-}10)$$

The reason for using *LOG* in Equation 5-10 is simply to damp the range of *wuSCORE* for plotting and scaling purposes. Note that *wuSCORE* is dimensionless and has no physical meaning.

Figure 5-42 shows an example of *wuSCORE* computed based on both all-hour UHII and all-hour absolute temperature averages for all years and intervals modeled in this study (Appendix D-2 provides a larger version of these maps). As can be seen, the pattern differs from that of UHII-only basis in scoring (in Figure 5-41).

The lowest score (Tier 1) includes AB617 communities D, G, H and surroundings, peripheral areas in Woodland and Davis, small areas in Marysville, Placerville, and parts of El Dorado Hills.

The second score (Tier 2) includes south and southeast Sacramento, some western parts of downtown Sacramento and surroundings, areas to the south of the American River, peripheral areas in Yuba City / Marysville, northwest Woodland, and central Davis. Some areas in Granite Bay are also included in this tier.

The next-to-top score (Tier 3) includes AB617 communities A, B, D, north Sacramento and parts of downtown, and an area extending east to include south Folsom and El Dorado Hills. Also

included in this tier are parts of Lincoln and Auburn. Finally, the top score (Tier 4) includes parts of AB617 community "D", parts of northeast Sacramento, Folsom, El Dorado Hills, Roseville, Rocklin, Lincoln, central parts of Yuba City / Marysville, and parts of Auburn.

Figure 5-42: Temperature-weighted UHII score (wuSCORE) for implementing UHI-reduction measures at the regional scale: Tiers 1 through 4 correspond to lowest to highest wuSCORE.
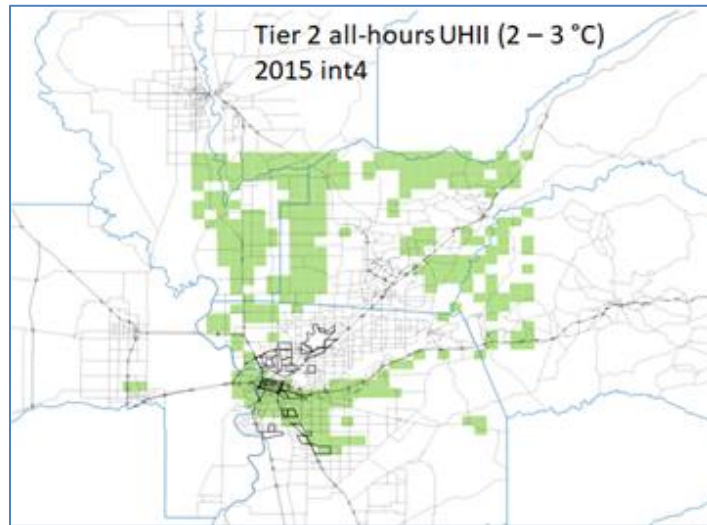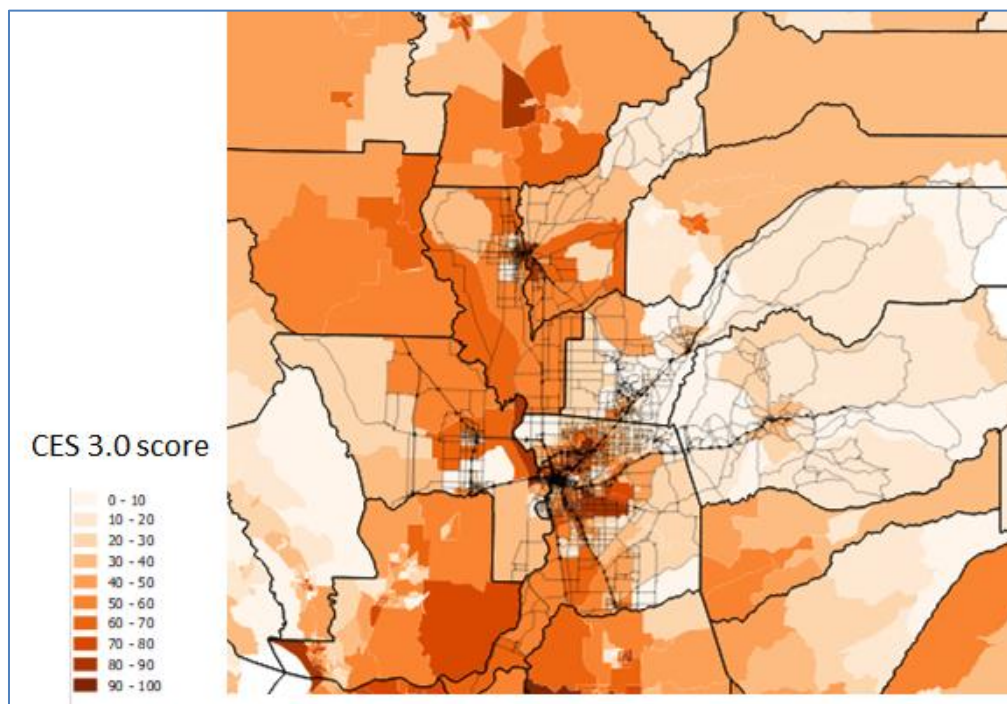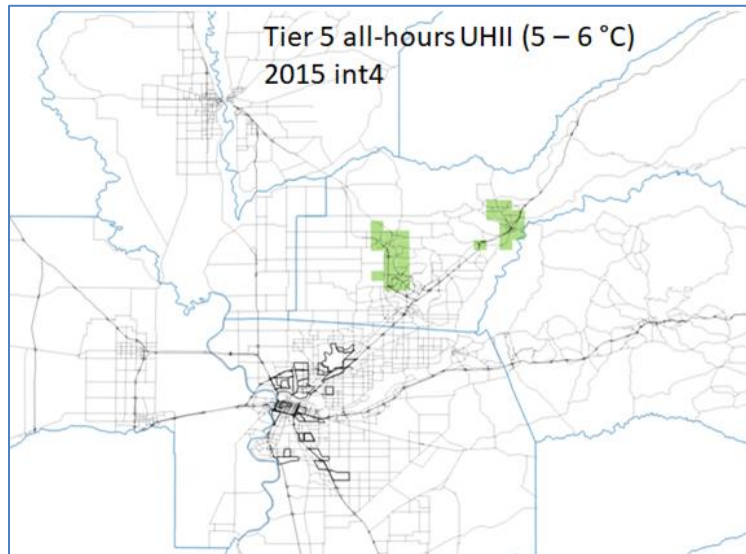

UHII-Tair weighted Tier 1: wuSCORE : 0.53 − 1.06

UHII-Tair weighted Tier 2: wuSCORE : 1.06 − 1.60

Figure 5-42, continued.

1: Yuba City / Marysville
2: Woodland
3: Davis
4: Sacramento
5: Elk Grove
6: Folsom
7: Placerville
8: Roseville
9: Lincoln
10: Auburn
11: El Dorado Hills

UHII-Tair weighted Tier 3: wuSCORE : 1.60 − 2.13

1: Yuba City / Marysville
2: Woodland
3: Davis
4: Sacramento
5: Elk Grove
6: Folsom
7: Placerville
8: Roseville
9: Lincoln
10: Auburn
11: El Dorado Hills

UHII-Tair weighted Tier 4: wuSCORE : 2.13 − 2.66
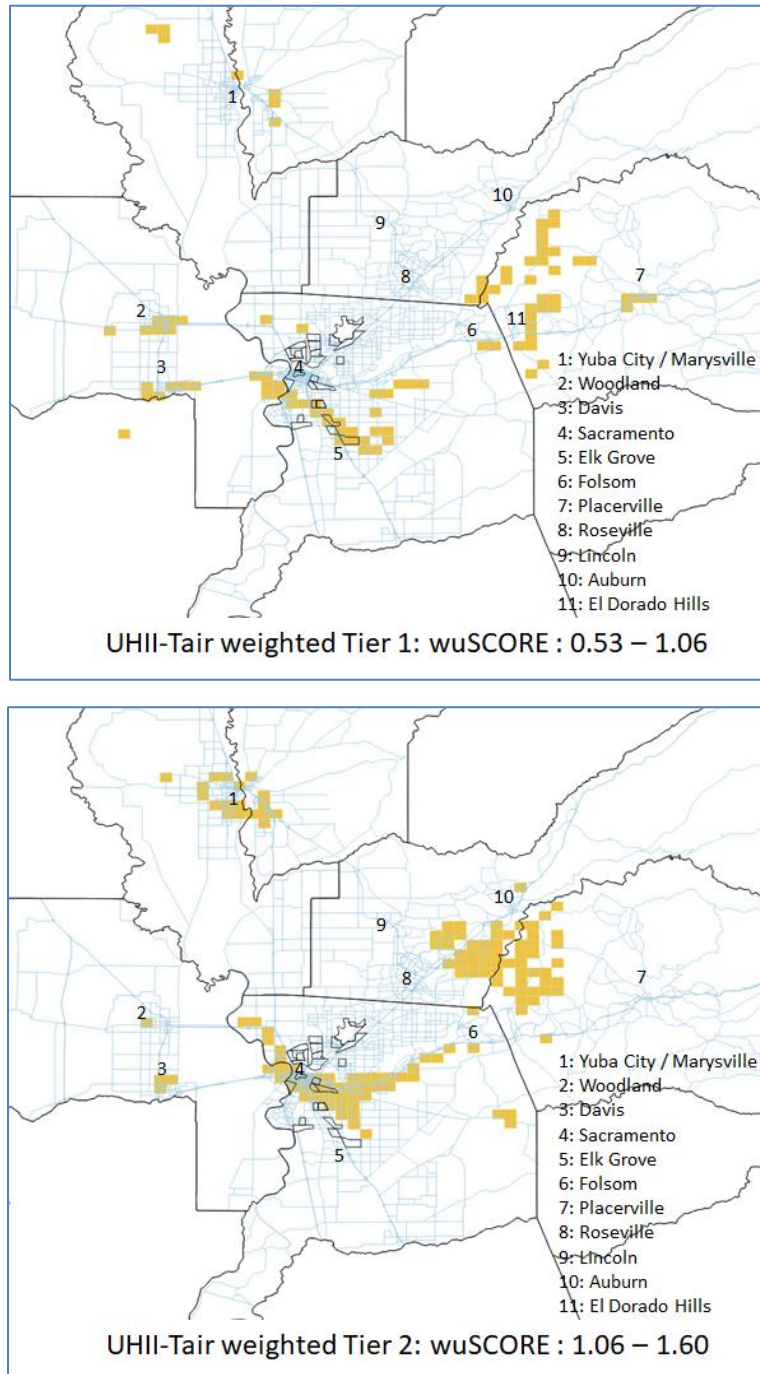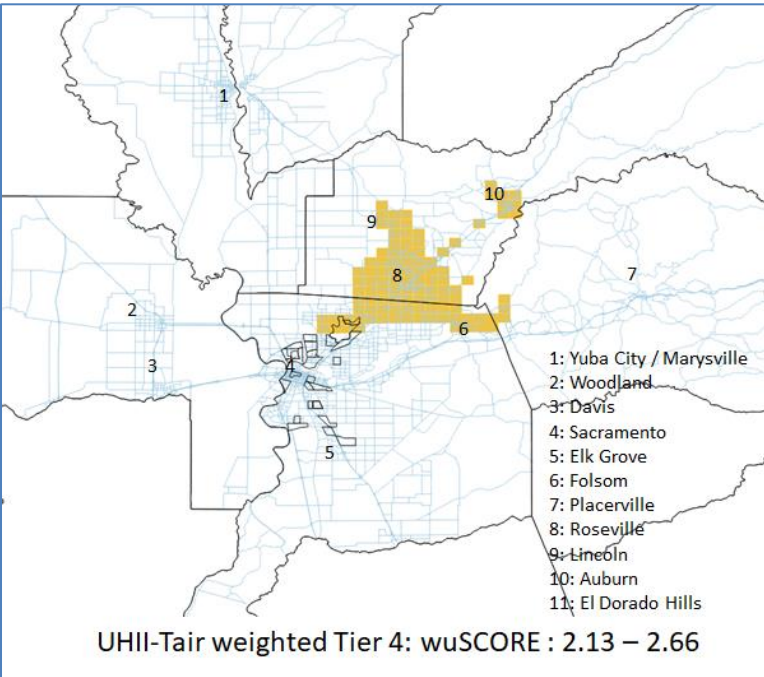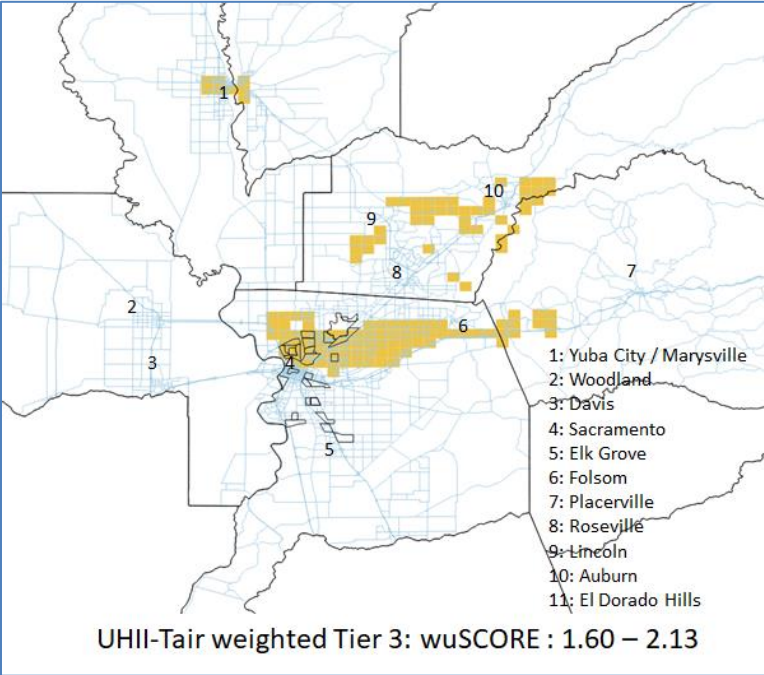
5.18 COMMUNITY-LEVEL, FINE-SCALE MODELING AND ANALYSIS

This section presents results from modeling community-scale or roadway project-specific mitigation measures. The goal of the simulations at 500-m resolution was to provide an assessment of the localized or site-specific changes in microclimate (excluding or including transported effects from neighboring communities) resulting from these measures. It was also the goal of the fine-scale modeling to evaluate certain mitigation strategies that were not tested at the 2-km level because they are project-, site-, or community-specific.

In other words, the simulations presented in this section answer the question: "What happens locally if a neighborhood or community implemented UHI-mitigation measures but the rest of the Capital region didn't do anything?"

The 500-m results were evaluated on a 5-dimensional matrix of:

(**v**)ariable (T_{air}, $T_{surface}$, T_{UCL}, RH, U, Zi, Solar);

(**i**)nterval (*year, month, interval*);

(**t**)ime of day or range of hours (*all hours, 0600 PDT, 0700 PDT, 1300 PDT, 1500 PDT, 1700 PDT, 1400-2000 PDT*);

(**m**)easure (*caseAA-00, caseBB-00, caseQF2-00, etc.,* see Section 5.19); and

(**a**)rea/site.

That is, changes from mitigation measures were given by:

$$\Delta_{v,i,t,m,a}$$

5.19 DEFINITIONS OF PROJECT-SPECIFIC AND COMMUNITY-LEVEL SCENARIOS

The following scenarios were modeled at the 500-m scale and in various combinations depending on domain and/or specific requests from the project participants, SMAQMD / LGC, and the project TAC:

- caseAA:
  - For the MTP projects defined by SMAQMD, LGC, the project TAC, or WSP, the roadway albedo was increased from a mean of 0.12 (average of current roadway albedo) to 0.35. The reason for imposing this upper limit was discussed earlier in the report.
  - For the AB617 communities, DAC areas, or other urban areas of interest to cities and project participants, such as downtown areas or specific projects, roof albedo was increased from a current mean of 0.17 to 0.5 and the roadway albedo from a

mean of 0.12 to 0.30 (this is a smaller increase than 0.35 above because these are mostly residential areas, compared to MTP projects that usually comprise major highways and freeways where increases in roadway albedo can be made larger). The reason for imposing these upper limits was discussed earlier in this report.

- caseQF2/QF3:
  - This is a vehicle-electrification scenario. In this case, heat flux from mobile sources was reduced by 25% (per CEC and SMAQMD studies that assume an electric-vehicle ownership of 25%). The maximum reduction (25%) was further modulated by (1) the distribution of urban fraction in the domain and (2) distance from charging stations. Furthermore, the hourly variations in heat emissions from mobile sources were approximated as in the following diurnal profile of traffic intensity (graph below) based on Sailor and Lu (2004). The red vertical line on the graph identifies the rush hour at 1700 PDT.
  - The reductions in mobile-source heat emissions were evaluated along the major highways in the region such as I-5, HWY 99, I-80, HWY 50, etc., depending on the sub-domain being modeled. This will be discussed when presenting results from various 500-m domain simulations in this report.
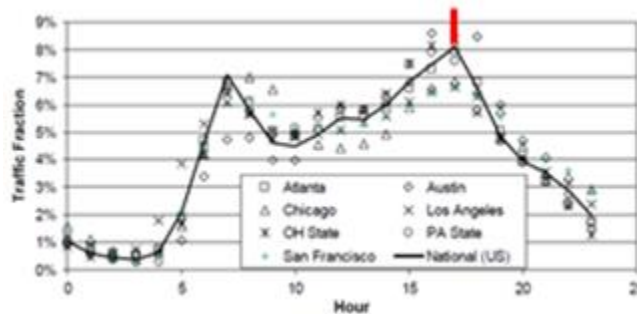
Source: Sailor and Lu (2004).

- caseSMAQMD_ZEV:
  - This is also a vehicle-electrification scenario, like cases QF2/QF3 above, except that the reductions in heat emissions were applied to and evaluated throughout the region, around the various charging stations identified in the SMAQMD's ZEV Readiness Plan (SMAQMD 2018).
  - In this modeling study, the reductions in heat emissions for this scenario were scaled using a Cressman weighting scheme that reduces electrification levels radially outward from each charging station location and further modified as a function of LULC, roadway density, and urban fraction.

- o At the charging stations, the reduction in heat emissions was assumed to be 25% (maximum reduction) which was then reduced radially outward of each station following a Cressman weighting scheme. For this analysis, the scheme was applied with a 10-km radius of influence, as discussed later in this report.

- caseBB_evapo:

  - o This is a vegetation-canopy scenario that increases cover and evapotranspiration, but is different from canopy-cover cases at the 2 km level (i.e., case01 through case02). Here, the increases in canopy cover were applied to areas of interest defined by the SMAQMD, LGC and project TAC, including AB617 communities, downtown areas, and DACs. This will be discussed on a domain-by-domain basis later in this report.

  - o For this case, 310 large trees were added to 0.25 km^2 cells, which is equivalent to an increase of 8% of the cell area. Thus, this is roughly equivalent to or smaller than case01 in domain D04 (2 km grid) but the increase in cover is concentrated in a smaller area (there also is a more extreme test case, caseBB_evapo3, where 940 trees were added to each 500-m cell, which is equivalent to an increase of 24% of cell area, thus roughly corresponding to case02 at the 2-km scale – but this was only a test scenario).

  - o Per literature, a large tree is 65 m^2 on average; a medium tree is 30 m^2; and a small tree is 10 m^2. The assumption made here is that the trees being planted are large (upon maturity), thus with a top-down view area of 65 m^2. However, compared to actual established trees, this may not be particularly large. For example, the trees in Cesar Chavez Park (between the LGC and Cal/EPA offices in Sacramento) have a top-down-view area of 120 – 150 m^2, thus twice or close to three times the size of the trees assumed in this modeling study.

  - o Another exercise that can help visualize the extent of increased canopy cover in this scenario is to compare to a well-known park, say, Central Park in New York. There are about 20,000 trees in that park and the total park area is ~3.6 km^2. This yields a tree-specific site area of 180 m^2 tree^{-1}. Thus, for a 500-m cell, this would translate into 1390 trees. On the other hand, the scenario modeled here adds only 310 trees per 500-m cell, which is quite reasonable.

- caseAA_BBevapo_QF

  - o This is a case combining cases AA, BBevapo, and QF2/QF3.

- caseAA_BBevapo_QF_CW:

  - o This is a cool-walls scenario where in addition to other measures, the albedo of walls is increased to 0.40 (from an average of 0.15).

Altostratus Inc.

- casePV01 through PV20:
  - These are solar PV scenarios explained in detail later in this report.

Out of the total number of grid cells in each 500-m domain D05 through D10, a subset of cells is designated as urban, each with a calculated urban fraction (per LULC analysis). These cells are where the Altostratus-modified modUCM model is triggered, i.e., where the urban fraction exceeds a certain pre-determined threshold. These will be discussed in Section 5.21. Furthermore, a subset of these urban cells was designated for application of the mitigation measures defined above. These cells were defined either by technical potential or by project locations of interest to the project TAC, cities, and communities in the region.

5.20 MODELED PERIODS AT 500 m SCALE

For the community-scale modeling and analysis at 500-m resolution, the following periods are presented in this report:

2013_int3:   Representing hottest periods (daily max: 38 – 45 °C)

2016_int5:   Representing mid-range periods (daily max: 34 – 37 °C)

2015_int1:   Representing lower-end periods (daily max: 27 – 35 °C)

It is to be noted that the hotter weather, e.g., with daily maximum air temperatures in the range of 38 – 45 °C, occurs in only about 10% of the time (out of the total number of hours examined in this study), but is weighted at 33% in this analysis (one of the three periods listed above). As such the results and discussions in the following sections are skewed towards hotter weather, i.e., they represent some of the worst-case conditions of urban heat and the UHII.

5.21 URBAN-CELL TRIGGERS FOR THE 500-m MODEL

As introduced earlier in this report, the fine-scale modeling at 500-m resolution was carried out in this study using modUCM, which is an Altostratus Inc. – modified WRF urban canopy model described in Taha (2008a-c, 2017, 2018). The modified model requires additional surface-characterization parameters as discussed in Section 2.

Per this Altostratus approach, the urban model is triggered (called) at specified grid cells in each domain. These cells can be defined per modeler's objectives and criteria – an approach that allows the triggering to occur not solely based on a cell's LULC class, as is done in the standard WRF model (although this is one of many available options) but also based on each cell's physical properties or combinations of properties (i.e., it often is the case that some areas are defined as urban but in fact have the same physical properties as a non-urban LULC, and vice-versa). Thus,

the Altostratus approach offers a more accurate basis for calling the urban modules in modUCM to ensure more area-specific simulations. When the modUCM is called at specified grid cells, various parameters are also weighted by urban fraction and meshed with non-urban properties and parameters based on LULC and physical characteristics in each cell. Figure 5-43 shows the modUCM trigger points for each 500-m domain (D05 through D10) based on urban fraction. Appendix A-2 provides a larger version of these maps.

Figure 5-43: Urban fraction as a modUCM trigger (trigger grid cells in 500-m domains). Note the contrast in urban extents and urban fraction ranges across these domains. Also note that the figures are not to the same scale.

Urban Fraction (933 trigger cells) Yuba City / Marysville area

Urban Fraction (501 trigger cells) Woodland area

Figure 5-43, continued.

Urban Fraction (3153 trigger cells) Sacramento / Elk Grove area

Urban Fraction (2251 trigger cells) Sacramento / Roseville area

Figure 5-43, continued.

Urban Fraction (1022 trigger cells) Folsom / El Dorado Hills area

Urban Fraction (845 trigger cells) Placerville area
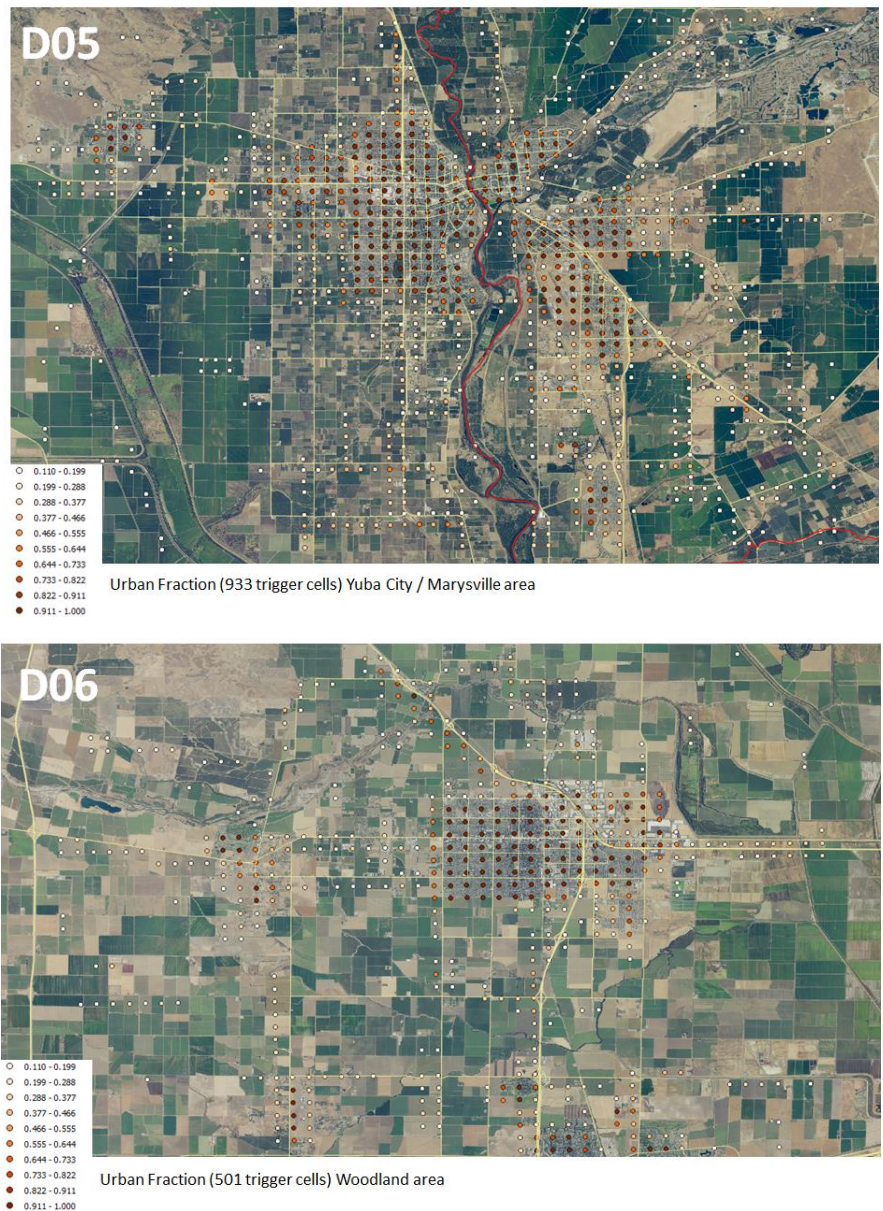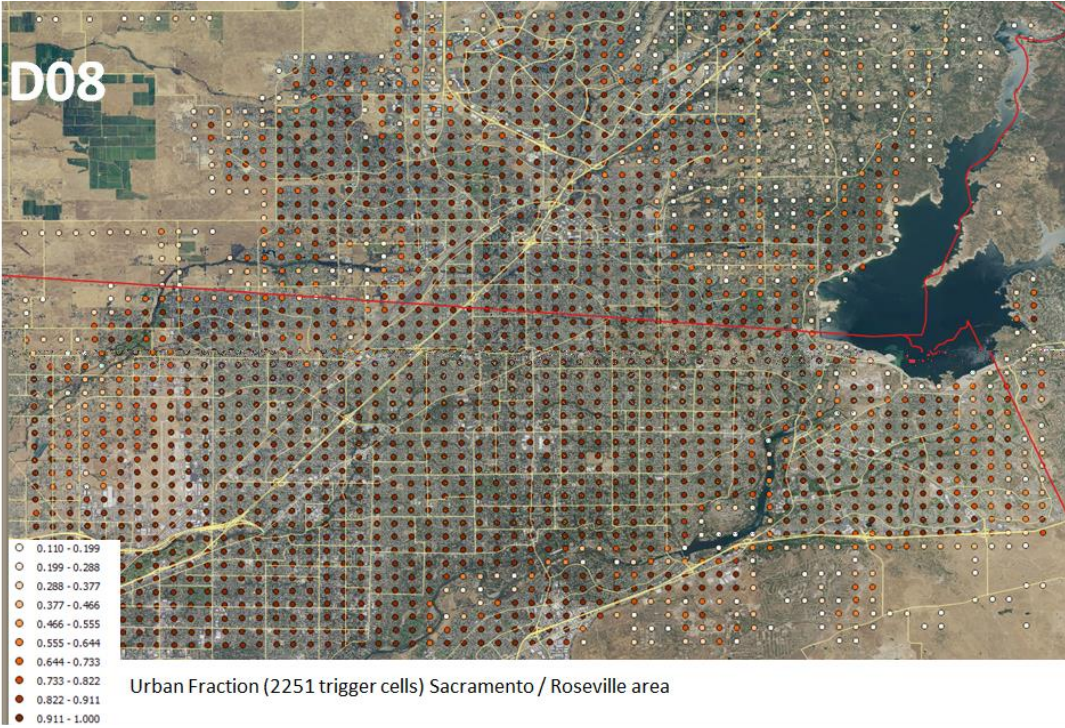
5.22 IMPACTS OF MITIGATION MEASURES AT THE COMMUNITY LEVEL

In this section, results from the fine-scale, community- or neighborhood-level simulations are presented. The analysis provides a quantification of effects from UHI-mitigation measures at the 500-m scale.

5.22.1 DOMAIN D05 (Yuba City / Marysville)

Figure 5-44 depicts the MTP project locations and other areas of interest that were modeled to evaluate the local-scale impacts of mitigation measures in domain D05. The 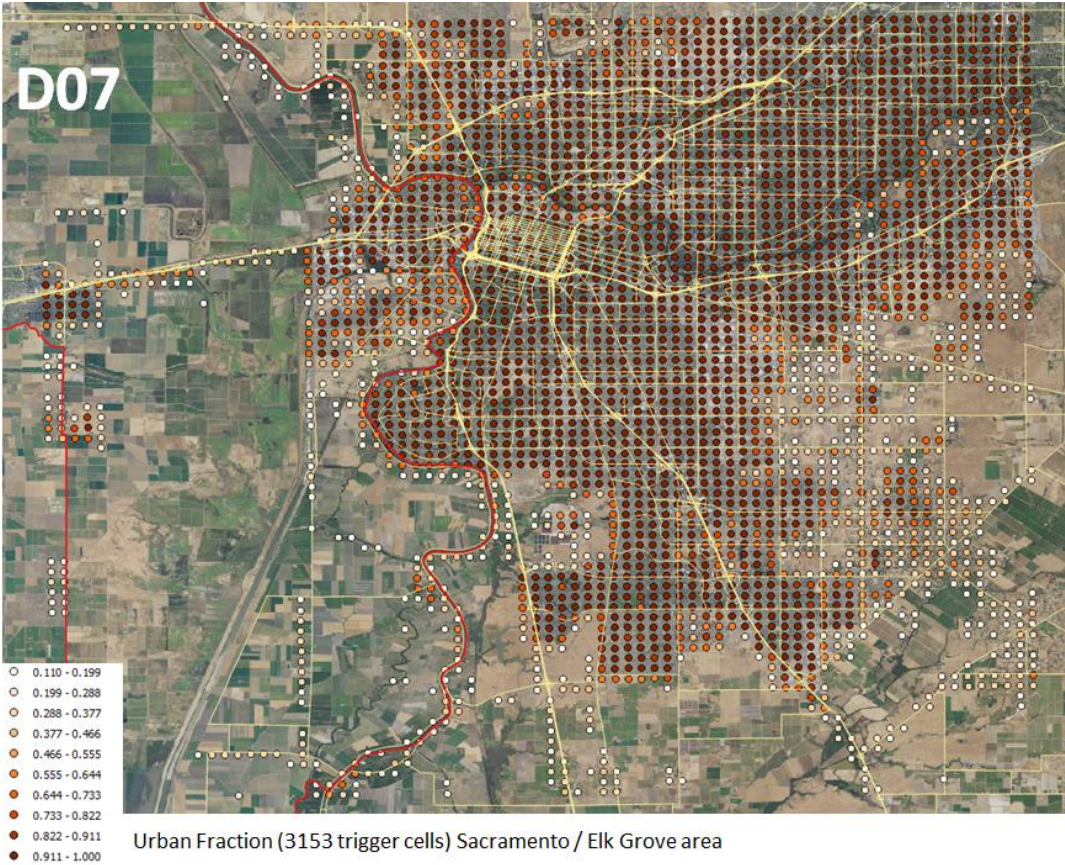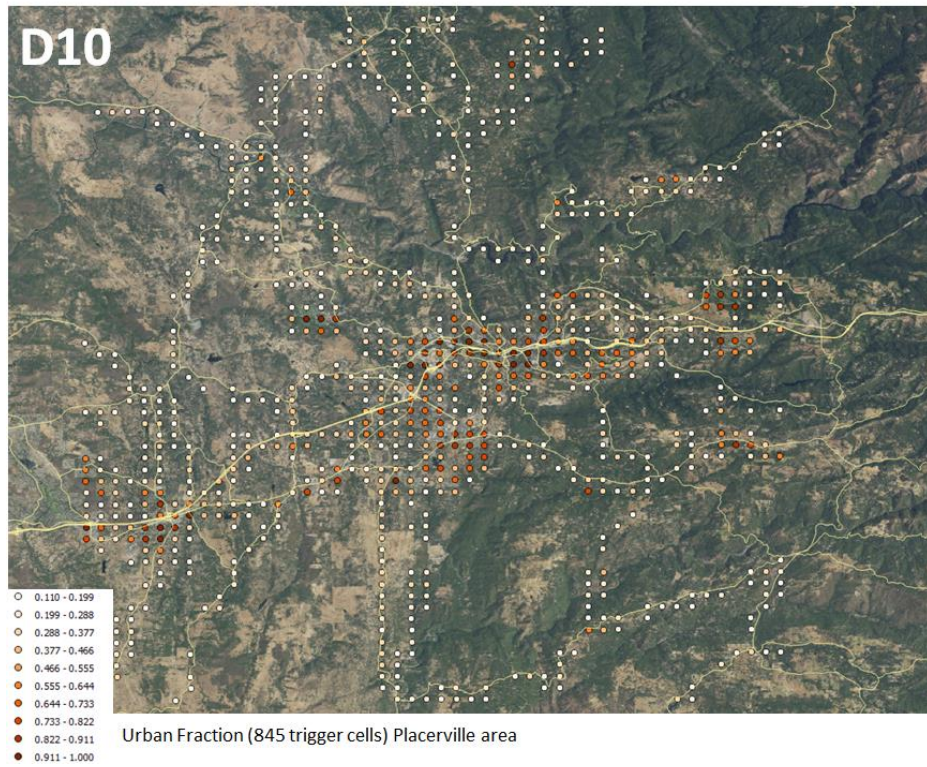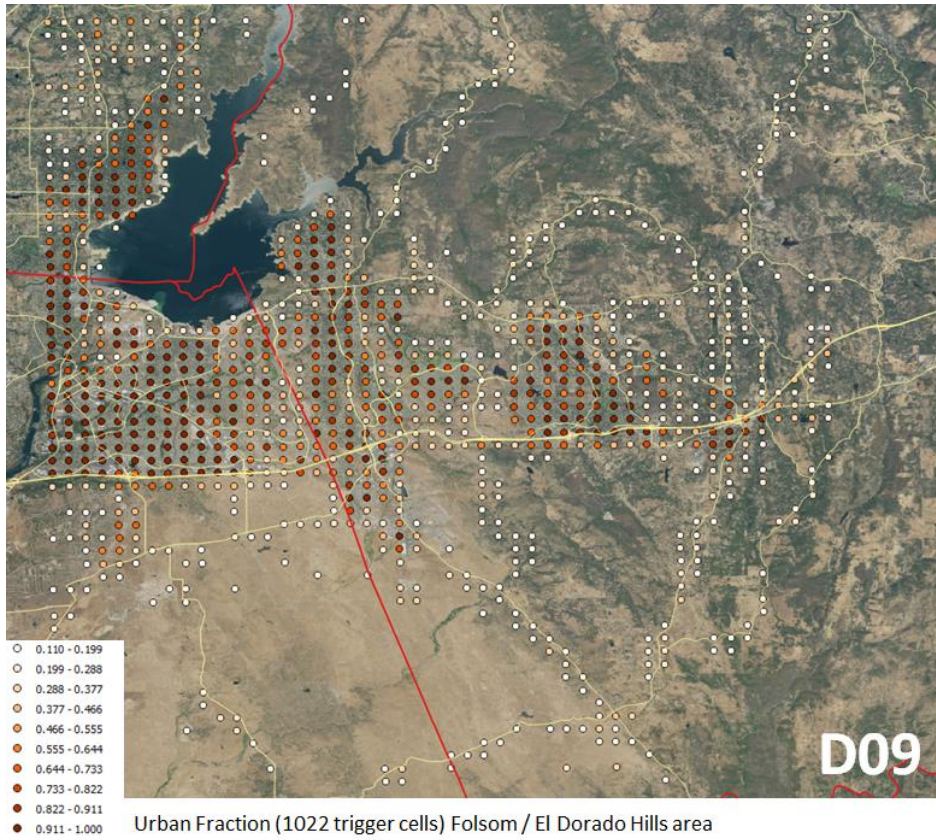yellow line defines downtown Marysville, an area of interest per project TAC, the orange lines are roadway and bridge projects identified by the City of Yuba City, and the red lines are MTP projects including point projects identified by WSP. The major highways of interest for electrification scenarios are also highlighted with bold black lines.

Figure 5-44: Locations of roadway projects and areas of interest in the Yuba City / Marysville domain.
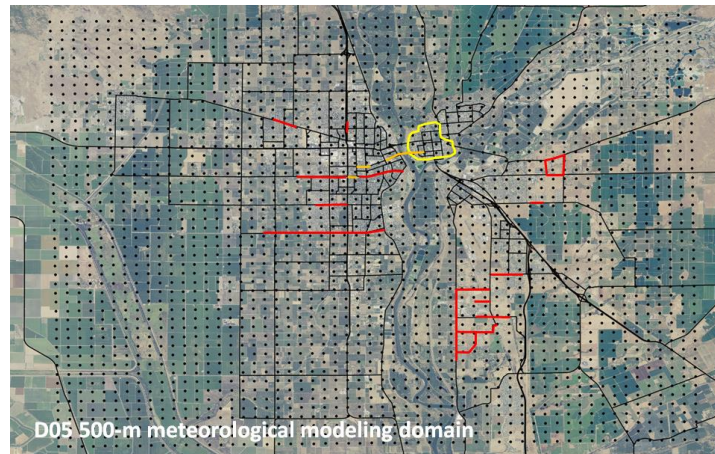
Scenario AA

Figure 5-45 depicts the urban-canopy air-temperature impacts of implementing caseAA (defined earlier) for a sample interval. In downtown Marysville, both cool roofs and pavements are implemented but in the MTP roadway project areas, only cool pavements are used. In the areas of interest (defined above), the urban canopy is cooled by up to a maximum of 4.5 °C, as an average over all 1500-PDT hours in the period August 1 – 15, 2016 (in this example). The largest cooling is seen in the downtown Marysville area and the MTP roadway projects in the southern part of the domain. These cooling effects are larger than the regional effects discussed earlier in Sections 5.10 and 5.13, as the former were averaged over 2 km whereas here, the effects are localized, at finer scales, and within the urban canopy. The roadway-temperature impacts of implementing cool

pavements are shown in Figure 5-46. The average maximum cooling (i.e., averaged over all 1500-PDT hours) in the period August 1 – 15, 2016 is 11.0 °C. The spatial pattern of the affected areas is similar to that in Figure 5-45 (since the measures are implemented at the same locations) but the temperature reductions are different.

Figure 5-45: Change in urban-canopy air temperature from cool roofs and pavements in the Yuba City / Marysville area. Example: average changes at 1500 PDT, August 1 – 15, 2016. Maximum average cooling is 4.5 °C (darkest blue).

Figure 5-46: Change in roadway temperature from cool pavements in the Yuba City / Marysville area. Example: average changes at 1500 PDT, August 1 – 15, 2016. Maximum average cooling is 11.0 °C (darkest blue).
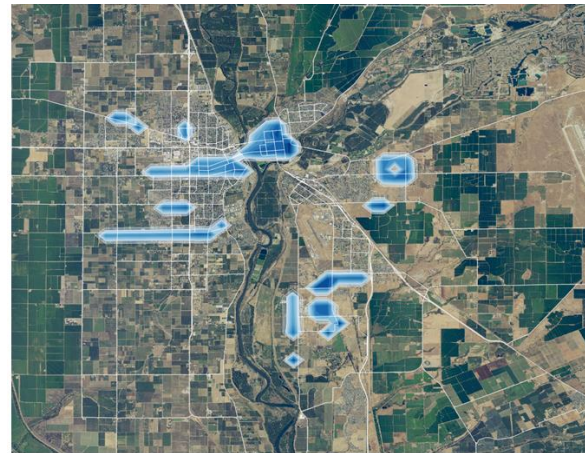
Scenario BBevapo

The air-temperature impacts of implementing vegetation canopy-cover increases in the downtown Marysville area were computed and an example is shown in Figure 5-47. The 24-hour average

cooling (in the sample interval June 1 – 15, 2015) reaches up to 1.8 °C in the north-central parts of downtown.
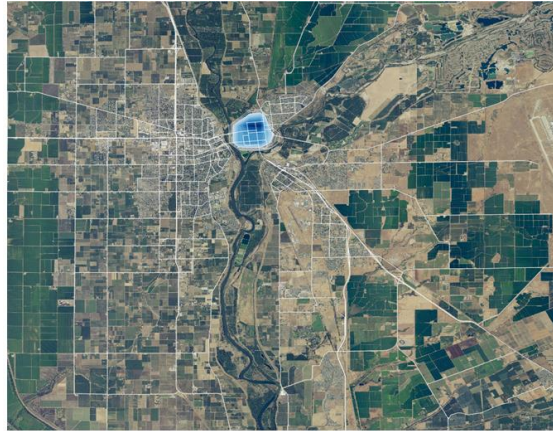
Figure 5-47: Change in air temperature from canopy in Marysville. Example: all-hour average change in the interval June 1 – 15, 2015. Maximum average cooling is 1.8 °C (darkest blue).

Scenario QF2

Figure 5-48 shows the near-surface temperature effects of vehicle electrification (25% EV ownership) along the major highways in the area, namely, HWY 20, HWY 99, HWY 70, and HWY 65. The 1700-PDT (rush-hour) average reduction reaches up to 1.8 °C, during the sample interval depicted in the figure (July 1 – 15, 2013). The largest cooling can be seen along highways 99 (N-S direction) and 20 (E-W direction) in Yuba City, as well as in the downtown Marysville area.

Figure 5-48: Change in near-surface temperature from vehicle electrification in the Yuba City / Marysville area. Example: 1700-PDT (rush-hour) average change in the interval July 1 – 15, 2013. Maximum average cooling is 1.8 °C (darkest blue).
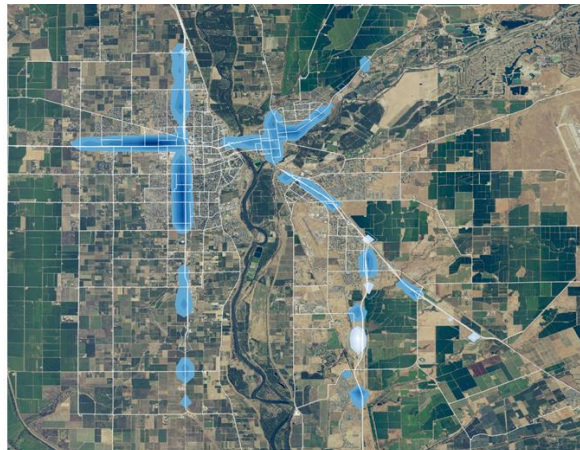
Thus, whereas the figures above provide samples of temperature impacts at selected hours during example time periods, Table 5-17 is a summary of temperature changes averaged (for various given hours or range of hours) over all modeled periods identified earlier in Section 5.20. As with the preceding analysis, the summaries in Table 5-17 are for localized effects only (no advective effects are accounted for). Later in this report, both localized and advective (transported) effects will be discussed and compared

It is important to note here (and in similar subsequent tables) that, unlike cool pavements and roofs, canopy cover affects air temperature above the canopy as well as both air temperature and surface temperature below the canopy. Similarly, for the electrification scenarios, the tail pipe exhaust occurs closer to the ground than to the upper parts of the urban canopy layer. Thus, for both canopy-cover and electrification scenarios, it is more accurate to account for (e.g., average) both air and surface temperature changes as will be shown later in the temperature summaries. However, for the purpose of Table 5-17 (and similar ones), the effects are reported separately.

Table 5-17: Changes in temperature as area-wide and time averages per given hour or range of hours (averaged over the 3 intervals defined earlier) for the Yuba City / Marysville area. In case of canopy cover and electrification scenarios, a better indicator of the effects is to average Tair and Tsfc (see text for explanation).

D05				
Marysville / Yuba City			Albedo scenario (avg. change in °C)	Canopy scenario (avg. change in °C)
0600 PDT				
	Tair	roofs and pavements	-0.24	-0.34
		roadways	-0.17	
	Tsf	roofs and pavements	-0.46	-2.23
		roadways	-0.35	
1300 PDT				
	Tair	roofs and pavements	-3.07	-0.43
		roadways	-2.09	
	Tsf	roofs and pavements	-8.28	-2.56
		roadways	-5.53	
1500 PDT				
	Tair	roofs and pavements	-2.68	-0.40
		roadways	-2.46	
	Tsf	roofs and pavements	-7.45	-2.50
		roadways	-6.33	
all hours				
	Tair	roofs and pavements	-1.38	-0.49
		roadways	-1.11	
	Tsf	roofs and pavements	-3.57	-2.87
		roadways	-2.68	

D05		
Marysville / Yuba City		Electrification scenario (avg. change in °C)
0700 PDT		
	Tair	-0.05
	Tsfc	-0.18
1700 PDT		
	Tair	-0.05
	Tsfc	-0.37
all hours		
	Tair	-0.04
	Tsfc	-0.24

5.22.2 DOMAIN D06 (Woodland)

In Figure 5-49, the yellow line highlights an area of interest (per TAC) in the northwestern part of Woodland where additional future urbanization is expected to occur. The red lines depict the MTP roadway projects including points identified by WSP. The highways of interest in electrification scenarios are highlighted with black lines.

Figure 5-49: Locations of roadway projects and areas of interest in the Woodland area.
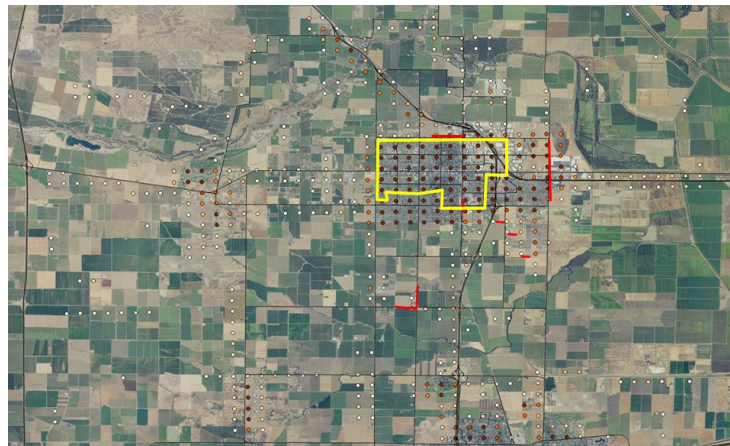
Scenario AA

Figure 5-50 shows the urban-canopy air-temperature impacts of implementing cool surfaces (as defined earlier) for a sample interval. Within the area defined by yellow boundaries (in Figure 5-49), both cool pavements and roofs are applied. In the roadway-project areas (red lines) only cool pavements are assumed to be implemented, as define earlier in Section 5-19. The urban canopy in these areas is cooled by up to a maximum of 4.5 °C, as an average over all 1500-PDT hours in the

sample period August 1 – 15, 2016. The largest cooling occurs in the northern part of the city (Figure 5-50). Again, and as discussed earlier, these cooling effects are larger than the regional ones, as the latter were averaged over 2 km whereas here the effects are localized.

The roadway-temperature impacts of implementing cool pavements are shown in Figure 5-51. The average maximum cooling (averaged over all 1500-PDT hours) in the period August 1 – 15, 2016 is 10.9 °C. The larger cooling occurs in the northern parts of Woodland as well as at the locations of the roadway projects. Figures 5-50 and 5-51 show the same spatial pattern in temperature change (as the different measures are implement in similar areas) but the magnitudes of the changes differ.

Figure 5-50: Change in urban-canopy air temperature from cool roofs and pavements in Woodland. Example: average changes at 1500 PDT, August 1 – 15, 2016. Maximum average cooling is 4.5 °C (darkest blue).

Figure 5-51: Change in roadway temperature from cool pavements in Woodland. Example: average changes at 1500 PDT, August 1 – 15, 2016. Maximum average cooling is 10.9 °C (darkest blue).

Scenario BBevapo

Figure 5-52 depicts the air-temperature impacts of increasing vegetation canopy-cover in the downtown Woodland area. The 24-hour average cooling (in the sample interval June 1 – 15, 2015) reaches up to 1.4 °C in the north-eastern parts of the urban area that was defined with yellow boundaries in Figure (5-49).

Figure 5-52: Change in air temperature from canopy in Woodland. Example: all-hour average change in the interval June 1 – 15, 2015. Maximum average cooling is 1.4 °C (darkest blue).

Scenario QF3

Figure 5-53 shows the near-surface temperature effects of vehicle electrification (25% EV ownership) in the Woodland area. The effects are quantified along the major highways in the area, namely, I-5, HWY 22/16, and HWY 113. The rush-hour (1700-PDT) average reduction in temperature reaches up to 2.2 °C during the sample interval depicted in the figure (July 1 – 15, 2013). The largest cooling is seen along highways 22/16, as well as in a central section of HWY 113.

Figure 5-53: Change in near-surface temperature from vehicle electrification in the Woodland area. Example: 1700-PDT (rush-hour) average change in the interval July 1 – 15, 2013. Maximum average cooling is 2.2 °C (darkest blue).

Table 5-18 provides a summary of temperature changes averaged (for various given hours or range of hours) over the three modeled periods identified in Section 5.20. Again, the summary is for localized effects only (both the localized and advective effects will be discussed later in this report). As explained above, for canopy-cover and electrification scenarios, both air and surface temperature changes should be accounted for, but are reported separately in Table 5-18.

Table 5-18: Changes in temperature as area-wide and time averages per given hour or range of hours (averaged over the 3 intervals defined earlier) for the Woodland area. For canopy cover and electrification scenarios, a better indicator of the effects is to average both Tair and Tsfc (see text for explanation).

D06

Woodland			Albedo scenario (avg. change in °C)		Canopy scenario (avg. change in °C)
0600 PDT					
	Tair	roofs and pavements	-0.25		-0.29
		roadways	-0.26		
	Tsf	roofs and pavements	-0.42		-1.73
		roadways	-0.46		
1300 PDT					
	Tair	roofs and pavements	-2.74		-0.23
		roadways	-3.31		
	Tsf	roofs and pavements	-6.61		-1.31
		roadways	-8.60		
1500 PDT					
	Tair	roofs and pavements	-2.51		-0.19
		roadways	-2.92		
	Tsf	roofs and pavements	-6.14		-1.70
		roadways	-7.55		
all hours					
	Tair	roofs and pavements	-1.29		-0.33
		roadways	-1.47		
	Tsf	roofs and pavements	-2.94		-2.01
		roadways	-3.66		

D06

Woodland		Electrification scenario (avg. change in °C)
0700 PDT		
	Tair	-0.05
	Tsfc	-0.26
1700 PDT		
	Tair	-0.01
	Tsfc	-0.40
all hours		
	Tair	-0.04
	Tsfc	-0.25

5.22.3 DOMAIN D07 (Sacramento)

Figure 5-54 identifies the locations of MTP project and other areas of interest for modeling and analysis in the Sacramento area. The yellow zones are AB617 communities defined by SMAQMD that also are of interest to the project TAC and the cities in this area. The red lines are MTP projects including those identified by WSP and the major highways of interest in electrification scenarios are highlighted with bold black lines.

Figure 5-54: Locations of roadway projects and areas of interest in the Sacramento region.
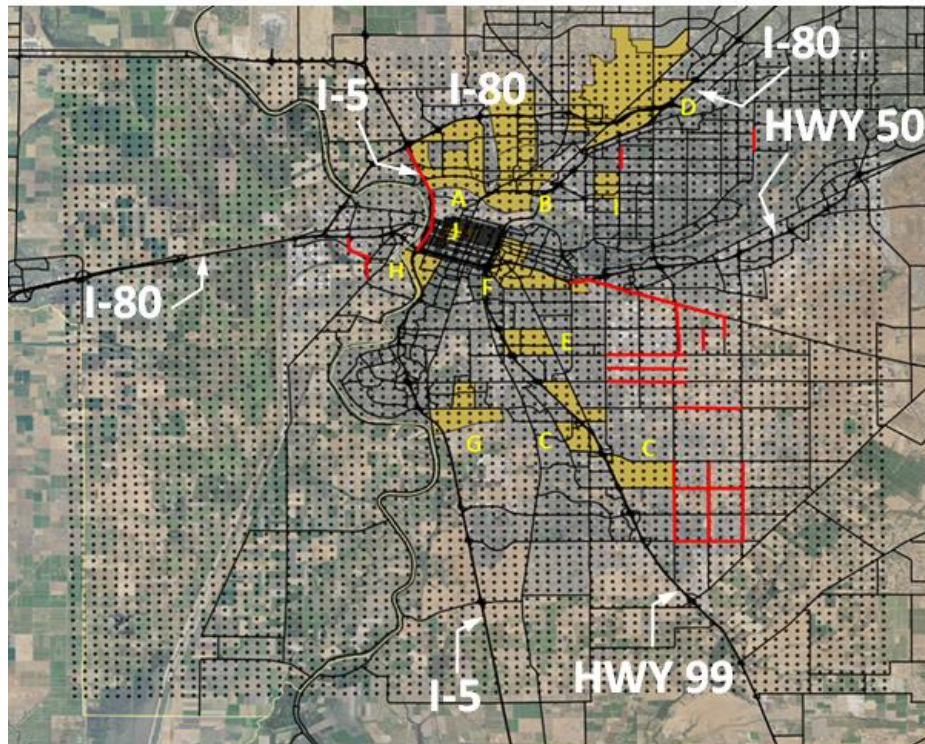
Scenario AA

In Figure 5-55, the urban-canopy air-temperature impacts of implementing caseAA (defined earlier) are shown for the sample interval August 1 – 15, 2016. It is assumed that in the AB617 communities (yellow areas in Figure 5-54), both cool roofs and cool pavements are implemented, whereas in the roadway project corridors (red lines), only cool pavement are applied. The average cooling in the urban canopy reaches up to a maximum of 5.2 °C as a result of implementing cool roofs and pavements (as an average over all 1500-PDT hours in this period). The largest cooling is seen in various parts of the AB617 communities as well as along the MTP roadway projects (Figure 5-55). Again, it should be recalled that these cooling effects are significantly larger than those at the 2 km scale because they are very localized and averaged over much smaller areas.

Figure 5-56 shows the roadway-temperature impacts of implementing cool pavements. The maximum average cooling of the roadways over all 1500-PDT hours in the period August 1 – 15, 2016 is 13.2 °C.

Figure 5-55: Change in urban-canopy air temperature from cool roofs and pavements in the Sacramento area. Example: average changes at 1500 PDT, August 1 – 15, 2016. Maximum average cooling is 5.2 °C (darkest blue).
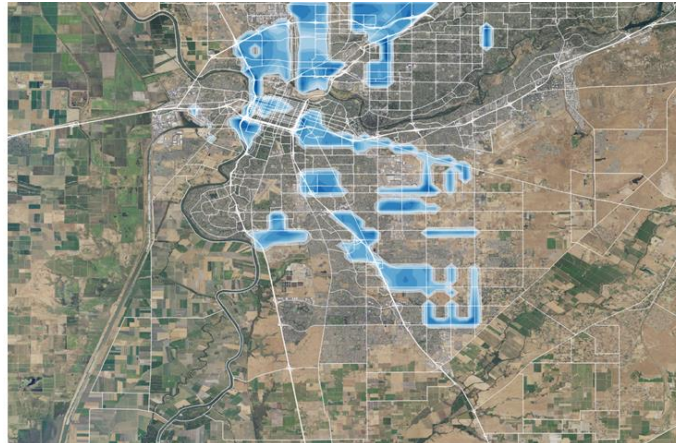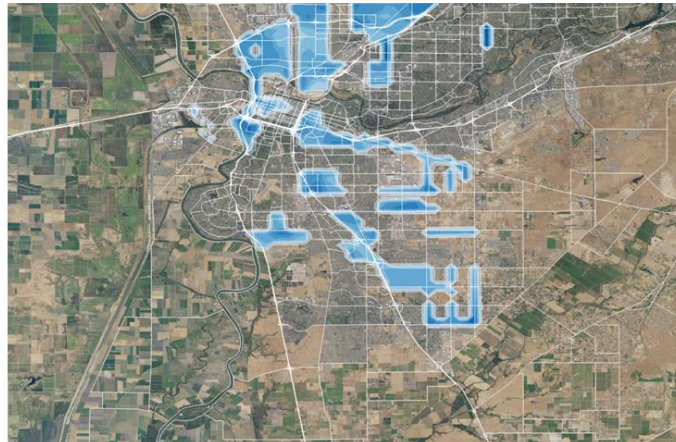

Figure 5-56: Change in roadway temperature from cool pavements in the Sacramento area. Example: average changes at 1500 PDT, August 1 – 15, 2016. Maximum average cooling is 13.2 °C (darkest blue).


Scenario BBevapo

The increases in canopy cover were assumed to be implemented in AB627 communities "A" in the north and "C" in the south of this domain. Figure 5-57 shows the air-temperature impacts of increasing vegetation canopy-cover in these two areas. The 24-hour average cooling (during the sample interval June 1 – 15, 2015) reaches up to 1.4 °C in community "C" and is larger than the cooling attained in community "A".

Figure 5-57: Change in air temperature from canopy cover in the Sacramento area. Example: all-hour average change in the interval June 1 – 15, 2015. Maximum average cooling is 1.4 °C (darkest blue).
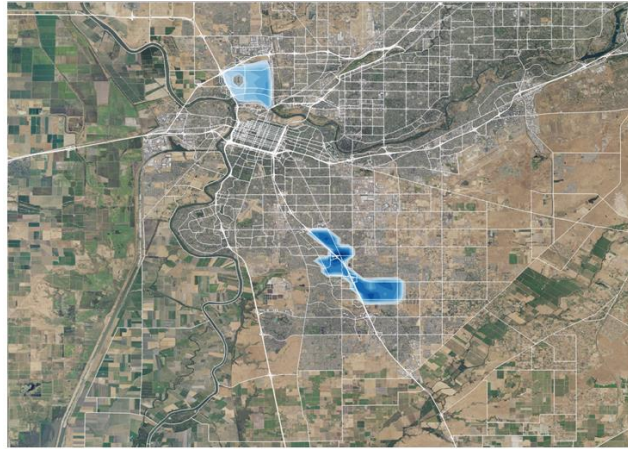
Scenario QF2

In terms of near-surface temperature effects from electrification (again, at the 25% level of EV ownership) in the Sacramento area, model results are shown in Figure 5-58. The effects are quantified along the major highways – I-80, HWY 50, I-5, and HWY 99. The 1700-PDT (rush-hour) average reduction in temperature reaches up to a maximum of 2.4 °C, during the sample interval depicted in the figure (July 1 – 15, 2013). The largest cooling occurs along HWY 50 and HWY 99, although all major highways do see significant cooling at different locations (see Figure 5-58).

Figure 5-58: Change in near-surface temperature from vehicle electrification in the Sacramento area. Example: 1700-PDT (rush-hour) average change in the interval July 1 – 15, 2013. Maximum average cooling is 2.4 °C (darkest blue).
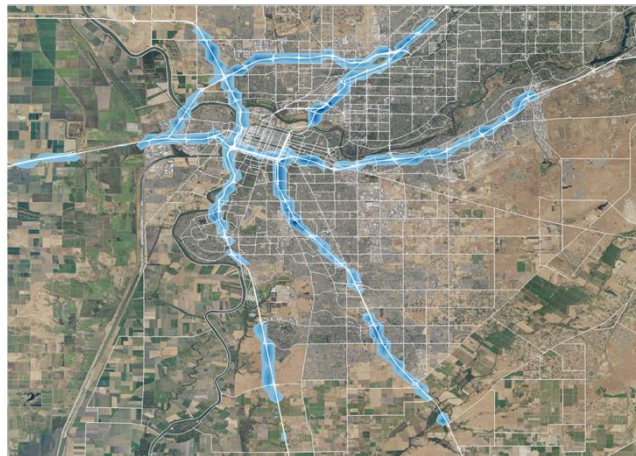
Table 5-19 provides a summary of temperature changes averaged (for various given hours or range of hours) over the three modeled periods identified in Section 5.20. Again, the summaries are for localized, non-advective effects only and, as explained above, for canopy-cover and electrification scenarios, both air and surface temperature changes should be accounted for. For the purpose of this table, however, the effects are reported separately.

Table 5-19: Changes in temperature as area-wide and time averages per given hour or range of hours (averaged over the 3 intervals defined earlier) for the Sacramento area. For canopy cover and electrification scenarios, a better indicator of the effects is to average both Tair and Tsfc (see text for explanation).

D07					
Sacramento area			Albedo scenario (avg. change in °C)		Canopy scenario (avg. change in °C)
0600 PDT					
	Tair	roofs and pavements	-0.25		-0.39
		roadways	-0.24		
	Tsf	roofs and pavements	-0.44		-2.25
		roadways	-0.45		
1300 PDT					
	Tair	roofs and pavements	-2.79		-0.14
		roadways	-3.14		
	Tsf	roofs and pavements	-6.98		-1.52
		roadways	-7.90		
1500 PDT					
	Tair	roofs and pavements	-2.67		-0.21
		roadways	-2.90		
	Tsf	roofs and pavements	-6.70		-2.03
		roadways	-7.39		
all hours					
	Tair	roofs and pavements	-1.31		-0.41
		roadways	-1.45		
	Tsf	roofs and pavements	-3.08		-2.54
		roadways	-3.46		

D07		
Sacramento area		Electrification scenario (avg. change in °C)
0700 PDT		
	Tair	-0.04
	Tsfc	-0.39
1700 PDT		
	Tair	-0.11
	Tsfc	-0.69
all hours		
	Tair	-0.07
	Tsfc	-0.43

5.22.4 DOMAIN D08 (Sacramento – Roseville – Granite Bay)

For the Sacramento – Roseville – Granite Bay areas, Figure 5-59 depicts the MTP project locations and areas of interest for analysis per project TAC recommendations. The yellow area is AB617 community "D" defined by SMAQMD. The red lines are MTP projects including those identified by WSP, and the major highways of interest in electrification scenarios are highlighted with white lines. The approximate outlines of the cities of Roseville and Granite Bay also are shown in the figure (with yellow and white lines, respectively).

Figure 5-59: Locations of roadway projects and areas of interest in the Sacramento – Roseville – Granite Bay area.
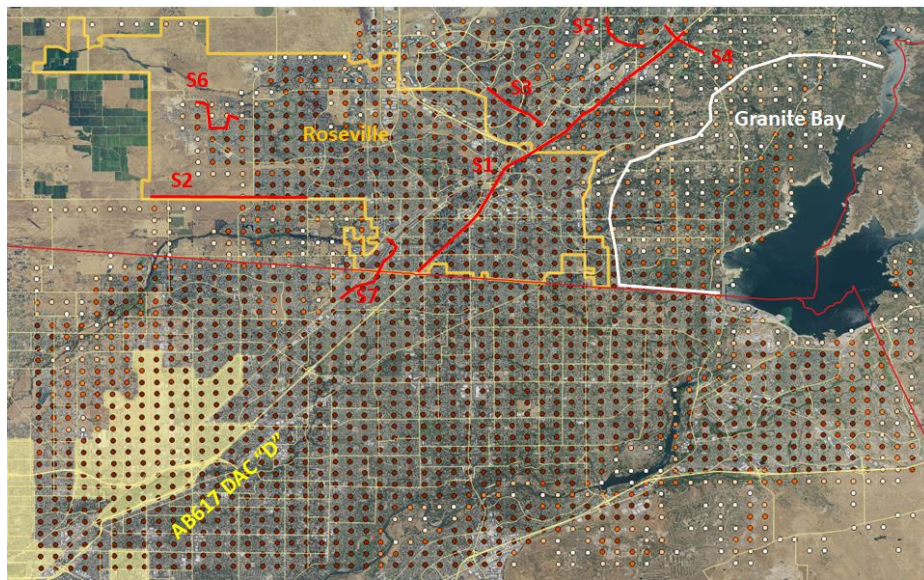
Scenario AA

In Figure 5-60, the urban-canopy air-temperature impacts of implementing caseAA (defined earlier) are shown for a sample interval. Again, it is assumed that in the AB617 community "D" (yellow area in Figure 5-59), both cool roofs and cool pavements are implemented, whereas in the roadway project areas (red lines), only cool pavement are applied. Thus, in the areas of interest, the urban canopy is cooled by up to a maximum of 4.6 °C as a result of implementing cool roofs and pavements, as an average over all 1500-PDT hours in the period August 1 – 15, 2016. The largest cooling effects are distributed throughout the modified urban area and along the major highways.

Figure 5-61 shows the roadway-temperature impacts of implementing cool pavements. The maximum averaged cooling of the roadways over all 1500-PDT hours in the period August 1 – 15, 2016 is 13.7 °C. The largest cooling, as expected, is seen relatively more along the main roadways in the area.

Figure 5-60: Change in urban-canopy air temperature from cool roofs and pavements in the Sacramento – Roseville – Granite Bay area. Example: average changes at 1500 PDT, August 1 – 15, 2016. Maximum average cooling is 4.6 °C (darkest blue).
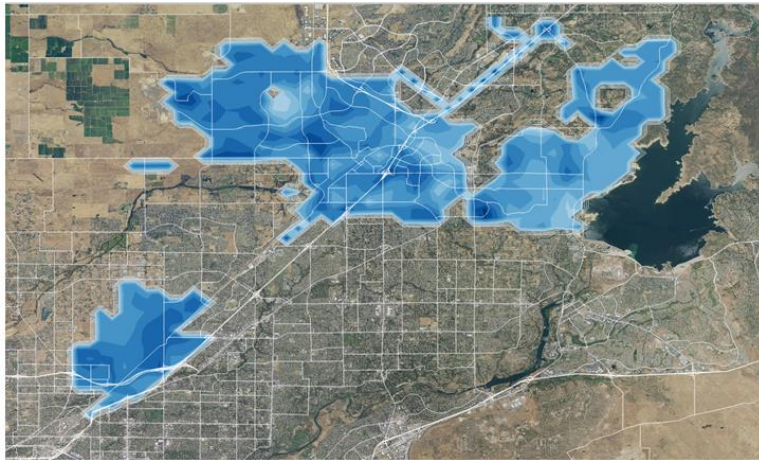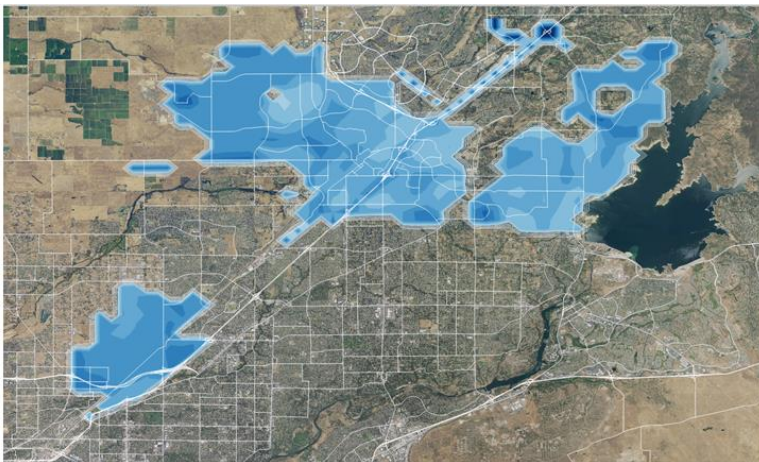

Figure 5-61: Change in roadway temperature from cool pavements in the Sacramento – Roseville – Granite Bay area. Example: average changes at 1500 PDT, August 1 – 15, 2016. Maximum average cooling is 13.7 °C (darkest blue).


Scenario BBevapo

The scenario of increased canopy cover was assumed to be implemented in the AB617 community "D" identified by the SMAQMD. Figure 5-62 depicts the air-temperature impacts of implementing vegetation canopy-cover increases during the sample interval June 1 – 15, 2015. The 24-hour average cooling (during this interval) reaches up to 0.9 °C mostly in the eastern and north-eastern parts of this community.

Figure 5-62: Change in air temperature from canopy in Sacramento AB-617 community "D": all-hour average change in the interval June 1 – 15, 2015. Maximum average cooling is 0.9 °C (darkest blue).
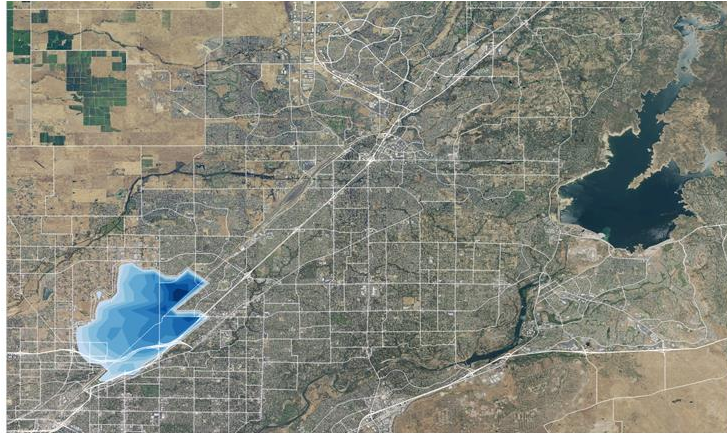
Scenario QF3

Figure 5-63 shows the near-surface temperature effects of automobile electrification (at the 25% level of EV ownership) in the Sacramento –Roseville – Granite Bay areas. The effects are quantified along the major highways in this region – I-80, HWY 65, HWY 50, and route E2. The 1700-PDT (rush-hour) average reduction in temperature reaches up to 2.3 °C, during the sample interval July 1 – 15, 2013. The largest average cooling occurs along HWY 50 and I-80.

Figure 5-63: Change in near-surface temperature from vehicle electrification in the Sacramento – Roseville – Granite Bay area. Example: 1700-PDT (rush-hour) average change in the interval July 1 – 15, 2013. Maximum average cooling is 2.3 °C (darkest blue).
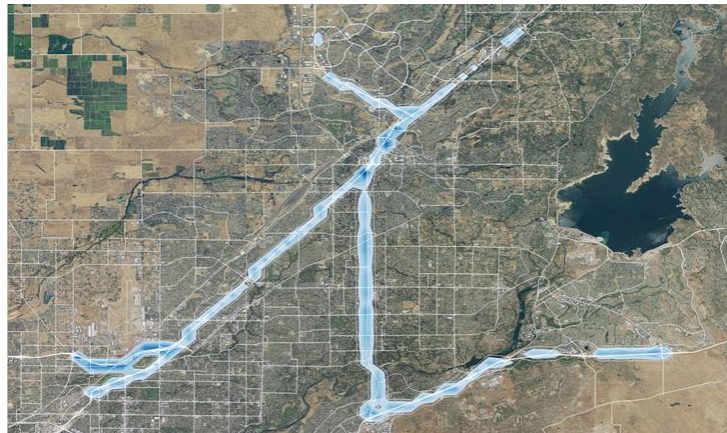
Finally, Table 5-20 provides a summary of temperature changes averaged (for various given hours or range of hours) over the three modeled periods identified in Section 5.20. As before, the summaries in Table 5-20 are only for the localized, non-advective effects. It is reiterated again that

for canopy-cover and electrification scenarios, both air and surface temperature changes need to be accounted for, e.g., averaged together. In Table 5-20, however, the effects are reported separately.

Table 5-20: Changes in temperature as area-wide and time averages per given hour or range of hours (averaged over the 3 intervals defined earlier) in the Sacramento – Roseville – Granite Bay areas. For canopy cover and electrification scenarios, a better indicator of the effects is to average both Tair and Tsfc (see text for explanation).

D08					
Sacramento – Roseville – Granite Bay			Albedo scenario (avg. change in °C)		Canopy scenario (avg. change in °C)
0600 PDT					
	Tair	roofs and pavements	-0.29		-0.34
		roadways	-0.36		
	Tsf	roofs and pavements	-0.49		-1.92
		roadways	-0.63		
1300 PDT					
	Tair	roofs and pavements	-3.02		-0.18
		roadways	-3.63		
	Tsf	roofs and pavements	-7.76		-1.57
		roadways	-10.04		
1500 PDT					
	Tair	roofs and pavements	-2.90		-0.22
		roadways	-3.61		
	Tsf	roofs and pavements	-7.35		-1.79
		roadways	-9.77		
all hours					
	Tair	roofs and pavements	-1.42		-0.34
		roadways	-1.72		
	Tsf	roofs and pavements	-3.43		-2.22
		roadways	-4.45		

D08		
Sacramento – Roseville – Granite Bay		Electrification scenario (avg. change in °C)
0700 PDT		
	Tair	-0.09
	Tsfc	-0.52
1700 PDT		
	Tair	-0.10
	Tsfc	-0.85
all hours		
	Tair	-0.08
	Tsfc	-0.55

5.22.5 DOMAIN D09 (Folsom – El Dorado Hills)

Figure 5-64 depicts the roadway projects and areas of interest in the Folsom – El Dorado Hills region that were modeled to evaluate the local-scale impacts of mitigation measure. As before, the red lines depict the MTP roadway projects including those identified by WSP and the approximate boundaries of the cities of Folsom and El Dorado Hills are highlighted with blue and yellow lines, respectively. The highways of interest to the electrification scenarios are also highlighted in white.

Figure 5-64: Locations of roadway projects and areas of interest in the Folsom – El Dorado Hills area.
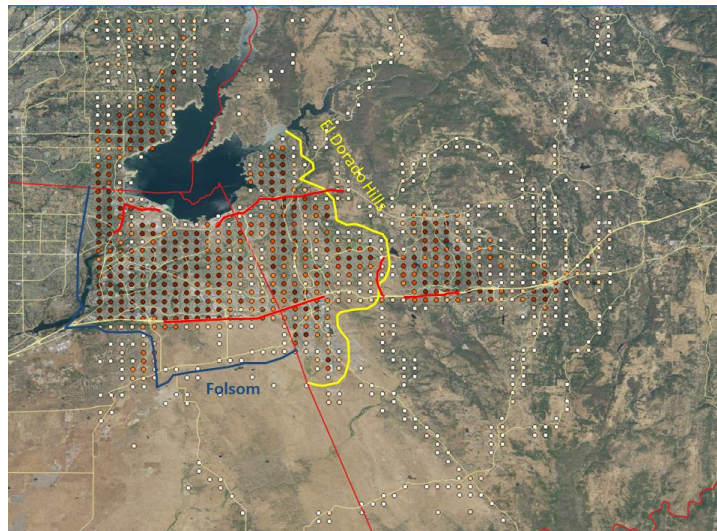
Scenario AA

In Figure 5-65 the urban-canopy air-temperature impacts of implementing caseAA (defined earlier) are shown for a sample interval. It is assumed in this scenario that both cool roofs and cool pavements are implemented throughout the urban areas whereas in the roadway project corridors (red lines), only cool pavement are applied. However, the roadway projects also occur within the urban areas that are modified and, as such, there is overlap in the reporting of effects. The urban canopy in these areas is cooled by up to a maximum of 4.9 °C as a result of implementing cool roofs and pavements, i.e., the largest average cooling over all 1500-PDT hours in the period August 1 – 15, 2016.

Figure 5-66 shows the roadway-temperature impacts of implementing cool pavements in the urban areas and at the locations of the MTP roadway projects. The average maximum cooling of the roadways over all 1500-PDT hours in the period August 1 – 15, 2016 is 12.6 °C. As expected, the largest cooling occurs in areas with higher densities of roadways (with larger modifications) as well as along major routes such as HWY 50.

Figure 5-65: Change in urban-canopy air temperature from cool roofs and pavements in the Folsom – El Dorado Hills area. Example: average changes at 1500 PDT, August 1 – 15, 2016. Maximum average cooling is 4.9 °C (darkest blue).
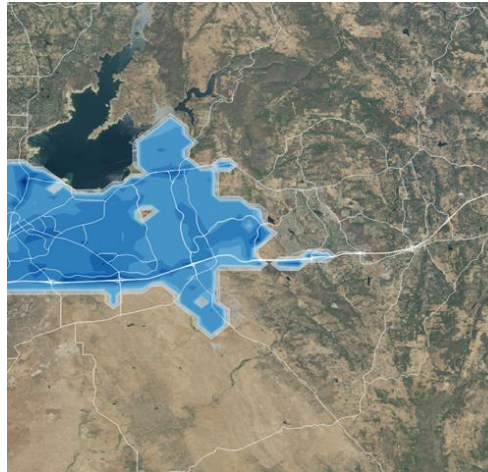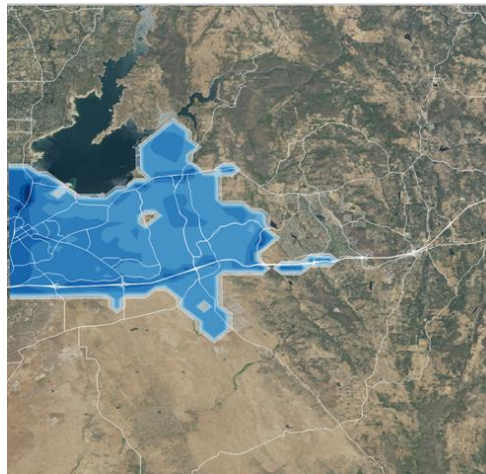

Figure 5-66: Change in roadway temperature from cool pavements in the Folsom – El Dorado Hills area. Example: average changes at 1500 PDT, August 1 – 15, 2016. Maximum average cooling is 12.6 °C (darkest blue).

Scenario BBevapo

The scenario of increased canopy cover was assumed to be implemented throughout the Folsom and El Dorado Hills urban areas, assuming an increase in cover that is proportional to the level of urbanization in each city. Figure 5-67 shows the air-temperature impacts of implementing vegetation canopy-cover during the sample interval June 1 – 15, 2015. The 24-hour average cooling (in this interval) reaches up to 1.5 °C mostly in the eastern parts of this urban area, and is relatively larger in the more urbanized parts in south Folsom and El Dorado Hills.

Figure 5-67: Change in air temperature from canopy in the Folsom – El Dorado Hills area: all-hour average change in the interval June 1 – 15, 2015. Maximum average cooling is 1.5 °C (darkest blue).
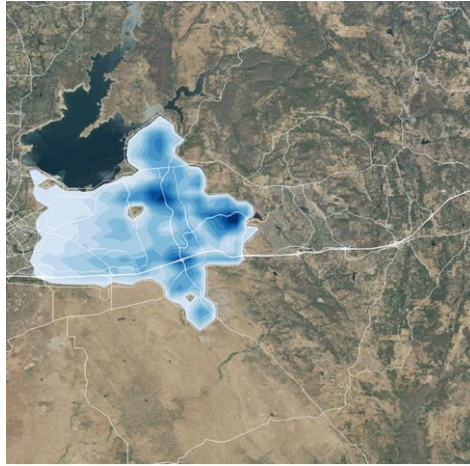
Scenario QF3

Figure 5-68 shows the near-surface temperature effects of automobile electrification (25% EV ownership) in the Folsom – El Dorado Hills area. The effects are quantified along the major highways – HWY 50 (running E-W in the figure), Folsom Blvd. (the left N-S route) and El Dorado Hills Blvd. (right N-S route in the figure). The 1700-PDT (rush-hour) average reduction in temperature reaches up to 1.8 °C, during the sample interval depicted in the figure (July 1 – 15, 2013). The largest cooling is seen along HWY 50.

Figure 5-68: Change in near-surface temperature from vehicle electrification in the Folsom – El Dorado Hills area. Example: 1700-PDT (rush-hour) average change in the interval July 1 – 15, 2013. Maximum average cooling is 1.8 °C (darkest blue).
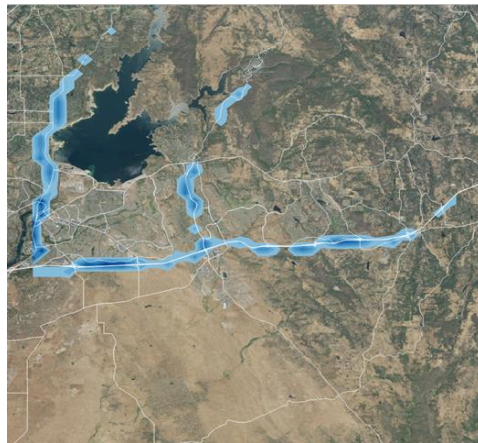
Table 5-21 provides a summary of temperature changes averaged (for various given hours or range of hours) over the three modeled periods identified in Section 5.20. While the summaries in this table are for localized effects only, the advective effects will be discussed later in this report. As explained above, for canopy-cover and electrification scenarios, both air and surface temperature should be accounted for, i.e., averaged, but are reported separately in Table 5-21.

Table 5-21: Changes in temperature as area-wide and time averages per given hour or range of hours (averaged over the 3 intervals defined earlier) in the Folsom – El Dorado Hills. For canopy cover and electrification scenarios, a better indicator of the effects is to average both Tair and Tsfc (see text for explanation).

D09			Albedo scenario (avg. change in °C)		Canopy scenario (avg. change in °C)
Folsom / El Dorado Hills					
0600 PDT					
	Tair	roofs and pavements	-0.27		-0.35
		roadways	-0.29		
	Tsf	roofs and pavements	-0.50		-1.71
		roadways	-0.54		
1300 PDT					
	Tair	roofs and pavements	-3.04		-0.21
		roadways	-3.46		
	Tsf	roofs and pavements	-8.10		-1.32
		roadways	-9.29		
1500 PDT					
	Tair	roofs and pavements	-3.15		-0.22
		roadways	-3.54		
	Tsf	roofs and pavements	-8.14		-1.52
		roadways	-9.18		
all hours					
	Tair	roofs and pavements	-1.49		-0.35
		roadways	-1.70		
	Tsf	roofs and pavements	-3.72		-1.86
		roadways	-4.30		

D09		Electrification scenario (avg. change in °C)
Folsom / El Dorado Hills		
0700 PDT		
	Tair	-0.06
	Tsfc	-0.32
1700 PDT		
	Tair	-0.08
	Tsfc	-0.53
all hours		
	Tair	-0.05
	Tsfc	-0.34

Altostratus Inc.

5.22.6 DOMAIN D10 (Placerville – Diamond Springs)

Finally, Figure 5-69 depicts the roadway project locations and areas of interest in the Placerville – Diamond Springs region that were modeled to evaluate the local-scale impacts of mitigation measures. As before, the red lines depict the MTP roadway projects including project point locations identified by WSP and the yellow lines delineate the urban areas of interest in (from north to south) Placerville, Diamond Springs, and El Dorado. The highways of interest to electrification scenarios are also identified.

Figure 5-69: Locations of roadway projects and areas of interest in Placerville – Diamond Springs area.
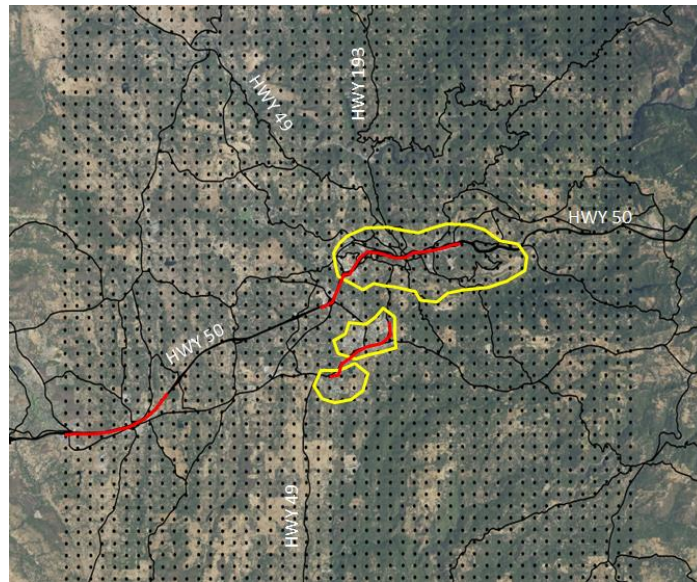
Scenario AA

In Figure 5-70 the urban-canopy air-temperature impacts of implementing caseAA (defined earlier) are shown for a sample interval. It is assumed in this scenario that both cool roofs and cool pavements are implemented throughout the above-defined urban areas whereas in the roadway project corridors (red lines), only cool pavement are applied. Since the roadway projects also occur in some of the urban areas that are modified, there is also an overlap in reporting the resulting effects. The urban canopy in these areas is cooled by up to a maximum of 4.4 °C as a result of implementing cool roofs and pavements, as an average over all 1500-PDT hours in the period August 1 – 15, 2016.

Figure 5-71 shows the roadway-temperature impacts of implementing cool pavements throughout the urban areas and at the locations of the MTP projects in the Placerville – Diamond Springs – El Dorado region. The average maximum cooling of the roadways over all 1500-PDT hours in the

period August 1 – 15, 2016 is 12.4 °C. The largest cooling occurs in areas with higher densities of roadways as well as along major routes such as HWY 50.

Figure 5-70: Change in urban-canopy air temperature from cool roofs and pavements in the Placerville – Diamond Springs area. Example: average changes at 1500 PDT, August 1 – 15, 2016. Maximum average cooling is 4.4 °C (darkest blue).

Figure 5-71: Change in roadway temperature from cool pavements in the Placerville – Diamond Springs area. Example: average changes at 1500 PDT, August 1 – 15, 2016. Maximum average cooling is 12.4 °C (darkest blue).
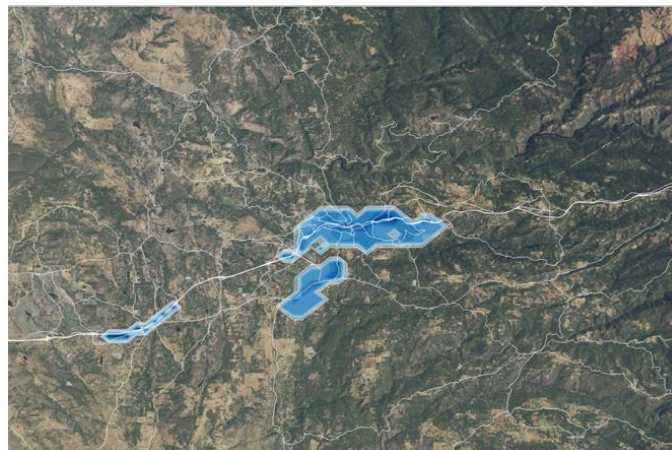

Scenario BBevapo

The scenario of increased canopy cover was assumed to be implemented throughout the Placerville, Diamond Springs, and El Dorado urban areas delineated in Figure 5-69, assuming that the increase in cover is proportional to the level of urbanization in each area. Figure 5-72 shows the air-temperature impacts of implementing vegetation canopy-cover during the sample interval

June 1 – 15, 2015. The 24-hour average cooling (in this interval) reaches up to 1.4 °C mostly in the central parts of Placerville.

Figure 5-72: Change in air temperature from canopy in Placerville – Diamond Springs – El Dorado area: all-hour average change in interval June 1 – 15, 2015. Maximum average cooling is 1.4 °C (darkest blue).
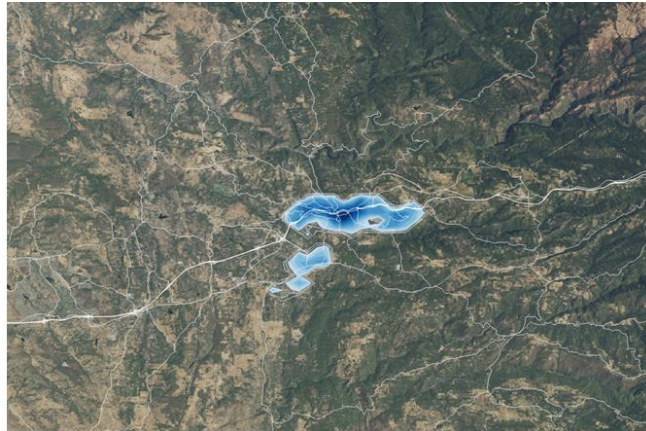
Scenario QF2

Figure 5-73 shows the near-surface temperature effects of automobile electrification (25% EV ownership) in the Placerville – Diamond Springs – El Dorado area. The effects are shown along the major highways – HWY 50, HWY 49, and HWY 193. The 1700-PDT (rush-hour) average reduction in near-surface temperature reaches up to 2.0 °C, during the sample interval depicted in the figure (July 1 – 15, 2013). The largest average cooling is seen along HWY 50 in the Placerville area (see Figure 5-69).

Figure 5-73: Change in near-surface temperature from vehicle electrification in the Placerville – Diamond Springs – El Dorado area. Example: 1700-PDT (rush-hour) average change in the interval July 1 – 15, 2013. Maximum average cooling is 2.0 °C (darkest blue).
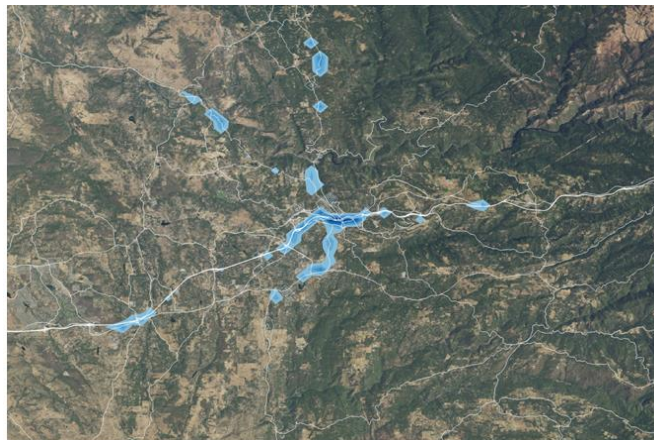
Finally, Table 5-22 provides a summary of temperature changes averaged (for various given hours or range of hours) over the three modeled periods identified in Section 5.20, above. The summaries in for localized effects only. Later in this report, the localized and advective (transported) effects will be discussed. As explained above, for canopy-cover and electrification scenarios, both air and surface temperature changes are accounted for. For the purpose of this table, the effects are reported separately.

Table 5-22: Changes in temperature as area-wide and time averages per given hour or range of hours (averaged over the 3 intervals defined earlier) in the Placerville – Diamond Springs – El Dorado area. For canopy cover and electrification scenarios, a better indicator of the effects is to average both Tair and Tsfc.

D10

Placerville			Albedo scenario (avg. change in °C)		Canopy scenario (avg. change in °C)
0600 PDT					
	Tair	roofs and pavements	-0.23		-0.44
		roadways	-0.33		
	Tsf	roofs and pavements	-0.47		-2.19
		roadways	-0.61		
1300 PDT					
	Tair	roofs and pavements	-2.51		-0.17
		roadways	-3.23		
	Tsf	roofs and pavements	-6.93		-1.36
		roadways	-8.93		
1500 PDT					
	Tair	roofs and pavements	-2.51		-0.29
		roadways	-3.21		
	Tsf	roofs and pavements	-6.77		-1.81
		roadways	-8.61		
all hours					
	Tair	roofs and pavements	-1.21		-0.39
		roadways	-1.57		
	Tsf	roofs and pavements	-3.12		-2.12
		roadways	-4.02		

D10

Placerville		Electrification scenario (avg. change in °C)
0700 PDT		
	Tair	-0.02
	Tsfc	-0.17
1700 PDT		
	Tair	-0.06
	Tsfc	-0.27
all hours		
	Tair	-0.02
	Tsfc	-0.15

5.23 TEMPERATURE SUMMARIES AND ATTAINMENT OF THE UHII

In this section, results from the modeling of localized cooling measures at community level (500-m scale) are summarized and compared to the local all-hours UHII computed for current climate conditions and urbanization levels. The goal here is to evaluate the effectiveness of local actions and the resulting microclimatic (e.g., temperature) changes at community scale in offsetting the area's UHII.

The local attainment of the UHII via each mitigation measures was evaluated for two situations, as shown in Table 5-23: (1) a scenario where only the community implements UHI-mitigation measures (which was presented in Section 5.22) and (2) a scenario where both the community and its neighbors implement the measures. In this second situation, the community also benefits from cooler air transported from upwind areas in addition to the local cooling resulting from the implementation of its own heat-mitigation measures. The length scale, or upwind distance of relevance to transport of cooler air, was defined as an average of 2 – 4 km per analysis in Section 5.8.

As discussed in previous sections, the attainment levels from implementing cool roofs and cool pavements were based on assessment of air temperature changes whereas attainment levels from vegetation-cover and vehicles-electrification measures were based on changes in both air and surface temperatures to more accurately capture their effects near the ground.

In Table 5-23, the all-hours UHII and the all-hours 500-m attainment of UHII were averaged over the same representative periods defined earlier in Section 5.20. The evaluations (in the table) are for each measure in standalone mode. The total effects of combinations of measures are non-linear (i.e., cannot be computed as simple sum of parts) and are typically smaller than the sum of the components (Taha 2015a,b). Still, the information in Table 5-23 can provide Caltrans and urban planners with rough information as to potential magnitudes of effects that can be anticipated if measures were combined.

From the summary table, it can readily be seen that (1) some measures, even in standalone fashion, can completely offset the UHII, with or without transport of cooler air from upwind urban areas and (2) when neighboring communities also implement UHI mitigation measures, the local benefits increase significantly (doubling, in general, but of course varying from one measure and location to another).

It is to be re-emphasized that these are localized effects, i.e., temperature changes at or near the surface of the modified roadways or he air temperature within the urban canyons of the selected communities. Hence, the cooling effects of pavements alone (in some locations) can be larger than the effects of pavements and roof albedo modifications because the levels of increase in pavement albedo for the main highways and freeways are larger than those for the local roadways in the selected communities (for the reasons stated in Section 5.6.4). In addition, there is a shading effect in the canyons that reduces the effectiveness of cool pavement measures there (Taha 2008a-c; Rosado et al. 2017). Refer, again, to the definitions of the scenarios in Section 5.19.

Table 5-23: Mitigation potential of local projects vs. regional all-hours UHII.

Project area	All-hours Tair UHII (°C)**		Localized/no advection UHII attainment local mitigation only	Localized+advection UHII attainment local mitigation+advection
D05 Yuba City / Marysville Downtown YC and M	2.41			
		Cool roofs / pavements	-58%	-82%
		Cool pavements	-46%	-70%
		Electric vehicles	-7%	-31%
		Vegetation cover	-71%	-95%
D06 Woodland DAC census tracts	2.14			
		Cool roofs / pavements	-60%	-93%
		Cool pavements	-69%	-101%
		Electric vehicles	-7%	-39%
		Vegetation cover	-51%	-84%
D07 Sac / SE Sac AB617 A, B, D	4.48			
		Cool roofs / pavements	-29%	-63%
		Cool pavements	-31%	-65%
		Electric vehicles	-6%	-39%
		Vegetation cover	-33%	-67%
D07 Sac / SE Sac AB617 C, E, G	2.33			
		Cool roofs / pavements	-56%	-93%
		Cool pavements	-60%	-97%
		Electric vehicles	-11%	-48%
		Vegetation cover	-63%	-101%

Project area	All-hours Tair UHII (°C)**		Localized/no advection UHII attainment local mitigation only	Localized+advection UHII attainment local mitigation+advection
D08 Granite Bay	5.07			
		Cool roofs / pavements	-28%	-48%
		Cool pavements	-34%	-54%
		Electric vehicles	-6%	-27%
		Vegetation cover	-21%	-41%
D08 Roseville	5.83			
		Cool roofs / pavements	-24%	-52%
		Cool pavements	-30%	-57%
		Electric vehicles	-5%	-33%
		Vegetation cover	-18%	-46%
D09 El Dorado Hills	4.91			
		Cool roofs / pavements	-30%	-47%
		Cool pavements	-34%	-51%
		Electric vehicles	-4%	-20%
		Vegetation cover	-23%	-39%
D09 Folsom	4.86			
		Cool roofs / pavements	-31%	-52%
		Cool pavements	-35%	-56%
		Electric vehicles	-4%	-25%
		Vegetation cover	-23%	-44%
		Doubled cover increase	-40%	-61%
D10 Placerville / Diamond Springs / El Dorado City	1.36			
		Cool roofs / pavements	-88%	-113%
		Cool pavements	-118%	-143%
		Electric vehicles	-6%	-31%
		Vegetation cover	-96%	-121%

## 5.24 ADDITIONAL COMMUNITY-LEVEL SIMULATIONS

The following additional modeling at 500-m resolution was carried out per requests from the project TAC, SMAQMD, LGC, and participating cities and communities, in no particular order:

- Solar PV deployment and interactions with effects of cool surfaces;

- Cool walls and their incremental impacts on combined mitigation measures;

- Combinations of measures (cool roofs, cool pavements, increased canopy cover, and fleet electrification); and

- Electrification of motor vehicles per SMAQMD's ZEV Readiness Plan.

5.24.1 Impacts of vehicles electrification

This set of simulations was undertaken to evaluate the potential temperature impacts from heat-emission reductions following the SMAQMD's ZEV Readiness Plan. The locations of charging facilities (per SMAQMD) are shown as black points in Figure 5-74 superimposed over the UHII tiles in the Capital region for a random time period (in this example for July 16 – 31, 2015).

Figure 5-74: Charging/H2 stations vs. UHII composite tiles for July 16-31, 2015.
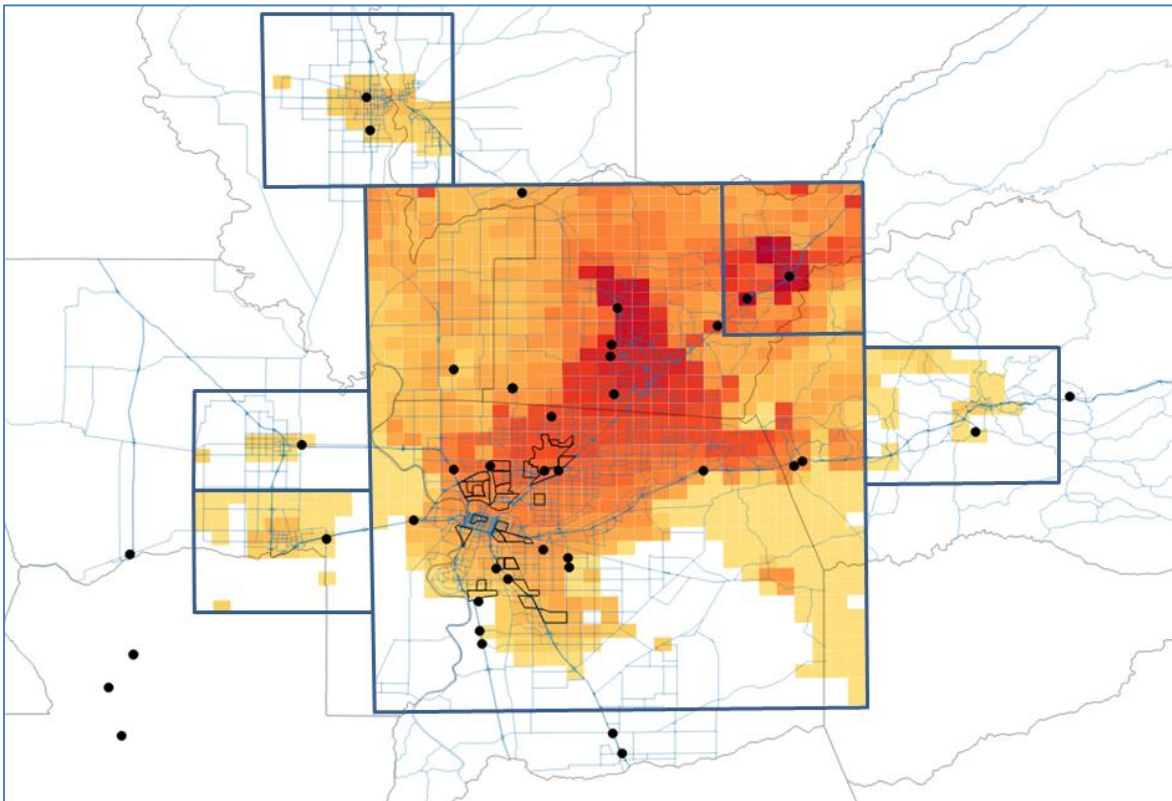
To calculate the reductions in heat emissions from this scenario, it was assumed in this study that maximum electrification would occur at and near the locations of the charging stations and decrease radially outwards following a Cressman weighting scheme:

$$W_{p,i} = \frac{R^2 - d_{p,i}^2}{R^2 + d_{p,i}^2} \qquad (5-11)$$

for $d_{p,i} \leq R$, and $W_{p,i} = 0$ for $d_{p,i} > R$.

In Eq. (5-11), $W_{p,i}$ is the weighting factor applied to heat emission rates (from mobile sources, in this case) at a model grid point, i, relative to a charging station point, p; R is a pre-determined radius of influence (e.g., 10 km); and $d_{p,i}$ is the distance from the grid point, i, to the charging station (point p). Note that heat emissions are not only weighted by this scheme, but also by land-use type, urban fraction, and the time of day relative to peak times, e.g., at 1700 PDT. The hourly profile for heat emissions was discussed in Section 5-19.

Thus, at the charging-station locations, electrification was assumed to be 25% and decreasing outwards until reaching zero at the 10 km radii of influence, as seen in Figure 5-75.

Figure 5-75: Charging/H2 stations vs. UHII composite tiles for July 16-31, 2015, and 10-km radii of influence. Source of station locations: SMAQMD / Frontier Energy ZEV Readiness Plan (2019).
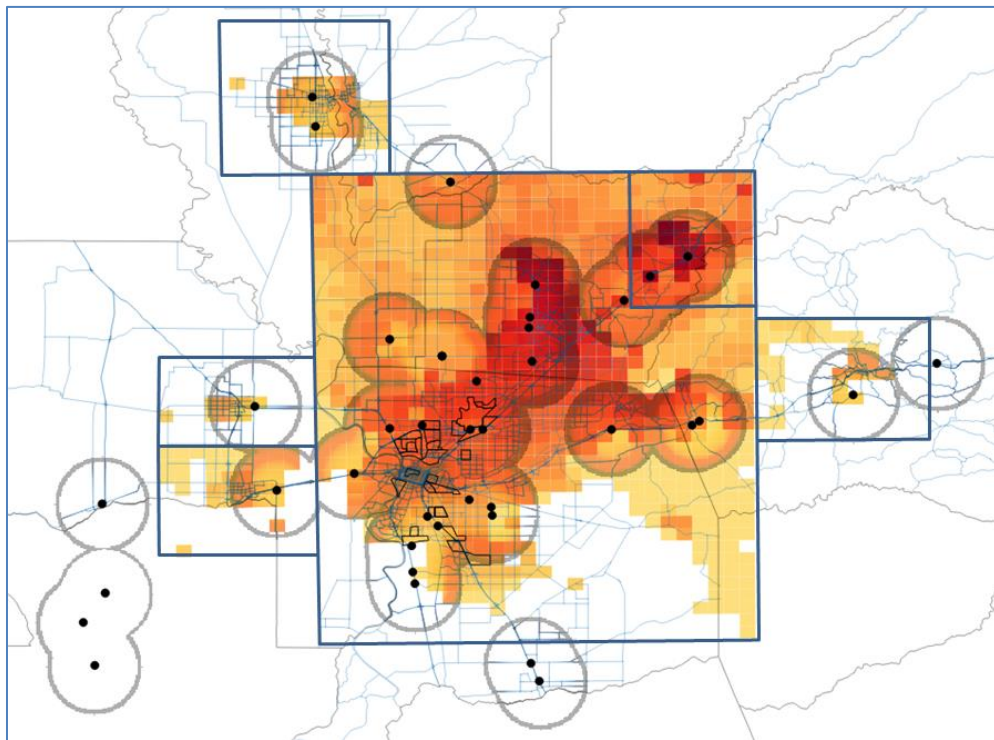
Figure 5-76: Charging stations and their locations relative to domains D07 and D08.
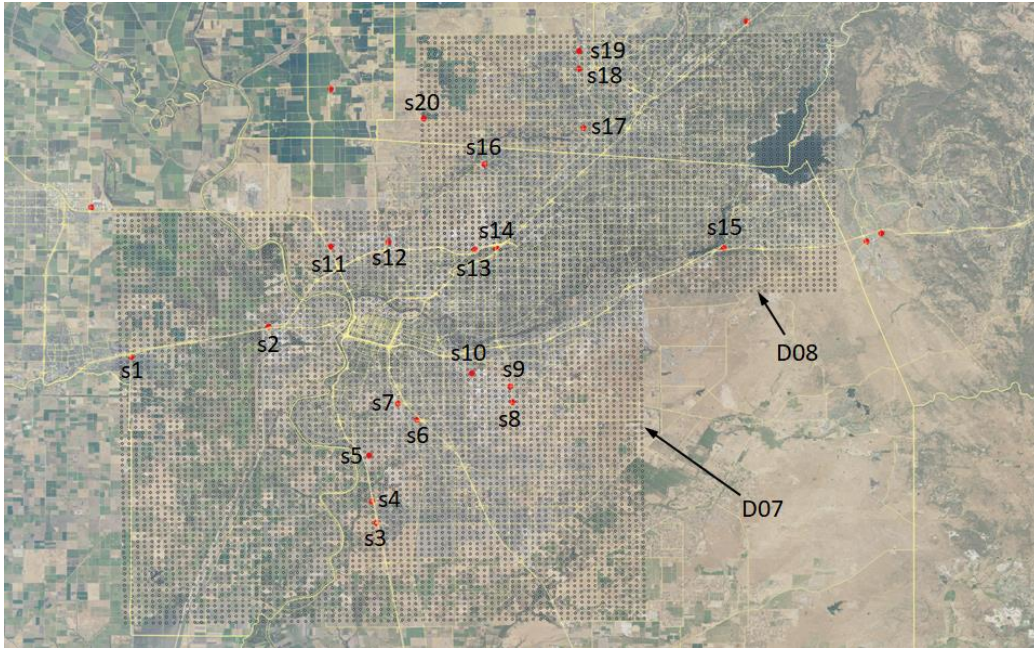
The simulations of this measure were carried out for domains D07 and D08, shown in Figure 5-76. Figure 5-77 depicts the resulting weighting ($W_{p,i}$, from Equation 5-11) for each grid cell as a function of distance from the charging stations. Thus, maximum electrification (25% EV ownership), i.e., $W_{p,i}=1$, is found at stations locations (black triangles) and zero electrification, i.e., $W_{p,i}=0$, at the perimeters of influence circles (no color).

Table 5-24 summarizes the results from this scenario (SMAQMD ZEV plan) as average reductions in 1700-PDT and all-hour temperature averages, that is, averaged over the time periods identified earlier and also averaged over all grid cells that were perturbed per given scenario. The results are presented for domains D07 and D08.

As previously discussed, surface temperature (Tsfc) may be a better indicator than Tair for the effects of tailpipe heat-emission reductions. Or, at the least, averaging both Tair and Tsfc should be done to more accurately capture those effects. However, in Table 5-24, these effects are still reported separately for Tair and Tsfc. The "average max cooling" column in the table is the average of the largest daily cooling over all days in the given period. The 1700 PDT averages columns are the averages of all 1700 PDT hours in the given period and the "all-hours" averages are averaged over every hour in the given period.

Figure 5-77: Charging stations and their locations relative to domains D07 (bottom-left) and D08 (top-right). The Cressman weight ranges from W=1 (maximum electrification) at the black triangles to W=0 (no electrification) at the yellow-white grid points.
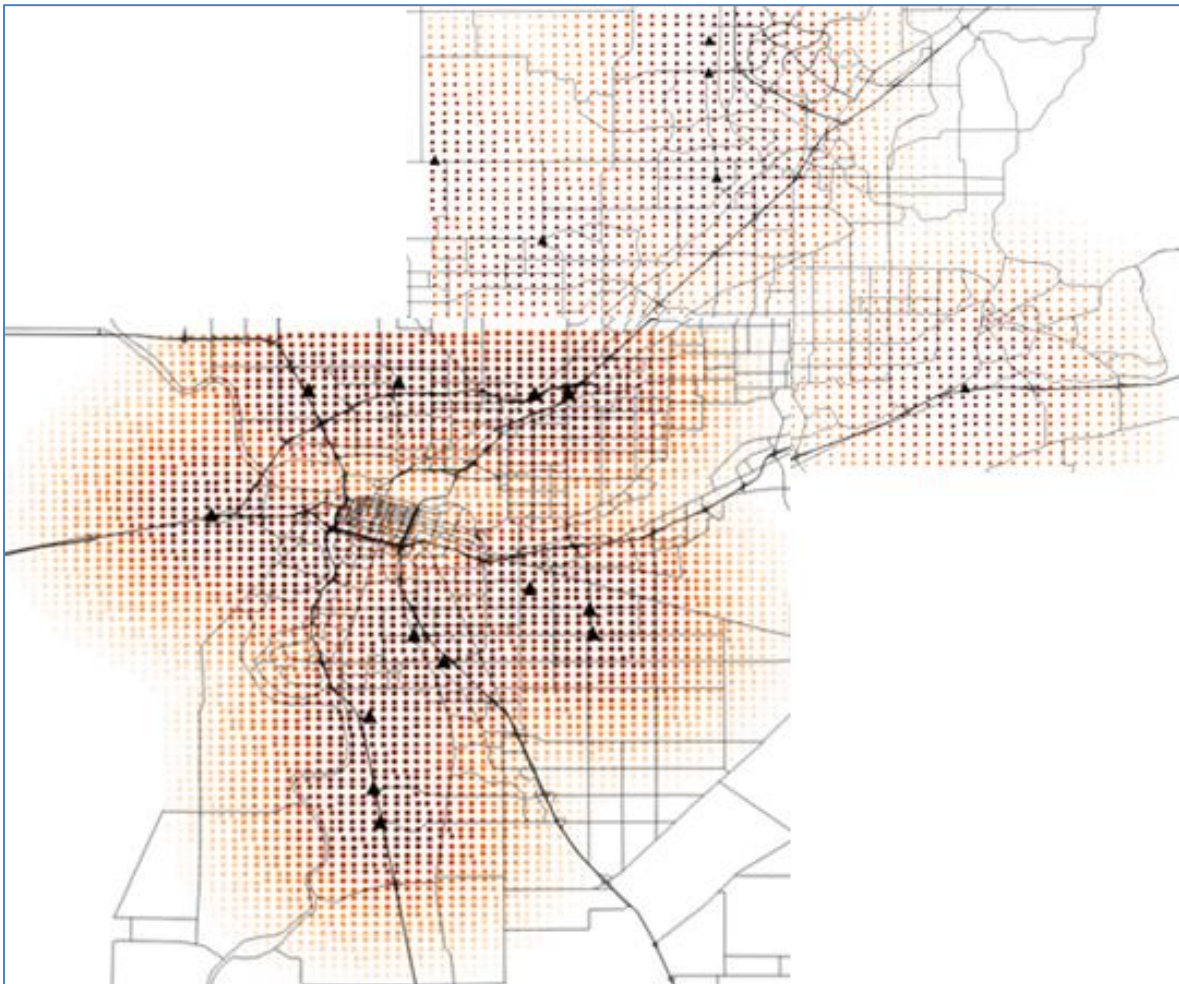

Table 5-24: SMAQMD ZEV measures impacts on temperature (changes in °C)

Domain and interval	1700 PDT			all hours		
	averages		average max. cooling (Tsfc)	averages		average max. cooling (Tsfc)
	Tair	Tsfc		Tair	Tsfc	
D07						
2013_int3	-0.32	-0.55	-2.97	-0.17	-0.28	-0.87
2015_int1	-0.20	-0.37	-2.81	-0.16	-0.27	-0.84
2016_int5	-0.24	-0.41	-3.34	-0.16	-0.27	-0.86
D08						
2013_int3	-0.27	-0.44	-1.58	-0.18	-0.29	-0.73
2015_int1	-0.25	-0.42	-2.17	-0.17	-0.27	-0.74
2016_int5	-0.26	-0.45	-1.79	-0.18	-0.30	-0.74

Figure 5-78 is a random sample showing the temperature effects from potential heat-emission reductions as a result of implementing the SMAQMD ZEV Readiness Plan in domains D07 and D08. For each domain, two examples are provided: (1) average change in Tsfc at 1700 PDT for sample periods and (2) all-hours average change in Tsfc (other intervals and averages are provided in Appendixes C-1 and C-2).

Surface temperature (Tsfc) in these examples can be reduced by up to a maximum of 2.81 °C as a 1700-PDT average and up to 0.84 °C as a 24-hour average in D07. In D08, the 1700-PDT average cooling reaches up to 1.58 °C and the 24-hour average cooling up to 0.73 °C. As stated above, the spatial temperature-reduction pattern is not only a result of the Cressman weighting scheme, but also affected by the LULC properties, urbanization density, locations of the major transportation routes, and other factors.

Note that the following figures are not to the same scale.

Figure 5-78: Samples from analysis of temperature impacts from the SMAQMD ZEV Readiness Plan. All other figures are included in Appendix C-1 and Appendix C-2. Caption below each figure provides additional information on content.
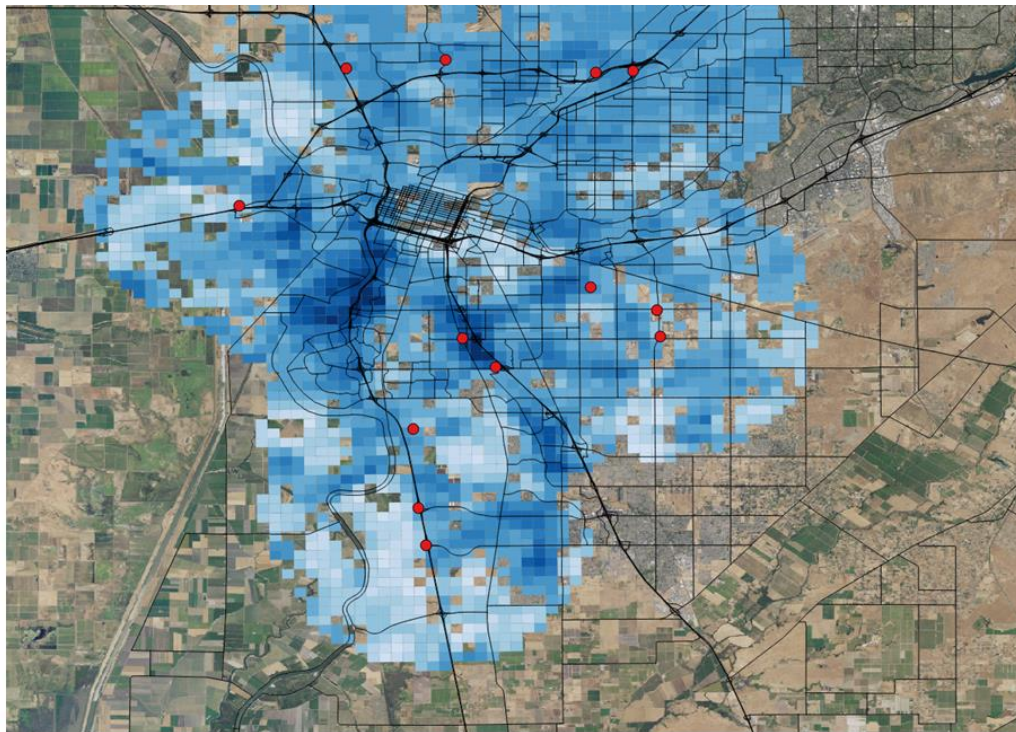
D07, average change in Tsfc at 1700 PDT, 2015_int1. Average maximum cooling: 2.81 °C (darkest blue), color step is 0.25 °C.

Figure 5-78, continued.
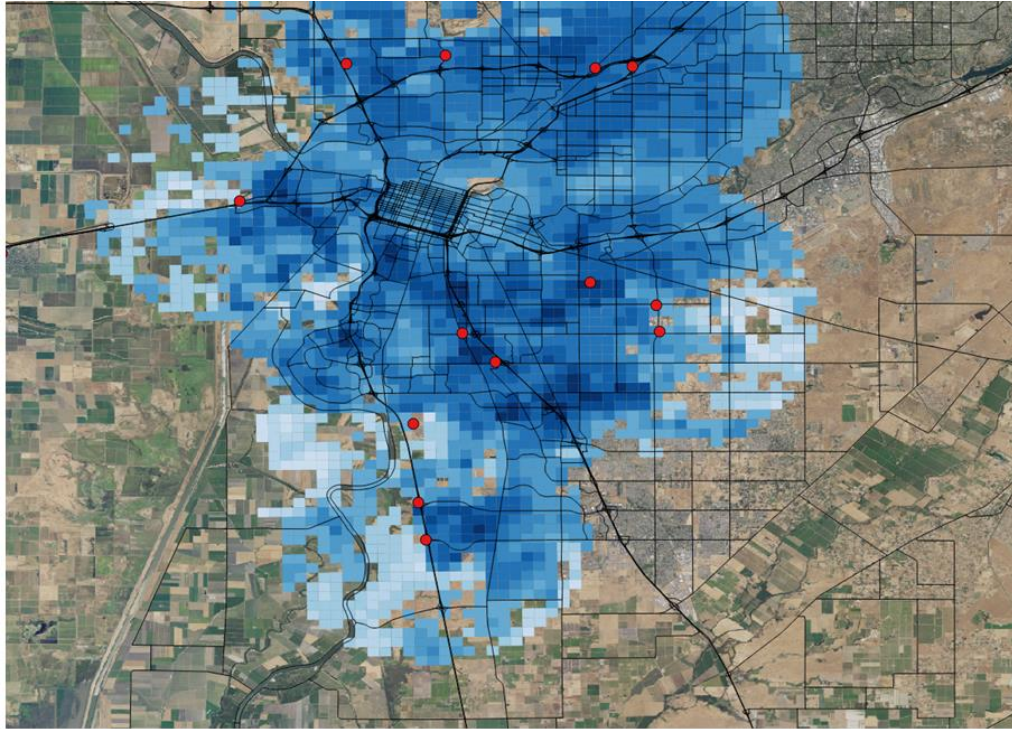
D07, all-hours average change in Tsfc, 2015_int1. Average maximum cooling: 0.84 °C (darkest blue), color step is 0.10 °C.
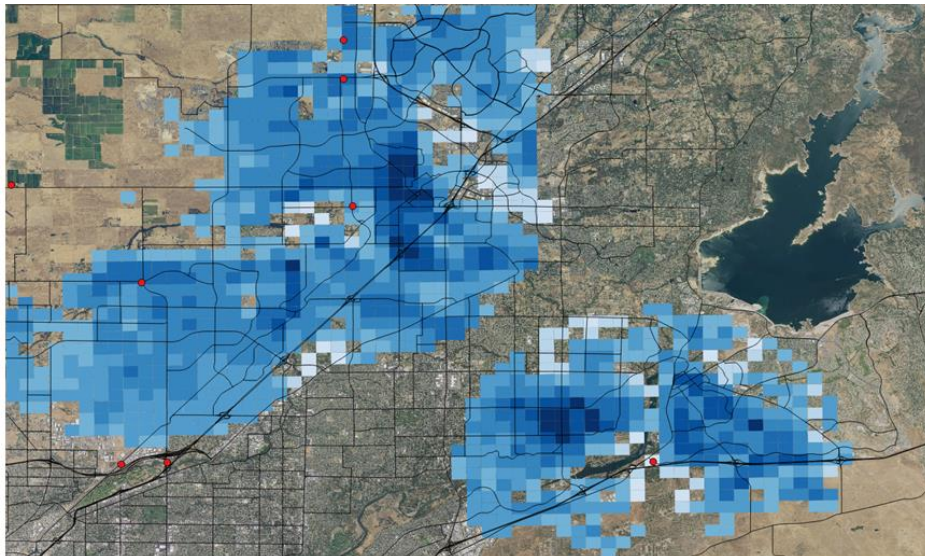
D08, average change in Tsfc at 1700 PDT, 2013_int3. Average maximum cooling: 1.58 °C (darkest blue), color step is 0.25 °C.

Figure 5-78, continued.
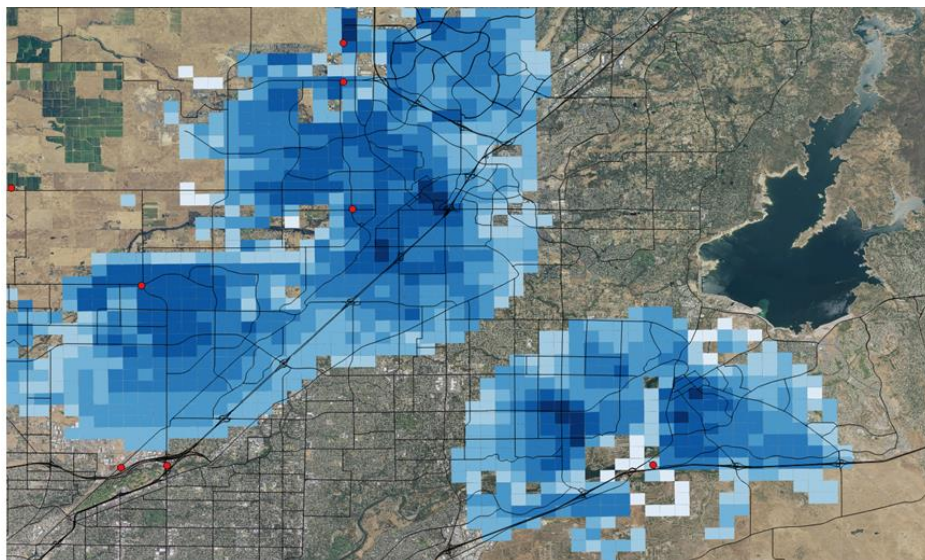
D08, all-hours average change in Tsfc, 2013_int3. Average maximum cooling: 0.73 °C (darkest blue), color step is 0.10 °C.

5.24.2 Solar photovoltaics

The City of Folsom and the SMAQMD expressed interest in evaluating the potential impacts of solar PV measures on air temperature near the ground and comparing their effects with those from tree cover on parking lots and from reflective materials. For this purpose, PV scenarios were modeled for domain D09, focusing on the City of Folsom.

Various parameters were considered in evaluating the standalone effects of ground-based (e.g., parking lots) and roof-based solar PV. While there are various approaches and levels of details involved in evaluating the effects of various solar PV configurations (e.g., Salamanca et al. 2016; Masson et al. 2014), Taha (2012) shows that, in general, the overall change in albedo after installation of a solar PV array can be estimated by:

$$\alpha'_s \;=\; \alpha_s\,(1-c) \;+\; (\rho + \varepsilon)\,c \qquad\qquad (5-12)$$

where α'_s is the new albedo of the surface s, e.g., roof, parking lot, wall, etc., α_s is the original albedo of the surface, in other words, the albedo of the surface upon which the solar PV is installed, c is the fraction of the surface s that is covered with the solar PV panels, ρ is the reflectivity of the solar panel, and ε is its conversion efficiency. As discussed in Taha (2012), ε typically ranges from an average of 0.15 currently to 0.30 in the near future. Thus, these two values were used as examples in the parameterizations examined here. For ρ, an average value is 0.08 and, from an evaluation of aerial imagery, c was found to range from 20% to 80% on residential and commercial roofs and from 50% to 100% on parking lots.

In the simulations discussed here, the current albedo (α_s) of various surfaces, e.g., roofs and pavements, were established based on the grid-cell-specific values obtained from the LULC and remote-sensed data analysis of albedo for each of the study domains (Section 2). Future values of albedo (α_s), to reflect scenarios of widespread implementation of cool roofs and cool pavements were assumed to be capped at 0.50 and 0.3, respectively. These realistic and feasible values are similar to those used in caseAA for the simulations discussed above (and defined in Section 5.19).

As there can be a large number of possible combinations of these parameters as well as their evolution over time, Table 5-25 identifies the scenarios that are discussed in this section. Table 5-26 presents a brief summary of the results followed by sample maps depicting the spatial characteristics of the temperature changes from widespread solar-PV deployment in the Folsom area.

Table 5-25: Scenarios of PV implementation.

Scenario	Surface = roof (#0)			Surface = paved / parking lot (0#)		
	roof albedo	ε	c	paved albedo	ε	c
casePV10	f(LULC) ~ 0.17 – 0.20	0.15	40%	-	-	-
casePV20	f(LULC) ~ 0.17 – 0.20	0.30	40%	-	-	-
casePV30	0.50	0.30	60%	-	-	-
casePV01	-	-	-	f(LULC) ~ 0.10 – 0.12	0.15	60%
casePV02	-	-	-	f(LULC) ~ 0.10 – 0.12	0.30	60%
casePV03	-	-	-	0.30	0.30	80%
casePV22	f(LULC) ~0.17 – 0.20	0.30	40%	f(LULC) ~ 0.10 – 0.12	0.30	60%

Table 5-26: Changes in near-surface temperatures (°C) resulting from various solar PV scenarios in the Folsom area. Note that scenarios PV03 and PV30 also include significant increases in background albedo, not just installation of solar PV.

	PV scenario							
	PV01	PV02	PV03	PV10	PV20	PV30	PV22	PV30vsAA
1500 PDT average								
Near-surface temperature	-1.17	-2.44	-4.04	-0.03	-0.08	-0.20	-2.49	+0.18
All hours average								
Near-surface temperature	-0.52	-1.18	-1.89	-0.01	-0.03	-0.09	-1.19	+0.08

As expected, the effects of solar PV on near-ground temperature are larger when the panels are implemented at ground level (ground-based) – e.g., over parking lots – than at roof level. This is because (1) rooftop modifications from solar PV occur at generally higher elevations above ground (or urban canyon) and as such, have smaller impacts on temperature in the lower parts of the urban canopy layer, (2) the albedo of roofs and effective albedo of solar panels are relatively similar and both larger than the albedo of pavements (e.g., parking lots), and (3) the effects of shading over parking lots (on near-surface temperature) are larger than the effects of shading at roof level (which is non-existent in some cases). Near the top of the canopy layer, on the other hand, both roof-based and ground-based solar PV have large effects on temperature.

With respect to current urban conditions, i.e., current typical albedo of roofs and pavements, the solar PV scenarios PV01 and PV02 (ground-based) produce average all-hours near-ground reduction (localized cooling) of 0.52 and 1.18 °C, respectively. This can reach a maximum of 1.17 and 2.44 °C, respectively, during peak hours. The larger cooling in case PV02 relative to that in case PV01 is entirely due to increased conversion efficiency (ε) and represents the range of possible cooling using today's technology in today's typical albedo ranges in urban areas.

The reductions in near-ground temperature as a result of roof-based solar PV installation (cases PV10 and PV20) are smaller, roughly up to 0.1 °C, for the reasons listed above. Nevertheless, these numbers show that the benefits from solar PV installations (electricity) at roof level can be attained without incurring negative atmospheric effects, i.e., increasing air temperature at street level. The averaged effects of scenarios PV01 and PV10 (i.e., cooling of 0.6 °C at 1500 PDT and 0.26 °C as all-hours average) are generally comparable to those from other studies, e.g., Salamanca et al. (2016) and Masson (et al. (2013) for rooftop PV effects, but the ground-based PV scenarios evaluated in this study produce larger cooling (which was not evaluated in those other studies).

The study by Salamanca et al. (2016), via detailed panel-level energy-balance calculations, estimated that the cooling effects of rooftop PV can be as large as 0.2 – 0.4 °C during the daytime. Using a relatively similar approach, Masson et al. (2014) estimated that the daytime cooling from solar PV reaches up to 0.2 °C. However, it is reiterated here that the cooling effects discussed in this section are for ground-based PV (not rooftop) and were quantified to evaluate the impacts on near-ground temperatures so as to compare with the effects of tree canopies on parking lots.

In a scenario where both roof and ground-based solar PV are implemented, e.g., case PV22, the cooling is slightly larger than in case PV02, but by a small amount. In this scenario, reductions in 1500-PDT and all-hours near-surface temperatures of 2.49 and 1.19 °C, respectively, are predicted. In cases PV03 and PV30, the background albedo (of roofs and pavements) was also increased significantly in addition to installing solar PV – hence the resulting larger cooling effects are attributable mostly to the increase in background albedo. These scenarios represent future conditions where roof albedo, pavement albedo, and solar PV cover (ground-based and roof-based) are all increased.

Finally, case PV30vsAA demonstrates the potential negative effects of solar PV if implemented widely in the future when cool roofs and cool pavements also would have been implemented at a large scale (a hypothetical scenario, at this time). In this case, the installation of solar PV can have the potential to increase air temperature by an average of 0.08 °C (all-hours) and 0.18 °C at the time of the peak (1500 PDT) relative to if only cool roofs and pavements were installed -- although still much cooler than the base scenario.

Another aspect of interest to the City of Folsom is evaluating the relative potential cooling benefits from ground-based solar PV versus increasing tree canopy cover on parking lots. As discussed elsewhere in this report (Section 5-23), the local cooling effects (not taking advection into consideration) of canopy cover in the Folsom area are an average of 1.11 °C (23% attainment of the all-hours averaged UHII). As seen in Table 5-26, the cooling potential from ground-based solar PV (local non-advective effects) is an all-hours average of 0.52 °C at $\varepsilon = 0.15$, under current conditions. Thus, ground-based solar PV at 60% cover are one half as effective as an increase of 8 – 12% in vegetation cover over parking lots (see definitions of case01 in Section 5.5 and case_BBevapo in Section 5.18). It is to be emphasized that these results and equivalences vary significantly from one area to another.

Figure 5-79 shows sample results for a random interval (July 1 – 15, 2013) for scenarios PV01, PV02, PV03, and PV22 in terms of changes in the all-hours near-surface temperature averages in the Folsom – El Dorado Hills area (domain D09).

Figure 5-79: All-hour average near-surface temperature change from implementation of solar PV measures in the Folsom – El Dorado Hills area. Maximum cooling is in dark blue areas.
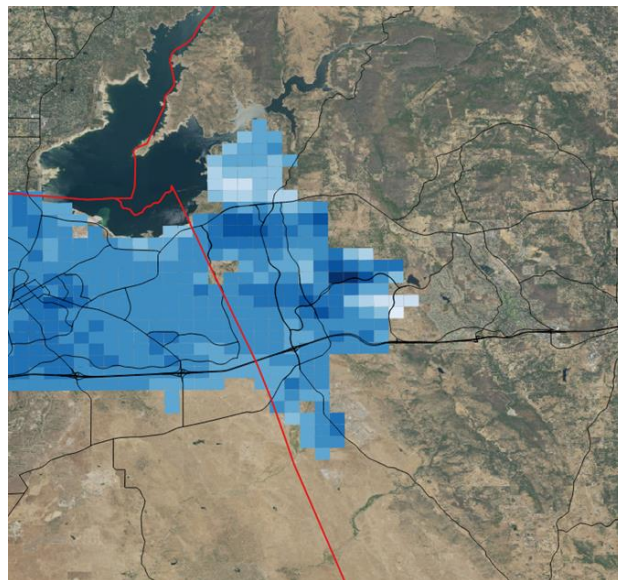
PV01: All-hours average impacts on near-surface temperature, 2013_int3. Range from white to dark blue: 0.0 to -0.90 ℃.

Figure 5-79, continued.
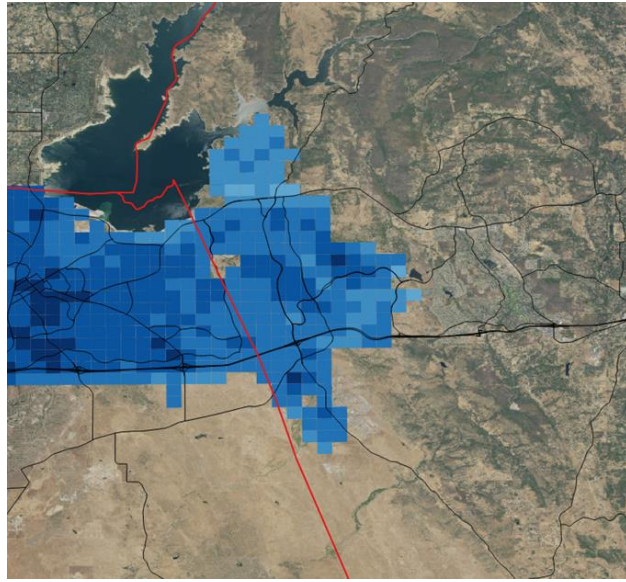
PV02: All-hours average impacts on near-surface temperature, 2013_int3. Range from white to dark blue: 0.0 to -1.6 ℃.
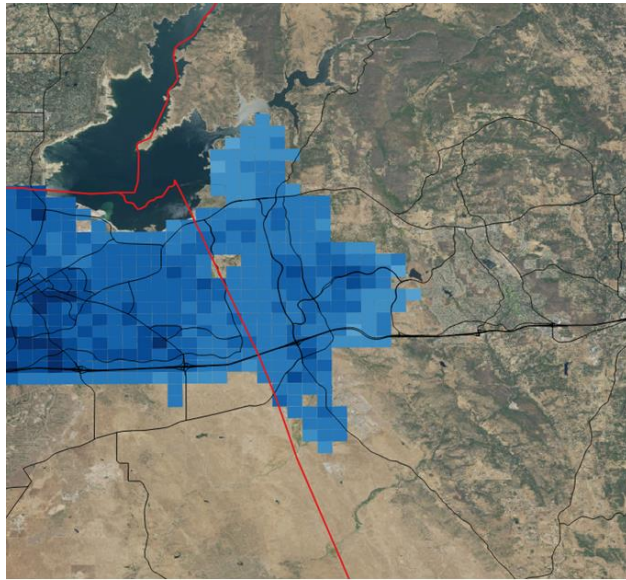
PV03: All-hours average impacts on near-surface temperature, 2013_int3. Range from white to dark blue: 0.0 to -2.6 ℃. This scenario also includes changes in background albedo.

Figure 5-79, continued.
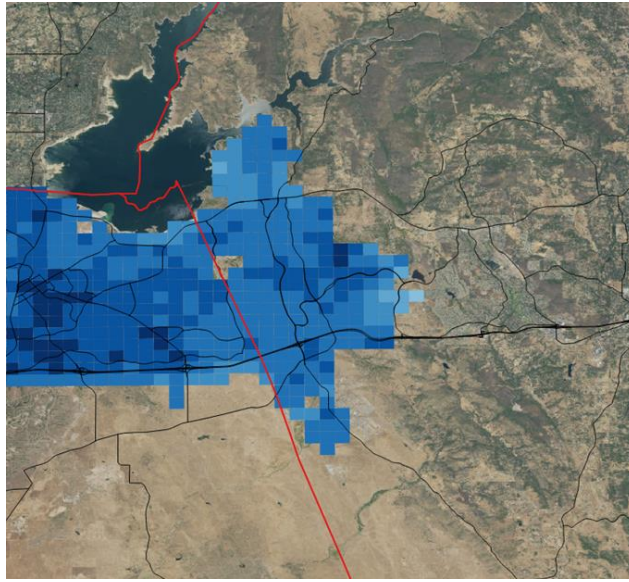
PV22: All-hours average impacts on near-surface temperature, 2013_int3. Range from white to dark blue: 0.0 to -1.64 ℃.

5.24.3 Combinations of measures

As discussed above, several mitigation measures were evaluated at the community scale (500-m resolution) in standalone mode. Combinations of measures were not presented as they would be arbitrary. However, per interest from the City of Elk Grove, an example of a combination scenario is provided (Figure 5-80).

This scenario was evaluated based on fine-scale modeling of the combined measures in domain D07, containing the City of Elk Grove. The results indicate that the combination measures provide significantly larger cooling benefits than each measure alone but, with two small exceptions, the total cooling (from combined measures) is smaller than the simple sum of the individual components (cooling from each standalone measure). In this domain, and for the modeled periods, the total cooling effects in the combination scenario are 5 – 15% smaller than the simple sum of the individual cooling effects.

Figure 5-80 summarizes some example findings and also shows the significant cooling benefits for the roadway surfaces ("Roadway temperature" column) during daytime hours, as well as for the 24 hours average. The other columns in this figure: "UCL temperature" is the air temperature within the urban canopy layer (canyon) and "surface temperature" is the average temperature of various surfaces making up the ground cover.

Figure 5-80: Temperature effects of combination of measures in D07. Vertical axis is change in temperature in degrees C.
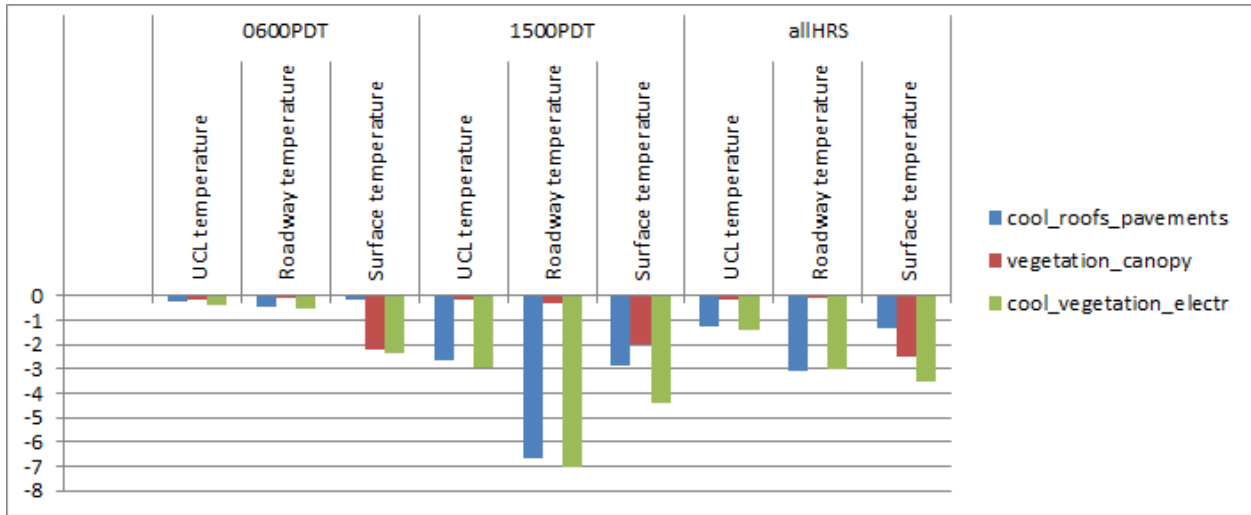
5.24.4 Cool walls

The potential impacts of cool walls were quantified for a scenario where wall albedo was increased from a current average of 0.15 to a maximum value of (capped at) 0.40. Figure 5-81 shows the cooling effects as averaged over time intervals (periods) of interest, representing various summer conditions in the City of Elk Grove. As expected, the albedo effects are largest during the daytime reaching up to a maximum average cooling of 1.4 ºC. The smaller effects in June 1 – 15, 2015, averaged 1500 PDT are caused by relatively larger cloud cover during this interval (first two weeks of June) relative to the other two intervals (which is also the reason behind the relatively lower air temperatures during that interval).

Figure 5-81: Averaged temperature effects of cool walls.
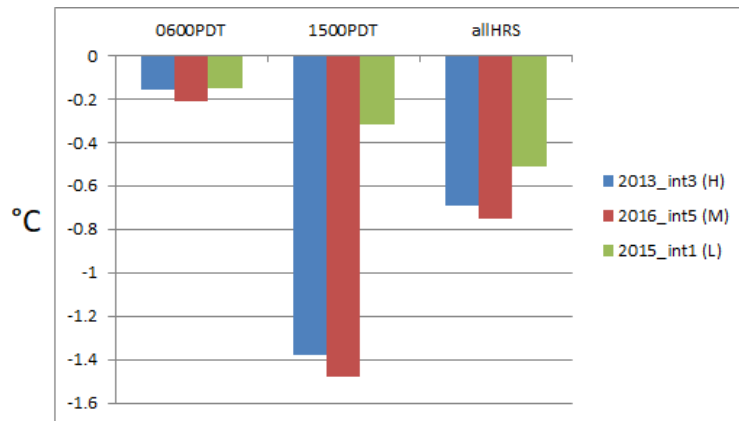
6. EFFECTS OF MITIGATION MEASURES IN FUTURE CLIMATE AND LAND USE

6.1 OBJECTIVES OF MODELING MITIGATION MEASURES IN FUTURE CLIMATE AND LAND USE

The goal of this task was to evaluate how urban heat and its indicators (e.g., UHI, UHII, and various metrics) are altered by changes in (1) climate and (2) urbanization levels. This is then followed by an evaluation of whether the proposed heat-mitigation measures would still be effective under those future conditions. For this purpose, the year 2050 was selected per input from SMAQMD, LGC, and the project TAC.

The objectives were to:

- Develop future climate scenarios via dynamical downscaling of CMIP5 / CCSM4 climate model with the Altostratus Inc.-customized urbanized WRF model and parameterizations;
- Develop future-year hourly meteorological initial and boundary conditions;
- Develop future physical urban surface properties characterizations based on LULC and urban morphology projections, future changes in the transportation system, roadways, and infrastructure (as available);
- Carry out future urban-climate simulations for year 2050 and two representative concentration pathways (RCP 4.5 and RCP 8.5);
- Characterize future climates in the 6-counties Capital region.;
- Evaluate changes in intra-urban climate variability, metrics, and thresholds under future conditions (of climate and land use) relative to present conditions; and
- Compute derivatives and metrics for heat health and the transportation system under future conditions.

6.2 EMISSIONS SCENARIOS

The representative concentration pathways (RCP, units of W m^{-2}) are indicators to the magnitudes of changes in radiative forcing. Four of the pathways, or scenarios, are defined as follows:

RCP 2.6:

This is the best scenario for limiting anthropogenic climate change, but likely unrealistic as it requires action very soon. CO_2 emissions peak by 2020 and decline to around zero by 2080. Atmospheric CO_2 peaks at 440 ppm in midcentury and then starts declining (Van Vuuren et al. 2011).

RCP 4.5:

In this scenario, emissions peak around mid-century at 50% higher than 2000 levels and then decline over 30 years to stabilize at half of 2000 levels. CO_2 concentrations rise to 520 ppm by 2070 beyond which the increase is much slower (Clarke et al. 2007).

RCP 6.0:

In this scenario, emissions double by 2060 and then decrease but stay above current levels. CO_2 concentrations increase to 620 ppm by 2100 but at a relatively slow rate (Hijioka et al. 2008).

RCP 8.5:

This is a scenario whereby emissions continue to increase. Atmospheric CO_2 concentrations reach 950 ppm by 2100 and continue increasing beyond that (Riahi et al. 2011).

In this modeling study, RCP 4.5 and RCP 8.5 were used. Output from the CCSM4 climate model (Bruyere et al. 2014) for these two scenarios was dynamically downscaled for the year 2050 using Altostratus Inc.'s modified urban models (AREAMOD and modUCM) discussed earlier in this report.

6.3 PROJECTIONS OF FUTURE URBANIZATION

In this study, the USGS LUCAS land-use projections of Sleeter et al. (2017a,b) were used to develop surface characterization input to the atmospheric model, including the development of surface physical properties in the new urban areas by 2050. The LUCAS dataset defines one business-as-usual (BAU) scenario and three other scenarios with population decrease, i.e., migration out of California. In this study, the BAU scenario was used in developing the model input for year 2050.

Figure 6-1 shows the expected urbanization levels in the Capital region by the 2050 under the BAU scenario per LUCAS. The green color-coded grid cells are current urban land use and the pink color-coded cells are new urban areas by 2050. These areas were developed in this study by vectorizing and remapping the LUCAS land-use datasets onto the model's 2-km domain. In this domain (D04), the urbanized area in 2050 is 1.68 times the urbanized area in 2015 (a 68% growth). In other words, the urban area in 2015 is 9.5% of the domain area whereas in 2050, the total urban area is 16% of the 2-km domain (dotted area in Figure 6-1).

In this project, the current land-use and land-cover distributions, including current urban cover (green areas), were derived from NLCD 2011 / 2016 datasets (MRLC 2011). This was then merged with the projected changes in urbanization from LUCAS to arrive at the 2050 urban LULC input to the atmospheric models.

The changes in land use corresponding to the BAU scenario, as defined by Sleeter et al. (2017a,b), include the following:

- Urban land cover will double by the year 2100, increasing by 182 km^2 yr^{-1} from 2001 to 2100;

- Agricultural expansion will occur at a rate of 155 km^2 yr^{-1}; Agricultural contraction will occur at 127 km^2 yr^{-1}; and

- Natural lands will decline by 13,842 km^2 by 2100.

Figure 6-2 is a translation of the BAU scenario (shown in Figure 6-1) into model grid-cell representations. The cells marked "1" represent current urban land use and those marked "99" represent expansion of urban land use by 2050. The number of urban cells in 2015 is 495, whereas in 2050 the number is 855 (i.e., 495+360).

Figure 6-1: Current (2015) and 2050 BAU urban land use scenario (per data from USGS LUCAS, Sleeter et al. 2017a,b and NLCD 2011).
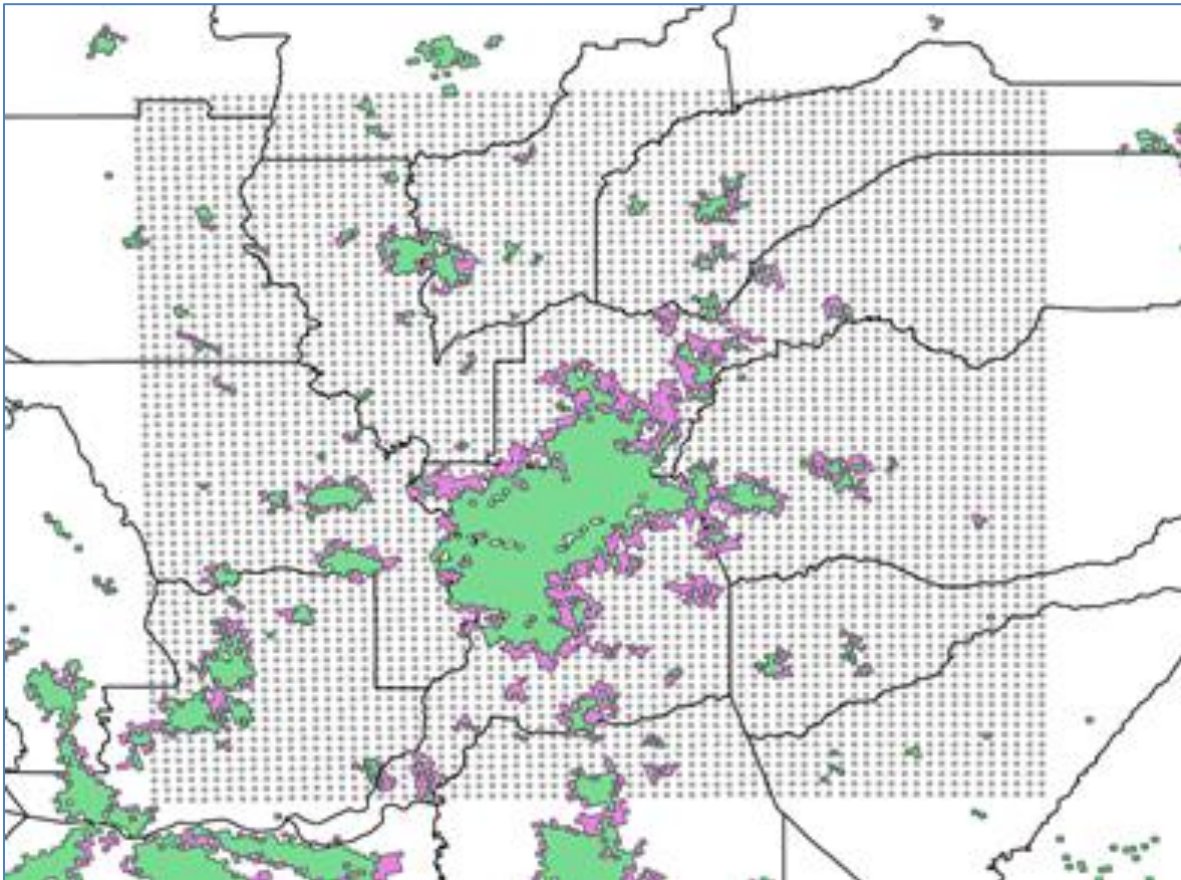
Figure 6-2: Translation of current and future urban land use into model-grid cell representations.
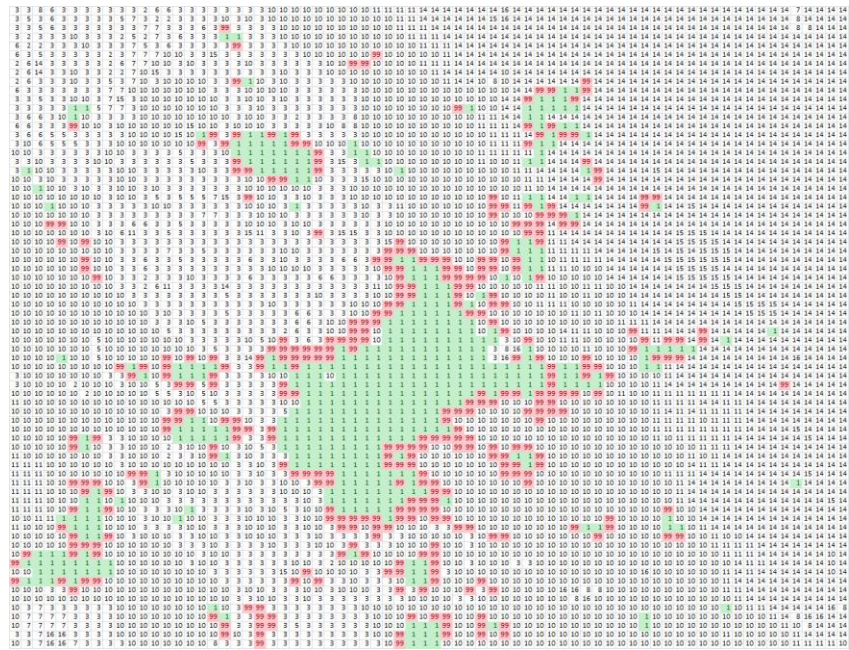
Having defined the new urban extent in 2050 (i.e., the pink areas in Figures 6-1 and 6-2), the next step was to develop a physical characterization for these urban areas to update the corresponding input to the land-surface and atmospheric models. Several properties were defined including (1) urban fraction, (2) various surface-cover types, vegetation, pervious / impervious cover, and (3) physical properties such as albedo, roughness length, etc., based on properties of nearby (current) urban areas. Since it is unknown what the physical and geometrical characteristics of these new urban areas would be, one way to characterize them is by extending the properties of existing nearby urban areas, i.e., near the outskirts of the current urban boundaries.

To do so, an algorithm was designed in this study to (1) "march" or "roam" through each and all new urban grid cells by 2050, (2) within a specified radius of influence, search for current urban cells and average their physical properties, then (3) project these properties onto the expanding, new urban areas (cells) based on average properties of current neighboring urban areas. In this analysis, the marching search window was assigned a radius of 6 km.

While the urban fractions and physical properties for the new urban areas by 2050 were derived based on neighboring-cells urban fractions (from 2015), the corresponding impervious fractions in 2050 were still needed in order to compute the changes in surface properties, e.g., albedo, roughness, soil moisture, etc., for developing the 2050 perturbation scenarios (mitigation measures). A first step in that direction was to evaluate whether some correlation exists (in current LULC conditions) between urban fraction and impervious fraction. If there were such correlation, then it could be used in deriving future gridded impervious fraction based on gridded urban fraction for those new urban cells by 2050.

Altostratus Inc.

A snapshot from this analysis is shown in Figure 6-3 where a correlation between current urban fraction and impervious fraction is evaluated.

Figure 6-3: Correlation between impervious (vertical axis) and urban fraction (horizontal axis) for current LULC (year 2015).
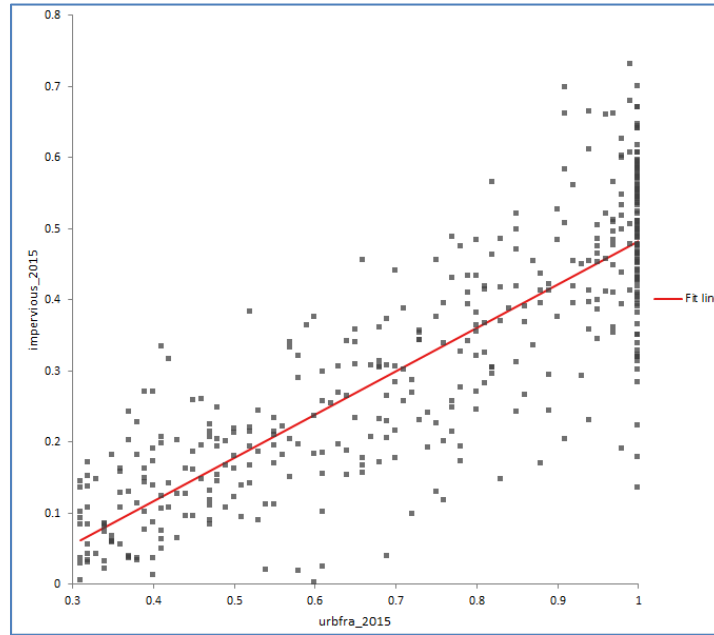
The analysis indicates that a reasonable correlation exists which can be used to estimate future impervious fraction from future urban fraction in 2050. In Figure 6-3, the correlation coefficient, R^2, is 0.7 and the P-value is <0.0001. The equation for the linear fit is:

$$I \ = \ -0.1257 \ + \ 0.6082\,U \qquad (6-1)$$

where I is the impervious fraction and U is the urban fraction as defined earlier, such as in Section 5.21 (equation 6-1 applies where $U > 0.30$). All projected thermo-physical properties were based on averages of current 2015 properties as discussed above and, where needed, weighted by urban fraction and / or impervious fraction as computed by equation 6-1.

Figures 6-4 and 6-5 show examples from characterizing the spatial distribution of changes in albedo for current (2015) and 2050 LULC (based on LUCAS), respectively. In both cases, the darkest color is the highest cell-level increase in albedo of +0.11. Contrasting the two figures also shows the larger extent of the urban area (and extent of albedo modifications) in 2050 relative to 2015.

Figure 6-4: Change in albedo for case10 in 2015

delta albedo for case10 in 2015
(darkest = +0.11) (projection= lat/lon)
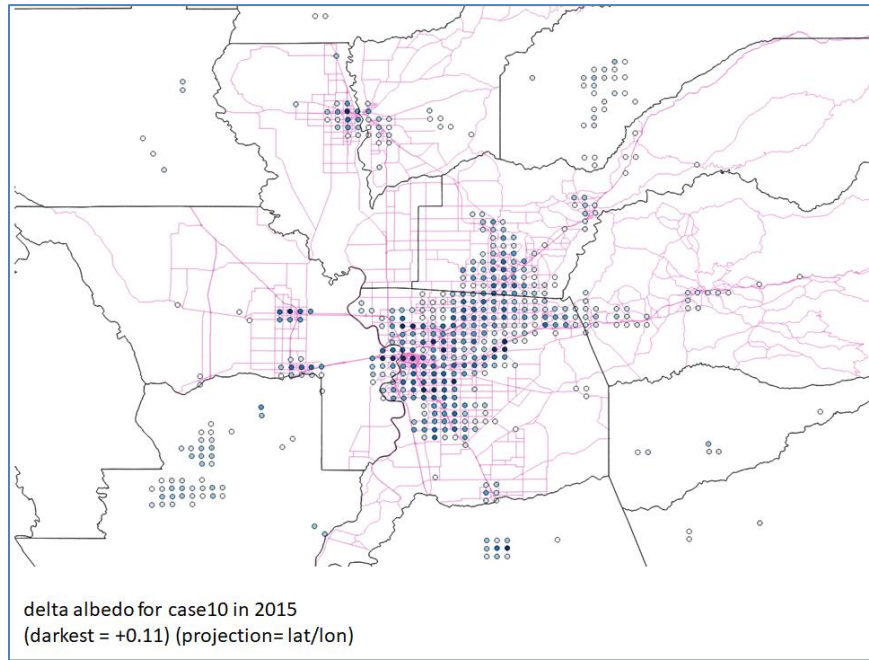
Figure 6-5: Change in albedo for case10 in 2050

delta albedo for case10 in 2050
(darkest = +0.11) (projection= LCC)
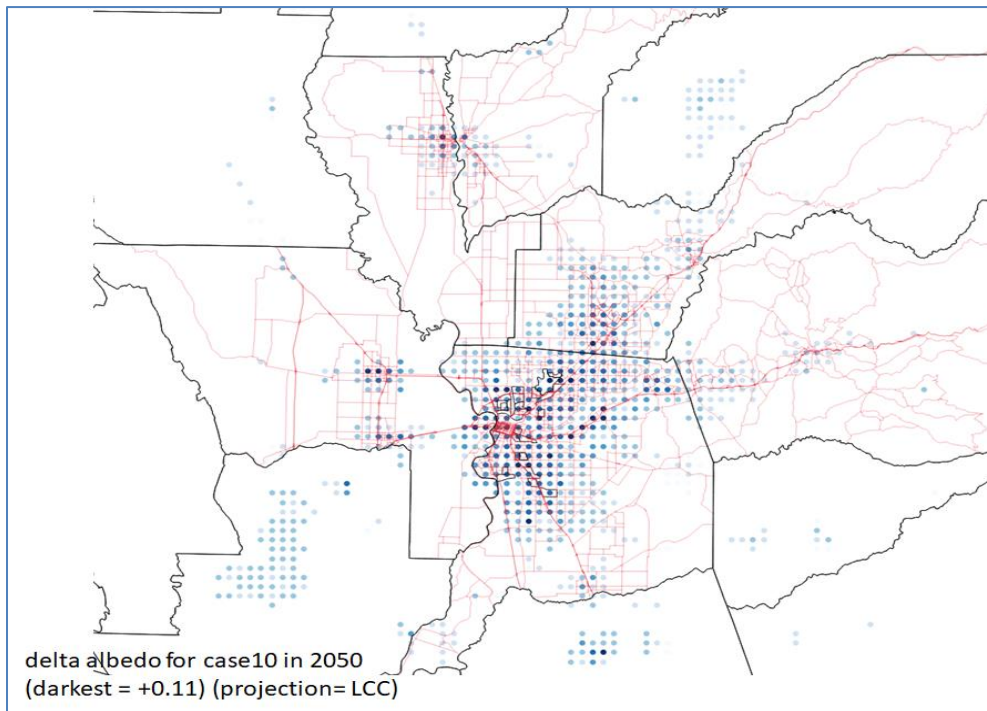
These changes in urban land-use properties were then used in the urban atmospheric model to dynamically-downscale the climate-model fields, i.e., with the Altostratus AREAMOD and modUCM approaches, and evaluate the combined impacts of climate and LULC changes on future meteorology in the study domains. The results are presented in the following sections. Here, two example snapshots are provided for the purpose of introducing this analysis.

In Figure 6-6, the temperature change (i.e., temperature equivalent DH hr^{-1} of the UHII) in 2050 RCP 8.5 at a random single hour (1600 PDT) relative to corresponding time and date in 2015 is presented. The range of change at that hour (dark green to dark red) is +1 to +5 °C. In the new urban areas (outskirts seen in pink in Figures 6-1 and 6-2), the change is up to +5 °C, which can be attributed to effects of both climate and LULC changes (urbanization), whereas the change in the existing (2015) urban areas is up to 3 °C, which is attributed to only the climate effects (since urbanization is assumed unchanged in these areas).

Thus, qualitatively at least, at this random hour, it can be said that the effects of climate are to warm the current urban areas by 3 °C whereas the effects of urbanization (changes in LULC only) are a warming of 2 °C (5 minus 3 °C). Thus this implies that (1) changes in urbanization and LULC are critical to account for and consider when developing regional land-use plans (since they have relatively similar local warming effects as the changes in climate) and (2) that UHI-mitigation measures will be critical in the future as they can locally offset the effects of climate change (e.g., in this case, 2 °C in potential cooling versus 3 °C in climate-induced urban warming).

Figure 6-6: Effects of climate and land-use changes at a random single hour. Example: Temperature equivalent, °C (DH hr^{-1}) difference between 2050 RCP 8.5 and current climate (2015) at 1600 PDT, July 27.
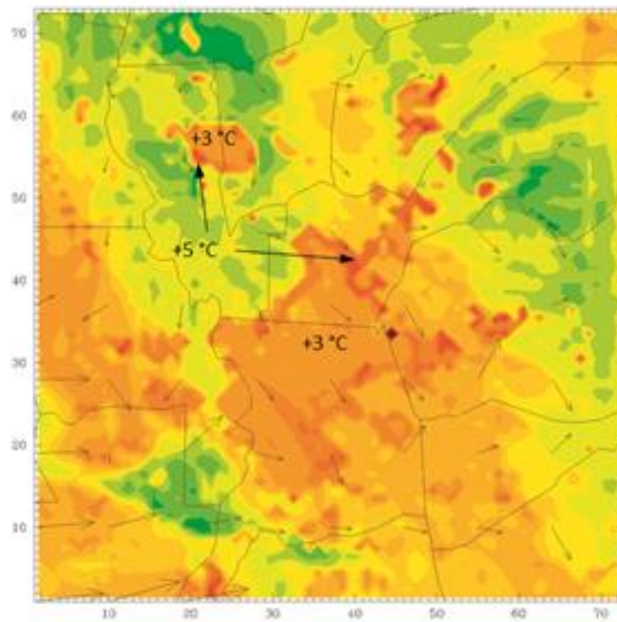
Figure 6-7: Temperature equivalent, °C (DH hr^{-1}) of the all-hours change in the UHII for all hours during the period July 16 – 31 of 2050 versus those in 2015.
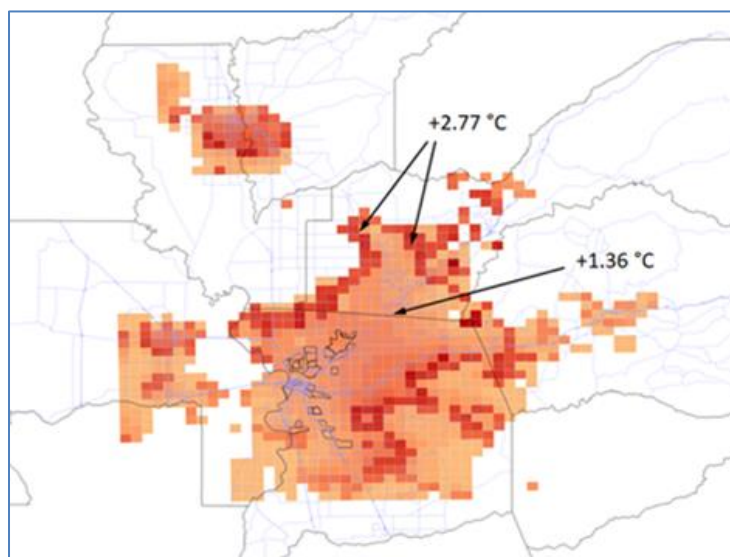
On the other hand, the examination of all intervals, not just a single hour as in the forgoing example, suggests that on the longer term, the local effects of changes in LULC and in climate on air temperature are of similar magnitudes. For example, Figure 6-7 shows the temperature equivalent (DH hr^{-1}) of the UHII change for all hours during the period July 16 – 31 of 2050 versus the same interval in 2015. In this case, the climate effect is +1.36 °C and the land-use effect is up to +1.41 °C (that is, 2.77 minus 1.36 °C), essentially of the same magnitude. Hence, the role of LULC change in warming and the role of UHI mitigation measures in cooling (under current and future climates) cannot be overstated in light of such similarities in magnitudes.

These are among a few points to bear in mind while the results are presented in more detail in the following sections.

6.4 MITIGATION MEASURES

The development of mitigation measures, e.g., increased albedo and canopy cover, among others, was discussed in Section 5.5, and needs not be repeated here. An example for increasing albedo was given above in Figure 6-5, where the darkest color represents the highest cell-level increase in albedo of +0.11. Similar patterns are seen in other mitigation measures that are proportional to technical potential. Because the urban area has expanded by 2050 (see Figures 6-1 and 6-2), there is increased technical potential as well, i.e., area available for implementation of albedo and canopy measures or, in other words, the modifiable urban area is larger. As will be discussed later in this report, this translates into larger potential cooling (because of the larger modified area) and thus provides a counterbalance to the warming effects from climate change and urbanization.

In addition to the scenarios defined in Section 5.5, this study also evaluated a scenario of smart growth whereby 15% less urbanization occurs in the future (2050) relative to the BAU scenario discussed above in Section 6.3. Figure 6-8 depicts the BAU scenario by 2050 (top) and the smart-growth scenario (bottom).

Figure 6-8: BAU (top) and smart growth (bottom) urbanization scenarios, by 2050, on the model 2-km grid (D04).
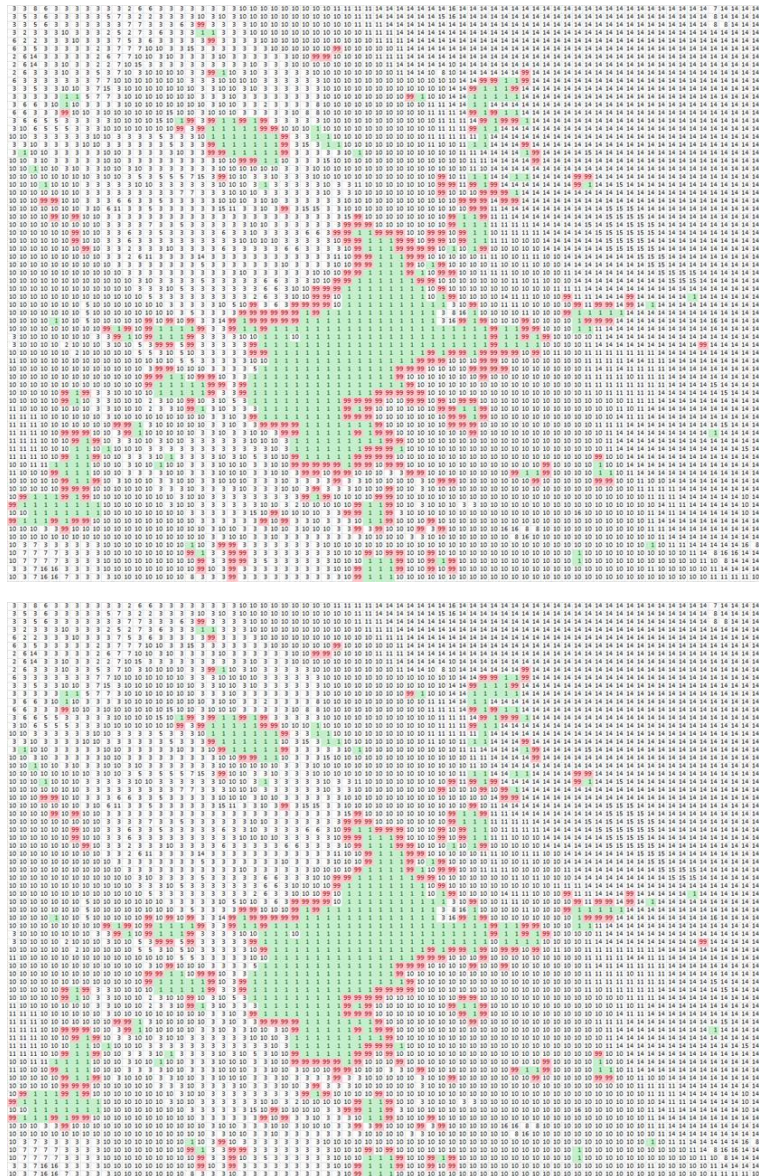
6.5 IMPACTS AND RANKING OF MITIGATION MEASURES IN FUTURE CLIMATE AND LAND USE

This discussion of the future impacts on the urban temperature field, UHI, UHII, and other metrics, largely follows the discussion of the same metrics for the current climate and land-use in Section 5-11. A such, definitions, concepts, and contexts will not be described again here.

6.5.1 Impact of mitigation measures on 0600 PDT temperature

In Figure 6-9, the average temperature reductions at 0600 PDT are presented, that is, temperature reductions averaged over all 0600 PDT hours (in each of the seven 2050 periods, int1 – int7) and over urban grid cells in each specified sub-domain. For each subdomain, two RCP scenarios are presented (RCP 4.5 and RCP 8.5, as defined in Section 6.2).

One can see from Figure 6-9 that the ranking (i.e., the order of measures' effectiveness) at this time interval is consistent and similar across all regions but that the magnitudes of reductions in temperature differ by location. This ranking (at this hour) is also exactly similar to the ranking (at 0600 PDT) in current climate.

As expected, the intra-measure differences within each area are different across the regions, i.e., how close or far apart the reductions are from different measures. Again, the caveat with case02 should be reiterated, i.e., an extreme canopy-cover increase scenario.

Figure 6-9: Average temperature reduction (°C) at 0600 PDT. Periods are identified on the horizontal axis and the ranking of measures on the right side of each graph.
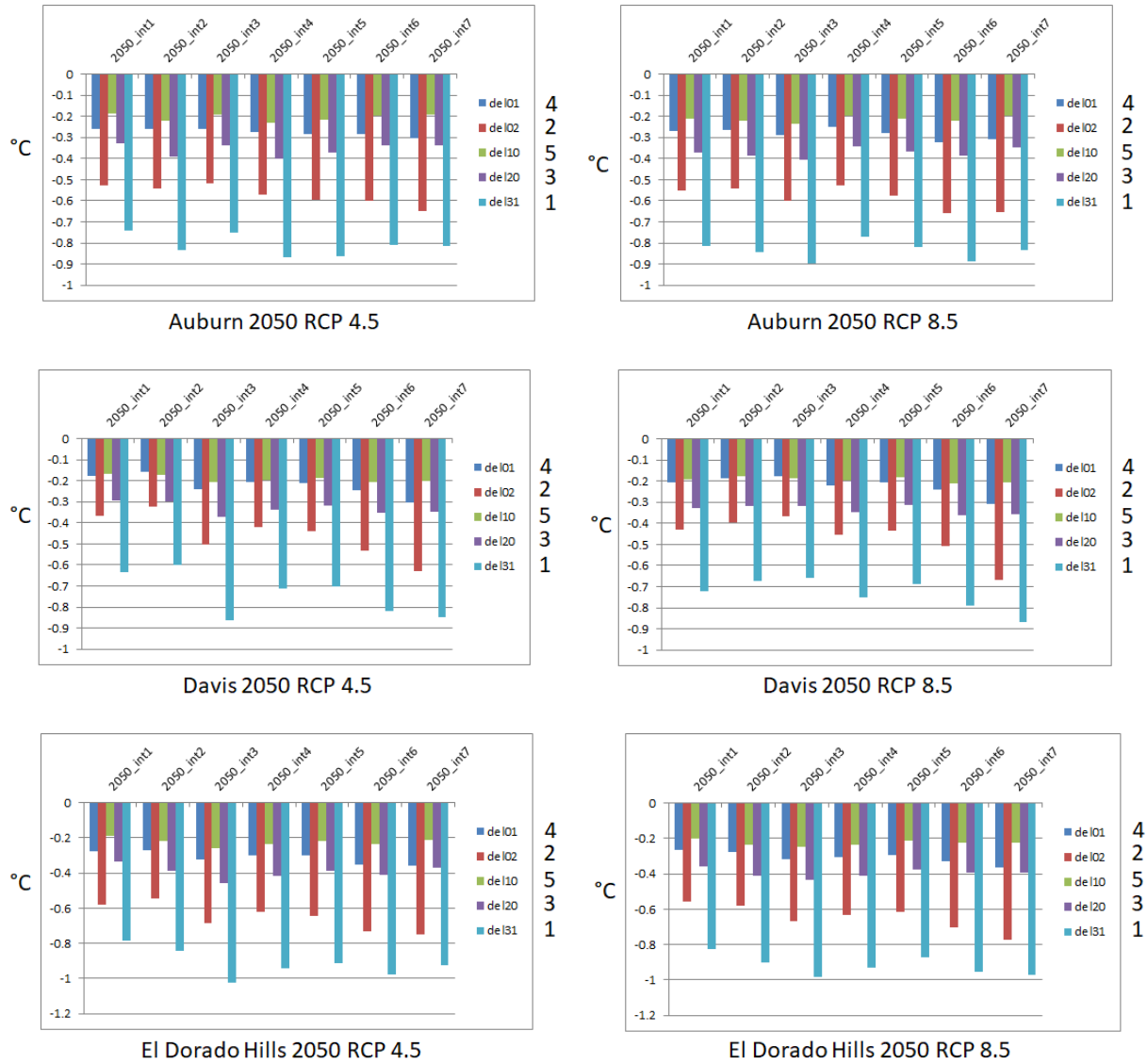
Figure 6-9, continued.

Davis 2050 RCP 4.5

Davis 2050 RCP 8.5

El Dorado Hills 2050 RCP 4.5

El Dorado Hills 2050 RCP 8.5

Placerville 2050 RCP 4.5

Placerville 2050 RCP 8.5

Sacramento 2050 RCP 4.5

Sacramento 2050 RCP 8.5

Figure 6-9, continued.

Woodland 2050 RCP 4.5

Woodland 2050 RCP 8.5

Yuba City 2050 RCP 4.5

Yuba City 2050 RCP 8.5
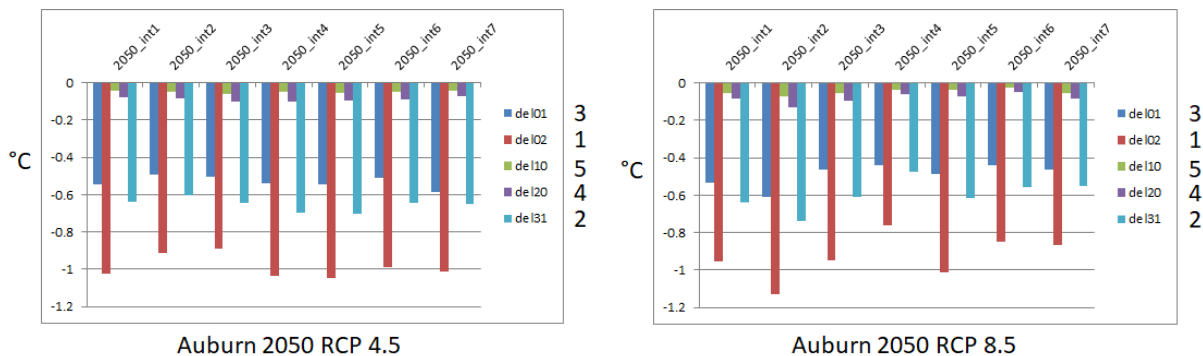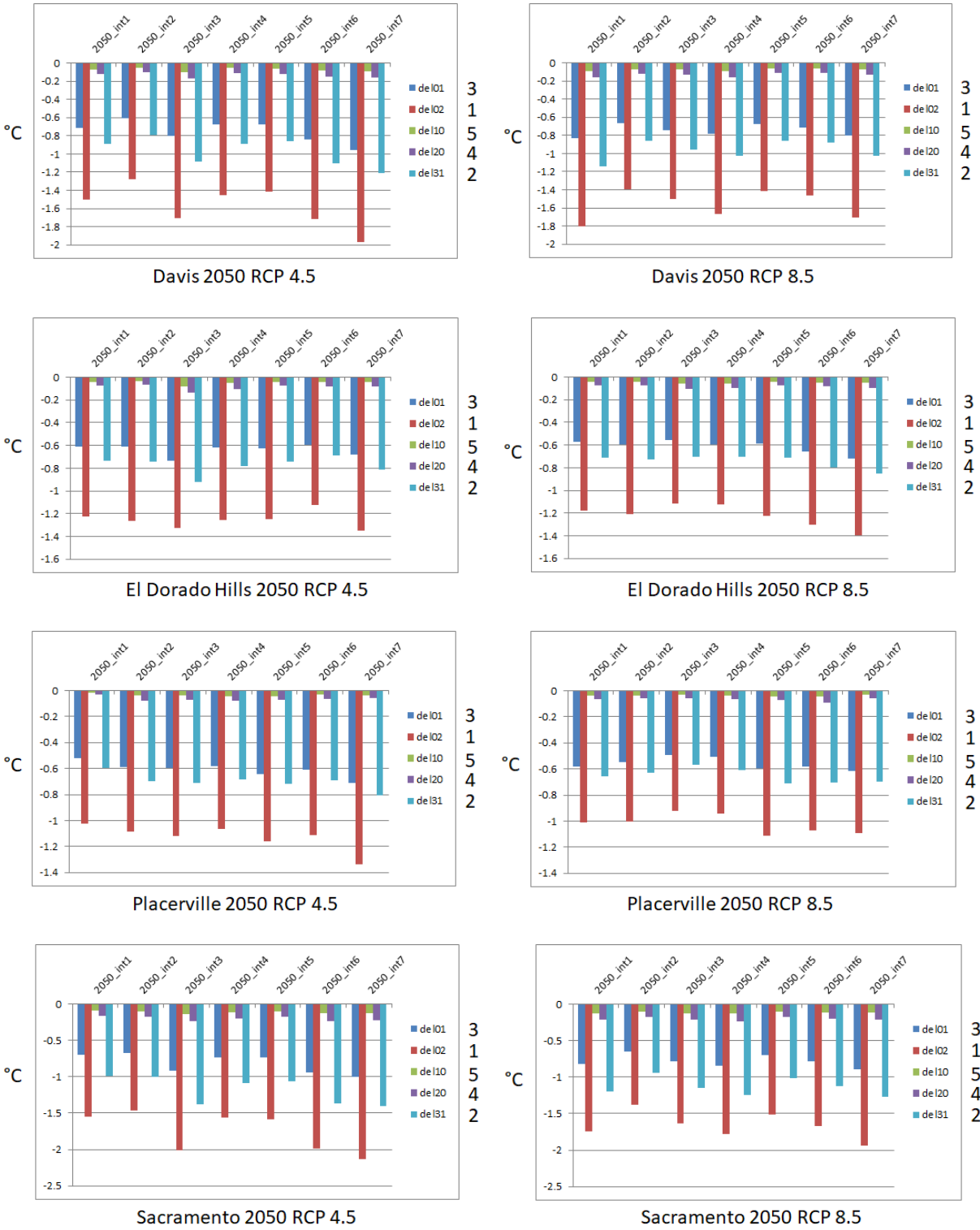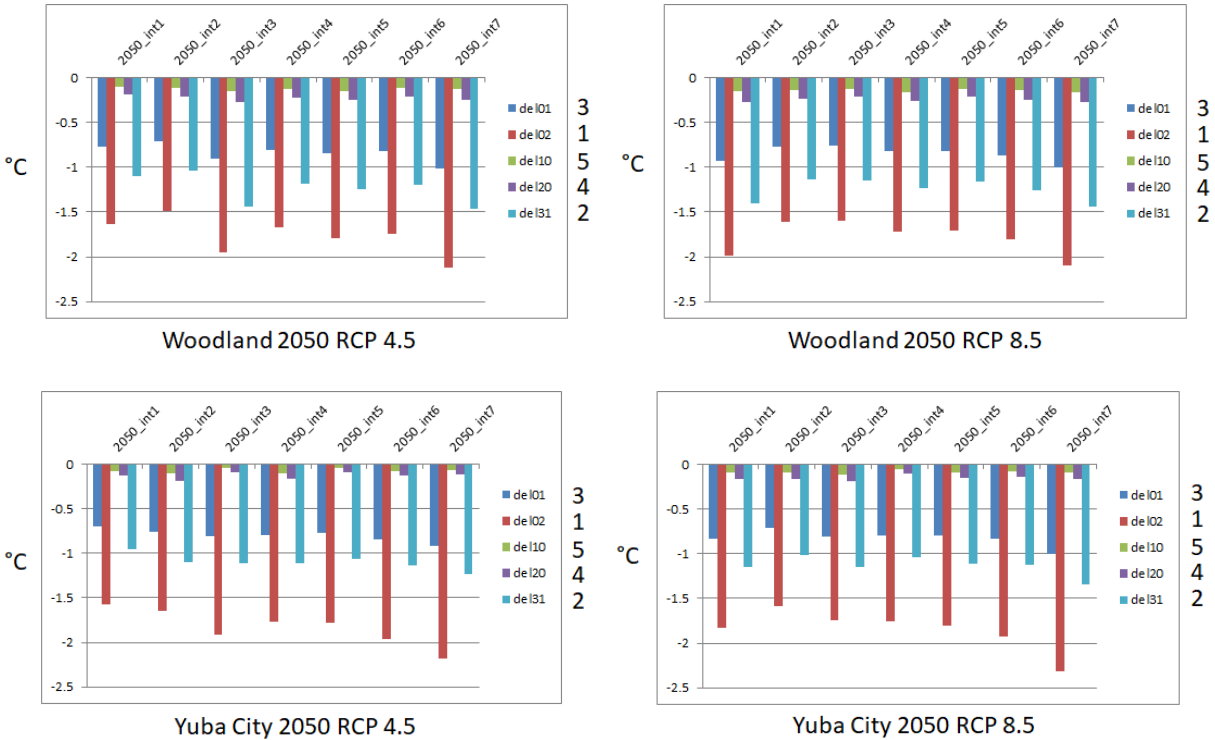
6.5.2 Impact of smart growth on 0600 PDT temperature

The impacts of the smart growth scenario defined in Section 6.4 were evaluated and compared against those of the BAU scenario in year 2050 (based on USGS LUCAS projections). While there are several ways these impacts could be quantified, including averaging over the entire region or each sub-domain, here the impacts are presented only for those locations (grid cells) where urbanization was prevented (compare the top and bottom parts of Figure 6-8). Clearly, applying this criterion would show much larger localized cooling impacts relative to, say, averaging over the entire domain including those areas that currently are urbanized (i.e., in 2013 – 2016).

Figure 6-10 shows that while there are variations by area and time interval, the overall average avoided warming at 0600 PDT is about 2 °C in the areas where urbanization was prevented. On the other hand, if averaged over each subdomain (not shown here), the effects of smart growth are smaller, as expected, i.e., an avoided warming of between 0.05 and 0.15 °C region-wide.

Figure 6-10: Impacts of smart growth on 0600-PDT air temperature in 2050: Avoided warming (°C) at new urban locations for RCP 4.5 and 8.5.
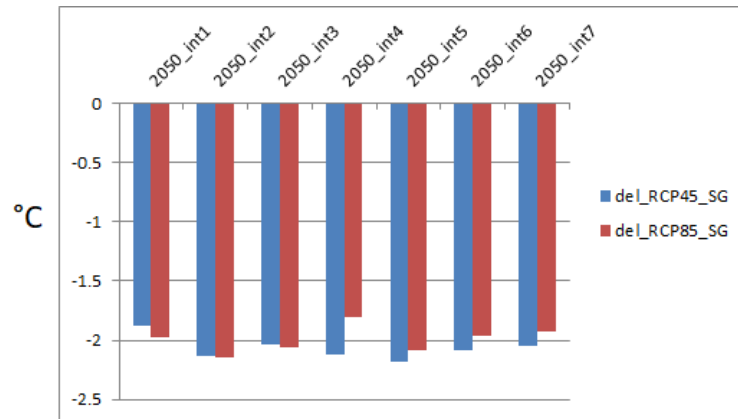
Auburn 2050 smart growth
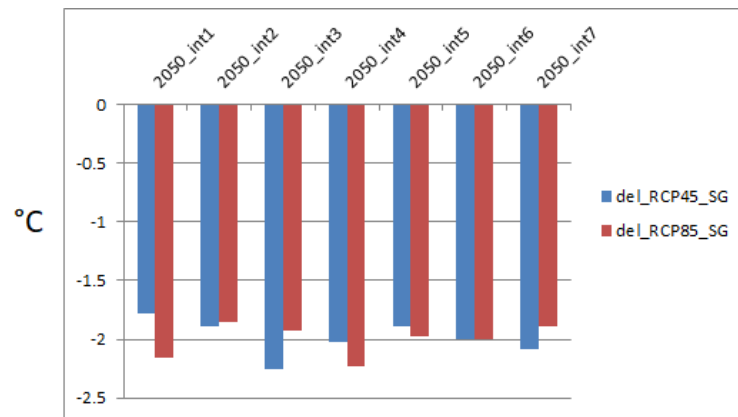
Davis 2050 smart growth
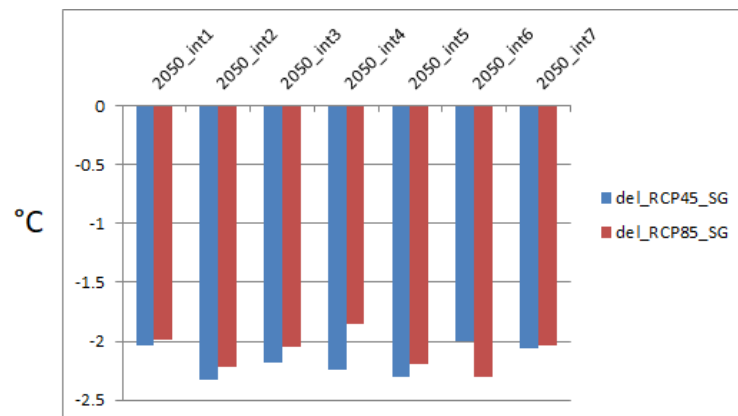
El Dorado Hills 2050 smart growth

Figure 6-10, continued.
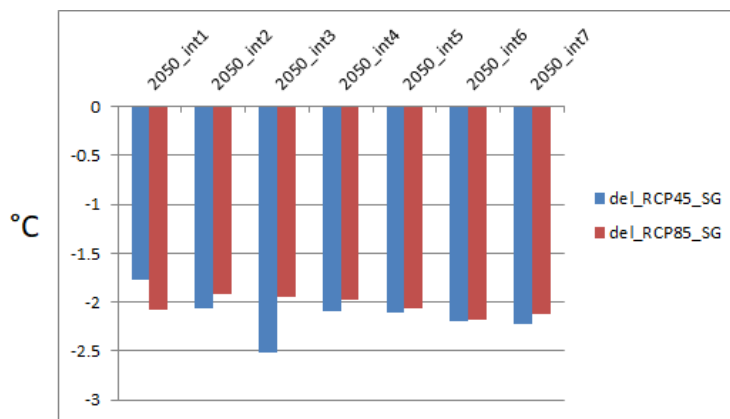
Sacramento 2050 smart growth
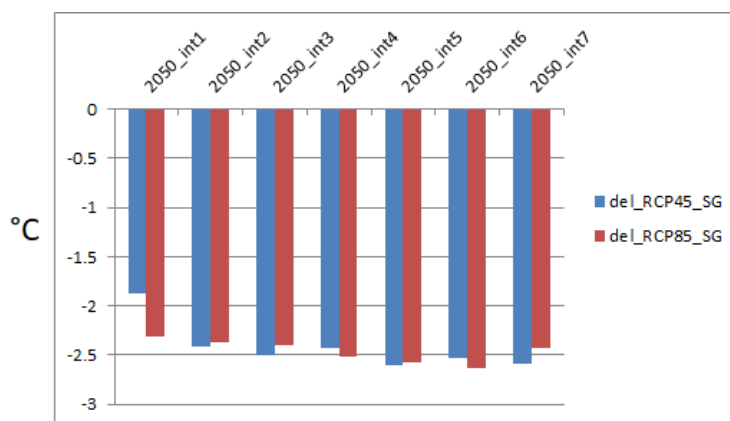
Yuba City 2050 smart growth

6.5.3 Impacts of mitigation measures on 1300 PDT temperature

In Figure 6-11, the average temperature reductions at 1300 PDT are presented, that is, temperature reductions averaged over all 1300 PDT hours (in each of the seven 2050 periods) and over urban grid cells in each specified sub-domain. For each area, two RCP scenarios are presented in the figure (RCP 4.5 and RCP 8.5).

Figure 6-11 shows that the ranking (i.e., the order of measures' effectiveness) at this time interval (1300 PDT) is (1) different from that at 0600 PDT, discussed above, and (2) also varies across different regions, unlike at 0600 PDT where they were similar across all sub-domains. At this time interval (1300 PDT), the effects of albedo measures are larger than those of canopy cover, as explained earlier, especially if case02 is excluded from the analysis (as an extreme). Furthermore, at Davis, the ranking of the measures is different in 2050 (for both RCPs) from the ranking in current climate. The magnitudes of reductions in temperature differ by location and so do the intra-

measure differences within each area, i.e., how close or far apart are the reductions resulting from different measures.

Figure 6-11: Average temperature reduction (°C) at 1300 PDT. Periods are identified on the horizontal axis and the ranking of measures on the right side of each graph.


Auburn 2050 RCP 4.5

Auburn 2050 RCP 8.5

Davis 2050 RCP 4.5

Davis 2050 RCP 8.5

El Dorado Hills 2050 RCP 4.5

El Dorado Hills 2050 RCP 8.5

Figure 6-11, continued.

Placerville 2050 RCP 4.5

Placerville 2050 RCP 8.5

Sacramento 2050 RCP 4.5

Sacramento 2050 RCP 8.5

Woodland 2050 RCP 4.5

Woodland 2050 RCP 8.5

Yuba City 2050 RCP 4.5

Yuba City 2050 RCP 8.5
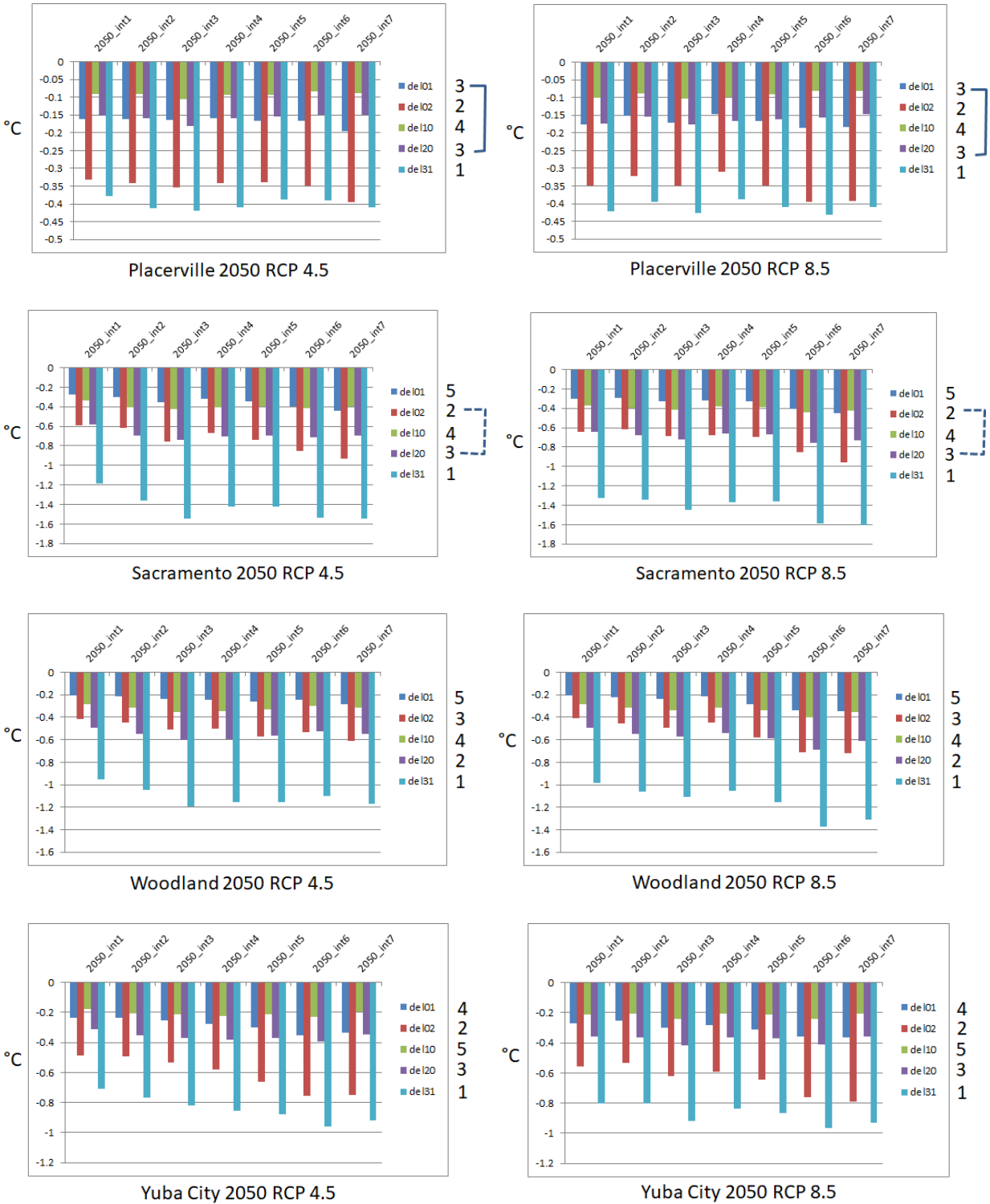
6.5.4 Impacts of smart growth on 1300 PDT temperature

The smart growth scenario (defined above) was also evaluated in terms of air-temperature impacts compared to those of the BAU LULC scenario in year 2050 at 1300 PDT. As discussed earlier, the impacts are presented only at those locations (grid cells) where urbanization was prevented.

Figure 6-12 shows that there are more variations across the regions than was the case at 0600 PDT (where all regions had about a 2 °C average avoided warming). In this case (at 1300 PDT), the avoided warming ranges from an average of 0.05 °C in Davis to up to an average of 0.4 °C in Auburn. There also is a single instance of increase of up to 0.06 °C in temperature (in Davis) as a result of smart growth, but this is likely an anomaly. Again, if averaged over each subdomain, the effects of smart growth are small, e.g., avoided warming of between 0.05 and 0.1 °C region-wide.

Figure 6-12: Impacts of smart growth on 1300-PDT air temperature in 2050: Avoided warming (°C) at new urban locations for RCP 4.5 and 8.5.
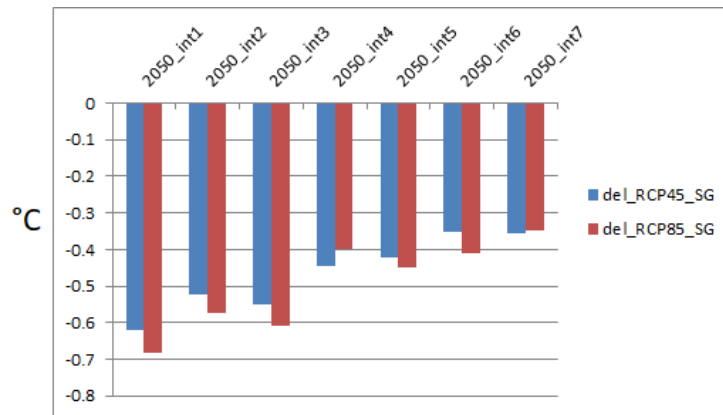
Auburn 2050 smart growth
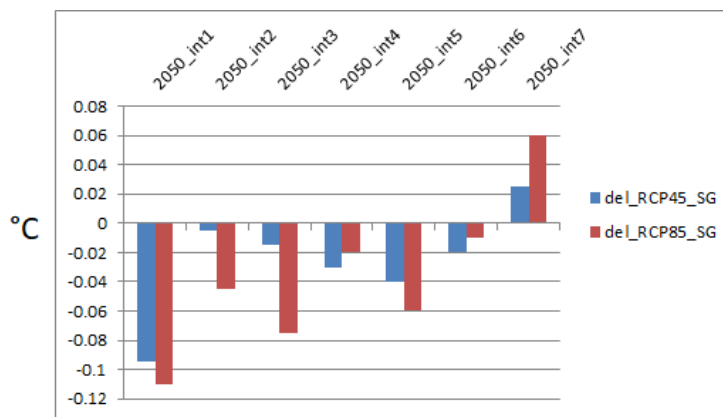
Davis 2050 smart growth

Figure 6-12, continued.
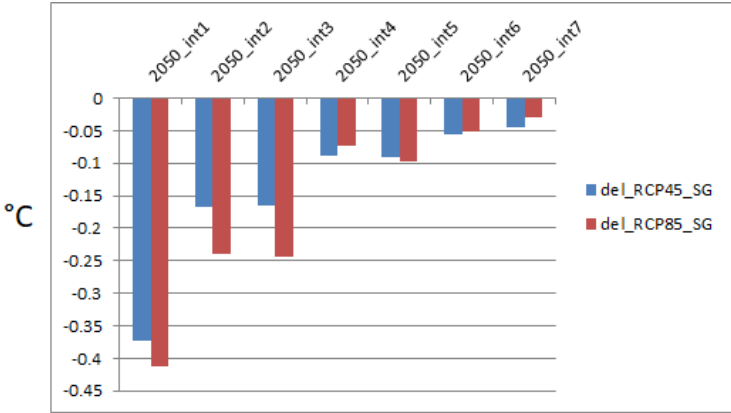
El Dorado Hills 2050 smart growth
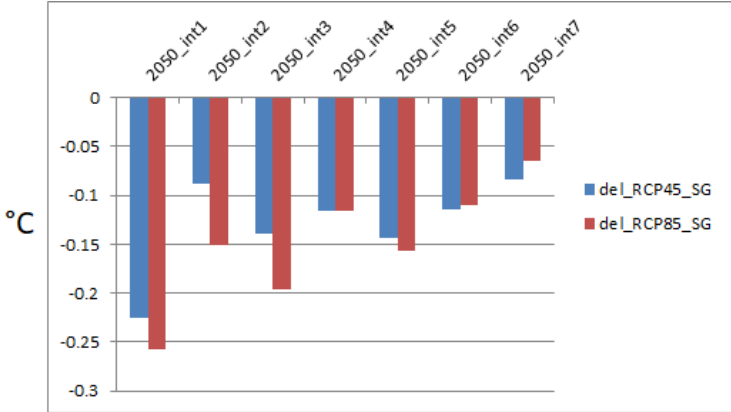
Sacramento 2050 smart growth
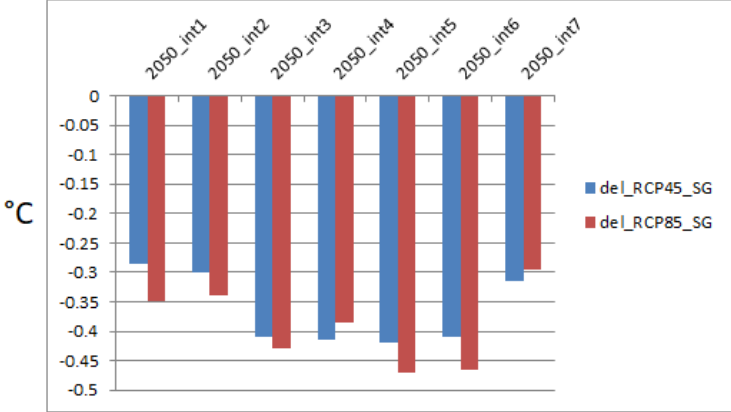
Yuba City 2050 smart growth

6.5.5 Impacts of mitigation measures on temperature during the period 1400 – 2000 PDT

Figure 6-13 shows the average temperature reductions for the interval 1400 - 2000 PDT (i.e., temperature reductions averaged over all 1400 to 2000 PDT hours in each period) and also averaged over urban grid cells in each specified sub-domain. As discussed earlier in the report, this range of hours is of interest to local utilities (SMUD) in peak-load planning and management.

Figure 6-13 shows that the ranking (i.e., the order of measures' effectiveness) at this time interval is (1) different from that at 0600 and 1300 PDT (although more similar to 1300 PDT) and (2) also varies across different regions, unlike at 0600 PDT. There is also the case in Woodland where the ranking of the mitigation measures in year 2050 differs from the ranking in current climate. At this time interval (1400 – 2000 PDT), the effects of albedo measures again are larger than those of canopy cover, excluding case02. The magnitudes of reductions in temperature and the intra-measure differences within each area differ by location, as was seen at hour 1300 PDT.

Figure 6-13: Average temperature reduction (°C) at 1400 - 2000 PDT. Periods are identified on the horizontal axis and the ranking of measures on the right side of each graph.
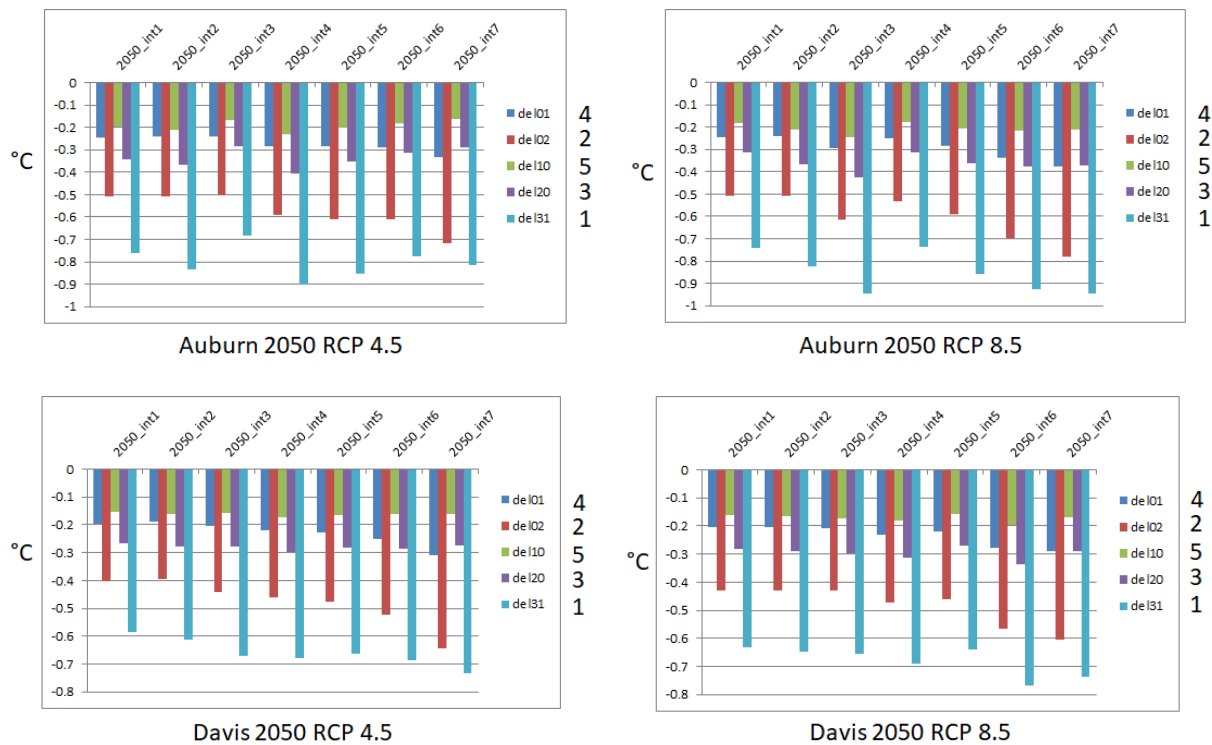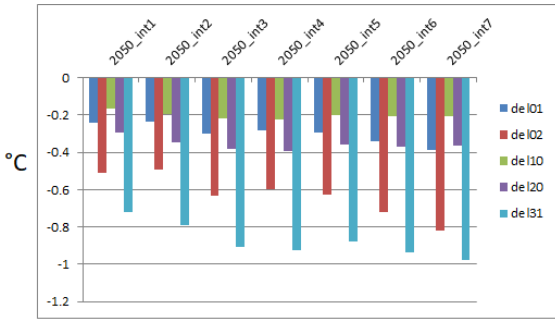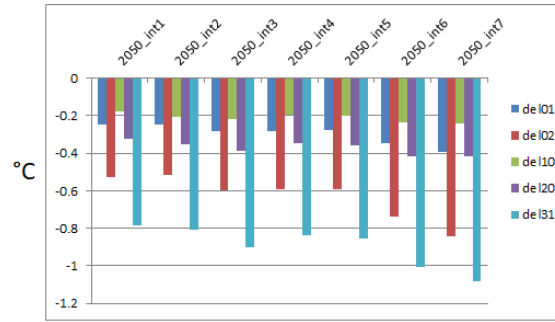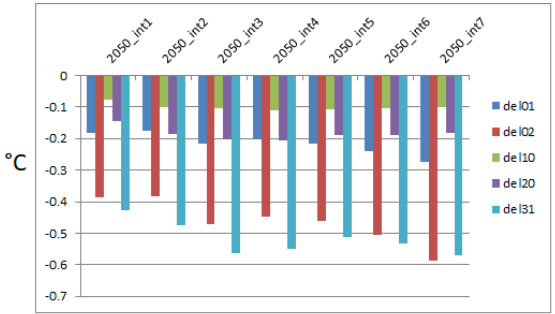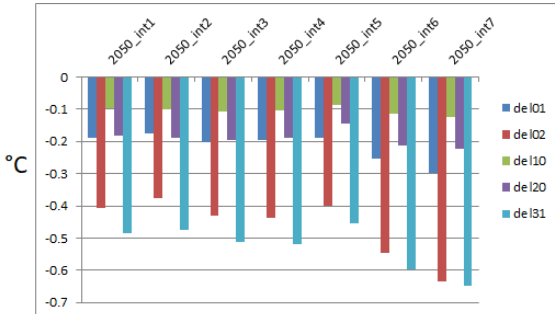
Figure 6-13, continued.

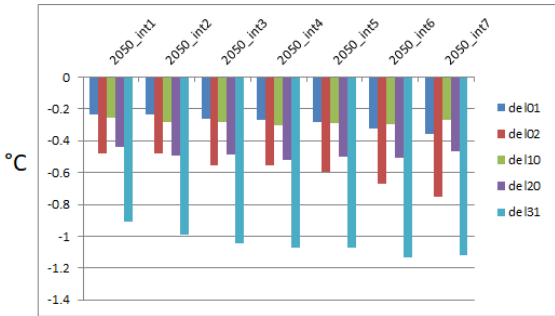

El Dorado Hills 2050 RCP 4.5
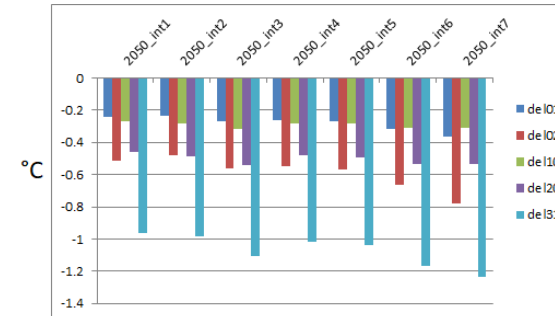
El Dorado Hills 2050 RCP 8.5
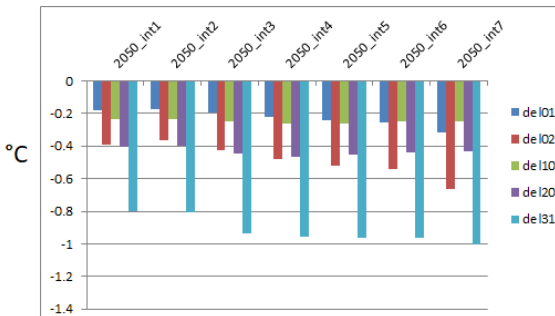
Placerville 2050 RCP 4.5
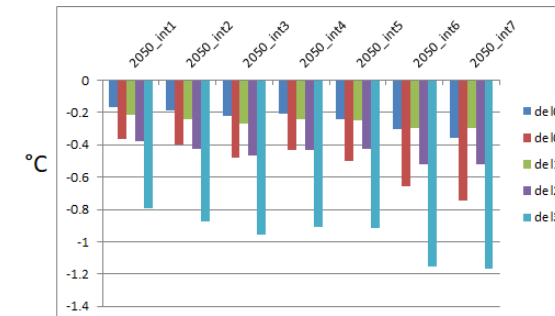
Placerville 2050 RCP 8.5

Sacramento 2050 RCP 4.5

Sacramento 2050 RCP 8.5

Woodland 2050 RCP 4.5

Woodland 2050 RCP 8.5

Figure 6-13, continued.

Yuba City 2050 RCP 4.5

Yuba City 2050 RCP 8.5
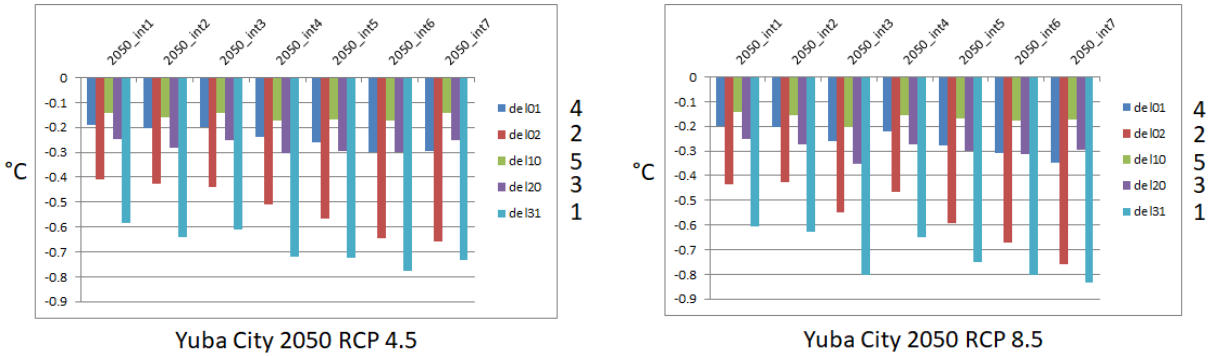
6.5.6 Impacts of smart growth on 1400 - 2000 PDT temperature

As with the time intervals discussed earlier, the smart growth scenario was also evaluated in terms of air-temperature impacts during the hours 1400 – 2000 PDT and compared against those of the BAU scenario in year 2050 (based on USGS LUCAS projections). As before, the impacts are presented (in this section) at those locations (grid cells) where urbanization was prevented.

Figure 6-14 shows that, similar to 1300 PDT, there are more variations in avoided warming across the regions than was the case at 0600 PDT. At 1400 – 2000 PDT, the avoided warming ranges from an average of 0.6 °C in Davis to up to an average of 1.2 °C in Auburn. If averaged over each subdomain, the effects of smart growth are an avoided warming of between 0.05 and 0.15 °C region-wide

Figure 6-14: Impacts of smart growth on 1400- 2000 PDT air temperature in 2050: Avoided warming (°C) at new urban locations for RCP 4.5 and 8.5.
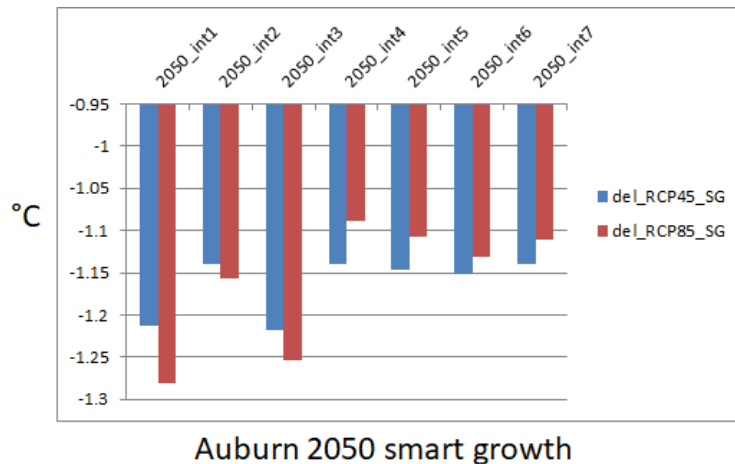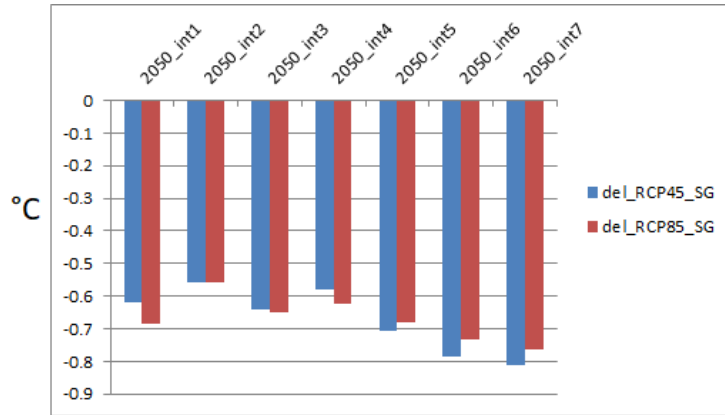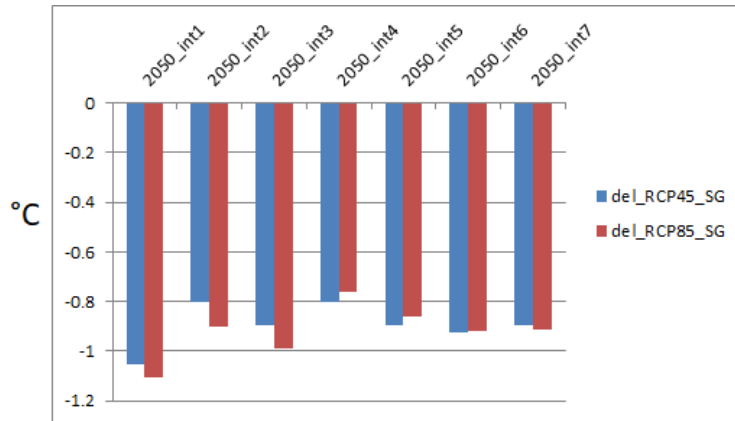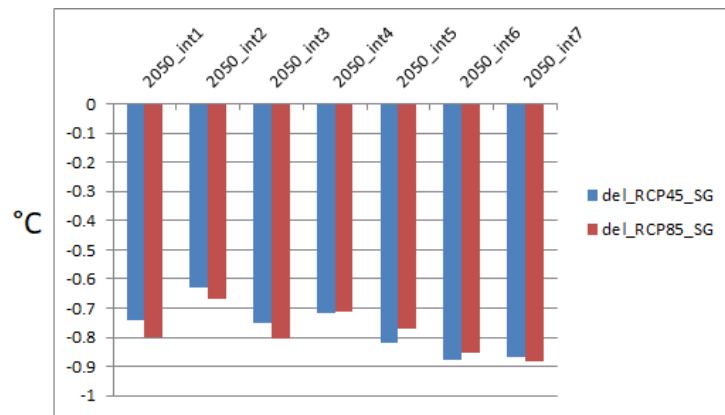

Auburn 2050 smart growth

Figure 6-14, continued.
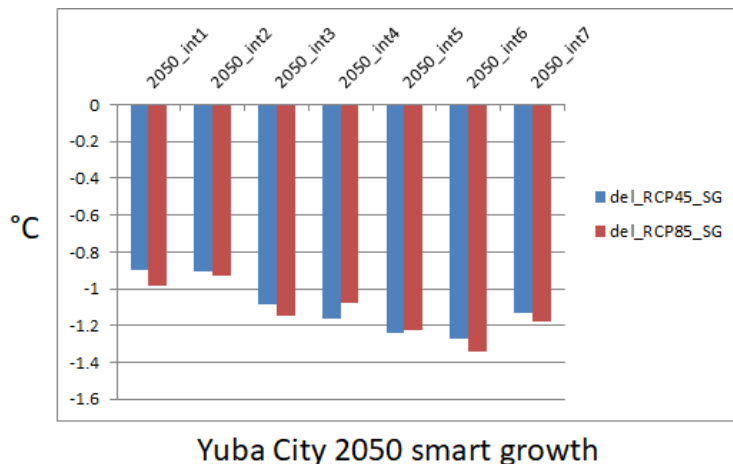

Davis 2050 smart growth

El Dorado Hills 2050 smart growth

Sacramento 2050 smart growth

Yuba City 2050 smart growth

6.5.7 Impact of mitigation measures on 1500 PDT temperature

In Figure 6-15, the average temperature reductions at 1500 PDT are presented, i.e., temperature reductions averaged over all 1500 PDT hours in each of the seven 2050 periods and over urban grid cells in each specified sub-domain. As before, two RCP scenarios are shown (RCP 4.5 and RCP 8.5) for each sub-domain.

Figure 6-15 shows that the ranking (order of measures' effectiveness) at this time interval (1500 PDT) is generally similar to that at 1300 PDT but at different magnitudes. At this time interval (1500 PDT), the effects of albedo measures are larger than those of canopy cover, as explained earlier, especially if case02 is excluded from the analysis as an extreme. However, some albedo measures are still more effective even if case02 were included. Furthermore, in Auburn, Davis, El Dorado Hills, and Yuba City, the ranking of the measures is different in 2050 (both RCPs) from the ranking in current climate.

The magnitudes of reductions in temperature differ by location and so do the intra-measure differences within each area, i.e., how close or far apart are the reductions from different measures.

Figure 6-15: Average temperature reduction (°C) at 1500 PDT. Periods are identified on the horizontal axis and the ranking of measures on the right side of each graph.
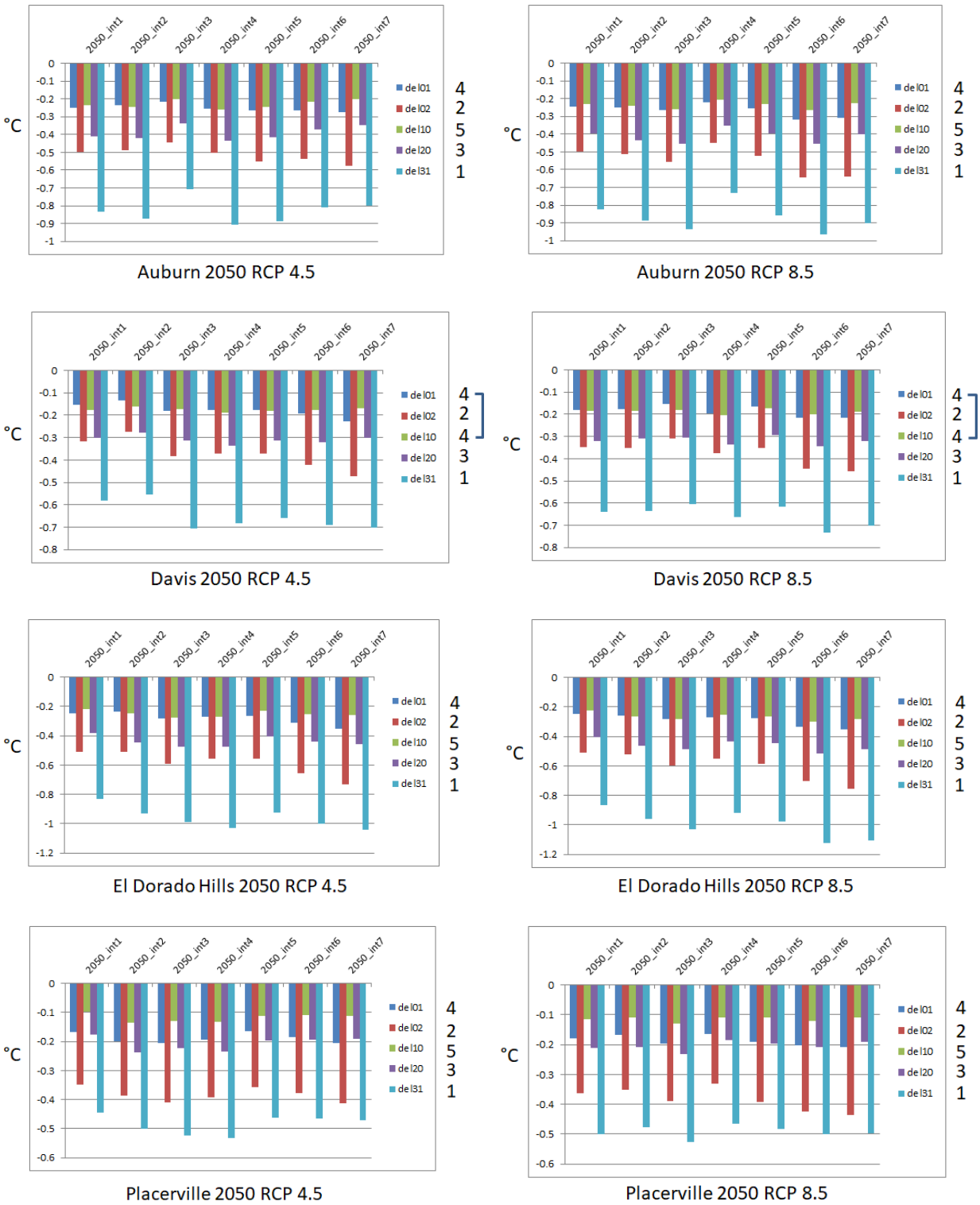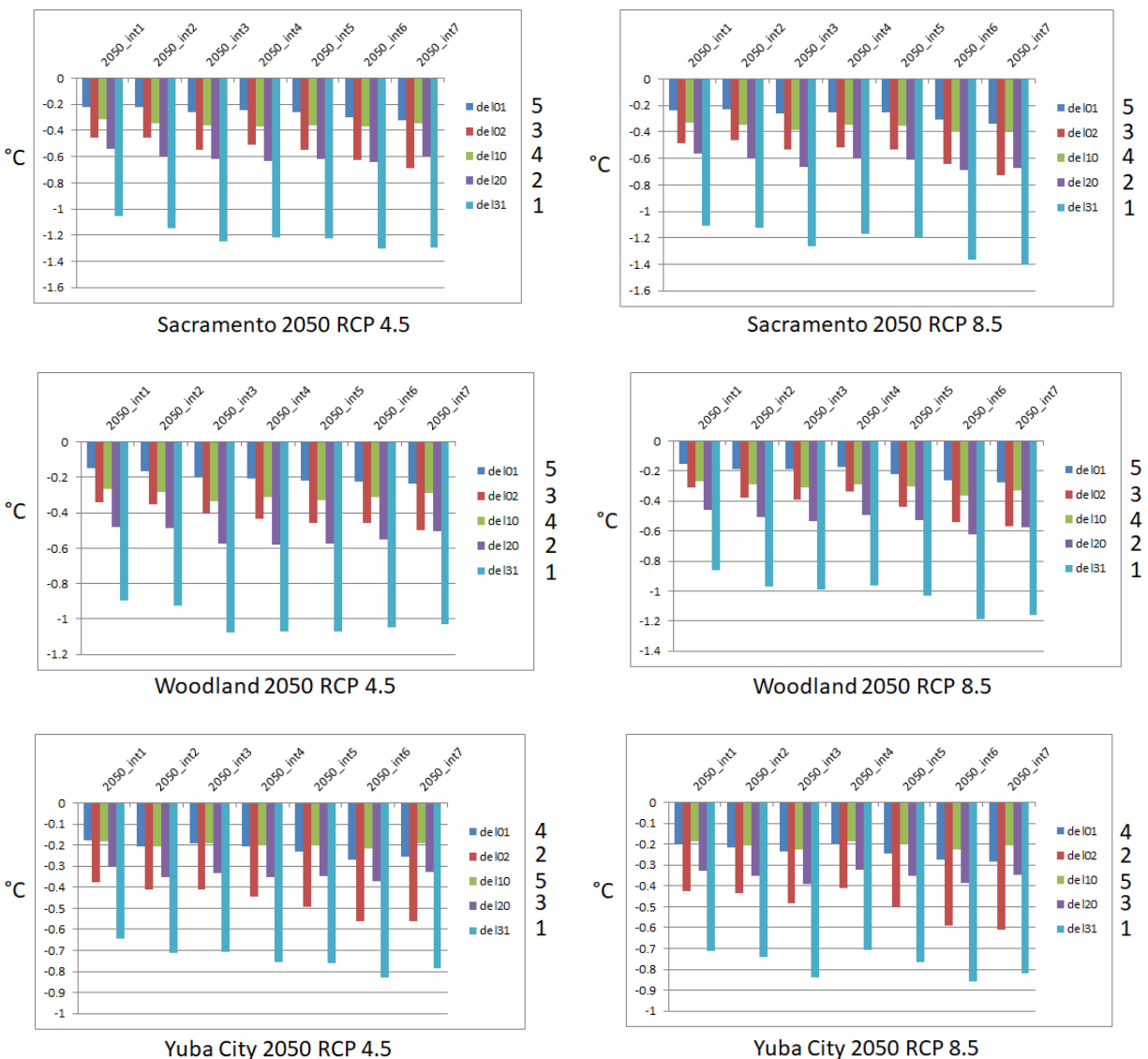

Auburn 2050 RCP 4.5

Auburn 2050 RCP 8.5

Davis 2050 RCP 4.5

Davis 2050 RCP 8.5

El Dorado Hills 2050 RCP 4.5

El Dorado Hills 2050 RCP 8.5

Placerville 2050 RCP 4.5

Placerville 2050 RCP 8.5

Sacramento 2050 RCP 4.5

Sacramento 2050 RCP 8.5

Woodland 2050 RCP 4.5

Woodland 2050 RCP 8.5
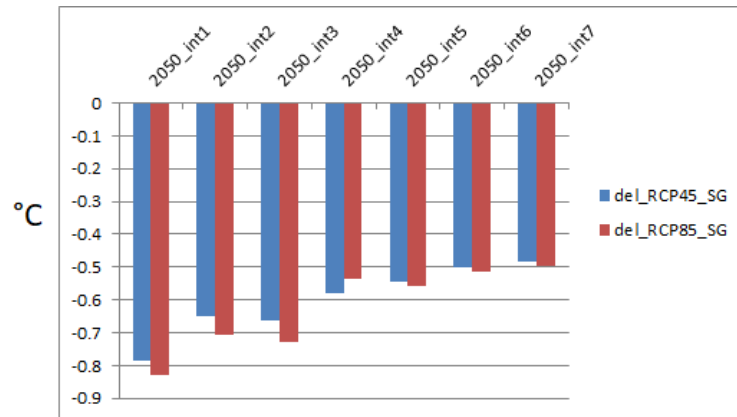
Yuba City 2050 RCP 4.5

Yuba City 2050 RCP 8.5

6.5.8 Impacts of smart growth on 1500 PDT temperature

The smart growth scenario (as defined earlier) was also evaluated in terms of air-temperature impacts and compared against those of the BAU scenario in year 2050 for the hour at 1500 PDT. As before, the impacts are presented here only for those grid cells where urbanization was avoided.

As with the hour at 1300 PDT, Figure 6-16 shows that there is significant variation across the regions. In this case, the avoided warming ranges from an average of 0.20 °C in Davis to up to an average of 0.6 °C in Auburn and Yuba City. However, if averaged over each subdomain, the effects of smart growth are smaller, e.g., an avoided warming of between 0.08 and 0.15 °C region-wide.

Figure 6-16: Impacts of smart growth on 1300-PDT air temperature in 2050: Avoided warming (°C) at new urban locations for RCP 4.5 and 8.5.

Auburn 2050 smart growth
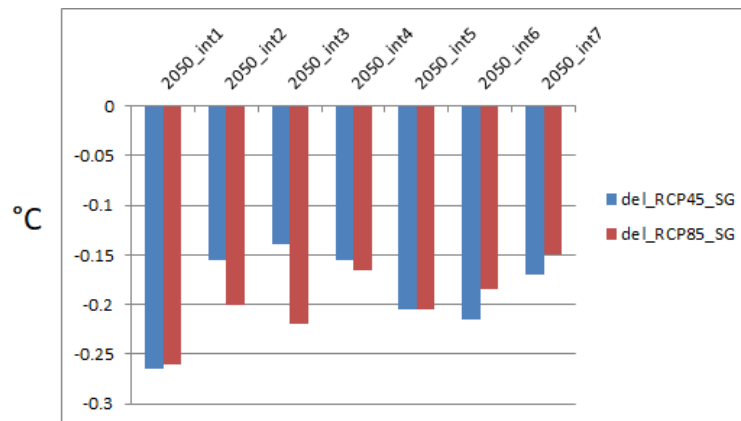
Davis 2050 smart growth
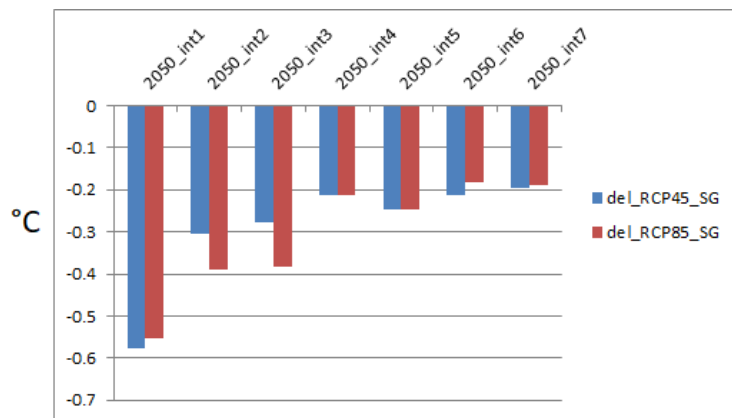
El Dorado Hills 2050 smart growth

Figure 6-16, continued.

Sacramento 2050 smart growth
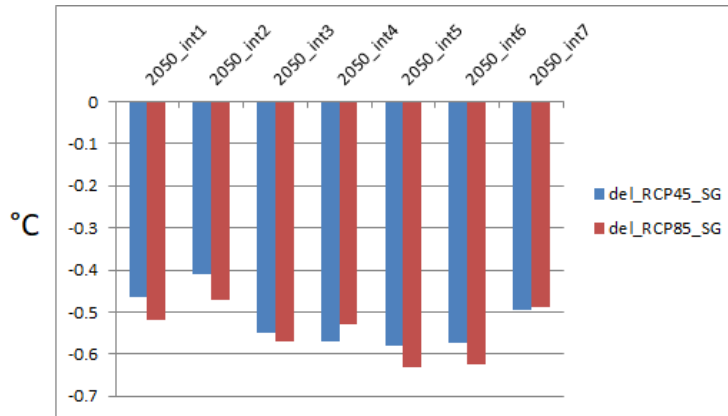
Yuba City 2050 smart growth

6.5.9 Impact of mitigation measures on all-hours average temperature

Figure 6-17 shows the all-hours average temperature reductions that are also averaged over urban grid cells in each specified sub-domain. It can be seen that the ranking of measures is uniform across all regions, but differs in Sacramento and Woodland. In the all-ours average, the effects of vegetation canopy cover are more dominant since this includes nighttime hours.

Figure 6-17: Average all-hours temperature reduction (°C). Periods are identified on the horizontal axis and the ranking of measures on the right side of each graph.

Auburn 2050 RCP 4.5

Auburn 2050 RCP 8.5

Davis 2050 RCP 4.5

Davis 2050 RCP 8.5

El Dorado Hills 2050 RCP 4.5

El Dorado Hills 2050 RCP 8.5

Placerville 2050 RCP 4.5

Placerville 2050 RCP 8.5

Figure 6-17, continued.

Sacramento 2050 RCP 4.5

Sacramento 2050 RCP 8.5

Woodland 2050 RCP 4.5

Woodland 2050 RCP 8.5

Yuba City 2050 RCP 4.5

Yuba City 2050 RCP 8.5
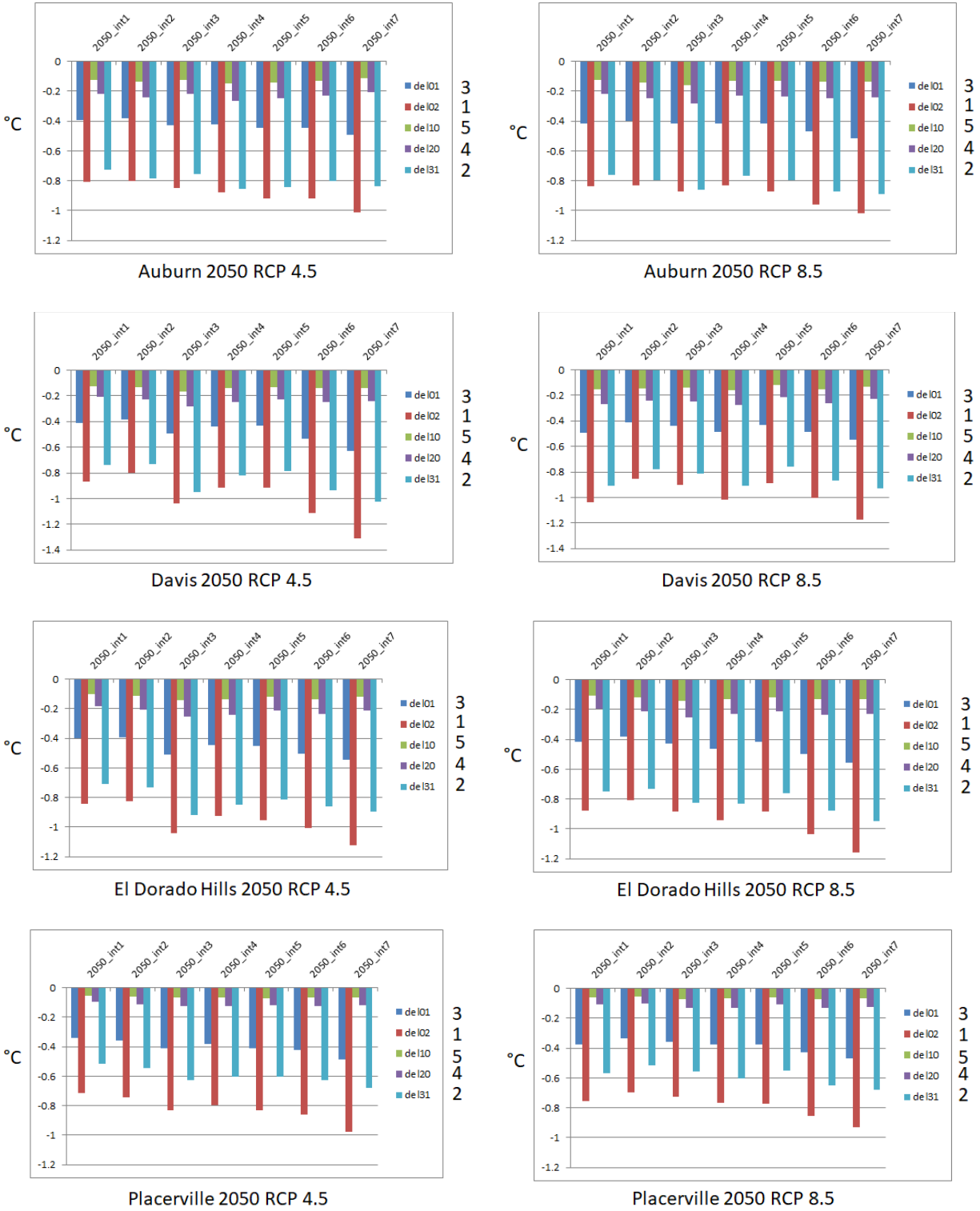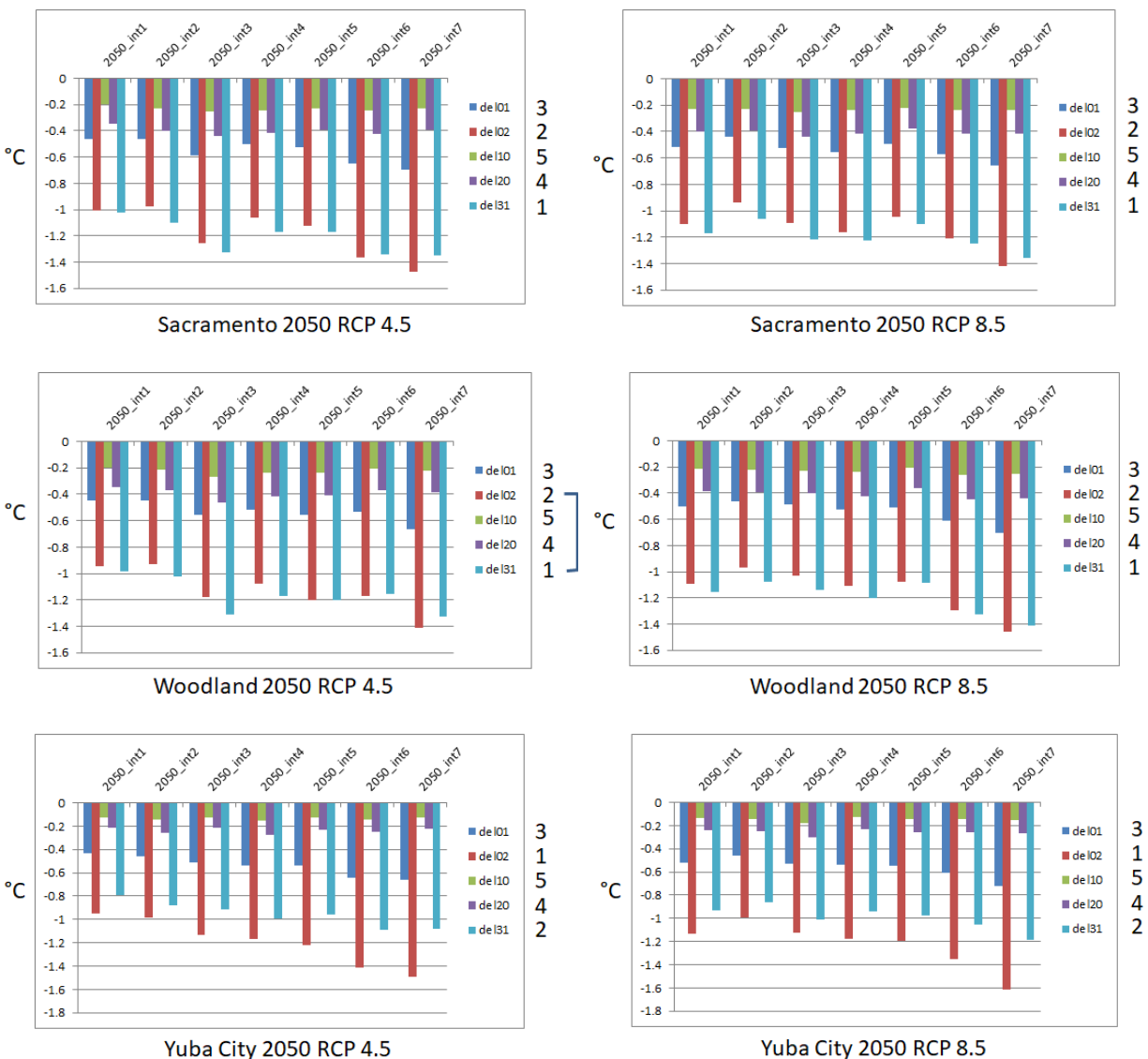
6.5.10 Impacts of smart growth on all-hours average temperature

Finally, the smart growth scenario was evaluated for the all-hours average impacts and compared against those of the BAU growth in year 2050. As before, the impacts are presented here only at those grid cells where urbanization was avoided. Figure 6-18 shows that except for Auburn and El Dorado Hills, there is less variation across the regions and a relatively similar avoided warming of between 1.2 and 1.6 °C. When averaged over sub-domains, the avoided warming is smaller, as discussed earlier.

Figure 6-18: Impacts of smart growth on all-hours average air temperature in 2050: Avoided warming (°C) at new urban locations for RCP 4.5 and 8.5.
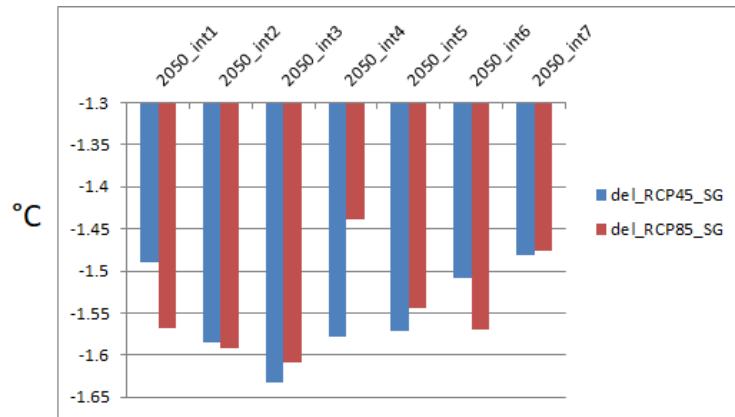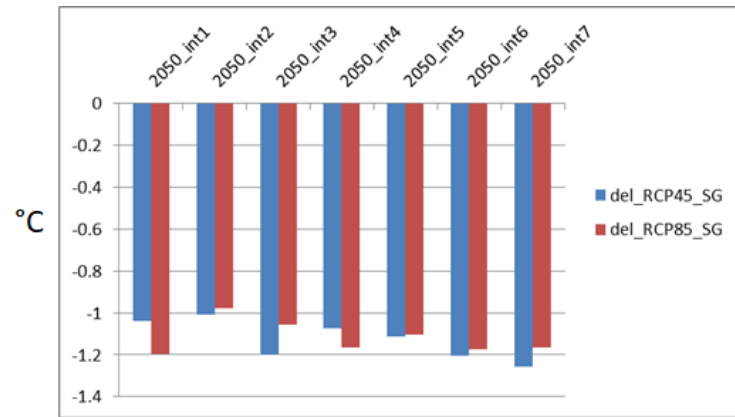
Auburn 2050 smart growth
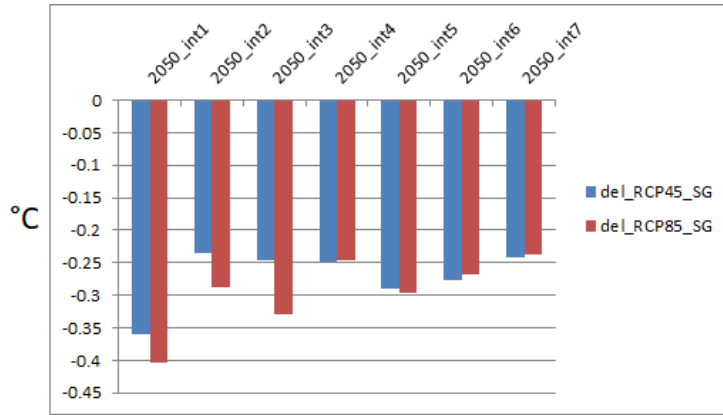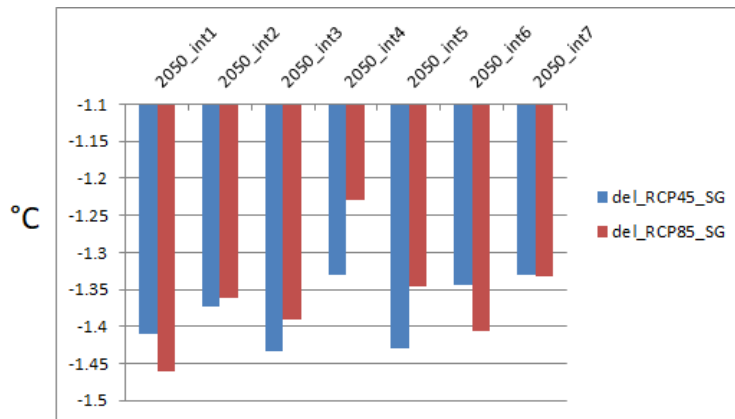

Davis 2050 smart growth

El Dorado Hills 2050 smart growth
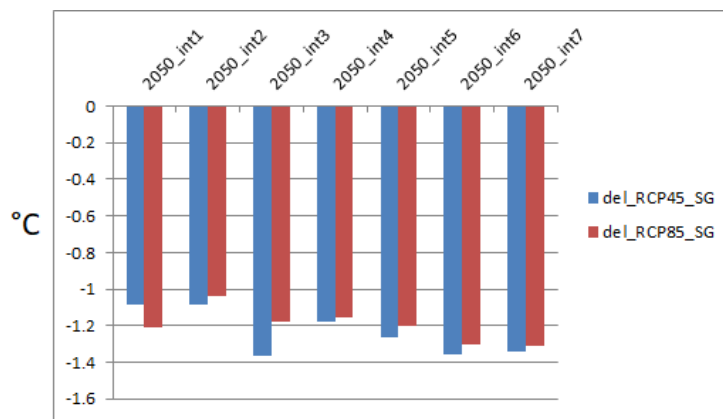
Sacramento 2050 smart growth
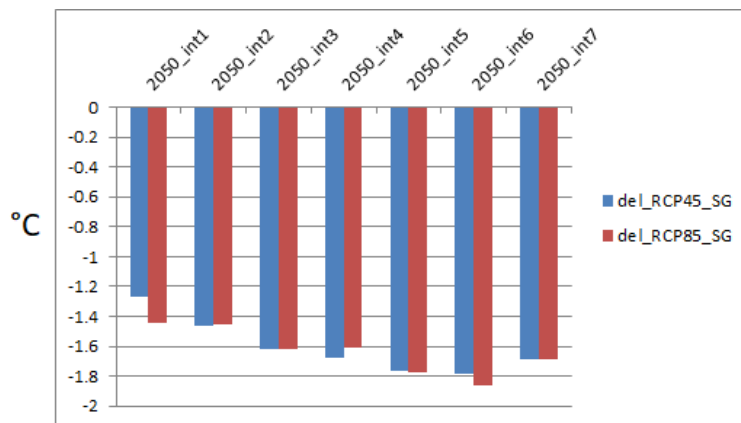
Yuba City 2050 smart growth

6.5.11 Summary of measures efficacies

Figure 6-19 summarizes the rankings of measures discussed above for 2050 RCP 4.5 and RCP 8.5 and provides a comparison with the efficacies under the current climate and land use. The chart is color-coded so that black is most effective measure (largest cooling) and near-white is smallest cooling effect. Note that these are impacts on air temperature, not the UHII. The following observations can be made:

1. For the 0600-PDT UHII:

   a. The rankings of mitigation measures (order) are similar and consistent across all regions.

   b. Within each region, the rankings are similar across current and future climates.

2. For the 1300-PDT UHII:

   a. The rankings are different across the regions.

Altostratus Inc.

b. In Davis and Sacramento, the rankings are different in future climate than they are in current climate.

3. For the 1400 – 2000 PDT UHII:

   a. The rankings are different across the regions.

   b. In Woodland, the rankings are different in future climate than they are in current climate.

4. For the 1500 PDT UHII:

   a. The rankings are different across the regions.

   b. In Auburn, Davis, El Dorado Hills, and Yuba City, the rankings are different in future climate than they are in current climate.

5. For the all-hours UHII:

   a. The rankings are different across the regions.

   b. Within each region, the rankings are similar across current and future climates.

This type of information may be useful to planners if they specifically target certain times of day, e.g., peak temperatures, or are interested in mitigating all-hour UHII averages. In Figure 6-19, the various time bands may be of interest yo different applications. For example, the 0600 PDT and allHRS bands could be of interest from a heat-wave perspective, the 1400-2000 PDT band may be of interest to utilities, the 1500-PDT band could be used in relation to peak cooling demand analysis, and the band at 1300 PDT may be of relevance to assessments of measures around solar noon.

Figure 6-19: Ranking of measures case01 through case31 at the regional scale.

6.6 IMPACTS OF CLIMATE AND LAND-USE CHANGES ON THE UHII

As demonstrated earlier and shown in Figures 6-6 and 6-7, for example, both climate and LULC changes have significant impacts on the temperature field. Here, we continue that discussion in some additional detail, by examining the impacts on the local all-hours UHII.

The characteristics of the future UHII are dictated mainly by two aspects: (1) in areas currently urbanized, the main impacts on the future temperature field and the UHII are those from local climate-change effects, whereas (2) in areas that will be urbanizing between now and 2050, the impacts on future air temperature result from changes in land use (urbanization) and changes in climate. In general, the UHII in 2050 RCP 8.5 is larger than in RCP 4.5, as one would like to expect – however, there are a couple of deviations from this tendency, as explained in this section.

The effects of (1) climate and (2) LULC changes can be seen, for example, in Figure 6-20, for the period July 16 – 31, 2050, RCP 8.5. The temperature equivalent of the changes in all-hour UHII in currently-urbanized areas in the metro Sacramento region (for that period) is a warming of 1.36 °C. On the other hand, for those urbanizing areas on the outskirts, the temperature equivalent is a warming of 2.77 °C, which is larger as it includes both effects from climate and LULC changes occurring between now and 2050.

Figure 6-20: Change in the all-hours UHII (°C) from 2015 to 2050 RCP 8.5. Example for July 16 – 31.
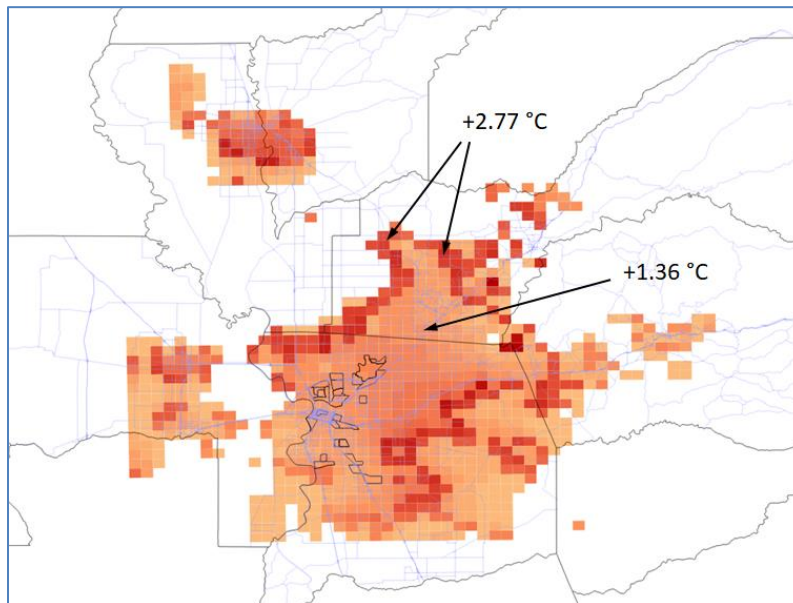
Table 6-1 provides a summary of the average all-hours UHII (averaged over all JJAS intervals 1 – 7, not just the sample period discussed above). It is noted from the table, and Figure 6-21, that the UHII is larger in 2050 RCP 4.5 than in current climates and is also larger in 2050 RCP 8.5 than it is in 2050 RCP 4.5, both of which are expected, except for domains D05 and D06. In these

domains, the UHII in the RCP 8.5 scenario is still larger than in the current climate but is slightly smaller than in RCP 4.5. The reason is that the non-urban areas surrounding Yuba City / Marysville (in D05) and Woodland (in D06) warm up faster (on the long run) than the urban areas. This might be the result of lower vegetation cover in the non-urban areas in these two regions (see discussion of vegetation cover in Section 2.3.2). Since the non-urban areas warm up slightly faster than the urban ones in this case, the UHII, by definition, becomes slightly smaller – despite the fact that the absolute urban temperatures are higher in RCP 8.5 than in RCP 4.5. This phenomenon was also discussed in Taha (2017) for various areas in California. Figure 6-21 summarizes these changes in the UHII from current climate to 2050.

Table 6-1. All-hours UHII and changes (temperature equivalent in °C) at each sub-region (derived from the 2-km level for locations of sub-regions where 500-m domains D05-D10).

Domain	Area	All-hours UHII (temperature equivalent °C)		
		2013-2016	2050 RCP 4.5	2050 RCP 8.5
D05	Yuba City / Marysville	2.41	2.96	2.64
D06	Woodland	2.14	2.80	2.57
D07	Sacramento AB617 A, B, D	4.48	5.00	5.13
D07	Sacramento AB617 C, E, G	2.33	2.67	2.99
D08	Granite Bay	5.07	5.55	5.72
D08	Roseville	5.83	6.42	6.63
D09	El Dorado Hills	4.91	5.02	5.22
D09	Folsom	4.86	5.46	5.62
D10	Placerville	1.36	1.59	1.60

Figure 6-21: Changes in the UHII from current climate and LULC to 2050.
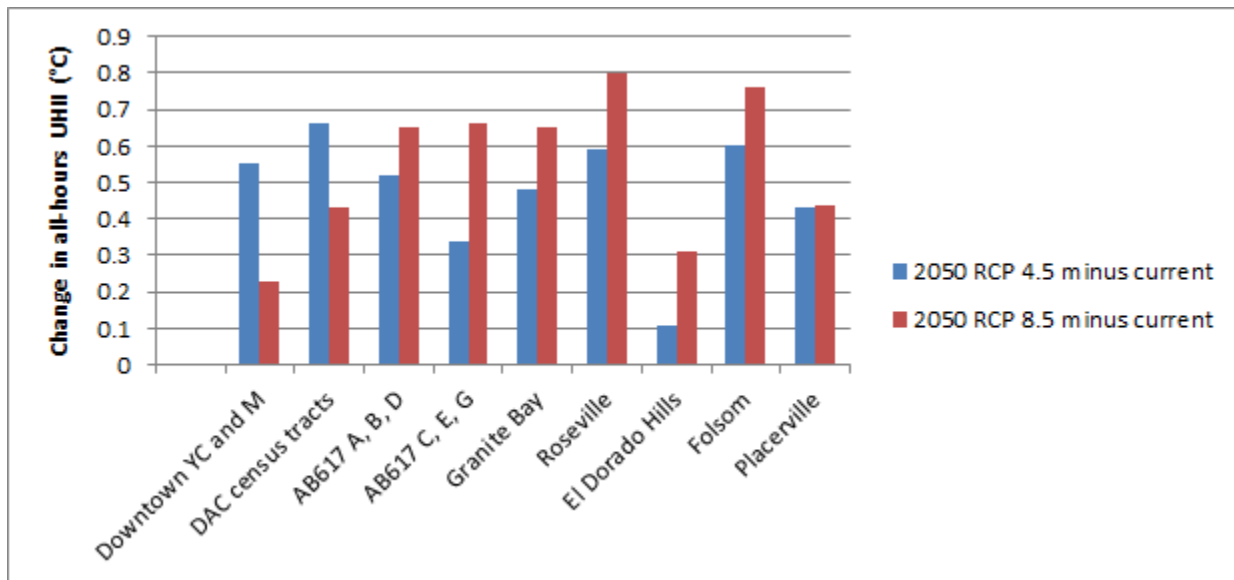
6.7 IMPACTS OF MITIGATION MEASURES ON THE 1300 PDT TEMPERATURE FIELD

As was done in Section 5.10, showing sample instantaneous effects of mitigation measures in current climate, a description of the spatial properties and distributions of the changes in the daytime UHII in 2050 as a result of heat-mitigation measures is provided in this section. Here, the instantaneous effects are presented, in Figure 6-22, for the random hour of 1300 PDT, July 27 or 28, of year 2050 (compared with the same dates in 2015, in Section 5.10, Figure 5-16).

Recall that this is the impact on the temperature field at sample hours (instantaneous impacts) not on the UHII per se or equivalent temperature. The scenarios (del##) presented in this figure were defined earlier in Section 5.5. The caption above each pair of graphs provides a description of the results and the potential cooling effects.

In general, the results show that the larger urban areas (i.e., total urbanization by 2050 relative to current) contribute to additional urban warming but at the same time provide increased technical potential, i.e., larger areas available for implementation of cooling measures – hence increased potential for cooling and canceling out the additional warming. A comparison between Figure 6-22 for 2050 (below) with Figure 5-16 (in Section 5.10 for current climate) shows a larger area affected by cooling in 2050 compared to 2013 – 2016.

Note that the cooling effect of vegetation canopy scenarios presented here is relatively the smallest (at the hour of 1300 PDT). It is shown here merely as an example to coincide with the same hour as the albedo effects shown in other figures but, as discussed earlier, the effects of urban greening are larger during later hours of the day and at night.

Figure 6-22: Example of instantaneous hourly impacts on temperature from mitigation measures at the 2-km level in the year 2050.

Case01. Left: 1300 PDT, July 27, 2050, RCP 4.5. Maximum cooling at this hour = 0.8 °C. Right: 1300 PDT, July 27, 2050, RCP 8.5. Maximum cooling at this hour = 0.9 °C.
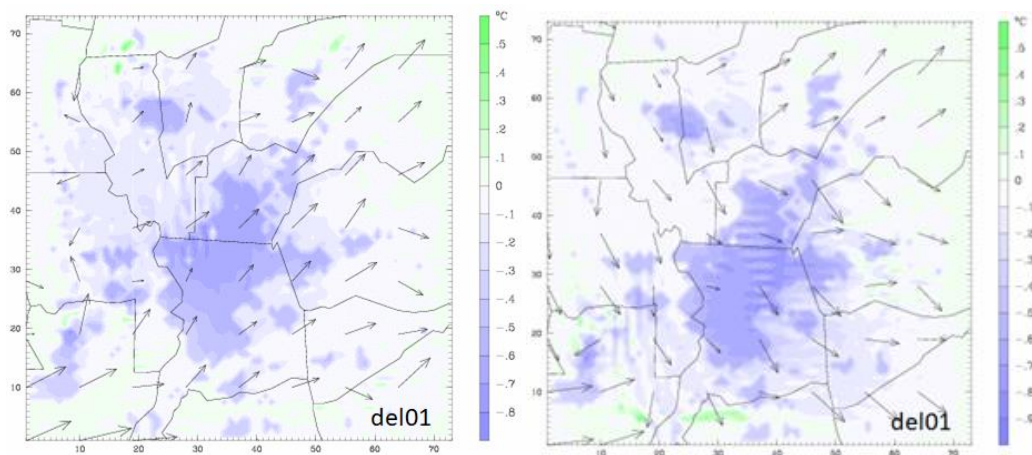
Case02. Left: 1300 PDT, July 27, 2050, RCP 4.5. Maximum cooling at this hour = 1.4 °C. Right: 1300 PDT, July 28, 2050, RCP 8.5. Maximum cooling at this hour = 1.6 °C.
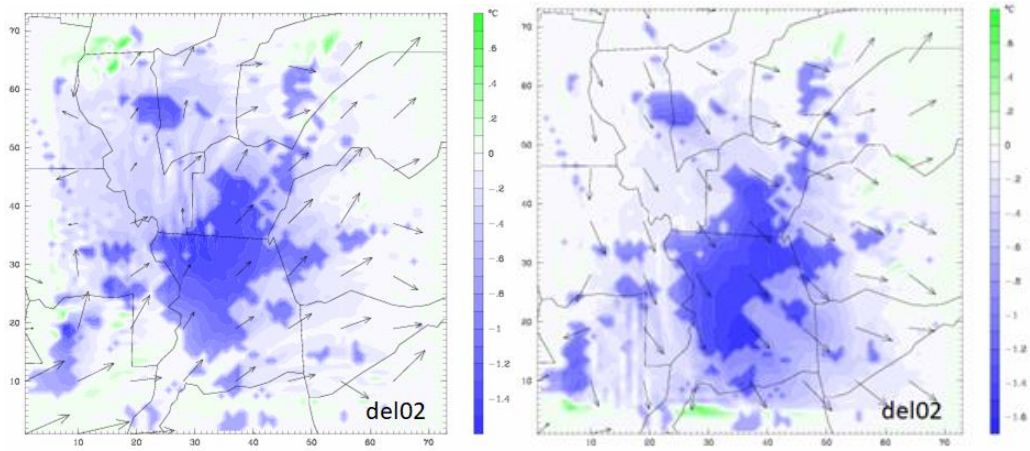
Case10. Left: 1300 PDT, July 27, 2050, RCP 4.5. Maximum cooling at this hour = 1.5 °C. Right: 1300 PDT, July 28, 2050, RCP 8.5. Maximum cooling at this hour = 1.3 °C.
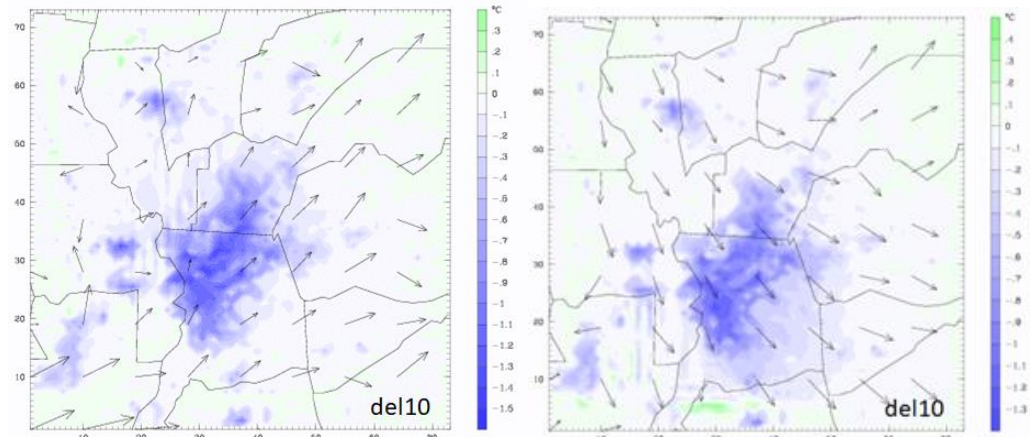
Case20. Left: 1300 PDT, July 27, 2050, RCP 4.5. Maximum cooling at this hour = 2.4 °C. Right: 1300 PDT, July 28, 2050, RCP 8.5. Maximum cooling at this hour = 2.2 °C.
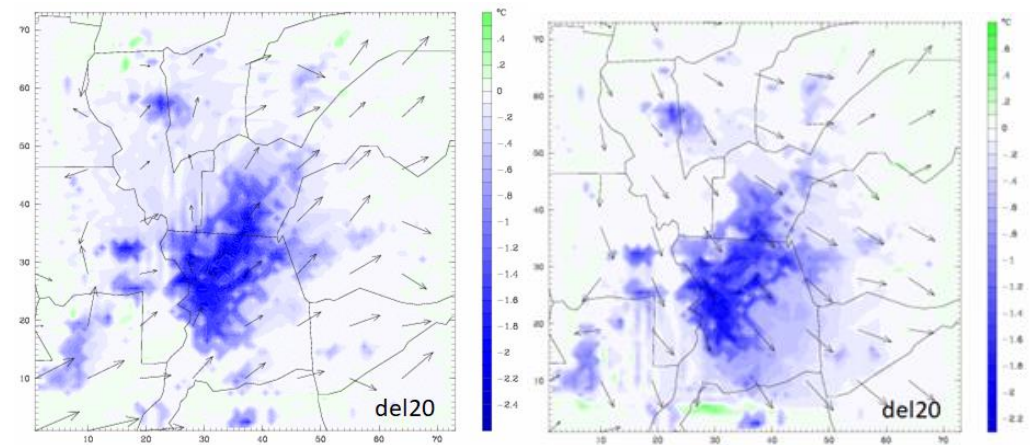
Case31. Left: 1300 PDT, July 27, 2050, RCP 4.5. Maximum cooling at this hour = 4.2 °C. Right: 1300 PDT, July 27, 2050, RCP 8.5. Maximum cooling at this hour = 4.2 °C.
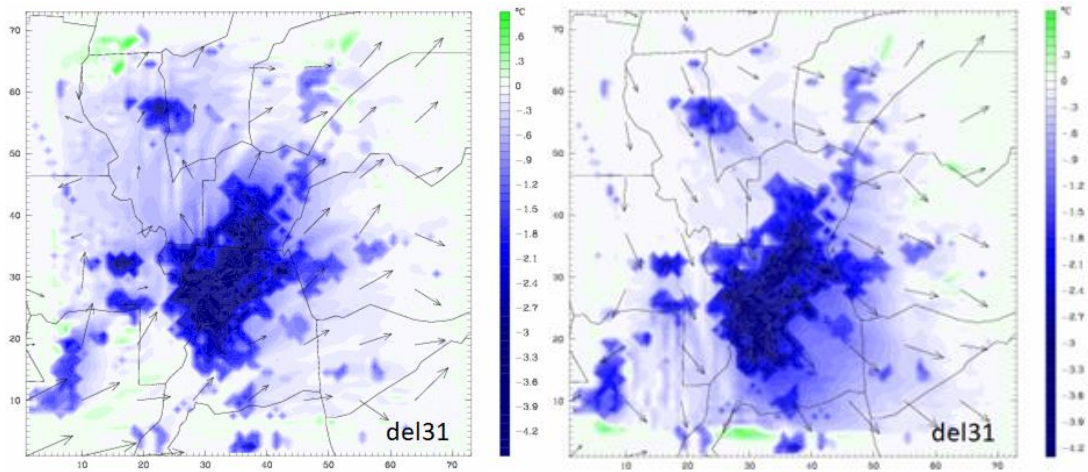
6.8 IMPACTS OF MITIGATION MEASURES ON THE UHI AND THE UHII IN FUTURE CLIMATE

6.8.1 Impact of mitigation measures on the 0600 PDT UHII in future climate

Figures 6-23 and 6-24 show the reductions (percentage-wise) in the 0600-PDT UHII averaged for all periods in 2050, for RCP 4.5 and RCP 8.5, respectively. Here, again, the caveat regarding case02 (as an extreme scenario) is to be born in mind.

The results show, in general, that the mitigation measures reduce the UHII in RCP 4.5 slightly more than in RCP 8.5 (because of the higher nighttime absolute temperatures in RCP 8.5 and the UHII definition as discussed earlier). The ranking of measures at the hour of 0600 PDT (including the extreme case02) is in the following order: 02, 31, 01, 20, and 10, in all sub-domains and in both RCP 4.5 and RCP 8.5. This ranking (order) of measures results from the larger nighttime effects of vegetation canopy cover relative to those from albedo modifications.

Figure 6-23: Impacts of mitigation measures on the 0600-PDT UHII in 2050 RCP 4.5. Vertical axis is percentage-wise reduction in the 0600-PDT UHII.

Figure 6-24: Impacts of mitigation measures on the 0600-PDT UHII in 2050 RCP 8.5. Vertical axis is percentage-wise reduction in the 0600-PDT UHII.

6.8.2 Impact of mitigation measures on the 1500 PDT UHII in future climate

Figures 6-25 and 6-26 summarize the reductions (percentage-wise) in the 1500-PDT UHII averaged for all periods in 2050, for RCP 4.5 and RCP 8.5, respectively.

The results from the 1500-PDT analysis show varying effects across scenarios and regions but also that, in general, the mitigation measures reduce the UHII in RCP 8.5 slightly more than in RCP 4.5 (which is the reverse of the effects during the hour at 0600 PDT). The ranking of measures at 1500 PDT (including the extreme case02) is in the following order: 31, 02, 20, then 10 and 01 tied, in all sub-domains and in both RCP 4.5 and RCP 8.5. This ranking (order) of measures is different from that at 0600-PDT (here the albedo measures are more effective) as this is for a daylight period.

Note that there is a single instance (anomaly) in Davis in RCP 4.5 where case10 causes a very small (1%) increase in the 1500-PDT UHII and a case in RCP 8.5 in Woodland where case01 has almost no effect on the UHII at this hour.

Figure 6-25: Impacts of mitigation measures on the 1500-PDT UHII in 2050 RCP 4.5. Vertical axis is percentage-wise reduction in the 1500-PDT UHII.

Figure 6-26: Impacts of mitigation measures on the 1500-PDT UHII in 2050 RCP 8.5. Vertical axis is percentage-wise reduction in the 1500-PDT UHII.
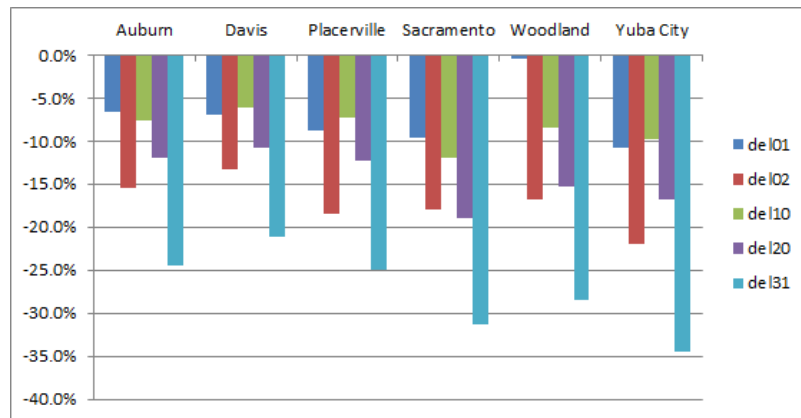
6.8.3 Impact of mitigation measures on the all-hours UHII in future climate

Finally, Figures 6-27 and 6-28 show the reductions (percentage-wise) in the all-hour UHII averaged for all periods in 2050, for RCP 4.5 and RCP 8.5, respectively.

The results indicate that the reductions are almost identical in RCP 4.5 and 8.5 (for each region) but that minor differences occur and that the reductions in RCP 8.5 are slightly smaller than those in RCP 4.5. The ranking of measures for the reduction in all-hours UHII (including extreme

case02) is in the following order: 02, 31, 01, 20, and 10, in all sub-domains and in both RCP 4.5 and RCP 8.5. This order of measures is influenced by the effects of vegetation canopy cover, including the nighttime effect.

Figure 6-27: Impacts of mitigation measures on the all-hours UHII in 2050 RCP 4.5. Vertical axis is percentage-wise reduction in the all-hours UHII.
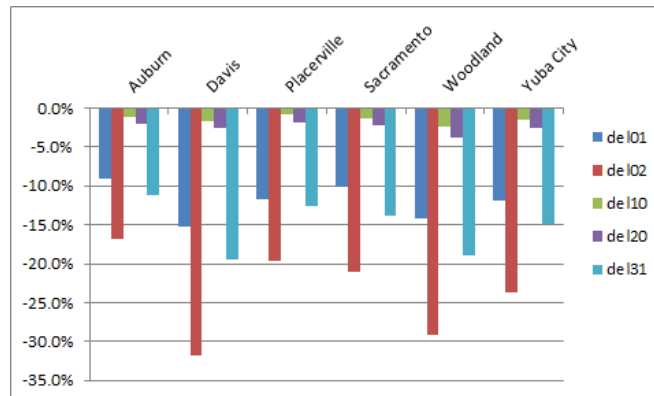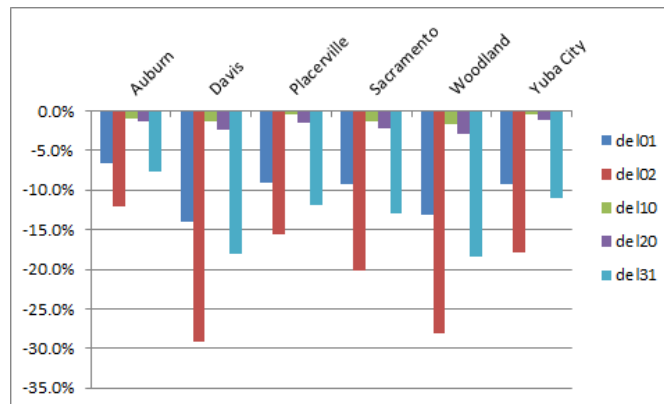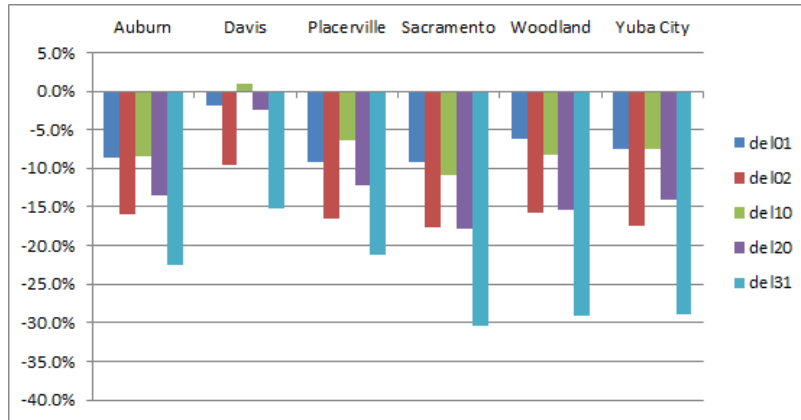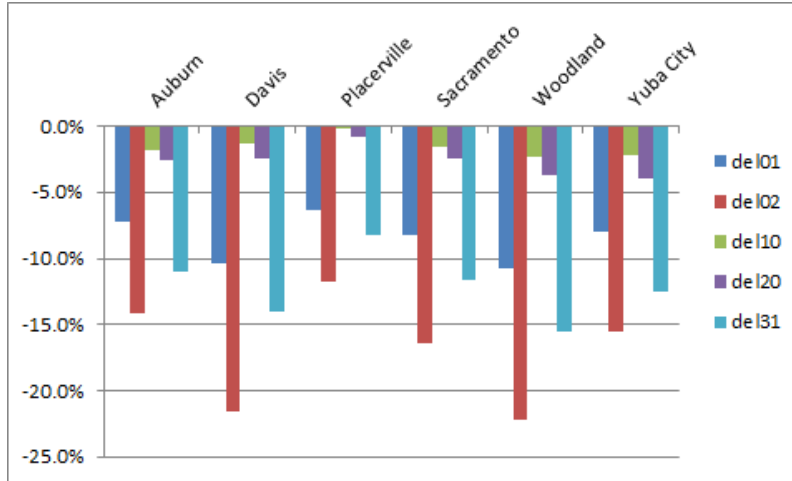

Figure 6-28: Impacts of mitigation measures on the all-hours UHII in 2050 RCP 8.5. Vertical axis is percentage-wise reduction in the all-hours UHII.
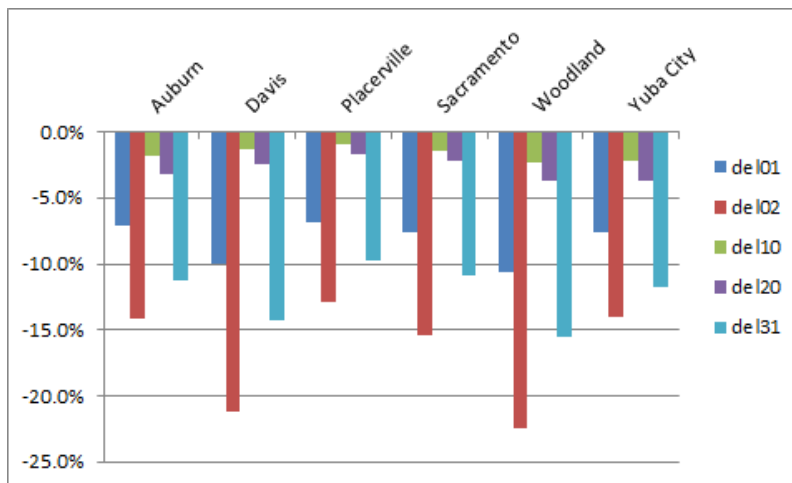
6.9 CHANGES IN THE NATIONAL WEATHER SERVICE HEAT INDEX (NWS HI) LEVELS IN FUTURE CLIMATE

Changes in the NWS HI warning levels resulting from changes in climate and urbanization, and the impacts of mitigation measures on the HI, were evaluated at the same probing locations defined in Section 5.15 (Figure 5-37). The analysis was carried out for all hours and ranges of hours. In this section, examples are provided for changes at 1700 PDT, i.e., averaged over all 1700 PDT hours in the period JJAS of 2050 for RCP 4.5 and RCP 8.5 for case00 and case31. The future-year NWS HI and its changes were also compared to the corresponding values in current climate (2013 – 2016) as seen in Figure 6-29 and Table 6-2, where the percentages of reductions in exceedances above specified NWS HI levels are given relative to thresholds "Danger", "Extreme caution", and "Caution".

Another goal of this analysis was to quantify the potential of heat-mitigation measures in "shifting down" the NWS HI from one warning level to a lower one, as was discussed in Section 5.15 for current climate. Several metrics are presented below that provide an assessment of these potential effects – some are specific to certain time intervals, others are more general indicators of averages.

In summary, it can be seen that the heat-mitigation measures can (1) shift down the NWS HI from one warning level to a lower one and (2) can offset the local-warming effects of urbanization and climate changes on the HI at all hours (compare the blue and red time series in Figure 6-29).

Figure 6-29: NWS HI and changes resulting from urban-cooling measures (case31) for the hour at 1700 PDT, year 2050, JJAS for RCP 4.5 and RCP 8.5.

RCP 4.5   RCP 8.5

At probing station P0004 in AB617 community

RCP 4.5   RCP 8.5

At probing station P0008 in AB617 community

RCP 4.5   RCP 8.5

At probing station P0011 in AB617 community

RCP 4.5   RCP 8.5

At probing station P0013 in Citrus Heights

RCP 4.5   RCP 8.5

At probing station P0014 in Roseville

RCP 4.5   RCP 8.5

At probing station P0018 in Lincoln

RCP 4.5   RCP 8.5

At probing station P0020 in El Dorado Hills

RCP 4.5   RCP 8.5

At probing station P0022 in Placerville

RCP 4.5   RCP 8.5

At probing station P0026 in Woodland

RCP 4.5

RCP 8.5

At probing station P0028 in Davis

Legend: HI_1700PDT_00, HI_1700PDT_31

RCP 4.5

RCP 8.5

At probing station P0029 in Marysville

Legend: HI_1700PDT_00, HI_1700PDT_31

RCP 4.5

RCP 8.5

At probing station P0032 in Yuba City

Legend: HI_1700PDT_00, HI_1700PDT_31

Altostratus Inc.

Table 6-2: NWS HI and changes resulting from UHI-mitigation measures (case31) at hours 1700 PDT, year 2050, JJAS for RCP 4.5 and RCP 8.5. Current-climate NWS HI and changes are also provided for comparison.

P0001 AB617

NWS HI values at **1700 PDT** and exceedances above thresholds

P0001 AB617	Percent of DH (out of total) above threshold		
NWS HI thresholds	2013-2016	2050 RCP 4.5	2050 RCP 8.5
> 80 °F (caution)	93.0%	94.3%	93.5%
> 91 °F (extreme caution)	45.6%	49.8%	51.2%
> 106 °F (danger)	0.9%	6.8%	8.1%

Changes (reductions) in exceedances after deployment of case31

P0001 AB617	Decrease in exceedance following case31		
NWS HI thresholds	2013-2016	2050 RCP 4.5	2050 RCP 8.5
> 80 °F (caution)	-5.8%	-4.7%	-7.6%
> 91 °F (extreme caution)	-31.9%	-20.2%	-23.4%
> 106 °F (danger)	-66.2%	-83.6%	-57.7%

P0004 AB617

NWS HI values at **1700 PDT** and exceedances above thresholds

P0004 AB617	Percent of DH (out of total) above threshold		
NWS HI thresholds	2013-2016	2050 RCP 4.5	2050 RCP 8.5
> 80 °F (caution)	92.8%	94.3%	92.7%
> 91 °F (extreme caution)	43.5%	48.9%	49.4%
> 106 °F (danger)	0.6%	5.7%	8.1%

Changes (reductions) in exceedances after deployment of case31

P0004 AB617	Decrease in exceedance following case31		
NWS HI thresholds	2013-2016	2050 RCP 4.5	2050 RCP 8.5
> 80 °F (caution)	-5.0%	-5.2%	-7.1%
> 91 °F (extreme caution)	-28.6%	-22.3%	-27.8%
> 106 °F (danger)	-49.7%	-80.4%	-57.8%

Altostratus Inc.

Table 6-2, continued.

P0008 AB617

NWS HI values at **1700 PDT** and exceedances above thresholds

P0008 AB617	Percent of DH (out of total) above threshold		
NWS HI thresholds	2013-2016	2050 RCP 4.5	2050 RCP 8.5
> 80 °F (caution)	90.6%	92.6%	90.1%
> 91 °F (extreme caution)	36.0%	43.2%	43.6%
> 106 °F (danger)	0.3%	4.6%	9.2%

Changes (reductions) in exceedances after deployment of case31

P0008 AB617	Decrease in exceedance following case31		
NWS HI thresholds	2013-2016	2050 RCP 4.5	2050 RCP 8.5
> 80 °F (caution)	-5.2%	-9.6%	-4.1%
> 91 °F (extreme caution)	-30.5%	-13.8%	-33.2%
> 106 °F (danger)	-100.0%	-100.0%	-100.0%

P0011 AB617

NWS HI values at **1700 PDT** and exceedances above thresholds

P0011 AB617	Percent of DH (out of total) above threshold		
NWS HI thresholds	2013-2016	2050 RCP 4.5	2050 RCP 8.5
> 80 °F (caution)	90.1%	90.8%	89.2%
> 91 °F (extreme caution)	32.1%	40.2%	39.8%
> 106 °F (danger)	0%	3.5%	8.1%

Changes (reductions) in exceedances after deployment of case31

P0011 AB617	Decrease in exceedance following case31		
NWS HI thresholds	2013-2016	2050 RCP 4.5	2050 RCP 8.5
> 80 °F (caution)	-9.4%	-7.7%	-4.1%
> 91 °F (extreme caution)	-28.0%	-9.7%	-29.2%
> 106 °F (danger)	N/A	-100.0%	100.0%

Table 6-2, continued.

P0013 Citrus Heights

NWS HI values at **1700 PDT** and exceedances above thresholds

P0013 Citrus Heights	Percent of DH (out of total) above threshold		
NWS HI thresholds	2013-2016	2050 RCP 4.5	2050 RCP 8.5
> 80 °F (caution)	92.3%	94.3%	93.5%
> 91 °F (extreme caution)	44.8%	47.7%	51.2%
> 106 °F (danger)	1.4%	6.8%	7.1%

Changes (reductions) in exceedances after deployment of case31

P0013 Citrus Heights	Decrease in exceedance following case31		
NWS HI thresholds	2013-2016	2050 RCP 4.5	2050 RCP 8.5
> 80 °F (caution)	-4.9%	-3.9%	-8.6%
> 91 °F (extreme caution)	-33.5%	-21.0%	-25.4%
> 106 °F (danger)	-79.8%	-100.0%	-50.9%

P0014 Roseville

NWS HI values at **1700 PDT** and exceedances above thresholds

P0014 Roseville	Percent of DH (out of total) above threshold		
NWS HI thresholds	2013-2016	2050 RCP 4.5	2050 RCP 8.5
> 80 °F (caution)	93.4%	94.3%	95.2%
> 91 °F (extreme caution)	47.7%	49.6%	52.2%
> 106 °F (danger)	1.7%	7.9%	7.1%

Changes (reductions) in exceedances after deployment of case31

P0014 Roseville	Decrease in exceedance following case31		
NWS HI thresholds	2013-2016	2050 RCP 4.5	2050 RCP 8.5
> 80 °F (caution)	-6.1%	-4.1%	-8.7%
> 91 °F (extreme caution)	-36.2%	-20.3%	-23.4%
> 106 °F (danger)	-83.2%	-100.0%	-51.1%

Table 6-2, continued.

P0018 Lincoln

NWS HI values at **1700 PDT** and exceedances above thresholds

P0018 Lincoln	Percent of DH (out of total) above threshold		
NWS HI thresholds	2013-2016	2050 RCP 4.5	2050 RCP 8.5
> 80 °F (caution)	93.9%	95.1%	95.2%
> 91 °F (extreme caution)	52.7%	48.4%	52.1%
> 106 °F (danger)	2.0%	4.5%	6.1%

Changes (reductions) in exceedances after deployment of case31

P0018 Lincoln	Decrease in exceedance following case31		
NWS HI thresholds	2013-2016	2050 RCP 4.5	2050 RCP 8.5
> 80 °F (caution)	-4.7%	-2.9%	-5.8%
> 91 °F (extreme caution)	-27.0%	-15.8%	-15.0%
> 106 °F (danger)	-85.5%	-75.3%	-40.2%

P0020 El Dorado Hills

NWS HI values at **1700 PDT** and exceedances above thresholds

P0020 El Dorado Hills	Percent of DH (out of total) above threshold		
NWS HI thresholds	2013-2016	2050 RCP 4.5	2050 RCP 8.5
> 80 °F (caution)	89.0%	93.4%	90.9%
> 91 °F (extreme caution)	29.3%	37.8%	38.5%
> 106 °F (danger)	0.3%	1.1%	3.7%

Changes (reductions) in exceedances after deployment of case31

P0020 El Dorado Hills	Decrease in exceedance following case31		
NWS HI thresholds	2013-2016	2050 RCP 4.5	2050 RCP 8.5
> 80 °F (caution)	-4.8%	-8.5%	-7.1%
> 91 °F (extreme caution)	-31.9%	-12.8%	-30.2%
> 106 °F (danger)	-100.0%	-100.0%	-35.6%

Table 6-2, continued.

P0022 Placerville

NWS HI values at **1700 PDT** and exceedances above thresholds

P0022 Placerville	Percent of DH (out of total) above threshold		
NWS HI thresholds	2013-2016	2050 RCP 4.5	2050 RCP 8.5
> 80 °F (caution)	71.3%	68.2%	80.0%
> 91 °F (extreme caution)	10.4%	16.0%	12.2%
> 106 °F (danger)	0%	0%	1.2%

Changes (reductions) in exceedances after deployment of case31

P0022 Placerville	Decrease in exceedance following case31		
NWS HI thresholds	2013-2016	2050 RCP 4.5	2050 RCP 8.5
> 80 °F (caution)	-4.8%	-10.6%	-5.8%
> 91 °F (extreme caution)	-23.3%	-40.0%	-10.2%
> 106 °F (danger)	N/A	N/A	-100.0%

P0026 Woodland

NWS HI values at **1700 PDT** and exceedances above thresholds

P0026 Woodland	Percent of DH (out of total) above threshold		
NWS HI thresholds	2013-2016	2050 RCP 4.5	2050 RCP 8.5
> 80 °F (caution)	94.1%	94.3%	94.4%
> 91 °F (extreme caution)	48.7%	48.7%	52.1%
> 106 °F (danger)	1.4%	5.6%	5.9%

Changes (reductions) in exceedances after deployment of case31

P0026 Woodland	Decrease in exceedance following case31		
NWS HI thresholds	2013-2016	2050 RCP 4.5	2050 RCP 8.5
> 80 °F (caution)	-4.2%	-2.9%	-4.9%
> 91 °F (extreme caution)	-22.3%	-13.9%	-16.7%
> 106 °F (danger)	-79.7%	-80.0%	-40.3%

Altostratus Inc.

Table 6-2, continued.

P0028 Davis

NWS HI values at **1700 PDT** and exceedances above thresholds

P0028 Davis	Percent of DH (out of total) above threshold		
NWS HI thresholds	2013-2016	2050 RCP 4.5	2050 RCP 8.5
> 80 °F (caution)	92.1%	91.8%	91.8%
> 91 °F (extreme caution)	38.2%	46.1%	48.4%
> 106 °F (danger)	0.3%	4.7%	8.0%

Changes (reductions) in exceedances after deployment of case31

P0028 Davis	Decrease in exceedance following case31		
NWS HI thresholds	2013-2016	2050 RCP 4.5	2050 RCP 8.5
> 80 °F (caution)	-4.8%	-7.4%	-5.6%
> 91 °F (extreme caution)	-18.7%	-18.8%	-29.7%
> 106 °F (danger)	-1.1%	-27.0%	-43.8%

P0029 Marysville

NWS HI values at **1700 PDT** and exceedances above thresholds

P0029 Marysville	Percent of DH (out of total) above threshold		
NWS HI thresholds	2013-2016	2050 RCP 4.5	2050 RCP 8.5
> 80 °F (caution)	94.6%	95.1%	93.5%
> 91 °F (extreme caution)	61.0%	47.3%	51.0%
> 106 °F (danger)	3.4%	1.1%	5.0%

Changes (reductions) in exceedances after deployment of case31

P0029 Marysville	Decrease in exceedance following case31		
NWS HI thresholds	2013-2016	2050 RCP 4.5	2050 RCP 8.5
> 80 °F (caution)	-2.6%	-2.6%	-2.0%
> 91 °F (extreme caution)	-22.1%	-17.9%	-20.5%
> 106 °F (danger)	-58.7%	-100.0%	-26.1%

Table 6-2, continued.

P0032 Yuba City
NWS HI values at **1700 PDT** and exceedances above thresholds

P0032 Yuba City	Percent of DH (out of total) above threshold		
NWS HI thresholds	2013-2016	2050 RCP 4.5	2050 RCP 8.5
> 80 °F (caution)	94.8%	95.9%	93.5%
> 91 °F (extreme caution)	62.5%	49.2%	53.0%
> 106 °F (danger)	3.4%	1.1%	6.1%

Changes (reductions) in exceedances after deployment of case31

| P0032 Yuba CIty	Decrease in exceedance following case31		
NWS HI thresholds	2013-2016	2050 RCP 4.5	2050 RCP 8.5
> 80 °F (caution)	-3.5%	-4.0%	-3.4%
> 91 °F (extreme caution)	-29.5%	-21.5%	-22.1%
> 106 °F (danger)	-75.2%	-100.0%	-40.0%

6.10 IMPACTS OF MITIGATION MEASURES ON THE UHII EXCEEDANCES RELATIVE TO A SPECIFIED TEMPERATURE THRESHOLD IN FUTURE CLIMATE

Figure 6-30 summarizes the percentage-wise reductions in the UHII (DH exceedances) relative to a specified temperature threshold of 35 °C (95 °F) which is a threshold commonly used by the electric utilities in calculating summertime cooling loads. This is shown in the figure for year 2050 and both RCP 4.5 and RCP 8.5.

The most effective measure at reducing the UHII above 35 °C is case31 (even if the extreme case02 is included in the analysis), followed by case02, then albedo (case20) and vegetation-canopy cover (case01) with relatively similar effects overall, and finally case10 (albedo). This order is seen across all regions and in both RCP 4.5 and RCP 8.5. The reductions are slightly larger in RCP 8.5 than in RCP 4.5 (as explained in the following section). The largest reductions (percentage-wise) are seen in Placerville because this area has only small UHII exceedances in the first place. It is important to reiterate again that the changes discussed in this section are changes in UHII not in absolute temperature.

Figure 6-30: Changes (percentage-wise) of the UHII exceedance above 35 C.

RCP 4.5
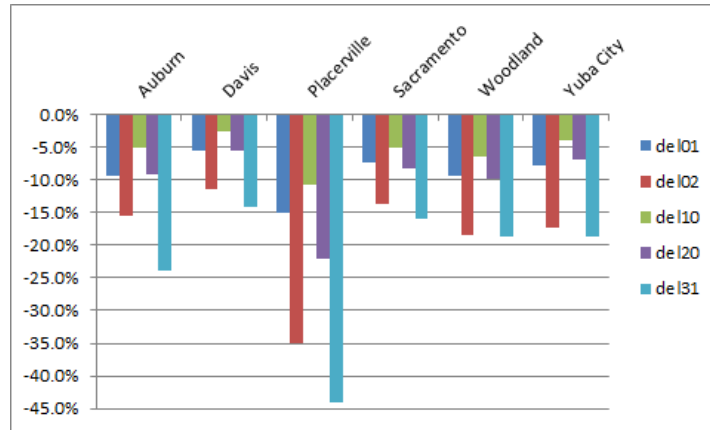
RCP 8.5
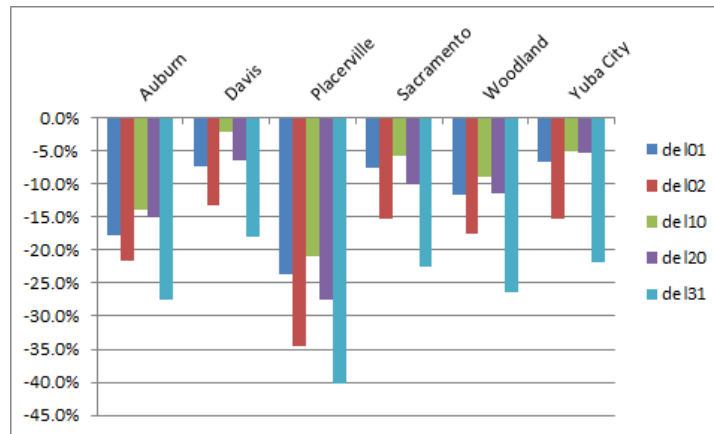
6.11 IMPACTS OF MITIGATION MEASURES ON TEMPERATURE EXCEEDANCES (DH) RELATIVE TO SPECIFIED THRESHOLDS IN FUTURE CLIMATE

In this section, the changes in temperature, e.g., cumulative DH, above certain thresholds, 35 and 38 °C, are discussed. It is noted here, again, that this analysis of temperature (DH) versus thresholds is different from a similar analysis of DH in terms of the NWS HI (discussed earlier, in Section 6.9) in that the NWS HI also includes humidity in the calculations whereas the analysis in this section is based only on dry-bulb temperature. This was also discussed in Section 5.14.

35 °C threshold

Figure 6-31 shows the percentage-wise changes in degree-hour (°C·hr) exceedances above 35 °C in sub-domains of interest, for all modeled time intervals (JJAS 2050), and for RCP 4.5 and RCP 8.5. For each time interval, the changes are presented for five scenarios or measures as an indication to their mitigation potentials relative to a corresponding base scenario. As before, the caveat related to case02 (as an extreme measure) should be reiterated.

Figure 6-31 shows that there is significant variation in the reduction of exceedances across different time intervals within each domain and variations from RCP 4.5 to RCP 8.5 within each region. There are also several cases (in different areas) where no exceedances occur above 35 °C in RCP 4.5 but significant exceedances are seen in RCP 8.5. As a result, the figures may be misleading in suggesting larger reductions in RCP 8.5 when there are none in RCP 4.5 (because there are no exceedances in RCP 4.5 to begin with).

The ranking (order) of measures in terms of effectiveness is as follows (applies to both RCP 4.5 and 8.5): in Auburn: 31, 02, 20, 01, 10; in Davis: 31, 02, 20, and 01/10 tied; in El Dorado Hills: 31, 02, 20, 01, 10; in Placerville: 31, 02, 20/01 tied, and 10; in Sacramento: 31, 02, 20, 01/10 tied; in Woodland: 31, 02/20 tied, 01/10 tied; and in Yuba City: 31, 02, 20/01 tied, then 10.

Figure 6-31: Changes in degree-hours above 35 °C
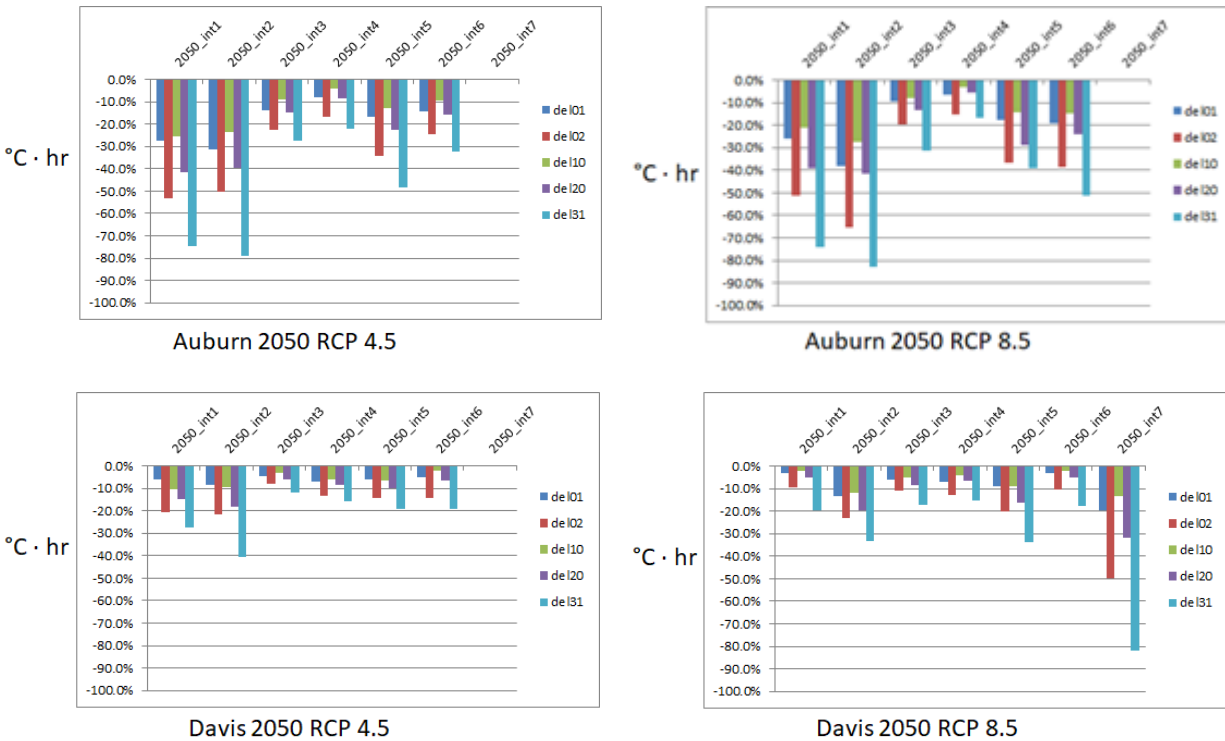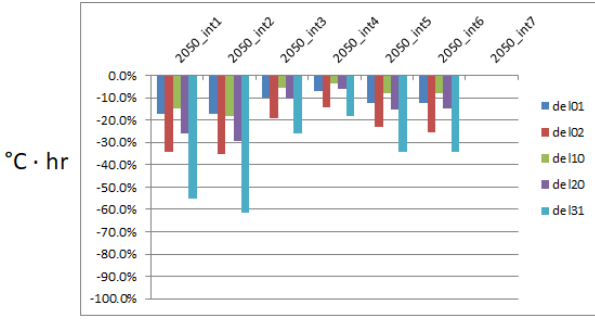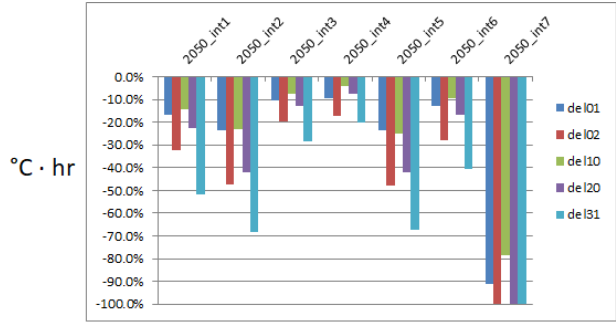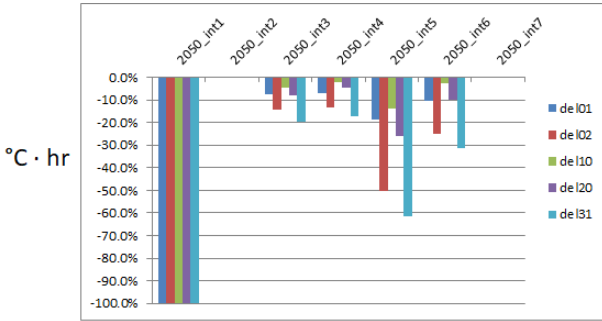
Figure 6-31, continued.

El Dorado Hills 2050 RCP 4.5

El Dorado Hills 2050 RCP 8.5

Placerville 2050 RCP 4.5

Placerville 2050 RCP 8.5

Sacramento 2050 RCP 4.5

Sacramento 2050 RCP 8.5

Woodland 2050 RCP 4.5

Woodland 2050 RCP 8.5

Yuba City 2050 RCP 4.5

Yuba City 2050 RCP 8.5
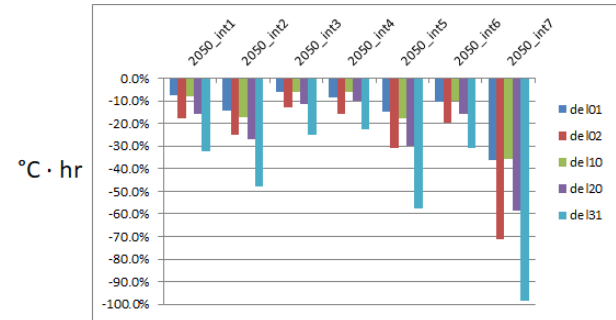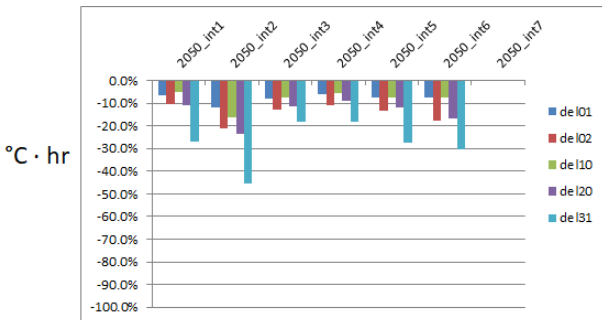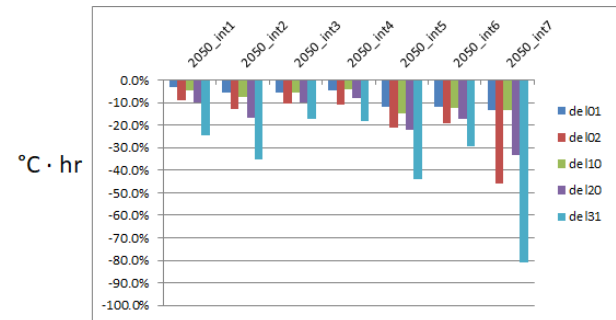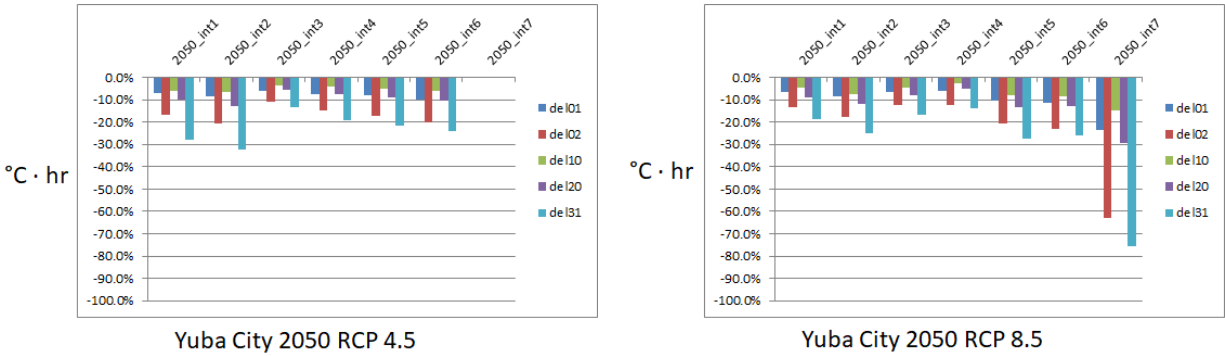
38 °C threshold

The threshold of 38 °C is of interest to utilities in the region (SMUD) in planning for electric demand. The percentage-wise reductions in exceedances above 38 °C are smaller than the corresponding reductions over 35 °C, or non-existent in some cases, since there are fewer exceedances over 38 than over 35 °C to begin with (compare Figure 6-32 to Figure 6-31).

Figure 6-32 shows the changes (percentage-wise) in degree-hour (°C·hr) exceedances above 38 °C in sub-domains of interest, for all modeled time intervals (JJAS 2050), and for both RCP 4.5 and RCP 8.5. As with the 35 °C threshold, the changes are presented for five scenarios or measures to characterize their mitigation potentials relative to a corresponding base scenario.

The ranking (order) of measures in terms of effectiveness is slightly different from that for the 35 °C threshold, and is as follows (applies to both RCP 4.5 and RCP 8.5): in Auburn: 31, 02, 20, 01, 10; in Davis: 31, 02, 20, and 01/10 tied; in El Dorado Hills: 31, 02, 20, 01, 10; in Placerville: 31, 02, 20, 01, 10; in Sacramento: 31, 02/20 tied, 01/10 tied; in Woodland: 31, 20, 02, 10, 01; and in Yuba City: 31, 02, 20, 01, 10.

Figure 6-32: Changes in degree-hours above 38 °C
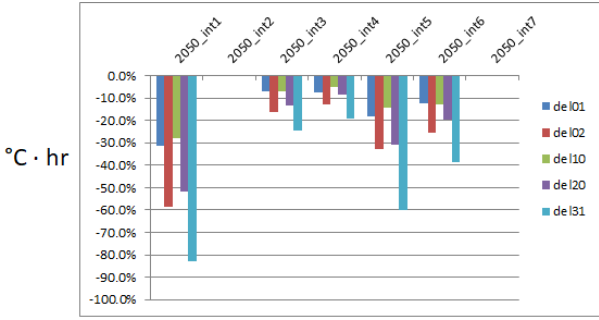
Auburn 2050 RCP 4.5

Auburn 2050 RCP 8.5

Figure 6-32, continued.
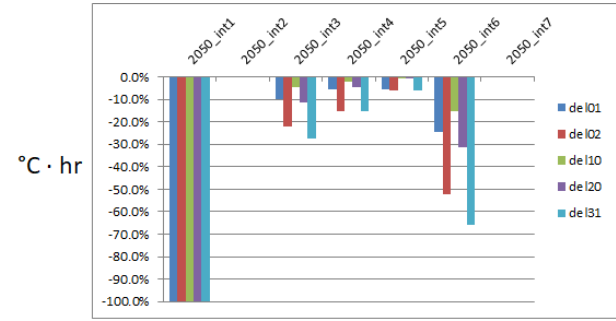

Davis 2050 RCP 4.5
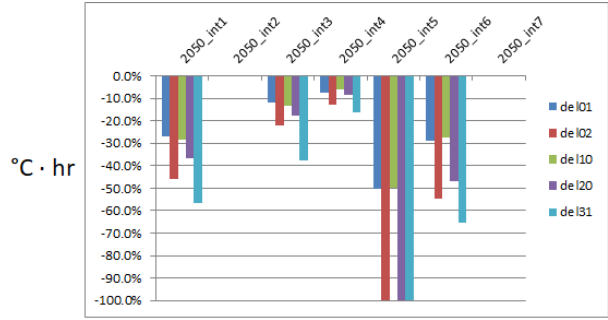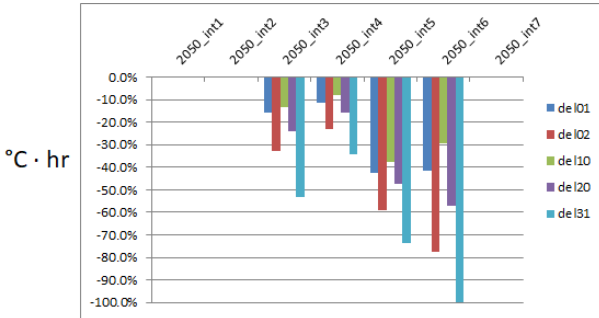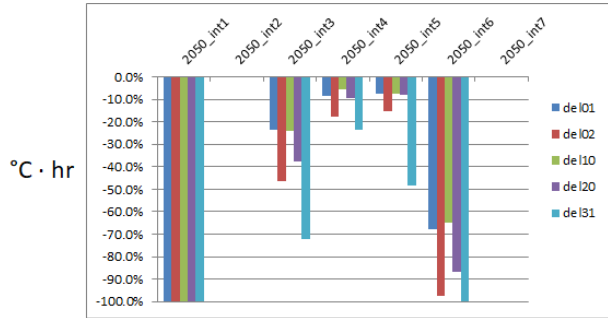
Davis 2050 RCP 8.5

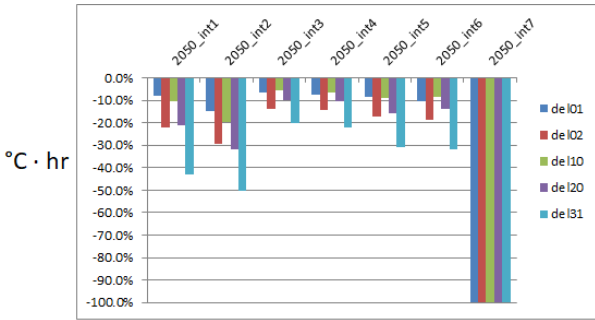El Dorado Hills 2050 RCP 4.5

El Dorado Hills 2050 RCP 8.5

Placerville 2050 RCP 4.5

Placerville 2050 RCP 8.5

Sacramento 2050 RCP 4.5

Sacramento 2050 RCP 8.5

Figure 6-32, continued.

Woodland 2050 RCP 4.5

Woodland 2050 RCP 8.5

Yuba City 2050 RCP 4.5

Yuba City 2050 RCP 8.5
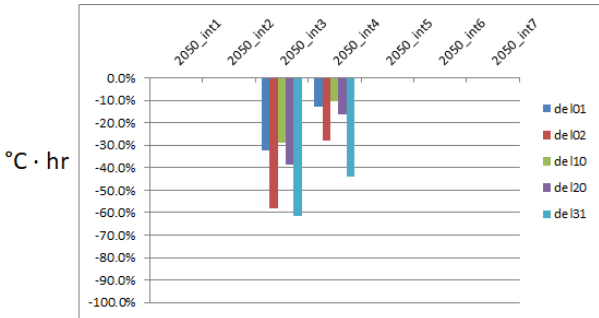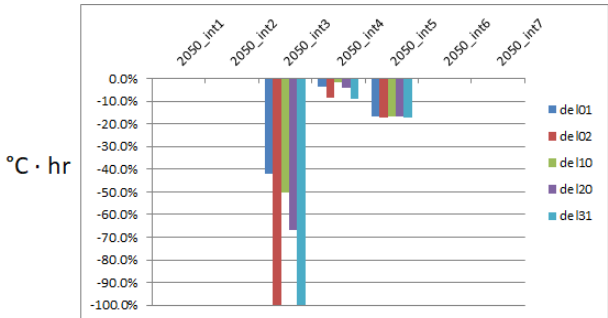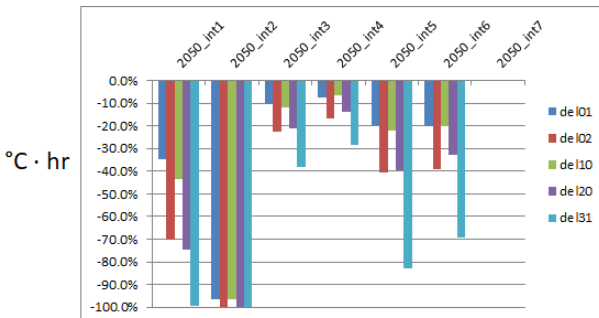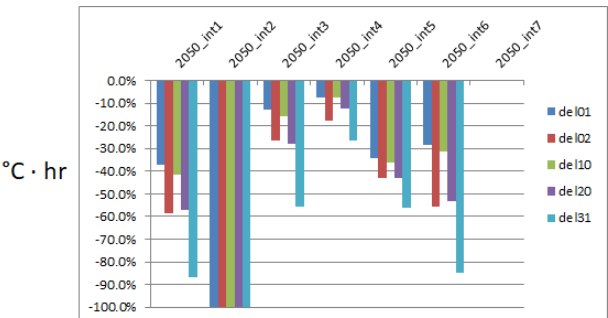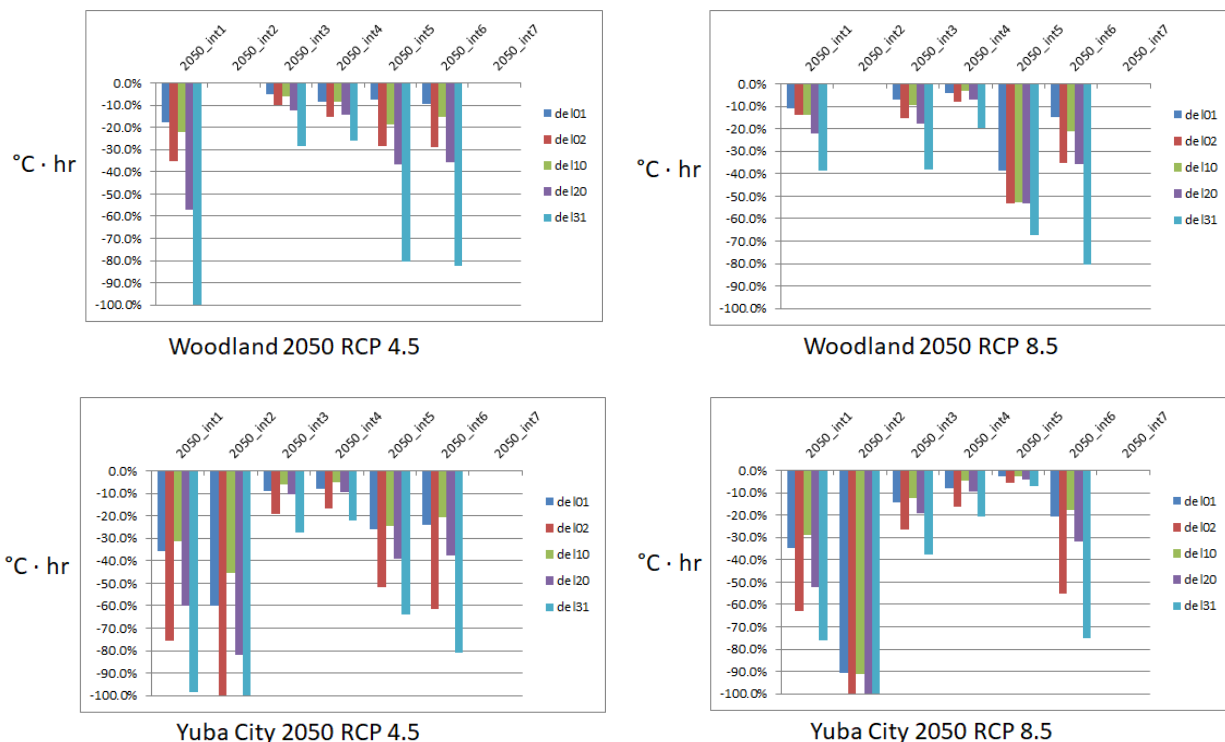
6.12 IMPACTS OF SMART GROWTH ON TEMPERATURE EXCEEDANCES RELATIVE TO SPECIFIED THRESHOLDS.

The 2050 smart growth scenario defined earlier (in Section 6.4) was evaluated for impacts on exceedances (DH) above two thresholds (35 and 38 °C) and compared against those of the BAU scenario for year 2050 based on the USGS LUCAS projections defined in Section 6.3. As discussed earlier, the impacts are evaluated (in this section) only at those grid cells where urbanization was avoided. If averaging over whole sub-domains, the effects are much smaller.

Figure 6-33 provides a summary of these impacts, presented as percentage-wise reductions in degree-hours (DH) over the thresholds. The reason behind the apparent larger reductions in exceedances above 38 °C (right-side charts) than above 35 °C (left-side charts) is because there is initially less exceedance above 38 compared to above 35 °C, hence relatively easier to offset a larger fraction of the exceedance above 38 °C.

An examination of the results presented in Figure 6-33 suggests that as a crude overall average, the avoided exceedances (DH) as a result of smart growth are: (1) in Auburn: 35% avoided exceedances over 35 °C and 40% avoided exceedances over 38 °C; (2) in Davis, the avoided

exceedances are 10% and 20%, respectively; (3) in El Dorado Hills, avoided exceedances are 25% and 35%, respectively; (4) in Sacramento, 20% and 40% respectively, and (5) in Yuba City, 30% and 60%, respectively.

Figure 6-33: Changes in degree-hours above 35 (left charts) and 38 °C (right charts) resulting from smart growth scenarios

Figure 6-33, continued.

Sacramento 2050 smart growth

Sacramento 2050 smart growth

Yuba City 2050 smart growth

Yuba City 2050 smart growth
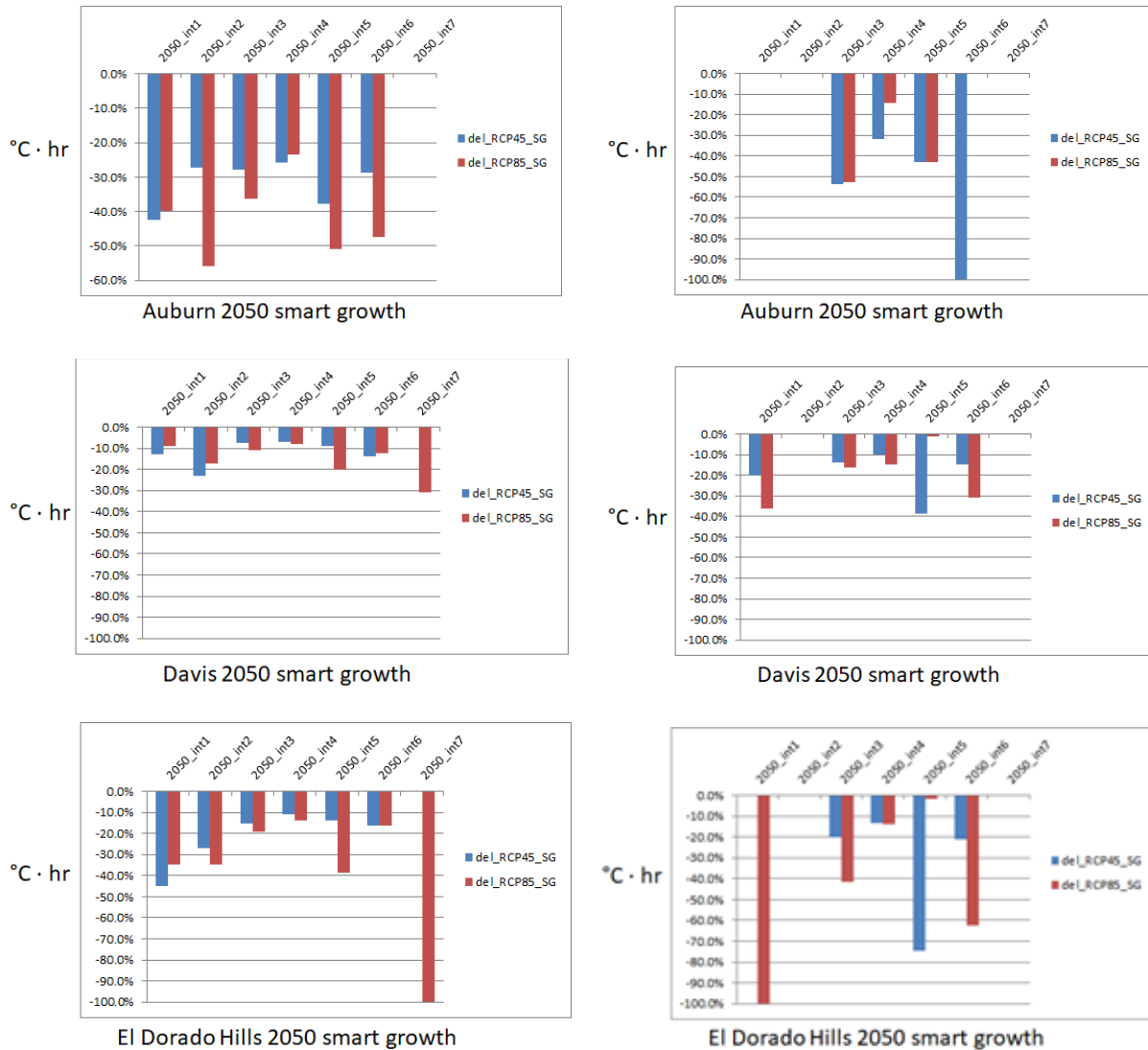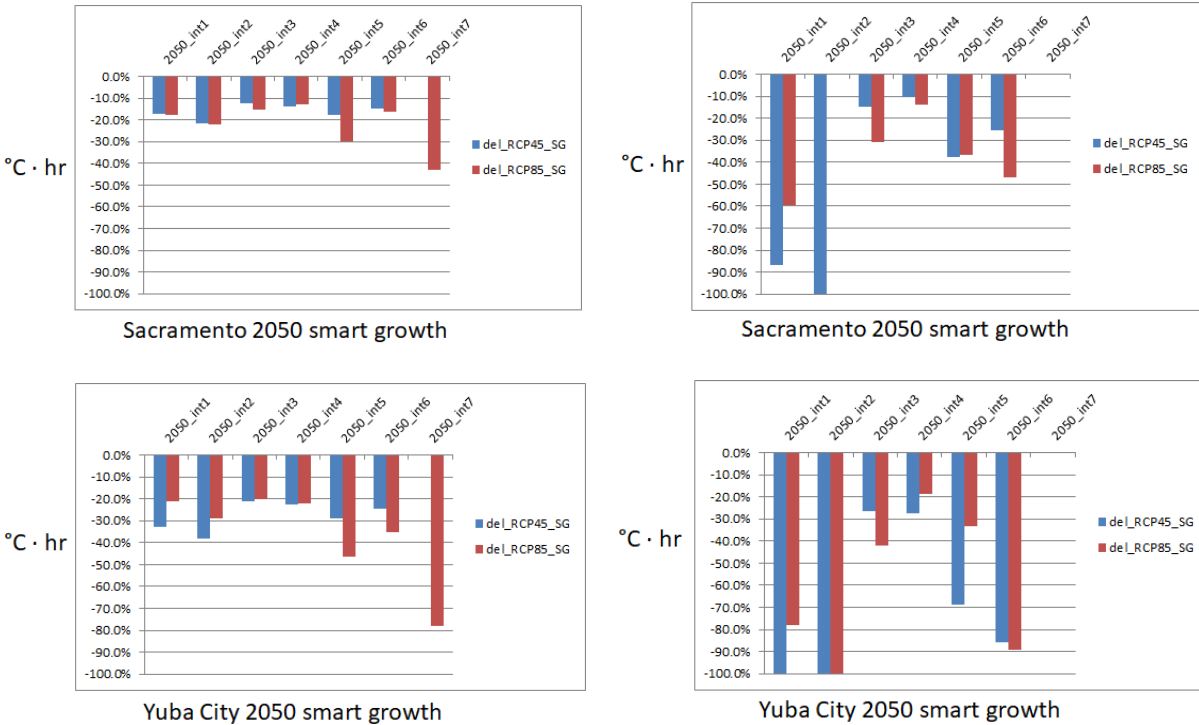
6.13 LOCAL OFFSETS TO THE UHII IN FUTURE CLIMATES

In this section, the 500-m simulations (discussed in Section 5) are revisited but this time in the context of future climate (2050). The goal is to evaluate the effectiveness of localized measures in offsetting the future-climate UHII that was characterized earlier in Section 6.6.

Tables 6-3 (for RCP 4.5) and 6-4 (for RCP 8.5) are structured in a manner similar to Table 5-23 (in Section 5.23), but for future climates. As before, these are the effects of mitigation measures in standalone mode of implementation at the geographical areas identified in the first column.

The model results show that the effectiveness of the mitigation measures in 2050 is generally similar to their effectiveness in current climate. In other words, the UHII attainment levels (percentages) for various measures are of the same magnitudes in 2050 (RCP 4.5 and RCP 8.5) as they are in current climate. Compare the last two columns in Tables 6-3 and 6-4 with the last two columns in Table 5-23. The reason, as explained earlier, is that increased urbanization, while contributing to additional local warming, also means an increase in technical potential, i.e., area available for the deployment of mitigation measures, thus keeping the UHII offset levels relatively similar to those in current climates or even slightly larger in some cases.

Table 6-3: 2050 RCP 4.5 temperature summaries and attainment of the UHII in future climate

Project area	All-hours Tair UHII (°C)**		Localized/no advection UHII attainment local mitigation only	Localized+advection UHII attainment local mitigation+advection
D05 Yuba City / Marysville Downtown YC and M	2.96	Cool roofs / pavements	-47%	-73%
		Cool pavements	-37%	-63%
		Electric vehicles	-6%	-31%
		Vegetation cover	-57%	-83%
D06 Woodland DAC census tracts	2.80	Cool roofs / pavements	-46%	-80%
		Cool pavements	-53%	-87%
		Electric vehicles	-5%	-39%
		Vegetation cover	-39%	-73%
D07 Sac / SE Sac AB617 A, B, D	5.00	Cool roofs / pavements	-26%	-62%
		Cool pavements	-28%	-64%
		Electric vehicles	-5%	-41%
		Vegetation cover	-30%	-66%
D07 Sac / SE Sac AB617 C, E, G	2.67	Cool roofs / pavements	-49%	-87%
		Cool pavements	-52%	-90%
		Electric vehicles	-9%	-47%
		Vegetation cover	-55%	-93%

Project area	All-hours Tair UHII (°C)**		Localized/no advection UHII attainment local mitigation only	Localized+advection UHII attainment local mitigation+advection
D08 Granite Bay	5.55	Cool roofs / pavements	-25%	-50%
		Cool pavements	-31%	-56%
		Electric vehicles	-6%	-30%
		Vegetation cover	-19%	-44%
D08 Roseville	6.42	Cool roofs / pavements	-22%	-54%
		Cool pavements	-27%	-59%
		Electric vehicles	-5%	-37%
		Vegetation cover	-16%	-48%
D09 El Dorado Hills	5.02	Cool roofs / pavements	-30%	-50%
		Cool pavements	-34%	-54%
		Electric vehicles	-4%	-24%
		Vegetation cover	-22%	-43%
D09 Folsom	5.46	Cool roofs / pavements	-27%	-53%
		Cool pavements	-31%	-57%
		Electric vehicles	-4%	-29%
		Vegetation cover	-20%	-46%
D10 Placerville / Diamond Springs / El Dorado City	1.59	Cool roofs / pavements	-75%	-99%
		Cool pavements	-101%	-125%
		Electric vehicles	-5%	-29%
		Vegetation cover	-82%	-106%

Table 6-4: 2050 RCP 8.5 temperature summaries and attainment of the UHII in future climate

Project area	All-hours Tair UHII (°C)**		Localized/no advection UHII attainment local mitigation only	Localized+advection UHII attainment local mitigation+advection
D05 Yuba City / Marysville Downtown YC and M	2.64	Cool roofs / pavements	-53%	-79%
		Cool pavements	-42%	-67%
		Electric vehicles	-6%	-32%
		Vegetation cover	-64%	-90%
D06 Woodland DAC census tracts	2.57	Cool roofs / pavements	-50%	-83%
		Cool pavements	-57%	-91%
		Electric vehicles	-6%	-39%
		Vegetation cover	-42%	-76%
D07 Sac / SE Sac AB617 A, B, D	5.13	Cool roofs / pavements	-25%	-61%
		Cool pavements	-27%	-63%
		Electric vehicles	-5%	-40%
		Vegetation cover	-29%	-64%
D07 Sac / SE Sac AB617 C, E, G	2.99	Cool roofs / pavements	-43%	-83%
		Cool pavements	-47%	-86%
		Electric vehicles	-8%	-47%
		Vegetation cover	-49%	-88%
Project area	All-hours Tair UHII (°C)**		Localized/no advection UHII attainment local mitigation only	Localized+advection UHII attainment local mitigation+advection
D08 Granite Bay	5.72	Cool roofs / pavements	-25%	-48%
		Cool pavements	-30%	-54%
		Electric vehicles	-5%	-29%
		Vegetation cover	-18%	-42%
D08 Roseville	6.63	Cool roofs / pavements	-21%	-53%
		Cool pavements	-26%	-57%
		Electric vehicles	-5%	-36%
		Vegetation cover	-16%	-47%
D09 El Dorado Hills	5.22	Cool roofs / pavements	-29%	-47%
		Cool pavements	-32%	-51%
		Electric vehicles	-4%	-22%
		Vegetation cover	-21%	-40%
D09 Folsom	5.62	Cool roofs / pavements	-27%	-51%
		Cool pavements	-30%	-55%
		Electric vehicles	-3%	-28%
		Vegetation cover	-20%	-44%
D10 Placerville / Diamond Springs / El Dorado City	1.6	Cool roofs / pavements	-75%	-100%
		Cool pavements	-100%	-125%
		Electric vehicles	-5%	-30%
		Vegetation cover	-81%	-106%

7. CONCLUDING REMARKS AND QUALITATIVE TAKEAWAYS

In concluding this report, a few qualitative takeaways are provided, in no particular order:

1. Significant urban-heat pollution exists in the 6-counties Capital region. The UHI and the UHII are larger in urban areas that (1) are more densely built up, (2) cover a larger geographical area, (3) located at the downwind end of an urban zone (trajectory-wise), (4) located at higher elevations, and (5) surrounded by non-urban areas that cool down significantly faster at night.

2. While temperature in the Capital region generally increases from current climate to future (e.g., to 2050 RCP 4.5 and then to 2050 RCP 8.5), the corresponding UHII also increases in this direction except for two urban areas where the UHII can be smaller in RCP 8.5 than in RCP 4.5 (although still larger than in current climate). This is a result of faster warming in the surrounding non-urban areas.

3. It is possible and highly feasible to mitigate the current UHI and offset the UHII (in some cases completely) using materials and practices that are reasonable and readily used throughout the 6-counties Capital region. The proposed UHI mitigation measures are reasonable – meaning they do not require hypothetical or extreme implementation levels, only what is already available and used in the current market and current construction and building practices.

4. Mitigation measures can offset the local UHII in standalone fashion, in some cases completely. Various combinations of measures can further attain or further offset the UHII, although the total effects of combinations of measures are not linear (not simple sums of individual cooling effects) and generally smaller than the sum of cooling effects from the individual UHI-mitigation measures.

5. The mitigation measures can have significant beneficial effects in terms of public heat health as indicated by their ability to lower the warning levels of the National Weather Service Heat Index (NWS HI). This was assessed by modeling various UHI-mitigation scenarios in this study.

6. The cooling measures can significantly reduce or completely erase the number of heat-wave days during several excessive-heat event periods identified in the study.

7. The mitigation measures are as effective under conditions of future climate and land use as they are under current conditions.

8. Different mitigation measures affect urban heat and temperature differently during different times of the day. Hence it is possible to target certain specific time intervals, e.g., peaks, night, day, or all hours (per a community or city's needs), if so desired, by choosing a specific mitigation measure or combinations of measures as suitable.

9. If, in addition to a community's own heat-mitigation actions, neighboring communities also implement UHI-mitigation measures, the local cooling effects could double (although there is a range of effects depending on location, time, specific measures, etc.).

10. Other measures that are not conventionally associated with urban cooling (or urban heat island mitigation), such as (1) vehicle electrification, (2) solar PV installations, and (3) smart urban growth, all appear to have significant urban-cooling effects.

11. The cooling effects are significant and beneficial across a range of urban areas in the Capital region, including AB617 and disadvantaged communities, which can help improve thermal comfort, reduce emissions of air pollutants, and improve air quality.

12. In this study, a ranking of measures' efficacy was done for each region, each measure, and each time interval (e.g., specific hours or a range of hours) for current and future climates and land use. Some areas or time intervals have a consistent ranking of measures, others vary by location, and, yet, others vary in future climate relative to current conditions. Some highlights are:

    a. For the 0600-PDT UHII:

        i. The rankings of mitigation measures (order) are similar and consistent across all regions.

        ii. Within each region, the rankings are similar across current and future climates.

    b. For the 1300-PDT UHII:

        i. The rankings are different across the regions.

        ii. In Davis and Sacramento, the rankings are different in future climate than they are in current climate.

    c. For the 1400 – 2000 PDT UHII:

        i. The rankings are different across the regions.

        ii. In Woodland, the rankings are different in future climate than they are in current climate.

    d. For the 1500 PDT UHII:

        i. The rankings are different across the regions.

        ii. In Auburn, Davis, El Dorado Hills, and Yuba City, the rankings are different in future climate than they are in current climate.

    e. For the all-hours UHII:

        i. The rankings are different across the regions.

        ii. Within each region, the rankings are similar across current and future climates.

13. Information generated in this modeling study can be used by Caltrans, SMAQMD, LGC, the cities and communities in the Capital region to prioritize projects and implementation of various measures or in the allocation of resources per urban-heat criteria under current climate conditions as well as in future climate and land use.

8. REFERENCES

Akbari H, Konopacki S, 2005. Calculating energy-saving potentials of heat-island reduction strategies. Energy Policy, 33, 721-756.

Akbari H, Rose S, Taha H, 1999. Characterizing the fabric of the urban environment: A case study of Sacramento, California. Lawrence Berkeley National Laboratory report LBNL-44688, Berkeley, California.

Alfaro E, Gershunov A, Cayan D, Steinemann A, Pierce D, Barnett T 2004. A method for prediction of California summer air surface temperature, EOS Transactions AGU, 85, 553–558 doi:10.1029/2004EO510001

Alfaro E, Gershunov A, Cayan D 2006. Prediction of summer maximum and minimum temperature over the central and western United States: The role of soil moisture and sea surface temperature. Journal of Climate 19, 1407-1421, doi: 10.1175/JCLI3665.1

Anderson JR, Hardy EE, Roach JT, Witmer RE, 2001. A land use and land cover classification system for use with remote sensor data. USGS Professional Paper 964, U.S. Government Printing Office, Washington, DC.

Ban-Weiss GA, Woods J, Millstein D, Levinson R, 2015. Using remote sensing to quantify albedo of roofs in seven California cities, Part 2: Results and application to climate modeling. Solar Energy, 115, 791-80, doi:10.1016/j.solener.2014.10.041

Benjamin M, Sudol M, Bloch L, Winer A, 1996. Low-emitting urban forests: A taxonomic methodology for assigning isoprene and monoterpene emission rates. Atmospheric Environment, 30, 1437 – 1452.

Berdahl P, Akbari H, Rose S, 2002. Aging of reflective roofs: Soot deposition. Applied Optics, 41, 2355. Also, Lawrence Berkeley National Laboratory Report No. 45367.

Berdahl P, Bretz S, 1997. Preliminary survey of the solar reflectance of cool roofing materials. Lawrence Berkeley National Laboratory Report No. 41294.

Bierwagen BG, Theobald DM, Pyke CR, Choate A, Groth P, Thomas JV, Morefield P 2010. National housing and impervious surface scenarios for integrated climate impacts assessments. PNAS 107, 20887-20892.

Bruyere C, Done JM, Holland GJ, Fredrick S, 2014. Bias corrections of global models for regional climate simulations of high-impact weather. Climate Dynamics, 43, 1847-1856, doi: 10.1007/s00382-013-2011-6

Burian S, Han WS, Brown M, 2003. Morphological analyses using 3-D building databases: Houston Texas. Department of Civil and Environmental Engineering, University of Utah.

Chen F, Kusaka H, Bornstein R, Ching J, Grimmond CSB, Grossman-Clarke S, Loridan T, Manning K, Martilli A, Miao S, Sailor D, Salamanca F, Taha H, Tewari M, Wang X, Wyszogrodzki A, Zhang C, 2010. The integrated WRF/urban modeling system: development, evaluation, and applications to urban environmental problems. International Journal of Climatology doi:10.1002/joc.2158.

Ching J, Brown M, Burian S, Chen F, Cionco R, Hanna A, Hultgren T, McPherson T, Sailor D, Taha H, Williams D, 2009. National urban database and access portal tool, NUDAPT. Bulletin of the American Meteorological Society doi:10.1175/2009BAMS2675.1

Clarke LE, Edmonds JA, Jacoby HD, Pitcher H, Reilly JM, Richels R, 2007. Scenarios of greenhouse gas emissions and atmospheric concentrations. Sub-report 2.1a of Synthesis and Assessment Product 2.1. Climate Change Science Program and the Subcommittee on Global Change Research, Washington DC.

Cooper CD, Alley FC, 1994. Air pollution control: A design approach. Waveland Press, Inc., Prospect Heights, IL, 694 pp.

Davey (2018). Urban tree canopy assessment, Sacramento, CA. Report prepared by Davey Resource Group for the City of Sacramento, pp. 56, Atascadero, California.

DuPont S, Mestayer PG, Guilloteau E, 2005. Parameterization of the urban water budget with the sub-mesoscale model. Journal of Applied Meteorology and Climatology, 45, 624 – 648.

Epstein SA, Lee S-M, Katzenstein AS, Carreras-Sospedra M, Zhang X, Farina SC, Vahmani P, Fine PM, Ban-Weiss G, 2017. Air-quality implications of widespread adoptions of cool roofs on ozone and particulate matter in southern California. PNAS August 7, 2017, https://doi.org/10.1073/pnas.1703560114.

Fallmann J, Forkel R, Emeis S, 2016. Secondary effects of urban heat island mitigation measures on air quality. Atmospheric Environment, 125, 199 – 211.

Fan H, Sailor DJ, 2005. Modeling the Impacts of Anthropogenic Heating on the Urban Climate of Philadelphia: A comparison of implementations in two PBL schemes. Atmospheric Environment, 39, 73-84.

Founda D, Santamouris M, 2017. Synergies between urban heat island and heat waves in Athens (Greece) during extremely hot summer (2012). Scientific Reports, 7: 10973. doi:10.1038/s41598-017-11407-6

Georgescu M, Morefield PE, Bierwage BG, Weaver CP. 2014. Urban adaptation can roll back warming of emerging metropolitan regions. Proceedings of the National Academy of Sciences 111, 2909-2914 doi: 10.1073/pnas.1322280111

Gershunov A, Cayan DR, Iacobellis SF, 2009. The great 2006 heat wave over California and Nevada: Signal of an increasing trend. Journal of Climate 22, 6181-6203.

Gery MW, Whitten GZ, Killus JP, 1988. Development and testing of the CBM-IV for urban and regional modeling. Report EPA-600/3-88-012, US EPA, Research Triangle Park, NC.

Gilbert HE, Rosado PJ, Ban-Weiss G, Harvey JT, Li H, Mandel BH, Millstein D, Mohegh A, Saboori A, Levinson RM, 2017. Energy and environmental consequences of a cool pavement campaign. Energy and Buildings, 157, 53-77, doi:10.1016/j.enbuild.2017.03.051

Grimmond CSB, Oke TR, 1999. Aerodynamic properties of urban areas derived from analysis of surface form. Journal of Applied Meteorology, 38, 1262-1292.

Hijioka Y, Matsuoka Y, Nishimoto H, Masui T, Kainuma M, 2008. Global GHG emission scenarios under GHG concentration stabilization targets. Journal of Global Environmental Engineering, 13, 97–108

Jacobson MZ, TenHoeve JE, 2011. Effects of urban surfaces and white roofs on global and regional climate. Journal of Climate, doi: 10.1175/JCLI-D-11-00032.1

Johnston B, Lehmer E, Gao S, Roth N, McCoy M. 2013. UPlan Land Use Allocation Model 2.6. University of California at Davis – Information Center for the Environment (http://ice.ucdavis.edu/project/uplan).

Kalkstein LS, Barthel CD, Green JS, Nichols MC,1996. A new spatial synoptic classification: Application to air-mass analysis. International Journal of Climatology, 16, 983-1004.

Kistler R, Kalnay E, Collins W, et al., 2001. The NCEP-NCAR 50-year reanalysis: Monthly means CDROM and documentation. Bulletin of the American Meteorological Society, 82, 247-267

Kusaka H, Kondo H, Kikegawa Y, Kimura F, 2001. A simple single-layer urban canopy model for atmospheric models: Comparison with multi-layer and slab models. Boundary-Layer Meteorology, 101, 329-358

Altostratus Inc.

Levinson R, Akbari H, Reilly JC, 2007. Cooler tile-roofed buildings with near-infrared-reflective non-white coatings. Energy & Buildings, 42, 2591-2605.

Levinson RM, Gilbert HE, Jin L, Harvey J, Kendall A, Li H, Mandel B, Millstein D, Rosado P, Saboori A, Lea J, Ban-Weiss G, Mohegh A, Santero N, 2017. Life-cycle assessment and co-benefits of cool pavements. Report prepared by the Lawrence Berkeley National Laboratory for the California Air Resources Board and the California Environmental Protection Agency under Contract 12-314.

Li D, Bou-Zeid E. 2013. Synergistic interactions between urban heat islands and heat waves: The impact in cities is larger than the sum of its parts. Journal of Applied Meteorology and Climatology 52, 2051-2064 doi: 10.1175/JAMC-D-13-02.1

Liu SC, Trainer M, 1988. Response of the tropospheric ozone and odd hydrogen radicals to column ozone change. Journal of Atmospheric Chemistry, 6, 221 – 233.

Macdonald RW, Griffiths RF, Hall DJ, 1998. An improved method for estimation of surface roughness of obstacle arrays. Atmospheric Environment, 32, 1857–1864

Martilli A, Clappier A, Rotach MW 2002. An urban surface exchange parameterization for mesoscale models. Boundary-Layer Meteorology, 104, 261-304

Masson V, Bonhomme M, Salagnac J-L, Briottet X, Lemonsu A, 2014. Solar panels reduce both global warming and urban heat island. Frontiers in Environmental Science, doi: 10.3389/fenvs.2014.00014

Multi-Resolution Land-Characteristics Consortium (MRLC) 2011. National Land Cover Databases. http://www.mrlc.gov/data/nlcd-2011-land-cover-conus-0

National Oceanic and Atmospheric Administration 2015. CM2 and CMIP5 models. https://www.ncdc.noaa.gov/data-access/model-data/model-datasets/climate-prediction

NOAA/MADIS. National Oceanic and Atmospheric Administration / Meteorological Assimilation Data Ingest System (https://madis.ncep.noaa.gov/)

OEHHA 2013. California Communities Environmental Health Screening Tool, Version 1 (CalEnviroScreen 1.0) Guidance and Screening Tool. Office of Environmental Health Hazard Assessment Report, Sacramento, California, oehha.ca.gov/ej/pdf/042313CalEnviroScreen1.pdf

Pleim J, Xiu A, Finkelstein P, Otte T, 2001. A coupled land-surface and dry deposition model and comparison to field measurements of surface heat, moisture, and ozone fluxes. Water, Air, and Soil Pollution, 1, 243-252.

Pretzsch H, Biber P, Uhl E, Dahlhausen J, Rotzer T, Caldentey J, Koike T, van Con T, Chavanne A, Seifert T, du Toit B, Farnden C, Apuleit S, 2015. Crown size and growing space requirements of common tree species in urban center, parks, and forests. Urban Forestry & Urban Greening, 14, 466 – 479.

Riahi K, Krey V, Rao S, Chirkov V, Fischer G, Kolp P, Kindermann G, Nakicenovic N, Rafai P, 2011. RCP-8.5: exploring the consequence of high emission trajectories. Climatic Change, doi: 10.1007/s10584-011-0149-y

Rosado PJ, Ban-Weiss G, Mohegh A, Levinson RM, 2017. Influence of street setbacks on solar reflection and air cooling by reflective streets in urban canyons. Solar Energy 144, 144-157, doi:10.1016/j.solener.2016.12.026

Rose S, Akbari H, Taha H, 2003. Characterizing the fabric of the urban environment: A case study of Greater Houston, Texas. Lawrence Berkeley National Laboratory report LBNL-51448, Berkeley, California.

Altostratus Inc.

Sailor DJ, Lu L, 2004. A top–down methodology for developing diurnal and seasonal anthropogenic heating profiles for urban areas. Atmospheric Environment, 38, 2737 – 2748.

Salamanca F, Martilli A, 2009. A new building energy model coupled with an urban canopy parameterization for urban climate simulations – Part II: Validation with one dimension off-line simulations. Theoretical and Applied Climatology, 99, 345-356, doi: 10.1007/s00704-009-0143-8

Salamanca F, Georgescu M, Mahalov A, Moustaoui M, Martilli A, 2016. Citywide impacts of cool roofs and rooftop photovoltaic development on near-surface air temperature and cooling energy demand. Boundary-Layer Meteorology, 161, 203-221.

Seinfeld JS, 1975. Air pollution – Physical and chemical fundamentals. McGraw Hill, New York, NY.

Seinfeld JS, Pandis SN, 1998. Atmospheric Chemistry and Physics. John Wiley & Sons, Inc., New York, 1326 pp.

Simpson J, McPherson G, 2007. Preliminary evaluation of the potential air-quality benefits of trees within SIP guidelines. Center for Urban Forest Research, PSW, USDA Forest Service.

Skamarock W, Klemp J, Dudhia J, et al., 2008. A description of the Advanced Research WRF. NCAR Technical Note NCAR/TN-475+STR, National Center for Atmospheric Research, Boulder, Colorado.

Sleeter BM, Wilson TS, Sherba JT. 2017a. Land use and land cover projections for California's 4th Climate Assessment. US Geological Survey Data Release, doi: 10.5066/F7M61HFP. IP-083329.

Sleeter BM, Wilson TS, Sharygin E, Sherba JT, 2017b. Future scenarios of land change based on empirical data and demographic trends. Earth's Future, 5, 1068–1083, doi: 10.1002/2017EF000560

SMAQMD 2018. Final Assessment of Proposed Monitoring Locations for AB 617 Community Air Protection Action. Report prepared by the Sacramento Metropolitan Air Quality Management District, July 31, 2018.

Stern AC, Boubel RW, Turner DB, Fox DL, 1984. Fundamentals of air pollution. Academic Press, Inc., 530 pp.

Taha H, 2018. Intra-urban enhancements to probabilistic climate forecasting for the electric system. Contract CEC-15-070; report to be published online on the California Energy Commission Website.

Taha H, 2017. Characterization of urban heat and exacerbation: Development of a heat island index for California. Climate 5, 59. doi:10.3390/cli5030059.

Taha H, 2015a. Cool cities: counteracting potential climate change and its health impacts. Current Climate Change Reports, doi: 10.1007/s40641-015-0019-1.

Taha H, 2015b. Meteorological, air-quality, and emission-equivalence impacts of urban heat island control in California. Invited Paper, Sustainable Cities and Society, doi: 10.1016/j.scs.2015.03.009

Taha H, 2013a. Meteorological, emissions, and air-quality modeling of heat-island mitigation: Recent findings for California, U.S.A. International Journal of Low Carbon Technologies, doi: 10.1093/ijlct/ctt010

Taha H, 2013b. Multi-episodic and seasonal meteorological, air-quality, and emission-equivalence impacts of heat-island control and evaluation of the potential atmospheric effects of urban solar photovoltaic arrays. Final report prepared by Altostratus Inc. for the California Energy Commission, PIER Environmental Research Program, Sacramento, California.

Altostratus Inc.

http://www.energy.ca.gov/2013publications/CEC-500-2013-061/CEC-500-2013-061.pdf

Taha H, 2012. The potential for air-temperature impact from large-scale deployment of solar photovoltaic arrays in urban areas. Solar Energy, 91, 358 – 367.

Taha H, 2008a. Meso-urban meteorological and photochemical modeling of heat island mitigation. Atmospheric Environment, 42, 8795-8809, doi:10.1016/j.atmosenv.2008.06.036.

Taha H, 2008b. Episodic performance and sensitivity of the urbanized MM5 (uMM5) to perturbations in surface properties in Houston TX. Boundary-Layer Meteorology 127, 193-218. doi:10.1007/s10546-007-9258-6.

Taha H, 2008c. Urban surface modification as a potential ozone air-quality improvement strategy in California: A mesoscale modeling study. Boundary-Layer Meteorology, 127, 219-239 doi:10.1007/s10546-007-9259-5.

Taha H, 2007. Urban surface modification as a potential ozone air-quality improvement strategy in California -- Phase 2: Fine-resolution meteorological and photochemical modeling of urban heat islands. Final report prepared by Altostratus Inc. for the California Energy Commission, Sacramento, California, PIER Environmental Research.
http://www.energy.ca.gov/2009publications/CEC-500-2009-071/CEC-500-2009-071.PDF

Taha H, 2005. Urban surface modification as a potential ozone air-quality improvement strategy in California -- Phase 1: Initial Mesoscale Modeling, Final report prepared by Altostratus Inc. for the California Energy Commission, Sacramento, California, PIER Environmental Research, 169 pp. http://www.energy.ca.gov/2005publications/CEC-500-2005-128/CEC-500-2005-128.PDF

Taha H, 2001. Potential impacts of climate change on tropospheric ozone in California: A preliminary assessment of the Los Angeles basin and the Sacramento valley. Lawrence Berkeley National Laboratory Report LBNL-46695, http://escholarship.org/uc/item/5s41x609

Taha H, 1999. Modifying a Mesoscale Meteorological Model to Better Incorporate Urban Heat Storage: A Bulk-Parameterization Approach. Journal of Applied Meteorology, 38, 466-473.

Taha H. 1997. Modeling the Impacts of Large-Scale Albedo Changes on Ozone Air Quality in the South Coast Air Basin. Atmospheric Environment, 31, 1667-1676.

Taha H, 1996. Modeling the Impacts of Increased Urban Vegetation on the Ozone Air Quality in the South Coast Air Basin. Atmospheric Environment, 30, 3423-3430.

Taha H, Levinson R, Mohegh A, Gilbert H, Ban-Weiss G, Chen S, 2018. Air-temperature response to neighborhood-scale variations in albedo and canopy cover in the real world: Fine-resolution meteorological modeling and mobile temperature observations in the Los Angeles climate archipelago. Climate 6, 53 (25 pp). https://doi.org/10.3390/cli6020053

Taha H, Freed T 2015. Creating and mapping an urban heat island index for California. Prepared by Altostratus Inc. for the California Environmental Protection Agency. https://calepa.ca.gov/wp-content/uploads/sites/34/2016/10/UrbanHeat-Report-Report.pdf

Taha H, Wilkinson J, Bornstein R, Xiao Q, McPherson G, Simpson J, Anderson C, Lau S, Lam J, Blain C, 2015. An urban–forest control measure for ozone in the Sacramento, CA Federal Non-Attainment Area (SFNA), Sustainable Cities and Society, 21, 51-65 doi: 10.1016/j.scs.2015.11.004.

Taha H, Wilkinson J, Bornstein R, 2011. Urban forest for clean air demonstration in the Sacramento Federal Non-Attainment Area: Atmospheric modeling in support of a voluntary control strategy. Project final report prepared by Altostratus Inc. for the Sacramento Metropolitan Air Quality Management District (SMAQMD), Sacramento, California.

Taha, H. and Sailor, D. 2010. "Evaluating the effects of radiative forcing feedback in modeling urban ozone air quality in Portland, Oregon: Two-way coupled MM5 - CMAQ simulations". *Boundary-Layer Meteorology*, Volume 137, No. 2, (2010), pp. 291-305-- doi:10.1007/s10546-010-9533-9.

Taha, H., Konopacki, S., and Gabersek, S. 1999. "Impacts of large-scale surface modifications on meteorological conditions and energy use: A 10-region modeling study", *Theoretical and Applied Climatology*, Vol. 62, no. 3-4, pp. 175-185.

Tesche TW, McNally DE, Emery CA, Tai E 2001. Evaluation of the MM5 model over the Midwestern U.S. for three 8-hour oxidant episodes, Prepared for the Kansas City Ozone Technical Workgroup. Alpine Geophysics LLC and Environ Corp.

Thompson AM, 1991. Interaction of atmospheric chemicals and climate changes: Implications for tropospheric ozone. Chapter 4 in Sloane CS and Tesche TW (eds.) 1991. Atmospheric chemistry models and predictions for climate and air quality. Lewis Publishers, Inc. Michigan.

Thompson AM, 1992. The oxidizing capacity of the Earth's atmosphere: Probable past and future changes. Science, 256, 1157 – 1165.

Van Vuuren DP, Stehfest E, Den Elzen MGJ, Deetman S, Hof A, Isaac M, Klein Goldewijk K, Kram T, Mendoza Beltran A, Oostenrijk R et al., 2011. RCP2.6: Exploring the possibility to keep global mean temperature change below 2°C. Climatic Change. doi: 10.1007/s10584-011-0152-3